



SBQT

2 0 1 5

XVIII

**Simpósio Brasileiro
de Química Teórica**

22 a 25 de Novembro de 2015

sbqt-2015.net.br

**RESUMOS
ABSTRACTS BOOK**

22 à 25 de Novembro 2015

Hotel Pousada dos Pireneus - Pirenópolis - GO - Brasil



2 0 1 5



sbqt-2015.net.br

Simpósio Brasileiro de Química Teórica (18.: 2015: Pirenópolis, 2015)

S6121

2013 Livro de Resumos do 18º Simpósio Brasileiro de Química Teórica – SBQT,
22 à 25 de Novembro 2015. Pirenópolis: Editora da UnB, 2015.

246 f.: il.

ISSN: 2237-2679

Coordenador: Kleber Carlos Mundim

1. Química Teórica - congressos. 2. Modelagem Molecular - congressos

I. Mundim, Kleber C., Coord. II. Título.

CDU 541 (06)

APRESENTAÇÃO

O Simpósio Brasileiro de Química Teórica (SBQT), na sua XVIII edição em 2015, completa 34 anos. O sucesso verificado nos encontros anteriores avaliza o fato de que esse evento se torna progressivamente a maior instância, nacional e latino americana, de expressão da comunidade de Química Teórica superando, inclusive, a barreira linguística dessa região americana. Este sucesso alcançado pelo SBQT reside no fato dele permitir a articulação dos grupos de pesquisa em Física, Química e áreas Biológicas direcionando e otimizando os esforços para o desenvolvimento de métodos teóricos e computacionais de interesse comum e para a utilização e aprimoramento de técnicas experimentais existentes no país, na busca de um entendimento mais completo de problemas em Química Moderna.

A Química Teórica, antes tida como uma área de interesse puramente acadêmico, passou a ser reconhecida como de grande importância na formação do Químico do Século XXI. Nessa última década, multiplicaram-se os cursos, tanto em nível de Graduação como de Pós-Graduação, em todo o país. Atualmente, a Química Teórica no Brasil engloba contribuições de diversas áreas específicas tais como Química Quântica, Dinâmica Atômica e Molecular, Simulação Computacional de Sistemas Líquidos e Sólidos, Modelagem Molecular de Sistemas de Interesse Biológico e Tecnológico, Catálise Química, Físico-Química Orgânica, entre outras. Nesse contexto, são inegáveis as contribuições do SBQT para o desenvolvimento da área no país. Portanto, nesse simpósio, bem como nos anteriores a programação terá um caráter diversificado visando contemplar as diferentes linhas de pesquisa existente na comunidade de química teórica do país.

A 18ª edição do SBQT será realizada na cidade histórica de Pirenópolis (GO) dando assim mais um salto ousado ao sair da região Sudeste para o interior do Brasil. É importante ressaltar que esse Simpósio ocorrerá à 50km da cidade de Anápolis que é o segundo maior polo da indústria farmacêutica e agrícola da América do Sul. Esta ação solidifica o SBQT como um evento de importância nacional tanto pela regularidade quanto pelo caráter de abrangência geográfica e científica que, no contexto geral, visa capacitar e formar pessoal especializado em química assim como facilitar o intercâmbio entre os diversos grupos de pesquisa nacionais ao setor produtivo como estabelece as metas do Governo Federal para as próximas décadas em CT&I.

Kleber Carlos Mundim

COVER PAGE

The Brazilian Symposium on Theoretical Chemistry (SBQT) in its seventeenth edition in 2015 is turning 34 years of existence. The success saw in previous meetings endorses the fact that this event becomes progressively the largest instance, national and in Latin America, expressions of Theoretical Chemistry Community, surpassing even the language barrier of the American region. The success of the SBQT lies in the fact that this event allows a large and direct articulation of research groups in Physics, Chemistry and Biological areas optimizing efforts to develop theoretical and computational methods of common interest and to use and improve experimental known techniques in the country searching a complete and better understanding of problems in Modern Chemistry.

The Theoretical Chemistry, before seen as a purely academic area of interest, was recognized with great importance in the development of Chemical of the XXI Century. In this last decade, multiplied the number of courses, as in undergraduate level as in Graduation and Pos Graduation degree in all country. Nowadays, Theoretical Chemistry in Brazil includes several specific areas of contributions such as Quantum Chemistry, Atomic and Molecular Dynamics, Computer Simulation of Liquids and Solids Systems, Molecular Modeling of Biological Interest and Technological, Catalysis Chemistry, Physical Chemistry Organic, and others. In this context, SBQT's contributions to the development of the area in the country are undeniable. Therefore, in this Symposium as well as in previous, the programming has a diverse character looking especially for different lines of existing research in Theoretical Chemistry Community in the country.

The 18th edition of SBQT will be held in the historic city of Pirenópolis (GO), taking another audacious leap out of the Southeast region to the internal of Brazil. Note that this Symposium will take place at 50 km from the city of Anapolis (GO), which is the second largest center of pharmaceutical and agricultural industry in South America. This action solidifies SBQT as a national important event, both for the regularity as the geographic and scientific scope. In the general context, that character aims to empower and train specialized staff in chemistry as well as facilitate the exchange between the various groups of national research to industry productive and also establish goals of the Federal Government for the next decades in CT&I.

Kleber Carlos Mundim

Comissão Organizadora:

Coordenador: Prof. Kleber Carlos Mundim (UnB)

Vice-coordenador: Profa. Kaline Rabelo Coutinho (USP)

Prof. André Gustavo Horta Barbosa (UFF)

Profa. Elizete Ventura do Monte (UFPB)

Prof. Heitor Avelino de Abreu (UFMG)

Prof. João Batista Lopes Martins (UnB)

Profa. Paula Homem de Mello (UFABC)

Comitê Local:

Prof. Marcos Antônio de Castro (UFG)

Prof. Solemar Silva Oliveira (UEG)

Prof. Hamilton B. Napolitano (UEG)

Prof. Demétrio Antônio da Silva Filho (UnB)

Profa. Maria Suely Pedrosa Mundim (UnB)

Comitê Científico:

Prof. Alfredo Mayall Simas (UFPE)

Prof. Marco Antonio Chaer do Nascimento (UFRJ)

Prof. Sylvio Canuto (USP)

Prof. Wagner Batista de Almeida (UFF)

SUMÁRIO

- 19 PROF. YUJI TAKAHATA
- 20 CRONOGRAMA
- PALESTRAS / LECTURES**
- 23 Oral 001 **Analyzing Proton Acidity with the Proton Propagator Approach**
Andrés Reyes , Laura Pedraza
- 24 Oral 002 **Directions of chemical change: reaction kinetics beyond Arrhenius and Eyring**
Nayara, Valter, Heibbe, Ademir, Mundim Vincenzo Aquilanti
- 25 Oral 003 **Covalence, not Resonance-Assistance, behind Cooperative Hydrogen and Halogen bonds**
Célia F. Guerra
- 26 Oral 004 **Controlling the Figure of Merit in some narrow band gap semiconductors: Density Functional theory study**
David Fuks, Yaniv Gelbstein
- 27 Oral 005 **Activation Strain Model (ASM) of Chemical Reactivity**
F. M. Bickelhaupt
- 28 Oral 006 **Alternative Physically Inspired Methodologies to Optimize the Long Range Separated Hybrid Density Functionals Based on the Maximum Hardness and Minimum Polarizability Principles**
Heibbe C. B. de Oliveira
- 29 Oral 007 **Following Chemical Reactions in Real Time**
Lars G.M. Pettersson
- 30 Oral 008 **A Quantum Chemical Approach to the Understanding of the Intrinsic Properties of Organic Donor-Acceptor Materials**
Terttu I. Hukka, Tuuva Kastinen, Outi Kontkanen, Mika Niskanen, Oana Cramariuc
- 31 Oral 009 **Protein Structure Prediction Combining Generalized Simulated Annealing and Molecular Dynamics Simulation**
Tacio V. A. Fernandes, Mariana F. R. Teixeira and Pedro G. Pascutti
- RESUMOS / ABSTRACTS**
- 35 Poster 001 **MRHFCI Calculations for BH molecule in the DZ base**
A. M. de C. Sobrinho , M. D. de Andrade , L. A. C. Malbouisson
- 36 Poster 002 **A Valence Bond Description of the Grignard Addition Reactions to a Ketone**
Henriques, A.M. , Barbosa A.G.H.
- 37 Poster 003 **Estudo teórico de adsorção de espécies gasosas em nanotubos de ZnO dopados com Cu**
Ademar Dourado Moitinho Neto a João B.L. Martins
- 38 Poster 004 **Estudo da Ligação e Ativação do O2 em Complexos do tipo FeN4: Um Estudo de DFT.**
Adilson L. P. Silva a , Jaldyr de J. G. Varela Júnior
- 39 Poster 005 **Theoretical and Experimental Study of Structural and Electronic Effects in DHMC.HCl**
Alberto dos Santos Marquesa , Gisele Franco de Castrob. Yuji Takahata
- 40 Poster 006 **Octopus: A Virtual High Throughput Screening Platform for Multi-Compounds and Targets**
Alex G. Taranto, Bianca dos R. Santos, Marina S. Costa, Vinícius A. Campos, Iann G. Lima, Sandro J. Greco, Rosy I. M. A. Ribeiro, Felipe M. Munayer, Alisson M. da Silva .
- 41 Poster 007 **Comparative Study of Asphaltene-Inhibitor Interactions by Density Functional Theory**
Alexandre N. M. Carauta , Michelle C. N. de Carvalho , Fernanda B. Silva, Julio C. C. Guedes, Maurício T. M. Cruze , Peter R. Seidl

- 42 Poster 008 **QSAR studies of combretastatin-like chalcones using PLS and ANN methods**
Célio F. Lipinski , Aline A. Oliveira , Albérico B. F. da Silva
- 43 Poster 009 **Theoretical Investigation of Carboxymethylcellulose/Glyceryl Monooleate Adsorption on Hematite**
Aline Carvalho Baruqui, Regina Sandra Veiga Nascimento, and Marco Antonio Chaer Nascimento
- 44 Poster 010 **1,2,4-Oxadiazole Esters as Aedes aegypti Larvicides**
Aluizio G. da Silva , João B. P. da Silva , Mozart N. Ramos , Geanne K.N.Santos, Daniela M. A. F. Navarro , Diana C. B. da Silva Alves , Janaína V. dos Anjos
- 45 Poster 011 **Análise Teórica do Efeito do Empacotamento do Líquido Iônico BMI-Br**
Ana Gabriela C. Oliveira , Davi A. C. Ferreira , Kleber C. Mundim
- 46 Poster 012 **Molecular dynamics simulations of MurA enzyme in complex with reaction products**
Anderson H. Lima, Alberto M. dos Santos, Isaque G. Medeiros, Cláudio Nahum Alves and Jerônimo Lameira
- 47 Poster 013 **Ab-initio Calculation of IR, UV-Vis and CD Spectra of Boron-nitrogen Azulenes**
Anderson José Lopes Catão , Alejandro Lopez-Castillo
- 48 Poster 014 **Time-Dependent Density Functional Theory (TD-DFT) Calculations of the Chiroptical Properties of Cds nanoparticles Functionalized with Cysteine**
André Farias de Moura, Nicholas A. Kotov
- 49 Poster 015 **Absorption Spectrum and Charge Transfer effects in dicyanovinyl-substituted quarterthiophene (DCV4T)/C60 materials for organic solar cells**
André Gonçalves de Oliveira , Lucas Modesto-Costa Itamar Borges Jr
- 50 Poster 016 **Application and development on the internally contracted Multireference Coupled-Cluster Theory**
Yuri Alexandre Aoto , Andreas Köhn
- 51 Poster 017 **Effects of Cholesterol Peroxidation on the Properties of Lipid Bilayers**
Antenor J. P. Neto, Rodrigo M. Cordeiro
- 52 Poster 018 **Transition Dipole Moments of PO**
Antonio Carlos Borin , Adalberto Vasconcelos Sanches de Araújo
- 53 Poster 019 **Bornite, Cu₅FeS₄ or Cu₈Fe₄S₈ - Experimental Versus Model Proposal.**
Antonio L. Soares Jr., Thomas Heine , Hélio A. Duartea and Heitor A. De Abreu .
- 54 Poster 020 **Study of the Electronic Properties of the Metallophthalocyanine as a Function of the Central Metal Atom**
Antonio Marcos Silva Santos , Tamires Lima Pereira , Demétrio Antonio da Silva Filho
- 55 Poster 021 **MRHFCl Calculations for BH molecule in the DZ base**
A. M. de C. Sobrinho , M. D. de Andrade , L. A. C. Malbouisson
- 56 Poster 022 **Local solvent properties of 1-alkyl-3-methylimidazolium ionic liquids**
Arno A. Veldhorst, Luiz F. O. Faria, Mauro C. C. Ribeiro
- 57 Poster 022 **Estudo do Efeito da Protonação da Norepinefrina na Sua Estrutura Eletrônica e Espectro de UV-vis**
Arsênio P. de V. Neto , Sara F. de A. Moraes , Davi A. C. Ferreira , Heibbe C. B. de Oliveira .
- 58 Poster 023 **MELQUIADES: A Monte Carlo program for simulation of multicomponent systems using arbitrary potential models**
Asdrubal Lozada Blanco , Luiz Carlos G. Freitas
- 59 Poster 024 **Estudo Químico-Quântico do Efeito da Cadeia Carbônica sobre Taxas de Dissociação em Reações Radicais do Tipo .H+H-R → H₂+R..**
Brenda S. Pauletti a, Thiago S. Castroa, Emília V. F. de Aragãoa, Sara F. de A. Moraisa , Kleber C. Mundima , Davi A. C. Ferreiraat
- 60 Poster 025 **The effect of spin-forbidden transitions in N(²D)+H₂ collisions: a trajectory surface hopping analysis**
B.R.L. Galvão , L.A. Poveda
- 61 Poster 026 **Substrate control in an intramolecular Heck-Matsuda reaction: a DFT Study**
Bruno M. Servilhaa , Carlos Roque D. Correiaab, Ataulpa A.C. Bragaa
- 62 Poster 027 **Calculation of Photoionization Cross-Section Using Square Integrable Basis Sets for Atoms and Molecules**
Bruno N. C. Tenório , Marco A.C. Nascimento , Alexandre B. Rocha
- 63 Poster 028 **Estudo teórico da molécula de água no Sol**
Bruno Silva Leite, Cristiano Costa Bastos, Antonio Carlos Pavão

- 64 Poster 029 **Molecular Dynamics Involving Ammonia and Noble-Gases**
Camila D. B. Silva, Rhuigi M. de Oliveira, Luiz F. Roncaratti, Geraldo M. E
- 65 Poster 030 **Optical Rotation Angle of S-4-phenyl-2-oxazolidinone: Importance of the Hydrogen Bonded Dimer**
C. M. B. Machado, and G. L. C. Moura,
- 66 Poster 031 **Propriedades Eletrônicas dos Peroxo Complexos de Molibdênio e de Tungstênio e Implicações na Oxidação de Sulfetos**
Camila S. de Avelar e Fabrício R. Sensato
- 67 Poster 032 **Structural Investigation of Dry Montmorillonite using Solid State NMR Simulations from ab initio Calculations**
Carla G. Fonseca, Gustavo S. G. de Carvalho, Renata Diniza (PQ), Alexandre A. Leitão
- 68 Poster 033 **Simulação de Processos de Adsorção Molecular em Material Nanoporoso Constituído por Tereftalato e Zircônio**
Carla V. Soares, Alexandre A. Leitão, Naseem A. Ramsahye, Guillaume Maurin
- 69 Poster 034 **Charge Transfer Dynamics of Inner-Shell Excited States on Organic Films for Photovoltaics**
Carlos E. V. de Moura, Yunier Garcia-Basabe (PQ), Maria Luiza Rocco, Alexandre Rocha
- 70 Poster 035 **Estudo teórico das propriedades estruturais e eletrônicas da junção Au/1,4-Benzenodiamina/Au**
Carlos Eduardo Silva, Renato Borges Pontes
- 71 Poster 036 **DTF Investigation of the optical Properties of Isoalloxazine Macrocycal Dervatieves**
C. E. Silva, M. A. San-Miguel
- 72 Poster 037 **Theoretical studie of porphyrins for application in Dye-Sensitized Solar Clls**
Cassiano M. Aono,
Paula H. de Mello
- 73 Poster 038 **¹OH Projection: the Latest Frontier to Define Geometry of Carbohydrates**
Clarissa O. da Silva (PQ), Leandro G. Alves (PG), Renato R. Andrade
- 74 Poster 039 **Estudo Teórico de Propriedades Estruturais e Elétricas de Politiofenos**
Eliziane da Silva Santos (G), Clebio Soares Nascimento Jr.
- 75 Poster 040 **Free Energy Calculations of Phenothiazine Dyes in Homogeneous and Micro-Heterogeneous Media**
Cleiton Maciel, Maurício Domingues Coutinho-Neto
- 76 Poster 041 **Highly Accurate Bound Rovibrational Eigen-energies of Ozone Using the ScallIT Software Suite**
Corey Petty , Bill Poirier b , Francisco B. C. Machado
- 77 Poster 042 **Syntheses of europium complexes: ligand displacement order, inversion or retention of configuration, and reaction pathways via RM1 orbital model for lanthanides**
Cristiano E.L. Jr, Monique F. Pereira, Isabella M. S. Rosado, Nathália B. D. Lima , and Alfredo M. Simas
- 78 Poster 043 **Theoretical Study of Structural, Electronic and Magnetic Properties of Platinum(II) Salicylidenes**
Cristina A. Barboza , Franklin Ferraro Gomez , José C. Germino , Pedro A. M. Vazquez , Tereza D. Z. Atvars
- 79 Poster 044 **Computational Studies of Spectroscopic Properties of Hydrocarbons at the Air-Ice Interface**
Dana Nachtigalova
- 80 Poster 045 **Optimization of Long-Range Corrected Functionals through The Minimum Polarizability and Maximum Hardness Principles in Polibutatriene Oligomers**
Daniel F. S. Machado, Demétrio A. S. Filho , Heibbe C. B. de Oliveira
- 81 Poster 046 **DFT studies of the interactions between the [Ca(H2O)5]2+ cation and monofunctionaloxo, aza, sulfur and phosphorous ligands**
Daniel G. S. Quattrociocchi, Marcos Vinicius M. Meuser, Glaucio B. Ferreira, Leonardo M. Costab and José Walkimar de M. Carneiro
- 82 Poster 047 **QSAR models applied to the anti-depression activity of hexahydro-pyrrolo-isoquinoline**
Daniela R. Silva , Lucas A. Santos , Letícia C. de Assis , Giovanna C. Gajo , Letícia S. Garcia , Tamiris M. de Assis , Elaine F.F. da Cunha
- 83 Poster 048 **Thermochemical and Kinetics studies of the H (2S) + CH3SH reaction**
Daniely V. V. Cardoso , Leonardo A. Cunha, Rene F. K. Spada , Luiz F. A. Ferrão , Corey A. Petty , Orlando Roberto-Neto , Francisco B. C. Machado
- 84 Poster 049 **Electronic and Conformational Structure of Ortho-Aminobenzoic Acid in Solution Combining the Sequential QM/MM and the Free Energy Gradient Methods**
Danillo P. Valverde , Herbert de C. Georg

- 85 Poster 050 **Dengue fusion peptide interacts with model membranes: an experimental and in silico study.**
Danilo Olivier, Neus Garcia, Ilja Voets, Amando Siuiti Ito
- 86 Poster 051 **Mechanical response under ballistic impact of penta-graphene**
David L. Azevedo
- 87 Poster 052 **Is There a Quadruple Bond in C2?**
David Wilian Oliveira de Sousa, Marco Antonio Chaer Nascimento
- 88 Poster 053 **Electronic structure and Raman spectra of Cyclohexanamine, Dicyclohexanamine and Ethanolamine: A comparison of theoretical and experimental results**
Deiver A. Teixeira, David L. Azevedo, Vanessa L. S. Teixeira, Marco A. G. Valente, Assis V. Benedetti, Cecílio S. Fugivara.
- 89 Poster 054 **Ab initio study of a new class of covalent organic frameworks: RIO**
Deyse G. Costaa, Pierre M. Esteves, Camilla D. Buarque, Leonardo Carneiro, Rodrigo B. Capaz
- 90 Poster 055 **Molecular Dynamics of Jaburetox in a POPC Bilayer**
William K. Nitschke, Celia R. Carlini, Hubert Stassen
- 91 Poster 056 **Computational Models for Fluorescence Study on Presence of Metallic Nanoparticles**
Edison Franco-Junior, Hueder P. M. de Oliveira, Janaina de Souza Garcia, Paula Homem-de-Mello
- 92 Poster 057 **Theoretical Investigation on the Reaction of CO₂ with Amines**
Ednilsom Orestes, Célia M. Ronconi and José Walkimar de M. Carneiro
- 93 Poster 058 **Modeling zigzag CNT: dependence of structural and electronic properties on the length and application to the encapsulation of HCN and HCCH**
Eduardo C. Aguiar, Ricardo L. Longo, João Bosco P. da Silva
- 94 Poster 059 **Chemical stability of a new h-CuS lamellar chalcogenide – A computational investigation**
Egon C. Santos, Antônio L. Soares Júnior, Heitor A. Abreu and Hélio A. Duarte.
- 95 Poster 060 **Electronic Structure and Optical Properties of Diblock Polymers for Solar Cell Applications**
Eliezer Fernando Oliveira, Francisco Carlos Lavarda
- 96 Poster 061 **Assessment of the Reliability of the SMD Model to Predict Activation Barriers for Classical SN₂ Reactions in Organic Solvents**
Elizabeth L. M. Miguel, Calink I. L. Santos, Carlos M. Silva, Josefredo R. Pliego Jr
- 97 Poster 062 **Efeito da temperatura sobre a formação de padrões em um sistema quiral tipo reação-difusão**
Emerson Boscheto, Alejandro López-Castillo
- 98 Poster 063 **Estudo Cinético e de Estrutura Eletrônica do Efeito da Água sobre a Racemização da Talidomida**
Emília V. F. de Aragão, Thiago S. Castro, Sara F. de A. Morais, Kleber C. Mundim, Davi A. C. Ferreira
- 99 Poster 064 **Study of Constitutional Isomers in Ru(II) Polypyridinic Complexes**
Érica de Liandra-Salvador, Paula Homem-de-Mello
- 100 Poster 065 **Periodic DFT Investigation on the Adsorption and Catalytic Desulfurization of Thiophene over VC(001) and VN(001) via Hydrogenation and Direct Pathways**
Eugenio Furtado de Souza, Teodorico de Castro Ramalho, Ricardo Bicca de Alencastro
- 101 Poster 066 **A Theoretical Study of Intramolecular Reaction Paths of α -hydroxynitrosamine in Gas Phase**
Ezequiel Fragozo V. Leitão, Silmar A. do Monte, Elizete V. do Monte
- 102 Poster 067 **Effects of different substituents on the stability of compounds derived from triphenylimidazol**
Carvalho, F., Bartoloni, F. H., Homem-de-Mello, P.
- 103 Poster 068 **Interações estereoeletrônicas e efeito Perlin em 2-flúor- cicloexanonas e cicloexanotionas**
Fátima M. P. de Rezende, Matheus P. Freitas, Teodorico C. Ramalho
- 104 Poster 069 **Estudo comparativo entre clorinas com diferentes substituintes**
F.C.T. Antonio, Paula Homem-de-Mello
- 105 Poster 070 **DFT study of Li, Na and K positions in mordenites: implication for the adsorption properties**
Felipe de S. Vilhena, Ramiro M. Serra, Alicia V. Boix, Glaucio Braga, José Walkimar Carneiro
- 106 Poster 071 **Revisiting Cyclobutadiene: Insights from Valence Bond Theory under the Quantum Interference Perspective**
Felipe Fantuzzi, T. M. Cardozo, Marco A. C. Nascimento
- 107 Poster 072 **Dimerização de Propano em Zeólitas Contendo Gálio**
Felipe M. Fernandes, Márcio S. Pereira, Marco A. C. Nascimento

- 108 Poster 073 **Efeito da excitação molecular sobre a transferência de energia roto-vibracional em colisões Ar+Cl₂, Ar+HCl e Ar+CO**
Felipe S. Carvalho, Emilio Borges, João P. Braga
- 109 Poster 074 **Estudo Mecanístico sobre a N-acilação de Aminas por Ácidos Carboxílicos Catalisada por ZrCl₄**
Felipe V. Z. Assad, Fabrício R. Sensato
- 110 Poster 075 **O Energetic and structural profile of liquid phase dimers of the green-solvent Gamma-valerolactone (GVL)**
Felippe M. Colombari, Luiz Carlos G. Freitas
- 111 Poster 076 **Evaluating the dependence of electronic properties of dyes with environment using a PCM-based model for lipid monolayer**
Fernanda Bettanin, Paula Homem-de-Mello, Benedetta Mennucci
- 112 Poster 077 **Obtenção de parâmetros cinéticos de reações de oxidação do felandreno em fase gasosa**
Fernando Renato Vicente Ferreira, Leonardo Baptista
- 113 Poster 078 **A computational study of molybdates and polyoxomolybdates.**
Fernando Steffler, Hélio A. Duarte
- 114 Poster 079 **Electronic States Generated by Single and Double Carbon Defects in Pyrene, Extended Pyrene and 7a,7z-Periacene as a Model for Graphene Sheet**
Daniely V. V. Cardoso, Adélia J. A. Aquino, and Hans Lischka, Francisco B. C. Machado
- 115 Poster 080 **Electronic energy levels engineering of ICBA employing chemical substitutions**
Eliezer Fernando Oliveira, Lucas Cartorino Silva, Francisco Carlos Lavarda
- 116 Poster 081 **Towards Improving the Fitting Ability of NDDO Semiempirical Methods with q-Multipole-Multipole Interactions**
Frederico T. Silva and Alfredo M. Simas
- 117 Poster 082 **Electronic structure and stability of Al_nC (n = 1 – 7) clusters**
Gabriel F.S. Fernandes, Luiz F. A. Ferrão, Francisco B.C. Machado
- 118 Poster 083 **Probing Cross Sections for Electron-Methyl Formate Collisions with EPolyScatD**
Gabriel L. C. de Souza, Leonardo M. F. Oliveiraa and Wagner J. C. Sousa
- 119 Poster 084 **Theoretical study on C9131 group of dyes for dye-sensitized solar cells - the effect of different solvent and different ligand groups.**
Gabriel M. Zanotto, Josene M. Toldo, Paulo F. B. Gonçalves.
- 120 Poster 085 **Investigation of substitution reactions on Selenuranes relevant to their biological activity on cysteine proteases**
Gabriela D. da Silva, Rodrigo L. O. R. Cunha e Mauricio D. Coutinho-Neto
- 121 Poster 086 **Difusão de Pólarons em Polímeros Condutores**
Gabrielle Gomes da Silva, Pedro Henrique de Oliveira Neto
- 122 Poster 087 **Conformational analysis, NBO and QTAIM Study of the Antimony Complexes with Mesoionic 1, 3-Thiazolium-5-thiolate**
Gerd Bruno da Rocha, Evandro Paulo S. Martins
- 123 Poster 088 **Study of UV-Photoexcitation and Ultrafast Dynamics of HCFC-132b (CF₂ClCH₂Cl)**
Gessenildo P. Rodrigues, Elizete Ventura, Silmar A. do Monte, Mario Barbatti
- 124 Poster 089 **Theoretical Investigation of the Butanol Combustion Mechanism**
Gladson de Souza Machado, Glauco F. Bauerfeldt
- 125 Poster 090 **Study of Aromatic + OH Reactions at the Density Functional Theory Level**
Thanízia Ferraz Santos, Luís Gustavo de Moraes, Glauco F. Bauerfeldt
- 126 Poster 091 **TD-DFT Study of Chalcones with Potential Pharmacological Activity against Alzheimer's Disease**
Graziele S. Pereira, Thiago O. Lopes, Murilo M. dos Anjos, Guilherme R. de Oliveira, Valter H. Carvalho da Silva c, Heibbe C. B. de Oliveira a
- 127 Poster 092 **The Nuclear Quadrupole Moment of Xenon**
Guilherme Arantes Canellaa, Régis Tadeu Santiagoa, Roberto Luiz Andrade Haidukea
- 128 Poster 093 **Computational Investigation of Water Glass Behavior Around DNA**
Gonzatti, Guilherme K., Netz, Paulo A.
- 129 Poster 094 **Development a Two Point Extrapolated Method Based on B3LYP/cc-pVDZ and cc-pVTZ Energies, Aiming a CBS Methodology.**
Guilherme Luiz Chinini, Rogério Custodio.

- 130** Poster 095 **Electronic structure and reactivity of a mechanically unfolded metalloprotein**
Guilherme Menegon Arantes
- 131** Poster 096 **Understanding the molybdenum oxodiperoxo complexes reactivities through of the IR and 17O–NMR DFT calculations**
Gustavo H. L. de Souza, Leonardo L. dos Santos, Lucelma P. de Carvalho, Marcus Vinicius Pereira dos Santos, Juliana A. B. Silvae, Ricardo L. Longo
- 132** Poster 097 **Substituent effects on the ESIPT process in 2-Hydroxy-1,4-Naphthoquinones**
Henrique A. Rodrigues, Eduardo P. Rocha, Livia C. T. Lacerda, Mateus A. Gonçalves, Maíra S. Pires, Telles C. Silva, Teodorico C. Ramalho
- 133** Poster 098 **Reaction Rate of HX+Y systems, with X, Y = H, F, Cl or Br and X≠Y**
H. O. Euclides, P. R. P. Barreto
- 134** Poster 099 **Understanding the solid-state phosphorescence of a new class of Tellurophenes compounds**
Inara de Aguiara, Eric Rivard, Alex Brown and Gabriel L. C. de Souza
- 135** Poster 100 **Assessing the Mesoionic Compounds Definitions by QTAIM, NBO and Spackman charge models**
Italo Curvelo dos Anjos, Gerd Bruno Rocha
- 136** Poster 101 **Estudo teórico de adsorção de CO₂ em ZnO("r")**
Ítalo Pimentel de Lima, João B. L. Martins
- 137** Poster 102 **Elucidating the photophysics of organic photovoltaic systems**
Itamar Borges Jr., Lucas Modesto-Costa (PD), Elmar (Uhl), (PD), Adelia J. Aquino, Hans Lischka
- 138** Poster 103 **Evaluation of Lennard-Jones Potentials in Calculations of Transport Properties of Near Critical Argon**
Jakler Nichele, Leonardo S. de Brito Alves, Itamar Borges Jr
- 139** Poster 104 **Synthesis, Spectroscopic Characterization and Crystal Structure of Asymmetric Azine C₁₅H₁₃N₃O₄**
Jhonata de Jesus Silva, Ademir João Camargo, Ricardo Rodrigues Ternavisk, Gilberto Lúcio Benedito de Aquino, Miriã Moreira Costa, Thalita Nátali Salamão dos Santos, Hamilton Barbosa Napolitano
- 140** Poster 105 **The importance of kinetic energy coupling in the vibrational spectra of small cluster dimers**
Monteiro, J.G.S., Barbosa, A.G.H.
- 141** Poster 106 **MRCI Characterization of the Low Lying Quintet States of MoO Radical**
Gabriel Lopes, Marcelo A. P. Pontes, Francisco B.C. Machado, Luiz A. Ferrão, Harley P. Martins Filho and Joaquim D. Da Motta Neto
- 142** Poster 107 **LUMPAC LUMinescence PACKage: New methods and implementations**
José Diogo Lisboa Dutra, Ricardo Oliveira Freire
- 143** Poster 108 **Mechanism of Dimethyl Sulfide Oxidation by Hydrogen Peroxide with Niobium Oxyhydroxide Heterogeneous Catalyst**
Carlos M. Silva and Josefredo R. Pliego Jr
- 144** Poster 109 **Photophysical study of Tröger's base molecular scaffolds**
Josene M. Toldo, Rodrigo R. Descalzo, Débora M. P. Aroche, Fabiano S. Rodembusch, Paulo F. B. Gonçalves
- 145** Poster 110 **Docking de novos derivados do Ácido Kójico com potencial atividade Anti-tirosinase**
Joyce Lima Vale, Nelson Alencar, Tainá Barros, Davi Brasil.
- 146** Poster 111 **Adsorption of Water and Oxygen on Arsenopyrite (001) Surface**
Silva, J. C. M., Heine, T., De Abreu, H. A. and Duarte, H. A.
- 147** Poster 112 **Theoretical investigation on the mechanism of corrosion inhibition of the (001) iron surface by imidazole and imidazoline: a surface coverage study.**
Juliana O. Mendes, Alexandre B. Rocha, Marco Antonio Chaer Nascimento
- 148** Poster 113 **Estudo de Interação do Cardanol com Mineral Albitapor Meio de Modelagem Molecular para Utilização na Etapa de Resinagem de Rochas Ornamentais**
Julio C. G. Correia, Alexandre N. M. Carauta, Danielle da S. Rosa, Letícia M. Prates, Kelly F. Pessôa, José Walkimar de M. Carneiro, Maurício T. M. Cruz, Elaine R. Maia
- 149** Poster 114 **Adsorption of Drugs in Metal-Organic Frameworks: A Combined Grand Canonical Monte Carlo and DFT-D Study.**
Júlio C. S. Da Silva, Amanda L., Roberta P. Dias and Thereza A. S.
- 150** Poster 115 **Purificação da Matriz Densidade Usando Operações de Álgebra Linear Esparsas baseadas em Orbitais Moleculares Localizados para GPUs.**
Júlio Daniel de Carvalho Maia, Gerd Bruno Rocha

- 151 Poster 116 **Insights Regarding the Irreversible Molecule Pulling in Complex Fluid Systems by Means of Molecular Dynamics Simulations**
Kalil Bernardino , Andre Farias de Moura
- 152 Poster 117 **Influence of DFT functionals in the molecular structure and thermodynamic properties of the molybdenum oxodiperoxo complexes.**
Kayo F. da Silva, Lucelma P. de Carvalho, Marcus Vinicius Pereira dos Santos , Juliana A. B. Silva , Ricardo L. Longo
- 153 Poster 118 **Estudo Químico-Quântico do Rearranjo do tipo McLafferty durante a Fragmentação Molecular do 1-Nitropropano**
Laís de S. Barbosa , Sara F. de A. Morais , Kleber C. Mundim , Davi A. C. Ferreira
- 154 Poster 119 **Estudos teóricos da fotoisomerização de butadieno com substituintes CHO e Cl**
Laís Petra Machado; Márcio Soares Pereira
- 155 Poster 120 **Desenvolvimento e Parametrização do Método Semiempírico RM1 para Níquel.**
Larissa Tavares de Jesus , José Diogo Lisboa Dutraa , Manoel Alves Machado Filho , Alfredo Mayall Simas e Ricardo Oliveira Freire
- 156 Poster 121 **Comparative Analysis of Docking Programs Using Distinct Protein-Ligand Test Sets**
Lucas A. Vizani , Isabella A. Guedes , Diogo A. Marinho, Camila S. de Magalhães and Laurent E. Dardenne
- 157 Poster 122 **Theoretical Investigations of the Effect of Solvent in the IR Absorption via Density Functional Theory Calculations for a Series of Systems Theobromine-Water.**
SANTIN, L.G. , ALBERNAZ, A , CAMARGO, A.J. , OLIVEIRA, S.S. , GARGANO, R.
- 158 Poster 123 **Combined use of Sequential QM/MM and Free Energy Gradient methods in the study of electronic and conformational structure of molecules with acceptor-donor groups**
Leandro R. Franco, Idney R. Brandão Tertius L. Fonseca , Herbert de C. Georg
- 159 Poster 124 **DFT Study on the Influence of the Cluster Size and Noncovalent Interactions in the CO Adsorption on Au/MOR Catalyst**
Lenin Díaz Soto, Aníbal Sierralta, and Marco A. C. Nascimento
- 160 Poster 125 **Antioxidant Activity of Isolated Interglycosidic O-(1→3) Flavonols: a DFT study**
Leonardo M. F. de Oliveira, Rafael G. Vicari and Gabriel L.C de Souza
- 161 Poster 126 **Estudo Computacional sobre a Formação da Ligação Amídica Catalisada pela Superfície (100) da -Al₂O₃**
Lethícia Ramos Santos e Fabrício R. Sensato
- 162 Poster 127 **A Density Functional Theory Study of NO Adsorption on Pd₄ and Pd₄/ -Al₂O₃ Clusters**
Leticia Maia Prates , Maurício Tavares de Macedo Cruz
- 163 Poster 128 **Equilibrium and non-equilibrium effects on the local order of water at metallic electrode surfaces**
Luana S. Pedroza
- 164 Poster 129 **Probing the nature of Halogen-Aromatic Interactions by empirical potential**
Lucas de Azevedo Santos , Daniela Rodrigues Silva , Teodorico C. Ramalho
- 165 Poster 130 **Multiple Pathways in the Hydrolysis of Phosphate Esters Catalysed by a Synthetic Model of Catechol Oxidase - Catalytic Promiscuity in Biomimetic Systems.**
Lucas F. Esteves , Hélio F. dos Santos , Luiz A. S. Costa
- 166 Poster 131 **Effect of Intramolecular Hydrogen Bond OH...O in 1,3-butanediol and 3-methoxybutanol**
Lucas José Karas , Patrick Rodrigues Batista , Renan Vidal Viesser , Luciano Nassif Vidal , Paulo Roberto de Oliveira
- 167 Poster 132 **Charge Transfer and Excitation Energy of TICT Molecules upon Solvation**
Lucas Modesto-Costa (PD), Itamar Borges Jr.
- 168 Poster 133 **All-electron segmented contraction basis sets of triple zeta valence quality for the fifth-row elements**
L.S.C. Martins , F.E. Jorge and S.F. Machado
- 169 Poster 134 **Chemoselectivity of the molybdenum oxodiperoxo complexes in oxidation reactions**
Lucelma Pereira de Carvalho, Marcus Vinicius Pereira dos Santos , Juliana Angeiras Batista da Silva , Ricardo Luiz Longo
- 170 Poster 135 **On the Interaction Energy among Propellant Components: A Carbon Black Model**
Luiz F.A. Ferrão , José A.F.F. Rocco , Francisco B.C. Machado

- 171 Poster 136 **Secondary Structure Stabilization of three different peptides by glycerol/water mixtures using molecular dynamics.**
Weverson R. Gomes, Luiz C.G. Freitas
- 172 Poster 137 **Cyclization of lapachol in acidic aqueous media: regioselectivity and interconversion mechanism study**
Maicon Delarmelina, Gláucio B. Ferreira, Vitor F. Ferreira, José Walkimar de M. Carneiro
- 173 Poster 138 **A Software for Designing SCC-DFTB Repulsion Parameters Automatically: The Framework for Automatization of SLAKO Parameterization (FASP)**
Maicon P. Lourença, Maurício C. Silva, Matheus Quintão, Hélio A. Duarte
- 174 Poster 139 **Estudo por Dinâmica Molecular de PVA em água com variação de parâmetros ambientais**
Maíra Theisen, Hubert K. Stassen, Rosane M. D. Soares
- 175 Poster 140 **Metaloenzimas Envolvidas na Hidrólise de Compostos Organofosforados: Uma abordagem teórica via modelos de sítios ativos para Zn(II)-Zn(II), Cd(II)-Cd(II) e Zn(II)-Cd(II) de Pseudomonas diminuta (pdPTE)**
M. A. Chagas, W. R. Rocha
- 176 Poster 141 **A MRCI comparative study of the electronic states of AsX⁺ (X=F, Cl, Br and I)**
Marcelo A. P. Pontes, Marcos H. de Oliveira, Luiz F. A. Ferrão, Joaquim D. Da Motta Neto, Orlando Roberto-Neto e Francisco B. C. Machado
- 177 Poster 142 **Effect of 1,10-Phenanthroline Aromaticity in Carboxylic Acids: GIAO Calculations and ¹H NMR Spectroscopy**
Márcia K. D. L. Belarmino, Camila M. B. Machado, Nathália B. D. Lima and Gustavo L. C. Moura
- 178 Poster 143 **Effects of the complexation energy on the thermochemistry and kinetics of oxidation reactions with oxodiperoxo complexes**
Marcio Marcos da Silva, Marcus Vinicius Pereira dos Santos, Juliana Angeiras Batista da Silva, Ricardo Luiz Longo
- 179 Poster 144 **Beryllone: a Novel Divalent Beryllium Lewis Base**
Felipe Fantuzzi, Marco A. C. Nascimento
- 180 Poster 145 **Second hyperpolarizability of the lithium salt electride Li-H₃C₄N₂...Na₂**
Marcos A. Castro, Orlando Silveira, Salviano A. Leão, Tertius L. Fonseca
- 181 Poster 146 **A DFT-D2 study of BTEX adsorption on rutile TiO₂ (110) surface**
Marcos dos Reis Vargas, Elton Anderson Santos de Castro, José Roberto dos Santos Politi, João B. L. Martins
- 182 Poster 147 **The Spin-Orbit effects on the CB, SiB and GeB molecules**
Marcos H. de Oliveira, Marcelo A. P. Pontes, Luiz F. A. Ferrão, Joaquim D. Da Motta Neto, Orlando Roberto Neto, Francisco B. C. Machado
- 183 Poster 148 **Computational study of the interaction between the [Pb(H₂O)₃]⁺cation with ligands containing oxygen, nitrogen and sulfur donors atoms**
Marcos Vinicius M. Meuser, Daniel G. S. Quattrociocchi, Gláucio B. Ferreira, Leonardo M. da Costab and José W. de M. Carneiro
- 184 Poster 149 **PICVib: An Accurate, Fast and Simple Procedure to Investigate Selected Vibrational Modes at High Theoretical Levels**
Marcus Vinicius Pereira dos Santos, Yaicel G. Proenza, Eduardo C. Aguiar, João Bosco P. da Silva, Ricardo Luiz Longo
- 185 Poster 150 **Estudo ab initio da interação de compostos análogos do alcaloide marinho teoneladina C com o grupo heme [Fe(III)PPIX]:**
Marília L.A e Costa, Clebio S.Nascimento Jr, Gustavo H.R. Viana, Luciana Guimarães
- 186 Poster 151 **Hydrazine decomposition reactions on the small platinum cluster Pt₄**
Pelegri M, Parreira RT, Ferrão LFA, Caramori GF, Machado FBC, Roberto-Neto O
- 187 Poster 152 **Estudo comparativo da atividade antimalárica de triterpenos pentacíclicos**
Marlon Marques V. de Melo Filho, Kelson Mota T. Oliveira, Jefferson R. A. Silva, Noam S. Gadelha, Aristeu S. da Fonseca
- 188 Poster 153 **Computational Studies on Dodecylsulfate-Quaternary Ammonium Herbicides Ion-Associate Formation in Water: A DFT Study**
Kassem Kalife Nege, Mateus Ribeiro Lage, Jonas Oliveira Vinhal, Ricardo Jorgensen Cassella, José Walkimar de M. Carneiro
- 189 Poster 154 **Free Solvation Energy of Aqueous Aluminium(III) species**
Matheus C. Quintão, Guilherme F. de Lima and Hélio A. Duarte

- 190 Poster 155 **DFT Approach of CO and NO Adsorption on LaFeO₃ Perovskite Doped with Pd and Co**
Maurício Tavares de Macedo Cruz , Letícia Maia Prates
- 191 Poster 156 **All-electron double zeta basis sets for the most fifth-row atoms: Application in DFT spectroscopic**
Mauro Lúcio Franco , Antônio Canal Neto, Francisco Elias Jorge
- 192 Poster 157 **New Double Zeta Bases Sets for Boron and Carbon Obtained by HF Gauss – GSA**
M. D. de Andrade , A. M. de C. Sobrinho , L. A. C. Malbouisson
- 193 Poster 158 **Theoretical Investigation of the Formaldehyde Gas-Phase Reaction with Chlorine Atoms**
Michel Braga Garcia , Glauco F. Bauerfeldt
- 194 Poster 159 **DFT studies on degradation mechanisms of chlorhexidine**
Michele A. Salvador , Camila Pinheiro Souza , Pedro de Lima-Neto , Adriana N. Correia , Paula Homem-de-Mello
- 195 Poster 160 **Theoretical Insights of Metallic Ag Growth on -Ag₂WO₄ upon Electron Irradiation**
Miguel A. San-Miguel, Juan Andrés, Elson Longo, Edison Z. da Silva
- 196 Poster 161 **Elastic scattering of low-energy electrons by CH₃CN and CN₃NC Isomers**
Milton Massumi Fujimoto , Erik V. R. de Lima and Jonathan Tennyson
- 197 Poster 162 **Study of Isomer and Conformer effects in electron scattering using R-Matrix Method**
Milton Massumi Fujimoto , Erik V. R. de Lima and Jonathan Tennyson
- 198 Poster 163 **Identificando os sítios preferenciais de solvatação da xilose**
Miqueias M. Peixoto , Clarissa O. da Silva
- 199 Poster 164 **Electronic and structural properties of B phase of Nb₂O₅ bulk – A DFT study**
Mirele Bastos Pinto , Hélio A. Duarte and Heitor A. De Abreu .
- 200 Poster 165 **Molecular Dynamics Simulation to design an Enzyme-based Nanobiosensor using Atomic Force Microscopy to detect Glyphosate herbicide**
Moacir F. Ferreira Jr.1, Eduardo F. Franca1, Fábio L. Leite
- 201 Poster 166 **Hybrid QC/MM potential simulations of iron-containing proteins**
Murilo H. Teixeira and Guilherme M. Arantes
- 202 Poster 167 **Structure and thermochemical properties of C₆ volatile unsaturated alcohols**
Natália Aparecida Rocha Pinto, Stella Maris Resende
- 203 Poster 168 **Europium Luminescence: Electronic Densities and Superdelocalizabilities for a Unique Adjustment of Theoretical Intensity Parameters**
Nathalia B. D. Lima , José D. L. Dutra , Ricardo O. Freire and Alfredo M. Simas
- 204 Poster 169 **Design de um catalisador baseado em éter-coroa e ligações de hidrogênio seletivas para promover reações de fluoração nucleofílica**
Nathália F. Carvalho , Josefredo R. Pliego Jr.
- 205 Poster 170 **Charge, Charge Flux and Dipole Flux Contributions for Infrared Intensities of the Stretching Modes during Protonation**
Natieli A. da Silva , Roberto L. A. Haiduke
- 206 Poster 171 **Simulation of Reactive channels for Inorganic Cycle SNP₂ Formation: A Study via ab Initio Molecular Dynamics**
COUTINHO,N.D.C., OLIVEIRA,H.C.B , CARVALHO, V.H.
- 207 Poster 172 **Electronic structure studies of Fe₂O₄**
Nelson Henrique Morgon
- 208 Poster 173 **Comparative theoretical studies of energetic and structural properties of betulinic and melaleucic acids and the stability of clusters of these special metabolites**
Noam Gadelha da Silva , Kelson Mota Teixeira de Oliveira , Jefferson Rocha Andrade Silva
- 209 Poster 174 **Theoretical Study of Geometric and Electronic Properties of Theophylline Using Car-Parrinello Molecular Dynamics**
Núbia Maria Nunes Rodrigues , Lauriane Gomes Santin , Ademir João Camargo e Solemar Silva Oliveira
- 210 Poster 175 **Chemical kinetics of the CH₃CH₂SH + H abstraction and bond breaking reactions: influence of the methodology on the tunneling effects**
Leonardo A. Cunha, Daniely V. V. Cardoso , Luiz F. A. Ferrão , Rene F. K. Spada (PD), Orlando Roberto-Neto , Francisco B. C. Machado

- 211 Poster 176 **Polysulfides species: formation mechanism in acid and basic environment.**
Pâmella V. B. de Pinho , Maurício C. Silva , Guilherme S. Rodrigues , Guilherme F. de Limac , Hélio A. Duarte
- 212 Poster 177 **Theoretical Studies of HS+HX=H2S+X, with X = H, F, Cl and Br**
P R P Barreto , H O Euclides, A C P S Cruz
- 213 Poster 178 **Conformational Analysis of 3-amino-1-propanol and 3-N,N-dimethylamino-1-propanol using QTAIM and NBO**
Patrick Rodrigues Batista , Lucas José Karas, Renan Vidal Viesser , Luciano Nassif Vidal , Paulo Roberto de Oliveira
- 214 Poster 179 **Investigação das conformações mais estáveis da molécula de -naftilxilose**
Paula do Nascimento Goulart , Clarissa Oliveira da Silva
- 215 Poster 180 **SAR analysis of phthalocyanines, porphyrins and chlorins using properties obtained with density functional calculations**
Fernanda Bettanin , Káthia M. Honório, Paula Homem-de-Mello
- 216 Poster 181 **Adaptive Resolution Simulation of Oligonucleotides**
Paulo Augusto Netz , Raffaello Potestio , Kurt Kremer
- 217 Poster 182 **Pyrite oxidation mechanism in the presence of oxygen and water**
Egon C. Santos , Paulo R. G. Gonçalves Júnior , and Hélio A. Duarte .
- 218 Poster 183 **Theoretical Study on the Substitution of Tungsten by Vanadium on Keggin Structures $[XW_{12-n}V_nO_{40}]^{-(q+n)}$
X=Si, P; 0<n<4**
Pedro. S. Pinheiro , Alexandre. B. Rocha , Jean. G. Eon .
- 219 Poster 184 **Photo-thermal activation study of ruthenium Keppler-type complexes with focus on the release of the nitrosyl ligand using TD-DFT and AIM theories**
Priscila C. Rocha, James A. Platts , Luiz Antônio S. Costa
- 220 Poster 185 **Protonated N-Nitrosodimethylamine: a comparative MR-CISD and EVPT2 study**
R. B. de Andrade, E. Venturaa, S. A. do Monte, M. A. F. de Sousa
- 221 Poster 186 **Theoretical study of the H₂ + PtO⁺ reaction by relativistic methods**
Régis T. Santiago , Roberto L.A. Haiduke
- 222 Poster 187 **Electronic and structural properties of engineering CdSe@TiO₂ nanotubes arrays**
R. G. Freitas, R. A. Mendes, F. W. S. Lucas, M. A. Santanna , G. L. C. Souza , L. H. Mascaro, E. C. Pereira
- 223 Poster 188 **Aromaticity in Complex Consisting of Thiocarbonyls**
Eder H. da Silva , Giovanni F. Caramori , Renato L. T. Parreira
- 224 Poster 189 **Influência da Presença de Moléculas do Solvente Explícitas no Estudo Conformacional de Monossacarídeos**
Renato Andrade , Clarissa Silva .
- 225 Poster 190 **Hydrogen Abstraction from the Hydrazine Dimer by an Oxygen Atom**
Rene F. K. Spada , Luiz F. A. Ferrão, Orlando Roberto-Neto, Hans Lischka , Francisco B. C. Machado
- 226 Poster 191 **Spectroscopic Study of the Ng-CCl₄, O₂-CCl₄, D₂O-CCl₄ and ND₃-CCl₄ Systems.**
Rhuaiago Mendes de Oliveira , Gabriel Fávero , Luiz F. Roncaratti , Geraldo Magela e Silva and Ricardo Gargano .
- 227 Poster 192 **The influence of the first series of transition elements in the electronic properties of Pd clusters: a study based on Density Functional Theory**
Ricardo de Almeida , Maurício Tavares de Macedo Cruz
- 228 Poster 193 **Catalytic hydrogenation of acrylic acid by molybdenum carbide**
Ricardo R. Oliveira, Victor Teixeira da Silva, Leandro Sousa, Alexandre B. Rocha
- 229 Poster 194 **Structural Characterization and Theoretical Study of Asymmetric Azines C₁₇H₁₇N₃O₂ and C₁₆H₁₆N₄O₂.**
Ricardo R. Ternavisk, Hamilton B. Napolitano, Ademir J. Camargo, Jhonata J. Silva, Francisco B. C. Machado
- 230 Poster 195 **Estimativa teórica da constante de velocidade da reação CH + CO → HCO + C em função da temperatura**
Roberto L. A. Haiduke , Rafael M. Vichiatti , Albérico B. F. da Silva
- 231 Poster 196 **Rovibrational Energies and Spectroscopic Constants for Buckyball Dimer**
Rodrigo Aparecido Lemos Silvaa , Luciano Ribeiroa , Valter Henrique Carvalho Silvaa , Daniel Francisco Scalabrini Machadob , Heibbe C. B. de Oliveirab

- 232 Poster 197 **On the fluxional behavior of [CpMn(CO)₂(-alkane)] complexes**
Rodrigo Silva Bitzer , Marco Antonio Chaer Nascimento
- 233 Poster 198 **Theoretical studies of adsorption on the surface of zeolite ZSM-5**
Costa, R. J., Martins, J. B. L., Politi, J. R. S. , Castro, E. A. S.
- 234 Poster 199 **Insight into the Spontaneity of Hydrogen Bond Formation between Formic Acid and Phthalimide Derivatives**
Rogério V. A. Júnior, Nathália B. D. Lima , and Alfredo M. Simas
- 235 Poster 200 **Characteristic behavior of carbonyl stretching IR absorption intensities**
Wagner Eduardo Richter , Arnaldo Fernandes da Silva , Roy Edward Bruns
- 236 Poster 201 **Spectroscopic Constants and Rovibrational Energies of the Helium-Antihydrogen System: A Study by Discrete Variable Representation Method**
Sandro F. Brito, Daniel F. S. Machado, Valter H. Carvalho , Heibbe C. B. de Oliveira
- 237 Poster 202 **Efeitos Cooperativos Como Abordagem Alternativa ao Tunelamento Quântico no Entendimento do Rearranjo de Hidroximetileno a Temperaturas Ultrabaixas**
Sara F. de A. Morais , Kleber C. Mundim, Davi A. C. Ferreira
- 238 Poster 203 **Investigação Teórica do Processo de Inclusão Envolvendo a Prilocaina e o Ácido p-Sulfônico Calix[6]areno**
Sara Maria Ribeiro de Sousa , Clebio Soares Nascimento Jr.
- 239 Poster 204 **Investigation of Chemical Bonds of the Interactions Cation- π in Ruthenophanes**
Sergio Emanuel Galembeck and Renato Pereira Orenha
- 240 Poster 205 **Solvent Effect on the Structure and Electronic Transition Energy of Enrofloxacin**
Queiroz, Nayhara B. D. F, Alcantara, Isabella C. Garcia, M. V. R, Preza, Sergio L. E, Amaral, Marcos S.
- 241 Poster 206 **Computational Simulation of C60 Embedded in Amino Acid Ionic Liquids**
Sidney R. Santana , Jefferson L. Medeiros, Dayse N. Moreira
- 242 Poster 207 **OH radical initiated oxidation of the volatile organic compound 3-methyl-3-buten-1-ol under atmospheric conditions**
Stella Maris Resende , Sara M. Ribeiro de Sousa
- 243 Poster 208 **Kinetic Analysis of the 2,5-Dimethylfuran Combustion Chemistry**
Suelen S. da S. F. Pessanha, Alessandra Rohr Fernandes de Amorim, Gladson de Souza Machado , Glauco F. Bauerfeldt
- 244 Poster 209 **Second hyperpolarizability of the lithium salt of pyridazine calcium doped Li-H₃C₄N₂...Ca**
Suélio Marques , Marcos A. Castro , Salviano A. Leão, Tertius L. Fonseca
- 245 Poster 210 **Molecular properties and spectroscopy along the phase diagram**
Marcelo H. Cardenuto, Kaline Coutinho Benedito J. C. Cabral, Sylvio Canuto
- 246 Poster 211 **Study of the Impact of the Central Atom on the Geometrical Parameters of Phthalocyanines**
Tamires Lima Pereira, Antonio Marcos Silva Santos, Demétrio Antonio da Silva Filho
- 247 Poster 212 **OH Addition Reactions to 1-pentene and 1-hexene: A Multi-Path Variational Transition State Study.**
Tatiane Nicola Tejero, Luís Gustavo de Moraes, Glauco F. Bauerfeldt
- 248 Poster 213 **Maghemita dopada com cobre (Cu-Fe₂O₃) para aplicação em reações Fenton heterogêneo: estudo experimental e teórico**
Teodorico Castro Ramalho , Maíra dos Santos Pires , Livia Clara Tavares Lacerda , Telles Cardoso Silva, Silvana Corrêa , Francisco Guilherme Esteves Nogueira , Eduardo Pereira da Rocha , Mateus Aquino Gonçalves .
- 249 Poster 214 **Theoretical Study of the Mechanism of Co-Mutagenicity of AminoPhenylNorharman**
Thayná Borges da Silva, Alberto dos Santos Marques
- 250 Poster 215 **Quantum Reactive Scattering Study of the Mu⁺ Li₂, D⁺ Li₂, and T⁺ Li₂ Isotopic Reactions**
Thiago F. da Cunha, Henrique V. R. Vila, Rhuigo Mendes de Oliveira, Geraldo M. e Silva, Ricardo Gargano
- 251 Poster 216 **Challenges for the ab initio simulation of the spectra of large molecules: Absorption and fluorescence spectra of poly(p-phenylenevinylene) oligomers**
Thiago Messias Cardozo , Adélia A.J. Aquino, Mario Barbatti, Itamar Borges Jr., Hans Lischka
- 252 Poster 217 **Substituent Effect in the Mesoionic Ring on Optical and Electric Properties of Mesoionics Compounds**
Thiago O. Lopes , Grazielle S. Pereira , Guilherme R. de Oliveira , Heibbe C. B. de Oliveira

253	Poster 218	Relaxation of Optically Excited States of p-Nitroaniline Valdemir Ludwig (PQ) and Zélia M. da Costa Ludwig XVIII Simpósio Brasileiro de Química Teórica – SBQT 2015 Pirenópolis – GO, 22-25 Novembro de 2015
254	Poster 219	Estudo Teórico das bases catalíticas -isocupreidina e Quinidina na Reação Assimétrica Morita-Baylis-Hillman Verônica M. Nascimento, Renan S. Galaverna, Gabriel Heerd, Marcos N. Eberlin ² , Fernando Coelho, Atualpa A. C. Braga ¹
255	Poster 220	Theoretical Study on Electron Collisions with Dimethyl Disulfide Victor A. S. da Mataa and Gabriel L. C. de Souza
256	Poster 221	DMBE potential energy surface for the 12A' excited state of the ClO₂ system Vinícius C. Mota, Oswaldo B. M. Teixeira, José Manoel Garcia de la Vega and António Joaquim de Campos Varandas
257	Poster 222	Absorption Spectra Shift of Tetrasubstituted Phthalocyanine due to Dimerization: evaluation of the environment Vinícius Fernandes, Maurício D. Coutinho Neto, Paula Homem-de-Mello
258	Poster 223	A Theoretical Model for Chiral-Induced Spin Selectivity Vladimiro Mujica
259	Poster 224	Atomic decomposition of carbonyl stretching IR absorption intensities Wagner Eduardo Richter, Arnaldo Fernandes da Silva, Roy Edward Bruns
260	Poster 225	Estudo teórico da adsorção de gases leves nas MOFs SIFSIX-2-Cu e SIFSIX-2-Cu-i Walber Gonçalves Guimarães Junior, Guilherme Ferreira de Lima.
261	Poster 226	Conformational Analysis of 1,2-Ethandiol through NBO, QTAIM and NCI Methods Wesley G. D. P. Silva, Josué M. Silla, Matheus P. Freitas
265		LISTA DE PARTICIPANTES

Prof. Yuji Takahata

27 de janeiro de 1941 a 13 de outubro de 2015

O Prof. Yuji Takahata (foto) nasceu em 27 de fevereiro de 1941 em Nagano-ken, região rural do Japão, cercado por montanhas e a 200 km de Tóquio. Era o segundo filho de Sozaburo Takahata e Shigeru Takahata em uma família de cinco irmãos. A família perdeu o primogênito. Mas, apesar das dificuldades da vida no campo, os pais garantiram a formação dos filhos até o ensino médio e todos chegaram a ter formação superior.

O Prof. Takahata graduou-se como Bacharel em Química pela Universidade de Tóquio Kyoiku em 1963. Descobriu seu interesse pela Química Quântica no terceiro ano da graduação ao ler um livro introdutório sobre o tema escrito pelo eminente Prof. Kenichi Fukui. Iniciou na sequência seu Mestrado pela mesma instituição trabalhando com "Espectro de ressonância paramagnética eletrônica de complexos de cobre" sob orientação do Prof. Keizo Suzuki. Em 1965 mudou-se para os Estados Unidos (EUA) e trabalhou no Depto. de Física da University of Pacific sob a supervisão do Prof. Carl E. Wulfman. Estudou com muito entusiasmo durante praticamente um ano nessa instituição. No ano seguinte se transfere para o Depto. de Química da John Hopkins University para realizar seu PhD sob orientação do Robert G. Parr com a tese: "Investigações teóricas da forma de moléculas poliatômicas simples", concluída em 1970.

Na sequência, realizou pós-doutorado com o Prof. David Bishop da University of Ottawa, Canada em 1970; com o Prof. Gerald Segal da University of Southern California em 1971-1972 e com o Prof. Delano P. Chong da University of British Columbia em 1975-1976. Chegou a retornar ao Japão na busca por emprego, mas sem sucesso. Finalmente, recebeu de um amigo, Prof. George Csanak, que estava trabalhando no Instituto de Física da Universidade Estadual de Campinas - Unicamp, informação sobre a possibilidade de ser contratado por esta instituição. No segundo semestre de 1976, o Prof. Takahata recebe carta do Prof. Jair P. Campello, Diretor Associado do Instituto de Química, indicando que a Instituição possuía uma vaga para sua contratação. Em janeiro de 1977 assina contrato com a Unicamp e tem início a sua nova vida, agora no Brasil. No Depto. de Físico-Química obteve sua Livre-docência pela Instituição em 1996 e tornou-se Professor Titular no Instituto de Química em 2003. Após sua aposentadoria tornou-se professor da Escola Superior de Tecnologia da Universidade Estadual do Amazonas (UEA) no período de 2009 -2011.

Em sua trajetória acadêmica dedicou grande parte dos

Foto: UNICAMP



seus esforços no estudo da estrutura eletrônica no estado fundamental e estados excitados de moléculas orgânicas e inorgânicas com métodos de natureza semi-empírica, baseados na teoria do funcional de densidade e de natureza ab initio. Tinha especial interesse por compostos orgânicos com atividade farmacológica. Procurou desenvolver metodologia baseada na teoria do funcional de densidade para possibilitar o cálculo de energias de ionização de camadas internas. Com o objetivo de agregar conhecimentos para solucionar problemas relacionados com seus interesses, visitou diversas Universidade e Instituições de Pesquisa no exterior, mantendo contato com cientistas de diferentes ramos da Química Teórica.

O docente aposentou-se da Unicamp em 2008, tendo orientado nove mestrados e 11 doutorados. Escreveu 107 artigos científicos em revistas de alto impacto. Era um entusiasta dos eventos no país, sempre disposto e extremamente participativo, tendo coordenado o 2º Simpósio Brasileiro de Química Teórica em Campinas no ano de 1983.

Este relato, não pretende traduzir toda a contribuição do Prof. Takahata como acadêmico. É apenas um breve relato da sua trajetória e uma maneira singela de prestar um tributo a um acadêmico como cientista e ser humano a todos que tiveram o privilégio e a alegria de conhecê-lo.

Rogério Custodio

Programação do Evento

Horário	Domingo 22/11/2015	Segunda Feira 23/11/2015	Terça Feira 24/11/2015	Quarta Feira 25/11/2015	Quinta Feira 26/11/2015
8:30-9:10		Plenária (PL2)-40 min Prof. Vincenzo Aquilanti	Plenária (PL3)- 40 min Prof. F. Matthias Bickelhaupt	Plenária (PL4) - 40 min Prof. Lars G.M. Pettersson	Partida dos ônibus
9:10-9:40		Palestra (PA1)- 30 min Prof. Patricia Barreto	Palestra (PA10) - 30 min Prof. Andrés Reyes Velasco	Palestra (PA16) - 30 min Prof. Mauricio Coutinho	
9:40-10:10	Chegada ao Local do Evento	Palestra (PA2)- 30 min Prof. David Fuks	Palestra (PA11) - 30 min Prof. Clarissa O. da Silva	Palestra (PA17) - 30 min Prof. Heibbe C Oliveira	
10:10-10:40		Palestra (PA3)- 30 min Prof. Pedro G. Pascutti	Palestra (PA12) - 30 min Dr. Célia Fonseca Guerra	Palestra (PA18) - 30 min Prof. Luana S. Pedroza	
10:40-11:00		Coffee Break - 20 min	Coffee Break - 20 min	Coffee Break- 20 min	
11:00-11:20		Sessão Coordenada 11:00h-12:20 4 apresentações de 15+5 minutos	Sessão Coordenada 11:00h-12:20 4 apresentações de 15+5 minutos	Sessão Coordenada 11:00h-12:20 4 apresentações de 15+5 minutos	
11:20-12:00					
12:00-12:20					
12:20-14:00		Almoço- 12:20 h - 14:00 h	Almoço- 12:20h - 14:00h	Almoço- 12:20h - 14:00h	
14:00-14:30		Palestra (PA4) - 30 min Dr. Vladimiro Mujica	Palestra (PA13) - 30 min Dr. Dana Nachtigallová	Palestra (PA19) - 30 min Prof. Terttu Hukka	
14:30-15:00		Palestra (PA5) - 30 min Dr. Mathieu Linares	Palestra (PA14) - 30 min Prof. Enrico Bodo	Palestra (PA20) - 30 min Dr. Pooria Farahani	
15:00-15:30		Palestra (PA6) - 30 min Prof. Hubert Stassen	Palestra (PA15) - 30 min Prof. Laurent E. Dardenne	Palestra (PA21) - 30 min Prof. Luiz Antônio Ribeiro Junior	
15:30-16:00		Coffee Break	Coffee Break	Coffee Break	
16:00-16:30		Palestra (PA7) - 30 min Prof. Francisco Machado	Sessão Coordenada 16:00h-17:20 4 apresentações de 15+5 minutos	Palestra (PA22) - 30 min Prof. Valter H. Carvalho	
16:30-17:00		Palestra (PA8) - 30 min Prof. Milton M. Fujimoto		Plenária (PL5) - 40 min Prof. Sylvio Canuto	
17:00-17:10		Palestra (PA9) - 30 min Prof. Itamar Borges Jr.		Pausa (20 min)}	
17:10-17:30				Assembléia Geral	
17:30-18:00		Sessão de Poster 17:30h - 19:00 h	Sessão de Poster 17:30h - 19:00 h		
18:00-19:00					
19:00-19:30	Abertura	Pausa - 19:00 h - 19:30 h			
19:30-20:30	Plenária (PL1) Prof. Marco Antônio Chaer	Mesa Redonda: <i>Universidade e Setor Produtivo</i>	Livre - 19:00 h - 21:00 h	Livre - 19:00h - 21:00h	
21:00-22:00				Confraternização de Encerramento 21:00h	



PALESTRAS

LECTURES

Analyzing Proton Acidity with the Proton Propagator Approach

Andrés Reyes^a (PQ), Laura Pedraza^a (PQ)

^a *Address Universidad Nacional de Colombia, Department of Chemistry, Calle 44 45-67, Bogotá - COLOMBIA - areyesv@unal.edu.co*

Keywords: APMO/PT, Proton Acidity and Proton Propagator Approach

Abstract

We have extended the electron propagator theory [1] using an Any Particle Molecular Orbital (APMO) reference wavefunction [2,3]. This approach, called APMO/PT is capable of describing the binding energies of any type of quantum species. In this work we present an overview of the applications of APMO/PT to study proton binding energies in molecular systems. Results obtained so far demonstrate the potential of APMO/PT to provide a common framework to study and understand one particle properties in composite systems (system containing several types of particles)

References:

- ¹ J. V. Ortiz, WIREs Comput. Mol. Sci. 2012, 3, 123
- ² J. Romero, E. Posada, R. Flores-Moreno, A. Reyes, J. Chem. Phys. 2012, 137, 074105
- ³ M. Diaz-Tinoco, J. Romero, J. V. Ortiz, A. Reyes, R. Flores-Moreno, J. Chem. Phys. 2013, 138, 194108

Directions of chemical change: reaction kinetics beyond Arrhenius and Eyring

Nayara, Valter, Heibbe, Ademir, Mundim Vincenzo Aquilanti^{1,2,3} E-mail: vincenzoaquilanti@yahoo.it

¹Dipartimento di Chimica, Biochimica e Biotecnologie, Università di Perugia, Italy ²Instituto de Física, Universidade Federal da Bahia, Salvador, Brazil, ³Istituto di Struttura della Materia, CNR, Rome, Italy.

Add

Introduction- Rigorous molecular quantum mechanics [1] and the theoretical description of polarization, orientation and alignment in molecular dynamics [2,3] are vigorously assisting experimental progress, a milestone having been benchmark temperature dependent rate constants for the prototypical F + H₂ reaction [4], recently validated by experiments in the moderate tunnelling regime [5].

Results and discussion. Experimental advances involve photochemical and molecular-beams techniques, combined with tools for specific state preparation, mode selection and detection, and are permitting to explore new trends on physico-chemical processes [6,7]. The ample phenomenology that has been accumulated is selectively illustrated, as time will permit.

- (i) In our recent and current work of photodissociation processes [8-10], novel paths are discovered by ion imaging and time resolved FTIR emission spectroscopy: they evolve through roaming roads away from transition states on potential energy surfaces and may involve nonadiabatic transitions at conical intersections.
- (ii) Our computational and theoretical attention is being addressed specifically to new aspects of reaction stereodynamics, namely chirality effects in collisions [11,12], a topic particularly relevant in astrochemistry and in the debate for the origin of life.
- (iii) For the characterization of the various facets of non-linear Arrhenius behavior in the temperature dependence of reaction rate constants [1]. The F+ HD variant permits exploring tunnel as well as isotopic effects [13].
- (iv) Finally, a numerical experiment is described, regarding a four-atom reaction [14], for which the potential energy surface is generated on-the-fly by quantum chemistry, and the low vs high temperature anti-Arrhenius reactivity is interpreted by a stereodynamical mechanism,

Conclusions- (i) is an example of four-center photodissociation phenomena, (ii) chirality manifests only for systems of more than four atoms, (iii) exact four-atom quantum treatment are a current challenge, the technique in (iv) can hopefully be extended to provide four-center quantum rates, and all examples point at need of overcoming the Wigner-Eyring transition state theory. A presentation at this conference tackles this issue. The senior author (VA) thanks Capes for a PVE position at UFBA.

References

- [1]- S Cavalli, V Aquilanti, K C Mundim, D De Fazio, Theoretical reaction kinetics astride the transition between moderate and deep tunneling regimes: the F + HD case, *J Phys Chem A*, **394**. 6632–6641 (2014), and references therein.
- [2] D. De Fazio, M. de Castro-Vitores, A. Aguado, V. Aquilanti, S. Cavalli “ The He + H₂⁺ → HeH⁺ + H reaction: Ab initio studies of the potential energy surface, benchmark time-independent quantum dynamics in an extended energy range and comparison with experiments” *J. Chem. Phys.* **137**, 244306 (2012)

Covalence, not Resonance-Assistance, behind Cooperative Hydrogen and Halogen bonds

Célia Fonseca Guerra

Amsterdam Center for Multiscale Modeling (ACMM), VU University Amsterdam;
e-mail: c.fonseca Guerra@vu.nl

Halogen bonds are shown to possess the same characteristics as hydrogen bonds: charge transfer, resonance assistance and cooperativity. This follows from computational analyses of the structure and bonding in N-halo-base pairs and quartets (see Figure 1). The objective was to achieve understanding of the nature of resonance-assisted halogen bonds (RAXB): how they resemble or differ from the better understood resonance-assisted hydrogen bonds (RAHB) in DNA.

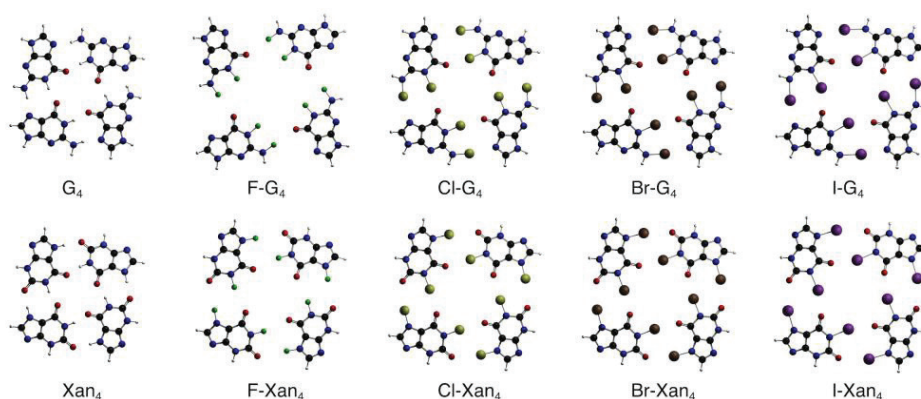


Figure 1. Hydrogen and halogen bonded quartets, X-G₄ and X-Xan₄ of X-G and X-Xan.

An accurate physical model of the RAXB based on molecular orbital theory is presented, which is derived from corresponding energy decomposition analyses and study of the charge distribution. The RAXB arise from classical electrostatic interaction and also receive strengthening from donor–acceptor interactions within the σ -electron system. Similar to the RAHB, there is also a small stabilization by π -electron delocalization. This resemblance leads to prove cooperativity in N-halo-guanine quartets, which originates from the charge separation that goes with donor–acceptor orbital interactions in the σ -electron system.

References:

- [1] G. Paragi, Y. Konijn, C. Fonseca Guerra, submitted.
- [1] L. P. Wolters, N. W. G. Smits, C. Fonseca Guerra, *Phys. Chem. Chem. Phys.*, **2015**, *17*, 1585.
- [2] L. Guillaumes, S. Simon, C. Fonseca Guerra, *ChemistryOpen* **2015**, *4*, 318.
- [3] C. Fonseca Guerra, H. Zijlstra, G. Paragi, F. M. Bickelhaupt, *Chem. Eur. J.*, **2011**, *17*, 12612.
- [4] L. P. Wolters, F. M. Bickelhaupt, *ChemistryOpen* **2012**, *1*, 96.
- [5] C. Fonseca Guerra, F. M. Bickelhaupt, *Angew. Chem. Int. Ed.* **1999**, *38*, 2942.
- [6] C. Fonseca Guerra, F. M. Bickelhaupt, *Angew. Chem. Int. Ed.* **2002**, *41*, 2092.

Controlling the Figure of Merit in some narrow band gap semiconductors: Density Functional theory study

David Fuks, Yaniv Gelbstein

Materials Engineering Department, Ben Gurion University of the Negev,

Beer Sheva, Israel

e-mail: fuks@bgu.ac.il

Narrow band gap semiconductors such as PbTe or TiNiSn half-Heusler (HH) alloys are considered as promising materials for application in thermoelectric devices. Improving their figure of merit may be achieved by increasing the Seebeck coefficient and/or by reduction of thermal conductivity. The magnitude of Seebeck coefficient depends on the shape of the electron Density of states (DOS) in the vicinity of Fermi energy, therefore engineering of DOS may improve thermoelectric figure of merit. Morphology of material influences the thermal conductivity, and this is an additional way to manage the thermoelectric efficiency. The promising method is to reduce the thermal conductivity by varying the average grain size in the sintering of nano-particles. The important question in this context is how the nanocrystalline structure influences their electronic properties. The aim of this presentation is to examine the improving thermoelectric figure of merit by Density Functional theory (DFT) calculations and statistical thermodynamics.

The analysis of the stability of TiNiSn with growing Ni contents is carried out for $T \neq 0$ by combining the DFT calculations with statistical thermodynamics. The approach bridges the gap between the quantum mechanical calculations of the phase stability in the ground state and the behavior of the alloys at elevated temperatures. Decomposition of the off-stoichiometric Ni-rich HH alloy and existence of the miscibility gap between TiNiSn and TiNi₂Sn leads to phase separation in the nano-scale and to reduction of thermal conductivity recently found in experiments.

It is demonstrated also that alloying of PbTe with small amount of Na substituting for Pb leads to *p*-type conductivity, while Cl substituting for Te makes PbTe an *n*-type material. Similar calculations for TiNiSn demonstrate that alloying with Cu makes the material of *n*-type, and alloying with Fe leads to *p*-type conductivity.

We show how the formation of PbTe or TiNiSn compounds with grain boundaries may influence the conductivity of these materials. The effect of impurities segregating to the grain boundaries in nano-structured materials is discussed.

Activation Strain Model (ASM) of Chemical Reactivity

F. M. Bickelhaupt

Amsterdam Center for Multiscale Modeling (ACMM), VU University Amsterdam, and Institute for Molecules and Materials (IMM), Radboud University Nijmegen;
e-mail: f.m.bickelhaupt@vu.nl

The aim of this work is to understand [1] the factors that determine the activity and selectivity of transition-metal catalysts in oxidative-addition steps that occur in bond activation and cross-coupling reactions. We studied the effect of varying the metal M along the d^{10} metals of groups 9, 10 and 11, in combination with varying the number as well as the type of ligands, using relativistic density functional theory (DFT) [2] and the activation strain model (ASM) [1].

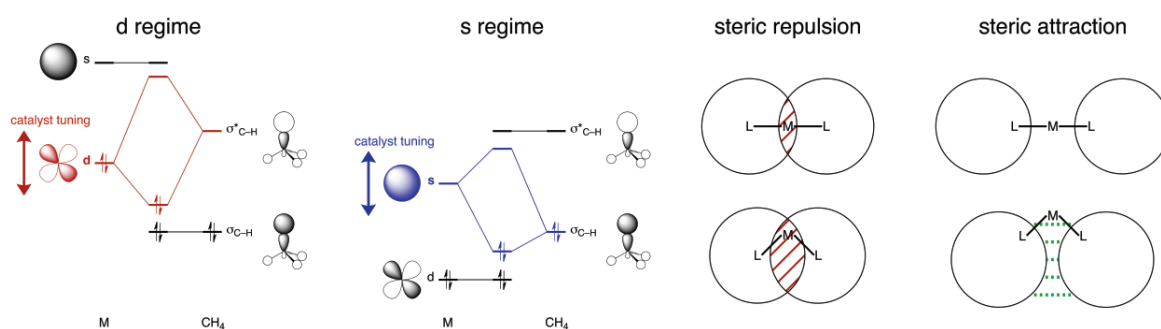


Figure 1. Schematic illustration of concepts presented in this lecture.

Three concepts for tuning a catalyst's activity emerge: (i) d-regime catalysts; (ii) s-regime catalysts; and (iii) bite-angle flexibility (see Figure 1, left). These concepts explain why the effect of one and the same ligand on a catalyst's activity can be completely different, even opposite, for catalysts from different electronic regimes. Furthermore, I will point out why not the bite angle itself, but its flexibility is decisive for the catalyst's activity. Finally, I show how the latter is influenced not only by steric repulsion but also by what we designate "steric attraction" (see Figure 1, right).

References:

- [1] (a) L. P. Wolters, W. J. van Zeist, F. M. Bickelhaupt, *Chem. Eur. J.* **2014**, *20*, 11370-11381; (b) L. P. Wolters, F. M. Bickelhaupt, *Chem. Asian J.* **2015**, *10*, online.
- [2] (a) G. te Velde, F. M. Bickelhaupt, E. J. Baerends, C. Fonseca Guerra, S. J. A. van Gisbergen, J. G. Snijders, T. Ziegler, *J. Comput. Chem.* **2001**, *22* 931; (b) F. M. Bickelhaupt, E. J. Baerends, In: *Reviews in Computational Chemistry*; K. B. Lipkowitz and D. B. Boyd, Eds.; Wiley-VCH: New York, **2000**, Vol. 15, pp. 1; (c) C. Fonseca Guerra, J.-W. Handgraaf, E. J. Baerends, F. M. Bickelhaupt, *J. Comput. Chem.* **2004**, *25*, 189.
- [3] (a) L. P. Wolters, F. M. Bickelhaupt, *WIREs Comput. Mol. Sci.* **2015**, *5*, 324-; (b) I. Fernandez, F. M. Bickelhaupt, *Chem. Soc. Rev.* **2014**, *43*, 4953; (c) F. M. Bickelhaupt, *J. Comput. Chem.* **1999**, *20*, 114.

Alternative Physically Inspired Methodologies to Optimize the Long Range Separated Hybrid Density Functionals Based on the Maximum Hardness and Minimum Polarizability Principles

Heibbe C. B. de Oliveira

Laboratório de Modelagem de Sistemas Complexos, Instituto de Química, Universidade de Brasília, 70919-970, Brasília, DF, Brazil.

In the last two decades, density functional theory¹ (DFT) based on the Kohn–Sham (KS) approach^{2,3} has been attracting considerable attention. Special attention has been devoted to the so-called Long-Range (LR) corrected (LRC)-DFT⁴⁻⁶ methods, which offer a possibility to restore the correct asymptotic exchange potential behavior and, simultaneously, avoid the inclusion of 100% Hartree-Fock exchange. LR separated hybrid functionals split the Coulomb operator r_{12}^{-1} into a short-range (SR) component and along-range (LR) complement, with the help of the standard error function (erf): $1/r = \text{erf}(\omega r)/r + \text{erfc}(\omega r)/r$. In this equation, the range separation is obtained by a single parameter, ω , which is usually obtained empirically. There are alternative strategies to optimize the ω parameter. In so-called IP-tuned LRC hybrids, the optimal ω is found by minimizing the difference between HOMO eigenvalue and the computed IP. The gap tuning schemes of LC-DFT demand that the molecule, and its corresponding anion, obey the Koopmans' theorem. In this seminar we will present a new alternative way to optimize the ω tuning parameter by minimization of average linear polarizability or by the maximization of molecular hardness. The underlying motivation is based on two important and fundamental principles: Maximum Hardness (MHP) and Minimum Polarizability (MPP) Principles.⁸ A discussion about the validity of these new alternative physically inspired methodologies as well as a comparison between the results obtained using them and the IP-tuning procedure will be presented.

1. P. Hohenberg and W. Kohn, Phys. Rev. 136, B864, 1964.
2. W. Kohn and L. J. Sham, Phys. Rev. 140, A1133, 1965.
3. L. J. Sham and W. Kohn, Phys. Rev. 145, 561, 1966.
4. T. Yanai, D. P. Tew and N. C. A. Handy, Chem. Phys. Lett. 393, 51, 2004.
5. O. A. Vydrov, J. Heyd, A. V. Krukau and G. E. Scuseria, J. Chem. Phys. 125, 074106(1-9), 2006.
6. O. A. Vydrov and G. E. Scuseria, J. Chem. Phys. 125, 234109(1-9), 2006.
7. T. Stein, L. Kronik and R. Baer, J. Am. Chem. Soc. 131, 2818, 2009
8. R. G. Parr and P. K. Chattaraj, J. Am. Chem. Soc. 131, 1854, 1991.

Following Chemical Reactions in Real Time

Lars G.M. Pettersson

*FYSIKUM, AlbaNova University Center, Stockholm University, S-106 91
Stockholm*

**email: Lars.Pettersson@fysik.su.se*

X-ray spectroscopies allow atomic resolution through tuning the energy to be resonant with the selected element in a molecule. With the advent of free-electron lasers producing tunable femtosecond x-ray pulses allowing atomic-scale both spatial and temporal resolution a new era in heterogeneous catalysis has opened up. Here I will discuss our recent studies of CO desorption from and oxidation on Ru(0001) where, for the first time the long-speculated precursor state to desorption and adsorption was directly observed [1]. The interpretation of x-ray absorption (XAS) and emission (XES) data was provided by density functional theory (DFT) calculations of spectra and computed free-energy surfaces. In particular, an entropic barrier was found dividing the potential energy surface into chemisorbed and precursor wells at finite temperature. The coadsorption system of oxygen and CO on Ru(0001) was studied in optical laser pump/x-ray laser probe experiments [2]. After about 1 ps we observe a new state associated with formation of the new C—O bond in the formation of CO₂. Based on computed spectra along the reaction pathway we assign this to molecules in the transition state (TS) region. In agreement with the picture of kinetic energy being converted to potential energy at the barrier we find that the reacting molecules "slow down" as they pass through TS. This demonstrates the possibility to capture molecules in the transition state region of a chemical reaction and there measure changes in electronic structure as the new bond is formed.

[1] Dell'Angela *et al.*, *Real-Time Observation of Surface Bond Breaking with an X-ray Laser*, *Science* **339**, 1302 (2013)

[2] Öström *et al.*, *Probing the Transition State Region in Catalytic CO Oxidation on Ru*, *Science* **347**, 978-982 (2015).

A Quantum Chemical Approach to the Understanding of the Intrinsic Properties of Organic Donor-Acceptor Materials

Terttu I. Hukka¹ (PQ), Tuuva Kastinen¹ (PG), Outi Kontkanen¹ (PG), Mika Niskanen¹ (PD), Oana Cramariuc² (PD)

¹*Department of Chemistry and Bioengineering, Tampere University of Technology, P.O. Box 541 (Korkeakoulunkatu 8), Tampere, FI-33101, Finland*

²*Department of Physics, Tampere University of Technology, P.O. Box 692, FI-33101 Tampere, Finland*

Keywords: donor-acceptor copolymer, dye-sensitized solar cell, DFT, TDDFT

INTRODUCTION

Organic solar cells (OSCs) and their applications have been a center of great interest¹ in the past few decades, due to their advantages such as tunable optical properties (color and transparency), light-weight, flexibility, and large-scale processability that lowers the manufacturing costs over the conventional inorganic silicon-based devices. Most successful OSCs make use of a so-called bulk heterojunction (BHJ) structure in the photoactive layer. In the BHJ structure a light-harvesting electron donor (eD) material is blended with an electron acceptor (eA) material, which reduces the diffusion length of the charge carriers and maximizes the interfacial contact and surface area for efficient charge separation. Several organic materials ranging from polymers to small molecules have been employed as eDs, whereas fullerene derivatives, e.g. [6,6]-phenyl-C₆₁-butyric acid methyl ester (PC₆₁BM) or [6,6]-phenyl-C₇₁-butyric acid methyl ester (PC₇₁BM) have typically been used as eAs. Solar-to-electric power conversion efficiencies (PCEs) exceeding 10 %^{1,2} have been achieved with the BHJ-OSC devices having polymers or small molecules as the eD materials. The donor (D) and acceptor (A) parts can be brought into a close contact with each other also by covalently binding them inside the same molecule as is done in organic, light-harvesting D–A dye molecules in the thin films of dye-sensitized solar cells (DSSCs). The PCE of the best n-type DSSC has reached 13 %³ and that of the p-type DSSC 2.5 %⁴. By combining the n- and p-type dyes into a pn-DSSC, i.e. a tandem cell, theoretical PCEs over 40 % have been predicted⁵. However, before the commercially viable organic photovoltaic (OPV) devices with over 20 %

PCEs are realized, a more detailed understanding of the intrinsic properties of the organic molecules used in these solar cells is required to shed light on the future material design considerations. Thus, we have employed theoretical approaches to gain insight into the ground and excited state and charge transfer (CT) properties of several organic eD, eA, and D–A materials used in both BHJ-OPVs and DSSCs and to find applicable methods to predict suitable material characteristics for viable solar cells.

METHODS

The studied systems include a series of conjugated copolymers with alternating D and A units in their backbones and p-type D–A dyes used in solar cells. The molecular geometries and electronic structures of the ground states of oligomers and dye molecules were optimized using density functional theory (DFT) with the Gaussian 09 program package.⁶ The excited state properties and the UV–Vis spectra were investigated with the time dependent (TD) DFT. Trimer models of the copolymers were combined with PC₇₁BM to study the CT properties. In addition to the common global hybrid functional B3LYP, we make use of both non-tuned long range corrected (LRC) functionals, ω B97X and ω B97X-D, and their optimally tuned counterparts, OT- ω B97X and OT- ω B97X-D. The 6-31G* basis set was used for the dye molecules and for tuning the range-separation parameter (ω) in the OT-LRC-functionals, whereas 6-31G** was used for the other calculations. The dye molecules were also studied with a CRYSTAL09⁷ program at the DFT/B3LYP/TZVP level of theory.

Protein Structure Prediction Combining Generalized Simulated Annealing and Molecular Dynamics Simulation

Tacio V. A. Fernandes, Mariana F. R. Teixeira and Pedro G. Pascutti

*Instituto de Biofísica Carlos Chagas Filho
Universidade Federal do Rio de Janeiro, Brasil
pascutti@biof.ufrj.br*

The genome sequencing of various organisms has revealed the amino acid sequence of about 188 million proteins and this number is growing rapidly. However, only about 113,000 proteins structures have been determined so far, mainly by x-ray diffraction and nuclear magnetic resonance, costly and slow techniques that present several obstacles along the process of determining protein folding. These difficulties, allied to the large discrepancy between the number of sequences and known structures reinforce the urgent need to develop new methods. Since the 1960's decade it is known that the information needed to achieve the three-dimensional structure of a protein, associated with its biological activity, is stored in the amino acid sequence, which enables computational approaches to tackle the problem. Advances in both computing power and the understanding of physical and chemical processes related to protein folding, as well as the emergence of new methods for structural prediction, have opened an promising perspective for protein structure prediction by computational methods. Consequently, the folding of small proteins has been reported in the literature using molecular dynamics (MD) on the time scale of hundreds of microseconds. In this work, we propose a method that combines Generalized Simulated Annealing (GSA) and MD for the protein folding prediction. The GSA, proposed by Tsallis, is a very efficient method for global optimization of functions with astronomical number of local minima. We have applied GSA calculations on polypeptide chains, finding intermediate folding states subsequently submitted to MD, leading to the complete folding of proteins (up to 60 amino acid residues) to their native state in considerable less simulation time. The knowledge of protein structure is of great interest, not only in which concerns basic science, but also in the field of drug design and medicinal chemistry, since it is essential to better characterize the interaction between the drugs and their targets.

Melo M. C. R., Bernardi R. C., Fernandes T. V. A., Pascutti, P. G., GSAFold: A new application of GSA to protein structure prediction. *Proteins*, v.80, p.2305 - 2310, 2012.

Moret, M. A., Santana, M. C., Zebende, G. F., Pascutti, P. G., Self-similarity and protein compactness. *Physical Review. E, Statistical, Nonlinear, and Soft Matter Physics*, v.80, p.041908 - , 2009.

Moret, M. A., Pascutti, P. G., Bisch, P. M., Mundim, M. S., MUNDIM, K. C., Classical and quantum conformational analysis using Generalized Genetic Algorithm. *Physica. A.*, v.363, p.260 - 268, 2006.

Agostini, F. P., Soares-Pinto, D. O., Moret, M. A., Osthoff, C., Pascutti, P. G., Generalized simulated annealing applied to protein folding studies. *Journal of Computational Chemistry*, v.27, p.1142 - 1155, 2006.

Moret, M. A., Bisch, P. M., Mundim, K. C., Pascutti, P. G., New Stochastic Strategy to Analyze Helix Folding. *Biophysical Journal*, v.82, p.1123 - 1132, 2002.



RESUMOS

ABSTRACTS

MRHF CI Calculations for BH molecule in the DZ base

A. M. de C. Sobrinho (PQ), M. D. de Andrade (PQ), L. A. C. Malbouisson (PQ)

Instituto de Física da UFBA – Depto. de Física do Estado Sólido, Salvador – Ba, Brasil
e-mail: moreira@ufba.br

Keywords: Multi-Reference Hartree-Fock Configuration Interaction method, Non-orthogonal Configuration Interaction, Multiples Hartree-Fock solutions.

ABSTRACT

The Hartree-Fock (HF) equation is not linear and has, in principle, several solutions [1]. In former works [2, 3] we introduced a multi-reference configuration interaction method based on HF multiples solutions (MRHF CI). In this method, are employed several HF extremes as references to expand the state function. So, for each system, are determined several HF solutions with the adequate point and spin symmetry. With each of the ω^{th} HF extreme we can construct a base of the full CI space. With the ω^{th} HF extreme is construct the \mathbf{B}^{ω} base and the set of the \mathbf{B}^{ω} bases is a generator system, \mathbf{G} , of the full CI space. Although the \mathbf{B}^{ω} bases generates the same space, the correspondent configurations of these bases have distinct quantum-mechanical information contents (QMIC). Then, we can use mixed bases to formulate the CI problem, i. e., multi-reference HF bases (MRHF) that include vectors of \mathbf{G} originated of different \mathbf{B}^{ω} bases [2 – 5], to calculate the energy and properties of molecules using reduced MRHF bases. In this work we have nineteen ${}^1\Sigma^+$ HF solutions obtained for the BH molecule in the double zeta (DZ) base. Were construct several bases MRHF and in the present stage we are performing the corresponding MRHF CI calculations. Some initial results for the permanent electrical dipole moment are displayed in the table below.

Table I. MRHF CI calculations for BH with the DZ basis.*

CSFs	HF solutions	MRHF CI Energy	μ
139	A,F	-25.1268543	1.2686
63	A,E	-25.1210269	1.2803
213	A,B,C,D	-25.1234686	1.2745
171	A,B,C,D	-25.1191880	1.2889
265	A,B,C,D	-25.1265645	1.2717
184	A,H	-25.1359379	1.3012
241	A,G	-25.1252752	1.2791
302	A,F	-25.1405398	1.2537
Full CI: 2575 CSF's		-25.1740150	1.5246

* Energies of the used HF References (a.u.): A = -25.1133953; B = -24.2866430; C = -23.1832873; D = -22.8364870; E = -22.3616984; F = -21.0350312; G = -8.2243947; H = -6.5179617; Exp. Dipole Value: $\mu = 1.270$ debye; Interatomic distance: R = 2.329 bohr.

¹ L. A. C Malbouisson and J. D. M. Vianna. J. de Chimie Physique et de Physico-Chimie Biologique. 87, 2017 (1990).

² L. A. C. Malbouisson, M. G. R. Martins, N. Makiuchi. Int. Journal of Quantum Chem. 106, 2772 (2006).

³ A. M. de C. Sobrinho, M. A. C. Nascimento, M. D. de Andrade and L. A. C. Malbouisson. Int. J. Quantum Chem. 108, 2595 (2008).

⁴ L. A. C. Malbouisson, M. D. de Andrade and A. M. de C. Sobrinho. Int. J. of Quantum Chem., 112, 3409 (2012);

⁵ A. M de C. Sobrinho, M. D de Andrade, M. A. C. Nascimento and L. A. C. Malbouisson. J. Mol. Model. 20, 2382 (2014).

A Valence Bond Description of the Grignard Addition Reactions to a Ketone

Henriques, A.M.^a (PQ), Barbosa A.G.H.^b (PQ)^{a, b} Instituto de Química, Universidade Federal Fluminense, 20141-020, Niterói, RJ, Brazil
amh3082henriques@gmail.com

Keywords: Reaction Path, 4-Membered versus 6-Membered Cyclic Transition States

INTRODUCTION

With over a 100-year-old history, the Grignard reaction is one of the most versatile methods for C-C bond formation.¹ The complexity of the mechanism arises from the wide number of possibilities depending on the solvents used, alkyl group of the Grignard reagent, and several others factors. It is well known that the reaction of an allyl Grignard is faster than a methyl one with the same ketone.² Our goal here is to establish the rate controlling factors for the alkyl transfer mechanism in the reaction of the methyl and allyl Grignard reagents with acetone.

METHODS

All geometry optimizations and stationary point characterizations were obtained through DFT/M06 functional and the 6-311G** basis set using the polarizable continuum model (PCM) to mimic some of the solvent effects. The reaction path from the transition states (TS's) was followed both in reverse and forward direction to verify that the correct transition states, which connects the reactants and products, were obtained. Liquid-phase rate constants were calculated by equilibrium solvation path approximation with the GAMESSPLUSRATE interface using the SM8 solvation model. A multi-structure Valence Bond description of the TS's were obtained at the Multi-Configuration-Spin-Coupled, MC-SC/6-31G** level with the VB2000/GAMESS package.

RESULTS AND DISCUSSION

During the simulations, we found two type of TS's in the addition reactions: (i) A 4 - membered Cyclic TS (Fig.1a,b) that presents a considerable barrier reactions; (ii) A 6 - membered Cyclic TS with a barrierless path (Fig. 1c). The calculated rate constants (Table 1) demonstrated that the first type (i) is under thermodynamic control and the second is type (ii) is the kinetic reaction path. These results are consistent with the simple allyl

Grignard reagent tendency; they are often far too reactive to undergo to 1,3 - shifts.^{3,4}

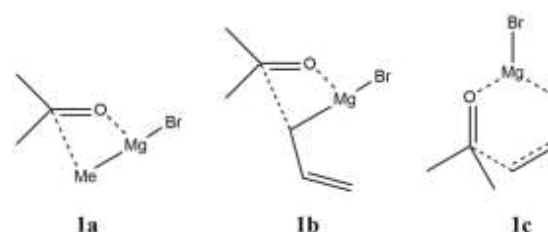


Figure 1. Possible transition states structures for Grignard addition reaction to the acetone: a) and b) 4-membered TS's, c) 6-membered TS.

T (K)	k _{1a}	k _{1b}	k _{1c}
273.15	4.91E-11	4.31E-03	3.81E+06
298.15	4.16E-09	4.19E-01	7.97E+06

Table 1. The forward rate constants (k) calculated at DFT/M06 level with the 6-311G** basis set in Et₂O. All evaluated with the SM8 model.

CONCLUSIONS

The calculations performed in this work reveal the 6 - membered cyclic TS as the responsible path for the great reactivity in the allylation reaction. The 4 - membered cyclic TS's pathways for the addition reactions have a larger $\Delta G^{0\ddagger}$ and present temperature dependence.

ACKNOWLEDGMENTS

The authors are grateful for the support given from the FAPERJ, CENPES-PETROBRAS.

¹ Handbook of Grignard Reagents: G. S. Silverman, P. E. Rakita, Eds; Marcel Dekker: New York, NY, (1996).

² T. Holm, G. Osztrovsky, R. Madsen, Org. Biomol. Chem., 8, 3402, (2010).

³ R. W. Hoffman, Pure Appl. Chem., 60, 123, (1988).

⁴ S. Yamazaki, S. Yamabe, J. Org. Chem., 67, 9346, (2002).

Estudo teórico de adsorção de espécies gasosas em nanotubos de ZnO dopados com Cu

Ademar Dourado Moitinho Neto^a (IC) João B.L. Martins^b (PQ)

^{a,b} Instituto de Química, Universidade de Brasília, CP 4478, Brasília, DF, CEP 70904-970
^a admneto20yy@gmail.com

Palavras-chaves: Nanotubos, ZnO, Adsorção, Dopado, Cu, PM6

INTRODUÇÃO

Dos óxidos metálicos, o óxido de zinco tem sido bastante estudado, visando aplicações em eletrônica, sensores de gases e catálise.[1] Pesquisas mais recentes envolvem o estudo de nanomateriais de ZnO, e alguns estudos teóricos foram desenvolvidos buscando contribuir com questões estruturais[2] e propriedades eletrônicas de interesse para materiais ópticos e eletrônicos.

MÉTODOLOGIA

Para tal estudo, utilizou-se um modelo de nanotubo de óxido de zinco na configuração cadeira, por ser a mais estável. O modelo finito do nanotubo utilizado apresenta nove camadas. Cada camada contendo 10 átomos de Zn e 10 de oxigênio. Dois átomos de Cu foram inseridos na estrutura, e diferentes distâncias foram testadas entre eles foram testadas.

Escolhida a estrutura mais estável, realizaram-se simulações, no vácuo, com os seguintes gases: CO, CO₂, H₂O, H₂ e CH₃OH. Com os resultados desses cálculos, foram obtidos valores termodinâmicos e dados estruturais, com os quais é possível analisar os processos de adsorção e os possíveis modos de interação dos gases com o substrato. Os cálculos foram realizados com o método semiempírico PM6 não-restrito.

RESULTADOS E DISCUSSÃO

Foram realizadas as otimizações das moléculas na camada do NT, com o método UPM6. Para cada molécula adsorvida, foi calculada a frequência e obtidos os valores de energia livre de Gibbs para os processos de adsorção dos gases. Em ordem decrescente do módulo dos valores de energia livre de Gibbs temos: CO, CH₃OH, CO₂, H₂O e H₂. As cargas de Mulliken das moléculas adsorvidas apresentaram a seguinte comportamento crescente: CO₂, H₂, H₂O, CO e

CH₃OH. Como se pode notar as duas tendências são distintas, provavelmente demonstrando uma interação diferente entre estas espécies.

Destas moléculas, apenas o CO₂ apresentou uma carga de Mulliken negativa, sendo que sua interação com o NT apresentava um carbono ligado a 3 oxigênios, em uma estrutura que se assemelha ao íon carbonato, em concordância com relatos da literatura.

CONCLUSÕES

Os cálculos preliminares permitiram a determinação dos valores de energia livre de Gibbs para os processos de adsorção dos gases. Em ordem crescente de valores de energia livre de Gibbs, encontrou-se a seguinte sequência de moléculas: CO, CH₃OH, CO₂, H₂O e H₂. Também foram determinadas as cargas de Mulliken das moléculas adsorvidas. Esta sequência responde parcialmente pela energia de adsorção, mostrando um comportamento intermediário as interações eletrostáticas e covalentes. CO₂ apresentou uma carga de Mulliken negativa, através de uma interação com três oxigênios do NT, em uma estrutura que se assemelha ao íon carbonato.

AGRADECIMENTOS

Os autores agradecem a FAPEG, CAPES, CNPq e FINATEC.

¹ V.A Coleman, C. Jagadish. Chaper 1: Basic Properties and Applications of ZnO. Zinc Oxide Bulk, Thin Films and Nanostructures, 1-20, (2006).

² E. Moraes, R.Gargano, J.R.S.Politi, et al, Curr Phys Chem, 3(4), 400-407, (2013)

Estudo da Ligação e Ativação do O₂ em Complexos do tipo FeN₄: Um Estudo de DFT.

Adilson L. P. Silva^a (PQ), Jaldyr de J. G. Varela Júnior^b (PQ)

^a Universidade Estadual do Maranhão, 65080-040, CP 09, São Luís, MA, Brasil

^b Universidade Federal do Maranhão, 65080-805, São Luís, MA, Brasil.

Palavras-chave: Complexos de Ferro, Oxigênio Molecular, DFT, Retro-doação.

INTRODUÇÃO

Nos últimos anos, muitos estudos químico-quânticos têm sido publicados para compreender a natureza da ligação Fe-O₂, para os sistemas Heme-O₂, os resultados dos cálculos sugerem, que na geometria de ligação *end-on*, o estado fundamental é o singlete de camada aberta (*open-shell singlet*), com formação do *aduto* Fe^{III}-O₂⁻. Jensen e Ryde¹, utilizando a DFT, mostraram o modelo Weiss (Fe^{III}-O₂⁻) como a melhor descrição para a natureza eletrônica da ligação Fe-O₂, em detrimento do modelo Pauling (Fe^{II}-O₂). Diante do exposto, no presente trabalho apresentamos um estudo em nível de DFT para verificar o efeito que diferentes ligantes do tipo tetraaza[14]anuleno desempenham no processo de ativação e ligação do oxigênio molecular (O₂), na formação dos *adutos* FeN₄-O₂.

METODOLOGIA

O modelo utilizado foi baseado em quatro complexos Fe^{II}N₄ (Fig. 1) e nos seus respectivos *adutos* FeN₄-O₂. A metodologia DFT aplicada nos cálculos baseou-se no funcional B3LYP, sendo o conjunto de base Lanl2TZ(f)/6-31G(d)² para os complexos FeN₄ e 6-311++G(d,p)³ para o O₂. Cabe destacar que a energia do estado *open-shell singlet* foi calculado pela correção de Yamaguchi e acordo com a equação:

$$E_S = \frac{(E_C - aE_{S+1})}{(1 - a)}; a = \frac{[(S^2)_C - s(s + 1)]}{2(s + 1)}$$

RESULTADOS E DISCUSSÃO

A partir dos cálculos observamos a preferência da geometria de ligação Pauling (*end-on*) em relação a geometria Griffith (*side-on*), bem como, o estado fundamental *open-shell singlet* para os *adutos* FeN₄-O₂ estudados, corroborando, desta forma, com o modelo Weiss (Fe^{III}-O₂⁻) para a descrição da natureza da ligação Fe-O₂.

Já com relação à distância (O-O) e a frequência de estiramento (O-O) nos *adutos* FeN₄-O₂,

observamos um aumento na d(O-O) e uma diminuição da ν (O-O) em relação ao O₂ livre, respectivamente. Este comportamento pode ser interpretado pela transferência de densidade de carga no sentido $d_{\pi}Fe \rightarrow \pi^*O_2$, ativando o O₂. Esta análise é suportada pelos dados de cargas NBO e da densidade de spin do O₂ no *adutos* FeN₄-O₂.

Finalizando, para verificar o efeito que os diferentes complexos exerciam na ativação do O₂, utilizamos o gap [HOMO(FeN₄)-LUMO(O₂)], e observamos que quanto menor era o gap maior era a retro-doação ($d_{\pi}Fe \rightarrow \pi^*O_2$).

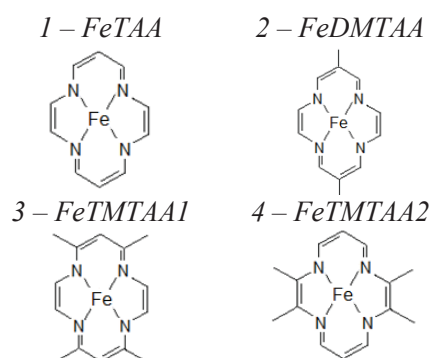


Figura 1. Estruturas dos complexos estudados.

CONCLUSÃO

Os nossos cálculos revelam uma ordem crescente de ativação para o processo de ligação dos complexos FeN₄ com o O₂, segue a sequência: FeTAA < FeDMTAA < FeTMTAA2 < FeTMTAA1, sendo o FeTMTAA1 mais ativo para a ligação com o oxigênio molecular com maior taxa de retro-doação ($d_{\pi}Fe \rightarrow \pi^*O_2$).

AGRADECIMENTOS

Os autores agradecem o suporte financeiro ao FINEP, a CAPES, ao CNPq e a FAPEMA.

¹ K. P. Jensen, U. Ryde, J. Biol. Chem. 279, 14561, (2004).

² A. L. P. Silva et al, Polyhedron 67, 36 (2014).

³ A. L. P. Silva et al, J. Mol. Model. 20, 2131 (2014).

Theoretical and Experimental Study of Structural and Electronic Effects in DHMC.HCl

Alberto dos Santos Marques^a (PQ), Gisele Franco de Castro^b (PQ), Yuji Takahata (PQ)

^a Universidade Federal do Amazonas, Laboratório de Tecnologia com Moléculas Bioativas, LTMB, Departamento de Química. E-mail: marquesalbertods@gmail.com.

^b Universidade do Estado do Amazonas, Centro de Estudos Superiores em Tefé, AM, e-mail: francogisele@gmail.com.

Keywords: Density Functional Theory, Molecular Electronic Spectroscopy, Photophysical Properties,

INTRODUCTION

Recently [1] 51 natural and synthetic coumarins have been tested to inhibit the mutagenicity of 2-amino-3-methylimidazo [4,5-f] quinoline (IQ), activated in *Salmonella typhimurium* TA98. Only six coumarins were inactive, one of them was 3-(diethylamine)ethyl-7-hydroxy-4-methyl-1,2-coumarin.HCl (DHMC.HCl), which exists in the form of a monocation, with protonation at N of the tertiary amine. The inactivity of (DHMC.HCl) was explained relating the molecular and electronic structures to the biological activity, and considering the geometrical conformations, the solvent effects ethanol and water, the protonation/deprotonation dynamics, the photophysical properties and solubilization in micelles solutions neutral and charged.

METHODS

Spectroscopic techniques: emission at 77K, were obtained in Lin Electronic Spectroscopic System (LESS), using the selected band 313 nm. The spectra: UV-Visible were recorded in Perkin-Elmer Lambda 19 UV-Visible and the infrared spectrum was made with the sample in KBr wafers and obtained in ATI Mattson Genesis FTIR spectrometer. The interpretation of the results was done with the aid, the Hartree-Fock method with base function 6-31G*. the excitation energies were calculated using the Time Dependent Density Functional Theory (TD-DFT) using functional B3LYP and base function 6-31G* and the theoretical absorption spectra.

RESULTS AND DISCUSSION

Most known coumarins [2] show a strong phosphorescence emission from emitting state $^3(\pi,\pi^*)$, with vibronic progression and it is more intense than the fluorescence emission and partially located on the (C₃ = C₄) bond of the pyrone ring. The DHMC.HCl dissolved in ethanol and water emits fluorescence but no

phosphorescence. The calculation of the electronic transition HOMO → LUMO to the free base and hydrogen bonded complex species, is assigned as a intramolecular charge-transfer character, originating from a non-bonding electron in the N tertiary amine group to the π^* orbital of benzene ring. This electronic transition is only possible, if the DHMC species, exist in an appropriate geometric conformation, in which the group tertiary amine of DHMC.HC is within close distance to the chromophore benzene, Figure 1. For monocation species, this transition is assigned as (π,π^*) , indicating that charge-transfer was interrupted by protonation in the N tertiary amine group, changing the absorptive and emitter chromophores. Their absorption and emission spectra show a dramatic change, compared to the spectra of the hydrogen bonded complex species.

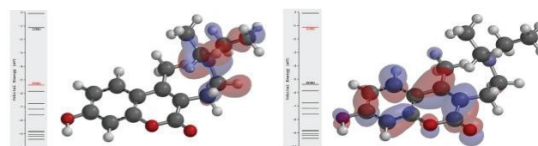


Figure 1. On the left, the molecular orbital HOMO, and on the right, the molecular orbital LUMO of free base DHMC. Calculated using Hartree-Fock method with base function 6-31G*.

CONCLUSIONS

The results show that inactivity of DHMC.HCl against IQ has several reasons, among which we highlight: (i) their photophysical properties are different from those of most coumarins, (ii) its non-planar molecular structure.

ACKNOWLEDGMENTS

We would like to thank CNPQ for its support.

¹R. Edenharder, C. Speth, M. Decker, H. Kolodziej, O. Kayser, K. L. Platt, Mutation Research 345, 57, (1995).

²A. D. S. Marques, C. T. Lin, J. Photochem. and Photobiol. B, Biology, 74, 63,(2004).

***Octopus*: A Virtual High Throughput Screening Platform for Multi-Compounds and Targets**

Alex G. Taranto^a(PQ), Bianca dos R. Santos^b (IC), Marina S. Costa^b (IC), Vinicius A. Campos^b (IC), Iann G. Lima^b (IC), Sandro J. Greco (PQ)^c, Rosy I. M. A. Ribeiro, Felipe M. Munayer, Alisson M. da Silva^b (PQ).

^a Universidade Federal de São João del-Rei - UFSJ, Campus Centro Oeste, Divinópolis- MG, Brazil.

^b Centro Federal de Educação Tecnológica de Minas Gerais – CEFET-MG, Divinópolis-MG, Brazil.

^c Universidade Federal do Espírito Santo – UFES, Vitória, Brazil.

labqf_ufsj@ufsj.edu.br

Keywords: Virtual Screening, Docking, Computational Drug Design, Drug Discovery, vHTS.

INTRODUCTION

Octopus is a software for virtual screening (VS) through AutoDock Vina. It can perform fast and friendly docking simulation. Differently from others VS platforms, *Octopus* can perform docking simulations of unlimited number of compounds into a set of molecular targets. In this work, we selected a successful case, which was addressed for biological assay.

METHODS

Any set of ligands can be submitted to *Octopus*. This is able to integrate MOPAC2012 and AutoDock Vina. After the ligands generated in any draw package in protein data bank (PDB) format, the *Octopus* has carried out geometry refinement using the semi-empirical method PM7 implemented on MOPAC2012. Docking simulation was carried out on Our Own Molecular Targets (OOMT)¹ databank by AutoDock Vina. AutoDock Vina performs stochastic optimization to search the binding conformation. Next, the Metropolis criterion is used to accept this or not. In addition, AutoDock Vina uses both knowledge-based potentials and empirical scoring functions². OOMT is composed by 34 targets, which were evaluated previously by redocking. All targets obtained a RMSD value equal or less than 2.0 angstroms¹. Finally, the proposed software compiles the best binding energy into standard table. The *Octopus* suggests the best bioassay among 34 targets, which were chosen considering the less binding energy in relation to crystallographic ligand energy. In this case, metalloproteinase target was chosen for experimental studies. This biological assay consists in the inhibition of gelatinolytic activity by Gelatin zymography.

RESULTS AND DISCUSSION

A sets of compounds were generated and submitted on *Octopus*. As a result, the molecular target under code PDB 1GKC was found by VS process with -9.5 Kcal/mol binding energy, against -6.6 Kcal/mol of crystallographic ligand. Figure 1 summarizes the intermolecular interaction between 1GKC and ligand. This molecular target is a metalloprotease involved in cancer pathology. Following, all compounds were addressed for biological assay. As a result, the compound LE007 was able to inhibit with 80% of enzymatic activity.

CONCLUSIONS

This successful example illustrated the performance of *Octopus* to find correct molecular targets. In other words, the software summarized the number of biological assay. Hence, it was able to find a new hit for lead compound optimization, that in this case, a new anti-neoplastic drug. Moreover, *Octopus* has a friendly gearing implemented on all Linux-based operation system for which MOPAC2012 and AutoDock Vina have been developed. Further development of molecular dynamics simulation routines are in progress.

Comparative Study of Asphaltene-Inhibitor Interactions by Density Functional Theory

*Alexandre N. M. Carauta^{a,d} (PQ), Michelle C. N. de Carvalho^b (PQ), Fernanda B. Silva^{c,d} (PQ), Julio C. C. Guedes^d (PQ), Maurício T. M. Cruz^e (PQ), Peter R. Seidl^c (PQ)

^aFundação Técnico-Educacional Souza Marques. Rio de Janeiro- RJ. Brazil

^bPetróleo Brasileiro S.A – PETROBRAS. Rio de Janeiro – RJ. Brazil

^cDepartamento de Processos Orgânicos, Escola de Química, Universidade Federal do Rio de Janeiro - UFRJ. Rio de Janeiro – RJ. Brazil.

^dCentro de Tecnologia Mineral – CETEM. Rio de Janeiro- RJ. Brazil

^eDepartamento de Química Geral e Inorgânica, Instituto de Química, Universidade do Estado do Rio de Janeiro – UERJ. Rio de Janeiro – RJ. Brazil

Keywords: Asphaltenes, Inhibitor, Molecular Modeling, Density Functional Theory

INTRODUCTION

Asphaltenes are responsible for causing major losses in petroleum industry and an effective method of prevention of this problem is the use of aggregation inhibitors¹. Molecular modeling can play an important role in the investigation of association phenomena of asphaltenes but the majority of the standard semiempirical, density functional theory (DFT) and ab initio methods does not properly account for the dispersion term¹.

METHODS

Two structures of asphaltenes (BB and BD) and two potential inhibitor molecules, p-nonylphenol and cardanol were used for computational simulations. Conformational analysis was realized by molecular dynamics using the COMPASS force field for each asphaltene and inhibitor structure. Docking between the most stable structures of each asphaltene molecule to each inhibitor molecule was carried out and conformational analysis of asphaltene-inhibitor structures obtained was made by molecular dynamics using the same force field. Calculations of most stable asphaltene-inhibitor structures (Fig.: 1) obtained by docking were done by Density Functional Theory (DFT) using the SVWN and ω B97X-D functional.



RESULTS AND DISCUSSION

The interaction energy calculated by SVWN and ω B97X-D functionals for the asphaltene-inhibitor system can be seen in the Table 1.

Table 1. ΔE (kcal/mol) obtained for asphaltene-p-nonylphenol interactions.

Interaction	SVWN	ω B97X-D
BB	-20.2	-29.9
BD	-25.8	-36.9

The Table 1 shows that calculated interaction energies to BD-p-nonylphenol are larger than BB-p-nonylphenol. Calculated energies by the local exchange-correlation functional SVWN are larger than calculated ones by functional ω B97X-D that has atom-atom dispersion corrections. These are important results because normally functional with local exchange-correlation overestimate binding energies of weakly bound systems. The calculations to asphaltene-cardanol structure are being realized.

CONCLUSIONS

The simulations suggest that the interaction of the p-nonylphenol with BD-asphaltenes is better than BB-asphaltenes, for both functional studied, although the energies are relatively close.

ACKNOWLEDGMENTS

The authors are grateful for the support given from the CNPQ and CETEM.

¹Costa. L.M., *et al.*; J. Phys. Chem.A, 118, 896-908 (2014).

*email of principal author: ancarauta@gmail.com

QSAR studies of combretastatin-like chalcones using PLS and ANN methods

Célio F. Lipinski (PG), Aline A. Oliveira (PG), Albérico B. F. da Silva (PQ)

Instituto de Química de São Carlos, Universidade de São Paulo, São Carlos, SP, Brazil.
alineoliveira@iqsc.usp.br

Keywords: chalcone, QSAR, PLS, MLP-ANN

INTRODUCTION

Several compounds with antimetabolic properties have been studied for the cancer treatment and most of them interact with components of the microtubules¹. Although many drugs are available for the cancer treatment, the high toxicity and resistance limit their use. Therefore, it is necessary to develop new therapeutic alternatives. For this purpose, chalcones have been extensively studied since they inhibit the polymerization of microtubules in cancer cells by interacting with β -tubulin². In order to obtain predictive mathematical models for the biological activity of 87 combretastatin-like chalcones³ and to identify structural features associated to their biological activity we have developed QSAR studies using Partial Least Square (PLS) and Artificial Neural Network (ANN) methods.

METHODS

Gaussian 09 software was used to perform optimization and frequency calculations on the chalcones structures using DFT/B3LYP with 6-31G++(d,p) basis set. Molecular descriptors were obtained by Dragon software and electronic descriptors were obtained by the quantum calculations. Correlation coefficients between descriptors and biological activity and genetic algorithm analysis (BuildQSAR software) were used to select the most relevant descriptors. Pirouette and Matlab softwares were used to perform PLS and Multilayer Perceptron ANN (MLP-ANN) analysis, respectively. Additional validation tests were performed on QSARModeling software.

RESULTS AND DISCUSSION

Correlation coefficients and genetic algorithm analysis allowed us to select the following descriptors: RDF045e, RTv, RDF155u,

RDF035m, SP02, UNIP, PI and $E_{\text{HOMO}-3}$. We have obtained an acceptable PLS model using the selected descriptors ($r^2 = 0.756$, $q^2 = 0.681$ and $r^2_{\text{test}} = 0.843$; Figure 1a). The validation tests showed that the PLS model is robust and it was not obtained by chance correlation. An ANN model was also obtained by training a MLP-ANN with 8-12-1 architecture ($r^2 = 0.803$, $q^2 = 0.761$ and $r^2_{\text{test}} = 0.663$; Figure 1b).

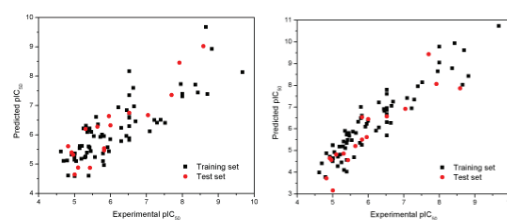


Figure 1. Biological activity prediction by (a) PLS and (b) ANN models.

CONCLUSIONS

The PLS and ANN models were able to predict the biological activity of the studied combretastatin-like chalcones and the PLS model showed better results indicating a linear behavior for the selected descriptors. Additionally, the selected descriptors have shown important features of the combretastatin-like chalcones structures that can be used for the rational drug design of new analogues.

ACKNOWLEDGMENTS

CNPq, CAPES and FAPESP.

¹Wilson, L. and Jordan, M. A. *Nature* 4 (2004) 252-265.

²Bergstrahl, D. T. and Ting, J. P. *Cancer Treat. Rev.* 32 (2006) 166-179.

³Ducki, S. *et al.* *Bioorg. Med. Chem.* 17 (2009) 7698-7710.

Theoretical Investigation of Carboxymethylcellulose/Glyceryl Monooleate Adsorption on Hematite

Aline Carvalho Baruqui, Regina Sandra Veiga Nascimento, and Marco Antonio Chaer Nascimento

Instituto de Química, Universidade Federal do Rio de Janeiro, Cidade Universitária, CT Bloco A, Rio de Janeiro, RJ 21949-900, Brazil. alinebaruqui@gmail.com

Keywords: Carboxymethylcellulose, glyceryl monooleate, hematite adsorption.

INTRODUCTION

Understanding the behavior of polymer/surfactant mixtures at the interface is very important because of their widespread industrial applications such as painting, detergency, water treatment, and oil recovery.¹ Density functional theory was used to study the polysaccharide carboxymethylcellulose (CMC) [Fig.1], the surfactant glyceryl monooleate (GMO) [Fig.2], the CMC-GMO system, and their interaction with hematite. The results showed that CMC adsorbs preferentially on hematite and that the GMO interacts with CMC by hydrogen bonds and van der Waals forces. Based on these results molecular dynamics calculations were performed to better understand how polymer/surfactant interacts on the interface with hematite.

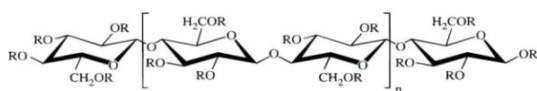


Figure 1. CMC.

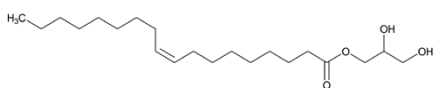


Figure 2. GMO.

METHODS

The interaction surface-polymer-surfactant was investigated with adiabatic molecular dynamics using the Dreiding II force field, trajectories of 1000ps with the CMC connected to the surface through the oxygen atom of the carboxymethyl group, and the (001) surface of hematite from the database of Cerius 2. The dynamics were performed in the presence or absence of surfactant, varying the size of the CMC fragments and their degree of substitution (DS). A preliminary study of the degree of surface coverage was also performed, considering two CMC fragments bounded to the hematite surface.

RESULTS AND DISCUSSION

The binding energy per fragment of CMC on hematite surface [Fig.3] ranges from 327.4 to 490.7 kcal/mol for dimers; 576.3 to 937.5 kcal/mol for tetramers; 914.3 to 1525.8 kcal/mol for octamers, becoming larger as the polymer chain increases. For the dimers the DS does not appear to affect the degree of interaction, however for the tetramers and the octamers an increase in the binding energy with increasing the DS is observed.

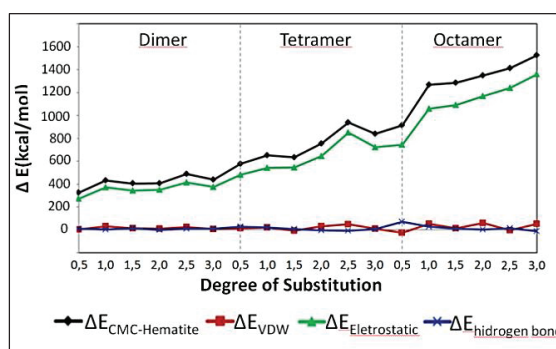


Figure 3. Binding Energy of CMC to Hematite.

The addition of the GMO increased the system stability in most cases by 100-200kcal/mol. The increase in binding energy of CMC to hematite in the presence of GMO can be explained by the reduction of the polymer intramolecular interactions such as hydrogen bonding.

CONCLUSIONS

The results indicate that CMC-hematite interaction is mainly governed by electrostatics forces. The molecular dynamics calculations showed that the addition of GMO increases the binding energy of CMC on hematite.

ACKNOWLEDGMENTS

The authors are grateful for the support from the CNPq, FAPERJ, and INOMAT.

¹Grządka, E., 2011. Materials Chemistry and Physics, 126(3), pp.488–493, (2011).

1,2,4-Oxadiazole Esters as *Aedes aegypti* Larvicides

Aluizio G. da Silva (PG), João B. P. da Silva (PQ), Mozart N. Ramos (PQ), Geanne K.N. Santos (PG), Daniela M. A. F. Navarro (PQ), Diana C. B. da Silva Alves (PG), Janaína V. dos Anjos (PQ)

^aDepartamento de Química Fundamental, Centro de Ciências Exatas e da Natureza, Universidade Federal de Pernambuco 50740-540, Recife (PE), Brazil
 aluiziogaldino@ipojuca.ifpe.edu.br

Keywords: *Aedes aegypti*, Larvicidal Activity, 1,2,4-oxadiazol and QSAR studies

INTRODUCTION

Compounds containing the 1,2,4-oxadiazole ring have been extensively studied because of their biological properties.¹ Recently, our group have successfully introduced a new application for methyl 3-(3-aryl-1,2,4-oxadiazol-5-yl)propanoates as larvicidal agents against the larvae of *Aedes aegypti*, the vector of the Dengue fever disease. The intensity of this activity, in turn, depends not only on the nature of the substituent attached to the phenyl ring, as well as their position. Larvicidal bioassays performed on DQF/UFPE² showed that the compound with a chlorine substituent at the *para* position of the phenyl ring has a $LC_{50} = 23.6 \mu\text{mol L}^{-1}$, whereas the compound substituted with a bromine in the same position has a $LC_{50} = 16.3 \mu\text{mol L}^{-1}$. Therefore, the aim of the current study is to investigate the Quantitative Structure-Activity Relationships (QSAR) between the larvicidal activity and molecular descriptors for the series of methyl 3-(3-aryl-1,2,4-oxadiazol-5-yl)propanoates.

METHODS

B3LYP/6-311G(d,p) calculations, using the standard internal criteria of the Gaussian 03 program, were performed to obtain the electronic properties: i) atomic charge or sum of atomic charges, ii) the electric dipole moment, iii) HOMO and LUMO energies. To evaluate the lipophilicity the parameter LogP was calculated using the program Kowwin 1.67³. Multiple Linear Regression (MLR) was used to obtain the QSAR model using the software STATISTICA 6.0. Only low correlated descriptors were employed.

RESULTS AND DISCUSSION

The QSAR model between the experimental LC_{50} values ($7.5 - 132.0 \mu\text{mol L}^{-1}$) and the molecular descriptors is given in the equation below:

$$\log\left(\frac{1}{LC_{50}}\right) = -15.22 + 67.60qC_3 - 0.94\Sigma q_{benzene} + 0.62\log P$$

with, $n = 11$, $R^2 = 0.98$ and $F = 63.39$. The quality of this model can also be appreciated in Figure 1 by the comparison between predicted and experimental activities.

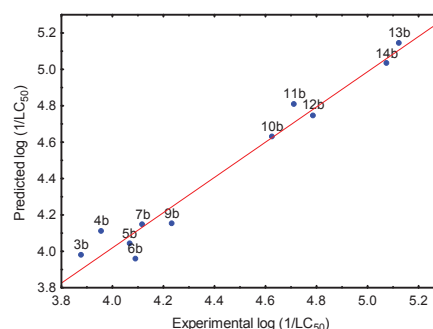


Figure 1. Predicted versus experimental activities.

Using the QSAR model, it was possible to predict a new compound that showed a best larvicidal activity ($6.07 \mu\text{mol L}^{-1}$).

CONCLUSIONS

Our QSAR studies indicate that substituents more hydrophobic and with larger charge at C_3 positively influence the larvicidal activity. We were also able to predict one new compound that exhibited better activity in the series. This result has encouraged us toward new generations of methyl 3-(3-aryl-1,2,4-oxadiazol-5-yl)propanoates with improved larvicidal activity against the larvae of *Aedes aegypti* mosquito.

ACKNOWLEDGMENTS

The authors are grateful for the financial support of FACEPE, CNPq and CAPES.

¹F. Eloy, Fortchr. Chem. Forsch., 4, 807, (1965).

²D.C.B.S. Alves, Dissertação de Mestrado, Universidade Federal de Pernambuco (2001).

³ Program Kowwin TM v.1.67, U.S. Environmental Protection Agency, (2000).

Análise Teórica do Efeito do Empacotamento do Líquido Iônico BMI-Br

Ana Gabriela C. Oliveira^{a*} (PG), Daví A. C. Ferreira^a (PQ), Kleber C. Mundim^a (PQ)

^a Laboratório de Modelagem de Sistemas Complexos, Instituto de Química, Universidade de Brasília, Campus Darcy Ribeiro, CP 04478, CEP: 70904-970, Asa Norte - Brasília-DF, Brasil.

*anagabrielac.oliveira@gmail.com

Palavras-chave: Líquidos Iônicos, Ligação de Hidrogênio, Condutividade Elétrica, DFT

INTRODUÇÃO

A condutividade elétrica, de maneira geral, é dita como uma migração de carga elétrica mediante um gradiente de potencial elétrico.¹ Essa propriedade vem sendo explorada em diversos sistemas moleculares, como os líquidos iônicos (LIs), que por possuírem boa condutividade elétrica são amplamente utilizados em processos eletroquímicos. Os LIs são formados a partir de diferentes combinações de cátions e ânions, e estas influenciam na natureza e efetividade das propriedades físico-químicas, como a condutividade elétrica, e na estrutura molecular destes compostos, resultando em diferentes tipos de interações intermoleculares entre essas combinações, no qual a ligação de hidrogênio (LH) possui um grande impacto.²

MÉTODOS

Neste estudo foram realizados cálculos baseados na Teoria do Funcional de Densidade (DFT) através do Funcional PBE1PBE e base atômica do tipo cc-pVDZ. Objetivando comparar os efeitos da vizinhança molecular, realizamos cálculos para uma cela unitária expandida contendo 1-butil-3-metil-imidazólio brometo (BMI-Br) na forma de tetrâmero, e conservando sua identidade cristalográfica, na forma monomérica onde foi realizada a otimização da geometria. Para a observação desses efeitos de vizinhança molecular, realizamos análises NBO (em andamento) e QTAIM.

RESULTADOS E DISCUSSÃO

Na análise do efeito do empacotamento do BMI-Br, na forma tetramérica, foi possível observar uma estabilização da ordem de 23,603 kcal.mol⁻¹ em relação ao monômero. Também foi observado que, em função da simetria de empacotamento, a polarizabilidade do sistema aumenta relativamente do monômero para o tetrâmero (de 111,937 bohr³ para 427,894 bohr³), enquanto que o comportamento inverso é

observado para o momento de dipolo (15,2735D para 2,0354D). Análises QTAIM foram realizadas, tomando como parâmetro de interação a laplaciana de densidade eletrônica ($\nabla^2\rho$) em alguns pontos selecionados, como exposto na Figura 1 (preto para monômero e vermelho para tetrâmero).

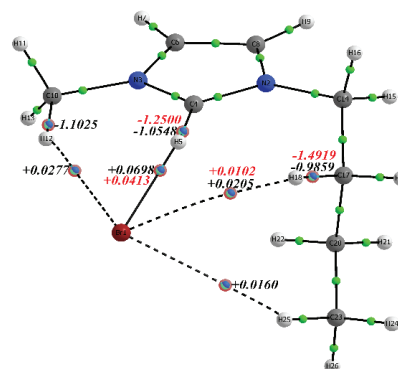


Figura 1. Principais $\nabla^2\rho$ para pontos críticos de ligação no BMIBr monomérico e tetramérico.

Como exposto na Figura 1, o aumento do número de moléculas proporciona uma redução na magnitude da interação entre o par BMI⁺Br⁻, o que indica o caráter deslocalizador da vizinhança molecular e, conseqüentemente, o provável comportamento condutor em fase líquida em sistemas semi-organizados como os LI.

CONCLUSÕES

O aumento de deslocalização nas interações entre os pares BMI⁺Br⁻, do monômero para o tetrâmero, é um indício do comportamento condutor do BMIBr em fase líquida, além de justificar o baixo ponto de fusão desses sais.

AGRADECIMENTOS

CAPES e CNPQ.

¹ Kittel, C., *Introduction to solid state physics*. 8th ed.; Wiley: Hoboken, NJ, 2005; p xix, 680 p.

Molecular dynamics simulations of MurA enzyme in complex with reaction products

Anderson H. Lima^{a,*}(PG), Alberto M. dos Santos^a(PG), Isaque G. Medeiros^a(PG), Cláudio Nahum Alves^a(PQ) and Jerônimo Lameira^a(PQ)

^a Laboratório de Planejamento e Desenvolvimento de Fármacos, Instituto de Ciências Exatas e Naturais, Universidade Federal do Pará, Belém, PA, Brasil.

*e-mail: anderson@ufpa.br

Keywords: Molecular Dynamic, MurA enzyme, MMGB-SA calculations.

INTRODUCTION

MurA(UDP-N-acetylglucosamine enolpyruvyl transferase, EC 2.5.1.7) is an essential enzyme in the biosynthesis of the peptidoglycan layer of the bacterial cell. The x-ray structure of the C115S mutant of *Enterobacter cloacae* MurA depicts the product state of the enzyme with enolpyruvyl-UDP-N-acetylglucosamine (EP-UNAG) and inorganic phosphate (PO₄) trapped in the active site. Kinetic analysis revealed that the Cys-to-Ser mutation results in an enzyme that appears to perform a single turnover of the reaction¹. Opposing the common view of Cys115 as a key residue in the chemical reaction of enolpyruvyl transfer², the wild-type cysteine is essential for product release only. Thus, the aim of this work was to employ molecular dynamics simulations of both native and C115S MurA in complex with PO₄ and EP-UNAG in order to understand the molecular differences on release or not the reaction products.

METHODS

The Amber 12 suite of programs was employed using the ff12SB force field to run a total of 21ns MD simulations. The trajectories with 2100 snapshots were used to compute the binding free energy of the PO₄ ligand at the active site of MurA enzyme along the simulation using the MM-GBSA method as implemented in amber 12.

RESULTS AND DISCUSSION

The results show that the native enzyme release the PO₄ product in the first steps of the simulation. In contrast, MurA C115S shows retaining the PO₄ molecule at the active site along the simulation. MMGB-SA calculations show an increase in free energy of PO₄ binding along the MD simulations of the native enzyme, which suggest repulsion interactions with the active site residues as supposed by experimental analysis¹.

Both complexes show stable values of binding free energy after 0,5ns. However, as can be seen in Figure 1, the mutant form appears with smaller binding free energy values, whereas the main interactions seen in the beginning of the simulation were maintained.

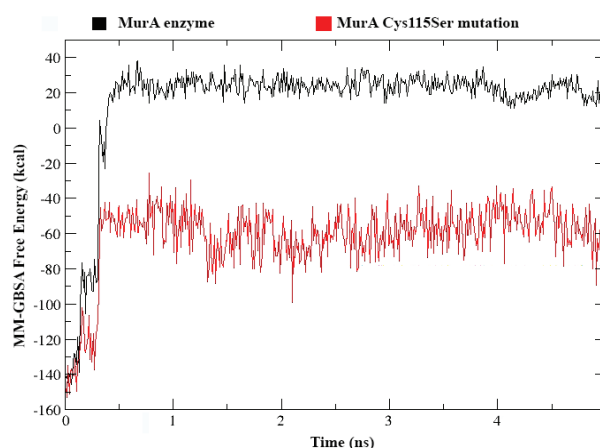


Figure 1. Free-energy profile for the first 5ns of MD simulations.

CONCLUSIONS

The simulations performed in this work are in agreement with experimental data analysis that reveal PO₄ releasing in MurA native form. Once we have serine instead of the wild-type cysteine in position 115, the products are trapped in the active site. Per-residue decomposition analysis are being carried out in order to investigate which residues contribute to the instability that leads to phosphate releasing.

ACKNOWLEDGMENTS

The authors are grateful for the support given from the CAPES, CNPQ and LPDF/UFPA.

¹ Eschenburg S, Priestman M, Schönbrunn E. J Biol Chem. 4,3757, (2005).

² Marquardt, J. L., Brown, E. D., Lane, W. S., Haley, T. M., Ichikawa, Y., Wong, C. H., and Walsh, C. T. Biochemistry 33, 10646, (1994).

Ab-initio Calculation of IR, UV-Vis and CD Spectra of Boron-nitrogen Azulenes

Anderson José Lopes Catão^a (PG), Alejandro Lopez-Castillo^a (PQ)

^a Departamento de Química, Universidade Federal de São Carlos

Keywords: Ab Initio, Circular Dichroism, Infrared, Azulene, Boron-Nitrogen.

INTRODUCTION

Azulene is an isomer of naphthalene. The isomerization of azulene to Naphthalene occurs at high temperature and is exothermic, nearly 40 Kcal/mol¹. Boron-nitrogen azulene, the equivalent boron-nitrogen compound of azulene, can exist in two isomers. BN-azulene is the one that has a boron-boron linkage and NB-azulene, the one that has a nitrogen-nitrogen linkage. These compounds have not been synthesized yet, so little information is available. The aim of this study is characterize the isomers of boron-nitrogen azulene providing information about the absorption spectra and stability of the isomers.

METHODS

All calculations were performed using *TURBOMOLE* software². The geometries of molecules were optimized in gas-phase at CC2 (Second-Order Approximate Coupled-Cluster) level using TZVPPD basis set. The spectra were also calculated at this level of theory. UV-Vis and CD spectra were obtained using 24 excitations and the Random Phase Approximation.

RESULTS AND DISCUSSION

Figure 1 shows the general structures of the two isomers discussed here. We note that both isomers are planar, which is usually a requirement for aromaticity.

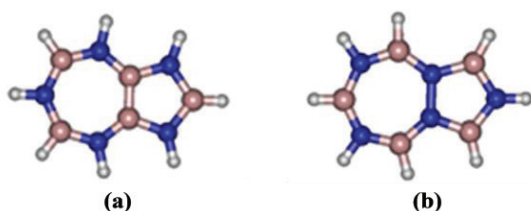


Figure 1. General structures of (a) BN-Azulene and (b) NB-azulene.

The values of total energy were: -402.592 eV (BN-Azulene) and -402.535 eV (NB-Azulene). BN-azulene appears to be more stable since it has the most negative value of total energy.

Figure 2 presents infrared, UV-Vis, CD absorption spectra for both isomers.

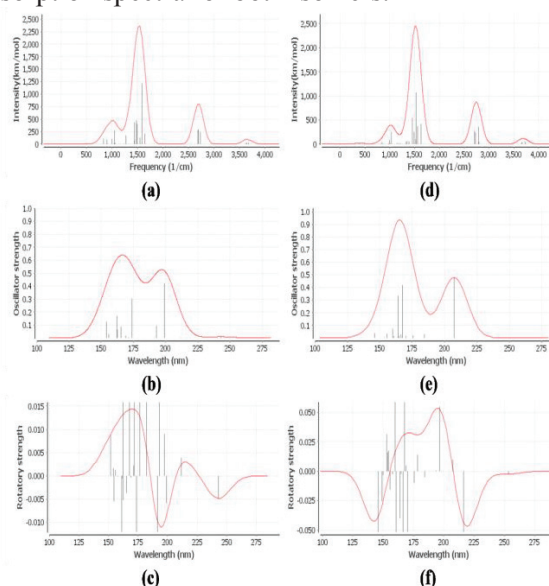


Figure 2. Predicted IR, UV-Vis and CD Spectra of BN-Azulene (a, b, c) and NB-azulene (d, e, f), respectively.

CONCLUSIONS

The calculation performed in this work enable the characterization of boron-nitrogen models to the azulene molecule. Both molecules are planar. However, BN-azulene presents higher stability.

ACKNOWLEDGMENTS

The authors are grateful for the support given from the CAPES.

¹ L. T. Scott and M. A. Kirms. J. Am. Chem. Soc. 1981, 103, 5875-5879.

² R. Ahlrichs, M. Bär, M. Häser, H. Horn, and C. Kölmel, Chem. Phys. Lett. 162, 165 (1989).

Time-Dependent Density Functional Theory (TD-DFT) Calculations of the Chiroptical Properties of CdS Nanoparticles Functionalized with Cysteine

André Farias de Moura^a (PQ), Nicholas A. Kotov^b (PQ)

^a Department of Chemistry, Federal University of São Carlos, São Carlos, SP, Brazil.
(Corresponding Author: moura@ufscar.br)

^b Department of Chemical Engineering, University of Michigan, Ann Arbor, MI, USA.

Keywords: TD-DFT, Chiral Nanoparticles, Chiroptical Properties, Circular Dichroism.

INTRODUCTION

One of the most important properties of chiral materials, whether natural or synthetic, is their optical activity. Although it is well established that chiroptical responses depend on geometric properties of the chiral units comprising the material, a full understanding of the factors affecting them are still missing. In order to fill some of these information gaps, we have performed an extensive series of electronic circular dichroism (ECD) calculations using time-dependent density functional theory (TD-DFT) for CdS nanoparticles (NPs) with cysteine molecules as stabilizers.

METHODS

The model systems consisted of truncated tetrahedral NPs ($\text{Cd}_{31}\text{S}_{40}^{-18}$) functionalized with 24 cysteine molecules. Geometry optimization was performed with the semiempirical Hamiltonian PM7 (as implemented in MOPAC2012) and TD-DFT calculations were performed at the B3LYP/LANL2DZ level (as implemented in Gaussian 09, revision C.01). We defined a representative set of structural and environmental features whose effects on the ECD spectra are not known yet. Among many possibilities, we have chosen to study in this preliminary investigation the two cysteine enantiomers (either D or L), their arrangement on the NPs faces (either clockwise or counterclockwise), their protonation state (anionic, neutral, zwitterionic or cationic), the solvent effect and the distribution of counterions.

RESULTS AND DISCUSSION

The most difficult and tricky part of the investigation was the evaluation of the

electrostatic screening of the counterions around the NPs. We sampled the sodium cations distribution around a negatively charged NP using a Metropolis sampling Monte Carlo to place the ions at physically meaningful positions, and performed the TD-DFT ECD calculation for 400 excited states (Fig. 1). The band just below 300 nm was the most conserved ECD signal, with negative peaks for all configurations, whereas other spectral regions presented bands of varying intensity and algebraic signal.

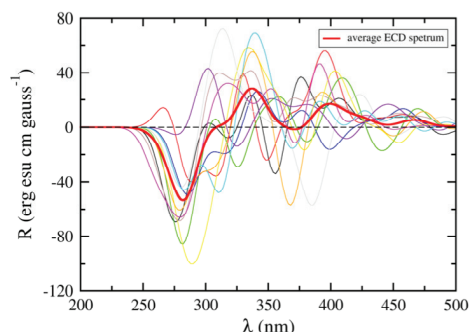


Figure 1. ECD spectra (counterclockwise anionic L-cysteine). Thin lines stand for spectra with 10 different arrangements of sodium cations around the NP.

CONCLUSIONS

The TD-DFT ECD calculation yielded spectra in excellent agreement with experimental results. Chiroptical properties are responsive to changes in the chirality and arrangement of the organic ligands, as well as to the protonation state of ligands and the electrostatic screening of the environment.

ACKNOWLEDGMENTS

The authors are grateful for the support from FAPESP (grant 2012/15.147-4). AFM also thanks PET-MEC for a fellowship.

Absorption Spectrum and Charge Transfer effects in dicyanovinyl-substituted quarterthiophene (DCV4T)/C60 materials for organic solar cells

André Gonçalves de Oliveira (PG), Lucas Modesto-Costa (PQ) Itamar Borges Jr (PQ)

Programa de Pós Graduação em Engenharia de Defesa e Departamento de Química, Instituto Militar de Engenharia, Rio de Janeiro, RJ, Brazil.

Keywords: Solar Cells, DCV4T, Fullerene, TDDFT, ADC(2).

INTRODUCTION

Renewable energy sources is nowadays a necessity. For this reason, developing new materials for converting light into electricity via photovoltaic effect is an increasingly important scientific field. Organic solar cells made of conjugated polymers are promising materials due to their low cost and flexibility. However, their fundamental electronic processes are still not clearly understood.

In this work, we investigate a promising polymeric material, the bulk heterojunction (BHJ) combining donor dicyanovinyl-substituted quarterthiophene (DCV4T) and acceptor fullerene C₆₀.¹ For seven different conformers of this BHJ, the absorption spectrum and charge transfer effects in excited states were investigated.

METHODS

Time-dependent density functional theory (TDDFT) with the PBE functional and the SV(P) base set were used to fully optimize the structures and compute the electronic spectrum. The algebraic-diagrammatic method to second order - ADC(2), an ab initio wave function, was also used and successfully employed before in similar systems.² The software Turbomole 6.6 was used for all calculations.

RESULTS AND DISCUSSION

Figure 1 shows the so called DH configuration, the lower energy one.

The energy difference between the seven conformers is small: the largest was 4 kcal/mol. To illustrate the computed results, Table 1 displays data from 5 out of the 7 studied structures.

Configurations	DH	DN	TIS	Tiot	Tit
Relative (kcal/mol)	0.0	3.79	3.46	3.57	3.82
Gap (ev)	1.20	1.37	1.05	1.26	1.24
First excitation	1.21	1.41	1.06	1.26	1.24

Table 1. Computed PBE/SV(P) properties of five out of seven studied structures.

The computed relative energies excepting the lower energy DH structure are very close. The gap calculated as the HOMO-LUMO energy difference has a very good agreement with the PBE excitation energies, hence indicating the dominant single configuration character of this state.

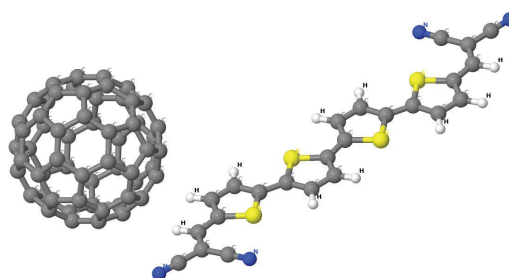


Figure 1. PBE/SV(P) converged DH conformer.

CONCLUSIONS

ADC(2) calculations are underway and will be compared with PBE results. The charge transfer character of the first excited states, which are of interest for organic solar cells, are being quantified.

ACKNOWLEDGMENTS

Faperj, CAPES and CNPq.

¹ B. Baumeier, D. Andrienko, M. Rohlfing. *J. Chem. Theory Comput.* 2012, 8, 2790-2795.

² I.Jr. Borges, A.J.A. Aquino, A. Köhn, R. Nieman, W.L. Hase, L.X. Chen and H. Lischka. *J. Am. Chem. Soc.* 2013, 135, 18252-18255.

Application and development on the internally contracted Multireference Coupled-Cluster Theory

Yuri Alexandre Aoto (PQ), Andreas Köhn (PQ)

*University of Stuttgart, Institute for Theoretical Chemistry
 Pfaffenwaldring 55, D-70569, Stuttgart, Germany
 yuri.aoto@theochem.uni-stuttgart.de*

Keywords: icMRCC, F + HCl Reaction, multi-state calculation

INTRODUCTION

The internally contracted multireference coupled-cluster method (icMRCC) is a promising tool to describe chemical systems with strong static correlation effects with the accuracy of an exponential *ansatz*. However, due to the complexity of the working equations, only recently this method became feasible. In the present work we show the application of the icMRCC method to the F + HCl reaction and the development of a multi-state extension of the theory.

METHODS

The icMRCC method is based on the *ansatz* $|\Psi\rangle = e^T \sum_{\mu} c_{\mu} |\Phi_{\mu}\rangle = e^T |\Psi_0\rangle$. The reference wave function, $|\Psi_0\rangle = \sum_{\mu} c_{\mu} |\Phi_{\mu}\rangle$, is of a CAS type for a selected electronic state, upon which the cluster operator, T , acts. The equations are obtained by a procedure similar to the single-reference case, but an orthogonalization procedure is needed to eliminate linear dependencies in the excitation manifold. This process is the main difficulty of the method and a procedure that leads to a size extensive theory was proposed by our group¹.

The implementation of the icMRCC approach is carried out using the *General Contraction Code* (GeCCo) to automated generate the equations. The orbitals and required integrals are calculated with the DALTON and Molpro codes.

RESULTS AND DISCUSSION

The application of the icMRCC theory to the reaction F + HCl showed a much better agreement to experimental values for the exothermicity and transition state energy than the MRCI method². This leads us to the development of a potential energy surface for this reaction, obtained scaling an MRCI-based PES to reproduce the transition

state geometry and energy calculated with icMRCC. Contrary to the original PES, the newly developed surface is able to correctly describe the experimental vibrational distribution for the products of this reaction.

We also propose a multi-state extension of the icMRCC theory, able to describe situations of quasi-degeneracy. The current approach treats each state in a separate calculation, controlling the target state through the reference wave function. This makes the convergence of the equations for excited states very difficult in near-degeneracy situations. The developed approach deals with this problem solving the coupled residual equations for several states. The results show that accuracy can be obtained without relaxing the reference coefficients, what is not true for the state-specific case.

CONCLUSIONS

Among the several multireference coupled-cluster theories, the icMRCC method keeps the desired features from the single reference case and it has been showing very accurate results. The present work shows the application of this theory on a system whose chemical dynamics is not satisfactorily described by standard methods. A large effort is also being done on extensions of the current approach and a multi-state procedure is being developed.

ACKNOWLEDGMENTS

Y.A.A acknowledges the CAPES and the Humboldt foundations and A.K. acknowledges the Deutsche Forschungsgemeinschaft for the support.

¹ M. Hanauer and A. Köhn, *J. Phys. Chem. A*, 134, 204111 (2011);

² A. Li, H. Guo, Z. Sun, J. Kłos and M. H. Alexander, *Phys. Chem. Chem. Phys.*, 15, 15347 (2013)

Effects of Cholesterol Peroxidation on the Properties of Lipid Bilayers

Antenor J. P. Neto^a, Rodrigo M. Cordeiro^a

^a Centro de Ciências Naturais e Humanas Universidade Federal do ABC - S. André (SP)

Keywords: molecular dynamics simulations, lipid peroxidation, singlet oxygen, oxidative stress

INTRODUCTION

Cholesterol (ChH) is naturally found in all eukaryotic cells and is susceptible to peroxidation. Photodynamically generated singlet oxygen molecules ($^1\text{O}_2$) can react directly with ChH via ene addition, producing cholesterol hydroperoxides (ChOOH). The cytotoxic and apoptotic effects of ChOOH can be partly attributed to their effects on the biophysical properties of phospholipid membranes,¹ as well as their ability to disseminate oxidative stress. These abilities relate strongly to the chemical structure of these hydroperoxides, but the underlying molecular mechanisms are not well understood. For this reason, in this work we use molecular dynamics simulations to study the structure-property relations that affect the cytotoxicity of different cholesterol hydroperoxides and peroxy radicals (ChOO \cdot) at phosphatidylcholine (POPC) bilayers.

METHODS

Atomistic molecular dynamics simulations were used to calculate the properties of the studied systems. Simulation results were analyzed based on the distributions, orientations and degrees of hydration of cholesterol hydroperoxides in

Simulations showed that after peroxidation, the rigid sterol backbone tilted with respect to the membrane and the generated -OOH groups engaged in H-bond interactions with phospholipids carbonyl ester groups. The orientation of cholesterol hydroperoxides with respect to the membrane normal depended on the peroxidation site. As a result, some properties of the lipid bilayer were modified such as the thickness, area, deuterium order parameter and the isothermal compressibility module.

CONCLUSIONS

The orientation of cholesterol hydroperoxides with respect to the normal vector of the bilayer showed to be dependent peroxidation site. The effect was analogous to the previously reported “floating” of -OOH groups in phospholipid hydroperoxides.² However, the whole sterol was forced to reorient due to its rigid structure. Based on these results, it can be inferred that cholesterol hydroperoxides may decrease the rigidity and destabilize membranes liquid-ordered domains. In the case of cholesterol peroxy radicals, the -OO \cdot groups did not migrate to the region of polar groups. This may facilitate the hydrogen abstraction reactions and the spread of oxidative stress.

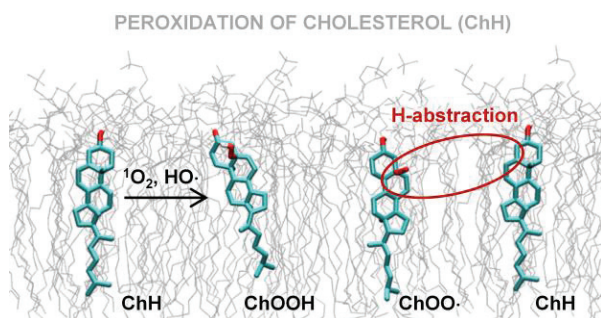
ACKNOWLEDGMENTS

FAPESP is acknowledged for financial support (grant no. 2012/50680-5), as well as CNPq (grant no. 459270/2014-1). A.J.P.N. acknowledges UFABC for the scholarship granted.

¹ L. Iuliano, Chem. Phys. Lipids 164 (2011) 457-468.

² Garrec, J.; Monari, A.; Assfeld, X.; Mir, L. M.; Tarek, M. J. Phys. Chem. Lett. 2014, 5, 1653-1658.

³ Paulista Neto, A. J.; Cordeiro, R. M.; Neto, M. C.; Molecular Simulations of the Effects of Cholesterol Peroxidation on Lipid Membrane Properties, in preparation.



membranes.

RESULTS AND DISCUSSION

Figure 1. Qualitative scheme of the structure of a POPC bilayer containing cholesterol (ChH) and the peroxidation products: ChOOH and ChOO \cdot .

Transition Dipole Moments of PO

Antonio Carlos Borin^a (PQ), Adalberto Vasconcelos Sanches de Araújo^b (PG)Universidade de São Paulo, Instituto de Química
Av. Prof. Lineu Prestes 748, 05508-000, São Paulo, SP, Brazil
(e-mail: ancborin@iq.usp.br^a, avsa2@hotmail.com^b)

Keywords: MRCI, Transition Dipole Moments, PO

INTRODUCTION

Phosphorus monoxide (PO) is a very important interstellar species found¹, for instance, in the circumstellar envelop of the VY CMA star and of the asymptotic giant branch oxygen star IK Tau, either characterized as rich oxygen environment. Despite of its relevance, little is known about the chemistry of PO formation. To understand it in the interstellar space, the rate coefficients for radiative association of P and O atoms is a need, for which the transition dipole moment function is a key information. In this work, the lowest-lying electronic states of PO and the most relevant electronic transitions were investigated by *ab initio* calculations at the MRCI level with extended basis sets. For the first time, transition dipole moment functions were also computed, which will be of great value for understanding the chemical aspects of PO formation in interstellar environments.

METHODS

Potential energy curves and transition dipole moments were calculated at the multireference configuration interaction (MRCI) level and full electron cc-pVQZ² basis sets, augmented with³ three s, three p, three d, and three f diffuse functions on the P atom. All P and C valence electrons and orbitals, plus one extra set of σ and π orbitals, were included in the active space. The calculations were carried out in the C_{2v} point group symmetry, with the MOLPRO⁴ software.

RESULTS AND DISCUSSION

The computed potential energy curves and transition dipole moment function are plotted in Figure 1. The $X^2\Pi$ is the ground electronic state ($R_e = 1.489 \text{ \AA}$, $\omega_e = 1243 \text{ cm}^{-1}$), with the $B^2\Sigma^+$ electronic state being the lowest-lying doublet excited state ($T_e = 3.75 \text{ eV}$, $R_e = 1.494 \text{ \AA}$, $\omega_e = 1042 \text{ cm}^{-1}$), in agreement with experimental findings⁵. As to the transition dipole moment, its

value at the asymptotic atomic limit is zero, because both electronic states dissociate into the same atomic dissociation channel.

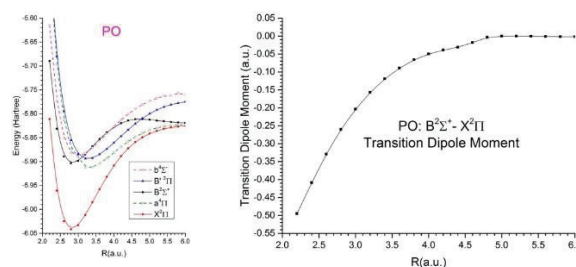


Figure 1. Potential energy curves for the lowest-lying electronic states of PO and the $B^2\Sigma^+ - X^2\Pi$ dipole transition moment function.

CONCLUSIONS

The results presented in this contribution are relevant for the computing the rate coefficients for radiative association of P and O atoms, from which the chemical aspects related to P and O association can be better understood. Franck-Condon factors, Einstein coefficients, and radiative lifetimes for the first excited electronic states.

ACKNOWLEDGMENTS

The authors are grateful for the support given from the CNPq.

¹ T. Kamiński, C. A. Gottlieb, K. H. Young, K. M. Menten, N. A. Patel, 2013, *Ast. Journal*, 209, 38 (2013).

² T. H. Dunning, *J. Chem. Phys.*, 90, 1007, (1989); D. E. Woon, T. H. Dunning, *J. Chem. Phys.*, 98, 1358, (1993).

³ H.-J. Werner, P. J. Knowles, G. Knizia, F. R. Manby, M. Schütz, *WIREs Comput. Mol. Sci.*, 2, 242, (2012).

⁴ A. Spielfiedel, N. C. Handy, *Phys. Chem. Chem. Phys.*, 1, 2401, (1999).

⁵ K. P. Huber, G. Herzberg, *Molecular Spectra and Molecular Structure. IV Constant of Diatomic Molecules*. Van Nostrand Reinhold, New York, 1979.

Bornite, Cu_5FeS_4 or $\text{Cu}_8\text{Fe}_4\text{S}_8$ - Experimental Versus Model Proposal.

Antonio L. Soares Jr.^{a,b} (PG), Thomas Heine^b (PQ), Hélio A. Duarte^a (PQ) and Heitor A. De Abreu^a (PQ).

^aUniversidade Federal de Minas Gerais, Departamento de Química – GPQIT, Belo Horizonte - Brazil. ^bJacobs University Bremen, Campus Ring, Bremen - Germany.
e-mail: antoniolsj@ufmg.br or alsoaresjr@gmail.com

Keywords: Sulfide Minerals, Bornite, Chalcopyrite, Acid Rock Drainage, Metal Extraction, DFT.

INTRODUCTION

Bornite (Cu_5FeS_4 ^[1] or $\text{Cu}_8\text{Fe}_4\text{S}_8$ ^[2]) is one of the minerals detected on the chalcopyrite surface during its leaching process^[3] for copper extraction. It is observed a dramatic decrease in the rate of leaching of copper and its mechanism at a molecular level is not well understood. Understanding the electronic structure of the bulk and surfaces of bornite is important for the proposal of a leaching mechanism. The orthorhombic Cu_5FeS_4 ^[1] (160 atom/cell) system is the best molecular formula proposed by experimental results and the cubic $\text{Cu}_8\text{Fe}_4\text{S}_8$ ^[2] (80 atom/cell) is a theoretical proposal which fixes some deviations found in the experimental results and crystallization. The aim of this work is the theoretical comparison between both structures with elucidation of the nature of the chemical bonding, structural and electronic properties through Density Functional Theory formalism.

METHODS

Quantum Espresso package in its parallel implementation with plane wave basis, PBE and PBESOL exchange–correlation (χ c) functional with core electrons described by US and PAW pseudopotentials were used. In both arrangements, kinetic energy was set to 80 Ry and charge density cutoff was 400 Ry. The k-points density $2 \times 2 \times 2$ integrals by Monkhorst and Pack for $\text{Cu}_8\text{Fe}_4\text{S}_8$ and Gamma point for Cu_5FeS_4 were used.

RESULTS AND DISCUSSION

X-ray diffraction results for Cu_5FeS_4 exhibit fractional occupation in metallic centers, however our theoretical results show that occupation 4 and 5 in asymmetric unit of the cell is 30 kcal.mol⁻¹ more stable than any other possible positions of iron atoms. Adopting these preferential positions to the iron atoms all other results were obtained. The PBE functional and US pseudopotential provided better results with structural properties variation less than 2% in both molecular proposals. Both structures show antiferromagnetic

behavior as detected in experimental results. Band gap of 0.86 eV was measured for Cu_5FeS_4 nanoparticles, but our results indicate metallic behavior in both cases, justified by the underestimated value of energy gap in DFT calculation. Although they had similar electronic behavior, as indicated by the DOS and band structure, PDOS results reveal that Cu_5FeS_4 presents large contributions from *d* orbitals localized on the iron atoms above the Fermi Level (FL) and $\text{Cu}_8\text{Fe}_4\text{S}_8$ exhibits some more contribution below the FL (Figure 1), suggesting the oxidation states +3 and +2, respectively, for the iron atoms. Charge distributions based on Bader's theory (AIM) confirm PDOS information, and suggest Cu^+ and S^{2-} . The AIM topological analysis and ELF shows the ionic character for M–S bond. The bulk compressibility of Cu_5FeS_4 is close to S and Cu local compressibility basins: $\kappa(\text{S}) \approx \kappa(\text{Cu}_5\text{FeS}_4) \approx \kappa(\text{Cu}) = 10.65 \text{ TPa}^{-1}$.

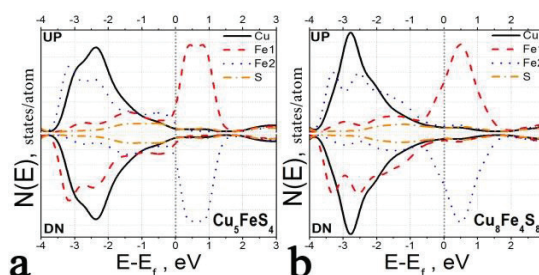


Figure 1. Projected Density Of States (PDOS)/atom for (a) Cu_5FeS_4 and (b) $\text{Cu}_8\text{Fe}_4\text{S}_8$.

CONCLUSIONS

Theoretical results of both structures could be described with accuracy. It was identified the metal occupation in Cu_5FeS_4 and it was shown that the $\text{Cu}_8\text{Fe}_4\text{S}_8$ does not represent a good model for the description of electronic distribution in native bornite (Cu_5FeS_4).

ACKNOWLEDGMENTS

The authors are grateful for the support given from the INCT-acqua, FAPEMIG, CAPES, CNPq and European Commission FP7-PEOPLE-2011-IRSES TEMM1P, GA 295172.

[1] K. Koto and N. Morimoto, *ACTA CRYSTALLOGR B* **1975**, *31*, 2268-2273.

[2] Y. Ding, et al., *AM MINERAL* **2005**, *90*, 1265-1269.

[3] a) D. Majuste, et al., *HYDROMETALLURGY* **2012**, *111*, 114-123; b) D. Majuste, et al., *HYDROMETALLURGY* **2013**, *131*, 54-66.

Study of the Electronic Properties of the Metallophthalocyanine as a Function of the Central Metal Atom

Antonio Marcos Silva Santos^a (PG), Tamires Lima Pereira^a (PG), Demétrio Antonio da Silva Filho^a (PQ)

^a Institute of Physics, University of Brasilia, 70.917-970, Brasília, Brazil.

Keywords: Phthalocyanine, Electronic Properties, Frontier Orbital Energies

INTRODUCTION

Phthalocyanines (Pcs) comprise a large class of compounds with many interesting properties. Several studies have addressed the impact of the position of the central metal atom relative to the organic cage of the phthalocyanine¹ and the possibility of exploiting it in numerous applications. Quite often, this central atom has *d* orbitals that may or may not interact with the π electron system of the molecule, thus contributing only to the geometrical properties or to the electronic properties of Pcs as well. Organic compounds, such as metallophthalocyanines have emerged as important candidates to be used as active materials in numerous applications such as, electrochromic display device, organic light emitting diodes (OLEDs) and organic photovoltaics (OPVs). Here, we analyze the effects of the metal on key properties of the molecule, such as the frontier orbital energies and first excitation energy ($S_0 \rightarrow S_1$). These properties are key in the selection of which metallophthalocyanine should be used for particular technological applications making use of this interesting compound.

METHODS

We started our study extracting phthalocyanines from the X-Ray coordinates available in the Cambridge Structural Database (CSD). With these geometries, we proceeded with the following steps: we added *-H* atoms in the cases where those atoms were missing; we replaced any saturated chains by *-CH₃*. These adapted geometries were used in the following calculations: **i**) a TD-DFT calculation to compute vertical excitation energies ($S_0 \rightarrow S_1$) using the original (X-Ray) geometry; **ii**) a Single Point calculation to compute the frontier orbital energies with the original (X-Ray) geometry; **iii**) a geometry optimization, followed by a Single Point and TD-DFT calculations to recompute the properties listed before for the optimized geometries.

RESULTS AND DISCUSSION

We analyze the first absorbing excited state energy for the various molecules investigated in this study. We can conclude that the energy of this state in both the molecules have values next comparing the values obtained with X-Ray geometries and the optimized geometry. We show the orbital energies of the highest three occupied orbitals and lowest three unoccupied molecular orbitals, both using the X-Ray and optimized geometries. The HOMO→LUMO energy are very comparable in all the molecules studied.

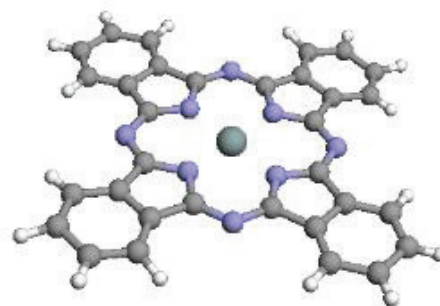


Figure 1. Molecule of metallophthalocyanine

CONCLUSIONS

In this study, we investigated the impact of the central atom on the electronic properties of phthalocyanines. These preliminary results show that the central atom can promote from little to major changes in the electronic properties of MePcs, depending on the interaction of its electronic structure with the π electron system of the Pc.

ACKNOWLEDGMENTS

The authors are grateful for the support given from the University of Brasília and from the Brazilian Research Councils CNPq and CAPES.

¹ Ruan, C., Mastryukov, V., Fink, M., *Journal of Chemical Physics*, 111, 3035-3041 (1999).

Molecular Dynamics of Jaburetox in a POPC Bilayer

William K. Nitschke^a (PG), Celia R. Carlini^{b,c} (PQ), Hubert Stassen^{a*}(PQ)

^a *Grupo de Química Teórica, Instituto de Química, Universidade Federal do Rio Grande do Sul, Porto Alegre, Brazil;*

^b *Department of Biophysics and Center of Biotechnology, Federal University of Rio Grande do Sul, Porto Alegre, Brazil;*

^c *Instituto do Cérebro, Pontifícia Universidade Católica do Rio Grande do Sul, Porto Alegre, Brazil*

**gullit@iq.ufrgs.br*

Keywords: Jaburetox, POPC, insecticidal, intrinsically disordered peptide

INTRODUCTION

Jaburetox (Jbtx) is an insecticidal peptide derived from the *Canavalia ensiformis* urease (JBU).¹ Its mechanism of action involves disruption of the cell membrane, especially in the stomach walls of the insect. Through NMR studies², Jbtx was shown to be an intrinsically disordered peptide. Jbtx forms cation-selective pores inside POPC bilayers³. It is interesting, therefore, to analyze the interaction of Jbtx with membrane bilayers.

METHODS

Jbtx was modeled initially by homology in the PHYRE2 server. The molecular dynamics and analysis were performed with the Gromacs 4.5 suite. The peptide was initially inserted in an aqueous box with physiological concentration of NaCl. After energy minimization and position restrained equilibration steps, the system was subjected to 200 ns molecular dynamics simulation. After 50 ns, the peptide structure was then inserted in two geometries inside a POPC bilayer with the *g_membed* algorithm of the Gromacs suite.

RESULTS AND DISCUSSION

Jbtx was correctly modeled as an intrinsically disordered peptide. Its backbone consists mostly of coils and transient regions as inferred from DSSP analysis. The only three regions with permanent secondary structure are consistent with NMR² studies and X-ray⁴ experiments with JBU.

When inserted into the POPC bilayer, Jbtx anchors into the bilayer surface. When inserted in transmembrane fashion, Jbtx remained anchored to both interfaces. When inserted completely

submerged in the hydrophobic region, it migrated into one of the interfaces. In both cases, Jbtx attracts some polar heads of the phospholipids, forming a ionic pathway, resembling a pore. Water molecules are present inside this pore throughout the simulation. The last snapshot of both simulations are shown in Figure 1.

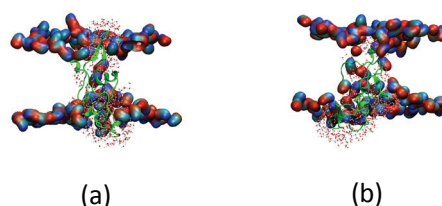


Figure 1. Last snapshot of the bilayer simulations. (a) Transmembrane insertion; (b) Submerged insertion.

CONCLUSIONS

The molecular dynamics simulations performed display formation of a pore, even when the peptide is completely submerged in the hydrophobic region of the bilayer. The presence of the peptide draws the polar heads of the POPC molecules inside of the bilayer itself, thus allowing water molecules to flow inside.

ACKNOWLEDGMENTS

The authors are grateful for the support given from CAPES.

¹ F. Mulinari *et al.* Peptides 28, 2042 (2007)

² Lopes, F. C. *et al.* FEBS J. 282, 1043 (2015)

³ Piovesan, A. R. *et al.* Arch. Biochem. Biophys. 547, 6 (2014)

⁴ Balasubramanian, A.; Ponnuraj, K. J. Mol. Biol. 400, 274 (2010)

Local solvent properties of 1-alkyl-3-methylimidazolium ionic liquids

Arno A. Veldhorst, Luiz F. O. Faria, Mauro C. C. Ribeiro

Laboratório de Espectroscopia Molecular, Instituto de Química, Universidade de São Paulo, CP 26077, CEP 05513-970 São Paulo, Brasil

Keywords: Ionic Liquids, Solvent Properties, Molecular Dynamic, Structural Heterogeneities, Internal Pressure, Cohesive Energy Density.

INTRODUCTION

Room temperature ionic liquids (IL) containing 1-alkyl-3-methylimidazolium cations are well known for the mesoscopic liquid structure¹. Their structure shows polar domains containing mostly the charged parts of the ions, and non-polar domains containing the alkyl groups. This heterogeneous structure has been linked to the peculiar solvent properties of ionic liquids, such as the ability to dissolve both polar and non-polar substances in a single solvent².

In this study we aim to quantify the solvent properties of polar and non-polar domains in the liquid. We do this by calculating the cohesive energy density *ced* and the internal pressure p_i of the domains. The *ced* is the square of Hildebrand's solubility parameter, and the miscibility of two substances is generally inversely proportional to the difference of their *ced*. Another measure for the stiffness of a solvent is the internal pressure p_i . Moreover, the difference between the *ced* and p_i indicates if a liquid is associated; for non-associated liquids, $p_i \approx ced$, while for associated liquids, $ced - p_i \gg 50\text{MPa}^3$.

METHODS

The ionic liquids were simulated using Molecular Dynamics simulations of 1-alkyl-3-methylimidazolium cations [$C_x\text{mim}$], with $x = 2, 4, 6, 8$, and nitrate [NO_3] and hexafluorophosphate [PF_6] as anions. We used the CL&P force field, which has been developed specifically for ionic liquids containing imidazolium cations⁴.

The cohesive energy density is calculated from the energy of vaporization $ced = \Delta_v U/V$. The internal pressure was calculated in two different ways, either from its definition (the partial derivative of the internal energy with respect to the volume on an isotherm), or using the fluctuation formula for the thermal pressure coefficient γ_V :

$$p_i = T\gamma_V - p = \frac{\langle \Delta U \Delta P \rangle}{k_B T} + k_B T \rho - p$$

RESULTS AND DISCUSSION

For the non-polar domains we find *ced* values in the range 280-350MPa, which is a common range for organic liquids, but slightly higher than experimental values for *n*-alkanes. The polar domains have a much higher *ced* values which are reminiscent of molten salts.

The p_i values of the domains are similar to the *ced* values, typical for non-associated liquids. However, for the liquid as a whole, $ced - p_i$ is typical for an associated liquid.

The chain length barely affects the values for the separate domains, but its effect on the liquid as a whole is large.

CONCLUSIONS

We find that the polar and non-polar domains of the ionic liquids have significantly different solvent properties. This confirms that the mesoscopic structural heterogeneities are indeed the cause of the fact that these ionic liquids are able to dissolve both polar and non-polar solutes.

ACKNOWLEDGMENTS

The authors are grateful for financial support from FAPESP.

¹ A. Hayes, G. G. Warr and R. Atkin, *Chem. Rev.* **115**, 6357 (2015).

² L. P. N. Rebelo, J. N. Canongia Lopes, J. M. S. S. Esperança, H. J. R. Guedes, V. Łachwa, V. Najdanovic-Visak, Z. P. Visak, *Acc. Chem. Res.* **40**, 1114 (2007).

³ Y. Marcus, "The Properties of Solvents", Wiley, Chichester (1999).

⁴ J. N. Conongia Lopes, A. A. H. Pádua, *Theor. Chem. Acc.* **131**, 1129 (2012)

Estudo do Efeito da Protonação da Norepinefrina na Sua Estrutura Eletrônica e Espectro de UV-vis

Arsênio P. de V. Neto^a (PG), Sara F. de A. Morais^a (PG), Davi A. C. Ferreira^a (PQ), Heibbe C. B. de Oliveira^a (PQ).

^a Universidade de Brasília, Instituto de Química, Campus Darcy Ribeiro, Brasília, DF.

Palavras-chave: Norepinefrina, TD-DFT, NBO, Efeito de Protonação.

INTRODUÇÃO

A norepinefrina, é uma importante catecolamina que atua como hormônio e neurotransmissor e tem sido associada à alguns processos fisiológicos como ansiedade e stress. Ela é secretada a partir dos neurônios noroadrenérgicos no sistema nervoso central e no sistema nervoso simpático e interage com seus biorreceptores na forma protonada.

Devido a sua grande importância em sistemas biológicos e para melhor entender os efeitos da sua protonação, o objetivo deste trabalho foi estudar a estrutura na norepinefrina neutra (Nep-N) e protonada (Nep-P) por uma análise de carga e análise NBO e observar o efeito de sua protonação do espectro de UV-vis.

METODOLOGIA

Os cálculos de estrutura eletrônica foram realizados no programa Gaussian09, usando o nível de cálculo M062X/6-311+G(d,p) para otimização das estruturas e cálculo de NBO e PBE1PBE/cc-pvdz a sua vertente dependente do tempo (TD-DFT), para o cálculo de UV-vis onde todas as moléculas foram otimizadas.

RESULTADOS E DISCUSSÃO

Ao analisar a estrutura eletrônica da norepinefrina observa-se que a protonação ocorre especificamente sobre o átomo de nitrogênio frente aos grupos –OH. Essa observação é consequência direta da disponibilidade eletrônica do grupo amina. Analisando a distribuição de cargas NBO na Nep-N e Nep-P observou-se maior deslocalização de carga do tipo $n_O \rightarrow \pi_{C-C}^*$ na Nep-P o que indica uma deslocalização de carga para o anel devido ao polarização da densidade eletrônica do anel em função do momento de dipolo criado pela protonação; que leva a um efeito indutivo retirador em direção à amina protonada em busca de estabilizar a carga positiva. Essa deslocalização de carga, em função da protonação, diminui a energia necessária para transições eletrônicas no anel

catecólico, corroborando dados experimentais (Figura 1).

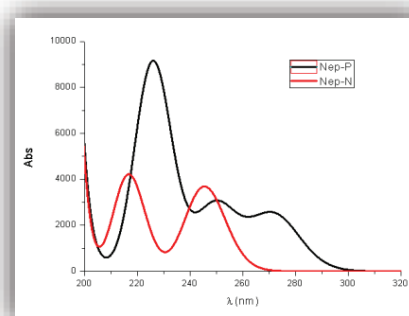


Figura 1. Espectro de UV-vis da norepinefrina neutra e protonada.

Experimentalmente observa-se uma banda de absorção no UV-vis na faixa de 280 nm o que é observado no espectro teórico calculado para a Nep-P, o que mostra que a estrutura eletrônica desta é a que mais se assemelha de dados experimentalmente observados, em que o solvente (água) desempenha papel fundamental. Cálculos de estado de transição com efeito de solvente explícito em meio ácido apontam forte tendência à protonação; indicando que em meio solvente, em sistemas biológicos, que deveriam apresentar uma certa $pH < 7,0$ a protonação é favorecida.

CONCLUSÕES

Os cálculos prévios e análise de NBO apontam tendência de protonação da epinefrina em meio ácido em um favorecimento das transições eletrônicas no anel catecólico na Nep levando a um deslocamento batocrômico no espectro de UV-vis. Comportamento que se aproxima mais dos resultados experimentais

AGRADECIMENTOS

Os autores agradecem à CAPES e CNPq.

¹ Pradhan, T.; Jung, H. S.; Jang, J. H.; Kim, T. W.; Kang, C.; Kim, J. S. Chem. Soc. Rev., 43, 4684, (2014).

MELQUIADES: A Monte Carlo program for simulation of multicomponent systems using arbitrary potential models

Asdrubal Lozada Blanco^a (PG), Luiz Carlos G. Freitas^a (PQ)

^a *Laboratorio de Química Teórica, Departamento de Química, Universidade Federal De São Carlos. Rodovia Washington Luis s/n, km 235 -São Carlos - SP – Brasil*
alozada@ufscar.br

Keywords: Monte Carlo Method, Multicomponent systems, Interaction Energy Potential

INTRODUCTION

A general purpose Metropolis Monte Carlo program, for the simulation of multicomponent system is presented.

METHODS

MELQUIADES is a serial and stand-alone FORTRAN 90/95 program for simulation of multicomponent systems using Metropolis Monte Carlo Algorithm¹. It can be compiled using the GNU Fortran Compiler (gfortran) 4.8 in different GNU/Linux distributions and hardware. In the current version some capabilities implemented are: i) besides Coulombic potential, Lennard-Jones, Buckingham or Yukawa potentials^{1,3} to can be used to calculate intermolecular interaction energy; ii) the configuration space is sampled either in canonical or isothermal-isobaric ensembles; iii) allows the multicomponent system energy calculation and building of diverse neighbor list depending on the molecular size; iv) the trajectories can be saved in xyz and/or xtc format file; v) interfaces with the plotting tools gnuplot or xmgrace and molecular visualization program vmd, molden are available. The source code of MELQUIADES was written in modular format as to facilitate the inclusion or adaption of other potential models or analysis tools.

RESULTS AND DISCUSSION

In this work, the capacity to simulate multicomponent systems is shown through the calculation of the intermolecular interaction energy between water molecules using the TIP3P transferable model. The calculations were carried out on the canonical ensemble at 298 K, using periodic box boundary conditions with a central box filled with 2048 TIP3P molecules.

Fixing the total number of molecules, the test consisted on the calculation of the average interaction energy per molecule assuming that the simulation box is divided into 1, 2, 4, and 8 components with the same number of molecules.

Therefore, in such arrangement, the average interaction energy per molecule must be the same within the statistical error. In all calculations the average energy per molecule obtained was -9.81 kcal/mol with standard deviation 0.00106, in good accord with the values reported in the literature. The figure 1 show the run-time value in seconds for calculations performed with different number of components and size of the markov chain. In figure 1, blue and red lines represents, respectively, markov chain with 1×10^5 and 2×10^5 configurations. One observes that, for a given markov chain size, the computer time is independent of the number of components. Some fluctuations, in the order of microseconds, associated to machine architecture were observed.

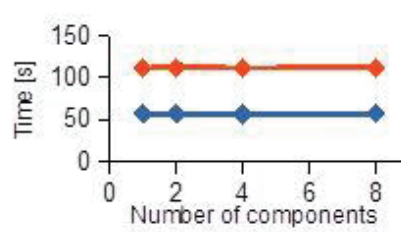


Figure 1. Run-time in markov chain

CONCLUSIONS

The MELQUIADES program can be used for the simulation of complex mixtures. The present test indicate negligible influence of the number of components on the average values and the computer run time.

ACKNOWLEDGMENTS

Financial support from CAPES is acknowledged.

¹ Frenkel, D.; Smit, B.; Understanding Molecular Simulation, Academic Press: San Diego, 2002.

² Ellis, T.M.R.; Philips, I.R.; Lahey, T. M. Fortran 90 Programming, Pearson: 1994.

³ Giccotti, G, Frenkel, D. McDonald, I.R.; Simulation of liquids and Solids, North-Holland: 1987

Estudo Químico-Quântico do Efeito da Cadeia Carbônica sobre Taxas de Dissociação em Reações Radicais do Tipo $\cdot\text{H}+\text{H}-\text{R} \rightarrow \text{H}_2+\text{R}\cdot$.

Brenda S. Pauletti^{a*} (IC), Thiago S. Castro^a (IC), Emília V. F. de Aragão^a (IC), Sara F. de A. Morais^a (PG), Kleber C. Mundim^a (PQ), Davi A. C. Ferreira^{a†} (PQ)

^a Laboratório de Modelagem de Sistemas Complexos, Instituto de Química, Universidade de Brasília, Campus Darcy Ribeiro, CP 04478, CEP: 70904-970, Asa Norte - Brasília-DF, Brasil. E-mail:

*brendaspauletti@hotmail.com/†dacf@unb.br

Palavras chave: Taxas de Reação, Radicais, Efeito do Substituinte, CBS-QB3

INTRODUÇÃO

Um dos mais destacados fenômenos observados em Química é o efeito de substituintes sobre a reatividade. Em reações radicais, a natureza do substituinte conectado diretamente ao radical é uma das principais variáveis que definem a reatividade do radical, estabilização do substrato/estado de transição e, conseqüentemente, a taxa de reação do processo químico estudado. Neste campo se destacam as observações sobre reações do tipo $\cdot\text{H}+\text{H}-\text{R} \rightarrow \text{H}_2+\text{R}\cdot$, que são bastante relatadas, porém muito pouco exploradas. Neste estudo mostramos uma análise sistemática do efeito eletrônico do substituinte sobre a velocidade de reações de dissociação de hidrocarbonetos.

MÉTODOS

Para a realização deste estudo foi aplicado o método CBS-QB3, para a descrição termoquímica da coordenada de dissociação. A partir das geometrias, realizamos cálculos *single point* MP2(Full)/aug-cc-pVDZ objetivando a exploração de propriedades eletrônicas QTAIM e NBO para as reações com R= CH₃, C₂H₅ e n-C₃H₇. Todas as taxas foram determinadas usando o modelo cinético de Mulyava² modificado com a correção *d-exponencial*.

RESULTADOS E DISCUSSÃO

Nossa análise cinética das reações de pirólise nos conduziu aos resultados listados na Tabela 1.

Tabela 1 – Observáveis cinéticas para as reações estudadas a 600K a 1.0 bar. Unidades em cal, K, mol, L, s.

R	E [‡]	ΔS [‡]	A	k
CH ₃	11780	-19.544	2.45x10 ¹¹	1.66x10 ⁷
C ₂ H ₆	7300	-11.155	1.68x10 ¹³	5.00x10 ¹⁰
n-C ₃ H ₇	8280	-18.570	4.00x10 ⁹	5.26x10 ⁸

Cineticamente, verificamos que a reação com etano ocorre cerca de 100 e 1000 vezes mais rápido, quando comparado com propano e metano, respectivamente, dentro dessas condições de análise. A validação da técnica aqui empregada pode ser feita pela reprodutibilidade das propriedades cinéticas descritas por Mulyava e Shevchuk¹ (A=2.00x10¹¹ M⁻¹.s⁻¹ e E[‡]=11.5 kcal.mol⁻¹). Para compreender melhor as tendências observadas através da análise cinética, verificamos as elipticidades nos pontos críticos de ligação (BCP) nos respectivos complexos do tipo van der Waals, destacados na Figura 1; onde verificamos que o radical é melhor estabilizado no etano.

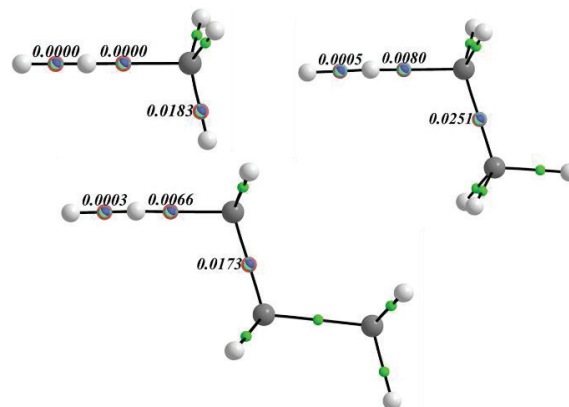


Figura 1. Elipticidades das densidades eletrônicas nos BCP's destacados.

CONCLUSÕES

O modelo cinético de Mulyava ajustado dá uma boa descrição de reações radicais envolvendo pequenas moléculas de hidrocarboneto. O Efeito do aumento da cadeia carbônica não proporciona variação linear de propriedades eletrônicas.

AGRADECIMENTOS

CAPES, CNPQ e PIBIC/ProIC-UnB.

The effect of spin-forbidden transitions in $N(^2D)+H_2$ collisions: a trajectory surface hopping analysis

B.R.L. Galvão (PQ), L.A. Poveda (PQ)

Centro Federal de Educação Tecnológica de Minas Gerais, CEFET-MG,
Av. Amazonas 5253, 30421-169, Belo Horizonte, Minas Gerais, Brazil
brenogalvao@gmail.com

Keywords: Spin-Orbit Coupling, Surface-Hopping, Quasiclassical Trajectories

INTRODUCTION

The reactions of $N(^2D)$ play an important role in plasma and atmospheric chemistry.¹ The rate constants for the quenching of such radical have been measured via multiple reactions¹, and the specific case of quenching via $N(^2D)+H_2 \rightarrow NH(X^3\Sigma^-)+H$ has found good agreement among different experiments.

Theoretically, there are 5 electronic potential energy surfaces (PESs) that correlate to the $N(^2D)+H_2$ channel, but normally only the lowest ($^2A''$) state of NH_2 is considered. However, nonadiabatic effects can play a role in reaction dynamics in multiple ways. For example, the first two electronic PESs of NH_2 ($^2A''$ and $^2A'$) are Renner-Teller coupled, and this effect has been studied in reaction dynamics². In this work we study, for the first time, another nonadiabatic coupling on this benchmark system: the spin-orbit induced transitions. This will allow the prediction of how much $N(^2D)$ can be quenched to the ground $N(^4S)$ state by the title collision, which may be experimentally detectable.

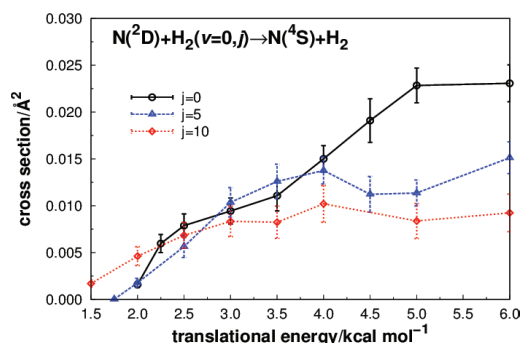
METHODS

In this work we employ two accurate analytic PESs for NH_2 ^{3,4}: the $^2A''$ and $^4A'$. These PESs are eigenvalues of the spin-free Hamiltonian. The coupling between them comes from the spin-orbit operator (H_{so}), and its matrix elements are computed at the MRCI level with the aug-cc-pVQZ basis set over a set of 600 NH_2 geometries, which were fitted to a Gaussian-type function. The dynamics are then performed with the quasiclassical trajectory method, and whenever a doublet/quartet crossing is reached, the Landau-Zener transition probability is calculated in order to determine whether a hopping occurs.

RESULTS AND DISCUSSION

The cross sections for the spin-forbidden reaction⁵ is given in Figure 1. It is found that the

reaction threshold is reduced by rotational excitation on H_2 . For higher translational energies, this excitation inhibits the spin-forbidden cross section, due to a lower hopping probability⁵. The formation of long-lived complexes is also studied, which enhances reaction probability for specific initial conditions. Further details on the collision



will also be explored.

Figure 1. Excitation function for the spin-forbidden reaction.

CONCLUSIONS

We have performed the first theoretical predictions of the spin-orbit coupling for the NH_2 system. High level *ab initio* calculations of the SO coupling were performed and fitted to an analytic function. This fit was employed to study the dynamics of the $N(^2D)+H_2 \rightarrow N(^4S)+H_2$ reaction.

ACKNOWLEDGMENTS

The authors are grateful for the support given by FAPEMIG, CAPES, and CNPQ.

¹ J. T. Herron, J. Phys. Chem. Ref. Data, 28, 1453 (1999).

² F. Santoro, C. Petrongolo, and G. C. Schatz, J. Phys. Chem. A, 106, 8276 (2002)

³ A. J. C. Varandas and L. A. Poveda, Theor. Chem. Acc., 116, 404 (2006).

⁴ L. A. Poveda and A. J. C. Varandas, Phys. Chem. Chem. Phys., 7, 2867 (2005).

Substrate control in an intramolecular Heck-Matsuda reaction: a DFT Study

Bruno M. Servilha^a (PG), Carlos Roque D. Correia^b (PQ), Ataulpa A.C. Braga^a (PQ)

^a Instituto de Química, Universidade de São Paulo, CP 26077, CEP 05513-970, São Paulo – SP

^b Instituto de Química, Universidade de Campinas, CP 6154, CEP 13084-970, Campinas - SP

INTRODUCTION

The development of new synthetic methodologies for heterocyclic compounds is a constant issue in organic synthesis. In 2010 Correia's Group reported the first examples of intramolecular Heck-Matsuda employing *o*-diazo aryl allyl ethers as substrates. The Heck-Matsuda reaction of **1**, an allylic ester, was completely regioselective for the benzopyran product at room temperature. At higher temperatures and catalyst loadings, regioisomer mixtures were obtained (Scheme 1). We have performed DFT calculations on the migratory insertion step of this reaction in order to understand the origin of regioselectivity for the benzopyran product at milder conditions. We are considering here a cationic mechanism, with methanol as a spectator ligand.



Scheme 1 Regioselective intramolecular Heck-Matsuda reaction of allylic ester **1**

METHODS

All calculations were performed on Gaussian 09 suite of quantum chemistry programs employing the M06 functional² with the SDD pseudopotential for Pd and the 6-31+G(d,p) basis set for all other atoms. All geometries were optimized in the gas phase and characterized either as local minima or transition states. Single point energies in methanol on the gas-phase optimized structures were calculated with the SMD model. Relative energies are reported as Gibbs free energies in methanol at 298.15K

RESULTS AND DISCUSSION

The starting complexes, **2** and **3**, for the regioisomeric migratory insertion steps are essentially isoenergetic. In both compounds the palladium-aryl bond is almost perpendicular to the alkene double bond and there is a weak coordination of the sp^2 carboxyl oxygen of the ester moiety to palladium. In order to **2** adopts the structure of **TS2**, the palladium-alkene bond must

be parallel, weakening the back-bonding stabilization of this complex. On the other hand, in **TS3**, the lowest energy transition state, this weakening of the back-bonding interaction is less pronounced than in **TS2**, even though, in this structure the palladium-oxygen bond is lost.

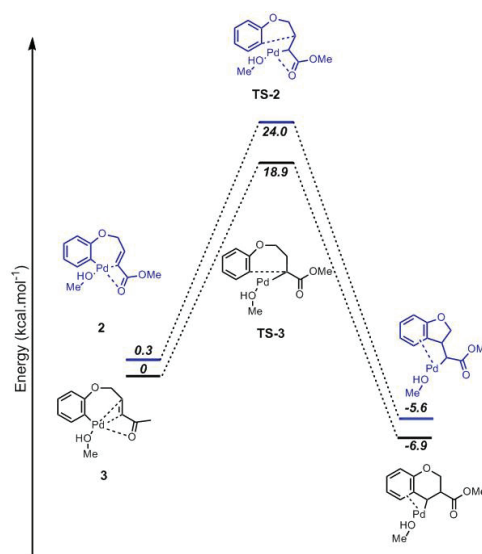


Figure 1 Energy profiles for the regioisomeric migratory insertion pathways. Relative Gibbs free energies (in methanol) are in kcal.mol⁻¹. Charges were omitted for clarity.

CONCLUSIONS

In this work DFT calculations successfully rationalized the regioselectivity in a model substrate-controlled intramolecular Heck-Matsuda reaction. Further studies regarding on the complete catalytic cycle will be reported in due course.

ACKNOWLEDGMENTS

The authors thank FAPESP (grant #2015/01491-3), CNPq and CAPES for financial support and fellowships. We also thank LCCA-USP and CENAPAD for computational facilities.

REFERENCES

- 1 Siqueira, F.A.; Taylor, J.G.; Correia, C.R.D. Tetrahedron Lett. 2010, 51, 2102
- 2 Zhao, Y. T.; Truhlar, D.G. Theor Chem Accounts, 2006, 120 215

Calculation of Photoionization Cross-Section Using Square Integrable Basis Sets for Atoms and Molecules

Bruno N. C. Tenório* (PG), Marco A.C. Nascimento (PQ), Alexandre B. Rocha (PQ)

Universidade Federal do Rio de Janeiro
*(bruno@pos.iq.ufrj.br)

Keywords: Photoionization cross section, Correlated wave functions, Stieltjes Imaging Method.

INTRODUCTION

Photoionization cross-section and dynamic polarizabilities are very important to understand a large number of phenomena, such as optical refractivity and for interpreting the photoelectron spectra of free and adsorbed species. The main difficulty in determining the photoionization cross-section resides in the calculation of continuum wave functions. Langhoff¹ proposed a procedure for constructing the photoionization cross-section from an approximate spectral representation of the dynamic polarizability using L^2 basis functions. The complex dynamic polarizability contains both the absorptive and dispersive information about the system. Thus, photoionization cross-section and dynamic polarizability can be obtained simultaneously, once a representation is found for the complex polarizability. This can be achieved by using a discrete basis set L^2 to represent both the bound and the continuum states of the system. This discrete representation of the continuum is used to construct an approximation to the complex dynamic polarizability, $\alpha(z) = \sum_{n \neq 0} \frac{f_{0n}}{w_{0n}^2 - z^2}$ (eq.1) which is used in an analytical continuation using Padé approximants².

METHODS

Ab initio wave functions of Li and Na were constructed at CASSCF/MRCI level with the basis set cc-pv5z augmented with diffuse primitives according to Kauffmann procedure³ in order to correctly represent the region of the continuum. In both systems, transitions of the type $^1P \leftarrow ^1S$ were studied. The spectra of the discrete distribution of oscillator strengths and transition energies are used to construct an approximation to (eq.1) from which the photoionization cross-section is obtained.

RESULTS AND DISCUSSION

One way of verifying if the discrete distribution of oscillator strengths, obtained with L^2 basis set, furnishes a good representation for $\alpha(z)$ (eq.1) is to determine whether it is able to reproduce the sum rules² and our results have revealed to be very accurate in this respect. Figure 1 shows our results for the photoionization cross-section of Li compared to the experimental curve⁴.

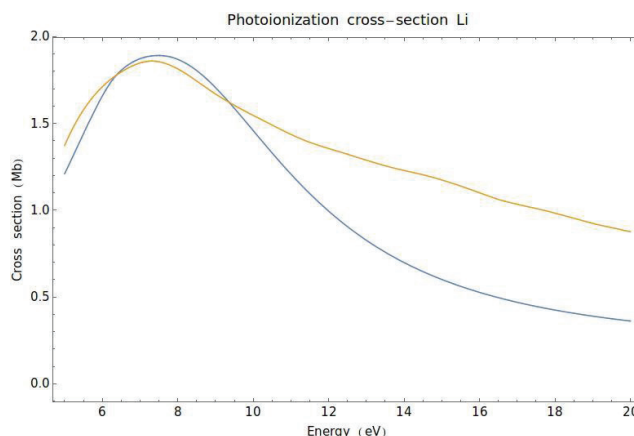


Figure 1. Photoionization cross-section of Li. In blue: our results. In yellow: experimental curve⁴.

CONCLUSIONS

The results obtained with the present method show a reasonable agreement with experiments from the onset up to 10 eV. The less pronounced decay of the experimental curve can be attributed to the presence of vapor of Li_2 in the experiment. Our method uses L^2 basis set and correlated wave function what makes it potentially applicable for molecules.

¹ P. W.Langhoff, Chem. Phys. Lett. 22, 60 (1973).

² M.A.C. Nascimento, W.A. Goddard III, Phys. Rev. A 16, 1559, (1977).

³ K. Kauffmann, W. Baumeister, M. Jungen, J. Phys. B: At. Mol. Opt. Phys. 22, 2223 (1989).

⁴ R.D. Hudson, V.L. Carter, J. Opt. Soc. Am. 57, 651 (1957).

Estudo teórico da molécula de água no Sol

Bruno Silva Leite^a (PG), Cristiano Costa Bastos^a (PQ), Antonio Carlos Pavão^b (PQ)

^a Universidade Federal Rural de Pernambuco

^b Universidade Federal de Pernambuco

bruno.leite@uast.ufrpe.br

Palavras-chave: Cálculos DFT, Espectro rotacional, água no Sol

INTRODUÇÃO

Em 1969, Wöhl¹, observando manchas solares, reportou a existência de água no Sol. Estudos dos espectros das manchas solares buscam relacionar certas bandas com modos roto-vibracionais da água². Não é uma tarefa simples calcular o espectro roto-vibracional da água nas condições do Sol. Considerando que o campo magnético, temperatura, pressão e outras condições existentes no ambiente solar podem ter influência na geometria dessa molécula, apresentamos neste trabalho os resultados de cálculos de Química Quântica para a geometria e o espectro rotacional da água.

MÉTODO

Na perspectiva de mimetizar a geometria da molécula de H₂O nas condições do Sol, realizamos cálculos DFT WB97XD/6-311++G** para o estado singlete ¹B₁ variando o ângulo de ligação e otimizando distâncias. Também analisamos o estado tripleto A₁B₁, no qual incluímos a otimização completa. Consideramos ainda as geometrias dos estados ³B₁ e ¹A₂ que são citadas na literatura^{3,4}. A partir da energia rotacional

$$E = \frac{J_a(J_a+1)h^2}{2I_a} + \frac{J_b(J_b+1)h^2}{2I_b} + \frac{J_c(J_c+1)h^2}{2I_c} \quad (1)$$

obtivemos novos números quânticos que podem ser atribuídos para transições observadas no espectro de manchas solares².

RESULTADOS E DISCUSSÃO

A Tabela 1 apresenta alguns resultados para a molécula de H₂O em diferentes estados eletrônicos.

Tabela 1. Geometrias otimizadas para H₂O.

Estado	Ângulo (deg)	Distância (Å)
¹ A ₂	91,8	1,23
³ B ₁	108,5	1,10
A ₁ B ₁	117,7	1,12

Observando o espectro das manchas solares, Tennyson e Polyansk² atribuem os números quânticos 26_{10 17}, 25_{9 16} e 24_{14 10}, 23_{13 11} para as transições 774,2 cm⁻¹ e 842,9 cm⁻¹, respectivamente. Usando a eq. 1 e as geometrias da Tabela 1, a Tabela 2 mostra outros possíveis números quânticos obtidos para estas duas transições.

Tabela 2. Números quânticos rotacionais para duas transições observadas no espectro de manchas solares.

	$J_{J_a J_b} \rightarrow J_{J_a' J_b'}$	λ_1	$J_{J_a J_b} \rightarrow J_{J_a' J_b'}$	λ_2
¹ B ₁	26 _{17 5} → 25 _{16 4}	772	25 _{5 13} → 24 _{4 12}	843
¹ B ₁	30 _{10 17} → 29 _{9 16}	777	24 _{8 5} → 23 _{7 4}	846
A ₁ B ₁	26 _{2 3} → 25 _{1 2}	772	26 _{3 12} → 25 _{2 11}	843
³ B ₁	29 _{13 15} → 28 _{12 14}	776	24 _{18 6} → 23 _{17 5}	844
¹ A ₂	26 _{19 16} → 25 _{18 15}	774	26 _{17 10} → 25 _{16 9}	842
Exp.	26 _{10 17} → 25 _{9 16}	774,2	24 _{14 10} → 23 _{13 11}	842,9

Portanto, pode existir água no Sol em estados eletrônicos e geometrias diferentes daquelas usualmente observadas na Terra.

CONCLUSÃO

O cálculo de transições rotacionais da água em diferentes estados eletrônicos indica a possibilidade da ocorrência da molécula com geometria não usual no Sol. Esta metodologia pode ser aplicada para outras moléculas presentes no ambiente solar, contribuindo assim para uma melhor caracterização do seu espectro.

AGRADECIMENTOS

CNPq e LEUTEQ-UFRPE.

¹ H. Wöhl. Solar Phys. 9, 394–396, (1969).

² J. Tennyson and O. L. Polyansky. Contemporary Physics, 39, 4, 283–294, (1998).

³ J. Páleníková, et al. Molecular Physics, 106, 20, 2333-2344, (2008).

⁴ Z. Cai, et al. The Journal of Chemical Physics 113, 7084-7096, (2000).

Molecular Dynamics Involving Ammonia and Noble-Gases

Camila D. B. Silva (PG), Rhuaiago M. de Oliveira(PG), Luiz F. Roncaratti(PQ), Geraldo M. e Silva(PQ), Ricardo Gargano(PQ)

Instituto de Física, Universidade de Brasília, Brasília-DF
camiladavila@ymail.com

Keywords: Ammonia, noble-gases, potential energy curves, molecular dynamics.

INTRODUCTION

Ammonia was the first polyatomic molecule detected in interstellar medium space, and has proved to be an invaluable spectroscopic tool in the study of interstellar medium [1]. And besides, the detailed characterization of intermolecular potentials and the development of suitable analytical functions for their formulation provide the foundation on which microscopic and macroscopic properties of matter can be described and extensive molecular dynamics simulations can be built. Specifically, the study of the intermolecular interaction between hydrogenated molecules and neutral species is of great interest for understanding presence and role of hydrogen bonding in various environments [2]. In this work, we present a study about the dynamics of the systems that involve ammonia (NH₃) and noble-gases (Ar, He, Kr, Ne, and Xe). More precisely, we determined the ro-vibrational energies and spectroscopic constants of these systems. All this study was based on the potential energy curves (PEC) of the kind Improved Lennard-Jones (IJL) with experimentally adjusted parameters.

METHODS

Ro-vibrational spectroscopic constants involving ammonia and noble-gases were determined by using two different approaches: discrete variable representation (DVR) and Dunham methods. In both cases, it was used the ILJ PEC given by the following expression:

$$V(r) = \varepsilon \left[\frac{6}{n(r)-6} \left(\frac{r_m}{r} \right)^{n(r)} - \frac{n(r)}{n(r)-6} \left(\frac{r_m}{r} \right)^6 \right] \quad (1)$$

where $n(r) = \beta + 4 \left(\frac{r}{r_m} \right)^2$. In the equation (1),

the first and second terms represent the repulsion and the attraction, respectively. The parameter ε is the depth of the potential well, r_m the equilibrium distance and β is associated with the resistance of the chemical species involved.

RESULTS AND DISCUSSIONS

The ro-vibrational constants (ω_e , $\omega_e x_e$, $\omega_e y_e$, α_e , and γ_e) obtained using Dunham and DVR methodologies are in an excellent agreement. This fact indicates a good quality of our results and the suitability of both methods to treat the NH₃-Ng

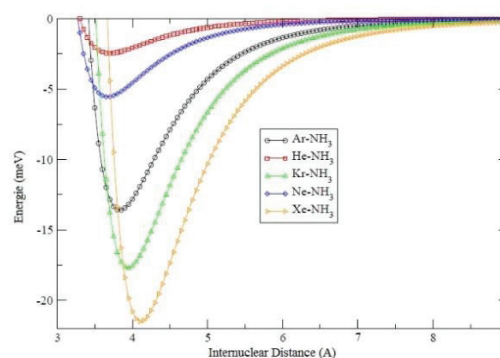


Figure 1: Potential energy curves for the interaction of ammonia with noble-gases.

systems. Furthermore, we determined the first fifteen vibrational states for these systems using the DVR approach. From these calculations, it was observed that the NH₃-He system can remain bonded even with a small dissociation energy.

CONCLUSIONS

It was the first time that the NH₃-Ng ro-vibrational energies and spectroscopic constants calculations are presented in the literature. The current predictions are expected to be useful in the future experimental investigations.

ACKNOWLEDGMENTS

The authors are grateful for the support given from the CAPES, CNPQ and FINATEC.

- [1] M. Bultski, P. E. S. Wormer and A. van der Avoird, *J. Phys. Chem.* 94, 491 (1991).
 [2] F. Pirani, L. F. Roncaratti, L. Belpassi, F. Tarantelli and D. Cappeletti, *J. Phys. Chem.* 135, 194301 (2011).

Optical Rotation Angle of *S*-4-phenyl-2-oxazolidinone: Importance of the Hydrogen Bonded Dimer

C. M. B. Machado, (PG)* and G. L. C. Moura, (PQ)

Departamento de Química Fundamental, Universidade Federal de Pernambuco, Recife-PE, Brazil.

**camila.machado@ufpe.br*

Keyword: Chirality, Optical Rotation, Absolute Configuration, Dimers, DFT Methods

INTRODUCTION

The Chemical, biological and pharmaceutical properties of chiral molecules depend on their stereochemistry. Therefore, there is great interest in determining the absolute configuration of these compounds. However, even the determination of the absolute configuration of simple molecules might be challenging, involving spectroscopic procedures or crystallographic methods. Indeed, it may even require the partial or total synthesis of the molecule. In this work, we studied the *S*-4-phenyl-2-oxazolidinone (SPO) molecule (see Fig. 1) and its hydrogen bonded dimer. We performed full geometry optimizations followed by optical rotation (OR) angle calculations with several DFT methods looking for one of low computational cost, which can best provide the OR angle values that will be used to assist the determination of the absolute configuration of other chiral molecules.

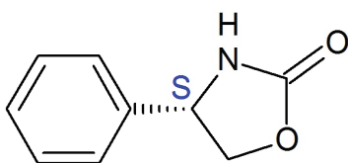


Figure 1. Chemical structure of *S*-4-phenyl-2-oxazolidinone (SPO).

METHODS

First, we employed molecular mechanics to generate the conformers of SPO. We took the two generated conformers, optimized their geometries and calculated the OR angle with four DFT methods (B3LYP, PBE, PBE0 and ω B97XD¹) with nineteen basis sets for the monomer. The dimer was calculated employing the B3LYP, PBE0 and ω B97XD methods with only six basis sets. All calculations were performed for the isolated molecule, and for the molecule in chloroform, using PCM. The OR angles were obtained performing a Boltzmann average over all conformations.

RESULTS AND DISCUSSION

The experimentally observed value of the OR angle for SPO is 48°. For all methods employed, the OR angles calculated for the isolated monomer give the correct sign but the wrong magnitude, yielding values between 120° and 200°. The results with the chloroform solvent are smaller but still considerably overshoot the experimental value, as in ω B97XD/cc-pVTZ with 115,56°. These results might originate from the formation of dimers between molecules of SPO in solution, which can affect the outcome of the value of the OR angle. Indeed, the OR angles calculated for the dimers are compatible with this possibility, since the calculated signs and magnitudes are closer to the experimental value, resulting in calculated OR angles between 35° and 70° for the ω B97XD method.

CONCLUSIONS

Our best results were for the ω B97XD method, where the dimer had OR angle values of 59,46° and 66,31° with the cc-pVDZ basis set and 38,73° and 69,43° with the def2-TZVP basis set for calculations performed for the isolated and solvated molecules, respectively. For the SPO molecule, calculating only the monomer is not enough to correctly assign its absolute configuration. Consequently, for the case of molecules with unknown absolute configuration, the possibility of dimer formation must be taken into consideration for the assignment of their absolute configuration.

ACKNOWLEDGEMENTS

The authors acknowledge the support provided by UFPE, FACEPE, PRONEX and CNPq.

¹ J.-D. Chai and M. Head-Gordon, “Long-range corrected hybrid density functionals with damped atom-atom dispersion corrections,” *Phys. Chem. Chem. Phys.*, **10**(2008) 6615-20.

Propriedades Eletrônicas dos Peroxo Complexos de Molibdênio e de Tungstênio e Implicações na Oxidação de Sulfetos

Camila S. de Avelar (IC) e Fabrício R. Sensato (PQ)

Universidade Federal de São Paulo, UNIFESP, Campus Diadema, e-mail: camilinha2211@gmail.com

Palavras-chave: Complexos de Mimoun, AIM, DFT, Reatividade Química, Química Verde,

INTRODUÇÃO

Oxo-diperoxo complexos de Mo ou de W (Figura 1) são comumente empregados em reações OAT (*oxygen atom transfer reactions*), sobretudo na oxidação de alquenos e sulfetos. Neste estudo, a reatividade química desses complexos é racionalizada em termos das propriedades eletrônicas do próprio complexo (e não da reação). Os resultados são, então, correlacionados com as energias de ativação calculadas.¹

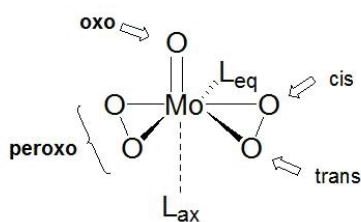


Figura 1. Estrutura molecular genérica para os peroxo complexos de molibdênio

Dentre as propriedades investigadas, destacam-se aquelas derivadas da análise topológica da densidade eletrônica (cargas atômicas e propriedades dos pontos críticos de ligação: densidade eletrônica, laplaciana da densidade eletrônica e densidade de energia), efeitos de doação e retrodoação nos complexos (CDA, *charge decomposition analysis*), e superfície molecular de potencial eletrostático.

MÉTODOS

Todos os cálculos foram realizados em nível DFT/B3LYP. Para descrever o caroço atômico dos átomos de molibdênio e tungstênio nos cálculos de funções de ondas, empregou-se o pseudopotencial relativístico de Hay e Wadt. Os elétrons externos ao caroço foram descritos com

os conjuntos de base de valência [8s6p7d2f] e [8s8p7d2f], respectivamente, para os átomos de Mo e W. O conjunto de base *standard* 6-311+G(2df,2p) foi utilizado para descrever os centros de H, C, N, O, P. A análise topológica da densidade eletrônica no âmbito da teoria AIM foi efetuada com os programas AIMC-UC e Multiwfn. Os cálculos de estrutura eletrônica foram feitos com o programa Gaussian09.

RESULTADOS E DISCUSSÃO

Os resultados revelam que em todos os complexos investigados o grau de covalência para as principais ligações químicas do complexo aumenta na seguinte ordem (M = Mo or W): $MO_{lig} \ll M-O_{cis} \approx M-O_{trans} < O_{cis}-O_{trans} < M-O_{oxo}$. Em particular, a covalência do grupo peroxo nos complexos de Mo é maior que nos congêneres de W. As análises AIM e CDA indicam que a ligação química metal-ligante, em todos os complexos investigados, pertence ao tipo de interações de camada fechada. A maior reatividade do O_{trans} , em detrimento ao O_{cis} , pode ser racionalizada em termos da Laplaciana da densidade eletrônica do grupo peroxo. A energia de ativação do processo de oxidação diminui de uma maneira aproximadamente linear com as seguintes propriedades do ponto crítico da ligação MO_{cis} : i) aumento de Δ_b , ii) aumento de $\nabla^2 \rho_b$ e iii) diminuição de H_b . A barreira de ativação também se correlaciona de uma maneira aproximadamente linear com a carga atômica do O_{cis} e com a nucleofilicidade do O_{trans} : quanto menor a carga sobre o O_{cis} e quanto menor for a nucleofilicidade do O_{trans} , mais reativo é o complexo.

CONCLUSÃO A reatividade dos peroxo complexos de Mo e W é fortemente influenciada pelas propriedades eletrônicas da ligação $M-O_{cis}$.

¹ P. Gonzalez-Navarrete, F.R. Sensato, J. Andres, E. Longo, J. Phys. Chem. A 118, 6092, (2014).

Structural Investigation of Dry Montmorillonite using Solid State NMR Simulations from *ab initio* Calculations

Carla G. Fonseca^{a*} (PG), Gustavo S. G. de Carvalho^a (PQ), Renata Diniz^a (PQ), Alexandre A. Leitão^a (PQ)

^a Department of Chemistry, Universidade Federal de Juiz de Fora, Juiz de Fora-MG, Brazil
*e-mail: carla.grijo@ice.uff.br

Keywords: Montmorillonite, Cationic Clays, *Ab Initio* Calculations, Solid State NMR calculations.

INTRODUCTION

Montmorillonite (MMT) is a 2:1 phyllosilicate with layer structure. It is one of the most useful of all layered silicates and this kind of material is important for industrial and technological applications. Due to the complexity of the MMT structure and the difficulty of acquiring or interpreting experimental results because of low crystallinity and structural heterogeneity, characterizing the geometrical disorder becomes a challenge. When NMR experiments are supported by *ab initio* calculations, there is a significant improvement in the description of the structure.¹ The aim of the present work was by means of DFT calculations, to obtain the energy corresponding to each cation arrangement in intralayer and to show how Si⁴⁺/Al³⁺ and Al³⁺/Mg²⁺ isomorphous substitution in tetrahedral and octahedral sheets respectively affect the dry Na-MMT structure and the Na, Al, Si, H and Mg chemical environments, computed by ²³Na, ²⁷Al, ²⁹Si, ¹H and ²⁵Mg by solid state NMR.

METHODS

This work was developed with the Quantum Espresso package, performing electronic structure calculations based on DFT, with the generalized gradient approximation and Vanderbilt ultrasoft pseudopotentials. The wave functions were expanded by plane wave basis. The NMR calculations were performed by means of gauge-including projector augmented wave (GIPAW) method.²

RESULTS AND DISCUSSION

The structures were generated by different substitutions of Al³⁺ by Mg²⁺ in alumina sheet (M) and/or Si⁴⁺ by Al³⁺ in silica sheet (A) followed by full optimization of the geometries. The sodium atom is more sensitive to replacements in Si-sheet than in Al-sheet. *Ab initio* NMR calculations can

provide an unambiguous peak assignment and good agreement between theoretical (Fig. 1) and experimental spectra was found^{1,3}. We did not identify severe changes in the spectra of both ²⁹Si and ²⁷Al nuclei for different compositions with q=1.0e, as it happened in the ²³Na simulated spectra. The combination of NMR simulations and total-energy calculations indicates a nonrandom Mg/Al occupation within Al-sheet and Al/Si occupation within Si-sheet and a preferred location of Na⁺ counter-ions.

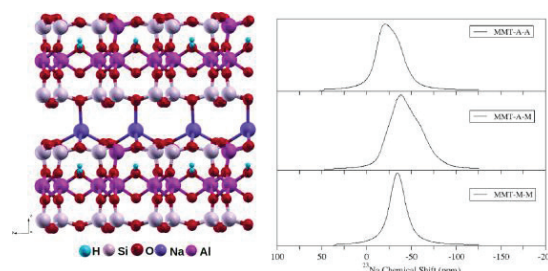


Figure 1. Optimized structure of Na-MMT-A3-A7 and theoretical ²³Na NMR spectra of Na-MMT.

CONCLUSIONS

This result demonstrates the potential of Na cation as a probe of their local structure in dehydrated clays. ²³Na solid state NMR data are very important to understand the molecular structure of Na-MMT.

ACKNOWLEDGMENTS

The authors are grateful for the support given from the FAPEMIG, CAPES and CNPQ. CENAPAD-SP for the computational support.

¹ Cadars, S.; Guégan, R.; *et al.* Chem. Mater.; 24, 4376-4389, (2012).

² J. Giannozzi, P.; Baroni, S.; Bonini, N.; *et al.* J. Phys. Condens. Matter.; 21, No.395502, (2009).

³ Ohkubo, T.; Saito; *Sci. et. al*; Technology of Advanced Mater.; 5, 693-696, (2004).

Simulação de Processos de Adsorção Molecular em Material Nanoporoso Constituído por Tereftalato e Zircônio

Carla V. Soares^{a*} (PG), Alexandre A. Leitão^a (PQ), Naseem A. Ramsahye^b (PQ), Guillaume Maurin^b (PQ)

^a Departamento de Química, Universidade Federal de Juiz de Fora, Juiz de Fora, Brasil.

^b Institut Charles Gerhardt Montpellier, UMR 5253 CNRS, École Nationale Supérieure de Chimie de Montpellier, Montpellier, France.

*e-mail: carlavieira@ice.ufjf.br

Palavras-chave: Metal-Organic-Frameworks, Adsorção, Cálculos *Ab initio*.

INTRODUÇÃO

Metal organic frameworks (MOFs) são constituídos por uma extensa rede de íons ou *clusters* metálicos coordenados a moléculas orgânicas multidentadas em dimensões porosas bem definidas. Esses materiais agrupam características relevantes, como: alta porosidade; elevada área superficial interna e existência de forte interação metal-ligante.¹ MOFs têm atraído muito interesse devido à aplicações em purificação, separação e estocagem de gases. Recentemente MOFs constituídos por metais tetravalente e carboxilato têm despertado interesse devido a alta estabilidade da unidade secundária de construção (SBU) que sugere uma elevada estabilidade química, térmica e forte resistência à água. Neste trabalho foi utilizado a Teoria do Funcional da Densidade (DFT) afim de propor um modelo estrutural para o MIL-140A² (Fig. 1) e em seguida investigar a adsorção das moléculas: CO₂, CO, N₂, CH₄, H₂S e C₄H₄S, avaliar a seletividade e a estabilidade em água.

METODOLOGIA

Este trabalho está sendo desenvolvido com o pacote *Quantum-ESPRESSO*, cujo programa principal *Pwscf* permite calcular a estrutura eletrônica de moléculas e sólidos com condições de contorno periódicas. Este pacote é baseado na DFT e utiliza pseudopotenciais e um conjunto de bases de autofunções dado por ondas planas³.

RESULTADOS E DISCUSSÃO

O modelo proposto otimizado a partir de uma estrutura cristalográfica experimental². No intuito de verificar a validade do modelo foram realizados as seguintes simulações: difratograma de raios X por policristais, espectro vibracional e parâmetros de RMN de ¹³C. Os resultados estão

em boa concordância com os experimentais. Em seguida foram selecionados os melhores sítios onde as moléculas foram adsorvidas. Uma simples comparação da energia eletrônica mostra que seletividade decresce na seguinte ordem: C₄H₄S > CO₂ > H₂S > CH₄ > CO > N₂ > H₂. Afim de verificar a estabilidade foi proposto a reação de hidrólise (Fig. 1), no limite p_{H₂O}/p₀=0 a temperatura tende ao infinito, logo, o material se mostra estável a consideráveis pressões relativas de água e altas temperaturas.

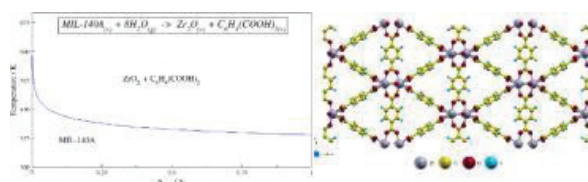


Figura 1. Diagrama de fases e estrutura otimizada do MIL-140A.

CONCLUSÃO

Os resultados demonstram que o MIL-140A é estável na presença de moléculas de água e portanto pode servir como plataforma ideal na remoção de gases como CO₂ proveniente de gases de combustão, gás de síntese e biogás.

AGRADECIMENTOS

FAPEMIG, CAPES, CNPQ pelo apoio financeiro e CENAPAD-SP pelo suporte computacional.

¹ V. Guillermin, F. Ragon, M. Dan-Hardi.; *et al.* *Angew. Chem.* 51, 9267, (2012).

² Z. Hasan, S. H. Jung. *J. Hazardous. Mater.* 283, 329, (2015).

³ J. Giannozzi, P.; Baroni, S.; Bonini, N.; *et al.* *J. Phys. Condens. Matter.* 21, 395502, (2009).

Charge Transfer Dynamics of Inner-Shell Excited States on Organic Films for Photovoltaics

Carlos E. V. de Moura (PG), Yunier Garcia-Basabe (PQ), Maria Luiza Rocco (PQ),
Alexandre Rocha (PQ)

Instituto de Química - Universidade Federal do Rio de Janeiro
carlosemoura@iq.ufrj.br

Keywords: Inner-Shell States, Excited States, Charge Transfer, Spectroscopy, Photovoltaics

INTRODUCTION

Organic optoelectronic devices constitute an important class of materials, which can be applied in renewable sources of energy. The fundamental physical process is the charge transfer dynamics of an *exciton* generated after solar radiation absorption. Donor-acceptor polymers, for example, presents moieties with distinct functions in this process.¹ In this work, the structure of thin-films of PFO-DBT and PSiF-DBT are studied by means of inner-shell spectroscopy and *ab initio* methods.

METHODS

Experiments were done at soft X-ray spectroscopy beamline (SXS) at the Brazilian Synchrotron Light Source (LNLS). Spectra in NEXAFS and RAS were measured. Films were deposited by spin coating on indium tin oxide (ITO) coated glass. Charge transfer was evaluated using different temperatures at annealing treatment, which changes the film ordering.

As the excited states are intrinsically localized, the monomer was used as model system to rationalize the polymer inner-shell spectrum. Geometries for monomers were obtained using optimization procedures with DFT methods for systems with five monomer units to represent the polymer structure, from which the monomer is extracted.

The electronic structure was performed with Molpro package. Contracted Configuration Interaction Singles and Doubles excitations method (CISD) was applied to calculate first states at excitation edge for each chemical element. Core relaxation effects on molecular orbitals was obtained by restricted open-shell Hartree-Fock method (HF), constraining the core orbital occupation. We got transition energies and intensities at silicon, nitrogen and sulphur *K*-

edges. Non-adiabatic coupling coefficients between excited states were also evaluated to indicate possible channels for charge transfers.

RESULTS AND DISCUSSION

Calculated transition energies and intensities are in good agreement with spectroscopic experimental data, as exemplified at Figure 1, corroborating our analysis concerning charge transfer in those excited states as will be shown in the symposium presentation.

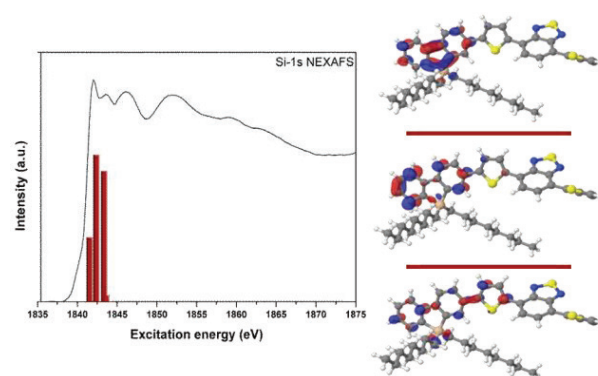


Figure 1. Absorption spectra at Silicon *K*-edge and representation of molecular orbitals involved in three more intense transitions.

CONCLUSIONS

Our methodology presents promising results in order to describe the electronic structure of inner-shell states in polymers. Associated with experiments, it's contributing to understand charge transfer processes in photovoltaics.²

ACKNOWLEDGMENTS

The authors are grateful for the support given by CNPq, CAPES and LNLS.

¹ J. L. Brédas, et al., *Acc. Chem. Res.*, 42 (11), 1691-1699, (2009)

² Y. Garcia-Basabe, et al., *J. Phys. Chem. C.*, 118 (41), 23863-23873, (2014)

Estudo teórico das propriedades estruturais e eletrônicas da junção Au/1,4-Benzenodiamina/Au

Carlos Eduardo Silva^a (PG), Renato Borges Pontes^a (PQ)

^aInstituto de Física, Universidade Federal de Goiás, CP 131, 74001-970, Goiânia, GO, Brasil. Email: carloseduardofisica@yahoo.com.br

Palavra Chave: 1,4-Benzenodiamina, Junção Molecular, Teoria do Funcional da Densidade.

INTRODUÇÃO

A nano-eletrônica molecular visa utilizar moléculas individuais como elementos ativos em dispositivos eletrônicos. Para o seu desenvolvimento é fundamental entender, do ponto de vista atômico, as propriedades físicas da junção molecular, cujos constituintes são: a molécula (elemento central) e os eletrodos (superfícies metálicas). Neste trabalho apresentamos uma investigação por meio de cálculos de primeiros princípios das propriedades mecânicas e eletrônicas da junção molecular Au/1,4-Benzenodiamina(BDA)/Au.

MÉTODOS

Nesse trabalho estudamos a molécula 1,4-benzenodiamina na fase isolada, e também ligada a superfícies de átomos de ouro na direção Au(111). Para a realização dos cálculos de estrutura eletrônica utilizamos o pacote SIESTA. Utilizamos um conjunto de funções base numérico finito para expandir as autofunções dos elétrons de valência. Também fizemos de pseudopotenciais de norma conservada para descrever as interações entre os elétrons de caroço e entre os elétrons de valência e de caroço.

RESULTADOS E DISCUSSÕES

Com as simulações realizadas para a molécula BDA, observamos que a mesma sofre pequenas mudanças conformacionais comparada com a molécula na fase isolada, durante o processo de alongação. No caso a distância entre o C-N (tanto superior quanto inferior) aumentam e também ocorre um pequeno decréscimo no ângulo θ_{H-N-H} (tanto superior quanto inferior). Pode ser observado na Figura 1 a energia e a força necessária para romper a junção Au/BDA/Au em

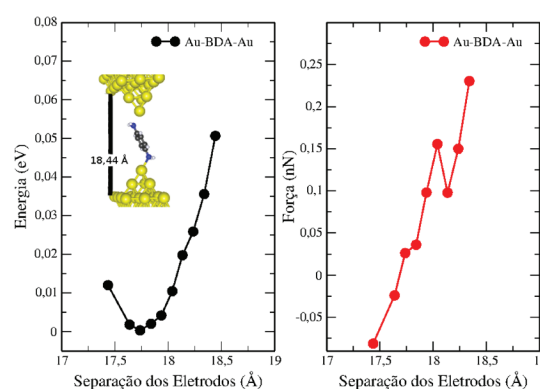


Figure 1. Energia (painel esquerdo) e a força (painel direito) em função do estiramento da junção Au/BDA/Au. A figura inserida, no painel esquerdo, ilustra a conformação do sistema na máxima alongação.

função da separação das superfícies. Como pode ser observado, a energia para a quebra da ligação corresponde à 0,05 eV e a força à 0,23 nN, a uma alongação de 0,7 Å a partir da configuração de menor energia.

CONCLUSÕES

Investigamos as propriedades estruturais e eletrônicas da molécula BDA em fase gasosa, bem como, acoplada a eletrodos de Au(111). Determinamos a força para ruptura desta junção. Estes resultados apresentam um bom acordo quando comparados com recentes medidas experimentais.

AGRADECIMENTOS

Os autores gostariam de agradecer as agências brasileiras de fomento à pesquisa: CAPES, CNPq e FAPEG.

DFT investigation of the Optical Properties of Isoalloxazine Macrocyclical Derivatives

C. E. Silva^a (PG), M. A. Farrán^b (PQ), M. A. San-Miguel^a (PQ)

^aInstituto de Química, Universidade Estadual de Campinas, 13083-970, Campinas – SP, Brazil

^bDepartamento de Química Orgánica y Bio-Orgánica, UNED, 28040, Madrid, Spain

kdusilva@gmail.com

Keywords: Flavin derivatives, DFT, NLO, Rayleigh scattering

INTRODUCTION

Organic materials are specially attractive for the design of optoelectronic devices since their electronic and optical properties can be easily modulated from chemical manipulation.¹ Additionally, they present better integration with the conventional microelectronic in comparison with the major photonic materials based on inorganic compounds.¹ In the research of materials with large non-linear optical response (NLO), the recognition of organic molecules that have higher molecular dipole moment and donor-acceptor electron systems (push-pull) is important.¹ In this sense, this work presents the investigation of the polarizability, the first hyperpolarizability and the depolarized light scattering of two isoalloxazine-anthraquinone adducts² (Figure 1) through DFT calculations.

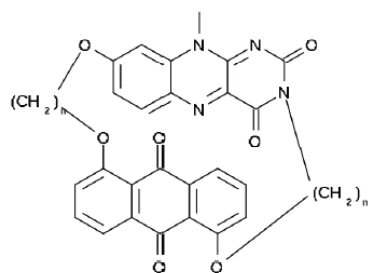


Figure 1. Molecular structure of the MQ4 (n=4) and MQ6 (n=6) macrocycles.

METHODS

The molecular geometry and all properties were obtained at M06-2X/6-311++G** theory level. Vertical electronic transitions were computed using a TD-DFT approach and the solvent effect included by the polarized continuum model ($\epsilon=8.93$). The static first hyperpolarizability (β_0), the projection of β on the dipole moment direction (β_{vec}), as well as the Rayleigh scattering activities (R_{\parallel} and R_{\perp})

were computed in the CPKS approach. Additionally, the Two Level Model (TLM) was also taken into account in the analysis of the first hyperpolarizability.¹

RESULTS AND DISCUSSION

TD-DFT calculations reveals a charge transference (CT) process involving the HOMO-LUMO excitation with the energy gap (ΔE_{gCT}) at about 3.08 eV for both compounds. The β_0 values comparison (29.30×10^{-30} esu and 38.17×10^{-30} esu for MQ4 and MQ6, respectively) shows that the extension of the side aliphatic chains induces changes in this NLO parameter. Moreover, these values are higher than the obtained for the *p*-nitroaniline at the same theory level (26.22×10^{-30} esu). Similar behavior was observed in the analysis of the $|\beta_{vec}|$ values. However, these ones have negative signals; which can be understood as result of the reduction in the polarity of these compounds upon the excitation to the CT state ($\Delta\mu_{gCT} < 0$). On the other hand, the change in the extension of the carbon chains does not produce expressive variations in the R_{\parallel} and R_{\perp} parameters.

CONCLUSIONS

A transition involving intramolecular charge transfer has been characterized in both compounds. The results show that the macrocycles formed between isoalloxazine and anthraquinone are good candidates for applications involving materials with higher NLO response.

ACKNOWLEDGMENTS

Fapesp, CENAPAD

1. Silva, D. L. *et al.* *J. Chem. Phys.* **142**, 064312 (2015).
2. Farrán, A. *et al.* *Photochem. Photobiol. Sci.* **12**, 813–22 (2013).

Theoretical study of porphyrins for application in Dye-Sensitized Solar Cells

Cassiano M. Aono (*cassiano.aono@gmail.com*) (IC),

Paula H. de Mello (*paula.mello@ufabc.edu.br*) (PQ)

Centro de Ciências Naturais e Humanas, Universidade Federal do ABC, Santo André, SP, Brasil

Keywords: DFT, DSSC, porphyrins, Hammett constant

INTRODUCTION

Porphyrins form a promising class of natural dyes to be applied in DSSC (Dye-Sensitized Solar Cells) since they absorb radiation in visible spectra [1]. The conjugated system π cause a shift to visible region of the spectra and works as a bridge connecting donor (D) and acceptor (A) groups, forming the system D- π -A. In this work, we studied porphyrins bonded to different electron donor groups, focusing on the effects of substitution in meso and β position.

METHODS

Density functional theory (DFT) was employed in geometry optimization, as well as to obtain the vibrational frequencies for porphyrins with one acceptor group, BTD, and the following donor groups: hidroxyl, amine (primary and tertiary), methyl, tert-butyl, methoxy and ethyl. We examined the effects of those substitutions, taking into account meso and β positions. To study the electronic excited states, time dependent DFT (TD-DFT) calculations were performed. M06 functional [2] and 6-311G(d,p) basis set were used in all calculations. Solvent effects (THF) were included with IEFPCM.

RESULTS AND DISCUSSION

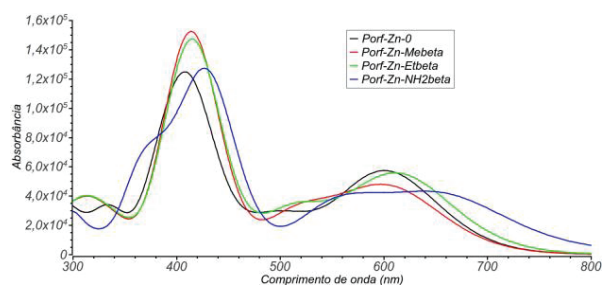


Figure 1: Absorption spectra for studied porphyrins with different substituents in β position

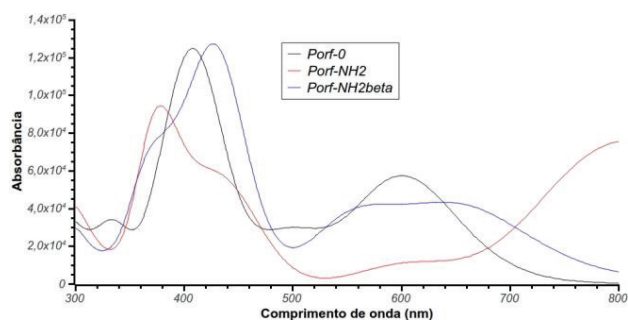


Figure 2: Absorption spectra for porphyrin with -NH_2 in meso and β position.

Figure 1 present the absorption spectra obtained for the BTD-porphyrin and for BTD-porphyrin bonded to three different acceptors at β position. These kind of substitution has small effect on the absorption maxima, being the -NH_2 responsible for the most significant shift. On the other hand, substitutions on meso positions have greater effect on the spectra (Fig. 2), since the gap HOMO-LUMO decreases. We observed that this group influences mainly the HOMO energy. This corroborates the red shift in spectra caused by this group and demonstrates his strong donor character. There is a direct correlation between the value of group's Hammett constant and the energy of the orbital.

CONCLUSION

Substitutions on meso positions of porphyrins conducts to greater modifications on absorption spectrum than β substitutions, being the amine groups responsible for the most significant shifts.

ACKNOWLEDGEMENT

The authors are grateful for the support given from the FAPESP, CNPq, UFABC, ABCSim.

¹ LI, L.-L.; DIAU, E. W.-G. Chemical Society reviews, v. 42, n. 1, p. 291–304, jan. 2013.

² ZHAO, Y.; TRUHLAR, D. G. Theoretical Chemistry Accounts, v. 120, n. 1-3, p. 215–241, 2007;

~OH Projection: the Latest Frontier to Define Geometry of Carbohydrates

Clarissa O. da Silva (PQ), Leandro G. Alves (PG), Renato R. Andrade (PG)

Dep. de Química-ICE, Universidade Federal Rural do Rio de Janeiro, Seropédica, RJ -Brazil
e-mail: clarissa-dq@ufrj.br

Keywords: Monosaccharides Conformation, Carbohydrate Conformation

The high relative abundance of different conformations of carbohydrates in aqueous solution at room conditions is due to their energy values, which differ from each other within a range of 0.5 kcal/mol. It happens because these compounds have several hydroxyl groups that interact in different orientations, generating several conformations. Since only *ab initio* descriptions may get close to this precision for energy difference values, we present a simple computational code (CONFPO) able to univocally classify and generate input files for *ab initio* calculations of all conformational possibilities for pentoses. D-Ribose was used as a test case, and within the set of stable conformers found some were not identified by common samplings. To do so, we developed a 1-3-6 numerical identification code that works as a univocal representation of the hydroxyl groups for each orientation possible, in a way that these degrees of freedom may properly receive attention (Figure 1).¹

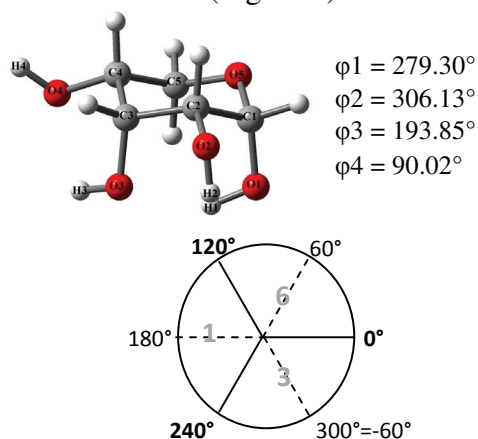


Figure 1. Dihedral angle values that establish each hydroxyl group orientation ($\varphi_1 = \text{H1-O1-C1-O5}$, $\varphi_2 = \text{H2-O2-C2-C1}$, $\varphi_3 = \text{H3-O3-C3-C2}$ and $\varphi_4 = \text{H4-O4-C4-C3}$), define the name of ribose conformation: 3316. The circle is a transversal section across the axis

of the $\text{O}_x\text{-C}_x$ bond, $x=1, 2, 3$ or 4 . The arrows in indicate the hydroxyl groups orientation, in this proposed OH projection.

The absence of an experimental property able to distinguish these conformations has left this issue untouched in the literature, but recently a theoretical *ab initio* description may support such a discussion. It starts with the investigation of all conformation possibilities for pentoses in aqueous solution, and is followed by the calculation of the specific rotation values of the conformers found as the most abundant in aqueous solution.

ACKNOWLEDGMENTS

The authors are grateful for the support given from the CNPq, CAPES and FAPERJ.

¹. (a) R. R. Andrade, C. O. Silva, *Carbohydr. Res.*, 2012, 350, 62; (b) B. A. França, C. O. Silva, *Phys. Chem. Chem. Phys.*, 2014, 16, 13096; (c) A. V. Orlova, A. I. Zinin, R. R. Andrade, C. O. Silva, L. O. Kononov, *ChemPhysChem*, 2014, 15, 195.

Estudo Teórico de Propriedades Estruturais e Elétricas de Politiofenos

Eliziane da Silva Santos (G), Clebio Soares Nascimento Jr. (PQ)

LQTC: Laboratório de Química Teórica e Computacional - Departamento de Ciências Naturais, Universidade Federal de São João del-Rei (UFSJ), Campus Dom Bosco, São João del-Rei, MG

eliziane2silva@yahoo.com.br

Palavras chave: Politiofenos, Push-pull groups, band gap energy.

INTRODUÇÃO

Como é de conhecimento, a capacidade dos polímeros conjugados, PCs, em conduzir eletricidade está relacionada, fundamentalmente, com a diferença de energia entre os orbitais de fronteira HOMO/LUMO, o qual é conhecido como lacuna de energia ou *band gap energy* (E_g). Assim, dependendo da diferença energética HOMO/LUMO, os PCs podem ser classificados como isolantes, condutores ou semicondutores¹. Nesse contexto, os objetivos que nortearam este trabalho foram: (i) Estimar os valores de E_g , via cálculos DFT, para os Politiofenos não substituídos (PTs) (Figura 1), o qual é considerado um PC semiconductor, variando o número de monômeros (n) de 4 à 20 unidades, buscando assim, estabelecer uma metodologia adequada para se obter estruturas e os orbitais HOMO/LUMO dos PTs (ii) Modificar quimicamente as extremidades dos PTs por grupos substituintes doadores e retiradores de elétrons, chamados de *push-pull groups*, para verificar se introdução e a variação de tais grupos substituintes na cadeia polimérica dos PTs modificariam sua condução elétrica.

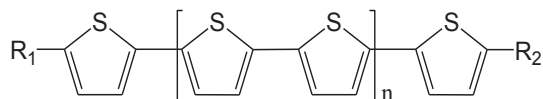


Figura 1. Estrutura geral dos politiofenos, com n variando de 4 ou 20 unidades monoméricas e R_1 e $R_2 =$ H, OH, HSO₃, NH₂, NO₂, OCH₃, CF₃.

METODOLOGIA

Foram realizados cálculos de otimização de geometria, frequências harmônicas e de energia dos orbitais HOMO/LUMO, por meio da Teoria do Funcional de Densidade (DFT), utilizando o funcional B3LYP e conjunto de bases, com qualidade triple zeta, 6-311G(d,p).

RESULTADOS E DISCUSSÃO

Na primeira etapa do trabalho, foram calculados os valores de E_g para os PTs, variando-se as unidades monoméricas de 4 a 20 (com intervalos de 2 em 2 unidades). Observou-se que conforme se aumentava o número de monômeros da cadeia polimérica dos PTs, os valores de E_g decresciam exponencialmente até um limiar, onde o PT apresentava 14 unidades monoméricas. Em seguida, os PTs tiveram suas extremidades substituídas por pares de grupos *push-pull* (NH₂ e SO₃H); (OCH₃ e NO₂); (OH e CF₃). De uma forma geral, para os três pares analisados, observou-se, sistematicamente o mesmo comportamento do PT não substituído, ou seja, conforme há um aumento da cadeia polimérica, os valores de E_g diminuem até um limiar e depois se mantém constante. Além disso, a presença dos grupos *push-pull* levaram a uma diminuição sensível dos valores de E_g , o que implica, teoricamente, numa melhora de condutividade, especialmente para um caso onde o valor de E_g de 2,21eV para o PT não substituído diminuiu para 0,94eV no PT substituído pelo conjunto *push-pull* (OCH₃ e NO₂), contendo 16 unidades monoméricas.

CONCLUSÃO

De acordo com os resultados obtidos, no nível B3LYP/6-311G(d,p), constatou-se que o controle teórico do *band gap* dos PTs, por meio da variação do número de unidades monoméricas, além da inserção de grupos *push-pull* nas posições terminais das cadeias, podem ser uma boa estratégia para a construção de novos PTs com propriedades de condutância melhoradas.

AGRADECIMENTOS

FAPEMIG, RQ-MG

¹ LYTHER, A. R. *Electrical properties of polymers*. New York: Cambridge University Press, 1979.

Free Energy Calculations of Phenothiazine Dyes in Homogeneous and Micro-Heterogeneous Media

Cleiton Maciel^a (PQ), Maurício Domingues Coutinho-Neto^a (PQ)

^a Centro de Ciências Naturais e Humanas, Universidade Federal do ABC, Rua Santa Adélia, 166, Bloco B, Santo André, 09210-270, BRAZIL
email: cleiton.maciel@ufabc.edu.br

Keywords: Phenothiazines, Aggregation, Methylene Blue, Free Energy, Molecular Dynamics.

INTRODUCTION

Photosensitizers (PS) are light-sensitive chemical compounds that have been used in several areas. In medicine occurs the most promising application of PS in Photodynamic Therapy (PDT), a therapy for neoplastic diseases. Upon irradiation, PS can be promoted to excited states and induce the formation of reactive oxygen species (ROS) such as singlet oxygen ($^1\text{O}_2$),¹ and are responsible by the cell death.² However, the aggregation of PS can decrease the photochemical efficiency of these compounds. In this work, we used molecular dynamics simulations to investigate the molecular aggregation of phenothiazine derivatives: Methylene Blue (MB), a well-known phenothiazine dye and DO15. Both compounds present desirable properties for PS in homogeneous and micro-heterogeneous media.

METHODS

Molecular dynamics simulations were carried out for monomers and dimers of PS. Cubic cells were built with 4000 solvent molecules in NPT ensemble using GROMOS 53a6 force field. The micro-heterogeneous solutions were modeling adding urea in aqueous media. The properties was obtained in a running-length of 20 ns. Free energy of solvation was estimated by using the Thermodynamic Integration method. All simulations were performed using GROMACS 4.5 suite.

RESULTS AND DISCUSSION

The free energy computed using TI for the dimer formation process in water at 298K produces a value of $-114.9 \text{ kJ.mol}^{-1}$ for ΔG_{dimer} , with ΔH_{dimer} and $T\Delta S_{\text{dimer}}$ being -91.2 and 23.7 kJ.mol^{-1} respectively. These values are in line with the ones computed for the same process using several distinct solvation methods and reproduce the experimental finding that dimerization in

water is mostly driven by enthalpy. For urea aqueous solutions, MD simulations reveal a clear preferential solvation effect of urea in both monomeric and dimeric forms of MB. Calculations for the $\Delta\Delta H$ shift when adding urea presented a clear enthalpic contribution of 14.0 kJ mol^{-1} favoring the monomer. Qualitatively, this result is in agreement with experimental observations.³

CONCLUSIONS

Structural analysis of the solutions indicate a increasing density of urea molecules around MB at high concentrations. Preliminary results suggests that the methodology overestimates the desestabilization effects of urea in MB monomers. Comparing to the water, the energetic cost to solvate the dimer is higher than solvate the monomers in water/urea mixtures, in a enthalpic point of view. Further calculations for DO15 molecule will be performed in order to understand its molecular mechanism of aggregation and the impact of urea on the stabilization of these dimers.

ACKNOWLEDGMENTS

The authors acknowledge CAPES and UFABC for financial support.

[1] Kamat, et al. *The Journal of Physical Chemistry*, 85, 814-818, (1981).

[2] Dougherty, et al. *Journal of the National Cancer Institute*, 90, 889-905, (1998).

[3] Nuñez, S. Maciel, C. et al. *Journal of the Photochemistry and Photobiology B: Biology*, Accepted, (2015).

Highly Accurate Bound Rovibrational Eigen-energies of Ozone Using the *ScalIT* Software Suite

Corey Petty^a (PQ), Bill Poirier^b (PQ), Francisco B. C. Machado^a (PQ)

^a Departamento de Química, Instituto Tecnológico de Aeronáutica, São José dos Campos, São Paulo, Brazil.

^b Department of Chemistry and Biochemistry, Texas Tech University, Lubbock, Texas, USA

Keywords: Exact Quantum Dynamics, Rovibrational Spectroscopy, *ScalIT*, Ozone

INTRODUCTION

In recent years, ozone and its isotopologues have been a topic of interest amongst many fields of research, due to its importance in atmospheric chemistry and its anomalous isotopic enrichment, or the so-called mass independent fractionation (MIF) effect. In the field of potential energy surface (PES) creation, debate of the existence of a potential barrier just under the dissociation energy (referred to as a potential “reef”) has plagued researchers for many years. Recently, Dawes *et al.*¹ created a highly accurate PES, which attributes this reef to an avoided crossing. Subsequent calculations on this surface have shown improved agreement with experiment, but have been focused on only the vibrational spectrum. It is well known that reaction dynamics require extensive knowledge of the *ro*-vibrational spectrum, not just the vibrational states, especially in cases like ozone that assume a Lindemann-type mechanism. This work represents the start of the complete characterization of the rovibrational spectrum for various isotopologues of ozone on Dawes’ newly created PES, using a highly parallelized suite of exact quantum dynamics codes, *ScalIT*².

METHODS

ScalIT is a highly parallelizable modularized software suite, written in Fortran90 and MPI, that can create triatomic and tetraatomic full dimensional rovibrational Hamiltonians, and solve the time-independent nuclear Schrödinger equation for highly accurate bound rovibrational spectra. All calculations are exact to within the Born-Oppenheimer approximation. By default, *ScalIT* employs Jacobi coordinates, which represents an AB₂ molecule (Fig. 1), thus not incorporating all possible symmetry of an A₃ molecule. By plotting the wavefunctions in hyperspherical coordinates, one can identify the

physically real states as those exhibiting a totally symmetric six-fold azimuthal symmetry.

RESULTS AND DISCUSSION

This work calculates the entire bound vibrational and choice rovibrational spectrum of ¹⁶O₃ to high accuracy ($< 10^{-4}$ cm⁻¹), and compares to available theoretical and experimental results.

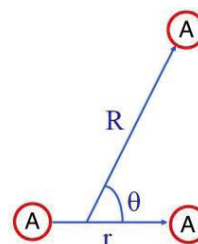


Figure 1. Schematic of a generic A₃ molecule described by Jacobi coordinates. Here, r represents the distance between the A₂ dimer, and R is the distance from the center of mass of r to the third A atom, with θ being the angle between.

CONCLUSIONS

Choice rovibrational states up to $J = 10$, and the entire vibrational spectrum of ¹⁶O₃ was calculated and converged to $< 10^{-4}$ cm⁻¹ using the Dawes PES and *ScalIT* software suite. This represents a starting point for the entire rovibrational spectrum for various isotopologues of ozone to serve as a database for future ozone research.

ACKNOWLEDGMENTS

The authors are grateful for the support given from FAPESP, ITA, as well as Texas Tech University for the computational resources.

¹ R. Dawes, P. Lolur, A. Li, B. Jiang, H. Guo. *J. Chem. Phys.* 139. 201103 (2013).

² C. Petty, B. Poirier. *Applied Mathematics.* 5. 2756-2763 (2013).

Syntheses of europium complexes: ligand displacement order, inversion or retention of configuration, and reaction pathways via RM1 orbital model for lanthanides

Cristiano E.L. Jr (IC), Monique F. Pereira (IC), Isabella M. S. Rosado (IC),
Nathália B. D. Lima (PG), and Alfredo M. Simas (PQ)

Departamento de Química Fundamental, CCEN, UFPE, 50590-470 - Recife, PE, Brazil.

Keywords: RM1, europium complexes, inorganic synthesis, thermodynamic properties

INTRODUCTION

We show that the thermodynamic properties calculated for chemical reactions involving lanthanide complexes with the recently introduced RM1 orbital model for lanthanides are consistent with established experimental results involving europium complexes. Subsequently, we use this model for the elucidation of synthetic pathways aiming at the design of new and more efficient synthetic routes for mixed ligand luminescent europium complexes².

METHODS

All calculations were carried out in a version of MOPAC we modified to include the RM1 orbital model for lanthanides. The RM1 orbital model for lanthanides does not treat them as sparkles. For europium, it assumes that the neutral atom is represented by $\{[\text{Xe}4f^6]6s^25d^16p^0\}$ with a semiempirical basis set comprised of 5d, 6s and 6p orbitals, introduced to allow a degree of covalency to occur between the ligands and the europium ion. The semiempirical core stands for $\{[\text{Xe}4f^6]\}$ and corresponds to the core of the trication.

Calculations of enthalpy and entropy were carried out by using standard MOPAC algorithms.

Syntheses were carried out according to the methodologies we developed².

RESULTS AND DISCUSSION

Syntheses of mixed ligand luminescent europium complexes involve a number of displacement reactions of a nonionic ligand by another, each one leading to either a retention or inversion of configuration. The europium complexes calculated were all of the form $\text{Eu}(\beta\text{-diketonate})_3(\text{L},\text{L}')$, where the β -diketonates were DBM, TTA, and BTFA; and L and L' were TPPO, PTSO, DBSO, and H₂O. Accordingly, we calculated the variation of enthalpy and entropy of all imaginable reactions of displacements of L by L', with both products and reagents in either cis or trans configurations. We then simulated the complete stepwise reaction

pathways for ligand exchange. Results were in exact agreement with the displacement capability

of nonionic ligands with respect to each other, we also determined experimentally: TPPO > PTSO > DBSO > H₂O. The calculations likewise accurately reproduced the observed inversion of configuration in the synthesis of $\text{trans-Eu}(\beta\text{-diketonate})_3(\text{L})_2$, from $\text{cis-Eu}(\beta\text{-diketonate})_3(\text{H}_2\text{O})_2$. Finally, calculations predicted the retention of configuration in the synthesis of $\text{trans-Eu}(\beta\text{-diketonate})_3(\text{L},\text{L}')$ from $\text{trans-Eu}(\beta\text{-diketonate})_3(\text{L})_2$, (Fig. 1).

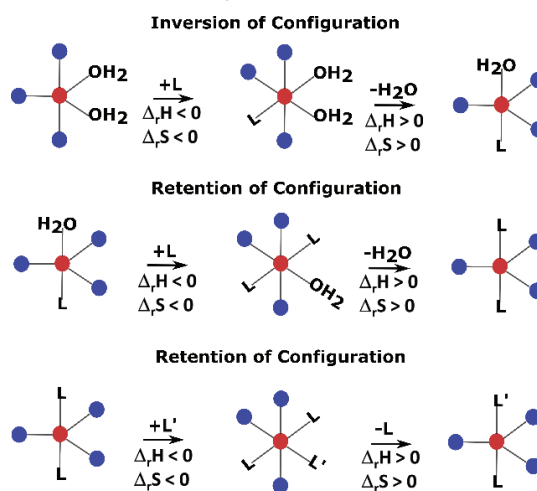


Figure 1. Predicted and already partially confirmed stepwise reaction pathways in the synthesis of $\text{Eu}(\beta\text{-diketonate})_3(\text{L},\text{L}')$.

CONCLUSIONS

Our results indicate that the thermodynamic properties calculated via RM1 orbital model for europium have predictive value and can be useful for the design of new synthetic routes of mixed ligand luminescent europium complexes involving ligand displacement reactions.

ACKNOWLEDGMENTS

The authors acknowledge support from CNPq, PET-Química UFPE and FACEPE/PRONEX.

Theoretical Study of Structural, Electronic and Magnetic Properties of Platinum(II) Salicylidenes

Cristina A. Barboza^a (PQ), Franklin Ferraro Gomez^b (PQ), José C. Germino^a (PG),
Pedro A. M. Vazquez^a (PQ), Tereza D. Z. Atvars^a (PQ)

^a *Chemistry Institute, State University of Campinas - UNICAMP, Campinas, Brazil*

^b *Departamento de Ciencias Básicas, Fundación Universitaria Luis Amigó, SISCO,
Transversal 51A 67B 90, Medellín, Colombia*

Keywords: platinum salicylidene, TD-DFT, ZORA, magnetically induced currents

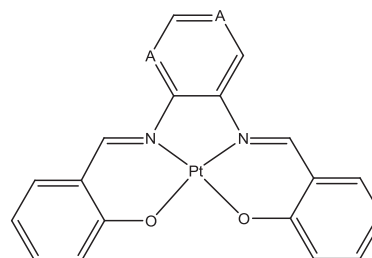
INTRODUCTION

Salicylidenes containing transition metal atoms have been intensively studied for applications in the field of organic electronics and material science. Platinum(II) Schiff base compounds constitute an attractive class of phosphorescent materials that are easily synthesized, structurally diverse. The strong spin-orbit coupling displayed by these metal ions remove partially the forbidden nature of the $T_1 \rightarrow S_0$ transition resulting in a fast intersystem crossing, leading to a high phosphorescence quantum yield. They can be used as phosphorescent materials for high efficiency and white light electroluminescent devices.

In this study electronic and magnetic properties of two salicylidene ligands, salophen and sal-4,5-pym and their respective platinum(II) coordination compounds (Figure 1) were evaluated within the DFT/TD-DFT framework, in order to evaluate the effect of the metal coordination and also the functionalization of its framework over the luminescent properties of the ligand.

METHODS

Ground and first excited state (S_1 and T_1) structures were obtained at PBE0/TZVP level using the ADF software. Electronic transitions were obtained at the same level of calculation. In order to evaluate the ligand electronic delocalization, magnetically induced current density were calculated using the DIRAC 14.04 code.



Molecular structure of the ligands, (A = C and N for salophen and sal-4,5-pym, respectively).

RESULTS AND DISCUSSION

The current density maps shows that the coordination of the Pt(II) atom to both ligands leads to an increment of the electronic delocalization of their structure, leading to a redshift of both emission and absorption bands. The presence of the pyrimidine leads to an increment of electronic charge over the iminic nitrogen, favoring the occurrence of the ESIPT, leading to a dual fluorescence emission.

CONCLUSIONS

Our results suggest that both the modification in the ligand framework and the coordination of a platinum atom, allowing the phosphorescence, improves significantly its luminescent properties, making these compounds suitable to be used in wOLEDs.

ACKNOWLEDGMENTS

The authors acknowledge FAPESP, UNICAMP (FAEPEX), CNPq, INEO and CAPES for financial support and fellowships.

REFERENCES: ¹C. A. Barboza, J. C. Germino, A. M. Santana, F. J. Quides, P. A. M. Vazquez, T. D. Z. Atvars, *J. Phys. Chem. C*, 119, 6152 (2015). ²C.-M. Che, S.-C. Chan, H.-F. Xiang, M. C. W. Chan, Y. Liu, Y. Wang, *Chem. Comm.* 1484 (2004).

Computational Studies of Spectroscopic Properties of Hydrocarbons at the Air-Ice Interface

Dana Nachtigallova

Institute of Organic Chemistry and Biochemistry AS CR v.v.i, Czech Republic

The interfacial non-covalent interactions between ice surface and organic molecules have been studied by different experimental techniques and computational approaches. The understanding of these physical phenomena is critical for modeling of chemical processes occurring in polar regions.

The ground state molecular dynamics simulations and DFT calculations, as well as the excited state ADC(2) calculations are used to discuss the occurrence of ground- and excited-state complexes (excimers) and other associates of benzene, naphthalene and methyl-naphthalene on the ice surface. The results of these calculations are used to interpret the excitation and emission spectra obtained in aqueous solution and at the air-ice surface.

Optimization of Long-Range Corrected Functionals through The Minimum Polarizability and Maximum Hardness Principles in Polibutatriene Oligomers

Daniel F. S. Machado^{a,†} (PG), Demétrio A. S. Filho^b (PQ), Heibbe C. B. de Oliveira^a (PQ)

^a Laboratório de Modelagem de Sistemas Complexos, Instituto de Química, Universidade de Brasília, 70919-970, Brasília, DF, Brazil.

[†] danieu_scalabrin@hotmail.com

Keywords: PBT, DFT, Maximum Hardness Principle, Minimum Polarizability Principle

INTRODUCTION

Range-separated hybrid functionals split the Coulomb operator into short (SR) and long-range (LR) components with the help of the standard error function (erf): $1/r = \text{erf}(\omega r)/r + \text{erfc}(\omega r)/r$. In this equation, the range separation is obtained by a single parameter, ω , which is usually obtained empirically.

There are a number of alternative strategies to optimize the ω parameter. In so-called IP-tuned LRC hybrids, the optimal ω is found by minimizing the difference between HOMO eigenvalue and the computed IP. In this work we propose an alternative way to optimize the ω tuning parameter by minimization of linear polarizability or by the maximization of hardness. The motivations of this propose is based on two important and fundamental principles: Maximum Hardness (MHP) and Minimum Polarizability (MPP) Principles.

METHODS

MHP asserts that molecular systems at equilibrium tend to the state of maximum hardness (η) and MPP states that the natural evolution of any system is toward a state of minimum polarizability (α). Based on these principles, we propose here an alternative procedure aiming to optimize the range-separation parameter. The first procedure is based on the possibility to find a ω value that maximizes the hardness:

$$\eta(\omega) = \frac{E(N-1, \omega) - E(N, \omega) - [E(N, \omega) - E(N+1, \omega)]}{2}$$

The second procedure is obtained from the ω value that minimizes the linear polarizability:

$$\langle \alpha(N, \omega) \rangle = \frac{\alpha_{xx}(N, \omega) + \alpha_{yy}(N, \omega) + \alpha_{zz}(N, \omega)}{3}$$

Herein, results for polibutatriene oligomers (PBT) from 2 up to 6 repeating monomers are

presented but the methodology will be applied to other molecular systems. All calculations were performed using the LC- ω PBE/6-31G(d) level as implemented in the G09 suite of programs. We compare our results with other calculated via other LRC hybrids, MP4 and CCSD(T) as well.¹

RESULTS AND DISCUSSION

The ω that minimizes α (maximizes η) for the PBT oligomers are: 0.514 (0.371), 0.510 (0.360), 0.518 (0.343), 0.518 (0.327), 0.518 (0.314) for N=2,3,4,5,6 repeating units, respectively.

Table 1. Longitudinal linear polarizability for increasingly large PBT oligomers calculated using the 6-31+G(d) basis set and different levels of calculation.

N	Max- η - Tuned- LC- ω PBE	Min- α - Tuned- LC- ω PBE	Tuned- IP-LC- BLYP	Default- LC- BLYP	CAM- B3LYP	MP4	CCSD(T)
α (a.u.)							
2		273.11	319.47	309.11	322.64	277.46	271.51
3	580.98	569.57	692.97	637.04	688.64	562.22	542.83
4	999.71	959.57	1237.87	1069.77	1196.79	935.66	894.28
5	¹ 514.54	¹ 432.87	1964.66	1587.59	1836.38		
6			2866.67	2170.70	2589.79		

CONCLUSIONS

The α values calculated with our procedures are in closer agreement with *ab initio* calculations (MP4 and CCSD(T)) than IP-tuned LCR methodology and default ω LC functionals.

ACKNOWLEDGMENTS

The authors are grateful for the support given from the CAPES and CNPQ.

¹ Nénon, S.; Champagne, B.; Spassova, M. Phys.Chem. Chem. Phys., 2014. 16: p. 7083.

DFT studies of the interactions between the $[Ca(H_2O)_5]^{2+}$ cation and monofunctionaloxo, aza, sulfur and phosphorous ligands

Daniel G. S. Quattrociochi^a(PG), Marcos Vinicius M. Meuser^a(PQ), Glaucio B. Ferreira^a(PQ), Leonardo M. Costa^b(PQ) and José Walkimar de M. Carneiro^a (PQ)

^aUniversidade Federal Fluminense, Outeiro de São João Batista, s/n, 24020-141 Niterói - RJ, Brazil, ^b Programa de Pós-Graduação em Ciência e Tecnologia Ambiental, Centro Universitário Estadual da Zona Oeste -UEZO, Campo Grande, Rio de Janeiro - RJ, Brasil.

Keywords: $[Ca(H_2O)_5]^{2+}$ cation, neutral ligand, interaction strength, DFT, EDA.

INTRODUCTION

The calcium cation is involved in chemical scaling formation in petroleum industry. The formation of $CaCO_3$ and $CaSO_4$ results in surface blockage that cause decline in the permeate flux, reducing the process efficiency and increasing operational costs.¹ During the past two decades, considerable efforts in the development of chemical additives have been made, which leads to antiscalant molecules like polycarboxylates, polyacrylates and polyphosphonates.¹

METHODS

All the structures were optimized using quantum chemical calculations with the B3LYP/6-311++G(d,p) method and the affinity of the $[Ca(H_2O)_5]^{2+}$ cation for several monofunctional ligands were determined. Four sets of ligands were studied: with oxygen, nitrogen, sulfur and phosphorous (phosphine) binding atom (table 1).

RESULTS AND DISCUSSION

Complexes that bind via a double bonded oxygen atom have the strongest metal-ligand interaction shown in table 1, followed by the nitrogen compounds, singly bonded oxygen interacting atom, sulfur ligands and phosphine. The ligand with the strongest interaction, phosphoryl, has an ionic resonance form with a negative charge on the binding oxygen atom that highly contributes to the hybrid geometry, that favors the interaction. The metal-ligand distance, the MerzKollman atomic charges and the HOMO energy of the ligands show high correlation ($r^2 > 0.9$) with the interaction strength. The Energy Decomposition Analysis (EDA) of the interaction energy between the $[Ca(H_2O)_5]^{2+}$ cation and the ligand shows that the electrostatic term is the major component of the interaction and represents at least 43.7% of the total interaction energy, due to charge attraction. The covalent component represents at least 28.1% of the total interaction energy, due to the ligand

electronic donation effect. Along the set of compounds studied, the electrostatic component varies more than twice the covalent term.

Ligand	ΔH	ΔG^{298}	qL
O=PH ₃	-18.77	-16.40	0.070
O=CHNH ₂	-15.97	-13.92	0.053
O=CHOH	-14.90	-13.13	0.051
O=C(CH ₃) ₂	-12.49	-12.16	0.045
O=CH ₂	-9.50	-9.01	0.045
HN=CH ₂	-8.72	-8.83	0.045
O(CH ₃) ₂	-2.68	-2.09	0.025
HO-CH ₃	-2.57	-1.88	0.023
S=CH ₂	2.63	3.73	0.021
PH ₃	10.60	11.23	0.005

Table 1. Affinity and charges on the ligand.

CONCLUSIONS

The interaction enthalpy order is: phosphoryl > C=O > C=N > C≡N > C-O > C-N > NH₃ > C=S > C-S > PH₃. This interacting order is mainly due to the electronic nature inherent to the atoms that interact with the metal center. The oxygen and nitrogen atoms are small, with a higher electronegativity, favouring polarization to them and increasing the interaction strength with the metal center. In the phosphoryl molecule, which binds more strongly to the cation, a Lewis resonance form with a formal charge on the oxygen atom is the one with the highest contribution to the final hybrid.

ACKNOWLEDGMENTS

The authors are grateful for the support given from the FAPERJ, CAPES and CNPQ.

¹M. Kim, J. Au, A. Rahardianto, C. Gabelich, Ind. Eng. Chem. Res. 48, 3126, (2009).

²L. M. Costa, J. W. M. Carneiro, A. G. Romeiro, L. W. C. Paes, Journal of Molecular Structure. Theochem, 911, 46-51, (2009).

QSAR models applied to the anti-depression activity of hexahydro-pyrrolo-isoquinoline

Daniela R. Silva (PG), Lucas A. Santos (PG), Letícia C. de Assis (PG), Giovanna C. Gajo (PG), Letícia S. Garcia (PG), Tamiris M. de Assis (PG), Elaine F.F. da Cunha (PQ)

Federal University of Lavras – Department of Chemistry, 3720000, Lavras/MG, Brazil

Keywords: Depression, serotonin transporter, hexahydro-pyrrolo-isoquinoline compounds, 4D-QSAR

INTRODUCTION

According to World Health Organization, millions of people worldwide suffer from depression¹. The current medications have been associated with some drawbacks like slow onset of action, undesirable side effects and poor efficacy. In this sense, Apodaca and coworkers developed hexahydro-pyrrolo-isoquinoline compounds (Figure 1) that block serotonin receptors². In this work, a quantitative structure-activity relationship study in four dimension (4D-QSAR)³ was performed on serotonin inhibitors in order to identify characteristics that enhance the activity of these compounds.

METHODS

The RM1 optimized structures were used as starting point in the 4D-QSAR analysis. Molecular dynamics simulation was performed to construct the conformational ensemble profile of each ligand. After that they were aligned inside a cubic box using the atoms 4-7-10, Figure 1. The interaction pharmacophore elements (descriptors) were calculated and genetic function approximation (GFA) analysis were performed to generate the mathematical models.

RESULTS AND DISCUSSION

The models were valuated according to the statistic measures and the best model from Alignment 1 is outlined below:

MODEL 1
$\text{pKi} = 8.5569 - 7.2674(\text{GC1_any}) + 4.8241(\text{GC2_np}) + 37.2096(\text{GC3_np}) - 17.8005(\text{GC4_arom}) - 3.2314(\text{GC5_any})$
$n=86; r^2=0.73; q^2=0.70; r^2_{\text{test}}=0.62; \text{LSE}=0.150; \text{LOF}=0.173$

GC = grid cells

Interactions: np=non polar; arom=aromatic; any=any type

The model has five descriptors, three of them with negative value coefficients and two with positive value coefficients (Figure 2). The descriptors GC1, GC2 and GC3 indicated that

compounds with substituent at position R_7 have lower activity than those at position R_3 . Furthermore, non-polar interactions in this position favor the activity.

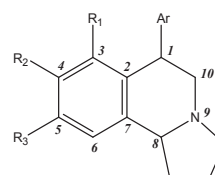


Figure 1. General structure of the hexahydro-pyrrolo-isoquinoline compounds³.

GC4 and GC5 have negative value coefficients suggesting that when the substituent at position *Ar* is *trans* or *para*-substituted the biological activity of the compounds decreases.

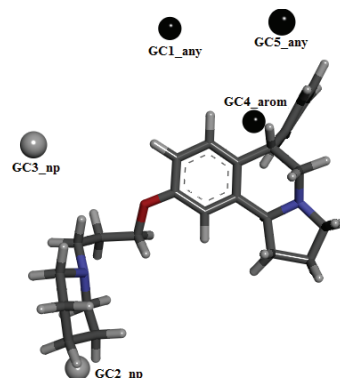


Figure 2. Descriptors of Model 1 represented in the most active compound.

CONCLUSIONS

Model 1 presents descriptors with important pharmacophore groups for serotonin inhibitors suggesting structural modification towards the synthesis of new compounds.

ACKNOWLEDGMENTS

CAPES, CNPQ, FAPEMIG and UFLA.

¹ L. Yu et al., J. Med. Chem., 57, 8204-8223, (2014).

² R. Apodaca et al., (2012) US2012/0321559A1

³ A. J. Hopfinger et al., J. Am. Chem. Soc., 119, 10509-10524, (1997).

Thermochemical and Kinetics studies of the H (²S) + CH₃SH reaction

Daniely V. V. Cardoso¹ (PG)^{*}, Leonardo A. Cunha¹ (IC), Rene F. K. Spada¹ (PQ), Luiz F. A. Ferrão¹ (PQ), Corey A. Petty¹ (PQ), Orlando Roberto-Neto² (PQ), Francisco B. C. Machado¹ (PQ)

¹ Departamento de Química, Instituto Tecnológico de Aeronáutica, São José dos Campos-SP, Brazil

² Departamento de Química, Instituto de Estudos Avançados (IEAv), São José dos Campos-SP, Brazil

*daniely@ita.br

Keywords: methanethiol, CCSD(T), DFT, elementary reactions, rate constants.

INTRODUCTION

Sulfur-containing molecules have a significant impact on the atmosphere and biosphere [1]. In this work, we study the reaction system formed by the methanethiol molecule (CH₃SH) and a hydrogen atom. Specifically, the elementary reaction of hydrogen abstractions (R1 = CH₃SH + H → CH₃S + H₂; R2 = CH₃SH + H → CH₂SH + H₂) and cleavage (R3 = CH₃SH + H → CH₃ + H₂S). These elementary reactions are studied by utilizing electronic structure and chemical kinetics methodologies.

METHODS

The geometrical structures of the reactants, products, and transition states for the three reaction paths were optimized using BB1K with the aug-cc-pV(T+d)Z basis set. The thermochemical properties were refined using single-point coupled-cluster (CCSD(T)) calculations on the BB1K geometries, followed by extrapolation to the complete basis set (CBS) limit. For each reaction path, the thermal rate constants were calculated using the Improved Canonical Variational Transition State (ICVT) including the zero-curvature tunneling (ICVT/ZCT) and the small-curvature tunneling (ICVT/SCT). All electronic structure calculations were carried out with the Gaussian G09 code and the thermal rate constants were computed with the Polyrate program.

RESULTS AND DISCUSSION

Figure 1 presents the adiabatic energy profile of studied reaction paths obtained with BB1K and single-point CCSD(T). The lowest adiabatic barriers calculated with these methods are 2.17 and 2.33 kcal.mol⁻¹, respectively, which correspond to the hydrogen abstraction from the thiol group (R1).

Figure 2 shows the Arrhenius plot of the overall rate constants for this reaction system (CH₃SH+H). The kinetic parameters obtained are of the same order of magnitude of previous experimental and theoretical data [2-4].

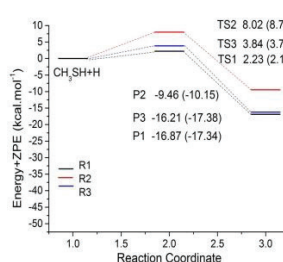


Figure 1: Adiabatic energy profile for the three reaction paths.

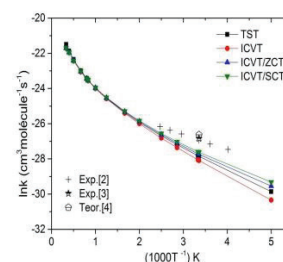


Figure 2: Overall rate constants for the CH₃SH + H reaction.

CONCLUSIONS

The reaction path R1, corresponding to the hydrogen abstraction from the thiol group (-SH) is the most important in all temperatures. The ICVT/SCT results for the overall rate constants at 298 K ($k_{\text{ICVT/SCT}} = 1.0 \times 10^{-12} \text{ cm}^3 \text{ molecule}^{-1} \text{ s}^{-1}$) are in good agreement with the available experimental data ($k_{\text{exp}} = 2.0\text{--}2.2 \times 10^{-12} \text{ cm}^3 \text{ molecule}^{-1} \text{ s}^{-1}$).

ACKNOWLEDGMENTS

The authors are grateful for the support given from the FAPESP, CNPQ and CAPES.

¹ T. E. Graedel, Chemical Compounds in the Atmosphere, Academic, New York, 1978.

² P. H. Wine, et al. J. Phys. Chem., v. 85, n. 18, p. 2660–2665, (1981).

³ D. Martin, et al. Int. J. Chem. Kinet., v. 20, n. 11, p. 897–907, (1988).

⁴ Y. X. Wang et al. Acta Physico-Chimica Sinica, v. 26, n. 1, p. 183-187, (2010).

Electronic and Conformational Structure of Ortho-Aminobenzoic Acid in Solution Combining the Sequential QM/MM and the Free Energy Gradient Methods

Danillo P. Valverde (PG), Herbert de C. Georg (PQ)

Instituto de Física, Universidade Federal de Goiás, CP 131, 74001-970, Goiânia, GO
danillo280991@gmail.com

Keywords: Sequential QM/MM, Free Energy Gradient, ASEC-FEG.

INTRODUCTION

In the last years, the use of an iterative Sequential QM/MM method with an average solvent field as electrostatic embedding [1] together with the Free Energy Gradient method [2], called the ASEC-FEG method, has provided interesting results for the conformational structure and properties of molecules in solution. In this work, we make use of that methodology to investigate the electronic structure of the ortho-aminobenzoic acid (o-Abz) in water, acetonitrile and cyclohexane. The o-Abz molecule has a considerably broad absorption band in the UV region and a long fluorescence lifetime. Therefore, o-Abz is frequently used as a fluorescent label in peptides whereas some derivatives are used in membranes. The o-Abz has two rotamers in gas-phase which differ by 180° rotation of the carboxylic group. We studied the solvent effect in the geometry of the neutral, anionic and cationic species.

METHODS

In each step of the iterative geometry optimization process, we generate an ensemble using Monte Carlo Metropolis simulations at room temperature with empirical Lennard-Jones-Coulomb potential, and we select hundreds of uncorrelated configurations. Then, we superpose all configurations with scaled charges to include the solvent average field in the solute's Hamiltonian. We perform only one quantum mechanics calculation of the atomic forces and an approximate Hessian to obtain a new geometry through the Newton-Raphson method. Lastly, a calculation of the charge distribution in the new geometry in the presence of the solvent is performed. With the new geometry and atomic charges, the next step of the simulation is initiated.

RESULTS AND DISCUSSION

In gas phase, we found two stable rotamers differing by 2.9 kcal/mol for the neutral species. Vibrational frequencies for the rotamer I (more stable) are in good agreement with the experimentally observed values. We also found that protonation occurs preferentially in the amino group, while deprotonation occurs in the carboxylic group. The cation also has two stable rotamers whereas in the anion they are the same rotamer.

In solution, the polarizable continuum model predicts no significant difference in the geometry of the o-Abz species. In contrast, using the ASEC-FEG method, we found remarkable structural changes in aqueous solution. The pyramidalization of the amino group is further increased (~20°) in the two rotamers of the neutral species. In rotamer II, the internal hydrogen bond is broken, in favour of intermolecular bonds with water, whereas it is maintained in rotamer I. In the anionic species, the hydrogen bond is also broken. In the cationic species, only one minimum was found, related to the rotamer I.

CONCLUSIONS

The results obtained indicate that the ASEC-FEG method is capable of describing accurately the structure of the molecules in solution.

ACKNOWLEDGMENTS

The authors are grateful for the support from the FAPEG, CAPES and CNPQ agencies, and the computer resources from LCC-UFG.

¹ K. Coutinho, H. C. Georg, T. L. Fonseca, V. Ludwig, S. Canuto. *Chem. Phys. Lett.* **437**, 148 (2007).

² N. Okuyama-Yoshida, M. Nagaoka, T. Yamabe. *Int. J. Quantum Chem.* **70**, 95 (1998).

Dengue fusion peptide interacts with model membranes: an experimental and in silico study.

Danilo Olivier^a(PG), Neus Garcia^b(PQ), Ilja Voets^b(PQ), Amando Siuiti Ito^a (PQ)

^a*Faculdade de Filosofia Ciências e Letras de Ribeirão Preto, Universidade de São Paulo*

^b*Department of Chemical Engineering and Chemistry, TU/e – The Netherlands
doliviercg@gmail.com*

Keywords: Dengue Peptide, Molecular Dynamics, Fluorescence, SAXS,

INTRODUCTION

Membrane fusion is one of the most important steps in flavivirus infection. Understanding how the fusion step occurs could help us design strategies to combat viral infection. We studied the interaction of dengue fusion peptide (DEN.II 88-123) with different membrane models. The peptide is located at the tip of the trimer and its sequence: KRFVC.KHSM.VDRGW.GNGCG.LFGKG.GIVTC.AMFTCKK. Our goal in this work is try to understand how the peptide affects the lipid vesicles and lipid membranes. To this end, we conducted a series of experiments (Fluorescence, SAXS, DLS) and molecular dynamics simulations (MDS) with different lipid composition (DMPC, DMPG) in presence and absence of DEN.II 88-123 peptide.

METHODS

All the experiments were measured at 40°C. The peptide-to-lipid ratio was 1%. For fluorescence studies the lipid concentration was 1 mM, while for DLS and SAXS it was 5 mM. For MDS the peptide was placed in water near the lipid bilayer (DMPC, DMPC:DMPG 4:1) and the simulations ran over 500 ns. The NpT ensemble were used with temperature of 313K, and 1 bar of pressure. These simulations were done with NAMD software using CHARMM 36 Force Field.

RESULTS AND DISCUSSION

Both experimental results (DLS and Fluorescence) have shown differences in the size of the vesicles, as well as in the position of the peptide after interaction. For DMPC

vesicles, the size changed from 40.3 to 40.8 nm, while for DMPG vesicles it changed from 42.0 to 47.8 nm. Fluorescence of tryptophan residue (W101) had a blue-shift when interacting with anionic vesicles (349 nm) compared with zwitterionic ones (358 nm). SAXS measurements for pure DMPC vesicles and vesicles in presence of peptides revealed that changes in structure of the bilayer was not affected. The thickness of the membrane was 4.1 nm. The electronic density profile of MDS has shown that the peptide interacts with the membrane and the W101 residue is buried into the bilayer. It is placed near the polar head. Furthermore, the area per lipid did not change significantly over time, with a average value of 62.2 Å. The acyl chain parameter order was also not affected by the peptide, with a average value of 0.17.

CONCLUSIONS

Combining experimental and computational techniques is a powerful way to study biomolecular systems. DLS data gave information about changes in size of the vesicles, while fluorescence measurements brought some information about position of tryptophan residue. MDS and SAXS revealed that despite the interaction between the peptide and membrane model the changes in structural parameters (area per lipid, thickness) are not significant.

ACKNOWLEDGMENTS

The authors are grateful for the support given from the Capes, CNPq, INCT-Fcx, FAPESP and NAP-Fcx USP.

Mechanical response under ballistic impact of penta-graphene

David L. Azevedo

Instituto de Física, Universidade de Brasília- UnB, Brasília, DF, Brazil

Keywords: Penta-graphene, reactive molecular dynamics, mechanical response.

INTRODUCTION

Recently, Shunhong Zhang et al¹ proposed a new class of carbon-based nanostructures, named ‘penta-graphene’ (Fig. 1a-1b). In this work it is reported preliminary impact molecular dynamics results for a monolayer of penta-graphene. It was investigated the mechanical response of these structures under ‘ballistic’ impact of diamond fragment (entirely atomistic).

METHODS

The simulations were carried out using the LAMMPS², which is a very suitable and flexible package for high quality molecular dynamics simulations. The force field employed was AIREBO (Adaptative Intermolecular Reactive Empirical Bond-Order) force field^{3,4}. The choice of incident particle as a diamond fragment was because this material has a well-known large mechanical resistance.

It was simulated impact dynamics with several different velocities for incident diamond particle. It was compared results of impact dynamics for graphene and penta-graphene.

RESULTS AND DISCUSSION

In the Fig. 2, we show the kinetic energy evolution for a 4000 m/s (40A/ps) incident particle initial speed under collision. As can be observed, penta-graphene monolayer absorbs less impact energy than graphene monolayer. Our results show that penta-graphene monolayer is a good absorber of mechanical impact, although less efficient than graphene. While penta-graphene absorbed around 45% of impact energy, graphene absorbed around 95%.

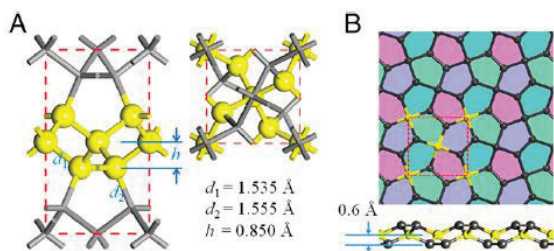


Figure 1. (a) Crystal structure, (b) top and side views of penta-graphene.

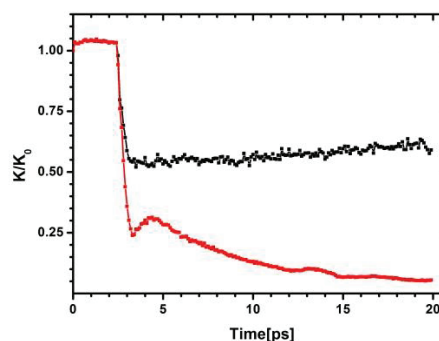


Figure 2. Temporal evolution of kinetic energy of incident particle of impact dynamics for a) black square, penta-graphene target, b) red circle, for graphene target.

CONCLUSIONS

The results presented here show that penta-graphene monolayer is a good absorber of impact, although is lesser efficient than graphene monolayer. The efficiency for penta-graphene energy absorption for this particular case of incident velocity(40A/ps) was around 45%.

ACKNOWLEDGMENTS

The authors are grateful for the support given from the CNPq, CAPES, FINATEC, FAP-DF and FAPEMA.

¹ Zhang, Shunhong; Zhou, Jian; Wang, Qian; et al., PNAS, 112, 2372 (2015).

² S. Plimpton, Fast Parallel Algorithms for Short-Range Molecular Dynamics, J. Comp Phys, 117, 1-19 (1995).

³ S. J. Stuart et al., J. Chem. Phys. 112, 6472 (2000).

⁴ D. W. Brenner, Phys. Rev. B 42, 9458 (1990).

Is There a Quadruple Bond in C₂?

David Wilian Oliveira de Sousa (PG), Marco Antonio Chaer Nascimento (PQ)

Instituto de Química - Universidade Federal do Rio de Janeiro. Avenida Athos da Silveira Ramos, 149, Cidade Universitária, CT Bloco A sala 412. Rio de Janeiro, RJ. CEP 21.941-909

Keywords: C₂, Chemical Bonding Theory, GPF-EP Method.

INTRODUCTION

The chemical structure of the C₂ molecule in its ground state (¹Σ_g⁺) has been the subject of intense debate in the literature¹ after the suggestion that the molecule could exhibit a fourth covalent bond, between the singlet-coupled orbitals φ₁ and φ₂ shown in the perfect-pairing diagram (Figure 1). However, the fact of the stretching mode frequency for the supposed quadruple bond in C₂ (1855 cm⁻¹) is smaller than the respective one for the triple bond in C₂H₂ (1974 cm⁻¹) gave rise to more debate. In this work we investigate this problem explicitly avoiding all the points of conflict from the previous papers to show that there is no quadruple bond in the C₂ molecule.

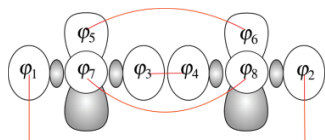


Figure 1. GVB-PP diagram of C₂ ground state.

METHODS

The Generalized Product Function Energy Partitioning (GPF-EP) method² was used in order to decompose the total electronic energy in quasi-classical (electrostatic) and interference (covalent) terms. Previous works have established a general rule concerning the nature of chemical bond – its formation leads to the lowering of interference energy, particularly its kinetic component. Potential energy curves were constructed at *full*-GVB/cc-pVTZ level with the programs GAMESS/VB2000. The GPF-EP code for GPF-EP, has been implemented into the VB2000 source code by our research group.

RESULTS AND DISCUSSION

For the standard σ and π bonds, interference acts like the expected for a regular covalent bond, while for the proposed “fourth bond”

interference is a destabilizing factor (Figure 2). In order to make sure that this misbehavior could not be attributed to a new kind of bond, we performed an equivalent analysis for the ³Σ_g⁻ excited state of the C₃ molecule in which a bond similar to the “fourth bond” of C₂ could be formed between the two carbon atoms at the ends of the linear chain (1-3 bond). The interference energy for this case shows exactly the same pattern of the equivalent one in C₂.

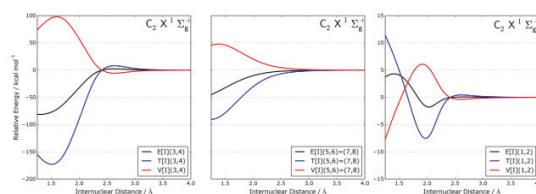


Figure 2. Interference energy and its components for the σ bond (a), the π bonds (b) and for the supposed fourth bond (c) of the C₂ molecule.

Analysis of the orbital overlaps along the internuclear axis shows that for C₂ there is an excess of charge density relative to C₂H₂. This explains the difference in the stretching frequencies of the C-C bonds in C₂ and C₂H₂. Although singlet coupling of the “fourth bond” in C₂ leads to energy stabilization, it also “weakens” the chemical bond in terms of the force constant.

CONCLUSION

The energy partition clearly shows that in C₂ only three electron pairs are contributing for the chemical bond, while the fourth pair exhibits exactly the opposite behavior expected for a covalent bond. Since the results are the same for the analogous C₃ state, unless one is ready to accept that there is a “1-3 bond” in C₃ one must conclude that there is no quadruple bond in C₂.

¹ See D. Danovich *et al*, Chem. Eur. J., 20, 6220, (2014) and references therein.

² T.M. Cardozo, M.A.C. Nascimento, J. Chem. Phys., 130, 14102, (2009).

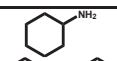
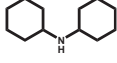

Electronic structure and Raman spectra of Cyclohexanamine, Dicyclohexanamine and Ethanolamine: A comparison of theoretical and experimental resultsDeiver A. Teixeira^{a,d}, David L. Azevedo^b, Vanessa L. S. Teixeira^c, Marco A. G. Valente^d, Assis V. Benedetti^d, Cecílio S. Fugivara^d.^a Instituto Federal de Mato Grosso, Cuiabá, MT, Brazil^b Instituto de Física, Universidade de Brasília – UNB, Brasília, DF, Brazil^c Secretaria de Educação do Mato Grosso, Cuiabá, MT, Brazil^d Instituto de Química, Universidade Paulista, UNESP, Araraquara, SP, Brazil

Keywords: Density functional theory (DFT), Raman spectrum, electronic structure, volatile corrosion inhibitors (VCI).

INTRODUCTION

In this present work, we report results of quantum chemical calculations of electronic structure and Raman spectra using DFT of the following molecules: ciclohexilamine, dicyclohexilamine, and ethanolamine that are volatile corrosion inhibitors¹, see below.

Table 1 – Chemical structure, molecular mass, name and abbreviation

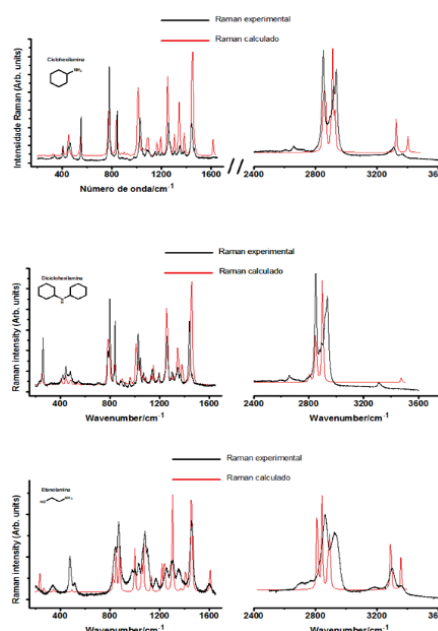
Structure	Molecular mass (g/mol)	Name (Abbreviation)
	99,2	Ciclohexilamine (CHA)
	181,3	Dicyclohexilamine (DCHA)
	61,1	Etanolamine (ETA)

METHODS

The molecular geometry, molecular orbitals and vibrational frequencies for each compound were calculated using density functional method with B3LYP exchange-correlation functional with a 6-311++G(d,p) basis as implemented in Gaussian 09. The Experimental Raman spectra were measured in micro-Raman equipment with He-Ne 632.81 nm laser. The potential energy distribution was obtained using VEDA program².

RESULTS AND DISCUSSION

In Fig 1, it is showed theoretical and experimental vibrational spectra. The correlation between these results was almost one. From experimental analysis, we suppose that molecule occupy several spatial orientations near the energetic minimum. In this situation, we perform a quantum chemistry calculation to elucidate which is the more favorable state.

Figure 1. Experimental and theoretical Raman spectra overlap for VCI: a) CHA; b) DCHA and c) ETA.

CONCLUSIONS

The chemical compounds here studied are volatile corrosion inhibitors¹. They present these properties due to the interaction of nitrogen atoms with metallic atoms of metallic surface. The overlap between experimental and theoretical data presented a correlation near unity. This give us confidence that the molecular structure analyzed was the same used in quantum chemical calculations.

ACKNOWLEDGMENTS

The authors are grateful for the support given by CNPq, CAPES and GRID-UNESP.

¹ TEIXEIRA, D. A. et al. J. Braz. Chem. Soc. V. 26, p. 434-450, 2015.

² LI, L. et al. Spectrochimica Acta: Molecular and Biomolecular Spectroscopy, v. 120, p. 106-118, 2014.

***Ab initio* study of a new class of covalent organic frameworks: RIO**

Deyse G. Costa^{a*}(PQ), Pierre M. Esteves^b(PQ), Camilla D. Buarque^c(PQ), Leonardo Carneiro^c(PG), Rodrigo B. Capaz^d(PQ)

^aDep. Química – UFV-MG, ^bInst. Química – UFRJ-RJ, ^cDep. Química – PUC-RJ, ^dInst. Física – UFRJ-RJ
deysegcosta@ufv.br

Keywords: *Ab initio*, COF, van der Waals, molecular modelling

INTRODUCTION

Covalent organic frameworks (COFs) are an emerging class of porous crystalline polymers with a wide variety of applications, including gas storage, sensing, energy storage and carriers for drug. Usually, COFs are composed of light elements, such as: H, B, C, N, and O, which crystallize into periodic two-dimensional (2D) layers or three-dimensional (3D) networks.

The interlayer interactions in 2D COFs can be attributed mainly to the weak van der Waals (vdW) forces. Consequently, 2D COFs can easily delaminate to single-layers, limiting their applications. Then, a chemically stable COF which combines permanent porosity and structural 3D ordering is highly desirable.

Here we report a new chemically stable COF, RIO-2, but due to its poor crystallinity, its structure is still unresolved.

In order to collaborate with this investigation, we perform *ab initio* calculations based on Density Functional Theory (DFT), for the structural and electronic properties of RIO-2. Geometrical analysis, including stacking sequence, interlayer distances, X-ray diffraction and Raman spectroscopy, were analyzed and presented.

METHODS

Calculations were performed with Quantum Espresso Code. We used ultrasoft pseudopotentials and plane waves with an energy cutoff of 60 Ry. To include weak vdW interactions, a semi-empirical dispersion terms (DFT-D), implemented in the Code, were included. The lattice dimensions were optimized simultaneously with the geometry.

RESULTS AND DISCUSSION

Based on experimental results, different 2D structural configurations were modeled and analyzed. The optimal model system has 102 atoms and a lattice constant of $a=b=19.57\text{Å}$ and $c=4.00\text{Å}$.

Van der Waals interactions play a crucial role in determining the structure, stability and dictate the optimal stacking mode and the interlayer sliding corrugation of RIO-2.

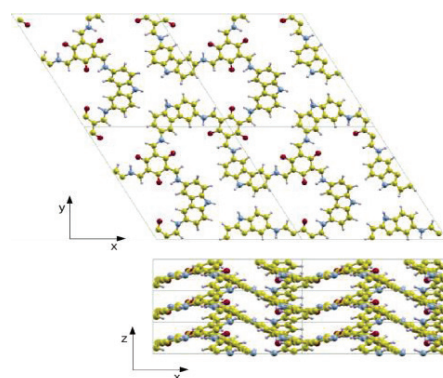


Figure 1. RIO-2 structure

Theoretical calculations indicate that RIO-2 behaves as a semiconductor, providing an additional advantage over its thiophene-based analogues, which are suggested to be insulators¹. Due to its relatively small band gap (calculated as 1.56eV), RIO-2 is a good candidate for optoelectronic devices.

CONCLUSIONS

Our calculations indicated that Rio-2 is a chemically stable material. Our results are in good agreement with experimental data.

ACKNOWLEDGMENTS

The authors are grateful for the support given from the FAPEMIG and FAPERJ.

¹ Guillaume H. V. et. al.; Proceedings of the National Academy of Sciences, 13, 4923, (2013).

Computational protocol to predict the Pt-195 NMR chemical shift

Diego Paschoal^{a*} (PQ), Marcone A. L. de Oliveira^a (PQ), Teodorico C. Ramalho^b (PQ), Hélio F. Dos Santos^a (PQ)

^aUniversidade Federal de Juiz de Fora, Departamento de Química, Campus Universitário Martelos, 36.036-900, Juiz de Fora – Brasil

^bUniversidade Federal de Lavras, Departamento de Química, 37.200-000, Lavras – MG, Brasil
 *diego paschoal@gmail.com

Keywords: Pt-195 chemical shift, Pt(II) complexes, NMR-TZPP-DKH basis sets, NMR spectroscopy

INTRODUCTION

Due the strong development in the last decades, NMR spectroscopy has played a key role in the discovery and design of new drugs. In addition of being widely used in the characterization of new structures, NMR has also been used in the optimization of complexes targets, in the elucidation of reaction mechanism, as well as in the studies of biomarkers and biosensors¹. In this present study a comprehensive analysis of relevant issues involved on the Pt-195 NMR chemical shift predictions are conducted. Non-relativistic and relativistic calculations are employed in distinct computations schemes to assess the most accurate method to use in a theoretical calculations of Pt-195 NMR. In addition to the existing methods, new relativistic NMR-TZPP-DKH Gaussian basis sets were constructed for H-He, Li-Ne, Na-Ar, K-Kr, Rb-Xe and Pt.

METHODS

DFT non-relativistic calculations were carried out by using the GAUSSIAN 09 program Rev. A.02. Figure 1, present the level of theory models used in this work. The NMR shielding constant was calculated through the GIAO approach and to calculate the $\delta^{195}\text{Pt}$, a simple linear regression model ($\delta_{\text{expt}} \times \sigma_{\text{calc}}$) was used. The calculated chemical shift was given by $\delta_{\text{calc}} = a \times \sigma_{\text{calc}} + b$. Besides, we have performed NMR relativistic calculations using the ADF 2012.01 program. Finally, 183 Pt(II) complexes were used for the development of models and other 73 Pt(II) complexes were used to validate the methodology.

Models	Level of Theory	NMR	Program
Model 1	PBEPBE/DZP-DKH/TZP-DKH/B3LYP/LANL2DZ/Def2-TZVPP	Linear regression	GAUSSIAN 09 Rev. A.02
Model 2	PBEPBE/SARC-ZORA/TZP-DKH/B3LYP/LANL2DZ/Def2-TZVPP	Linear regression	GAUSSIAN 09 Rev. A.02
Model 3	B3LYP/NMR-TZPP-DKH/B3LYP/LANL2DZ/Def2-TZVPP	Linear regression	GAUSSIAN 09 Rev. A.02
Model 4	PBEPBE/NMR-TZPP-DKH/B3LYP/LANL2DZ/Def2-TZVPP	Linear regression	GAUSSIAN 09 Rev. A.02
Model 5	PBEPBE/NMR-TZPP-DKH/B3LYP/LANL2DZ/Def2-SVP	Linear regression	GAUSSIAN 09 Rev. A.02
Model 6	PBEPBE-ZORA(SO)/TZ2P/B3LYP/LANL2DZ/Def2-TZVPP	Linear regression	ADF 2012.01
Model 7	PBEPBE-ZORA(SO)/TZ2P/B3LYP/LANL2DZ/Def2-TZVPP	$\delta_{\text{calc}} = \sigma_{\text{ref}} - \sigma_{\text{calc}}$	ADF 2012.01

Figure 1. Level of theory models used in this work

RESULTS AND DISCUSSION

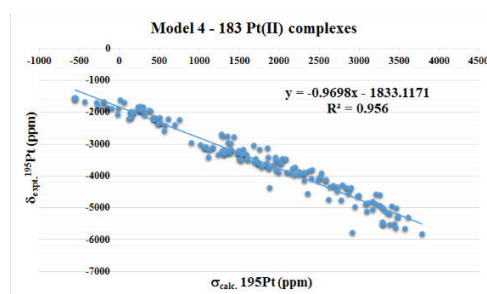


Figure 2. Simple regression linear model ($\delta_{\text{expt}} \times \sigma_{\text{calc}}$) used to development the Model 4.

Figure 2 present the data to the simple regression linear model used to development (183 Pt(II) complexes) the Model 4. The model 4 showed normal behavior of residues to the confidence interval of 95% (significance above 0.01). After we substitute the calculated shielding constants in the equation and found the calculated $\delta^{195}\text{Pt}$. For these 183 Pt(II) complexes an excellent coefficient of determination (R^2) of 0.9564 was obtained. The absolute and relative deviation were of 179 ppm and 6%, respectively. In the next step, other 73 Pt(II) complexes were used to validation the models. For Model 4, the absolute and relative deviation were of 190 ppm and 8%, respectively, showing an excellent agreement with the experimental data.

CONCLUSIONS

The results show that constructed models and the NMR-TZPP-DKH basis sets are an excellent alternative to predict the $\delta^{195}\text{Pt}$ even for complexes which were not used in the construction thereof.

ACKNOWLEDGMENTS

Computational Models for Fluorescence Study on Presence of Metallic Nanoparticles

Edison Franco-Junior (PG), Hueder P. M. de Oliveira (PQ), Janaína de Souza Garcia (PQ),
Paula Homem-de-Mello (PQ)

ABCSim, CCNH, Universidade Federal do ABC – UFABC, Santo André – SP

Keywords: DFT, TD-DFT, Platinum, PAH's, cluster.

INTRODUCTION

The optical properties of chromophores can be changed by the presence of metallic surfaces or metallic nanoparticles. It was shown to be possible to switch between quenching or enhancement of fluorescence brightness varying factors such as metal-chromophore distance, shape and size of the nanoparticle, among others.^{1,2} These phenomena could be used to develop new characterization techniques, however, there is no systematic study presented in literature.

METHODS

The electronic properties of four fluorophores (the PAH's pyrene, anthracene, diphenylanthracene and naphthalene) were studied using DFT and the TDDFT. To evaluate the effects of the presence of platinum nanoparticles in the emission spectrum of these compounds, we have employed a new type cluster based on the study of Piotrowski and Piquini³ (Figure 1). TDDFT calculations (B3LYP / 6-311G) were performed to optimize and obtain the energy of the first excited state of molecules studied in the gas phase and in aqueous solution (IEFPCM).

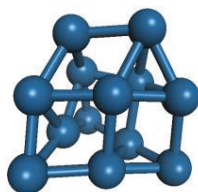


Fig. 1: Model of Piotrowski and Piquini³ for the Pt minimum cluster.

RESULTS AND DISCUSSION

Table 1 shows that emission wavelength (λ_{\max}) values obtained for the isolated PAH's with TDDFT calculations are in good agreement with experimental values. The inclusion of the solvent effect causes small bathochromic effect.

Experimental results⁴ indicate that the presence of Pt cubic nanoparticles (with edge about 2Å) induces quenching of the fluorescence spectrum. These results also show that the quenching is only observed if fluorophore and nanoparticle interacts. From our calculations, there is

interaction between the PAH and the metallic cluster until the distance of 8Å (Fig. 2).

Table 1: Emission wavelengths obtained with B3LYP/6-311G(d) and experimental values

	λ_{\max} (nm) gas- phase	λ_{\max} (nm) water	λ_{\max} (nm) exp.
Pyrene	368	377	373
Anthracene	446	451	420
Diphenylanthracene	481	489	410
Naphthalene	326	329	338

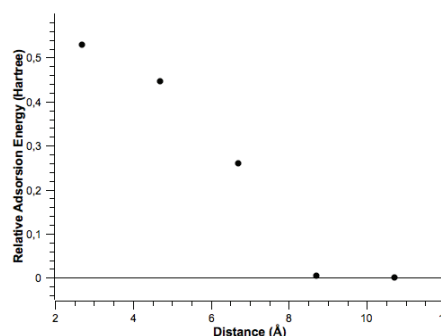


Fig. 2: Interaction energy dependence with the separation between pyrene and Pt cluster.

CONCLUSIONS

The methodology chosen for obtaining the wavelength of emission of isolated PAH's proved to be efficient. The use of Piotrowski and Piquini³ model allows to study the interaction between fluorophore and Pt-cluster, with reduced computational costs, but getting the excited state and the electronic transition to the ground state of the fluorophores in the presence of this cluster is still a problem to be overcome.

ACKNOWLEDGMENTS

FAPESP (2012/20653), CNPq and UFABC.

- ¹ K. H. Drexhage and M. Fleck, *Berichte der Bunsengesellschaft für Phys. Chemie*, 1968, **72**, 330.
- ² S. Vukovic, S. Corni and B. Mennucci, *J. Phys. Chem. C*, 2009, **113**, 121–133.
- ³ M. J. Piotrowski and P. Piquini, *Phys. Rev. B*, 2010, **81**, 1–14.
- ⁴ E. Franco-Junior, manuscript in preparation.

Theoretical Investigation on the Reaction of CO₂ with AminesEdnilsom Orestes^{a,b} (PG), Célia M. Ronconi^b (PG) and José Walkimar de M. Carneiro^b (PG)^a Departamento de Ciências Exatas, Escola de Engenharia Industrial Metalúrgica de Volta Redonda, Universidade Federal Fluminense^b Departamento de Química Inorgânica, Instituto de Química, Universidade Federal FluminenseKeywords: computational chemistry, CO₂ absorption, reaction mechanism.

INTRODUCTION

The high amounts of greenhouse gases, particularly CO₂, as a product of the fossil fuels combustion has been claimed as one of the main reasons for the fast global climate change.¹ This has motivated the search for methods able to capture and separate CO₂, among them, aqueous solutions of primary, secondary or tertiary alkanolamines, e.g., methylamine (MAM), monoethanolamine (MEA), and diethanolamine (DEA), have been widely used as chemical absorbents of CO₂.² It is known that the rate-determining step and favored reaction channel between alkanolamines and CO₂ to form carbamate involves a zwitterion as intermediate specie.³ In a recent communication, we have used MP2 and DFT methods to investigate the first step of the reaction between CO₂ and primary pure amines to form a zwitterion specie.⁴ Now, the second step of this reaction is under study, i.e., the proton abstraction of the zwitterion amino group by a second alkanolamine (1) to form a carbamate and its possible devolution to the carboxylic acid group to form a carbamic acid (2).



METHODS

Three alkanolamines were considered in this study; MAM, MEA, and DEA. After a conformational analysis using PM3 for MEA and DEA, the geometry of all species were fully optimized with the 6-311++G(2d,2p) basis set and CAM-B3LYP density functional followed by the frequency calculation including solvent effects through the IEFPCM and counterpoise correction for the basis set superposition error. The calculations were performed with Spartan and G09 packages.

RESULTS AND DISCUSSION

The conformational analysis revealed two energetically most stable geometries for MEA, chair (MEAr) and chain (MEAn), and three for

DEA: without hydrogen bonding (hb0) involving the hydroxyls; with one (hb1); and two (hb2).

Table 1: Energy barriers for each reaction in kcal/mol.

	MAM	MEAr	MEAn	DEAhb0	DEAhb1	DEAhb2
REAC1	0,60	0,86	1,40	1,57	1,77	2,45
REAC2	1,08	1,19	1,26	1,11	0,91	1,20

The reaction mechanism study shows that the energy barrier for the reaction (1) increases from MAM to MEA and from MEA to DEA. Particularly, the energy barrier for reaction (1) is higher for MEAn than for MEAr, and is higher for DEAhb2 than for DEAhb1 and DEAhb0. On the other hand, the energy barrier for the reaction (2) is in general, lower than that for the reaction (1) with no significantly differences among different conformations of the alkanolamines. Besides, the proton turned back in the reaction (2) always involve a different proton than that withdrew in the reaction (1).

CONCLUSIONS

Besides MAM, two different conformations for MEA e three for DEA were obtained and analyzed. The energy barrier for reaction (1) increases with the number of intramolecular hbs and is lower than that for reaction (2). The reaction (2) always involves a different proton than that involved in the reaction (1).

ACKNOWLEDGMENTS

The authors would like to thank CNPq and FAPERJ for financial support and UFF for the facilities.

¹ K. Sumida, D. L. Rogow, J. A. Mason, T. M. McDonald, E. D. Bloch, Z. R. Herm, T.-H. Bae, J. R. Long, *Chem. Rev.* 112, 724 (2012).

² Satyapal, S.; Filburn, T.; Trela, J.; Strange, J., *Energy Fuels*, 15, 250 (2001).

³ Davran-Candan, T.; *J. Phys. Chem. A*, 118, 4582 (2014).

⁴ Orestes, E; Ronconi, C. M.; Carneiro, J. W. de M., *Phys. Chem. Chem. Phys.*, 16, 17213 (2015).

Modeling zigzag CNT: dependence of structural and electronic properties on the length and application to the encapsulation of HCN and HCCH

Eduardo C. Aguiar^a (PQ), Ricardo L. Longo^b (PQ) João Bosco P. da Silva^b (PQ)

^a Unidade Acadêmica de Serra Talhada, Universidade Federal Rural de Pernambuco (UFRPE), 56909-535, Serra Talhada (PE), Brazil.
castro.eduardo@gmail.com

^b Departamento de Química Fundamental, Universidade Federal de Pernambuco (UFPE), 50740-540, Recife (PE), Brazil

Keywords: Carbon Nanotubes, DFT, encapsulated species, charge transfer, molecular model.

INTRODUCTION

Recently, carbon nanotubes (CNT) have been the focus of a lot of research efforts because their physical properties and potential applications. The first theoretical works on CNT used only one C=C bond length. When different C=C distances are considered the a most stable CNT is predicted^{1,2}. Experimental crystallographic results³ for zigzag CNT indicate that longitudinal C=C (CCL) bond lengths are shorter than tangential (CCT) ones. In this work we have performed B3LYP calculations in order to determine the minimal length of zigzag single wall CNT that reproduce the experimental C=C bond behavior and evaluated the effect of the model size on the encapsulation of the isoelectronic molecules HCCH and HCN.

METHODS

The set of calculated zigzag CNTs have chiral index of 6 to 9 and lengths of two ($\times 2$), three ($\times 3$) or four ($\times 4$) times the unit cell of repetition. The geometries were fully optimized with the B3LYP/6-31G(d) method using the Gaussian 09 program. The encapsulation energies (ΔE) were calculated according to the supermolecule approach corrected by the BSSE counterpoise method. All atomic charges were evaluated with the Natural Bond Orbital (NBO) partition. The effect of dispersion corrections on these systems was studied with the two parameters Grimme's empirical dispersion correction (GD2).

RESULTS AND DISCUSSION

We observed that C=C bond are larger at the CNT borders and decrease as approach to the center and when CNT length (L_i) reaches twice its diameter (d_i) the CCL < CCT experimental observation is fulfilled. The atomic charges that assume values close to zero at nanotube's center and negative values at the border due its saturation

with hydrogen atoms. Based in this observations we can define an useful region of CNT where the computational model behaviors as expected for the real system (see Figure 1 to the (7,0) $\times 4$ CNT).

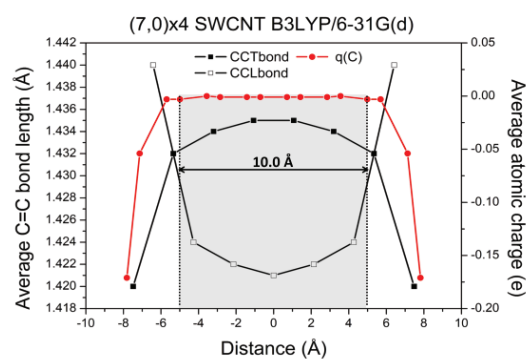


Figure 1. In black, average CCL (open squares) and CCT (filled squares), in Å. In red, average carbon charge, in electrons. Grey area refers to the CNT useful region.

The ΔE values are sensitive to the change of C=C bond pattern of CNT getting smaller as the tube length grows. Both ΔE and charge transfer, from CNT to dopants, decrease with the increase of tube diameter. The dispersion energy stabilize the supermolecule and shortens the C=C bonds.

CONCLUSIONS

CNT's with $L_i/d_i > 2$ reproduce, at its center, the experimental pattern of C=C bonds which affect the ΔE , stabilizing it, being an important parameter to model interacting system with CNT.

ACKNOWLEDGMENTS

The authors are grateful for the financial support of FACEPE, CAPES, CNPQ and inct-INAMI.

¹ R.K.F. Lee *et al.*, *Nanoscale* **2** (2010) 859.

² V.K. Jindal and A.N. Imtani, *Comput. Mater. Sci.* **44** (2008) 156.

³ J. Zhang, J.M. Zuo, *Carbon* **47** (2009) 3515.

Chemical stability of a new h-CuS lamellar chalcogenide – A computational investigation

Egon C. Santos (PG), Antônio L. Soares Júnior (PG), Heitor A. Abreu (PQ) and Hélio A. Duarte (PQ).

Grupo de Pesquisa em Química Inorgânica Teórica – GPQIT; Departamento de Química – ICEx, Universidade Federal de Minas Gerais (UFMG), 31.270-901 Belo Horizonte-MG.
 Email: egoncs@gmail.com.

Keywords: Covellite, Surfaces, Dichalcogenides, 2D materials, DFT

INTRODUCTION

We investigated copper sulfur (h-CuS) honeycomb sheet with similar structure of graphene. This structure was obtained by serendipity during the investigation of the covellite surface reconstruction. Figure 1 shows the (001) surface in which the h-CuS monolayer is formed by covellite reconstructions and stabilized with van der Waals interactions with the bulk. Due to its similarities to the graphene¹⁻³ and h-BN materials which are technologically important, we decide to investigate the properties and the stability of this material.

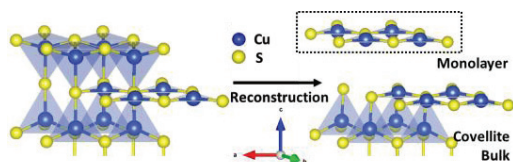


Figure 1. Fragment of the covellite structure showing the reconstruction to form a monolayer.

METHODS

The electronic structure of the systems were calculated by GGA/PBE exchange/correlation approximation of the Density Functional method (DFT) as implemented in Quantum-ESPRESSO package. Following the Monkhost-Pack scheme 12x12x1 special k-points meshes were carry out for all slabs, and Kohn-Sham (KS) electronic orbitals were expanded in a plane-wave basis set up to a kinetic cutoff of 680 eV (50 Ry). Bader analysis was evaluated in CRITIC2 software. The h-CuS layer are placed in xy plane and modeled with a vacuum space of 20 Å in z-axis to avoid the interactions between two adjacent sheets.

RESULTS AND DISCUSSION

Structural, electronic and mechanical properties were evaluated for the monolayer in vacuum, Figure 2. The calculated Cu-S distances are 2.16 Å (0.03 Å less than in covellite) and the lattice parameter for the monolayer was

determined to be $a=b=3.74$ Å (0.09 Å less than in covellite). This observation is in a good agreement with Bader analysis, which observed that electron density increases in Cu-S BCP, suggesting stronger bond in the monolayer than in covellite bulk. The system is non-magnetic, and the band structure (Figure 2) indicated a metallic behavior of the monolayer. Projected Density of States (PDOS) shows that the conduction band is formed predominantly by p_x , p_y , $d_{x^2-y^2}$ and d_{xy} orbitals, suggesting that the conduction of the system occurs along xy plane, in the direction of the Cu-S bonds. It is in a good agreement with topological analysis, where all critical points (BCP and RCP, Figure 2) is located in the sheet plane. Young modulus founded by our theoretical level was 1406 GPa, a value greater than for graphene³ (about 1000 GPa).

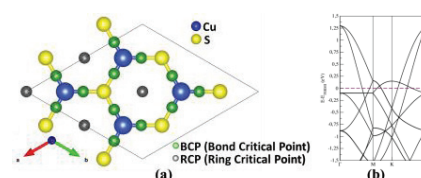


Figure 2. (a) Critical points analysis. (b) Band structure.

CONCLUSIONS

A new two-dimensional stable material is proposed. This material is metallic and has strongest Cu-S chemical bonds than graphene. Phonon density of states will be presented and the local structure stability discussed. Considering all development in the production of low-dimensional materials,³ we are optimistic that 2D CuS covellite based can be synthesized in the near future.

ACKNOWLEDGMENTS

The authors are grateful for the support given from the FAPEMIG, CAPES, CNPq and INCT.

¹ R. P. Gainov, I. A. Bryzgalov. *Phys. Rev. B*, 79, 075115, (2009).

² L. Yang, E. Ganz. *J. Am. Chem. Soc.*, 137, 2757, (2015).

³ F. Liu, J. Li. *Phys. Rev. B*, 76, 064120, (2007).

Electronic Structure and Optical Properties of Diblock Polymers for Solar Cell Applications

Eliezer Fernando Oliveira^a (PG), Francisco Carlos Lavarda^b (PQ)

^aUNESP - Univ Estadual Paulista, POSMAT - Programa de Pós-Graduação em Ciência e Tecnologia de Materiais, Bauru, SP, Brazil

^bDF-FC, UNESP - Univ Estadual Paulista, Av. Eng. Luiz Edmundo Carrijo Coube 14-01, 17033-360 Bauru, SP, Brazil.

Keywords: Conducting Polymers, Electronic Structure Calculation, Organic Solar Cells

INTRODUCTION

The search for cheaper sources of renewable and efficient energy has led the scientific community to the improvement of organic solar cells¹. A less common polymer used as the active layer is the diblock polymer, which consists of two types of homopolymers connected to each other by its ends. Experimental data show that these types of polymers have an improved morphology compared to the homopolymer that constitute the diblock; however, for electronic structure no improvement was observed². In this work we investigate theoretically the electronic structure of diblock polymers in order to understand the electronic structure of these types of polymers and try to understand why is not observed improvements in the properties arising from electronic structure in relation to homopolymers.

METHODS

We study six diblock polymers built from eight known polymers: polifenileno vinileno (PPV), politiofeno (PTh), polipirrol (PPy), polisilole (PSi), polifosfol (PPh), policiclopentadieno (PCP), poli(2-metóxi-5-(2'-etil-hexiloxi)-1,4-fenileno vinileno (MEH-PPV) e Poli(3-hexiltiofeno) (P3HT). We employ a semiempirical Hartree-Fock PM6 method for geometry optimization and Density Functional Theory for the electronic structure analysis. All calculations was performed by MOPAC2012, GAMESS and ORCA programs.

RESULTS AND DISCUSSION

Our results show that the HOMO and LUMO levels for diblock polymer was always approximately the HOMO of the homopolymer

that had the highest HOMO and LUMO of the homopolymer that had the lowest LUMO. The bandgap of the diblock polymer decreased compared to homopolymers in which they were built, but we found these the frontier orbitals were not extended throughout the main chain (See Figure 1 for the PCP-block-PTh case). Due to this fact, there was no HOMO-LUMO optical transition in diblock polymer.

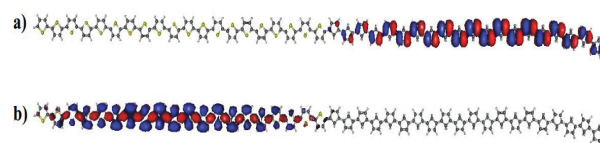


Figure 1. Kohn-Sham orbitals representation for a) HOMO e b) LUMO of PCP-*block*-Pth polymer.

CONCLUSIONS

In general, diblock polymer showed to be a low bandgap material but with no improvements regarding to the optical response.

ACKNOWLEDGMENTS

We would like to thank the Brazilian agency FAPESP (proc. 2012/21983-0 and 2014/20410-1) for financial support and the resources supplied by the Center for Scientific Computing (NCC/GridUNESP) of the São Paulo State University (UNESP).

¹ H. Zhou, L. Yang, and W. You, *Macromolecules* 45, 607 (2012).

² D. Gao, J. Hollinger, and D. S. Seferos, *ACS Nano* 6, 7114 (2012).

Assessment of the Reliability of the SMD Model to Predict Activation Barriers for Classical S_N2 Reactions in Organic Solvents

Elizabeth L. M. Miguel (PG), Calink I. L. Santos (PG), Carlos M. Silva (PG), Josefredo R. Pliego Jr (PQ)

*Laboratório de Química Teórica e Computacional, Departamento de Ciências Naturais, Universidade Federal de São del Rei, São João del-Rei, MG, Brazil
elizabethmmiguel@gmail.com*

Keywords: S_N2 reaction, continuum model, Free energy barrier, solvent effect

INTRODUCTION

Bimolecular nucleophilic substitution reactions (S_N2) are classical processes in organic chemistry and the correct prediction of the activation barriers by theoretical calculations constitutes an important test of computational methods.¹ In this work, our aim was to evaluate how able is a standard DFT method (X3LYP) combined with a universal continuum solvation model (SMD) to predict absolute and relative activation barriers in different solvents. The investigated systems are presented in Table 1:

Table 1: Reactions studied in this work.

Number	Reaction
1	CH ₃ Cl + N ₃ ⁻ → CH ₃ N ₃ + Cl ⁻
2	CH ₃ Cl + SCN ⁻ → CH ₃ SCN + Cl ⁻
3	CH ₃ Br + Cl ⁻ → CH ₃ Cl + Br ⁻
4	CH ₃ CHBrCH ₃ + PhS ⁻ → (CH ₃) ₂ CH-SPh + Br ⁻

METHODS

Geometry optimization and harmonic frequency calculations were obtained using the X3LYP functional and the DZV+P(d)+diff basis set. The optimizations were done in solution through the SMD solvation model. This method was also used to compute the final solvation free energy. More reliable single point energy calculations were done at X3LYP/TZVPP+diff level of theory.

RESULTS AND DISCUSSION

The activation free energy barriers of four S_N2 reactions in solvents like methanol, formamide, water, DMF, acetonitrile and acetone, resulting in 11 free energy barriers, are presented in Figure 1. We have included the results with (solution phase) and without (gas phase) the solvent effect. We can notice that calculated gas phase barriers are in

considerable deviation in relation to solution phase experimental barriers, as expected. When the solvent effect is included, there is a considerable improvement in the barriers, and the SMD model is able to catch the most important solvent effect. However, analyzing the effect of changing the solvent from protic to dipolar aprotic, the SMD model is not able to predict the classical rate acceleration effect. These details will be presented in the event.

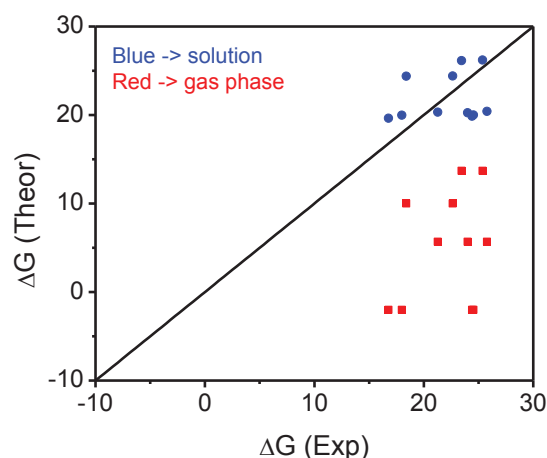


Figure 1. Relation between experimental and theoretical values of activation free energy.

CONCLUSIONS

The SMD model includes the most important solvent effect, but it is not able to describe finer details like rate acceleration involving protic and dipolar aprotic solvents. More reactions are being studied.

ACKNOWLEDGMENTS

The authors are grateful for the support given from the CAPES, CNPQ and FAPEMIG.

¹ D.W. Tondo and J. R. Pliego Jr, J. Phys. Chem. A, 109, 507, (2005).

Efeito da temperatura sobre a formação de padrões em um sistema quiral tipo reação-difusão

Emerson Boscheto^a (PQ), Alejandro López-Castillo^a (PQ)

^a Depto. De Química, Universidade Federal de São Carlos, São Paulo - Brasil

Palavras-chave: Formação de padrão, Reação-difusão, Brusselator, Gradiente de temperatura

INTRODUÇÃO

Em sistemas tipo reação-difusão é possível observar, sob determinadas condições, a formação espontânea de padrões de concentração estacionários ou dinâmicos. Esta classe de sistemas tem sido proposta, por exemplo, para auxiliar o entendimento da dinâmica da morfogênese¹. Neste trabalho estudamos a influência da temperatura sobre a formação de padrões em uma versão do conhecido modelo Brusselator² modificada por Iwamoto para estudar a quebra de simetria quiral³.

MÉTODOS

O sistema de equações diferenciais parciais foi resolvido pelo método de integração numérica das diferenças finitas⁴ com código implementado em linguagem FORTRAN. Para as simulações assumiu-se um perfil inicial de concentração randômico distribuído em um domínio de 1 cm².

RESULTADOS E DISCUSSÃO

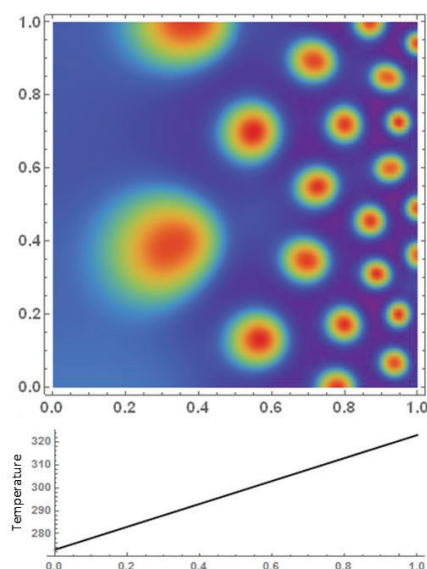


Figura 1. Padrão de ilhas formado sob efeito de um gradiente linear de temperatura, ilustrado na parte inferior da figura.

Durante as simulações encontramos que a submissão do sistema a um gradiente linear de temperatura, entre 273 K na posição 0 cm em 323 K na posição 1 cm (Fig. 1), pode introduzir diferenças no tamanho e na distribuição de padrões de ilhas de concentração.

CONCLUSÕES

Encontrou-se que gradientes de temperatura podem afetar o processo de formação de padrões de concentração em um sistema de reação-difusão simples. Estudos como estes podem proporcionar meios de controle externo da fabricação de padrões de interesse ou auxiliar no entendimento de como gradientes espontâneos de temperatura podem contribuir para a disposição de padrões em sistemas naturais.

AGRADECIMENTOS

Os autores agradecem o apoio concedido pela FAPESP, processo 2013/25210-8.

¹ Turing, A.M., *Philosophical Transactions of the Royal Society of London. Series B, Biological Sciences*, 237(641),37,(1952).

² Prigogine, I. e R. Lefever, *The Journal of Chemical Physics*, 48(4), 1695, (1968).

³ Iwamoto, K., *Physical Chemistry Chemical Physics*, 4(16), 3975, (2002).

⁴ Smith, G.D., *Numerical Solution of Partial Differential Equations: Finite Difference Methods*, Estados Unidos da América: Oxford University Press. 350 p, (1986).

Estudo Cinético e de Estrutura Eletrônica do Efeito da Água sobre a Racemização da Talidomida

Emília V. F. de Aragão^a (IC), Thiago S. Castro^a (IC),
 Sara F. de A. Morais^{a*} (PG), Kleber C. Mundim^a (PQ), Davi A. C. Ferreira^{a†} (PQ),

^a Laboratório de Modelagem de Sistemas Complexos, Instituto de Química, Universidade de Brasília, Campus Darcy Ribeiro, CP 04478, CEP: 70904-970, Asa Norte - Brasília-DF, Brasil. E-mail: ^{*}emiliaragao@hotmail.com/[†]dacf@unb.br

Palavras chave: Talidomida, Taxas de Reação, DFT, Efeitos Cooperativos.

INTRODUÇÃO

No início dos anos 50, um novo fármaco com propriedades sedativo-hipnóticas foi descoberto pela indústria alemã Chemie Grünenthal e em seguida comercializado com a promessa de aliviar a sensação de enjoo em gestantes: era o nascimento da talidomida. Graças à sua eficácia, a talidomida foi prescrita em diversos países, no entanto não demorou muito para que os casos de teratogenia comesçassem a aparecer; perfil manifestado até mesmo em pH fisiológico devido ao processo de racemização proporcionado pela reação de hidrólise¹, que converte o enantiômero R em S, esquematizado na Figura 1.

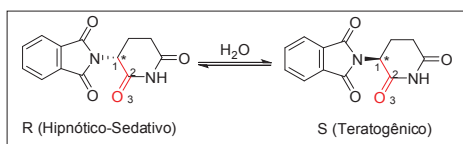


Figura 1 – Formas Canônicas da Talidomida em equilíbrio aquoso.

Neste trabalho realizamos uma análise cinética e de estrutura eletrônica para o mecanismo de racemização da talidomida em meio aquoso, através de transferência protônica concertada.

METODOLOGIA

Para o estudo mecanístico empregamos a Teoria do Funcional de densidade, através do funcional PBE1PBE e base 6-31+G(d,p), e Teoria Quântica de Átomos em Moléculas, para avaliação da estabilidade eletrônica relativa dos passos representativos na coordenada de reação proposta.

RESULTADOS E DISCUSSÃO

Nossos cálculos indicaram que o processo de racemização da talidomida em água ocorre por transferência protônica concertada, com barreiras

da ordem de 24.3 kcal.mol⁻¹, como mostrado na Figura 2.

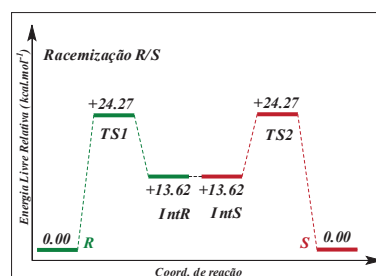


Figura 2. Coordenada de racemização da talidomida através de hidrólise.

Nesta proposta, o processo de isomerização ocorre devido à possibilidade de um equilíbrio ceto-enólico entre R e IntR ($k_{direta} = 6,6 \times 10^{-5} \text{M}^{-2} \cdot \text{s}^{-1}$ e $k_{inversa} = 2,6 \times 10^{-5} \text{M}^{-2} \cdot \text{s}^{-1}$) ou S e IntS. Assim, uma vez formado o enol (IntR ou IntS) pela desprotonação do carbono assimétrico, o sistema rapidamente se interconverte em talidomida R ou S. Análises NBO, e QTAIM (Tabela 1), apontaram maior facilidade de racemização por interferência da água; com destaque para a deslocalização do tipo $\sigma_{C1-H1} \rightarrow \pi^*_{C2-O3}$. (0.66 kcal.mol⁻¹ em fase gás e 8.03 kcal.mol⁻¹ solvatado).

Tabela 2 – Densidades eletrônicas nos pontos críticos de ligação.

LIGAÇÃO	$\rho_C(\text{GAS})$	$\rho_C(\text{SOLV})$
C1-H1	0.2802	0.2800
C1-C2	0.2548	0.2572
C2-O3	0.4138	0.4040

CONCLUSÕES

Os cálculos realizados neste trabalho indicam que a racemização da talidomida ocorre através de um equilíbrio ceto-enólico, cuja etapa determinante é a desprotonação do carbono assimétrico.

AGRADECIMENTOS

Study of Constitutional Isomers in Ru(II) Polypyridinic Complexes

Érica de Liandra-Salvador^a (PG), Paula Homem-de-Mello (PQ)

ABC₂Sim, CCNH, Universidade Federal do ABC, SP, Brasil
^a ericaliandra@gmail.com; erica.liandra@ufabc.edu.br

Keywords: DFT, Ruthenium(II) complexes, Isomers

INTRODUCTION

Dyes based on ruthenium(II) polypyridine complexes¹ may be used as sensitizers in dye sensitized solar cells (DSSC). In order to improve the efficiency of these cells, one can replace a ligand, what can interfere in spectroscopic properties. N3 (cis-Ru[(dcbH₂)₂(NCS)₂) is one of the most efficient dyes² and, in this work, we have evaluate the substitution of withdrawing groups -COOH by donating groups -CH₃.

METHODS

The studied structures (Figure 1) were divided into isomers of group 1: (H), (I), (J) and (K) and group 2 (L) (M) (N) and (O). All calculations were carried out with Gaussian 09 program, by using DFT and TD-DFT approaches, with B3LYP functional and LANL2DZ basis set. Effects of solvent, acetonitrile, were simulated by means of IEFPCM continuum model.

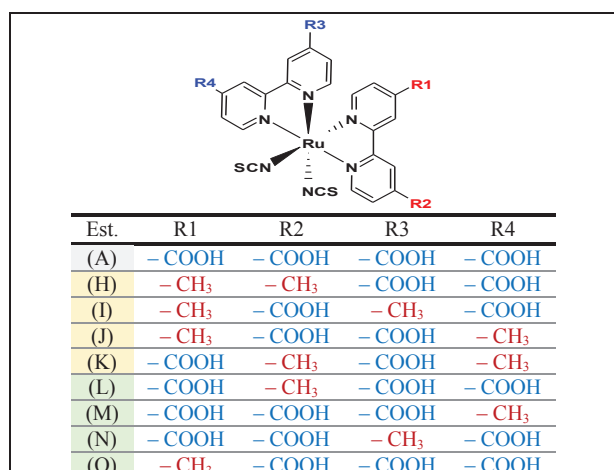


Figure 1. List of structures covered in this study.

RESULTS AND DISCUSSION

The lowest energy structures of each group of isomers are (J) and (K), of group 1, and (L) and (M) of group 2, that is substitutions at R2 and/or R4 positions.

Many electronic properties of these dyes have been studied. Molecular orbitals energy levels (Figure 2) analysis indicates that replacing one or two carboxylic groups by methyl groups, lead to increase energies of both lowest and highest levels. Reorganization energy is higher for these structures than for the N3 dye.

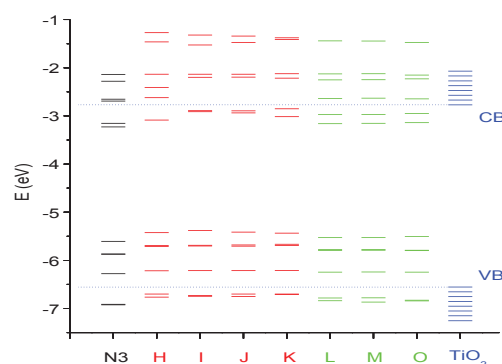


Figure 2. Orbitals energy from HOMO-5 to LUMO+5, compared with conduction bands (CB) and valence bands (VB) of TiO₂ semiconductor.

CONCLUSIONS

In this work, results indicate that the substitution of some groups of dye N3 lead to significant changes in the electronic structure of the studied compounds. Several other properties are being studied aiming to propose molecules that increase the DSSC performance.

ACKNOWLEDGMENTS

The authors are grateful for the support given from the UFABC, CAPES, FAPESP and CNPq.

¹ L. Vandenberg, M. R. Buck, D. A. Freedman, *Inorg. Chem.*, 47, 9134, (2008).

² T. P. Brewster, et al, *Inorg. Chem.*, 50, 11938, (2011).

Periodic DFT Investigation on the Adsorption and Catalytic Desulfurization of Thiophene over VC(001) and VN(001) *via* Hydrogenation and Direct Pathways

Eugenio Furtado de Souza^a (PQ), Teodorico de Castro Ramalho^b (PQ), Ricardo Bicca de Alencastro^a (PQ)

^a Universidade Federal do Rio de Janeiro. Rio de Janeiro, Instituto de Química. Programa de PG em Química. Laboratório de Modelagem Molecular-LABMMOL

^b Universidade Federal de Lavras, Departamento de Química.

Keywords: carbide, nitride, thiophene, hydrodesulfurization, DFT, catalysis.

INTRODUCTION

The imposition of stringent environmental restrictions on the S-content of petroleum derivatives makes necessary efforts in the development of new catalysts¹. Particularly, vanadium nitrides and carbides are active in desulfurization reactions². However, experimental and theoretical studies on the surface properties and reaction mechanisms are quite scarce. In this work, we carried out a detailed computational investigation on the aspects involved in thiophene adsorption and desulfurization processes over VC(001) and VN(001) surfaces. The effects of thiophene hydrogenation were also studied and possible mechanisms involved in bond breaking were discussed.

METHODS

Total-energy calculations were performed using the PWSCF computational code³. The Kohn-Sham states were expanded in plane-waves up to a kinetic energy cutoff of 30 Ry. The PBE functional was used to calculate the exchange and correlation contributions. Integrals over the Brillouin-zone were performed by sums of 2x2x1 Monkhorst-Pack. The slab was divided into four atomic layers and a vacuum region of ~15 Å was applied. The NEB method⁴ was used in order to locate energy barriers and transition states through the minimum energy path.

RESULTS AND DISCUSSION

Our theoretical calculations suggest that on VC(001) thiophene molecules adsorb preferentially in a partially-tilted η^1 configuration with the ring S atom forming a covalent bond with a $V_{(Surf)}$ atom and with small modification in the

intramolecular structure. On the other hand, on VN(001) thiophene molecules prefer to interact with the ring orthogonally located on a surface hollow site. The calculated energies indicated that adsorption on both surfaces (Fig. 1) are exothermic and that the catalytic activity are related to surface effects (corrugation and reconstruction). Our calculations confirm that the surfaces present resistance to sulfur deposition and the analysis of the electronic properties confirms the participation of the non-metal surface atoms in the adsorption.

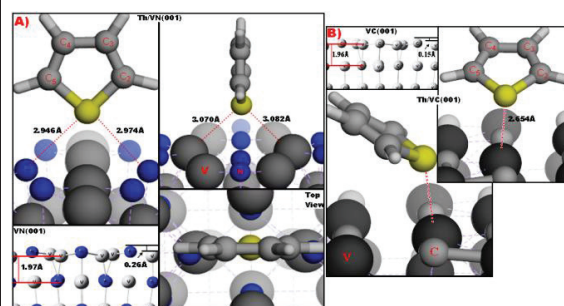


Fig 1 - Configurations of the most stable (Th@VN(001) (A) and the Th@VC(001) (B) adsorption systems.

Our calculations indicate that the removal of sulfur starts with the S-C² scission, followed by the cleavage of the S-C⁵ bond.

CONCLUSIONS

The present work indicates that the HYD pathway is more difficult to achieve for the S-C cleavage process. For both surfaces, the substantial increase of the energy barriers caused by ring hydrogenation clearly reveals a preference for the DDS pathway instead of HYD in close resemblance to noble metal surfaces⁵.

A Theoretical Study of Intramolecular Reaction Paths of α -hydroxynitrosamine in Gas Phase

Ezequiel Frago V. Leitão^a (PG), Silmar A. do Monte^b (PQ), Elizete V. do Monte (PQ)^c

^{a,b,c} Department of Chemistry, CCEN, Federal University of Paraíba, João Pessoa/PB 58059-900
Brazil,
kelfvl@yahoo.com.br

Keywords: α -hydroxynitrosamine, Intramolecular Reaction, reaction pathways

INTRODUCTION

Nitrosamines are generally considered potent carcinogens. The carcinogenic potential of nitrosamines such as N-nitrosodimethylamine (NDMA) is activated after their reaction with the OH group which is bound to the iron porphyrin cytochrome P450.¹ This reaction yields α -hydroxynitrosamine, which is then dissociated through release of carbonyl and OH⁻ to form the diazonium ion², as shown in Figure 1:

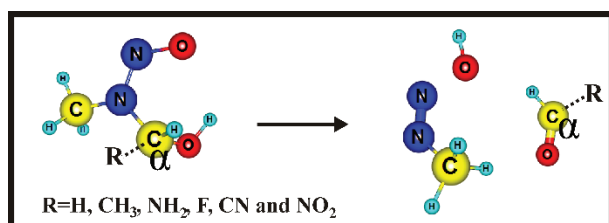


Figure 1. Molecular Structure of the Reactant Complex (RC) -Left- and Products Complex (PC) -Right- involved in the intramolecular hydrogen transfer reaction of the α -hydroxynitrosamine.

The aim of this work is to study the effect of the $C\alpha$ substituents on the possible reaction pathways for the formation of the diazonium species of α -hydroxynitrosamine. Both kinetic and Thermodynamic aspects of four reaction pathways were investigated.

METHODS

The reaction pathways studied in this work involve R= H, CH₃, NH₂, F, CN and NO₂ (see Fig.1). The stationary points along each reaction pathway have been optimized at the B2PLYP/aug-cc-pVDZ level, followed by single-point calculations with the aug-cc-pVTZ basis set. IRC calculations were performed to ensure the correct connection between transition states and minima. Frequency calculations were performed to ensure the correct nature of each stationary point and provide the vibrational zero-point energies (ZPE).

All calculations were performed with Gaussian 09 using its default criteria.

RESULTS AND DISCUSSION

According to potential energy profiles the barrier heights for the four reaction mechanisms are significantly dependent on the substituents. Among the four reaction pathways studied for R=H three of them yield products observed experimentally³, while the remaining one yields products in agreement with the work of Silva.⁴

CONCLUSIONS

The calculations performed in this work comprise four distinct reaction mechanisms which yield diazonium ions from intramolecular hydrogen transfer reaction of the α -hydroxynitrosamine. These reaction mechanisms are significantly dependent on the type of substituent connected to the $C\alpha$ atom. For R= H three of them are consistent with experiments.³

ACKNOWLEDGMENTS

The authors are grateful for the support given by CAPES, CNPq and UFPB.

¹ Li Ji and Gerrit Schüürmann, J. Phys. Chem. B, 116, 903, (2012).

² F. P. Guengerich, Chem. Res. Toxicol., 14, 611, (2001).

³ N. Kulikova *et al.*, Int. J. Mass Spectrometry, 75, 288, (2009).

⁴ G. Silva, Environ. Sci. Technol., 47, 7766, (2013).

Effects of different substituents on the stability of compounds derived from triphenylimidazol

Carvalho, F. (PG)^a, Bartoloni, F. H. (PQ), Homem-de-Mello, P. (PQ)

^afabricio.carvalho@ufabc.edu.br

Centro de Ciências Naturais e Humanas, Universidade Federal do ABC

Keywords: PCET, triphenylimidazol, hydrogen bonding, DFT.

INTRODUCTION

The proton coupled electron transfer reaction (PCET) is a formal class of hydrogen atom transfer reactions (HAT), which has shown a broad interest because it is applied to a wide range of chemical and biochemical processes, such as in enzymatic reactions, in photosynthesis and respiration processes¹. This study aimed at examining the tautomeric balance and stability of the intramolecular hydrogen bond occurring in this class of compounds towards different substituents as in some types of solvents.

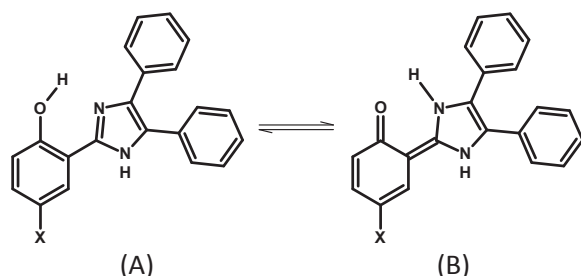


Figure 1. Scheme showing the proton transfer in compound derived from triphenylimidazol.

METHODS

A variety of theoretical approaches have been tested to study the PCET reactions², wherein the DFT has emerged as an appropriate tool³. In this work, we studied three triphenylimidazolic compounds. The geometry optimization and frequency calculations were performed with the functional M06-2X and the basis set 6-31G(2d,2p) as implemented in Orca software.

RESULTS AND DISCUSSIONS

Free energy values were used to analyze the stability of intramolecular hydrogen bonds that occur in some derivatives of triphenylimidazol, Fig 1. In principle, the free energies in gas-phase and in ethyl acetate (COSMO) were analyzed to three substituents: X = CH₃, H and NO₂. The keto

form (B) is less stable than the phenolic form (A), ie, this keto-enol equilibrium that occurs in triphenylimidazol is shifted to the enol form. However, note that for the –NO₂, that is an electron withdrawing group, the difference is significantly lower, probably due the more intense hydrogen bonding (Table 2).

Table 1. Free energy differences between the structures A and B for the three substituents obtained in ethyl acetate

X	ΔG_A° (Eh)	ΔG_B° (Eh)	$\Delta G_B^\circ - \Delta G_A^\circ$ (kJ.mol ⁻¹)
CH ₃	-1033,278	-1033,272	17,02
H	-994,006	-993,999	16,54
NO ₂	-1198,448	-1198,445	7,50

Table 2. Distance between the atoms involved in intramolecular hydrogen bond to the structures A and B to three substituents

X	O - H _A (Å)	N - H _A (Å)	O - H _B (Å)	N - H _B (Å)
CH ₃	0,970	2,335	1,657	1,030
H	0,970	2,319	1,645	1,030
NO ₂	0,976	2,098	1,654	1,038

CONCLUSION

The free energy analysis of the data shows that for all substituents analyzed, the A structures are the most stable. Comparing the free energy amounts, it can see that the stability increases in the following order: CH₃ > H > NO₂. Particularly, for –NO₂ as substituent, more effective hydrogen bonding approximate the free energy of both structures.

ACKNOWLEDGMENTS

Authors acknowledge the financial support provided by FAPESP, CAPES and CNPq.

- Hammes-Schiffer, S. *Acc. Chem. Res.* **34**, 273–281 (2001).
- Siegbahn, P. E. M. & Blomberg, M. R. A. *Chem. Rev.* **110**, 7040–7061 (2010).
- Yan, S., Kang, S., Hayashi, T., Mukamel, S. & Lee, J. Y. *J. Comput. Chem.* **31**, 393–402 (2010).

Interações estereoeletrônicas e efeito Perlin em 2-flúor- cicloexanonas e cicloexanotionas

Fátima M. P. de Rezende^a (PG), Matheus P. Freitas^a (PQ), Teodorico C. Ramalho^a (PQ)

^a Universidade Federal de Lavras, Departamento de Química CP 3037, 37200-000, Lavras, MG, Brasil

Palavras Chave: Efeito Perlin, Repulsão Estérica, Constante de Acoplamento, Cicloexanonas, Cicloexanotionas.

INTRODUÇÃO

É bem conhecido que constantes de acoplamento spin-spin são cruciais para determinar a estrutura e a estereoquímica das moléculas.¹ O efeito Perlin refere-se ao menor valor da constante de acoplamento spin-spin $J_{C-H_{axial}}$ em comparação com o correspondente $J_{C-H_{eq}}$ em anel de seis membros.¹ Nesse contexto, o objetivo do presente trabalho é avaliar a constante de acoplamento J_{C-F} (axial e equatorial) com base em parâmetros de interações estereoeletrônicas para as moléculas da Figura 1.

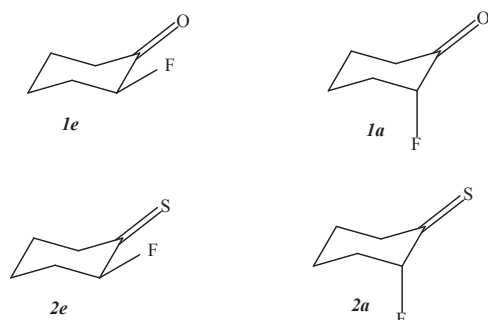


Figura 1. Estruturas estudadas computacionalmente.

METODOLOGIA

Cálculos de otimização e NBO com deleção de todos os orbitais antiligantes e de Rydberg foram realizados em nível B3LYP/aug-cc-pVDZ e os cálculos de constantes de acoplamento foram realizados em nível ω B97X-D/6-311+g(d,p). O efeito do solvente (água e DMSO) foi incorporado pelo modelo IEFPCM.

RESULTADOS E DISCUSSÃO

A molécula **2** apresenta maior estabilidade da forma axial em relação à equatorial em razão da repulsão entre os átomos volumosos S e F_{eq} . A estabilidade é dada devido a interação $\pi_{CS} \rightarrow \sigma^*_{CF}$, que é de 5,4 kcal.mol⁻¹. Valores de $^1J_{C-F}$ também foram maiores para os conformeros **2** ao invés dos conformeros de **1**, uma vez que para **2** a ligação vizinha é C=S, mais polarizável que C=O, dando origem ao maior valor de $^1J_{C-F}$.² Os cálculos foram

efetuados em gás, DMSO e água, porém não se obteve diferença significativa entre os três meios.

Tabela 1. Dados de $^1J_{C-F}$. Os dados separados por parênteses/ ponto e vírgula foram efetuados no gás, DMSO e água, respectivamente.

Conf	$^1J_{C-F}$
1e	(-185,7); (-185,6); (-185,6)
1a	(-168,0); (-168,2); (-168,2)
2e	(-212,4); (-212,4); (-212,4)
2a	(-207,9); (-208,1); (-207,9)

Para todas as estruturas observou-se $|^1J_{C-X_{axial}}| < |^1J_{C-X_{equatorial}}|$, Tabela 1, fornecendo evidências da manifestação do efeito Perlin. Segundo a literatura¹, dados experimentais de $^1J_{C-F}$ para o 2-flúor-4-terc-butilcicloexanona foram de -190,6 Hz para $C-F_{eq}$ e -176,5 Hz para $C-F_{axial}$, os quais estão bem próximos dos nossos dados teóricos, reportados na Tabela 1 para **1e** e **1a**.

CONCLUSÃO

Os cálculos de constante de acoplamento apontaram que derivados halogenados de cicloexanonas e cicloexanotionas podem manifestar o efeito Perlin. $\pi_{CS} \rightarrow \sigma^*_{CF}$ modula o efeito Perlin e é a principal interação responsável na estabilidade dos conformeros. O efeito do solvente sobre os valores de constante de acoplamento CF RMN foi desprezível.

AGRADECIMENTOS

Os autores agradecem a FAPEMIG e o CNPq pelo suporte financeiro e a CAPES pela bolsa de estudos de F.M.P.R.

REFERÊNCIAS

- SILLA, J. M.; FREITAS, M. P.; CORMANICH, R. A.; RITTNER, R. The reverse fluorine Perlin-like effect and related stereoelectronic interactions. *The Journal of organic chemistry*, v. 79, n. 13, p. 6385-6388, 2014.
- FREITAS, M. P.; RAMALHO, T.C. Princípios de estrutura eletrônica em orbitais em química orgânica. Lavras: Ufla, 2013, 126 p.

Estudo comparativo entre clorinas com diferentes substituintesF.C.T. Antonio^a (PG), Paula Homem-de-Mello^b (PQ)^a Universidade Federal do ABC; e-mail: fcesarta@gmail.com ^b paula.mello@ufabc.edu.br

Keywords: terapia fotodinâmica, PDT, teoria do funcional da densidade, clorinas.

INTRODUÇÃO

Neste trabalho foram empregados cálculos com base na teoria do funcional da densidade (DFT) para avaliar os efeitos de diferentes substituintes nas propriedades eletrônicas de clorinas não complexadas. Estas moléculas podem ser empregadas na terapia fotodinâmica, transformando a energia luminosa em energia química para induzir morte celular.

Nessa perspectiva, foi realizado um levantamento de moléculas e realizados cálculos baseados na teoria do funcional da densidade (DFT) de forma a tentar estabelecer uma relação da estrutura desses compostos com propriedades experimentais de interesse.

MÉTODOS

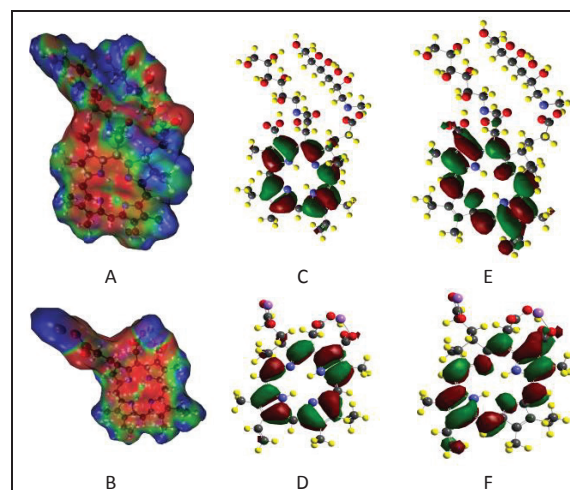
As estruturas das moléculas selecionadas foram otimizadas, utilizando o software Gaussian 09 com o funcional B3LYP e a base 6-311G (d, p). A escolha da base e funcional deveu-se à boa correlação entre os resultados obtidos em trabalhos anteriores. Entre as propriedades calculadas nos concentramos naquelas que podem auxiliar na avaliação de compostos para aplicação em terapia fotodinâmica, como momento de dipolo, cargas atômicas, a superfície de potencial eletrostático, espectros de absorção e orbitais moleculares envolvidos.

RESULTADOS E DISCUSSÃO

As moléculas do estudo foram selecionadas atentando-se à necessidade de que já houvessem anterior síntese e resultado de concentração citotóxica (IC₅₀) em condições comparáveis para que assim a viabilidade sintética e o IC₅₀ pudessem nortear as discussões e possíveis correlações com as observáveis computacionais.

Dentre as moléculas estudadas, são apresentados aqui alguns resultados obtidos para duas clorinas: (i) CloA detentora de IC₅₀ de 18 mg.mL⁻¹ e a CloE6 com IC₅₀ de 32 mg.mL⁻¹.

Ao observar que ambas possuem a transição HOMO-LUMO como principal excitação na banda de interesse para a terapia e densidade de carga variando no mesmo sentido nesta transição (na direção dos nitrogênios livres do anel central), a carga efetiva no anel clorínico e a carga nestes mesmos átomos se reduz, o que pode ser um dos responsáveis das diferenças de citotoxicidade. Ou seja, o anel menos carregado (-1,14 para CloA e -1,47 para CloE6) pode estar permitindo a aproximação do oxigênio molecular, que é apolar, permitindo a transferência de carga e posterior formação de espécies reativas.



Figuras: distribuição de carga da (A)CloA, (B)CloE6; HOMO de (C) CloA e (D) CloE6; e LUMO de (E) CloA e (F) CloE6.

CONCLUSÕES

As características que se relacionam com a transferência de energia são de interesse para a aplicação dessas moléculas em terapia fotodinâmica. Os resultados apresentados aqui para duas das moléculas estudadas indicam que há correlação entre o potencial de retirada de carga do núcleo do anel clorínico com o IC₅₀.

AGRADECIMENTOS

DFT study of Li, Na and K positions in mordenites: implication for the adsorption properties

Felipe de S. Vilhena^a (PG), Ramiro M. Serra^b (PQ), Alicia V. Boix^b (PQ), Glaucio Braga^a (PQ), José Walkimar Carneiro^a (PQ)
vilhenafs@gmail.com

^aInstitute of Chemistry, Universidade Federal Fluminense (UFF), Niterói, Brazil

^bInstituto de Investigaciones en Catálisis y Petroquímica, Santa Fe, Argentina

Keywords: mordenite, aluminium distribution, exchangeable ions, periodical calculation

INTRODUCTION

Zeolites are natural or synthetic microporous materials composed of tetrahedral $[\text{SiO}_4]$ and $[\text{AlO}_4]^-$ unities used in a broad range of processes¹. The substitution of silicon (Si^{4+}) for aluminium (Al^{3+}) causes a negative charge in the structures which is compensated by the presence of exchangeable cations. An important parameter in zeolites is the Si/Al ratio which is easy to control experimentally, whereas the exact position of Al atoms in the framework and, consequently, of the cations is much more difficult. The alkaline cations in the zeolites influences the adsorption properties and their positions are strongly related to the Al distribution. In this work we performed periodic calculations of Li, Na and K mordenites with Si/Al ratio of 5 and 11. The aim of this work is to describe the preferential positions of the alkaline cations and their effects on the adsorption properties.

METHODS

A hydrated crystalline mordenite structure was obtained from the database of zeolite structures². Two homogeneous Al distribution were assumed, according to the Lowenstein rule. Optimizations of the $\text{X}_8\text{Al}_8\text{Si}_{40}\text{O}_{96}\cdot 8\text{H}_2\text{O}$, $\text{X}_8\text{Al}_8\text{Si}_{40}\text{O}_{96}$ and $\text{X}_4\text{Al}_4\text{Si}_{44}\text{O}_{96}$ ($\text{X} = \text{Li}^+$, Na^+ and K^+) structures were performed using the cp2k program at periodical level (1x1x1) with the cell parameters $a = 18.256$; $b = 20.534$; $c = 7.542$ Å and $\alpha = \beta = \gamma = 90^\circ$. The plane wave method (PAW) with PBE exchange-correlation functional and the Ahlrichs-VDZ basis set was used.

RESULTS AND DISCUSSION

Optimization of Li+-MOR, Na+-MOR and K+-MOR (Si/Al=5) showed three preferential positions for the alkaline cations. In the hydrated

mordenites the cations surrounded by solvating water molecules prefer the lateral cavity (Fig. 1a). In the absence of water the alkaline cations moved to the main cavity leading to a third position (Fig. 1b). The alkaline cations move to the proximity of the Al atoms.

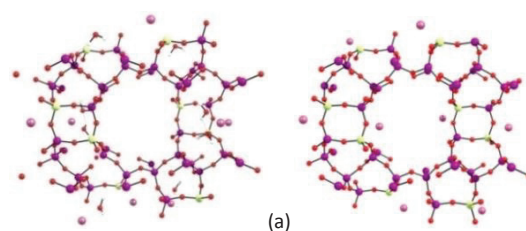


Figure 1. Periodical optimization (1x1x1) of Na⁺-mordenites. (a) $\text{Na}_8\text{Al}_8\text{Si}_{40}\text{O}_{96}\cdot 8\text{H}_2\text{O}$ and (b) $\text{Na}_8\text{Al}_8\text{Si}_{40}\text{O}_{96}$ (PAW/PBE/Ahlrichs-VDZ basis set).

In the K^+ -MOR structure, the Al-O-Si angles suffered bend to 129, 130, 157 and 157° compared its in the Na^+ -MOR and Li^+ -MOR. An alignment of the K atoms with the lateral cavity oxygen atom was observed. Although it has been suggested that the Al positions are controlled by experimental conditions³ our theoretical calculation of $\text{Li}_4\text{Al}_4\text{Si}_{44}\text{O}_{96}$ and $\text{Na}_4\text{Al}_4\text{Si}_{44}\text{O}_{96}$ (Si/Al=11) showed that alkaline cations prefer the lateral cavity by 27.3 and 39.0 kcal mol⁻¹, respectively. In the Na^+ -MOR, the $[\text{AlO}_4]^-$ site in the lateral cavity had an increase in the negative charge (-0.58) compared to its in the hydrated structure (-0.38).

CONCLUSIONS

The DFT periodical calculation results of the alkaline cations position is in agreement with the experimental data. Understanding the effects that the exchangeable cations causes in the structural and electronic properties of mordenites could be useful to preview the adsorption phenomena and to the developing of functional materials. The

Revisiting Cyclobutadiene: Insights from Valence Bond Theory under the Quantum Interference Perspective

Felipe Fantuzzi^a (PG), T. M. Cardozo^a (PQ), Marco A. C. Nascimento^a (PQ)

^a Dpto. Físico-Química, Instituto de Química, Universidade Federal do Rio de Janeiro

Keywords: Chemical Bond Theory, Generalized Valence Bond, Interference Energy, Molecular Structure, Cyclobutadiene

INTRODUCTION

Cyclobutadiene is one of the most intriguing systems in chemistry. For many decades it has been the focus of a great diversity of experimental and theoretical studies. Despite its apparently simple electronic structure, interesting and unexpected features were identified since the early works. Although it is widely accepted that the majority of its peculiar properties are due to a combination between electronic (antiaromaticity?) and structural (high angular strain) effects, their relative contributions and origin are still subjects of research.¹

METHODS

The Generalized Product Function Energy Partitioning (GPF-EP) method²⁻⁶ has been applied for the description of the cyclobutadiene molecule. The influence of quasi-classical and quantum interference contributions on each chemical bond of the system were analyzed along the automerization reaction coordinate for the lowest singlet and triplet states. In the GPF-EP ansatz, the total energy of the system can be separated as follows:

$$E[tot] = E[ref] + E[x] + E[I] + E[II] \quad (1)$$

where $E[ref]$ is the total reference energy, $E[I]$ and $E[II]$ are the first and second-order interference energies respectively, and $E[x]$ is the total intergroup exchange energy, which arises from the antisymmetrization of the GPF wave function.

RESULTS AND DISCUSSION

The results show that the interference effect reduces the electronic energy of the singlet cyclobutadiene relative to the second-order Jahn-Teller distortion, which takes the molecule from a D_{4h} to a D_{2h} structure. Our results also suggest that the π space of the ${}^1B_{1g}$ state of the square cyclobutadiene is composed of a weak 4c-4e

bond, while the ${}^3A_{2g}$ state has a 4c-2e π bond (Figure 1). Finally, we also show that, although strain effects are non-negligible, the thermodynamics of the main decomposition pathway of cyclobutadiene in the gas-phase is dominated by the π space interference.

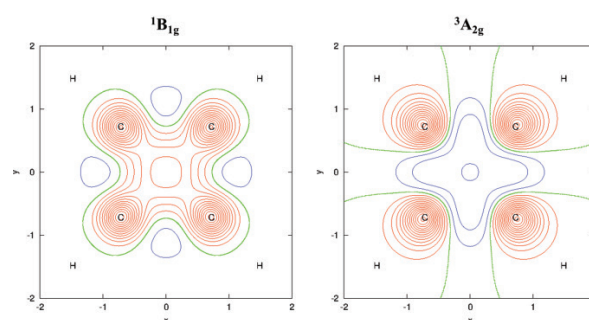


Figure 1. Interference density profile of the π space of singlet and triplet cyclobutadiene.

ACKNOWLEDGMENTS

The authors are grateful for the support given from CAPES, FAPERJ, and CNPq.

¹ J. I.-C. Wu, Y. Mo, F. A. Evangelista, P. v. R. Schleyer., *Chem. Comm.*, 48, 8437, (2012).

² T. M. Cardozo, M. A. C. Nascimento., *J. Chem. Phys.*, 130, 104102, (2009).

³ F. Fantuzzi, T. M. Cardozo, M. A. C. Nascimento. *Phys. Chem. Chem. Phys.*, 14, 5479, (2012).

⁴ T. M. Cardozo, F. Fantuzzi, M. A. C. Nascimento. *Phys. Chem. Chem. Phys.* 16, 11024, (2014).

⁵ F. Fantuzzi, M. A. C. Nascimento, *J. Chem. Theory Comput.*, 10, 2322, (2014).

⁶ F. Fantuzzi, T. M. Cardozo, M. A. C. Nascimento. *J. Phys. Chem. A*, 119, 5335, (2015).

Dimerização de Propano em Zeólitas Contendo Gálio

Felipe M. Fernandes¹ (IC), Márcio S. Pereira^{1,*} (PQ), Marco A. C. Nascimento²

¹DEQUIM/UFRRJ; ²IQ/UFRRJ;
*msoares@ufrj.br

Palavras Chave: Zeólita, Propano, Dimerização

INTRODUÇÃO

A reforma catalítica das naftas para produzir hidrocarbonetos aromáticos é um processo industrial amplamente utilizado.¹ Enquanto esta tecnologia está baseada na conversão do carbono C6+ parafínico em aromático, o uso de gás liquefeito de petróleo de baixo custo na dehidrociclodimerização com uso de zeólitas (em particular as que contém Gálio), gera uma nova forma de produção destes hidrocarbonetos.

A introdução de espécies metálicas em zeólita H-MFI fornece um acréscimo à atividade e à seletividade da aromatização das reações.² O uso de gálio parece ser preferencial às aplicações industriais devido à alta estabilidade do Gálio substituído na zeólita sobre certas condições de operação.³ Contudo, muitos aspectos do mecanismo de reação ainda não foram determinados.

MÉTODOS

A zeólita foi modelada pelo aglomerado T5 (com 5 átomos tetraédricos – Al, Si) e também pelo aglomerado T22 (com 22 átomos tetraédricos - Al, Si) que consegue reproduzir melhor os efeitos de cavidade. Todos os cálculos foram realizados através do programa Jaguar com o funcional de densidade B3LYP e base LACVP.

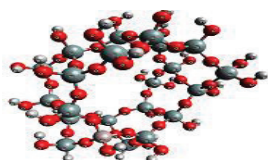


FIGURA 1: T22

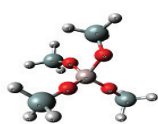


FIGURA 2: T5

RESULTADOS E DISCUSSÃO

As energias das estruturas otimizadas de reagentes e produtos (incluindo a energia de ponto zero) com o aglomerado T5 segue na tabela 1. Foi feito o cálculo de frequência a fim de confirmar

que as estruturas eram mínimos na superfície de energia potencial.

Tabela 1: Energias Relativas

Reagentes	Energia Relativa (kcal/mol)
T5 – Propano (C1)	0,4
T5 – Propano (C2)	0

Produtos	Energia Relativa (kcal/mol)
T5 – Hexano (C1)	-14,6
T5 – 2,3-Dimetil-Butano (C1)	-13,2
T5 – 2-Metil-Pentano (C1)	-12,5
T5 – isoMetil-Pentano (C2)	-17,7

*Onde C1 representa o hidrocarboneto ligado à zeólita através do carbono primário e C2 quando o hidrocarboneto está ligado à zeólita através do carbono secundário.

** Energia Relativa ao T5 – Propano (C2), contemplando, além da energia eletrônica, a energia de ponto zero.

É possível observar que todos os produtos são mais estáveis que os reagentes e que dentre os produtos, o mais estável é o T5 substituído com o iso-metilpentano.

CONCLUSÕES

Foi estudada a dimerização de propano em zeólitas contendo Gálio. Foram obtidas 4 possíveis produtos sendo o mais estável o T5 isometil-pentano. Estão sendo finalizados os cálculos com o aglomerado T22, incorporando o efeito da cavidade.

AGRADECIMENTOS: FAPERJ CNPq INOMAT

- (1) Seddon, D. Catal. Today 1990, 6, 351.
- (2) Brabec, L.; Jeschke, M.; Meusinger, J. Appl. Catal., A 1998, 167, 309.
- (3) Mowry, J. R.; Anderson, R. F.; Johnson, J. A. Oil Gas J. 1985, 83, 128.

Efeito da excitação molecular sobre a transferência de energia roto-vibracional em colisões Ar+Cl₂, Ar+HCl e Ar+CO

Felipe S. Carvalho¹, Emilio Borges¹, João P. Braga²

¹Universidade Federal de Viçosa, Av. P.H. Rolfs, s/nº, 36570-000, Viçosa, Minas Gerais, Brasil

²Universidade Federal de Minas Gerais, Av. Presidente Antônio Carlos, 6627, 31270-901, Belo Horizonte, Minas Gerais, Brasil
 felipe.s.silva@ufv.br

Palavras-chave: Energia, Colisões, Coriolis

INTRODUÇÃO

A interação roto-vibracional, também chamada acoplamento de Coriolis tem sido frequentemente investigada em processos espectroscópicos e de transferência de energia¹. A compreensão do acoplamento de Coriolis tem se mostrado relevante, por exemplo, para a descrição de mecanismos envolvendo reações de interesse ambiental e tecnológico². No presente trabalho relata-se o papel desta interação para a transferência de energia em processos não reativos envolvendo os sistemas Ar+CO, Ar+HCl e Ar+Cl₂.

METODOLOGIA

Utilizou-se uma metodologia semi-clássica em que as equações dinâmicas são clássicas e as condições iniciais quantizadas. Os potenciais utilizados foram o de Morse (intramolecular) e Lennard-Jones (intermolecular). As condições iniciais foram obtidas por meio das energias espectroscópicas e de um conjunto de coordenadas cartesianas acopladas aos modos normais. Desta forma foi possível analisar a transferência de energia para diferentes estados quânticos. Os cálculos foram realizados com um algoritmo desenvolvido pelo grupo e foram computadas 5000 trajetórias para obtenção dos valores médios da energia transferida.

RESULTADOS E DISCUSSÕES

Notam-se algumas tendências em todos os sistemas: a variação de energia aumenta com o aumento do número quântico rotacional, salvo para a energia colisional de 0.2 eV para o CO; na medida em que o momento de inércia aumenta observa-se uma diminuição da energia transferida. Observou-se a mesma tendência para os estados excitados vibracionalmente. Também observou-se que excitando-se as moléculas vibracionalmente a

energia transferida aumenta. Esses efeitos dos números quânticos sobre a quantidade de energia transferida para a componente de Coriolis já foi observado para outros sistemas¹.

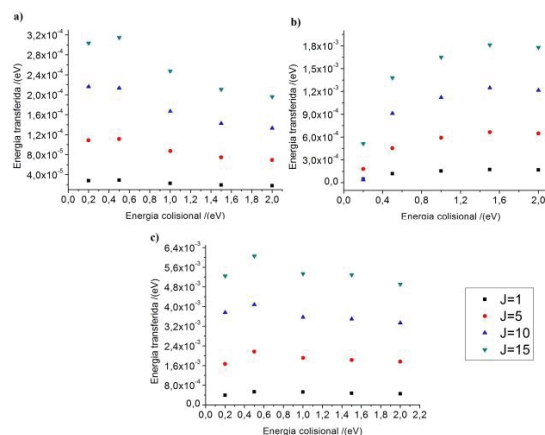


Figure 1. Transferência de energia para números quânticos $N=0$ e diferentes valores de J a) Ar+Cl₂ b) Ar+CO c) Ar+HCl.

CONCLUSÕES

Esses resultados preliminares mostram que os diferentes estados excitados das moléculas influenciam na transferência de energia roto-vibracional (ou Coriolis) aparentemente em concordância com um padrão que está sendo analisado no momento. Um próximo passo desse estudo será além da compreensão do padrão mencionado anteriormente, a análise da dependência do acoplamento de Coriolis com o número de modos normais.

REFERÊNCIAS

- ¹ E. BORGES, G. G. FERREIRA, J. P. BRAGA, J. C. BELCHIOR, *Journal of Quantum Chemistry*, **2006**, 106, 13.
- ² G. LIN, J. ATKINSON, *Dynamics of Atmospheres and Oceans*, **2000**, 31, 247-269.

Estudo Mecanístico sobre a *N*-acilação de Aminas por Ácidos Carboxílicos Catalisada por $ZrCl_4$

Felipe V. Z. Assad (PG), Fabrício R. Sensato (PQ)

Universidade Federal de São Paulo, UNIFESP, Campus Diadema. e-mail felipe.assad@globocom

Palavras-chave: *N*-acilação de aminas, Ligação Amídica, $ZrCl_4$, Cálculos de Estrutura Eletrônica

INTRODUÇÃO

A formação da ligação amídica através da *N*-acilação de aminas por ácido carboxílico é um processo que exerce em química orgânica. Entretanto, a união destes dois grupos funcionais não ocorre à temperatura ambiente e requer temperaturas da ordem de 160-180 °C.¹ Em 2012, Williams e colaboradores² reportaram um inédito e green protocolo de síntese de amidas via a reação direta de aminas e ácidos carboxílicos, catalisada por tetracloreto de zircônio ($ZrCl_4$). Não obstante a proeminência do referido procedimento, nenhuma explanação pormenorizada sobre o mecanismo molecular da reação tem sido oferecida. Assim, esse estudo tem como objetivo caracterizar computacionalmente o mecanismo de formação da ligação amídica através da *N*-acilação de aminas por ácidos carboxílicos catalisada por $ZrCl_4$.

MÉTODOS

Os mecanismos reacionais foram investigados em nível DFT/B3LYP em que o átomo de zircônio foi descrito pelo conjunto de base LANL2DZ e os demais átomos pelo conjunto de base *standard* 6-311+G(2df,2p). Estruturas de equilíbrio e de transição foram caracterizadas por cálculos de frequência vibracional. Efeitos de solvente foram descritos pelo modelo SMD. Os cálculos foram realizados com o programa Gaussian09.

RESULTADOS E DISCUSSÕES

Empregando-se a metilamina e o ácido fórmico, respectivamente, como modelos químicos para aminas e ácidos carboxílicos, sete mecanismos de reação foram investigados.

A Figura 1 ilustra o perfil energético para o mecanismo mais favorecido cineticamente (dentro os investigados), o qual é constituído pelas seguintes etapas: i) complexação entre o ácido fórmico e o catalisador levando à formação do aduto ($HCOOH$)- $ZrCl_4$; ii) ataque nucleofílico da

metilamina à carbonila do aduto ($HCOOH$)- $ZrCl_4$, via **TS1**, o qual conduz à formação do intermediário **I(1)**; iii) **I(1)** reage com uma molécula adicional de ácido fórmico, via **TS2**, o qual se decompõe em uma molécula de ácido fórmico e em um aduto entre o metilaminometanodiol e o $ZrCl_4$, **I(2)**; iv) **I(2)** sofre uma reação de desidroxilação, via **TS3**, formando assim duas espécies iônicas: a *N*-metilformamida protonada e o $ZrCl_4$ hidroxilado aniônico, e v) transferência de próton entre as espécies iônicas, via **TS4**, conduzindo à formação da amida.

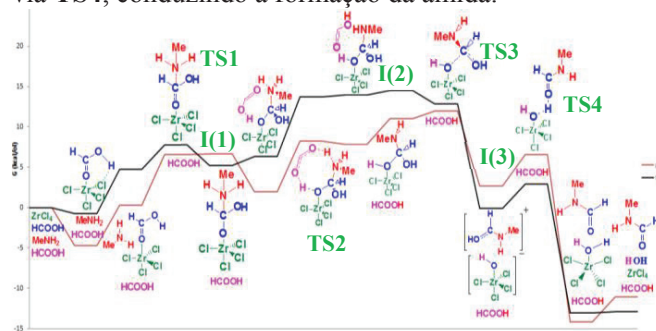


Figura 1. Perfil energético para a reação de formação da ligação amídica pela reação direta entre a metilamina e ácido fórmico, catalisada por $ZrCl_4$. O perfil energético em vermelho se refere ao processo livre de solvente, enquanto a linha negra, em meio de tolueno.

CONCLUSÃO

O mecanismo reacional cineticamente mais favorecido de formação da ligação amídica via reação direta, catalisada pelo $ZrCl_4$, entre o ácido fórmico e a metilamina envolve cinco etapas e exige uma energia livre de ativação de 12,0 kcal/mol em fase gasosa e 14,6 kcal/mol quando em tolueno.

AGRADECIMENTOS

CAPES

¹E. Valeur, M. Bradley, Chem. Soc. Rev. 38, 606, (2009).

²C.L. Allen, A.R., J.M. Chhatwal, J.M.J., Chem. Commun. 48, 666, (2012).

O Energetic and structural profile of liquid phase dimers of the green-solvent Gamma-valerolactone (GVL)

Felippe M. Colombari (PG), Luiz Carlos G. Freitas (PQ)

Depto. de Química - Centro de Ciências Exatas e Tecnologia -Universidade Federal de São Carlos
colombarifm@hotmail.com

Keywords: Green Chemistry, Gamma-valerolactone, Modeling of Greener Solvents, Chiral Solvents

INTRODUCTION

In the past years, the use of Gamma-valerolactone (also known as GVL) as solvent in chemical processes has presenting an increasing interest due to its chemical and environmental friendly properties. In this work an optimized force field was parameterized to reproduce available experimental data for the liquid phase. Chirality effects were also investigated. The simulations were performed using Metropolis Monte Carlo (MMC) methodology.

METHODS

The liquid phase of both R and S GVL pure isomers and its racemic mixture were studied. From an equilibrated simulation box containing 500 molecules and using periodic boundary conditions, the most stable R-R, S-S and R-S dimers were searched at distances corresponding to the first and second solvation shell. To ensure a representative sampling the following protocol was used: *i*) a 10k configurations trajectory was generated; *ii*) the most stable dimers were searched in the following 2k configurations. The procedure was repeated 800 times therefore generating 800 different dimers pairs. The running averages of interaction energies and angles between dipoles vectors were calculated. Calculations were performed with MMC method in the *NVT ensemble* with $T = 300$ K using DIADORIM software.¹ For comparison purposes, interaction energies were also calculated with the HF-3c method² implemented in ORCA 3.0.1 software³ for the dimers geometries obtained in the MMC search.

RESULTS AND DISCUSSION

The run average energies of R-R, S-S and R-S dimers are show in Fig. 1. One observes that R-R and S-S energies are statistically the same but the R-S dimers are energetically 10% more stable.

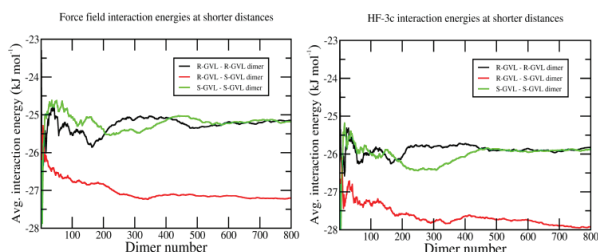


Figure 1: Average interaction energies from R-R, S-S, R-S most stable dimers extracted from MC simulations. Values were calculated using the GVL optimized force field (left) and the quantum chemistry method HF-3c (right).

Furthermore, analysis of the run average angle between dipole vectors are 147.5 degree for R-R and S-S and 153.3 degree for R-S species, showing a predominance of anti-parallel orientation leading to an

Evaluating the dependence of electronic properties of dyes with environment using a PCM-based model for lipid monolayer

Fernanda Bettanin^{a,c} (PG), Paula Homem-de-Mello^a (PQ), Benedetta Mennucci^b (PQ)

^a ABCSim, Centro de Ciências Naturais e Humanas, Universidade Federal do ABC, Brasil

^b Molecolab, Dipartimento di Chimica e Chimica Industriale, Università di Pisa, Italia

^c Instituto Tecnológico de Aeronáutica – ITA, Brazil

Keywords: IEFPCM, lipid layer, absorption, phtalocyanines, porphyrins, chlorins

INTRODUCTION

The interfacial region, as in a membrane, is a peculiar environment where many events occur, such as the absorption of ions and molecules by the cell, fundamental to the maintenance of the organism. In the case of photodynamic therapy (PDT), to understand how this environment affects the electronic absorption and emission of energy by macrocycles, as phthalocyanines (Ph) and porphyrins (Pc), is fundamental to increase the efficiency of the therapy itself.

Usually, the interaction of molecules with membranes is studied by Molecular Dynamics, but this method is computationally demanding and cannot provide electronic properties. As an alternative, this work used the Integral Equation Formalism Polarizable Continuum Model (IEFPCM) [1] to describe a lipid monolayer environment [2].

METHODS

The lipid monolayer environment was included in TD-DFT/OLYP/6-31g(d) calculations by using a PCM description based on a position dependent dielectric permittivity function (Fig. 1). Free Ph, Pc and Ch (chlorine) and different substituted or complexed Ph and Pc were studied.

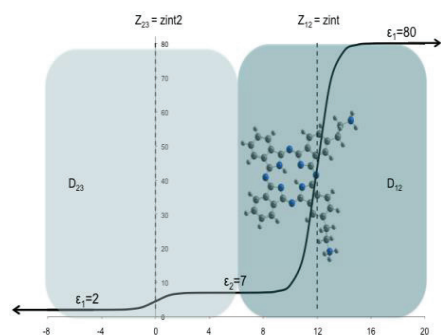


Figure 1. Position dependent dielectric permittivity used to represent a lipid monolayer. D's are the parameters that give the width of the first and second interfacial zones

RESULTS AND DISCUSSION

In a previous work [4], the absorption spectrum for the free Ph obtained with PCM-lipid layer was compared to QM/MMPol and experimental data. Both theoretical approaches showed satisfactory results.

So, we have extended the methodology to substituted and complexed macrocycles and the shift induced by the dielectric difference along the z axis of the simulated lipid monolayer was analyzed. For the free Ph and substituted with 1 or 2 amines in cis position, the Q_x band shift were about 3 nm and for Q_y band, 6 nm. For the trans substitution, the Q_x band shift was 25 nm and for Q_y band, 10 nm; and for the substitution with 3 amines, both bands shift about 10 nm. Free Pc and Ch (chlorine) had 6 nm of shift on Q_x and 5 nm on Q_y band. Pc complexed with Al⁺³ and Si⁺⁴ with methyl as axial ligand, was shifted by 5 nm, while for the Zn-Pc insignificant effect was observed. The band for Si-Pc with chloride as axial ligand shifted 10 nm and with phenyl, 74 nm.

CONCLUSIONS

The method here investigated was able to provide the shift in the absorption spectra of Pc, Ph and Ch in a dielectric gradient reproducing a lipid monolayer. In general the shift along the lipid monolayer z axis is not so significant and may not interfere in the PDT efficiency of the studied dyes, except for the Pc complexed with Si⁺⁴ with phenyl as axial ligand.

ACKNOWLEDGMENTS

FAPESP (2010/19790-3; 2012/50680-5), CNPq, CAPES and UFABC.

¹ E. Cancès, B. Mennucci, J. Tomasi, J. Chem. Phys. 107, 3032 (1997);

² L. Frediani, *et al.* J. Chem. Phys. 120, 3893 (2004);

³ A. B. Ormond and H. S. Freeman, Materials, 6, 817, (2013).

⁴ F. Bettanin, S. Juronovich, B. Mennucci, P. Homem-de-Mello, WATOC2014, PP078 (2014).

Obtenção de parâmetros cinéticos de reações de oxidação do felandreno em fase gasosa

Fernando Renato Vicente Ferreira^a, Leonardo Baptista^b

^a Instituto de Química, Universidade Estadual do Rio de Janeiro, Rua São Francisco Xavier, 524 – Maracanã, Rio de Janeiro, RJ, Brasil

^b Faculdade de Tecnologia, Departamento de Química e Ambiental, Universidade Estadual do Rio de Janeiro, Rodovia Presidente Dutra Km 298, Resende, RJ, Brasil

Palavras chave: felandreno, ozonólise, terpenos, cinética

INTRODUÇÃO

O estudo cinético das reações de oxidação com compostos insaturados, é útil como base de dados para criação de modelos cinéticos, os quais são usados para descrever a qualidade de ar urbano e rural. Em um nível mais fundamental, os dados fornecem algumas pistas para o mecanismo da reação e contribuem para um melhor entendimento da química da atmosfera, incluindo a formação de oxidantes em fase gasosa e a produção de aerossóis. A cinética das reações de ozônio e radical OH com alcenos de estrutura simples tem sido intensivamente estudada e para estes compostos, os dados estão sempre sendo atualizados. Entretanto, não existem muitos estudos para os alcenos de alta massa molar, apesar da sua importância para a química atmosférica, como precursores de compostos carbonílicos, ácidos carboxílicos, material particulado e nitrato de peroxiacetila, quando radicais nitratos estão presentes no meio.

METODOLOGIA

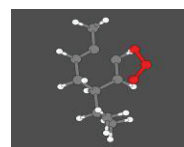
A etapa do trabalho consiste em iniciar a descrição do mecanismo de ozonólise do felandreno através do cálculo dos coeficientes de velocidade para decomposição dos POZs e dos intermediários Criegee, através do software Gabedit, e calculados pelo Gaussian 09, utilizando os funcionais BHandHLYP, B3LYP e PBE1PBE, e nas bases 6-311G e 6-31G.

RESULTADOS E DISCUSSÃO

Geometrias otimizadas. O α -felandreno e o β -felandreno são isômeros e espera-se reagir de forma semelhante, na presença de ozônio. Uma investigação conformacional foi a rotação ao longo do ângulo diedro $\theta_{C3C4C7C8}$ das moléculas desses isômeros e mostraram que o ângulo diedro em ambas as moléculas pode girar livremente porque a altura da barreira conformacional das mudanças é inferior a $1,0 \text{ kcal mol}^{-1}$.

	Reagentes	TS-POZ1	Barreira	POZ1	Termodinâmica
E	-615,844	-615,846	-0,8285	-615,961	-73,3927
E + ZPE	-615,594	-615,593	0,593624	-615,704	-68,5875
H	-615,579	-615,579	-0,00753	-615,69	-69,8205
G	-615,653	-615,633	12,28288	-615,742	-56,0465

Tabela com os resultados obtidos do POZ1, a partir da reação com o β -felandreno com seu estado de transição, em nível BHandHLYP/6-311G(d,p)



Geometria otimizada do estado de transição do POZ1 da reação de ozonólise do felandreno, em nível BHandHLYP/6-311G(d,p)

CONCLUSÃO

Os passos iniciais de reação para a ozonólise do felandreno foram estudados, a termoquímica e cinética. Foram avaliados os parâmetros que regem o processo. A formação de POZs é altamente exotérmica, e em todo o PES transição estrutura parece ser solto e permite a formação de um precomplexo. A complexidade do PES requer um método mais preciso para descrever as barreiras de energia para a formação de POZs. Os funcionais PBE1PBE e B3LYP descrever corretamente o geometrias de cada estrutura que participa no mecanismo, mas não conseguem prever corretamente os parâmetros termoquímicos e cinéticos. O funcional BHandHLYP proporciona uma descrição adequada para o passo limitante da velocidade e do mecanismo, podendo ser útil para a estimativa da taxa de coeficientes sem um elevado custo computacional.

AGRADECIMENTOS

CAPES, CNPq e FAPERJ

1) BAPTISTA, L.; PFEIFER, R.; SILVA, E.C.; ARBILLA, G. *Kinetics and Thermodynamics of Limonene Ozonolysis* – The Journal of Physical Chemistry, 201

A computational study of molybdates and polyoxomolybdates.

Fernando Steffler^a (PG), Hélio A. Duarte^a (PQ)

^a Grupo de Pesquisa em Química Inorgânica Teórica – GPQIT; Departamento de Química – ICEx, Universidade Federal de Minas Gerais. 31.270-901 – Belo Horizonte – MG. E-mail: Fernando.steffler@gmail.com.

Keywords: Ab Initio, Polyoxomolybdates and electronic structure.

INTRODUCTION

In the last decade the Polyoxometalates (POMs) have attracted attention as building blocks for synthesizing advanced materials¹. The polyoxomolybdates are the most studied POMs, which have been targeted for important technological applications in photocatalysis and nanotechnology². Mostly of the giant polyoxomolybdates are octahedrally coordinated by 6 oxygens. However, square pyramidal (or trigonal bipyramidal) species with 5 coordinated oxygens and tetrahedral species with 4 coordinated oxygens are common. The POMs normally possess high negative charges and are dependent of the pH of the solution^{1,2}. On the present work, the relative stability and the band gaps for the $\text{Mo}_x\text{O}_y^{6x-2y}$ ($x=1, 2, 4, 6, 7, 8; y=3, 4, 7, 12, 13, 18, 19, 24, 26$) have been calculated. The effects of the protonation of the different species have also been investigated.

METHODS

Density functional method with GGA-PBE exchange-correlation functional has been used as implemented in the deMon-2K package³. The effective core potential (ECP) for the Mo atoms has been used and DZVP basis sets for the oxygen atoms. The geometries have been fully optimized with no symmetry constraint. The relative stability was calculated based on the atomization energy taking as reference the ground state of Mo^{6+} and O^{2-} atoms.

RESULTS AND DISCUSSION

The main results are shown in the Table 1. The $[\text{Mo}_6\text{O}_{18}]$ species is the most stable. The neutral POMs are normally more stable than the charged structures. This is probably due to the fact that the solvent effects, was not taken into account in the present calculations. The band (BG) gap estimates are in the range between 1.81 eV for $[\text{Mo}_7\text{O}_{24}]^{6-}$ to 3.72 eV $[\text{Mo}_2\text{O}_7]^{2-}$. The structures investigated with more than 4 Mo present band gap between 1.81 – 3.0 eV.

Table 1. Relative Energy (RE) and Band Gap (BG) for the molybdate structures investigated.

Structure	RE in eV/at	BG in eV
$[\text{MoO}_3]$	0.67	1.91
$[\text{MoO}_4]^{2-}$	26.66	1.98
$[\text{Mo}_2\text{O}_7]^{2-}$	16.68	3.72
$[\text{Mo}_4\text{O}_{12}]$	0.01	3.07
$[\text{Mo}_4\text{O}_{13}]^{2-}$	9.52	2.94
$[\text{Mo}_6\text{O}_{18}]$	0.00	2.39
$[\text{Mo}_6\text{O}_{19}]^{2-}$	1.84	2.64
$[\text{Mo}_7\text{O}_{24}]^{6-}$	5.82	1.81
$[\text{Mo}_8\text{O}_{26}]^{4-}$	1.28	2.87

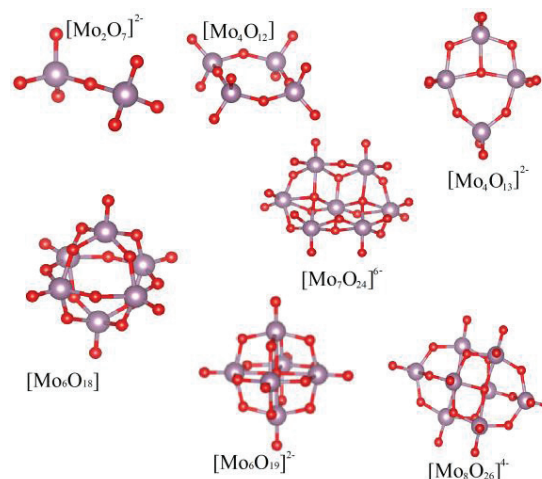


Figure 1. Optimized geometries of molybdates.

CONCLUSIONS

The multichannel reactions to form larger polyoxomolybdates have been calculated and will be discussed on detail. The effect on the protonation of the species to the BG, polarizabilities and hyperpolarizabilities will be presented.

ACKNOWLEDGMENTS

The authors are grateful for the support given from the GPQIT, FAPEMIG, CAPES, CNPQ and INCT-ACQUA.

¹ M. T. Pope, Springer-Verlag, vol 8, (1983).

² A. Davantès and G. Lefèvre, J. Phys. Chem. A, 117, 12922, (2013).

³ A.M. Koster et al, *deMon2k*, Version 3, The deMon developers, Cinvestav, Mexico City (2011).

Electronic States Generated by Single and Double Carbon Defects in Pyrene, Extended Pyrene and 7a,7z-Periacene as a Model for Graphene Sheet

Daniely V. V. Cardoso^a (PG), Adélia J. A. Aquino^b (PQ), and Hans Lischka^b (PQ), Francisco B. C. Machado^{a*} (PQ)

^a Departamento de Química, Instituto Tecnológico de Aeronáutica, São José dos Campos, SP, Brazil

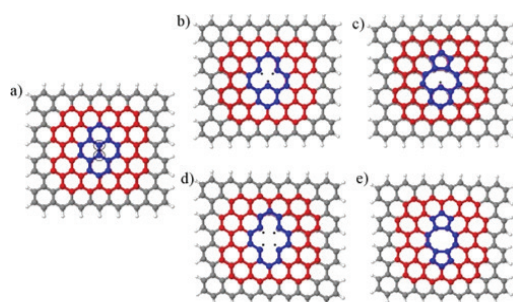
^b Department of Chemistry and Biochemistry, Texas Tech University Lubbock, USA

*fmachado@ita.br

Keywords: DFT, graphene, vacancy defects, electronic states

INTRODUCTION

Graphene consists of a single atomic layer of graphite and possesses exceptional electronic, thermal, and mechanical properties. A variety of defects can occur in graphene, often times through single or multiple vacancies of carbon atoms, yielding dangling bonds, which arise during defective growth or after irradiation of the material. The dangling bonds can associate with a multitude of closely spaced excited electronic states with different spin multiplicities, which leads to a very challenging theoretical description. This work focuses on prototypes of single and double vacancies in a graphene sheet using pyrene (blue), extended pyrene (red) and 7a,7z-periacene (gray) as model structures, as shown in Scheme 1.



Scheme 1. b,d) unrelaxed; c,e) relaxed.

METHODS

The pyrene, extended pyrene, and 7a,7z-periacene structures were optimized using the B3LYP density functional with the 6-31G* basis set. Next, the one and two innermost carbon atoms were removed from the structures. (U)DFT/B3LYP single point and geometry optimizations were performed for some low-lying electronic states with singlet and triplet multiplicities. Linear interpolation curves between the unrelaxed and relaxed structures were also performed. All calculations were carried out using the TURBOMOLE program.

RESULTS AND DISCUSSION

Recently, using pyrene as a model, we have shown^{1,2} by means of MRCI calculations, that single and double vacancy defects induce a complex set of several closely spaced electronic states leading to geometry relaxation effects with carbon-carbon bond formation. The B3LYP/6-31G* excitation energies for low-lying states in the relaxed structure are presented in Table 1.

Table 1. B3LYP/6-31G* excitation energies (eV).

State	Pyr-1C	Ext. Pyr-1C	Periac-1C
³ B ₂	0.000	0.000	0.017
¹ B ₂	0.114	0.111	0.017
³ A ₂	0.231	0.079	0.002
¹ A ₂	0.258	0.061	0.000
State	Pyr-2C	Ext. Pyr-2C	Periac-2C
¹ A _g	0.000	0.000	0.596
³ B _{2u}	0.441	1.218	1.523
¹ B _{2u}	0.479	1.435	1.595
³ B _{3u}	1.430	1.530	0.000

CONCLUSIONS

We have obtained a detailed picture of the manifold of electronic states occurring due to the removal of one and two carbon atoms from a graphene sheet based on the local environment of the defect. We found good agreement between the MRCI^{1,2} and DFT results using pyrene as a model, which give us confidence in the DFT accuracy for the investigation of larger graphene models. This will provide better insight into the embedding effects and their consequences on the electronic and geometrical structure of single and double vacancy defects.

ACKNOWLEDGMENTS

Support: FAPESP, CNPQ and CAPES.

¹ F.B.C. Machado, A.J.A. Aquino and H. Lischka, *ChemPhysChem.*, 15, 3334 (2014).

² F.B.C. Machado, A.J.A. Aquino and H. Lischka, *Phys.Chem.Chem.Phys.*, 17, 12778 (2015).

Electronic energy levels engineering of ICBA employing chemical substitutions

Eliezer Fernando Oliveira^a (PG), Lucas Cartorino Silva^b (G), Francisco Carlos Lavarda^c (PQ)

^aUNESP - Univ Estadual Paulista, POSMAT - Programa de Pós-Graduação em Ciência e Tecnologia de Materiais, Bauru, SP, Brazil

^bUNESP - Univ Estadual Paulista, Graduação em Física, Faculdade de Ciências, Bauru, SP, Brazil

^cDF-FC, UNESP - Univ Estadual Paulista, Av. Eng. Luiz Edmundo Carrijo Coube 14-01, 17033-360 Bauru, SP, Brazil.

Keywords: Fullerene Derivatives, Electronic Structure Calculation, Organic Solar Cells

INTRODUCTION

Currently, there is an intensive search for new materials to make more efficient organic solar cells. The use of chemical modifications capable of modifying the electronic properties of materials already known is an interesting approach [1,2], as it can, in principle, provide a more adequate adjustment of the frontier electronic levels while preserving properties such as solubility. Thus, we performed a theoretical study of the Indene-C₆₀-bisadduct (ICBA) (Figure 1) and 13 new derivatives obtained by substitution with electron acceptor and donor groups in order to understand how the energy levels of the frontier orbitals are modified.



Figure 1. Molecular structure of Indene-C₆₀-bisadduct (ICBA)

METHODS

Geometry optimizations and electronic Functional Theory (DFT), PBE functional, and basis set functions 6-311G(d,p). Chemical substitutions was made by replace the hydrogen atom of red point showed in Figure 1 below with chlorine (Cl), bromine (Br), fluorine (F), hydroxy (OH), cyano (CN), amino (NH₂), methyltio (SCH₃), trifluoromethyl (CF₃), methyl (CH₃), dimethylamino (N(CH₃)₂), metoxy (OCH₃), carboxy (COOH), and ethenyl (CH=CH₂). All calculations was performed by GAUSSIAN09 program.

RESULTS AND DISCUSSION

In figure 2 we show the results obtained for energies of highest occupied molecular orbital

(HOMO) and lowest unoccupied molecular orbital (LUMO). As can be observed, employing chemical substitutions allow to get a range of materials with very different electronic properties, an interesting fact for tuning the properties of the devices.

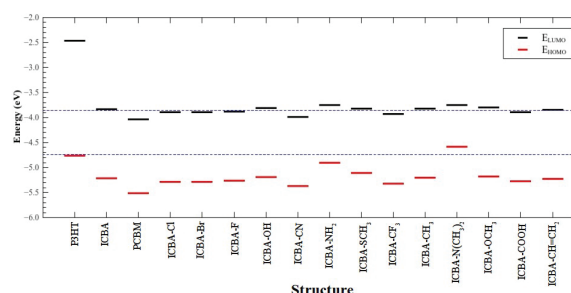


Figure 2. Electronic structure data for ICBA derivatives obtained from DFT/PBE/6-311G(d,p).

CONCLUSIONS

We show that by chemical substitutions it is possible to tune frontier electronic level energies and solubility of ICBA and find new acceptor materials that show improvements in open circuit voltage (V_{oc}) and morphology of active layer, potentially bringing better efficiencies of solar cell.

ACKNOWLEDGMENTS

We would like to thank the Brazilian agency FAPESP (proc. 2012/21983-0 and 2014/20410-1) for financial support and the resources supplied by the Center for Scientific Computing (NCC/GridUNESP) of the São Paulo State University (UNESP).

¹ E. F. Oliveira, A. Camilo-Jr., L. C. da Silva-Filho, F. C. Lavarda, *J. Polym. Sci. Part B: Polym. Phys.* 51, 842 (2013).

² E. F. Oliveira and F. C. Lavarda, *Mater. Chem. Phys.* 148, 923 (2014).

Towards Improving the Fitting Ability of NDDO Semiempirical Methods with q-Multipole-Multipole Interactions

Frederico T. Silva (PG) and Alfredo M. Simas^a (PQ)

^a *Departamento de Química Fundamental, CCEN, UFPE, 50590-470 - Recife, PE, Brazil.*

Keywords: Semiempirical models, NDDO, multipolar

INTRODUCTION

Present semiempirical methods have an important characteristic, which makes them applicable to very large systems: the NDDO approximation, which makes them scale, with traditional algorithms, with N^2 , in contrast with the N^4 scaling of Hartree-Fock-Roothaan for the calculation of the electron repulsion integrals, where N is the number of electrons. These diatomic integrals in NDDO methods are then expressed in terms of multipole-multipole interaction terms, all containing inverse square roots in their formulae².

q-Operations emerge from nonextensive statistical mechanics¹ and have been a source of investigation in deformed algebraic structures. In particular, q-deformed functions have been proven to be much more flexible and adaptable³, which makes them suitable for applications to problems where fitting is essential, such as in the development of semiempirical methods.

METHOD

We wrote a complete NDDO software from scratch, which allowed us to investigate the usage of (i) generalized q-exponentials, replacing exponentials in the overlap and core-core repulsions; (ii) q-Gaussians replacing the Gaussians in the core-core repulsion terms, and (iii) q-inverse square roots replacing inverse square roots in the multipole-multipole interactions.

As very preliminary test systems, we considered the closed shell hydrogen systems: H_2 , H_3^+ , H_4 and H_5^+ . The reference properties: total energies, fully optimized geometries, and vertical ionization potentials, were determined via GAMESS CCSD calculations with the aug-cc-pVTZ basis set.

RESULTS AND DISCUSSION

Initially, we derived the definition of the q-inverse square root, which, to the best of our

knowledge, is seemingly not otherwise available, as being:

$$\left(\frac{1}{\sqrt{x}}\right)_q = \left(\frac{3}{2} - \frac{x^{1-q}}{2}\right)^{\frac{1}{1-q}}$$

and, of course,

$$\lim_{q \rightarrow 1} \left(\frac{1}{\sqrt{x}}\right)_q = \lim_{q \rightarrow 1} \left(\frac{3}{2} - \frac{x^{1-q}}{2}\right)^{\frac{1}{1-q}} = \frac{1}{\sqrt{x}}$$

In this preliminary work, we considered a regular NDDO method, together with all fourteen different NDDO methods resulting from combinations of q-functions in the overlap, core-core repulsions (exponentials and Gaussians) and the monopole-monopole interaction term.

We parameterized all these fifteen methods for the total energies, ionization potentials and geometries of only H_2 and H_3^+ , which we took as the parameterization set. Subsequently, we used the parameters to compute the corresponding properties of H_4 , and H_5^+ systems to check the transferability of the parameters and the robustness of the methods.

Results indicated that the replacement of only the inverse square root in the monopole-monopole interaction by the q-inverse square root had a positive and significant effect on the transferability of the parameters from H_2 and H_3^+ to H_4 and H_5^+ .

CONCLUSION

Further investigation of the applicability of q-square root functions in the multipole-multipole expansions of NDDO methods for other chemical systems is therefore warranted, and is presently being carried out in our laboratories.

ACKNOWLEDGMENTS

The authors acknowledge support from CNPq, and FACEPE/PRONEX.

¹ Tsallis, C., J. Stat. Phys. **52**, 479 (1988).

Electronic structure and stability of Al_nC ($n = 1 - 7$) clusters

Gabriel F.S. Fernandes^{1,2}, Luiz F. A. Ferrão¹, Francisco B.C. Machado¹

¹Departamento de Química, - Instituto Tecnológico de Aeronáutica – São José dos Campos – SP, Brazil. ²UNESP, Guaratinguetá – SP, Brazil. email: gabrielsanzovo@hotmail.com; ferrao_lfa@yahoo.com.br; fmachado@ita.br

Keywords: Aluminum carbide, M06, DFT

Introduction

The properties of metal clusters containing few atoms are significantly different from the metallic bulk since. They show electronic, optical, and magnetic properties that do not converge monotonically to the bulk as a function of cluster size. Metal clusters show potential technological applications, like catalysts and new materials, because of the low dimensionality. Beyond the technological importance and applications in many areas of knowledge, the characterization of cluster properties are challenging. In this study, small aluminum clusters doped with one carbon atom with neutral and anionic charges were characterized. Some of them were characterized before, both experimentally and theoretically [1-2]. In these studies, anionic Al_7C presented high stability.

Methods

The electronic structure calculations were carried out using density functional theory (DFT) within the M06 approximation, and the basis sets used were aug-cc-pVTZ and 6-311++G(3df,3pd). Several starting geometries and spin multiplicities were considered to characterize the global minimum of each species. All calculations were carried out using Gaussian G09 package.

Results and discussions

The binding energies for the Al_nC ($n = 1 - 7$) clusters are presented in Figure 1.

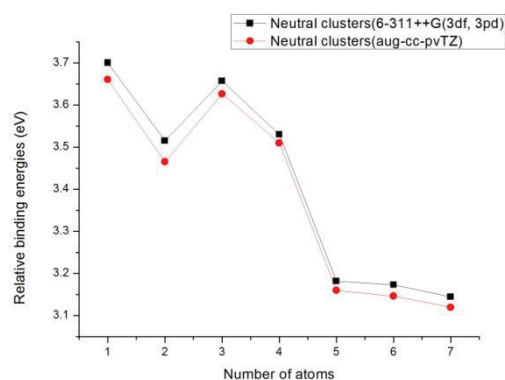


Figure 1- Binding energy trends of Al_nC ($n= 1 - 7$) obtained with M06 functional

Conclusions

The relative binding energies for the Al_nC cluster present two regions: From $n = 1$ to $n = 4$ the binding is covalent and there are hybridization processes in the carbon atom. From $n= 5$ to $n = 7$ there is a larger interaction between the aluminum atoms and the relative binding energies decrease.

ACKNOWLEDGMENTS

The authors are grateful for the support given from the FAPESP and ITA.

- [1] A. I. Boldyrev et al., J. Chem. Phys., **110**, 8980 (1999).
- [2] D. Y. Zubarev, A. I. Boldyrev, J. Chem. Phys., **122**, 144322 (2005).

Probing Cross Sections for Electron-Methyl Formate Collisions with EPolyScatD

Gabriel L. C. de Souza^a (PQ), Leonardo M. F. Oliveira^a (IC) and Wagner J. C. Sousa^b (PG)

^a Federal University of Mato Grosso, Department of Chemistry, 78060-900 Cuiabá-MT, Brazil

^b Federal University of Amazonas, ICET, 69100-000 Itacoatiara-AM, Brazil

gabriellcs@pq.cnpq.br

Keywords: Electron Scattering, Methyl Formate, Differential Cross Sections

INTRODUCTION

EPolyScatD is a series of programs for computing electron-molecule (e^- -molecule) scattering and molecular photoionization cross sections. It was originally developed by Lucchese *et al.*¹ and later modified by de Souza *et al.*² and by Lee *et al.*³ Since then, the suite of codes have become a tool capable to calculate cross sections for elastic scattering of molecules of any symmetry, at intermediate energies, with absorption effects included. During the last years, EPolyScatD has been applied to probe e^- -molecule cross sections for a variety of molecular targets.^{2,3} In the present work, as a new application, we present results of e^- -molecule cross sections computed for methyl formate (HCOOCH_3).

METHODS

The present study made use of a complex optical potential given by:

$$U_{\text{int}} = U_{\text{st}} + U_{\text{ex}} + U_{\text{cp}} + iU_{\text{abs}}$$

In our calculation, static (U_{st}) and exchange (U_{ex}) potentials are derived directly from a Hartree-Fock SCF target wavefunction. The parameter-free model potential introduced by Padiál and Norcross⁴ is used to account for correlation-polarization (U_{cp}) contributions while the model potential developed by Lee *et al.*⁵ is used for describing the absorption effects (U_{abs}).

Using the referred interaction potential, the scattering equations are solved iteratively using the Padé's approximant method, as in the manner described by Lee *et al.*³

RESULTS AND DISCUSSION

In Fig. 1 we show our calculated Differential Cross Sections (DCS) for elastic e^- - HCOOCH_3 scattering at 100 eV along with experimental data from Homem and Iga.⁶

DCS computed results are in good qualitative as well as quantitative agreement with the experimental data from Homem and Iga.⁶ This can be seen in the whole angular region covered by the experimental measurements.

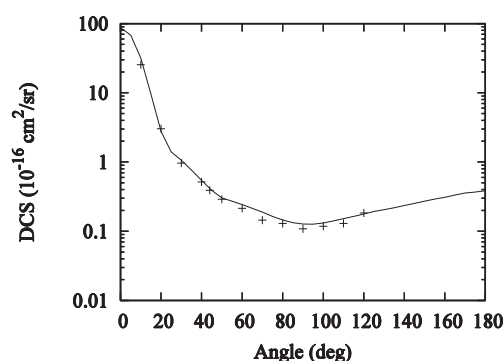


Figure 1. DCS for elastic e^- - HCOOCH_3 at 100 eV. Solid line: Present results; Crosses: Experimental data of Homem and Iga.⁶

CONCLUSIONS

The agreement between present computed results and experimental data indicates EPolyScatD can be successfully applied for probing e^- -molecule cross sections of targets belonging to the class of the esters. More results will be presented during the conference.

ACKNOWLEDGMENTS

The authors are thankful to CNPq and CAPES.

¹ R. R. Lucchese *et al.*, J. Chem. Phys., 102, 5743, (1995).

² G. L. C. de Souza *et al.*, Phys. Rev. A, 82, 012709, (2010).

³ M.-T. Lee *et al.*, J. Chem. Phys., 136, 114311, (2012).

⁴ N. T. Padiál and D. W. Norcross, Phys. Rev. A, 29, 1742 (1984).

⁵ M.-T. Lee *et al.*, J. Elec. Spectros. Rel. Phenom., 155, 14, (2007).

⁶ M. G. P. Homem and I. Iga (Private Communication) (2015).

Theoretical study on C9131 group of dyes for dye-sensitized solar cells - the effect of different solvent and different ligand groups.

Gabriel M. Zanotto¹, Josene M. Toldo (PG)¹, Paulo F. B. Gonçalves (PQ)¹.
gabriel.zanotto@ufrgs.br

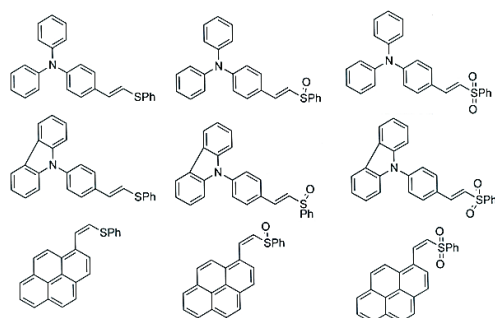
1 Universidade Federal do Rio Grande do Sul, Instituto de Química, Grupo de Química Teórica. Av. Bento Gonçalves, 9500, Porto Alegre-RS.

Keyword: TD-DFT, DSSC, Organic dye, CAM-B3LYP

INTRODUCTION

The search for efficient, low-cost and metal-free solar cells has aroused a great interest of researchers in dye sensitized solar cells. Since it is the dye that absorbs the light, generates and transports the charges, studies have focused on new conjugated organic dyes.^{1,2} In this work, a class of organic dye, namely C9131, with variations in donor and acceptor groups (Figure I), has been theoretically studied and their photophysical properties has been evaluated.

Figure I. Molecules in study.



METHODS

Time-Dependent Density Functional Theory (TD-DFT) was used to study the photophysical behavior of the molecules presented in Figure I, in the ground (S_0) and excited state (S_1). CAM-B3LYP functional was used at cc-pVDZ level for the optimization of S_0 and S_1 , and using jun-cc-pVTZ basis set for determination of the wavelength and oscillator strength of the absorption and emission. Compared to experimental data, this level of theory has described correctly these systems. The effect of solvent was evaluated by the PCM model, with acetonitrile, dichloromethane, 1,4-dioxane and ethanol as solvents.

RESULTS AND DISCUSSION

The solvent effect can be seen when comparing the difference between wavelengths of the same molecule. Blueshifts at the absorption and redshifts on the emission have been noted on all of the molecules as the solvent dielectric constant increases. Similar effects can be observed as the donor and acceptor group is changed. Comparing the change of the donor group, redshifts can be observed as the group becomes more rigid. Raising the acceptor group polarity causes redshifts to occur at the wavelength of absorption and blueshifts on the emission. These shifts can be explained as these changes vary the localization of HOMO and LUMO, which influences directly on the molecule dipole moment.

CONCLUSIONS

The positions of HOMO and LUMO and the variation in dipole moment is a strong indication for charge transfer, as it characterizes the conditions for a molecule to obtain the push-pull effect, placing C9131 and its derivatives on the list of possibilities as sensitizers for solar cells.

ACKNOWLEDGMENTS

The authors are grateful for the support given from the CAPES, CNPQ and Applied Organic Photochemistry Research Group.

¹ Saurabh Agrawal, Niall J. English, K. Ravindranathan Thampi. J. M. D. MacElroy; - Phys. Chem. Chem. Phys., 2012, 14, 12044–12056

Mariachiara Pastore, Edoardo Mosconi, Filippo De Angelis, and Michael Grätzel | - J. Phys. Chem. C 2010, 114, 7205–7212

Investigation of substitution reactions on Selenuranes relevant to their biological activity on cysteine proteases

Gabriela D. da Silva* (PG), Rodrigo L. O. R. Cunha (PQ) e Mauricio D. Coutinho-Neto (PQ)

^a *CCNH-Universidade Federal do ABC, Santo André*
mauricio.neto@ufabc.edu.br, silva.gdias@gmail.com

Keywords: DFT, Reaction Mechanism, Cathepsins and Chalcogenuranes

INTRODUCTION

Unregulated activity of cysteine proteases are related to the development of several pathologies, which makes them valuable targets for the design of inhibitors¹⁻³. Although hypervalent selenium compounds have shown potent inhibition of cysteine proteases, the mechanism of reaction is not yet well understood, and the nature of selenium reactive species in solution under physiological conditions is not known⁴. It has been proposed that the inhibition occurs through the ligand exchange reaction between enzyme's thiol group and the chalcogen atom⁴. Herein, efforts to clarify the reactivity profile of selenuranes in a multi-nucleophile medium were performed. In this approach, possible substitution reactions routes of a selenurane with H₂S, cysteine, glutathione and H₂O were studied. Effect of pH and the possibility of having water molecules explicitly participating in the reaction coordinate were also investigated.

METHODS

All optimized molecular geometries were obtained using Density Functional Theory along the B3LYP functional and 6-311+G(d) basis set using the Gaussian09 code. Reaction barrier estimates for the proposed mechanism were obtained by using relaxed geometry scans with the same basis set and functional as implemented in the Orca v3.03 code. Solvation effects were accounted for by using the SMD implicit solvent model.

RESULTS AND DISCUSSION

We found that the associative-dissociative mechanism is more favorable than the dissociative-associative mechanism for aliphatic and aromatic selenuranes. Results for the Cl⁻ by OH⁻ substitution reaction presented a barrierless path, whereas Cl⁻ by SH⁻ and OH⁻ by SH⁻

substitution have barriers. Our results suggest a two steps mechanism where the first step consists on the nucleophile attack while the second step consists on a subsequent rearrangement to seesaw geometry and departure of a leaving group. Nucleophile attack happens on the opposite side of the leaving group, except on the Cl⁻ by OH⁻ substitution reaction where the attack occurs on the same side. For OH⁻ by SH⁻ substitution reaction, a distinct oxidized intermediary is formed having Se bound to only three substituents, (CH₃)₂ and Oxygen.

CONCLUSIONS

Starting from R₂Se(Cl)₂, chlorine is rapidly substituted by OH forming a Selenodiol compound. Depending on environment conditions (low pH, excess thiol) a Selenothiol derivative can be formed with barriers in the range of 13 – 16 kcal/mol. In all cases the associative mechanism had a lower energy barrier. Changes in mechanism due to explicit water or H₃O⁺ participating in the reactive complex were minor for most systems. An exception happens for the Cl⁻ by OH⁻ substitution reaction where the explicit water has a stronger role in defining the orientation attack.

ACKNOWLEDGMENTS

The authors are grateful for the support given from CAPES and UFABC.

¹ V. Turk, V. Stoka, O. Vasiljeva, M. Renko, T. Sun, B. Turk, and D. Turk, *Biochim. et biophys. acta*, vol. 1824, no. 1, pp. 68–88, Jan. 2012.

² J. C. Powers, J. L. Asgian, Ö. D. Ekici, and K. E. James, *Chem. Rev.*, vol. 102, no. 12, pp. 4639–4750, Dec. 2002.

³ H. a Chapman, R. J. Riese, and G. P. Shi, *Annual rev. of physiol.*, vol. 59, pp. 63–88, Jan. 1997.

⁴ A. Albeck, H. Weitman, B. Sredni, and M. Albeck, *Inorg. Chem.*, vol. 37, no. 8, pp. 1704–1712, Apr. 1998.

Difusão de Pólarons em Polímeros Condutores

Gabrielle Gomes da Silva^a (IC), Pedro Henrique de Oliveira Neto^b (PQ)

Instituto de Física, Universidade de Brasília, C.P. 04455, DF, 70919-70, Brasil.

^a gabriellegomes.s@gmail.com

^b Pedrohenrique@unb.br

Palavras-chave: Polímeros condutores, Pólarons, Comprimento de difusão, Portador de carga.

INTRODUÇÃO

Polímeros condutores são utilizados na fabricação de OLED's (Organic Light Emission Diode), de OFET'S (Organic Field Effect Transistors) e dos OPV's (Organic Photovoltaic Cells). A tecnologia baseada em materiais orgânicos destaca-se devido ao baixo custo de processamento, a flexibilidade e leveza destes materiais, além do baixo impacto ambiental na sua produção em detrimento dos concorrentes inorgânicos. Para o desenvolvimento das novas tecnologias com base nestes materiais orgânicos é essencial que se conheça os mecanismos de transporte de carga dentro desses polímeros. Especificamente, saber quais os fatores que mais influenciam na condução de carga. Assim pode-se melhorar a eficiência destes materiais. Estudaremos efeitos de temperatura em macromoléculas de cis-poliacetileno sobre os portadores de carga, os pólarons. Vamos observar também o comportamento da quasi-partícula em diferentes regimes de densidade. Analisaremos a difusividade destes pólarons.

METODOLOGIA

Utilizamos o modelo SSH (Su-Schrieffer-Heeger) modificado. Especificamente foram incluídos efeitos de temperatura e o termo de quebra de simetria de Brazovskii-Kirova. A temperatura foi incluída a partir de uma equação de Langevin. Os estados iniciais foram obtidos a partir da resolução conjunta da equação de Schrödinger independente do tempo e das equações de Euler estacionárias. Para a determinação dos comportamentos difusivos simulamos a trajetória dos portadores de carga em vários regimes de densidade. Para a avaliação estatística fizemos aproximadamente 300 realizações para cada regime de densidade. Estudamos a distribuição das posições em função do tempo. O comportamento difusivo foi determinado a partir da análise da variância dessas distribuições em função do tempo.

RESULTADOS E DISCUSSÃO

As simulações foram feitas em cadeias de cis-poliacetileno contendo 120 sítios para cada regime de densidade. A temperatura utilizada foi de 200 K. As trajetórias foram determinadas a partir da evolução temporal da densidade de carga. O comportamento da distribuição foi analisado em relação aos coeficientes de linearidade da variância em função do tempo. Tratando-se de uma distribuição normal, obtivemos dados a respeito da difusividade dos pólarons. Para 2 pólarons na cadeia, por exemplo, obtivemos o coeficiente linear da variância em função do tempo igual a 0,99.

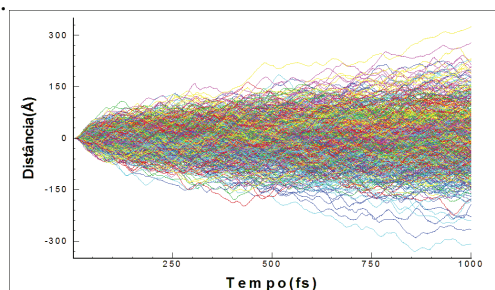


Figura 1. Posição(Å) de 2 pólarons em função do tempo(fs) a uma temperatura de 200K.

CONCLUSÕES

Através do coeficiente de linearidade encontrado para o caso de 2 pólarons, identificamos o regime de difusão normal e determinamos o coeficiente de difusividade. Percebemos ainda que o aumento na densidade de portadores de carga gera uma mudança de fase no transporte de carga passando de um regime subdifusivo para densidades menores que 2 pólarons por 120 sítios para superdifusivo partir de 3 pólarons por 120 sítios.

AGRADECIMENTOS

CNPq, CAPES e FAP-DF

¹ New Journal of Chemistry (1987), v. 37, p. 2829, 2013.

² Computational and Theoretical Chemistry, v. 1018, p. 91-94, 2013.

³ Chemical Physics Letters (Print), v. 580, p. 108-114, 2013.

Conformational analysis, NBO and QTAIM Study of the Antimony Complexes with Mesoionic 1, 3-Thiazolium-5-thiolate

Gerd Bruno da Rocha^a (PQ), Evandro Paulo S. Martins^a (PG)

^a Universidade Federal da Paraíba, Departamento de Química, João Pessoa, PB, Brasil

Keywords: Antimony complexes, mesoionic 1,3-thiazolium-5-thiolate, conformational analysis, NBO and QTAIM analysis

INTRODUCTION

In recent years, antimony complexes have been widely studied as antimicrobial agents, anticancer, and precursor of thin films¹. Mesoionic compounds have attracted interest because of their unusual electronic structure and application in medicine and nonlinear optics. In this work, we calculated molecular conformations, electronic structure, thermodynamic stabilities and chemical bonds properties for $\text{SbX}_3(\text{L})$ ($\text{X} = \text{F}, \text{Cl}, \text{Br}; \text{L} = \text{C}_{17}\text{H}_{14}\text{NS}_2\text{Cl}$) complexes in gas phase. Our objective was to get a detailed interpretation on the chemical bonds, in special, on the change in the electronic structure of mesoionic ligands after coordination.

METHODS

The potential energy curves (PECs) for all complexes were calculated from the 360° rotation around the Sb–S bond, using B3LYP, M06-2X and MP2 level with 6-31G(d) basis set with semi-relativistic pseudopotential (ECP) for Sb. After that, the minimum structures of the PECs were fully optimized and characterized by vibration analysis, using M06-2X/cc-pVTZ level with relativistic ECP for Sb. Besides, the basis set superposition errors were estimated using counterpoise protocol. Chemical bonds were studied by Quantum Theory of Atoms in Molecules (QTAIM)². NBO calculations were performed to compute atomic charges and hybrid natural orbitals. All the calculations were carried out with Gaussian 09 and AIMALL programs.

RESULTS AND DISCUSSION

The PECs calculated by using MP2 and M06-2X methods were quite similar. Thus, the method M06-2X was selected to study the complexes. The calculated thermodynamic parameters indicated that the formation of the complexes is spontaneous, with ΔG_r ranging from -33.43 to -27.27 $\text{kJ}\cdot\text{mol}^{-1}$. The analysis of NBO charges for the complexes indicated which the metal coordination led to the loss of mesoionic

character, producing large charge delocalization in the ring. The *s* character of Sb lone pair (Lp) increase from 83.0% in $\text{SbF}_3(\text{L})$ to 86.6% in $\text{SbCl}_3(\text{L})$, and to 89.1% in $\text{SbBr}_3(\text{L})$. Moreover, the NBO Lp orbital energies of the Sb change from -13.53eV [in $\text{SbF}_3(\text{L})$] to -15.37eV [in $\text{SbBr}_3(\text{L})$], indicating a greater stability for $\text{SbBr}_3(\text{L})$ lone pair electrons. Using the results from QTAIM, we were able to classify the Sb–S bonds as closed shell, with small degree of electrons sharing. Also, the intramolecular interactions in the complexes were classified by QTAIM into three types: i) hydrogen bonds, ii) halogen bonds and iii) Sb- π , as is shown in the following figure.

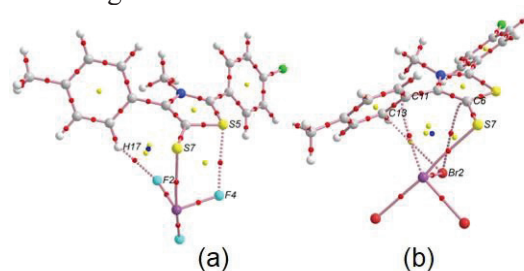


Figure 1. QTAIM path and bond critical points (in red) for: (a) $\text{SbF}_3(\text{L})$ and (b) $\text{SbBr}_3(\text{L})$.

CONCLUSIONS

Our study showed that the ground state geometries for all $\text{SbX}_3(\text{L})$ complex are stabilized by non-covalent interactions such as hydrogen bonds, halogen bonds, and Sb- π and Sb-S interactions. In addition, the NBO analysis indicated that the metal coordination produce a greater charge delocalization in the mesoionic ring, resulting in a larger stability.

ACKNOWLEDGMENT

The authors are grateful for the support given from the PRONEX/FACEPE, CAPES, CNPq and CENAPAD-SP.

¹ I. I. Ozturk and C.N. Banti, *J. Inorg. Biochem.*, 109, 57, (2012).

² F. C. Cortés, R. F.W. Bader. *Coord. Chem. Rev.*, 246, 633, (2005).

Study of UV-Photoexcitation and Ultrafast Dynamics of HCFC-132b (CF₂ClCH₂Cl)

Gessenildo P. Rodrigues^{a,b} (PG), Elizete Ventura^a (PQ), Silmar A. do Monte^a (PQ),
Mario Barbatti^b (PQ)

^a Universidade Federal da Paraíba, 58059-900, João Pessoa-PB, Brazil.

^b Max-Planck-Institut für Kohlenforschung, Kaiser-Wilhelm-Platz 1, Mülheim an der Ruhr, Germany.

Email: nildopr@kofo.mpg.de

Keywords: Atmospheric photochemistry, hydrochlorofluorocarbons, surface hopping, TD-DFT

INTRODUCTION

The issue of greenhouse gas emissions to the atmosphere and the ozone hole depletion phenomenon are topics of major importance. The main compounds reported as contributors to this fact are the chlorofluorocarbons (CFCs)¹. These were replaced by the hydrochlorofluorocarbons (HCFCs)². The understanding of HCFC's photodissociation is of great importance for the elucidation of their behavior in the upper atmosphere.

The aim of this research is to compute excited-states properties with TD-DFT methodology and compare with CASPT2 results. Nonadiabatic dynamics calculations were also performed to investigate the photochemical deactivation process of HCFC-132b (CF₂ClCH₂Cl).

METHODS

Static calculations and excited-states properties were calculated at TD-DFT (CAM-B3LYP and ω B97XD functional) and CASPT2 levels with Gaussian 09 and MOLCAS programs, respectively. In all calculations aug-cc-pVDZ (C, F and H)/d-aug-cc-pVDZ (Cl) basis set was used.

UV photoabsorption spectrum calculation was carried out and simulations of ultrafast gas phase nonadiabatic dynamics were performed, taking into account 25 electronic states at TD- ω B97XD level starting in two different spectral windows (8.5±0.25 and 10.0±0.25 eV), using Newton-X program interfaced with Gaussian 09.

RESULTS AND DISCUSSION

Excited states calculations at the TDDFT level are in good agreement with CASPT2 results, correctly predicting the main excited-states properties.

Experimental data measured at 147 nm (~8.43 eV)³ is in very good agreement with our simulations. The excited state lifetime is 106 and 191 fs for the 8.5 and 10.0 eV spectral excitation windows, respectively.

Internal conversion to the ground state occurred through several different reaction pathways with different products, where 2Cl, C-Cl bond breakage, and HCl are the main photochemical paths in the low-excitation region, representing 95% of all processes. On the other hand, HCl, HF, and C-Cl bond breakage are the main reaction pathways in the higher excitation region, with 77% of the total yield. Figure 1 shows the main decay process for HCFC-132b.

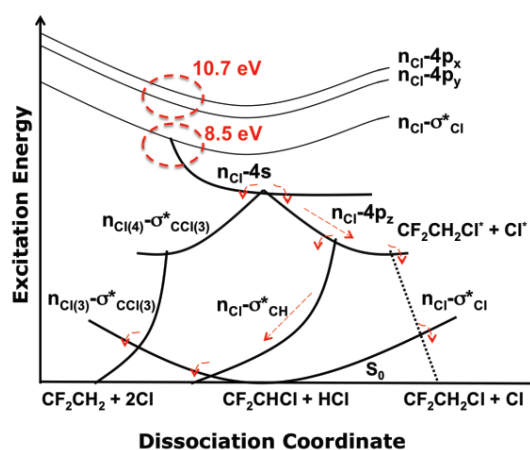


Figure 1. Main photochemical pathways for HCFC-132b.

CONCLUSIONS

For HCFC-132b, TD-DFT performed quite well in the description of excited states properties. Gas phase non-adiabatic dynamic simulations correctly predict the photochemical reaction paths. We have also observed a direct influence of spectral excitation window on products distribution and photodecay lifetime.

¹M. J. Molina, F. S. Rowland, Nature, 249, 810 (1974).

²Montreal Protocol, 1983 Report of the Technology and Economic Assessment Panel, New York (1993).

³T. Yano, E. Tschuikow-Roux, J Phys Chem, 83 (20), 2572 (1979).

Theoretical Investigation of the Butanol Combustion Mechanism

Gladson de Souza Machado (PG), Glauco F. Bauerfeldt (PQ)

Departamento de Química, Instituto de Ciências Exatas, UFRuralRJ

Keywords: rate analysis, sensitivity analysis, ignition delay time

INTRODUCTION

Attempts to avoid the dependence on fossil fuels and the search for sustainable and renewable energy sources are issues of great importance worldwide¹. An alternative fuel is butanol and, despite the apparent advantages over other biofuels, as ethanol, a systematic study of the combustion profile is needed. Hence, the main goal of this work is the investigation of the most important reactions in butanol combustion mechanism.

METHODS

The kinetic model proposed by Sarathy et al.,² modified to include the NO_x chemistry has been adopted to simulate the combustion of butanol. The coupled ordinary differential equations have been integrated using the numerical method DVODE available in the Kintecus[®] software.³ Rate Analysis (RA) and Sensitivity Analysis (SA) have been performed in order to identify the most important reactions to the initiation of the mechanism and to the ignition. The simulation has been done at 1332 K and 1.73 atm, with equivalence ratio one, four percent of oxygen in the mixture, using argon as bath gas and assuming constant volume, in order to reach the experimental shock tube conditions.

RESULTS AND DISCUSSION

The chemical kinetic model for the combustion of butanol is originally composed by 2335 reactions and 426 species. In this mechanism, 65 reactions are responsible for the consumption of butanol.

RA suggests that, at 1332 K, butanol is consumed, in the beginning of the reaction (at a time value corresponding to 0.5% of the ignition delay time), mostly by C-C bond cleavage and dehydration reactions (which sum up to 40.0% of the flux of butanol consumption). Other important channels are the hydrogen abstraction reactions by hydrogen atoms (28.5%) and hydroxyl radicals

(28.5%). At a time value corresponding to 2% of the ignition delay, this ranking is changed and hydrogen abstraction by hydrogen atoms is found as the most relevant (34.0%). Among O₂ reactions, O₂+CH₂OH→CH₂O+HO₂ is suggested to be the most important, followed by H+O₂→O+OH. It is important to notice that the CH₂OH is the main product of the unimolecular C-C bond dissociation. Similar analysis for other simulations performed at different initial conditions was done.

SA confirm that the C-C cleavage and dehydration reactions are the most important for the butanol consumption, but at the ignition delay time the reaction butanol is mostly removed by OH radicals, which arise from the H+O₂→O+OH reactions. The sensitivity coefficient for this reaction is high, also being the most important for the formation of oxygen atoms and for the raise of the temperature.

CONCLUSIONS

Our results suggest that the unimolecular reactions of butanol play a fundamental role in the initiation of the combustion. Moreover, the H+O₂→O+OH reaction was shown to be highly important in the ignition delay time. Hydrogen abstraction reactions showed the highest contributions to the rate of consumption of butanol at the ignition delay time.

ACKNOWLEDGMENTS

The authors thank the support given from CAPES.

¹ A.K. Agarwal, Prog. Energ. Combust, 33, 233, (2007).

² S.M. Sarathy, S. Vranckx, K. Yasunaga, M. Mehl, P. Oswald, W.K. Metcalfe, C.K. Westbrook, W.J. Pitz, K. Kohse-Hoinghaus, R.X. Fernandes, H.J. Curran, Combust and Flame, 159, 2028, (2012).

³ J.C. Ianni, Computational Fluid and Solid Mechanics, 1368, (2003).

Study of Aromatic + OH Reactions at the Density Functional Theory Level

Thanízia Ferraz Santos(PG), Luís Gustavo de Moraes (IC), **Glauco F. Bauerfeldt** (PQ)

Departamento de Química, Instituto de Ciências Exatas, UFRuralRJ

Keywords: 2,5-Dimethylfuran, Benzene, Toluene, Aromatic + OH, Variational Rate Coefficients

INTRODUCTION

Theoretical description of the reactions of OH radicals with unsaturated compounds has received great attention on the last years. OH addition is believed to be main channel, at atmospheric conditions, following a mechanism in which a pre-barrier complex is reversibly formed and further reacts, forming a radical. The successful performance of the BHandHLYP functional in describing OH reactions with alkenes has been demonstrated.¹

In this work, a more difficult case is evaluated: the OH reactions with aromatic compounds. Three models for aromatic + OH reactions were studied: 2,5-dimethylfuran (DMF), benzene (Bz) and Toluene (Tol). Our main goal is to assess the possibility of describing the reaction kinetics at the DFT level.

METHODS

Theoretical calculations for the DMF + OH, Bz + OH and Tol + OH reactions include geometry optimizations and vibrational frequencies and reaction path calculations at DFT level, adopting the BHandHLYP and M06-2X functionals and the aug-cc-pVDZ (ACCD) basis set. Single point calculations at the CCSD(T) level have also been performed. Variational rate coefficients were finally calculated in the range from 200 – 500 K.

RESULTS AND DISCUSSION

Our BHandHLYP calculations for the DMF + OH reactions suggest that a π -prebarrier complex is formed, stabilized by $2.78 \text{ kcal mol}^{-1}$ (including zero point energy corrections). Saddle points for the C2 and C3 additions have been located, with relative energies -1.37 and $2.22 \text{ kcal mol}^{-1}$, respectively. Differently, a σ -prebarrier complex has been located at M06-2X level, with relative energy $-5.68 \text{ kcal mol}^{-1}$. The Saddle points, despite the geometrical resemblance with the BHandHLYP saddle points, show relative

energies -5.27 and $-2.16 \text{ kcal mol}^{-1}$. CCSD(T) single point calculations have been performed, supporting the M06-2X results. Rate coefficients have been calculated on the basis of both CCSD(T)//BHandHLYP and CCSD(T)//M06-2X results, showing good agreement with the experimental value,² at 298 K ($k^{\text{predicted}}/k^{\text{literature}} = 2$).

For Bz and Tol, the BHandHLYP functional was unable to predict a prebarrier complex, and saddle points have been located above the isolated reactants. At the M06-2X level, the relative energies found for the prebarrier complex and saddle point for the OH addition to Bz were -5.15 and $0.24 \text{ kcal mol}^{-1}$, respectively. Rate coefficients have been predicted at the M06-2X level and compared to literature data.³ The ratio $k^{\text{predicted}}/k^{\text{literature}} = 30$, for $T = 298 \text{ K}$, has been achieved. Hydrogen abstraction shows minor contribution to the global rate coefficient at room temperature. Similar results for the Tol + OH reaction have been obtained.

CONCLUSIONS

The OH reactions with aromatic compounds can be satisfactorily described at the M06-2X level but not at the BHandHLYP level, despite the good performance of the latter function in describing OH reactions with simple alkene compounds. Kinetic results, based on a mechanism in which a σ -type prebarrier complex is formed, are generally found in good agreement with the experimental values.

ACKNOWLEDGMENTS

The authors thank the support given from CAPES.

¹ T. S. Barbosa et al. Phys. Chem. Chem. Phys., 17, 8714-8722 (2015).

² A. Bierbach, I. Barnes, K. H. Becker, Atmos Environ., 26, 813-817 (1992).

³ D. L. Baulch et al. J. Phys. Chem. Ref. data, 21, 411-429 (1992).

TD-DFT Study of Chalcones with Potential Pharmacological Activity against Alzheimer's Disease

Graziele S. Pereira^a (PG), Thiago O. Lopes^a (PG), Murilo M. dos Anjos^b (PG), Guilherme R. de Oliveira^b (PQ), Valter H. Carvalho da Silva^c (PQ), Heibbe C. B. de Oliveira^a (PQ)

^a LMSC, Instituto de Química, Universidade de Brasília, 70919-970, Brasília, DF, Brazil.

^b LQSA, Instituto de Química, Universidade Federal de Goiás, 74001-970, Goiânia, Brasil.

^c QTEA, Universidade Estadual de Goiás, 75001-970, Anápolis, Brasil

Keywords: Alzheimer; DFT; Chalcones; Absorption spectrum.

INTRODUCTION

One of the main diseases of the 21st century is Alzheimer's disease, a neurodegenerative disorder, which commonly attacks patients more than 65 years old. Its main feature is the progressive cell death of neurons, causing its main symptom: the loss of memory and cognitive ability of the patient. There is no cure for Alzheimer's disease, and its main method of palliative treatment is based on the cholinergic hypothesis, acting on the activity of acetylcholinesterase (AChE). By inhibiting this activity, the cholinergic deficit decreases.¹ Among the compounds developed to act as an AChE inhibitor are several chalcones, some that have already been used as prototypes for new drugs. With that in mind, our research group has synthesized and studied some new chalcones in order to observe the action of these new molecules face up to the action of AChE. The experimental work of synthesis and biological activity is being finalized and will be published soon. Here, we discussed about theoretical properties,¹ specifically, UV-vis theoretical calculations based on Time Dependent Density Functional Theory (TD-DFT). This theoretical study will supply us in important aspects related to the photophysical behavior of these new compounds.

METHODS

Figure 1 shows the chalcones studied in this work.²

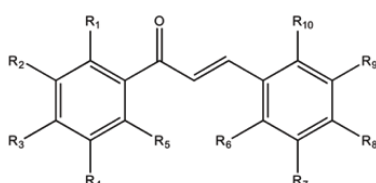


Figure 1: Representation of the base structure of Chalcones studied, with the following substituents: **R₁**: H, NH₂; **R₂**: H, NH₂; **R₃**: H, NH₂, NO₂; **R₄**: H, NH₂; **R₅**: H, NH₂; **R₆**: H, OH; **R₇**: H, OCH₃; **R₈**: H, OH, NO₂, OCH₃, CH₂CH₃, CH₃, OCH₂CH₃; **R₉**: H, OH, OCH₃; **R₁₀**: H, OH.

Based on similar structures, previously studied, all theoretical calculations were performed in G09 program suite at the TD-PBE1PBE/6-311+G(2d,p) //CAM-B3LYP/6-311G(d,p) level.

RESULTS AND DISCUSSION

The calculated data, such as the orbital energies and the theoretical UV-Vis spectrum for one of the 33 chalcones studied, are arranged in Figure 2, as well as the electronic densities of its HOMO and LUMO orbitals and electron density difference between the S₁ and S₀ states.

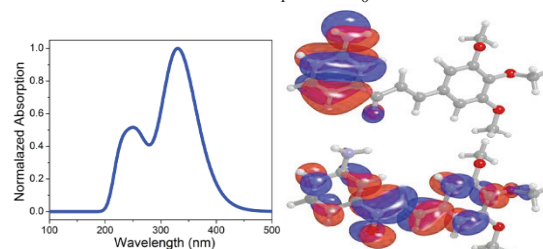


Figure 2: Electronic density of LUMO (top – right) and HOMO (bottom – right), and the theoretical UV-Vis spectrum (oscillator force vs. wavelength – to the left) at TD-PBE1PBE/6-311+G(2d,p)//CAM-B3LYP/6-311G(d,p) level.

In all molecules derivatives, HOMO orbitals is concentrated on the methoxyphenyl side, whereas the LUMO are more distributed, but clearly show a tendency towards the conjugated C=C-C=O moiety of the structure (Michael system). Also, as depicted in Figure 2, both HOMO and LUMO are of π type.

CONCLUSIONS

Theoretical results indicate an efficiency of the intramolecular charge transfer (ICT) process to stabilize the dye in the excited state.

ACKNOWLEDGMENTS

The authors are grateful for the support given from UEG, UFG, UnB, CAPES, CNPQ, FAPDF and FAPEG.

The Nuclear Quadrupole Moment of Xenon

Guilherme Arantes Canella^a (PG), Régis Tadeu Santiago^a (PG), Roberto Luiz Andrade Haiduke^a (PQ)

^a*Departamento de Química e Física Molecular, Instituto de Química de São Carlos, Universidade de São Paulo.
guilherme.canella@usp.br.*

Keywords: Xenon, Nuclear Quadrupole Moment, Electric Field Gradient, Relativistic Basis Set.

INTRODUCTION

Nuclear Quadrupole Moments (NQMs) have been systematically investigated in the last decades, since they are relevant to important spectroscopy techniques, *e.g.*, nuclear magnetic resonance, Mössbauer spectroscopy, etc.¹. The molecular method is one of the treatments used to determine this property. In this method, the NQM can be calculated based on a simple relation between the Nuclear Quadrupole Coupling Constants (NQCCs) and Electric Field Gradients (EFGs)²,

$$Q(X) = \frac{\nu_Q(X)}{0.2349647q(X)}, \quad (1)$$

where $Q(X)$, $\nu_Q(X)$ and $q(X)$ stand for the NQM (milibarns), NQCC (MHz) and EFG (a.u.) respectively.

Some years ago, Kellö *et al.* calculated the EFG and consequently determined the NQM, for the isotope ¹³¹Xe in the XeH⁺ molecule. They found values of 13.8183 a.u. and -114 mb respectively³. Here, we calculated the EFG for xenon in XeH⁺ by using a more advanced level of theory and a new relativistic basis set.

METHODS

All EFG calculations have been performed with fully uncontracted basis sets for Xe (25s20p14d11f3g) and H (6s3p2d1f). We used a new relativistic prolapse-free basis set of quadrupole- ζ quality (RPF-4Z) for xenon and the cc-pVTZ basis set for hydrogen. Moreover, we employed the Dirac-Coulomb Hamiltonian (DC), with a Gaunt correction estimated at the Hartree-Fock level. Møller-Plesset Perturbation Theory with second-order approximation (MP2) and Coupled-Cluster Theory (CCSD, CCSD(T) and CCSD-T) were also used to achieve a reliable description of electron correlation effects. The chosen active space accounts for 26 electrons in the 4s, 4p, 4d, 5s and 5p shells of xenon. The calculations also were done within a four-component formalism.

RESULTS AND DISCUSSION

As one can notice in Table (1), nice accordance with Kellö's results were obtained with DC+G-CCSD(T) and DC+G-CCSD-T treatments. This is surprising since they used Douglas-Kroll (DK) theory level (two-components).

Table 1: EFG and NQM for ¹³¹Xe in XeH⁺ as given by different theoretical treatments.

Method	EFG (a.u.)	NQM (mb)
DC-HF	14.1081	-111.8
DG-HF	14.0399	-112.3
DC-B3LYP	14.1898	-111.1
DC+G-MP2 (full)	13.4829	-117.0
DC+G-CCSD	13.9070	-113.4
DC+G-CCSD(T)	13.7595	-114.6
DC+G-CCSD-T	13.7590	-114.6

CONCLUSIONS

The results show that a more advanced theory level along with a quadrupole- ζ quality basis set still provide NQM values in nice agreement with Kellö's results (deviations smaller than 1%).

ACKNOWLEDGMENTS

The authors are grateful for the support from FAPESP (2010/18743-1 and 2014/23714-1), CNPQ and São Carlos Institute of Chemistry (USP).

¹ J.W. Zwanziger, *Computing Electric Field Gradient Tensors, in NMR of Quadrupolar Nuclei in Solid Materials*; R.E. Wasylshen, S.E. Ashbrook e S. Wimperis (Eds); Wiley: United Kingdom, (2012).

² R. T. Santiago and R. L. A. Haiduke, *Phys. Rev. A* 91, (2015), 042516.

³ V. Kellö, P. Pyykkö, A. J. Sadlej, *Chem. Phys. Lett.* 346, (2001), 155-159.

Computational Investigation of Water Glass Behavior Around DNA

Gonzatti, Guilherme K.*^a (PG), Netz, Paulo A.^a (PQ)

^a Dept. Physical-Chemistry, Universidade Federal do Rio Grande do Sul - Porto Alegre, Rio Grande do Sul, Brazil

* guilherme.gonzatti@ufrgs.br

Keywords: Waterlike Anomalies, Glass Behavior, Water Models, DNA

INTRODUCTION

Water displays interesting and unusual physico-chemical properties, many of which are necessary for the existence of life. Among these properties is water's polyamorphism, i.e. the fact that water displays two distinct amorphous solid phases, LDA (Low-Density) and HDA (High-Density Amorphous Water). Recent experimental studies¹ have shown that, upon cooling, DNA's hydration layer is made of LDA and HDA. Motivated by such findings, we've studied the molecular dynamics of this phenomena, which could be interesting for anti-freezing technologies and cryopreservation of biological matter.²

METHODS

Molecular Dynamics (MD) simulations were carried out using the GROMACS 4.5³ to study a system composed of a Dickerson-Dodecamer double strand in pure water molecules of TIP3P (called TIP3P-DNA) and TIP5P model (TIP5P-DNA) or in NaCl solution of physiological concentration (TIP5P-FISIO). The NpT ensemble was used to equilibrate the system at 300 K and then relevant dynamical and structural data was obtained by further simulation in the NVE ensemble. The system was then cooled by 10 K and the procedure repeated.

RESULTS AND DISCUSSION

Our findings show that TIP3P water is unable to produce dynamic glass transition either in bulk solution or around DNA's major and minor grooves, as shown in Figure 1. TIP5P model, however, could show such transition. It can be seen that (i) water further than 1 nm from DNA has its dynamics unaffected by the biomolecule; (ii) NaCl of physiological concentration has no relevant impact on the systems dynamics; (iii) water in DNA's grooves behaves very differently from bulk water, but similar to one another (major *versus* minor groove); (iv) groove water has non-

Arrhenius dynamics; (v) in low temperatures groove water has a slower dynamic than bulk water, but, as temperature decreases, an inversion occurs.

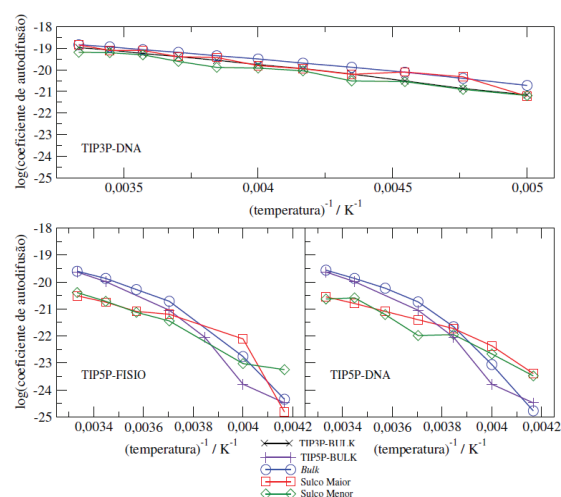


Figure 1. Arrhenius plot of logarithm of self-diffusion coefficient versus inverse temperature.

CONCLUSIONS

The simulations show that, at low temperatures, water in DNA's grooves is more mobile than bulk water at the same temperature. This suggests a possible interpretation for the glass formation of water around DNA, as verified by experiments: water cannot properly crystallize around DNA due to the fast dynamics of water in the grooves.

ACKNOWLEDGMENTS

The authors are grateful for the support given by CNPQ and CESUP.

¹ A. Paciaroni et al., J. Phys. Chem. B, 117, 2026 (2013).

² T. A. Berendsen et al., Nature Medicine, 20, 790 (2014).

³ S. Pronk et al., Bioinformatics, 7, 845 (2013).

Development a Two Point Extrapolated Method Based on B3LYP/cc-pVDZ and cc-pVTZ Energies, Aiming a CBS Methodology.

Guilherme Luiz Chinini^a (PG), Rogério Custodio^b (PQ).

^a Universidade de Campinas e-mai: guilherme.chinini@iqm.unicamp.br

^b Universidade de Campinas e-mai: roger@iqm.unicamp.br

Keywords: CBS Methods, Extrapolation Formula, Hierarchical Basis Set.

INTRODUCTION

Considering the current performance of computers along with the constant and growing need for high-level information, the quantum mechanical calculations applied for obtain molecular properties (equilibrium geometry, thermodynamic properties and more) using only a unique configuration and a minimal basis set do not represent an appropriate methodology, this problem is mostly caused for the difficult in describe a system with a *full*-CI and a CBS (Complete Basis Set) quality, with respect to the last, suitable extrapolation methods based on hierarchical basis set (ANO Almlöf, Dunning Correlation-Consistent Basis Set,¹ pc-n and others) can be employed for determine the CBS limite ($E_{infinite}$). The present work, describe the extrapolation method development based on a two points energies formula according with the B3LYP/cc-pV(n)Z ($n = D$ and T) approximation level.

METHODS

Firstly it was selected a test set containing 26 open and closed shell molecules, 14 atoms, 21 cationic and 19 anionic species (atoms and molecules) with a B3LYP/6-31G(d) equilibrium geometry and a series of B3LYP/cc-pV(n)Z ($n = D, T, Q$ and 5) single-point energies was calculate for each geometry and interpolated according the asymptotic exponential formula for E_{∞} : $E_n = E_{\infty} + A \exp(-n/t)$, that represent a good agreement and better results than cc-pVQZ for Hartree-Fock calculations.² The same was done using the inverse cubic extrapolation formula with cc-pVDZ and cc-pVTZ basis, including one additional term in the extrapolation formula, this term denoted by “b” was included in two different forms, as the sum in the n-zeta parameter and as a product in the exponent term: $E_n = E_{\infty} + D(n + b)^{-3}$ and $E_n = E_{\infty} + Dn^{-3b}$, this term “b” was obtained by minimizing the sum of squared differences

calculated by the exponential and the modify inverse cubic formula.

RESULTS AND DISCUSSION

The exponential model for extrapolation the CBS limite, show a good agreement with relation to calculated energies ($n = 2, 3, 4$ e 5) and it was used for adjust de parameter “b” in the modify inverse cubic function for extrapolation energies. The calculated OLS for modify inverse cubic form ($E_n = E_{\infty} + Dn^{-3b}$) compared with B3LYP/cc-pV(n)Z energies present the highest value (about $0,44 \text{ kcal.mol}^{-1}$) for ionized atoms, and the OLS differences estimated between the two models are greater for ionic molecules ($0,31 \text{ kcal.mol}^{-1}$).

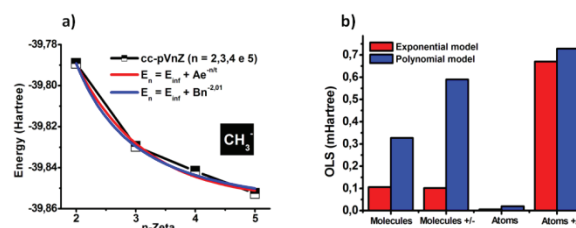


Figure 1: a) Single-point energies for modify inverse cubic and exponential extrapolated curves, b) OLS energies estimated between the two forms.

CONCLUSIONS

The two modify formulas $E_n = E_{\infty} + D(n + b)^{-3}$ and $E_n = E_{\infty} + Dn^{-3b}$ related in this work, with the parameter b adjust based on exponential extrapolation method, represent a good proposal to implement the E_{∞} on CBS methodologies.

ACKNOWLEDGMENTS

The authors are grateful for the support given from the IQ-Unicamp.

¹ T. H. Dunning Jr. J. Chem. Phys., 90, 1007, (1989).

² A. Halkier, T. Helgaker, W. Klopper and J. Olsen J. Chem. Phys. Lett., 302, 437, (1999).

Electronic structure and reactivity of a mechanically unfolded metalloprotein

Guilherme Menegon Arantes (PQ)

*Instituto de Química, Universidade de São Paulo, Av. Lineu Prestes 748, 05508-000, São Paulo, SP, Brazil.
Email:garantes@iq.usp.br*

Keywords: Hybrid QM/MM potentials. Density functional theory. Atomic force microscopy. Single-molecule spectroscopy. Mechanochemistry

INTRODUCTION

The function of iron-sulfur proteins, such as rubredoxin, depends in large part on the stability and reactivity of their ferric-thiolate bonds. Recent atomic force microscopy experiments unexpectedly showed that Fe-S dissociation in rubredoxin single molecules under mechanical stress occurred at relatively low forces¹.

METHODS

In order to probe the detailed mechanism of forced rubredoxin unfolding, we develop here an approximate molecular dynamics scheme to simulate unfolding trajectories with bond dissociation and employ density functional theory pure quantum chemical (QC) and hybrid quantum chemical molecular mechanical (QC/MM) potentials to describe in detail the mechanism of Fe-S rupture in stretched rubredoxin in the presence of competing chemical agents such as SCN⁻ and H⁺.

RESULTS AND DISCUSSION

In contrast to results previously observed in the absence of such agents², a heterolytic bond cleavage mechanism is obtained here with a ferric-thiolate dissociation product³. Calculated rupture forces are in good agreement with the

experimental values in the order of 200 pN. Analysis of hundreds of unfolding trajectories also explains the anisotropic response of stretched rubredoxin when force is applied at different points along the protein primary sequence.

CONCLUSIONS

We conclude that the stability of ferric-thiolate bonds decreases in the presence of electrophilic and nucleophilic agents. Finally, the combination of quantitative experiments such as single-molecule atomic force microscopy and molecular modeling with quantum chemical calculations can accurately describe the stability and reactivity of metalloproteins.

ACKNOWLEDGMENTS

Financial support from FAPESP is acknowledged.

¹ P. Zheng, H. Li, J. Am. Chem. Soc., 133, 6791-6798 (2011);

² G.M. Arantes, A. Bhattacharjee, M.J. Field, Angew. Chem. Int. Ed., 52, 8144-8146 (2013);

³ P. Zheng, G.M. Arantes, M.J. Field, H. Li, Nature Comm., 6, 7569, DOI: 10.1038/ncomms8569 (2015)

Understanding the molybdenum oxodiperoxo complexes reactivities through of the IR and ^{17}O -NMR DFT calculations

Gustavo H. L. de Souza^a (IC), Leonardo L. dos Santos^b (PG), Lucelma P. de Carvalho^a (IC), Marcus Vinicius Pereira dos Santos^a (PQ), Juliana A. B. Silva^a (PQ), Ricardo L. Longo^c (PQ)

^aCentro Acadêmico do Agreste, Universidade Federal de Pernambuco

^bDQ – Universidade Federal Rural de Pernambuco

^cdQF - Centro de Ciências Exatas e da Natureza, Universidade Federal de Pernambuco

Keywords: Oxo-diperoxo Complexes, DFT, Oxidation Reactions, Activation Energy

INTRODUCTION

Molybdenum oxodiperoxo complexes of type $[\text{MoO}(\text{O}_2)_2\text{L}_1\text{L}_2]$, $\text{L}_1 =$ pyrazole, N-oxo of pyridine, $\text{L}_2 = \text{H}_2\text{O}$, silica, are used in selective sulfide oxidation reactions, whereas active species transfer oxygen and it will be regenerated later. Albeit, there are some questions about how their reactivities are affected by different ligands (L_1 and/or L_2) effects. Quantum chemical (QC) methods can be useful to understand the behavior in oxygen transfer reactions, also in proposing mechanisms, which can explain the observed chemoselectivity and stereoselectivity, e.g., in case of chiral sulfoxides formation. In order to elucidate the mechanism of oxidation reactions, some NMR and IR spectroscopic properties were evaluated. The following complexes were chosen $[\text{MO}(\text{O}_2)_2\text{L}_1\text{L}_2]$, with $\text{L}_1 =$ HMPA, OPH_3 , N-oxo of pyridine, pyrazole, and $\text{L}_2 =$ none or H_2O .

METHODS

All calculations were performed with Gaussian 09 program (Rev. D.01). We applied four DFT functionals in this study: B3LYP, PBE1PBE, WB97XD and M062X. These functionals were used associated with the 6-31G(d) basis set for all atoms, except LanL2DZ applied for molybdenum (also effective core potential). For ^{17}O -NMR chemical shifts $\delta(^{17}\text{O})$, the DFT/LANL2DZ/IGLO3 was applied for all systems.

RESULTS AND DISCUSSION

The vibrational analysis showed invariance in the Mo-O(oxo) stretch (oxo) between the different ligands in the hexacoordinated (with $\text{L}_2 =$ none) and heptacoordinated complexes. In particular, for the complex $[\text{MoO}(\text{O}_2)_2(\text{pyrazole})(\text{H}_2\text{O})]$, our results are in good agreement with the experimental frequencies (errors $\sim 10\%$ - B3LYP).¹ For other functionals, the errors are higher. The order errors associated with vibrational frequencies values are: B3LYP < PBE1PBE < WB97XD < M062X, in special, for stretching modes.

For ^{17}O -NMR chemical shifts suggest that the oxygen atom present in the oxo group is less susceptible to the different ligands than peroxy group. For oxygen atoms in peroxy group, $\delta(^{17}\text{O})$ shifts decrease in those oxygen that are in the same side of ligand (*syn*). This result is explained in terms of increased electron density due to the coordination ligands.

The presence of another ligand heptacoordinated complexes ligands enhances the chemical shifts for oxygen (oxo) in relation to the hexacoordinated complexes. This result shows that the introduction of one more ligand at the axial position decreases the electron density and thus shielding of those oxygen atoms. In particular, ^{17}O -NMR chemical shifts $\delta(^{17}\text{O})$ of the oxygen atom (oxo) in the complex $[\text{MoO}(\text{O}_2)_2(\text{HMPA})]$ is 916ppm (B3LYP), whereas the experimental value (obtained by Postel *et al.*²) is 863ppm, a 6.1% error, suggesting B3LYP is the most suitable DFT functional to apply in order to obtain this kind of NMR properties.

CONCLUSIONS

The calculated vibrational frequencies of $[\text{MoO}(\text{O}_2)_2(\text{pyrazole})(\text{H}_2\text{O})]$ were used to assign the experimental vibrational spectrum. The spectroscopic analysis shows correlation of the vibrational frequencies and chemical shifts with the strengths of the ligands and the reactivity of the complexes. The oxo group is less susceptible to the presence of different ligands than the peroxy oxygen atoms.

ACKNOWLEDGMENTS

The authors would like to thank the FACEPE, CAPES and CNPq for the grant and scholarships.

¹Q. B. Cass, F. Batigaglia, M. Z. Hernandez, I. Malvestiti, A. G. Ferreira, *Tetrahedron*, 57, 9669 (2001).

²M. Postel, C. Brevard, H. Arzoumanian J. G. Riess, *J. Am. Chem. Soc.*, 105, 4922 (1983).

Substituent effects on the ESIPT process in 2-Hydroxy-1,4-Naphthoquinones

Henrique A. Rodrigues (IC), Eduardo P. Rocha (PG), Livia C. T. Lacerda (PG), Mateus A. Gonçalves (PG), Máira S. Pires (PG), Telles C. Silva (PG), Teodorico C. Ramalho (PQ)

Chemistry Department, Federal University of Lavras, Lavras, Minas Gerais, Brazil.
teodorico.ramalho@gmail.com

Keywords: ESIPT, Fluorescence, DFT, TD-DFT, Naphthoquinone.

INTRODUCTION

Despite recent technological advances, cancer is still one of the most serious problems of humanity [1,2]. In this line, the use of fluorescent probes for preoperative and postoperative cancer diagnoses is crucial to detect early tumors and increase the changes of treatment. The Excited State Intramolecular Proton Transfer (ESIPT) is usually the main mechanism for fluorescent probes used for the cancer diagnoses (Fig. 1).²

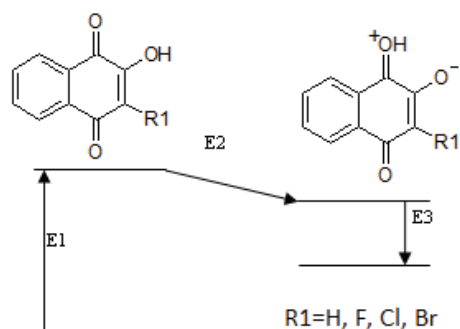


Fig. 1 - ESIPT process for the HNQ.

In spite of great importance associated to substituent effects on the ESIPT process, surprisingly little detailed computational work on this subject has appeared.³ Thus, the goal of the current work, is evaluate the substituent effects on the ESIPT process of 2-Hydroxy-1,4-Naphthoquinones.

METHODS

Firstly, molecules were optimized by DFT/DGTZVP calculations. The electronic properties were calculated at the DFT/B3LYP/DGTZVP level for ground state and TD-DFT/CAM-B3LYP/DGTZVP for excited state. The solvent effect (Water) was evaluated by means of the IEFPCM model.⁴

RESULTS AND DISCUSSION

2-hydroxy-1,4-Naphthoquinone (HNQ) showed ESIPT process and its derivatives too (Fig. 1). The energy values for the absorption (E1) and emission (E3) were evaluated by means of

DFT/B3LYP/DGTZVP and TD-DFT/CAM-B3LYP/DGTZVP techniques. For the HNQ analogues, E1 values are of 3.32, 3.60, 3.66 and 4.69 eV for Br, Cl, F and CN derivatives, respectively. The substituent CN is not favorable for the ESIPT process, because the absorption energy is higher. However, the Br derivative is the more favorable for the ESIPT process.

Table 1 – Energy values (eV) for 2-Hydroxy-1,4-Naphthoquinone derivatives for the ESIPT process.

R1	E1	E2	E3
Br	3.32	3.23	1.20
Cl	3.60	3.52	1.20
F	3.66	2.66	1.14
CN	4.69	5.30	1.22

The E2 values for the Br, Cl, F and CN derivatives were 3.2; 3.52; 2.66 and 5.30 eV, respectively. It should be kept in mind, however, that all compounds showed similar emission values, then, the E3 values are not modulated by the substituent effect.

CONCLUSIONS

The investigation of the ESIPT process for HNQ derivatives by DFT and TD-DFT calculations was satisfactory; however the CN derivative was less favorable in water solution.

ACKNOWLEDGMENTS

The authors are grateful for the support given from the FAPEMIG, CAPES, CNPQ and UFLA.

- Jali, B. R.; Baruah, J. B. *Dye. Pigment.* 2014, 110, 56–66.
- Zhao, J.; Ji, S.; Chen, Y.; Guo, H.; Yang, P. *Phys. Chem. Chem. Phys.* 2012, 14, 8803.
- Il'ichev, Y. V.; Kühnle, W.; Zachariasse, K. a J. *Phys. Chem. A* 1998, 102, 5670–5680.
- Arumugam, K.; Becker, U. *Computational Redox Potential Predictions: Applications to Inorganic and Organic Aqueous Complexes, and Complexes Adsorbed to Mineral Surfaces*; 2014; Vol. 4.

Reaction Rate of $HX+Y$ systems, with $X, Y = H, F, Cl$ or Br and $X \neq Y$

H. O. Euclides^a (IC), P. R. P. Barreto^a (PQ)

^a Instituto Nacional de Pesquisas Espaciais (INPE/MCT), Laboratório Associado de Plasma (LAP), São José dos Campos, SP, CEP 12247-970, CP515, Brasil
henriqueuclides@gmail.com

Keywords: Reaction Rate, Rovibrational Levels, Transition State Theory

INTRODUCTION

The knowledge of the thermodynamic properties of chemical species is of fundamental importance for studies such as combustion processes, the study of reactions occurring in the atmosphere as the greenhouse effect, knowing how quickly a drug works in the body, industrial problems such as the discovery of catalysts to accelerate the synthesis of a product, desorption of water from soybean, among others.

Since these applications, knowing the rate of these reactions, it is essential to know the speed with which they occur. Was writing a program in C language to calculate the reaction rate¹⁻⁴, with the correction of small curvature tunneling, correction using transmission coefficient Wigner and Eckart, and then the rate constant is presented in the Arrhenius form. We had, also, include the rovibrational levels⁵⁻⁶, when necessary, of the reactants and products in our calculation.

METHODS

We study a series of reactions $HX + H = H_2 + X$, $HX + H = H + HX$, $HX + Y = X + HY$ and $HX + Y = H + XY$, where $X, Y = F, Cl$, or Br , with $X \neq Y$. The geometries are optimized at MP2/6-61g(d), MP2/6-311++g(d,p) and MP2/aug-cc-pvtz and the energies are calculated in CCSD(T) and in a series of bases set, the difference in geometries and frequencies will be discussed.

RESULTS AND DISCUSSION

We compare the reaction rate to the type species $HF+X$, with $X = Cl$ or Br , including the rovibrational levels for the reactants, as shown in Figure 1. And to type reactions $HX+H = H_2+X$, with $X = F, Cl$ or Br , was calculate the reaction rate, and we compare with experimental data, as shown in Figure 2.

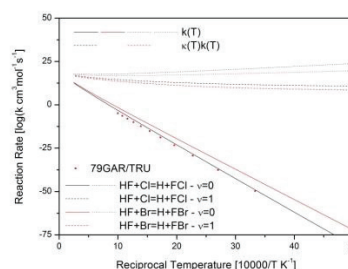


Figure 1. Reaction Rate for $HF+X$, with $X = Cl$ or Br .

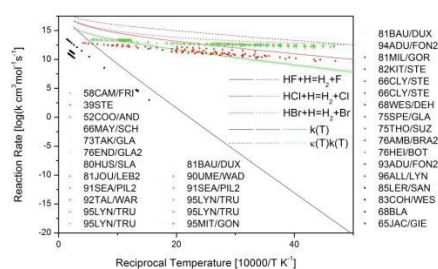


Figure 2. Reaction Rate for $HX+H = H_2+X$.

CONCLUSIONS

Our goal was to develop a code to determine the reaction rate for systems in general. Our code allows us to determine various reaction rates at once, provided all information about the reactions we want to analyze. Some changes still need to be implemented to make the most generic possible program, including other tunneling corrections to provide a better description of these effects at low temperatures, where it becomes critical.

¹Gonzalez-Lafont A., Truong T. N., Truhlar D. G. J. Chem. Phys. , 1991, 95, 8875.

²Duncan W. T., Bell R. L., Truong T. N. J. Comput. Chem. ,1998, 19, 1038.

³Barreto P. R. P.; Vilela, A. F. A.; Gargano, R. J. Mol Struct (Theochem) 2003, 639, 167.

⁴Barreto P. R. P.; Vilela, A. F. A.; Gargano, R. Int. J. Quantum Chem. 2005, 103, 685.

⁵Dunham J. L., Phys. Rev. , 1932, 41, 713.

⁶Dunham J. L., Phys. Rev. , 1932, 41, 721.

Understanding the solid-state phosphorescence of a new class of Tellurophenes compounds

Inara de Aguiar^{a*} (PQ), Eric Rivard^b (PQ), Alex Brown^b (PQ) and Gabriel L. C. de Souza^a (PQ)

^a Federal University of Mato Grosso, Department of Chemistry, 78060-900 Cuiabá-MT, Brazil

^b University of Alberta, Department of Chemistry, T6G 2R3 Edmonton, AB, Canada

*inara.aguiar@gmail.com

Keywords: Tellurophenes, Phosphorescence, DFT, ADF, Excited States

INTRODUCTION

In the last year, the first phosphorescent Tellurophenes compounds and their polymeric analogues in solid state were discovered.¹ These species can be applied in light-emitting diode technologies. Although Te compounds are generally non-emissive, these Te compounds containing pinacolboronate (BPin) showed long-lived triplet states in solid state, at room temperature and in the presence of water and oxygen. Several new Te, Se, and S containing compounds with similar spectroscopic features were synthesized and almost none of them exhibited phosphorescence. In order to better understand the excited states and the phosphorescence pathways of these molecules aiming to enhance the emissive properties of this new class of compound, computations studies using a variety of functional and basis sets were performed.

METHODS

Computations were carried out with Gaussian 09 and ADF suite of codes.^{2,3} The ground state structures of the Te compounds were determined at B3LYP, CAM-B3LYP and M06 functional with the cc-pVDZ basis set (in Gaussian 09) and at the B3LYP/TZ2P level of theory in gas-phase (in the case of ADF). Using the ADF, the relativistic calculations with the Zero Order Regular Approximation (ZORA) formalism including scalar relativistic (SR) and spin-orbit relativistic (SO) methods were performed.

Using all the functional and basis sets referred before, the twenty low-lying excited states were probed using TD-DFT in Gaussian 09 while the forty low-lying excited states were determined

using Self-Consistent Spin-Orbit Coupling Time-Dependent Density Functional Theory in ADF.

RESULTS AND DISCUSSION

Results obtained using the B3LYP functional showed one striking difference for the Te-BPin compound (emissive) compared to the Se-Bpin and the S-BPin compounds (non-emissive). In the Te heterocycle, there is a triplet state (T_3) which is nearly degenerated with the singlet state (S_1), while in the S and Se analogues, the T_3 state is about 1 eV higher in energy suggesting that the Te compound has energetically well-matched states to enable efficient singlet-triplet crossing to occur; once T_3 is populated, relaxation through the triplet manifold to the T_1 state is possible, followed by emission. The investigation was extended on the entire series of Te containing compounds synthesized by Rivard *et al.*¹

For all the functional and basis set used in the present work, the tendency reported by the previous study¹ was not observed anymore. No linear correlation between the singlet and triplet states were observed for the emissive and non-emissive compounds. The first results using the spin-orbit considerations through ADF were more consistent and the emission is correlated to the energy gap required to reach the first S_1 state.

CONCLUSIONS

The studies revealed that theoretical emissive properties of this type of compounds cannot be evaluated without spin-orbit coupling considerations.

ACKNOWLEDGMENTS

The authors thank CNPq and CAPES.

Assessing the Mesoionic Compounds Definitions by QTAIM, NBO and Spackman charge models

Italo Curvelo dos Anjos^a (PG), Gerd Bruno Rocha^a (PQ)

^aDepartamento de Química, Universidade Federal da Paraíba
Cidade Universitária - João Pessoa - PB - Brasil - CEP: 58051-900
italocurvelo@gmail.com

Keywords: mesoionic compounds, QTAIM, NBO, Spackman charge

INTRODUCTION

The mesoionic compounds have been widely studied since late 19th century. Despite this, the definition of these compounds is still controversial. Most authors agree that mesoionic compounds have an important π -bonding delocalization and a large charge separation, but there is no agreement about how the π -bonds and the positive and negative charges are (de)localized throughout these compounds. The two main models commonly used to describe these molecules are shown in Figure 1.

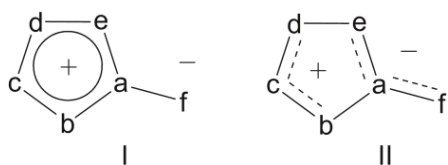


Figure 1. Mesoionic models I¹ and II²

In this work, we used three different charge models to evaluate the positive and negative charge distributions in these compounds: (i) Quantum Theory of Atoms in Molecules (QTAIM), (ii) Natural Bond Orbitals (NBO) and (iii) the Spackman's Geodesic scheme derived from Electrostatic Potential.

METHODS

We considered three different mesoionic rings: 1,3-diazole-4-thione (NNCS), 1,3-thiazole-5-thione (NSS) and 1,3-oxazol-5-one (NOO) and we also varied substituent groups to an overall of 48 structures. The structures were fully optimized to minimum geometries using M06-2X functional and cc-pVTZ basis set. Then, the charge calculations were performed with each method.

RESULTS AND DISCUSSION

The different charge models show some qualitative agreement in the mean charges of most

atoms; but a few cases exhibit large differences. In addition, the absolute values differ much from a method to another, QTAIM charges, in general, have larger absolute values. Finally, the three methods disagree with both mesoionic models regarding the individual charges (Table 1) in these compounds.

Table 1. QTAIM, NBO and Spackman mean charges for the 48 mesoionic compounds

		d	c	b	e	a	f
QTAIM	NNCS	-1.273	1.297	-1.229	0.485	0.099	-0.161
	NSS	-1.267	0.529	0.380	0.526	-0.393	-0.032
	NOO	-1.286	1.267	-1.086	0.448	1.402	-1.245
NBO	NNCS	-0.391	0.394	-0.337	0.049	-0.015	-0.372
	NSS	-0.370	0.041	0.458	0.046	-0.356	-0.232
	NOO	-0.366	0.386	-0.467	-0.125	0.676	-0.621
Spackman	NNCS	-0.074	-0.095	0.333	0.233	-0.249	-0.467
	NSS	0.011	-0.100	0.151	0.172	-0.163	-0.360
	NOO	-0.036	0.057	-0.231	-0.138	0.500	-0.496

CONCLUSIONS

Therefore, the results show that mesoionic compounds have a complex electronic structure and do not follow the models I or II. Thus, a new and improved definition of mesoionic compounds is still needed.

ACKNOWLEDGMENTS

The authors thank CAPES, CNPq and INCT-INAMI for financial support, and CENAPAD-SP for providing computational resources.

¹ W. Ollis, C. A. Ramsden, *Adv. Heterocycl. Chem.*, 19, 1 (1976)

² M. B. de Oliveira et al., *Phos. Sulf. Silic. Relat. Elem.*, 108, 75 (1996)

Estudo teórico de adsorção de CO₂ em ZnO(10 $\bar{1}$ 0)Ítalo Pimentel de Lima^a (PG), João B. L. Martins^a (PQ)^a Instituto de Química, Universidade de Brasília, CP 4478, Brasília, DF, CEP 70904-970
italoplima@gmail.com

Palavras chave: óxido de zinco, dióxido de carbono, ZnO, adsorção

INTRODUÇÃO

O estudo de catalisadores sempre foi de interesse, e esse interesse vem crescendo gradativamente na área de química ambiental e sustentável devido ao aquecimento global. Uma das potenciais fontes de energia para a substituição de combustíveis fósseis¹ e provavelmente a de utilização mais facilitada é o metanol. Sua produção é majoritariamente feita através de catalisadores contendo óxido de zinco (ZnO), sendo este a fase ativa do primeiro catalisador utilizado nessa síntese. Assim, análise de interações de moléculas precursoras envolvidas na síntese com o ZnO foi bastante estudado, havendo hoje um certo consenso² sobre como a síntese ocorre, mas nenhum mecanismo é completamente aceito. Neste trabalho é feita uma análise da interação da molécula de CO₂ com ZnO(10 $\bar{1}$ 0) em diversas conformações.

MÉTODOS

Este estudo foi realizado utilizando o software VASP³ (ver. 4.6.36) com pseudo-potenciais PAW utilizando o funcional PW91. A energia foi minimizada com convergência da ordem de 10⁻⁵ eV. A energia de interação, E_b, foi utilizada como:

$$E_b = E_{m+s} - E_m - E_s$$

Onde E_b é a energia de interação, E_{m+s} é a energia do sistema com a molécula adsorvida, E_m é a energia da molécula e E_s é a energia da superfície. Estas duas últimas energias são calculadas como “single point” utilizando a geometria de adsorção.

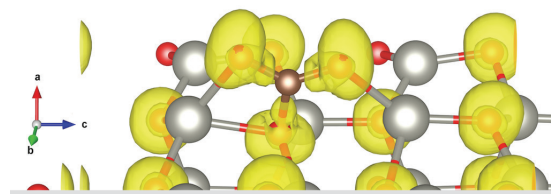
RESULTADOS E DISCUSSÃO

As energias de interação obtidas para as quatro conformações resultaram em três modos de interação distintos (Tabela 1). Duas das estruturas iniciais convergiram para uma mesma estrutura final. A interação ponte (Zn-Zn) indica que o CO₂ realiza uma interação por cada um dos oxigênios com zínco próximos. O monodentado (oxigênio) indica a interação com o zinco feita por um dos oxigênios. O carbonato é a interação do CO₂ com a

superfície, interagindo tanto pelos oxigênios quanto pelo carbono (Figura 1).

Tabela 1. Energias de interação (E_b) para as adsorções de CO₂.

Conformação	E _b (eV)	E _b (kJ.mol ⁻¹)
Ponte (Zn-Zn)	-0,3149	-30,4
Monodentado (oxigênio)	-0,3736	-36,1
Carbonato	-4,7335	-456,8

**Figura 1.** Electron localization function (ELF) para a interação de CO₂ com a superfície de ZnO(10 $\bar{1}$ 0) em isosuperfície de 0.75. O ELF mostra que os três átomos de oxigênio mais próximos ao carbono interagem de maneira similar. Átomos de oxigênio em vermelho, zinco em cinza e carbono em marrom.

A interação de CO₂ formando carbonato já foi observada por infravermelho². Acredita-se que, durante a síntese de metanol, esse intermediário não seja ativo por estar muito ligado à superfície.

CONCLUSÕES

Os resultados teóricos obtidos apresentam correlação com os dados experimentais disponíveis.

AGRADECIMENTOS

CNPq, FAPDF, DPP/UnB e Finatec.

¹ Olah, G. A., Angew. Chem. Int. Ed., 44, 2636, (2005).² Wöll, C., Prog. Surf. Sci. 2007, 82, 55, (2007).³ Kresse, G.; Hafner, J., Phys. Rev. B, 47, 558, (1993).

Elucidating the photophysics of organic photovoltaic systems

Itamar Borges Jr.^a (PQ), Lucas Modesto-Costa (PD), Elmar (Uhl),^a (PD), Adelia J. Aquino^b (PQ), Hans Lischka^b (PQ)

^a Departamento de Química, Instituto Militar de Engenharia, Rio de Janeiro (RJ), Brazil

^b Department of Chemistry and Biochemistry, Texas Tech University, Lubbock (TX), USA

Keywords: ADC(2), TDDFT, poly(thieno[3,4-b]-thiophene benzodithiophene), Charge transfer states

INTRODUCTION

Understanding the fundamental photophysics of organic photovoltaics is a challenge for theoretical chemistry. Their basic process after solar incidence is the production of excitons, bound electron-hole pairs that must be split via a charge transfer (CT) state to produce an electric current. In organic solar cells, exciton dissociation mostly happens at the interface between electron donor and electron acceptor distinct materials as in the bulk heterojunction (BHJ).

In this work, we used the ab initio wave function-based polarization propagator method algebraic diagrammatic construction to second order, ADC(2), to investigate and characterize the excited electronic states of different systems of practical interest including the recently synthesized poly(thieno[3,4-b]-thiophene benzodithiophene) donor polymer, PTB1, and two substituted derivatives either alone or combined with a C₆₀. PTB polymers display remarkable properties as electron donors in BHJs solar cells by combining the electron deficient thienothiophene (TT) and benzodithiophene (BDT) moieties in each oligomer unit.

METHODS

The ADC(2)/SV(P) and time dependent density function theory (TDDFT)/SV(P) methods were used to study the first 4 excited states of PTB1 and two substituted derivatives, PTB6 and PTB7, and PTB1/C₆₀. For TDDFT, five correlation exchange-potential with different degrees of Hartree-Fock exchange were used. The Turbomole Program version 6.6 was employed.

RESULTS AND DISCUSSION

For the PTB1, PTB6 and PTB7 copolymers, excitons can be trapped in the middle of the chain thereby degrading their performance in a BHJ (Figure 1a). Side chains in PTB6 and especially in PTB7 has a crucial role in the electronic spectra,

and not only on the easiness of synthesis of these polymers. Only the PBE functional, which does not include any amount of Hartree-Fock exchange, did not display trapping effects.

For the PTB1/C₆₀ model system, we showed that:¹ (1) CT states are localized below the bright interchain excitonic state and are directly accessible via internal conversion processes; (2) discrete bands of CT states originated by a lateral C₆₀ are also formed and; (3) interchain charge delocalization is important for the stability of the CT states (Figure 1b). In this case, a simple model for the charge separation step showed the energetic feasibility of the overall photovoltaic process in this BHJ.

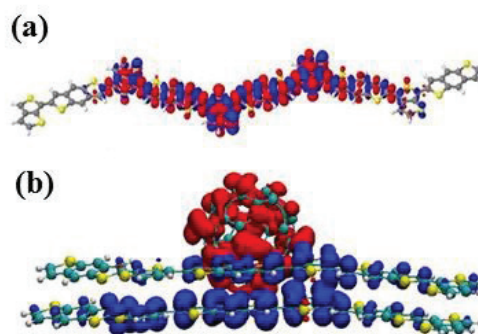


Figure 1. Isodensity plot of the density difference showing the S₀ → S₁ charge transfer transition. (a) PTB1; (b) PTB1/C₆₀. Red: Charge accumulation. Blue: Charge depletion.

CONCLUSIONS

A comprehensive study of donor polymers and a BHJ that lead to several new physical insights was done using an ab initio method and TDDFT. New results are going to be presented in SBQT.

ACKNOWLEDGMENTS

Faperj, CNPq and Capes.

¹ I. Borges *et al.*, JACS **135**, 18252 (2013).

Evaluation of Lennard-Jones Potentials in Calculations of Transport Properties of Near Critical Argon

Jakler Nichele^a (PG), Leonardo S. de Brito Alves^b (PQ) Itamar Borges Jr^a (PQ)

^a Defense Eng. Grad. Prog./Chem. Eng. Dept., Military Institute of Engineering, Rio de Janeiro, Brazil

^b Mechanical Engineering Department, Fluminense Federal University, Niteroi, Brazil

Keywords: Supercritical Fluids, Molecular Dynamics, Lennard-Jones potential, Transport Properties

INTRODUCTION

Supercritical fluids are an important class of fluids of great technological importance ranging from green chemistry to rocket fuel combustion. They are defined as the thermodynamic state that has temperature (T) and pressure (P) values above the critical point (T_c , P_c). Far from it, supercritical fluids behave quite similarly to a dense fluid or a gas depending on T and P values. However, the most notable behavior is in the neighborhood of the critical point. This region is characterized by critical anomalies due to long range interactions, which leaves several open questions.¹ Moreover, there are experimental difficulties to measure physical-chemical and thermodynamic properties for near critical fluids.

Molecular dynamics (MD) is a powerful technique that allows one to investigate in details the anomalous region. From suitable statistics of trajectories, interactions and velocities, properties of these fluids can be determined. In this work, focused on two transport properties of engineering interest: shear viscosity (η) and thermal conductivity (κ). Both can be computed from the Green-Kubo relations that are time-autocorrelation functions of momentum J_{xy} and heat fluxes S :

$$\eta = \frac{1}{Vk_B T} \int_0^\infty \langle J_{xy}(0)J_{xy}(t) \rangle dt \quad (1)$$

$$\kappa = \frac{1}{3Vk_B T^2} \int_0^\infty \langle S(0)S(t) \rangle dt \quad (2)$$

J_{xy} and S strongly depend on the pair potential which models the interatomic/intermolecular energies. Although it is possible to find very complex and extremely precise models for these interactions, the Lennard-Jones 12-6 (eq. 3) potential is still in use mainly for noble gases for which a spherically symmetric potentials is appropriate.

$$U(r_{ij}) = 4\varepsilon \left[\left(\frac{\sigma}{r_{ij}} \right)^{12} - \left(\frac{\sigma}{r_{ij}} \right)^6 \right] \quad (3)$$

η and κ were computed for Ar near its critical point using the Lennard-Jones potential with different pairs of parameters.²⁻⁵ Results were compared with NIST experimental data.

METHODS

We have used LAMMPS MD program to run systems with 10^4 atoms using the NVT ensemble and temperatures from 1.00 to 2.00 T_c . Each state was equilibrated for 2 ns and averaged for 1 ns. A time step of 1 fs was used.

RESULTS, DISCUSSION AND CONCLUSION

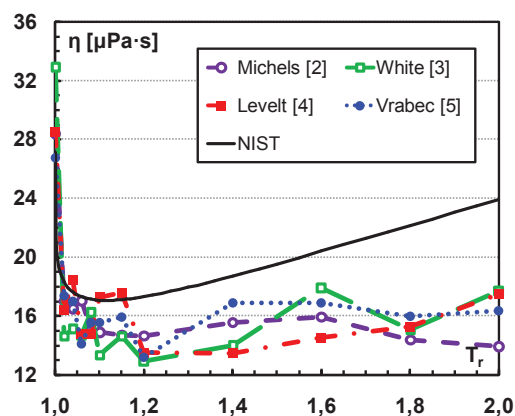


Figure 1. Shear viscosity of argon calculated via MD with different pairs of parameters for $P = P_c$.

The LJ potential presents errors of up 30% in predicting transport properties near the critical point. Although this agreement is quite good for these macroscopic properties, work is underway to improve this agreement including the use of other type of potentials.

ACKNOWLEDGMENTS

FAPERJ, CAPES, CNPq and Brazilian Army.

¹ J. Nichele, L. S. B. Alves, I. Borges Jr, High Temp. High Press. 43, 385-400 (2014).

² A. Michels, H. Wijker, H.K. Wijker. Physica, 15, 627-633, (1949).

³ J.A. White, J. Chem. Phys., 111, 9352-9356, (1999)

⁴ J. M. H. Levelt, Physica, 26, 361-377, (1960)

⁵ J. Vrabec, J. Stoll, H. Hasse, J. Phys. Chem. B, 105, 12126, (2001).

Synthesis, Spectroscopic Characterization and Crystal Structure of Asymmetric Azine $C_{15}H_{13}N_3O_4$

Jhonata de Jesus Silva^a (PG), Ademir João Camargo^a (PQ), Ricardo Rodrigues Ternavisk^b (PG), Gilberto Lúcio Benedito de Aquino^a (PQ), Miriã Moreira Costa^a (PG), Thalita Náatali Salamão dos Santos^a (PG), Hamilton Barbosa Napolitano^a (PQ)

^a Science and Technology Center, State University of Goiás Anápolis, GO 1

^b Department of Chemistry, Institute of Aeronautical Technology, São José dos Campos-SP 2

^ahamilton@ueg.br

Keywords: Asymmetric Azine, Crystal, X-ray

INTRODUCTION

Asymmetric azines are derived from hydrazones and they have present pharmacological activities. The hydrazones and their derivatives have many applications such as anti-inflammatory activity, analgesic, antibacterial and antifungal^{1,2}. This work aims to elucidate the structure of the synthesized and crystallized asymmetric azine (7E, 8E) -2- (3-methoxy-4-hydroxy-benzylidene) -1- (4-nitrobenzylidene) hydrazine by x-ray diffraction and IR, GC and NMR spectroscopy.

METHODS

The synthesis of asymmetric azine was carried out using the hydrazone (E) -1- (4-nitrobenzylidene) hydrazine, which may be obtained by reacting aldehydes / ketones with hydrazine. The method of slow evaporation of the solvent was employed in the crystallization process. The structure of the compound was determined by analysis of X-ray diffraction of a single crystal. It crystallized in the monoclinic crystal system; space group $P2_1 / n$ $Z = 4$. The structure solution was carried out using Direct Methods throughout SHELXS – 97 program. The refinement was further performed by SHELXL – 97 implemented in the WinGX suite of package.

RESULTS AND DISCUSSION

All the hydrogen and carbon atoms identified by NMR spectroscopy and the functional groups (NO_2 , $C=N$, OH) identified by IR spectroscopy were confirmed by X-ray diffraction analysis. The crystal molecular packing is driven mainly by classical (O-H---O) and non-classical (C-H---O) intermolecular

interactions. The molecule has a planar configuration and B3LYP/6-311++G** studies are been made to quantify the non-classical interaction energy.

CONCLUSIONS

In this study $C_{15}H_{13}N_3O_4$ crystal structure was analyzed and characterized. Theoretical calculation are underway in order to find out the molecular regions where it is more electrophilic or nucleophilic. A fully understanding of the nature of those sites will be of great help to shed light in the asymmetric azine biological activities. As a further study, the electrostatic potential maps are also being conducted on the compound. As it is well known, the electrostatic potential is the long range driven forces and therefore it represent the first kind of interaction between molecules.

ACKNOWLEDGMENTS

The authors thank the support from CAPES and UEG.

¹ROLLAS, S.; KÜÇÜKGÜZEL, S. G. Biological activities of hydrazone derivatives. *Molecules*, v. 12, p. 1910-1939, 2007.

²MOLDOVAN, C. M.; ONIGA, O.; PÂRVU, A.; TIPERCIUC, B.; VERITE, P.; PÎRNĂU, A.; CRISAN, O.; BOJITĂ, M.; POP, R. Synthesis and anti-inflammatory evaluation of some new acyl-hydrazones bearing 2-aryl-thiazole. *European Journal of Medicinal Chemistry*, [s.l.], v. 46, p. 526-534, 2011.

The importance of kinetic energy coupling in the vibrational spectra of small cluster dimers

Monteiro, J.G.S.^a(PG), Barbosa, A.G.H.^b(PQ)

Laboratório de Química Teórica – Instituto de Química – Universidade Federal Fluminense
^ajoao_guilherme@id.uff.br ^bandre@vm.uff.br

Keywords: Dimers, Cluster, VSCF, Watson Hamiltonian

INTRODUCTION

The Watson molecular Hamiltonian in normal coordinates for a non-rotating top is:

$$H = \frac{1}{2} \sum_{\alpha\beta} \hat{\pi}_\alpha \mu_{\alpha\beta} \hat{\pi}_\beta - \frac{1}{2} \sum_k \frac{\partial^2}{\partial Q_k^2} + V(Q_1, Q_2, \dots) - \frac{1}{8} \sum_\alpha \mu_{\alpha\alpha}$$

where $\hat{\pi}_\kappa$ is the vibrational angular momentum in normal coordinates. The $\mu_{\alpha\beta}$ tensor can be expanded into a power series and that for most cases the series can be truncated after the first term. [1] The mode coupling in the kinetic energy operator is usually neglected by many authors. This simplifies considerably the Watson Hamiltonian and it is also justified by the fact that the coupling is usually weak, being considered irrelevant for heavy molecules. Calculations performed by several authors [1,2] showed that the contributions of the kinetic energy couplings (also termed Coriolis coupling) to the fundamental frequencies may be of the order of tens of cm^{-1} . Hence for high level spectroscopy studies the inclusion of the full Watson Hamiltonian components is mandatory. In this work we use the VSCF formalism to investigate the importance of Coriolis coupling in the vibrational spectra of small dimers as $(\text{H}_2\text{O})_2$, $(\text{H}_2\text{O}_2)_2$ and $(\text{NH}_3)_2$. Our aim is to show how far the vibrational analysis may be taken without considering the coupling of normal modes in the kinetic energy operator.

METHODS

The electronic structure calculations were done with the GAMESS package at the MP2/aug-cc-pVTZ level of theory. Our VSCF code is an extended version of the GAMESS implementation that enables calculations including the Coriolis coupling discussed above. The potential energy operator used is based in the QFF representation. [3]

RESULTS AND DISCUSSION

The average and the maximum Coriolis contribution for each dimer are shown in table 1.

Table 1: Average and Maximum Coriolis contribution (in cm^{-1}) to the fundamental transitions of $(\text{H}_2\text{O})_2$, $(\text{H}_2\text{O}_2)_2$ and $(\text{NH}_3)_2$.

	Avg	Max
$(\text{H}_2\text{O})_2$	23,55	72,81
$(\text{H}_2\text{O}_2)_2$	1,28	4,97
$(\text{NH}_3)_2$	19,46	108,78

Coriolis may play an important role as it can cause a shift in frequencies as large as 100 cm^{-1} , although they usually do not exceed 50 cm^{-1} . For hydrogen peroxide dimer, the error in not including is negligible for most purposes, except for the lowest bending mode ν_{18} . The reason is the small rotational constants for this cluster. For ammonia and water dimer, the rotational constants are considerably larger. Hence the impact of Coriolis coupling is more pronounced.

CONCLUSIONS

In this work we investigated the importance of the vibrational mode coupling in the kinetic energy operator for three cluster dimers: $(\text{H}_2\text{O})_2$, $(\text{H}_2\text{O}_2)_2$ and $(\text{NH}_3)_2$. It was found that there can be considerably shifting in the fundamental transition frequencies, especially when the rotational constants are not very low. This coupling may be important not only for high level spectroscopy but also to correctly probe potential energy surfaces.

ACKNOWLEDGMENTS

The authors are grateful for the support given from the CAPES.

1. M. Neff, T. Hrenar, D. Oschetzki and G. Rauhut, J. Chem. Phys., 134, 064105, (2011).
2. P. Carbonniere and V. Barone, Chem. Phys. Lett., 392, 365, (2004).
3. K. Yagi, K. Hirao, T. Taketsugu, M. W. Schmidt, M. S. Gordon, J Chem. Phys., 121,1383, (2004).

MRCI Characterization of the Low Lying Quintet States of MoO Radical

Gabriel Lopes^a (IC), Marcelo A. P. Pontes^b (PG), Francisco B.C. Machado^b (PQ),
Luiz A. Ferrão^b (PQ), Harley P. Martins Filho^a (PQ) and Joaquim D. Da Motta Neto^a (PQ)

^a Department of Chemistry, Univ. of Paraná (UFPR), P.O. Box 19081, Curitiba, PR

^b Instituto Tecnológico de Aeronáutica (ITA), São José dos Campos, SP, Brazil.

e-mail: quim@ufpr.br

Keywords: molybdenum monoxide, CASSCF, MRCI, spectroscopic constants

INTRODUCTION

In recent years several studies have been published on the properties of MoO. Early MCPF calculations by Langhoff and Bauschlicher¹ on the electronic structure of MoO examined a small set of states and characterized the ground state as $^5\Pi$ with configuration $(2\delta)^2 (12\sigma)^1 (6\pi)^1 (13\sigma)^0$. Later, Hamrick and Morse² obtained a high resolution optical spectrum of jet-cooled MoO, and obtained several spectroscopic constants for several quintet states. Given the interest in these systems, we have studied them using multireference methods.

METHODS

The chosen basis was the aug-cc-pV5Z set for both atoms, with inclusion of ECP for Mo. The zeroth order wavefunction was obtained at the CASSCF level, and the resulting optimized MOs were used in MRCI calculations. The calculations were carried out using the MOLPRO program and the molecular constants have been calculated by solving the radial equation using the INTENSITY code.

RESULTS AND DISCUSSION

Table 1 shows our calculated spectroscopic constants, and Figure 1 shows our calculated potential curves for the quintet low lying states of MoO radical.

Table 1. Quintet electronic states of MoO.

state	r_e (Å)	T_e (cm ⁻¹)	ω_e (cm ⁻¹)	$\omega_e x_e$ (cm ⁻¹)
$X^5\Pi$	1.713	0	924.0	2.90
$(1)^5\Sigma^-$	1.742	10877	862.1	4.26
$(1)^5\Sigma^+$	1.757	11896	859.6	0.51
$A^5\Delta$	1.752	16214	886.7	2.51
$B^5\Pi$	1.795	21747	788.0	9.30

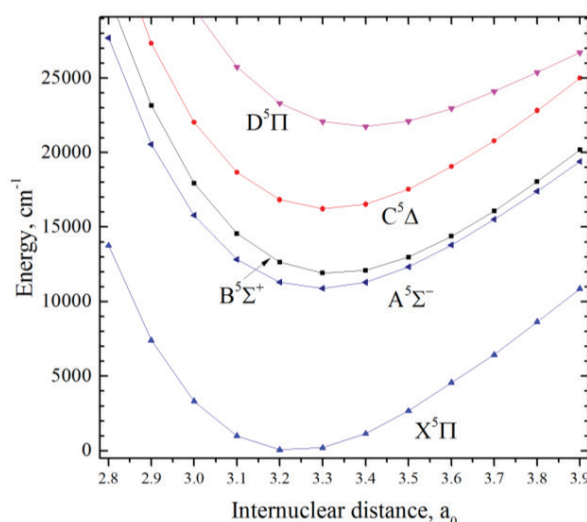


Figure 1. Calculated potential curves for MoO.

Our calculated harmonic frequency of 924 cm⁻¹ matches the MCPF value of 850 cm⁻¹ by Bauschlicher. We discuss the fact that this transition is apparently absent in the infrared spectrum obtained by Andrews and coworkers³.

CONCLUSIONS

We have studied MoO using multireference methods. We present a list of spectroscopic constants for this little known system.

ACKNOWLEDGMENTS

The authors are grateful for the support given by Brazilian agencies FAPESP, CNPq and CAPES.

¹ S.R. Langhoff, C.W. Bauschlicher and L.G.M. Pettersson, Chem. Phys. 132, 49 (1989).

² Y.M. Hamrick, S. Taylor and M.D. Morse, J. Mol. Spectrosc. 146, 274 (1991).

³ W.D. Bare, P.F. Souter and L. Andrews, J. Phys. Chem. A 102, 8279-8286 (1998).

LUMPAC LUMinescence PACKage: New methods and implementations

José Diogo Lisboa Dutra^{a,b} (PG), Ricardo Oliveira Freire^b (PQ)

^a Departamento de Química Fundamental, UFPE, 50.740-540, Recife, PE, Brazil

^b Pople Computational Chemistry Laboratory, Departamento de Química, UFS, 49.100-000 – São Cristóvão, SE, Brazil

Keywords: LUMPAC, Luminescence, Lanthanide, Europium Complexes

INTRODUCTION

The systems containing lanthanide have been widely studied due to their several applications such as in luminescent sensor, optical fibers, biologic markers, and luminescent devices. The search for new lanthanide systems can be carry out only by using theoretical methods. Due to lack of a computational tool with these methods implemented, the LUMPAC¹ (LUMinescence PACKage) software was developed and is available free of charge at <http://www.lumpac.pro.br>.

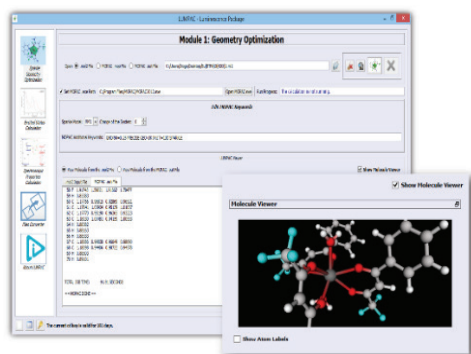


Figure 1. LUMPAC software.

LUMPAC is structured in modules. The first and second one are integrated to the MOPAC and ORCA programs, respectively, enabling the geometry optimization of the system and the excited states calculations of the ligand part. The third module calculates the luminescence properties, such as experimental and theoretical intensity parameters (Ω_λ), energy transfer rates, and theoretical emission quantum yield. The fourth module is a file converter. In the first version of LUMPAC were just implemented some of the main methods commonly applied to study luminescence properties of lanthanide systems. This work aims to present the new methods and implementations that were added to the second version of LUMPAC.

RESULTS AND DISCUSSION

Currently, we are reparameterizing the INDO/S-CIS semiempirical method, which is implemented into ORCA. At the end, we hope to obtain a method with similar accuracy compared to TD-DFT method for the excited states calculations of systems containing lanthanide. A new submodule that enables the phenomenological calculation of the Stark levels was added to the third module. From this calculation, the ligand field parameters (B_{kq}) are obtained. In the submodule regarding the calculation of energy transfer rates, we implemented the model developed by Malta and coworkers to calculate the energy transfer in systems with charge transfer band². Furthermore, the model improved by Malta to calculate the energy transfer rates between two lanthanide ions³ was also implemented into this new version of LUMPAC.

CONCLUSIONS

All these new implementations become LUMPAC a tool ever more useful for that research groups interested in understanding the photophysical properties of systems containing lanthanide ions. In a little more than one year, we already distributed more than 100 licenses throughout the world.

ACKNOWLEDGMENTS

The authors are grateful for the support given from the FAPITEC-SE, CAPES, INCT-INAMI, and CNPq.

¹ J.D.L. Dutra, T.D. Bispo, R.O. Freire, J. Comp. Chem. A, 35, 772,(2014).

² W.M. Faustino, O.L. Malta, G.F. Sá, J. Chem. Phys., 122, 054109,(2005).

³ O.L. Malta, J. Non-Cryst. Sol., 354, 4770,(2008).

Mechanism of Dimethyl Sulfide Oxidation by Hydrogen Peroxide with Niobium Oxyhydroxide Heterogeneous Catalyst

Carlos M. Silva (PG) and Josefredo R. Pliego Jr (PQ)

DCNAT, Universidade Federal de São João del-Rei, 36301-160, São João del-Rei, MG, Brazil
pliego@ufsj.edu.br

Keywords: Heterogeneous Catalysis, Niobium Oxyhydroxide, Oxidation, DMS, H₂O₂

INTRODUCTION

Experimental studies have shown that niobium oxyhydroxide (NbO₂OH) acts as support and active phase in various reactions to form highly oxidizing groups on its surface when in contact with H₂O₂.¹ However, reactions on surfaces are generally poorly understood by the difficulty to characterize unequivocally the structure of the adsorbed species and transition states (TS). In this respect, the computational chemistry methods have much to contribute. Thus, in this theoretical study, we have investigated the dimethyl sulfide (DMS) oxidation mechanism by H₂O₂ on the surface of NbO₂OH in order to better understand this catalytic process, since there is no computational study reported in the literature up to date.

METHODS

Equilibrium geometries and harmonic frequencies calculations have been obtained using the X3LYP functional with the SBKJC+P(d) basis set and ECP. More reliable single point energy calculations and solvation free energy using the SMD solvation model have been done at X3LYP/SVP+diff level. The potential of mean force (W(r)) has been calculated according to eq. (1), in order to predict relative rates among different reaction pathways.

$$W(r) = E_g + \Delta G_{\text{solv}} \quad (1)$$

RESULTS AND DISCUSSION

Fig. 1 shows that the catalytic route occurs in two steps: In the first one, the Nb atom of the catalyst surface is attacked nucleophilically by H₂O₂, via TS2a heptacoordinated, leading to the formation of hydroperoxo groups (HO–O–Nb). In the second step, these hydroperoxo groups formed on the surface promote the DMS oxidation (Fig. 2). The oxidation mechanism is similar to a nucleophilic substitution process on the oxygen of the peroxide group, with niobium acting as a

Lewis acid and the oxygen of the Nb–O–Nb group as a Brønsted base in the proton capture. At the end of this heterolytic process, the catalyst is regenerated and a new catalytic cycle starts.

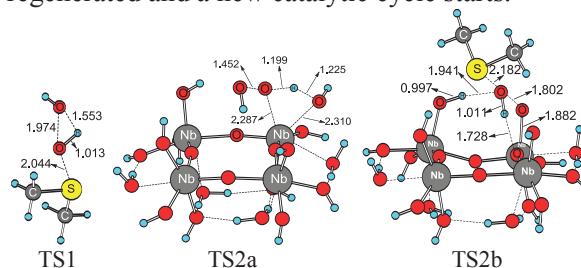


Figure 1. Uncatalyzed (TS1) and catalyzed (TS2a and TS2b) reactions for DMS oxidation by H₂O₂.

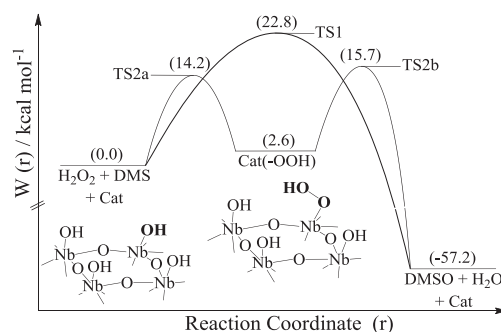


Figure 2. W(r) profile for the DMS oxidation by H₂O₂ catalyzed by NbO₂OH.

CONCLUSIONS

We have found the reaction pathway able to explain the catalytic effect of NbO₂OH on DMS oxidation by H₂O₂. There is formation of a hydroperoxo species on the surface, which is able to act as Lewis base and Brønsted acid, providing a decrease of the activation barrier by -7.1 kcal mol⁻¹ in relation to the free hydrogen peroxide reaction.

ACKNOWLEDGMENTS

The authors are grateful for the support of the agencies CAPES, FAPEMIG and CNPQ.

¹ L. C. A. de Oliveira, et al. Appl. Catal. B: Envir., 147, 43, (2014).

Photophysical study of Tröger's base molecular scaffolds

Josene M. Toldo^a (PG), Rodrigo R. Descalzo^a (IC), Débora M. P. Aroche^b (PG), Fabiano S. Rodembusch^b (PQ), Paulo F. B. Gonçalves^a (PQ)

^a Universidade Federal do Rio Grande do Sul, Instituto de Química, Grupo de Química Teórica.

^b Universidade Federal do Rio Grande do Sul, Grupo de Pesquisa em Fotoquímica Orgânica Aplicada.

^{a,b} Av. Bento Gonçalves, 9500, Porto Alegre – RS. Brazil

josene.toldo@ufrgs.br

Keywords: DFT, Photophysical, Tröger's base.

INTRODUCTION

Tröger's base (TB) is a chiral amine first synthesized by Julius Tröger in 1877. Its intrinsic concavity provides a rigid structure and its chirality results from the very high energy barrier for the inversion of the nitrogen atoms. Due to these characteristic, Tröger's base analogues have countless potential applications, such as molecular recognition, catalysis, medicinal chemistry, supramolecular chemistry and new materials.¹ Although there have been several reports of new Tröger's base analogues, there are few reports in the literature studying the electronic structure of these analogues.² In this work, we dedicate our efforts to the understand of the photophysical of Tröger's base structures shown in Figure 1 by comparing experimental and theoretical properties predicted with TD-DFT.

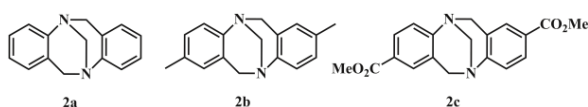


Figure 1. Structure of the studied Tröger's bases (2a-c).

METHODS

Time-dependent Density Functional Theory (TD-DFT) was used to study the photophysical behavior of Tröger's base structures. Geometry optimization and vibrational analysis of the ground (S_0) and first excited state (S_1) were done at PBE1PBE/cc-pVDZ level of theory and vertical transitions were calculated at PBE1PBE/aug-cc-pVDZ level. Solvent effects are included by IEF-PCM formalism using 1,4-dioxane (DIOX), ethyl acetate (AcOEt), dichloromethane (DCM), ethanol (EtOH) and acetonitrile (MeCN) as solvent. All calculations were carried out using Gaussian 09 Package.

RESULTS AND DISCUSSION

The theoretical results are very close to the experimental. Tröger's bases 2a-b present absorption maxima (λ_{abs}) located around 280 nm and emission maxima (λ_{em}) near to 350nm, while 2c presents a λ_{abs} around 315nm and λ_{em} around 425nm. A larger red-shift observed in 2c could be associated with the increase of π system length, due to the presence of C=O group. A small solvatochromic effect was observed in 2a-c absorption wavelength indicating an almost absence charge transfer in S_0 . However, 2c structure shows a higher solvatochromic effect in emission wavelength. In addition, a larger change in dipole moment from S_0 to S_1 in 2c (around 4 times) indicates an intramolecular charge transfer mechanism in S_1 , corroborates by Lippert-Mataga plot. The vertical transitions from S_0 to S_1 are $\pi \rightarrow \pi^*$ type, from HOMO to LUMO molecular orbitals.

CONCLUSIONS

The photophysical study show that i) TB 2a-c present a main absorption in UV region and emission at a violet-blue region; ii) the vertical transitions are ascribed to $\pi\pi^*$ electronic transitions; iii) the presence of substituents in 2-8 positions causes a bathochromic effect; iv) a small solvatochromic effect in S_0 points to an almost charge transfer, but in 2c a intramolecular charge transfer in excited state is expected.

ACKNOWLEDGMENTS

The authors are grateful for the support given from the CAPES and CNPq.

¹ D.M.P. Aroche, J.M. Toldo, R.R. Descalzo, P.F.B. Gonçalves and F. Rodembusch. *New J. Chem.*, (2015). DOI: 10.1039/c5nj01166c.

² O.V. Rúnarsson, J. Artacho and K. Wärnmark, *Eur. J. Org. Chem.*, 36, 7015 (2012).

Docking de novos derivados do Ácido Kójico com potencial atividade Anti-tirosinase

Joyce Lima Vale^a (PG), Nelson Alencar^b (PG), Tainá Barros^b (PG), Davi Brasil^a (PQ).

¹Laboratório de Modelagem Molecular e Materiais - Universidade Federal do Pará

²Laboratório de Planejamento de Desenvolvimento de Fármacos - Universidade Federal do Pará

joycelima@ufpa.br

Palavras Chave: *Docking*, Acoplamento molecular, Tirosinase, Ácido kójico, Tropolone, derivados

INTRODUÇÃO

A tirosinase (EC 1.14.18.1) é uma enzima binuclear que contém um cobre como cofator redox no seu sítio ativo, e através de reações de hidroxilação, (atividade monofenolase), oxidação (atividade difenolase), seguida de polimerização, forma melanina¹. A tirosinase, está envolvida tanto nos processos de escurecimento de frutos, quanto em mecanismos de neurodegeneração de Parkinson¹. O Ácido Kójico (AKJ) possui amplo perfil farmacológico, e é tido padrão positivo para tirosinase². Estes estudos ressaltam a importância do desenvolvimento de novos inibidores de tirosinase derivados do AKJ, pois, inúmeros compostos têm sido relatados, mas, a maioria não são potentes o suficiente, ou não possuem perfis terapêuticos adequados³.

MÉTODOS

Através do programa Molegro Virtual Docker (MVD®), foram realizados cálculos de energia de interação, do AKJ e 12 derivados, no sítio ativo da enzima tirosinase, utilizando o algoritmo MolDock ($E_{\text{Score}} = E_{\text{inter}} + E_{\text{intra}}$), onde E_{inter} é a energia de interação ligante-proteína e E_{intra} é a energia interna do ligante. A análise foi baseada no modelo cristalográfico da tirosinase tipo *Agaricus bisporus* (Data Bank Protein, código PDB: 2Y9X). A estrutura do Tropolone (OTR) foi submetida ao redocking e utilizada como guia para definir os parâmetros estruturais e validar a estratégia computacional no *docking* do AKJ e derivados.

RESULTADOS E DISCUSSÃO

Durante as simulações observou-se que as orientações vinculativas e geometrias para o OTR acoplado no sítio ativo 2Y9X pode ser sobreposta e são consistentes com a estrutura de raios-X publicada⁴.

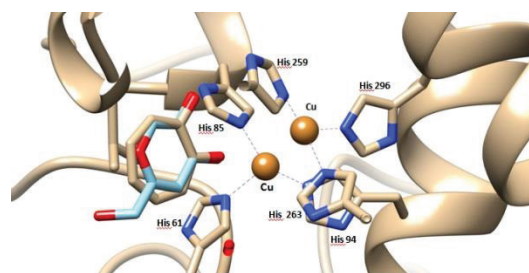


Figura 1. *Docking* do AKJ no sítio ativo da tirosinase.

O AKJ e os 12 derivados testados foram ancorados na mesma região que o inibidor OTR. Esses resultados são consistentes com modelos obtidos para ancoragem em tirosinase de *A. bisporus*². Além disso, demonstraram boa afinidade com o sítio receptor e menor energia quando comparados ao inibidor (OTR: -57.478 kcal.mol⁻¹). Os derivados 2,3,8 e 9 demonstraram valores de MolDock Score (kcal.mol⁻¹) de -71.3983, -70.0027, -71.6849 e -72.6554, respectivamente. Estes resultados são corroborados por estudos anteriores que sugerem que a introdução de elementos eletronegativos pode contribuir para a ligação do possível inibidor à cadeia lateral da enzima⁵.

CONCLUSÕES

Os resultados das simulações de *Docking* foram satisfatórios. Os valores de energia obtidos sugerem que os derivados 2,3,8 e 9 podem ser potenciais candidatos a novos inibidores da tirosinase.

AGRADECIMENTOS

Os autores agradecem o auxílio financeiro dado pela CAPES.

¹Yang, M.H.Chen, C.M.J.Biosci. Bioeng. 2013.

²Saghaie, M.; Res. in Pharm. Sci. 2013.

³You, A.O. Zhou, J. Eur. J. Med. Chem.2015.

⁴Wangsa T. I. Henriette J. Biochem. 2011

⁵Noh, J-M; Bioorg. & Med. Chem. 2009.

Adsorption of Water and Oxygen on Arsenopyrite (001) Surface

Silva, J. C. M.^a (PG), Heine, T.^b (PQ), De Abreu, H. A.^a (PQ) and Duarte, H. A.^a (PQ)

^a Universidade Federal de Minas Gerais, Department of Chemistry, Av. Antônio Carlos 6627, 31.270-901, Belo Horizonte – BRAZIL

^b Jacobs University, Physics and Earth Sciences, Campus Ring 1, 28759, Bremen – GERMANY
e-mail: julianacmsilva@gmail.com

Keywords: Density Functional Theory (DFT), Arsenopyrite, Surface, Adsorption, Oxidation.

INTRODUCTION

Arsenopyrite is a mineral present in gold mining tailings and, as the other mineral sulfides, it is responsible for Acid Rock Drainage (ARD) – a process in which the sulfide mineral in contact with water and oxygen oxidizes, yielding sulfuric acid – contaminating soils and waters. Therefore understanding the reaction process involved in ARD is very important and not yet completely understood. The reactions involved are much complex, leading to a lack of consensus in the literature¹. Therefore, theoretical calculations can contribute to the understanding of the reaction mechanism at a molecular level. In this work the adsorption of water and oxygen on the most stable arsenopyrite surface² was investigated in order to understand the first step of the oxidation mechanism of this mineral.

METHODS

Density Functional Theory (DFT) with plane waves approximation implemented in Quantum Espresso package was used for investigating the adsorption of water and oxygen on the (001) surface of arsenopyrite. The spin-polarized calculations were performed using PW91 XC functional, with an energy cutoff of 30 Ry, a **K**-point mesh of 2×2×1 and a vacuum layer of 15Å.

The Density of States (DOS) analysis of the surface indicate that the adsorption of a Lewis base is preferred at the Fe site². This is probably the site where the oxidation reaction starts.

RESULTS AND DISCUSSION

The results show that the molecular adsorption of one water molecule to a Fe atom on the surface is favorable, with adsorption energy of -11.04 kcal mol⁻¹, unlike the dissociative adsorption, which has an adsorption energy of 4.50 kcal mol⁻¹. Due to two different types of Fe sites on the surface model, the most stable configuration for a full coverage of water molecules on the surface is when 4 water

molecules bond to the iron atoms on the surface and other 4 molecules make hydrogen bonds with the adsorbed molecules. In this case the adsorption energy per water molecule is similar to the energy of a single molecule (-11.45 kcal mol⁻¹).

The adsorption of one oxygen molecule is also favorable with high energy, especially when it is dissociative (-59.41 kcal mol⁻¹). In the last case the oxygen atoms bond to Fe and As atoms of the surface in a 3 member ring. The effect of the co-adsorption of water and oxygen on the surface has been investigated and will be discussed in detail.

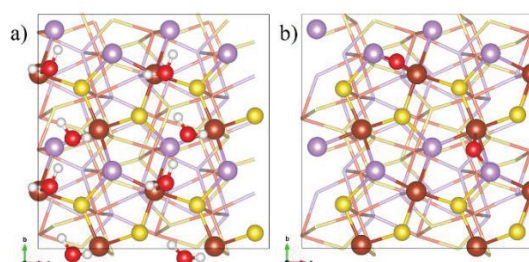


Figure 1. Adsorption on arsenopyrite (001) surface: a) water molecules, b) one dissociated oxygen molecule.

CONCLUSIONS

The adsorption of water and oxygen molecules on arsenopyrite surface was investigated using DFT/plane waves method. Water adsorbs molecularly up to 4 molecules to the surface and oxygen is strongly adsorbed.

ACKNOWLEDGMENTS

The authors are grateful for the support given from the CNPq, CAPES, FAPEMIG, INCT-Acqua, and the European Commission FP7-PEOPLE-2011-IRSES TEMM1P, GA 295172.

¹ C. L. Corkhill and D. J. Vaughan, Applied Geochemistry, 24, 2342, (2009).

² J. C. M. Silva, H. A. De Abreu, and H. A. Duarte, RSC Adv., 5, 2013, (2015).

Theoretical investigation on the mechanism of corrosion inhibition of the (001) iron surface by imidazole and imidazoline: a surface coverage study.

Juliana O. Mendes (PQ), Alexandre B. Rocha (PQ), Marco Antonio Chaer Nascimento (PQ)

*Instituto de Química, Universidade Federal do Rio de Janeiro, Brazil;
e-mail: mendesjuliana.juli@gmail.com*

Keywords: Corrosion inhibition, iron surface, protective film, periodic DFT calculations.

INTRODUCTION

Organic heterocyclic compounds containing nitrogen atoms are commonly used as corrosion inhibitors¹. Those inhibitors can adhere to a metal surface to form a protective film against corrosive agents in the environment. However, the mechanism of inhibition is not well understood yet. In the current work, we applied density functional theory (DFT) under periodic boundary conditions to evaluate the surface coverage of four organic heterocyclic compounds and predict a potential formation of a protective film on the (001) iron surface.

COMPUTATIONAL DETAILS

The calculations were performed within the DFT (Density Functional Theory) under periodic boundary conditions with a plane wave basis set and ultrasoft pseudopotentials. We used the Generalized Gradient Approximation (GGA) functional of Perdew, Burke and Ernzerhof (PBE)³ implemented in the PWSCF code of the Quantum Espresso⁴ suite of programs. The coverage was carried out varying from 2 to 6 the number of adsorbed molecules.

RESULTS AND DISCUSSION

For imidazole the highest surface coverage was achieved with four molecules adsorbed per unit cell, giving rise to a tetrameric structure (-1.62 eV) (Figure 1, left). For imidazoline, the highest coverage is achieved with only two molecules adsorbed, resulting in a dimeric structure (-2.68 eV) (Figure 1, right). The new structures (imidazole tetramer and imidazoline dimer), interact more strongly with the (001) iron surface than the respective monomers (-1.53 eV and -0.93 eV, respectively). These results can be understood as a cooperative effect that occurs during the adsorptions, leading to the formation of a film.

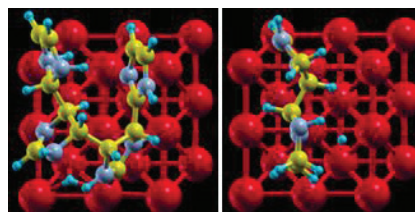


Figure 1. Structures yielded from the surface coverage: (left) imidazole tetramer and (right) imidazoline dimer.

CONCLUSIONS

In this work, a model is proposed to explain the inhibition performance of two organic heterocyclic compounds. Preliminary results show that the inhibition performance of imidazole and imidazoline molecules can be explained by the formation of a film. The formation of the films is due to a cooperative effect on the adsorption, caused by the breaking of double bonds on the rings and the formation of C–C sigma bonds between the molecules on the surface.

ACKNOWLEDGMENTS

The authors thank for the financial support given from the FAPERJ, CAPES, CNPQ and INOMAT.

¹ J. Cruz et al., *J. Electroanal. Chem.*, 566, 111, (2004).

² J. Cruz et al., *Int. J. Quant. Chem.*, 85, 546, (2001).

³ J. P. Perdew; K. Burke; M. Ernzerhof, *Phys. Rev. Lett.* 77, 3865, (1996).

⁴ P. Giannozzi et al., *Quantum Espresso (v. 5.0)*, *J. Phys.: Condens. Matter.*, 21, 395502 (2009).

Estudo de Interação do Cardanol com Mineral Albitapor Meio de Modelagem Molecular para Utilização na Etapa de Resinagem de Rochas Ornamentais

Julio C. G. Correia^a (PQ), Alexandre N. M. Carauta^{a,b} (PQ), Danielle da S. Rosa^a (PG), Letícia M. Prates^d (PG), Kelly F. Pessôa^a (IC), José Walkimar de M. Carneiro^e (PQ), Maurício T. M. Cruz^d (PQ), Elaine R. Maia^c (PQ)

^aCentro de Tecnologia Mineral – CETEM/ MCTI. Rio de Janeiro- RJ. Brazil

^bFundação Técnico-Educacional Souza Marques. Rio de Janeiro- RJ. Brazil

^cInstituto de Química, Físico- Química, Universidade de Brasília- UnB-Brasília-DF. Brazil.

^dDepartamento de Química Geral e Inorgânica, Instituto de Química, Universidade do Estado do Rio de Janeiro – UERJ. Rio de Janeiro – RJ. Brazil

^eDepartamento de Química Inorgânica, Instituto de Química. Universidade Federal Fluminense – UFF, Niterói- Rio de Janeiro – RJ. Brazil

Palavras-chave: cardanol, albita, modelagem molecular

INTRODUÇÃO

A etapa de resinagem de rochas ornamentais é um processo de beneficiamento de extrema importância, pois a resina tem como função estruturar o material e melhorar a qualidade da superfície da mesma. O cardanol presente no líquido da casca da castanha de caju (LCC) possui características físico-químicas diferenciadas que lhe permitem grandes combinações químicas podendo ser utilizadas nas mais diversas indústrias e é uma opção viável e de baixo custo para realizações de pesquisas de produtos poliméricos para a produção de resinas, já que ele possui propriedade de resistência à água e a produtos químicos. A modelagem molecular que se baseia em métodos computacionais para a simulação de sistemas o mais próximo possível do real, pode estudar antes da fabricação, se a resina derivada do líquido poderá ser favorável ao processo de resinagem.

METODOLOGIA

Uma análise conformacional das estruturas do cardanol e do sistema cardanol-albita foi realizada utilizando dinâmica molecular clássica em um *ensemble* (NVT), a 298 K, campo de força Dreiding, e 1 ns de tempo. A estrutura da albita foi obtida a partir do banco de dados do programa *Materials Visualizer* e foi mantida fixa, sendo suas cargas calculadas o método Qeq para equilíbrio das cargas com algoritmo Ewald para tratar as interações não ligadas. Após a análise da trajetória calculada, as estruturas de mais baixas energias foram selecionadas e submetidas a uma nova minimização de energia a fim de obter a

estrutura de menor energia. A partir da estrutura de energia mínima calculada pela dinâmica molecular, cálculos a partir da Teoria do Funcional de Densidade foram realizados com os métodos B3LYP/6-31G (d,p) para o cardanol e B3LYP/LANL2DZ para a albita.

RESULTADOS E DISCUSSÃO

A Figura 1 mostra a estrutura mais estável para o sistema albita-cardanol.

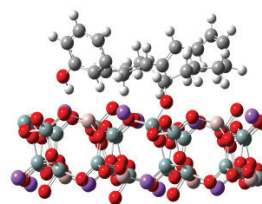


Figura 1 – Cardanol-Albita.

As distâncias entre o cardanol e a albita indicam que a interação ocorre. Os cálculos utilizando o campo de força COMPASS indicam que a energia de interação é favorável e que a análise dos termos do campo de força não ligados mostra que as interações eletrostáticas eram as principais responsáveis pela interação. Os cálculos com DFT com a correção para a sobreposição de bases estão em curso.

AGRADECIMENTOS

Os autores agradecem ao CNPq e ao CETEM pelo suporte dado.

Adsorption of Drugs in Metal-Organic Frameworks: A Combined Grand Canonical Monte Carlo and DFT-D Study.

Júlio C. S. Da Silva^a (PQ), Amanda L.^a (PG), Roberta P. Dias^b (PQ) and Thereza A. S.^a (PQ)

^a Departamento de Química Fundamental, UFPE.

^b Centro Acadêmico do Agreste, UFPE.

Keywords: Grand Canonical Monte Carlo, DFT-D, Metal Organic Frameworks.

INTRODUCTION

Metal-organic frameworks (MOFs) have drawn considerable attention in recent years due to their promising applications in gas technology, catalysis, sensors, electronic devices, and more recently, drug delivery.¹ In general, MOFs have excellent biodegradability, biocompatibility and guests loading capability, endowing promising candidates as nano-carrier platforms for drug delivery. Given the fact of the existence of many different MOF structures, a systematic study of their performance in drug delivery is crucial for identification of new promising structures. In order to get a detailed understanding about the adsorption of drugs in MOFs, is essential to get information about the nature of the interactions between the drug and specific sites of the material. Inside this context, molecular simulations emerge as an outstanding approach to predict the performance of the MOFs for drug delivery from the quantitative predictions with additional molecular level insight.²

METHODS

Grand Canonical Monte Carlo simulations were carried out to investigate the adsorption mechanism of some drugs (5-fluoracil, ibuprofen, cis-platinum and carbo-platinum) in different Metal-Organic Frameworks (MOFs) (three new nanocage-based MOFs of Zn, Cu, Sm and HKUST-1). Some configurations obtained during the GCMC simulations were used to estimate the binding energy of the drugs from DFT-D calculations.

RESULTS AND DISCUSSION

Figure 1(a), 1(b) and 1(c) shows some snapshots taken from GCMC simulation of the adsorption of 5-fluoracil (5-FU) in **ZnMOF**, **CuMOF** and **SmMOF** MOFs, respectively.

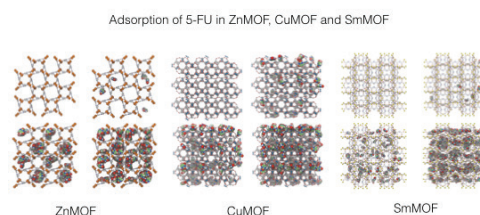


Figure 1. Snapshots of 5-FU in ZnMOF (a), CuMOF (b) and SmMOF (c).

According our GCMC results the 5-FU adsorption to **ZnMOF**, should occurs in two steps: (1) 5-FU molecules fill up the larger pore, forming well-structured aggregates. (2) Once the larger pores are occupied, 5-FU molecules bind to the smaller pore albeit in much smaller numbers. Our results also suggest that 5-FU binding preferences to **ZnMOF**, **CuMOF** and **SmMOF** reflect the diversity in pore types, chemical nature and size. The calculated drug payloads indicate that capacity of each material in adsorb the 5-FU is more related to the accessible volume than to the pore size. We calculated the bind energy of the drugs in the materials from DFT-D calculations performed with molecular models built from some configurations generated in the GCMC simulations. Details about these calculations as well as the results obtained will be presented and discussed during the event.

CONCLUSIONS

The GCMC simulations and DFT-D calculations carried out in this work revealed some insights into the fundamental aspects related to adsorption mechanism of some drugs in different Metal-Organic Frameworks.

ACKNOWLEDGMENTS

FACEPE, CAPES and CNPQ.

¹ MOFs special issue: Chem. Rev., 112, 2 (2012).

² R. Q. Snurr, et al, J. Mater. Chem. B, 2, 766-774, (2014).

Purificação da Matriz Densidade Usando Operações de Álgebra Linear Esparsas baseadas em Orbitais Moleculares Localizados para GPUs.

Júlio Daniel de Carvalho Maia^a (IC), Gerd Bruno Rocha^b (PQ)

^a Centro de Informática, UFPB, João Pessoa – PB, Brasil, CEP: 58051-900
juliodaniel.carvalho@gmail.com

^b Departamento de Química, UFPB, João Pessoa – PB, Brasil, CEP: 58051-900
gbr@quimica.ufpb.br

Keywords: Escalonamento Linear, PDM, GPU, matrizes esparsas e métodos semiempíricos

INTRODUÇÃO

Métodos de estrutura eletrônica baseados na purificação da matriz de densidade (PDM, do inglês *Purification of Density Matrix*) são empregados quando se deseja o cálculo químico quântico completo de sistemas com muitos átomos. Nesses métodos, operações de multiplicações de matrizes (ex. $P^2 = P \times P$) são necessárias durante o *updating* da matriz densidade no SCF. Nesse trabalho algoritmos paralelos para GPU e CPU são propostos para a multiplicação de matrizes esparsas armazenadas no formato SVBR (*Symmetrical Variable Block Row*) para a realização dessa etapa através das equações do algoritmo SP2 [Cawkwell, M. J., *et al*, J. Chem. Theory Comput. 2012, 8, 4094–4101] e usando métodos semiempíricos implementados no programa MOPAC [Maia, J. D. C., *et al*, J. Chem. Theory Comput. 2012, 8, 3072–3081].

METODOLOGIA

Todos os cálculos foram executados utilizando um processador Intel® Xeon® E5-2620, 12 núcleos, de 2.0 GHz e 64GB de RAM. A GPU utilizada foi uma NVIDIA Tesla K20c com 5.0GB de VRAM dedicada. Para testar a performance dos nossos algoritmos, usamos como *benchmark* um conjunto de caixas de simulação esféricas contendo moléculas de água, rotuladas de W_n , onde n representa o raio em angstroms da caixa ($n = 10$ a 37Å). Rotulamos de: i) **GPU**, para os cálculos que foram executados na GPU; ii) **12T**, para os que utilizaram os 12 núcleos do processador; iii) **1T**, para o cálculo serial de referência.

RESULTADOS E DISCUSSÕES

A figura 1 mostra o escalonamento do algoritmo proposto para a atualização da matriz densidade via o método PDM para os sistemas usados como *benchmark*.

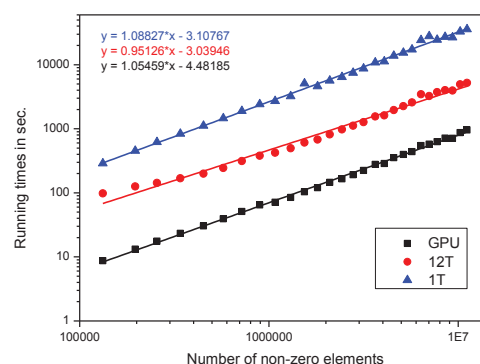


Figura 1. Somatório dos tempos de todas as chamadas do procedimento PDM durante a convergência do SCF para caixas com água, W_n , onde, $n = 10$ até 37Å , em escala log-log.

De acordo com os resultados da figura 1, percebemos que todos os protocolos escalonam o tempo de execução do procedimento PDM de forma linear com o aumento do número de elementos não-zeros. Podemos notar também que as equações do método SP2 resolvidas através do algoritmo de multiplicação de matrizes esparsas para GPUs possui um desempenho superior quando executado na CPU com **1T** e **12T**.

CONCLUSÃO

Com essa etapa finalizada podemos partir para acelerar outras partes do código do MOPAC, como a montagem da matriz de Fock e o cálculo de integrais de dois elétrons e, assim, aplicar os métodos semiempíricos para a modelagem de sistemas moleculares de grande complexidade, tais como proteínas e polímeros.

AGRADECIMENTOS

Os autores agradecem a PRONEX/FACEPE, CNPq e CAPES.

Insights Regarding the Irreversible Molecule Pulling in Complex Fluid Systems by Means of Molecular Dynamics Simulations

Kalil Bernardino^a (PG), André Farias de Moura^a (PQ)

^a Departamento de Química, Centro de Ciências Exatas e de Tecnologia, Universidade Federal de São Carlos, Rodovia Washington Luiz km 235, CP 676, CEP 13565-905, São Carlos, SP, Brasil.

Keywords: Steered Molecular Dynamics, Micelle, Free Energy, Irreversible Thermodynamics, Jarzynski Equality

INTRODUCTION

Although the Jarzynski equality (JE)¹ provides a way to obtain the equilibrium free energy difference from an ensemble of irreversible amounts of work, its convergence can be very poor, especially if the system is far from equilibrium, since the more negative contributions, although rare, have a greater weight in JE. Instead, if the distributions of irreversible amounts of work can be assumed to be normal, a simple relation emerges from JE relating the free energy to the more easily converging arithmetic average, $\langle w \rangle$, and variance, σ^2 .¹ (Equation 1)

$$\Delta F = \langle w \rangle - \frac{\sigma^2}{2k_B T} \quad (1)$$

This work aims to test this equation and the physical hypotheses behind it in complex fluid systems by calculating ensembles of the irreversible pulling of a surfactant ion from an equilibrated micelle at several pulling speeds.

METHODS

The model systems consisted of a coarse-grained SDS micelle (N=60) in aqueous solution. Starting with structures obtained from equilibrium simulations, several pulling experiments were performed in which a single surfactant ion was removed from the micellar cluster by defining a reaction coordinate between the head of the molecule to be removed and the center of mass of the remaining cluster, forcing the surfactant to move along this reaction coordinate at a constant speed from its initial position to the bulk solution. The integration of the force exerted on the pulling group along the reaction coordinate yielded the irreversible amount of work for the complete removal. This protocol was repeated at several speeds: 120 replicas at 0.01 m/s, 240 at 0.05, 240 at 0.1, 360 at 0.2, 480 at 0.5 and 960 at 1.0 m/s.

RESULTS AND DISCUSSION

The variance varied linearly with the average values calculated for the work ensembles at each pulling speed (Figure 1), as suggested in Eq. 1. However, the slope of the linear regression, (4.3 ± 0.3) kJ/mol, is significantly smaller than the $2k_B T$ value at 300 K (5.0 kJ/mol). Three main effects can explain this discrepancy and are currently being investigated: (1) a feedback control effect induced by the methodology itself, which, if present, should introduce a correction in Eq. 1, (2) The fact that surfactant may start at different positions along the reaction coordinate in the outset of each pulling simulation, due to the flexible nature of the micelle, and (3) small differences from the normal distribution that should also introduce corrections in Eq. 1.

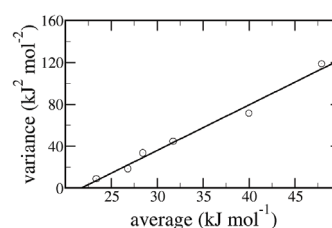


Figure 1. Linear regression of the variance as a function of average values of irreversible work distributions obtained at different pulling speeds.

CONCLUSIONS

Our results should be applicable to other complex fluid systems and suggest corrections in Eq. 1. and those corrections may provide physical insights on the behavior of these systems.

ACKNOWLEDGMENTS

The authors are grateful for the support from FAPESP (2012/15.147-4), CAPES and CNPq. AFM also thanks MEC/PET for a fellowship.

¹ C. Jarzynski, *Annu. Rev. Condens. Matter Phys.* 2, 329 (2011).

Influence of DFT functionals in the molecular structure and thermodynamic properties of the molybdenum oxodiperoxo complexes.

Kayo F. da Silva^a (IC), Lucelma P. de Carvalho^a (IC), Marcus Vinicius Pereira dos Santos^a (PQ), Juliana A. B. Silva^a (PQ), Ricardo L. Longo^b (PQ)

^a*Centro Acadêmico do Agreste, Universidade Federal de Pernambuco*

^b*dQF - Centro de Ciências Exatas e da Natureza, Universidade Federal de Pernambuco*

Keywords: Oxo-diperoxo Complexes, DFT, Oxidation Reactions, Activation Energy

INTRODUCTION

Metal transition oxodiperoxo complexes of type $[MO(O_2)_2L_1L_2]$, $M = Mo$ e W , $L_1 =$ pyrazole, N-oxo of pyridine, $L_2 = H_2O$, silica, are used in several selective oxidation reaction, e.g., of olefins and sulfides, in which the active species transfer oxygen and after can be regenerated, but these active species are not well established yet.

The use of quantum chemical computational methods to obtain the molecular and electronic structures of complexes of these kind and similar ones should be useful in understanding their behavior in oxygen transfer reactions and in proposing mechanisms which can also explain the observed chemoselectivity. For this purpose, in this work, ground state molecular and electronic structure calculations of some compounds with the general formula $[MoO(O_2)_2L_1L_2]$ with $L_1 =$ none, HMPA, OPH_3 , N-oxo of pyridine, pyrazole, silica, and $L_2 =$ none or H_2O , were performed.

METHODS

We have calculated all molecular and electronic structures of these complexes considered in this work and all critical points of the potential energy surface have been characterized by Hessian matrix. All calculations were performed with Gaussian 09 program (Rev. D.01). We applied four DFT functionals in this study: B3LYP, PBE1PBE, WB97XD and M062X. These functionals were used associated with the 6-31G(d) basis set for all atoms, except the LanL2DZ (basis set and effective core potential) applied for molybdenum.

RESULTS AND DISCUSSION

In terms of geometry parameters, functionals B3LYP, M062X and PBE1PBE presents same Mo-L bond distances. In addition, these values keep the same for heptacoordinated complexes with water in the axial position. These results corroborate with the experimental observation that

in this position, the ligand has a weaker coordination. Effects such inclusion interval correction and dispersion correction (via functional WB97XD) are not essential for describing these structures. Instead, they overestimate interactions. Nevertheless, B3LYP functional presented the closest results in comparison to X-ray crystallography¹ results. Using B3LYP, it easier to keep the Cs-asymmetric structure of pentacoordinated moieties, since previous experimental studies have reported that this symmetry is substantially maintained even in the presence of ligands L_1 and/or L_2 . However, for heptacoordinated complexes with the water ligand in the axial position, the bond distance Mo-OH₂ is not well described, since its coordinate at this position is weaker. This discrepancy between the calculated and experimental results was previously attributed,¹ at least partially, solid-state effects and these differences become larger when the ligand is weaker. Unlikely the results obtained for the geometrical parameters, it seems that the inclusion of dispersion and correction range are important for achieving stabilization energies results obtained for by other groups. However, it is needed further investigation to acquire quantitative information.

CONCLUSIONS

The results show that the methodology is suitable for the study of molybdenum oxodiperoxo complexes, since the values of the geometric parameters of the studied complexes are in good agreement with literature data. Our results may help in the investigation of their reactivities and chemoselectivities in order to determine the mechanisms involved in such reactions.

ACKNOWLEDGMENTS

The authors are grateful for the support given from the FACEPE, CAPES, CNPq.

¹D. V. Deubel, J. Sundermeyer, G. Frenking, *Inorg. Chem.*, 39, 2314, (2000).

Estudo Químico-Quântico do Rearranjo do tipo McLafferty durante a Fragmentação Molecular do 1-Nitropropano

Laís de S. Barbosa^{a*} (PG), Sara F. de A. Morais^a (PG), Kleber C. Mundim^a (PQ),
Daví A. C. Ferreira^{a†} (PQ)

^a Laboratório de Modelagem de Sistemas Complexos, Instituto de Química, Universidade de Brasília,
Campus Darcy Ribeiro, CP 04478, CEP: 70904-970, Asa Norte - Brasília-DF, Brasil.

*laisbsousa@gmail.com / †dacf@unb.br

Palavras chave: Rearranjo do tipo McLafferty, CBS-Q, Espectrometria de Massas, Fragmentação.

INTRODUÇÃO

A espectrometria de massas é uma importante técnica para análise de estruturas moleculares diversas, que se baseia na ionização e fragmentação, de maneira que o caminho de fragmentação se passa pela formação de intermediários estáveis naquelas condições de fragmentação. Assim, compreender os mecanismos de reações de fragmentações é de fundamental importância para elucidar o espectro de massa e, conseqüentemente, determinar a composição de amostras tomando como ponto de partida os intermediários catiônicos e/ou radiculares formados. Dentre os diversos mecanismos de fragmentação, destaca-se o Rearranjo do tipo McLafferty¹, um modelo mecanístico bastante aplicado na interpretação de surgimento de intermediários no espectro de massa. Neste trabalho foi investigado o rearranjo de McLafferty (de *b* para *c*) do 1-nitropropano (PrNO₂), descrito na Figura 1.

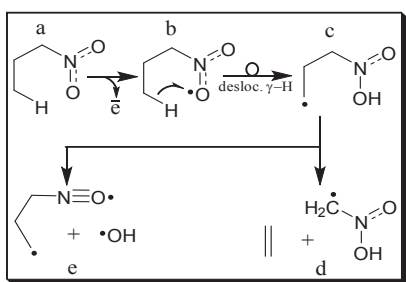


Figura 1. Mecanismo de fragmentação do PrNO₂.

MÉTODOS

Para a realização deste estudo foi aplicado o método CBS-Q, para a descrição da coordenada de fragmentação, e Dinâmica Semi-Clássica do tipo Born-Oppenheimer com a combinação HF/3-21G, para a verificação de complexos de van der Waals no processo de fragmentação molecular.

RESULTADOS E DISCUSSÃO

Na descrição das duas rotas de fragmentação do PrNO₂, verificamos que há um favorecimento termodinâmico para a ocorrência da fragmentação passando pelo rearranjo do tipo McLafferty, como descrito na Figura 2.

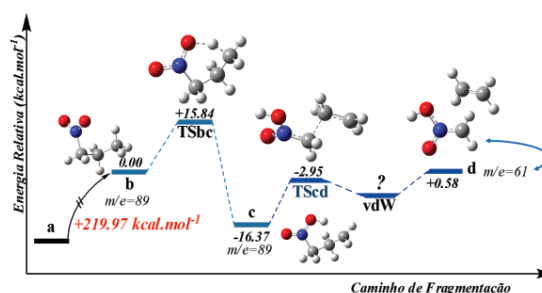


Figura 2. Coordenada de fragmentação do PrNO₂ para a formação do produto *d*.

A fragmentação que conduz ao produto *e*, ocorre através de uma barreira de ativação da ordem de +35.7 kcal.mol⁻¹, enquanto que para a fragmentação que conduz a *d*, a barreira foi da ordem de +13.4 kcal.mol⁻¹. Para a formação de *d*, foi identificado um complexo de van der Waals (*vdW*), que é cerca de 10.0 kcal.mol⁻¹ mais estável que o estado de transição anterior (*TScd*). A formação de *d* é eletronicamente guiada pela formação de apenas um radical, enquanto que o não favorecimento de *e* pode ser facilmente compreendida pela formação de um mono e um bi-radical. Análises QTAIM estão em andamento.

CONCLUSÕES

O rearranjo do tipo McLafferty é cinética e termodinamicamente favorecido na fragmentação do PrNO₂; ao mesmo tempo, a geração do produto *d* é eletronicamente favorecido por formar apenas uma espécie radicalar.

AGRADECIMENTOS

CAPES e CNPQ.

¹ N. M. M. Nibbering, J. Am. Soc. Mass. Spectrom., 15, 956, (2004).

ESTUDOS TEÓRICOS DA FOTOISOMERIZAÇÃO DE BUTADIENO COM SUBSTITUÍNTES CHO E Cl

Laís Petra Machado (IC); Márcio Soares Pereira (PQ)

DEQUIM/ICE/UFRRJ, msoares@ufrj.br

Palavras-chave: Fotoisomerização, butadieno, pentadienal

INTRODUÇÃO

A interação entre a luz e a matéria está presente nos mais importantes processos da natureza. Fótons são utilizados por sistemas naturais como doadores de energia ou como elementos de informação. A isomerização Z-E da ligação C=C é induzida pela energia proveniente dos fótons¹. Este é um processo fotoquímico amplamente explorado e forma a etapa fundamental em muitos processos fotobiológicos como, por exemplo, visão, bomba de íons induzida pela luz e fototaxia.²

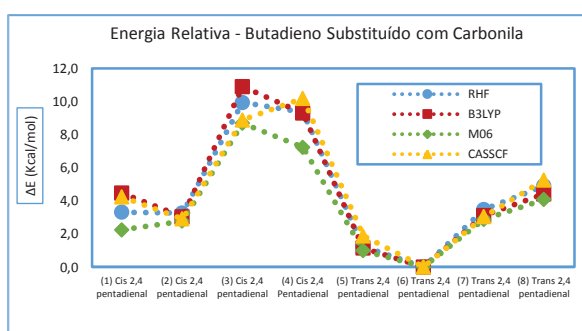
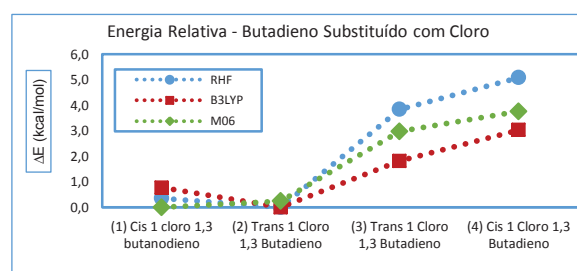
O projeto tem como objetivo obter pontos relevantes da superfície da energia potencial para as moléculas de butadieno substituído com grupo Cl e moléculas de butadieno substituídas com carbonila. Esta descrição da superfície pode gerar um modelo para a compreensão da influência dos grupos na geometria e no processo de fotoisomerização.

MÉTODOS

Foram estudadas as moléculas de cloro-butadieno e pentadienal. Como ponto de partida para as investigações no estado excitado, foram mapeadas as configurações das moléculas que correspondem a mínimos na superfície de energia no estado fundamental, através de quatro metodologias: o método Hartree-Fock (HF); funcional da densidade (DFT), com dois funcionais (B3LYP e M06) e o método CASSCF. Todos os cálculos foram realizados com o programa GAMESS. Os Cálculos DFT e HF foram realizados com a base 6-31G**, o os cálculos de CASSCF foram realizados com a base ACCD.

RESULTADOS

Os gráficos a seguir apresentam a energia relativa para os confôrmeros de cadeia aberta dos butadienos substituídos.



É possível observar que, tanto para o Cl-butadieno quanto para o pentadienal, o confôrmero que corresponde ao mínimo global é um isômero E (trans). Por outro lado as estruturas de maior energia correspondem a isômeros Z (cis).

CONCLUSÃO

Neste trabalho foram mapeados os mínimos na superfície de energia potencial para o butadieno substituído com CHO e Cl no estado fundamental. Estão sendo concluídos os cálculos dos estados de transição conectando os diferentes confôrmeros e estão sendo investigadas as estruturas no estado excitado.

AGRADECIMENTOS: CNPQ

Semeraro, M.; Silvi, S.; Credi, A. AIP Conf. Proc. 2007, 963, 603–606

Dugave, C.; Demange, L. Chem. Rev. 2003, 103, 2475–2532.

Desenvolvimento e Parametrização do Método Semiempírico RM1 para Níquel.

Larissa Tavares de Jesus^a (G), José Diogo Lisboa Dutra^{a,b} (PG), Manoel Alves Machado Filho^a (PG), Alfredo Mayall Simas^b (PQ) e Ricardo Oliveira Freire^a (PQ)

^a *Pople Computational Chemistry Laboratory, Departamento de Química, UFS, 49.100-000 – São Cristóvão, SE, Brasil.*

^b *Departamento de Química Fundamental, UFPE, 50.740-540, Recife, PE, Brasil.
larissatdejesus@hotmail.com*

Palavras-Chave: RM1, Parametrização, Métodos Semiempíricos, Níquel.

INTRODUÇÃO

O níquel, é um dos 5 elementos ferromagnéticos. Evidências sugerem que o níquel pode ser um elemento essencial para mamíferos¹. Ele ocupa o sítio ativo de seis dos diversos tipos de enzimas desidrogenases, tais como acetil-CoA e Urease, de grande importância nos mais diversos organismos². Atualmente, os métodos PM6 e PM7 são os únicos métodos semiempíricos capazes de tratar sistemas moleculares que contém átomos de níquel. Neste trabalho apresentamos a parametrização do método semiempírico RM1³ para o átomo de níquel com a inclusão explícita de orbitais do tipo s, p e d no conjunto de base.

METODOLOGIA

Através de uma pesquisa no banco de dados *Cambridge Structural Database – CSD*, 146 complexos contendo átomos de níquel foram selecionados. Utilizando a técnica estatística DIANA, realizamos uma análise de agrupamentos hierárquicos, com o objetivo de separar as estruturas para a formação dos conjuntos de parametrização. Foram selecionadas 13 estruturas para compor o conjunto de parametrização reduzido e 36 estruturas para compor o conjunto de parametrização expandido. O conjunto teste foi composto por todas as 146 estruturas. Após a parametrização do modelo que durou vários meses, procedemos com a validação dos parâmetros obtidos. Os Erros Médios Absolutos - EMA (Eq. 1) foram utilizados no procedimento de validação.

$$EMA = \frac{1}{n} \sum_{j=1}^n |R_j^{CSD} - R_j^{calc}| \quad (1)$$

RESULTADOS E DISCUSSÃO

O processo de validação do modelo considerou todos os métodos semiempíricos

disponíveis para cálculo de sistemas contendo átomos de níquel. Analisando os erros apresentados na tabela 1, verifica-se que o RM1 possui menores erros para a maioria dos tipos de ligação existentes nos sistemas que compuseram o conjunto teste.

Tabela 1: Comparação entre erros obtidos com os métodos RM1, PM6 e PM7.

	Nº de medidas	Erro Médio Absoluto (Å)		
		RM1	PM6	PM7
Ni – Ni	14	0,2792	0,7062	0,5502
Ni – O	112	0,0731	0,4626	0,2213
Ni – N	221	0,0763	0,1185	0,1986
Ni – C	71	0,1040	0,0638	0,0965
Ni – S	107	0,1336	0,1246	0,1084
Ni – P	107	0,1978	0,0348	0,1125
Ni – F	1	0,0268	0,1157	0,878
Ni – Cl	44	0,1003	0,1578	1,3705
Ni – Br	27	0,0460	0,0908	0,2264
Ni – L	711	0,1101	0,1681	0,246
L – L	1219	0,2292	0,3223	0,5064
Todas	1930	0,1853	0,2655	0,4105

CONCLUSÕES

A análise geral dos erros obtidos com os métodos PM6, PM7 e RM1 mostra que o RM1 apresenta uma redução de 30% e 55% em relação aos métodos PM6 e PM7 respectivamente.

AGRADECIMENTOS

FAPITEC-SE, FACEPE, CAPES, INCT-INAMI E CNPq.

¹ K.K. Das.; S.N. Das.; S.A. Dhundasi., *Indian J Med Res*, 128, 412, (2008).

² W.R. Stephen, *Current Opinion in Chemical Biology*, 2, 208, (1998).

³ G.B. Rocha.; R. O. Freire, A. M. Simas, J. J. P. Stewart, *J. Comput. Chem.* 27, 1101, (2006).

Comparative Analysis of Docking Programs Using Distinct Protein-Ligand Test Sets

Lucas A. Vizani¹ (PG), Isabella A. Guedes¹ (PG), Diogo A. Marinho¹, Camila S. de Magalhães² (PQ) and Laurent E. Dardenne¹ (PQ)

¹ *Laboratório Nacional de Computação Científica – LNCC/MCTI*

² *Universidade Federal do Rio de Janeiro – Campus Xerém – UFRJ*
dardenne@lncc.br

Keywords: Protein-Ligand Docking, Molecular Modeling, Rational Drug Design

INTRODUCTION

Protein-ligand docking methodologies are important tools for structure-based rational drug design studies. These methods aim to predict the experimental binding mode and affinity of a small molecule within the binding site of the protein target of interest. The DockThor program, developed by the Brazilian group GMMSB/LNCC, uses a grid based methodology and was implemented to deal with highly flexible ligands using a multiple-solution steady state genetic algorithm[1]. The scoring function is based on the MMFF94S classical force field.

In this work the Dockthor performance was evaluated through a comparative analysis of redocking experiments with three of the most used docking programs, i.e., GLIDE, GOLD and AutoDock Vina. The comparative analysis was performed using two receptor-ligand test sets: (i) the Astex Therapeutics Ltd test set[2], containing 85 diverse and curated protein-ligand complexes and (ii) the Iridium-HT[3], a high quality test set containing 120 diverse protein-ligand complexes.

METHODS

We observed that for some of the complexes of the Iridium-HT dataset the ligand and protein residues protonation and tautomeric states were not correctly taken into account. We curated this dataset using PROPKA, Epik and Protoss tools to predict the correct protonation states for both protein and ligand. For all complexes no protein-ligand pre-optimization was made (i.e., the crystallographic structures were maintained in their original conformation).

The GOLD program was evaluated using the ChemPLP scoring function. For all complexes, the docking programs were executed using their best docking protocols and using a grid of dimension of 22 Å in each dimension.

Best energy ligand pose predictions with RMSD values lower than or equals to 2.0 Å from the experimental structure were considered as a docking success.

RESULTS AND DISCUSSION

DockThor obtained very satisfactory results in the redocking experiments.

For the Astex test set, considering the top-scoring pose, Dockthor obtained a success of 77.7% and GOLD, Vina and GLIDE obtained 85.9%, 77.7% and 78.8% respectively.

For the Iridium-HT test set, DockThor obtained a success rate of 75.4% when considering only the top-scoring poses and 82.2% when considering multiple solutions with similar energies with the top-scoring one.

CONCLUSIONS

In this work, we performed a comparative analysis of redocking experiments for four docking programs: Glide, GOLD, AutoDock Vina and Dockthor. The analyses show that the DockThor (<http://www.dockthor.lncc.br>) program has a great potential to be widely used in real receptor-ligand studies showing a comparable overall performance with the other programs evaluated.

ACKNOWLEDGMENTS

The authors are grateful for the financial support from FAPERJ, CAPES and CNPQ

¹ C. S. de Magalhães, D. A. Marinho H. J. C. Barbosa, L. E. Dardenne, *Information Sciences*, 289, 206, (2014)

² Hartshorn, M. J., et al *J. Med Chem.* 50, 726 (2007)

³ Warren et al., *Drug Disc. Today*, 12, 1270, (2012)

Theoretical Investigations of the Effect of Solvent in the IR Absorption via Density Functional Theory Calculations for a Series of Systems Theobromine-Water.

SANTIN, L.G.^a (PG), ALBERNAZ, A.^a (PQ), CAMARGO, A.J.^b (PQ), OLIVEIRA, S.S.^b (PQ), GARGANO, R.^a (PQ)

^aInstituto de Física, Universidade de Brasília (UNB). CP 04455, Brasília, DF, CEP 70919-970, Brasil

^bUnidade Universitária de Ciências Exatas e Tecnológicas (UnUCET), Universidade Estadual de Goiás (UEG). BR 153, km 98, CEP 75001-970, Anápolis, GO, Brasil.

Keywords: Theobromine, DFT, Water, Hydrogen bonding.

INTRODUCTION

Molecular systems where there are hydrogen bonds are studied a long time due to its importance in the fields of physical-chemistry, biochemistry, materials science and other areas. These hydrogen bonds are responsible also for the molecular and macroscopic properties of materials. The analysis of hydrogen bonds that occur between water molecules and potential drug candidates is very important for medicine and pharmaceutical industry. Theobromine is one of the main active components of the seeds cocoa and chocolate, where is found in abundance, and is one of the main metabolites of caffeine.¹ Thereby it is very consumed by the world's population. This molecule has several medicinal properties, such as potential diuretic, antitussive, anti-inflammatory, antitumor, and is a stimulant of the peripheral physiology^{2,3}. The design of effective drugs implies the knowledge of some key properties, such as the molecular behavior in aqueous solutions and the main molecular sites of electrophilic attack, nucleophilic reactions. In this study, we analyzed the changes in infrared (IR) absorption frequencies, map electrostatic potential (MEP) and frontier orbitals for theobromine isolated and in aqueous solution, using DFT calculations. We analyzed 9 different systems: theobromine isolated, theobromine interacting with water molecules ranging from one to seven (solvent explicit), and other system considering only water dielectric constant (solvent implicit) in solvation. We want to observe the changes generated by the use of explicit and implicit solvent in the properties analyzed.

METHODS

We perform the computations using Gaussian package at B3LYP/6-31g(d,p) and M06L/6-31g(d,p) level.

RESULTS AND DISCUSSION

Our results indicate that for the observed frontier orbitals the main sites of electrophilic and nucleophilic attack vary with the inclusion of new water molecules, generating different energy gaps and modifying the calculation levels significantly alter these values. The vibrational frequencies were changed mainly in the region of 3000 cm⁻¹, as expected for water molecules.

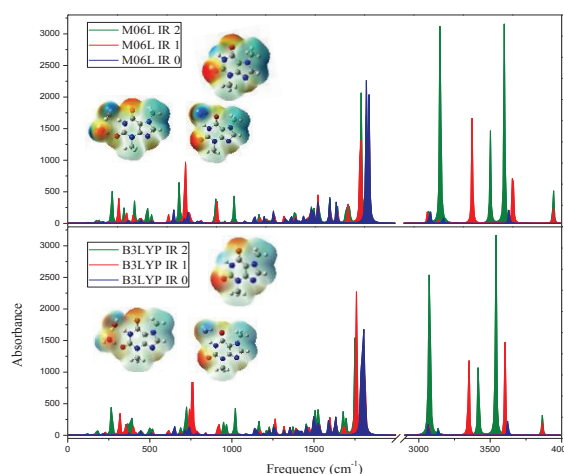


Figure 1. Infrared absorption frequencies for theobromine isolated and theobromine with one and two water molecules for M06L and B3LYP levels.

CONCLUSIONS

The present study shows that the inclusion of water molecules modifies the frontier orbitals. In the IR spectrum, the water molecules modify the absorption peaks.

ACKNOWLEDGMENTS

CAPES

¹ S. Gunasekaran et al. *Spectrochim. Acta Part A* 61 117–127 (2005).

² N. Sugimoto et al. *Nutrition and Cancer*. 66(3), 419–423 (2014).

³ Usmani et al. *The FASEB Journal*. 19 (2005).

Combined use of Sequential QM/MM and Free Energy Gradient methods in the study of electronic and conformational structure of molecules with acceptor-donor groups

Leandro R. Franco (PG), Idney R. Brandão (PG)
 Tertius L. Fonseca (PQ), Herbert de C. Georg (PQ)

Instituto de Física, Universidade Federal de Goiás, CP 131, 74001-970, Goiânia, GO
leofrancofisica@gmail.com

Keywords: Sequential QM/MM, Free Energy Gradient, ASEC-FEG.

INTRODUCTION

The combined use of the Sequential QM/MM method with a mean field approximation (ASEC) [1] and the Free Energy Gradient method [2] has been very successful in describing the electronic structure of molecules in solution [3]. In this work, we will show the results we recently obtained in applying that combination to study the structure of DMACA and Phenol Blue (PB) in several solvents, such as cyclohexane, acetonitrile, water and other protic and aprotic solvents covering a range of polarity. We studied the solvent effect in the geometry, the electronic absorption spectrum and the first hyperpolarizability.

METHODS

The methodology consists in an iterative process. In each step of the process we perform: (i) a Monte Carlo simulation with empirical Lennard-Jones-Coulomb potential to generate few hundreds of uncorrelated configurations; (ii) calculation of the ensemble average of the solvent potential to include in the solute's Hamiltonian; (iii) calculation of the atomic forces and the hessian matrix so that a new geometry can be obtained using a Newton-Raphson scheme; (iv) lastly, a calculation of the charge distribution of the molecules in the presence of the solvent in the new geometry. With the new geometry and atomic charges, the next step of the simulation is initiated. The geometry optimization and hyperpolarizability calculations were performed using the MP2 method. The electronic excitation calculations were obtained with TD-DFT.

RESULTS AND DISCUSSION

Covering a reasonable variety of solvents, we found that for low polarity solvents like cyclohexane, there are no significant changes in geometry, excitation energy and electrical properties in relation to the gaseous phase.

In aqueous solution, where the most significant changes are observed, PB has the typical conjugation of single and double N–C bonds between the rings slightly inverted. Also, the well characterized aromatic and quinonoidal rings of the molecule in vacuo are both deformed to something in between these two situations. In DMACA, the changes are less abrupt. The C=C bonds increase and the C–C bonds decrease, but they lie in the halfway to equalize themselves. But, in both solutes, the pyramidal angle of the dimethylamino group decreases almost 30 degrees in comparison with the vacuum, leading to a planar conformation of the amino group. Furthermore, our results are in accordance with the experimentally observed behavior of DMACA and PB in solution for solvatochromic shifts and hyperpolarizabilities.

CONCLUSIONS

The simulations performed in this work show that the ASEC-FEG method is able to capture efficiently the major solvent effects in the geometry of the molecules, giving results in good agreement with experiment for molecules with acceptor-donor groups connected by large conjugated or aromatic chains.

ACKNOWLEDGMENTS

DFT Study on the Influence of the Cluster Size and Noncovalent Interactions in the CO Adsorption on Au/MOR Catalyst

Lenin Díaz Soto,¹ Aníbal Sierralta,² and Marco A. C. Nascimento³

¹ PUC-Rio de Janeiro, Departamento de Física, 22451-900 Rio de Janeiro, RJ, Brazil

² Laboratorio de Química-Física y Catálisis Computacional, IVIC, Caracas 1020 A, Venezuela

³ Instituto de Química, UFRJ, CT Bloco A sala 412, Rio de Janeiro, RJ 21949-900, Brazil
diazlenin@gmail.com

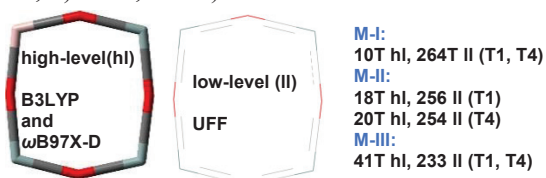
Keywords: Gold, mordenite, CO adsorption, noncovalent interactions.

INTRODUCTION

The discovery of the remarkable activity of gold nanoparticles in CO oxidation at low temperatures has stimulated the research of gold as a catalyst. Au⁺ and Au⁰ are considered responsible for CO activation, and the water gas shift (WGS) reaction at low temperature. Recently, it has been shown that protected Au⁺ inside the KLTL zeolite could favor the WGS reaction below 498 K.¹ Noncovalent interactions are important in determining the stability and reactivity of many different species. In this work, we employ the ONIOM-2 method and the density functional theory (DFT) to model the Au-exchange mordenite (MOR) catalyst, Au/MOR, in order to establish the influence of the noncovalent interactions on the CO adsorption energy ($E_{\text{ads}}\text{CO}$) and CO frequency (νCO).

METHODS

The tetrahedron (T) sites T1 and T4 inside MOR were represented by three models, varying the size of the high-level (hl) and low-level (ll): a) M-I, b) M-II, and c) M-III.



The calculations were done with the G09 program. UFF was employed for the ll calculations. Hl calculations were performed using B3LYP and $\omega\text{B97X-D}$ with: LANL2DZ for the atoms belonging to the MOR model, ACEP-121 effective potential for Au, and BS2 basis set for CO.² The BSSE and ZPVE correction was included in the reported $E_{\text{ads}}\text{CO}$.

RESULTS AND DISCUSSION

The Au-C and C-O distances for all the models, sites and DFT approaches are similar, $d(\text{Au-C}) \sim 1,86 \text{ \AA}$ and $d(\text{C-O}) \sim 1,14 \text{ \AA}$. Generally,

the Au-C-O angle is smaller at T4 than at T1, by 1 to 5°. Increasing the model has little effect on the $E_{\text{ads}}\text{CO}$, Figure 1a show $\Delta E_{\text{ads}}\text{CO} = E_{\text{ads}}\text{CO}(\text{B3LYP}) - E_{\text{ads}}\text{CO}(\omega\text{B97X-D})$.

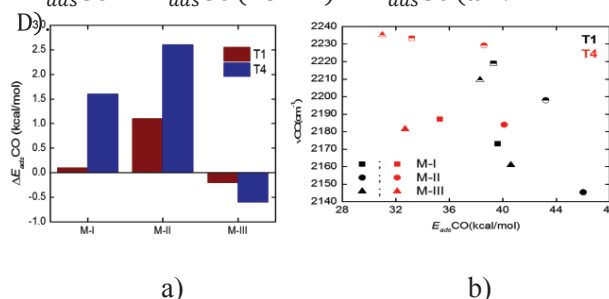


Figure 1. (a) $\Delta E_{\text{ads}}\text{CO}$ and (b) νCO ; fully-filled symbols represent the B3LYP results and half-filled the $\omega\text{B97X-D}$ results.

The νCO is larger, at T1 and T4 sites, when the $\omega\text{B97X-D}$ functional is used (Figure 1b). $\nu\text{CO}(\text{T4})$ does not change with the size of cluster but $\nu\text{CO}(\text{T1})$ does. The $\nu\text{CO}(\text{T1})$ follows the trend: M-I > M-III > M-II for both B3LYP and $\omega\text{B97X-D}$. The M-III model does not represent adequately the T1 site even though it has more Ts in hl.

CONCLUSIONS

The Au-C-O geometrical parameters and the $E_{\text{ads}}\text{CO}$, in the OC-Au/MOR do not change with the inclusion of noncovalent interactions. $\nu\text{CO}(\omega\text{B97X-D}) > \nu\text{CO}(\text{B3LYP})$ and T1 is sensitive to the size of the cluster.

ACKNOWLEDGMENTS

A. S. acknowledge the financial support given by the Misión Ciencia project. The rest of the authors acknowledge financial support from CNPq, FAPERJ, and INOMAT.

¹ M. Yang, S. Li, Y. Wang, J. A. Herron, Y. Xu, L. F. Allard, S. Lee, J. Huang, M. Mavrikakis, M. Flytzani-Stephanopoulos, Science (80-), 346, 1498, (2014).

Antioxidant Activity of Isolated Interglycosidic O-(1→3) Flavonols: a DFT study

Leonardo M. F. de Oliveira^a (IC), Rafael G. Vicari^a (IC) and Gabriel L.C de Souza^a (PQ)

^aFederal University of Mato Grosso, Department of Chemistry, 78060-900 Cuiabá-MT, Brazil
 Email: leonardomfoliveira@gmail.com

Keywords: DFT, Flavonols, Antioxidant Activity
 INTRODUCTION

Many properties of the flavonols are related to their antioxidant activities.¹ Recently, two new Quercetin and Kaempferol derived flavonols presenting the uncommon interglycosidic O-(1→3) linkage were isolated from *Loranthaceae* family plants extracts.² In this work, we present a computational study on *Kaempferol 3-O-α-L-arabinofuranosyl-(1→3)-α-L-rhamnoside* (Compound K) and *Quercetin 3-O-α-L-arabinofuranosyl-(1→3)-α-L-rhamnoside* (Compound Q).

The Hydrogen-Atom Transfer and the Single Electron Transfer mechanisms were probed for both compounds through the determination of the Bond Dissociation Enthalpies (BDEs) and Ionization Potentials (IPs), respectively. Present Kaempferol and Quercetin computations along with others results of computational studies on Kaempferol and Quercetin available in the literature as well as solvent effect computations were also used for comparisons.

METHODS

The geometries of the neutral molecules and all their radicals were fully optimized up to the B3LYP/6-31+G(d,p) level of theory.³⁻⁵ Computations for open-shell species were undertaken with UB3LYP. Vibrational frequencies were computed for both molecules and radicals, to characterize the conformations as minima. All the computations were performed in Gaussian 09 suite of codes.⁶

BDEs were determined as:

$$\text{BDE} = H_f(\text{ArO}\cdot) + H_f(\text{H}\cdot) - H_f(\text{ArOH})$$

where $H_f(\text{ArO}\cdot)$ is the enthalpy of the radical generated via H-atom abstraction, $H_f(\text{H}\cdot)$ is the enthalpy of the H atom and $H_f(\text{ArOH})$ is the enthalpy of neutral molecules. The IPs were determined as the difference between the ArOH and ArOH⁺ energies (electronic + ZPE) for each compound.

RESULTS AND DISCUSSION

As we can see in Figure 1, computed BDEs and IPs values for both Compounds K and Q are slightly lower when compared to Kaempferol and Quercetin, respectively. This indicate that the presence of the sugar O-(1→3) linkage moiety can lead to a small increase in the antioxidant activity for the studied compounds, when compared to their respective parental molecules.

Radicals	Compound K	Kaempferol	Compound Q	Quercetin
BDEs				
3'-ArO	-	-	73.08	75.39
4'-ArO	81.28	81.45	78.14	82.15
7-ArO	87.68	87.19	83.28	87.08
5-ArO	99.13	96.16	95.06	96.26
IPs				
	169.38	170.35	168.00	168.90

Figure 1. BDEs and IPs (in kcal.mol⁻¹) at 298 K for Compounds K and Q along with results computed for Kaempferol and Quercetin. All results were computed in the gas phase at B3LYP/6-31+G(d,p) level of theory.

CONCLUSIONS

BDEs and IPs obtained suggest both compounds studied are promising in presenting antioxidant activity. Thus, further experimental tests (e.g. IC50) are encouraged. Additional results will be presented at the Conference.

ACKNOWLEDGMENTS

The authors thank CNPq and CAPES.

- ¹ D. Flores *et al.*, Food. Chem., 141, 1497, (2013).
- ² A. C. Guimarães *et al.*, Nat. Prod. Commun., 7, 1, (2012).
- ³ A. D. Becke, J. Chem. Phys., 98, 5648, (1993).
- ⁴ C. Lee *et al.*, Phys. Rev. B, 37, 785, (1988).
- ⁵ J. S. Binkley *et al.*, J. Am. Chem. Soc., 102, 939, (1980)
- ⁶ M. J. Frisch *et al.*, Gaussian 09, Revisions D.01, (2009).

Estudo Computacional sobre a Formação da Ligação Amídica Catalisada pela Superfície (100) da γ -Al₂O₃

Lethícia Ramos Santos (PG) e Fabrício R. Sensato (PQ)

*Universidade Federal de São Paulo, UNIFESP, Campus Diadema,
e-mail: lethicia.ramosdossantos@yahoo.com*

Palavras-chave: Cálculos de Estrutura Eletrônica, Amidação, Química Verde, Alumina

INTRODUÇÃO

A formação da ligação amídica é uma das mais importantes reações em síntese orgânica, uma vez que amidas são empregadas em uma ampla variedade de aplicações industriais. Correntemente, o mais popular método industrial de síntese de amidas baseia-se na ativação do ácido carboxílico e subsequente acoplamento com uma amina. No entanto, esse tipo de protocolo reacional exibe muitos infortúnios, tais como emprego de reagentes de elevado custo e/ou toxicidade, baixa economia de átomos, formação de subprodutos não desejados, longo tempo reacional, baixo rendimento, condições severas de reação e o uso estequiométrico de reagentes de acoplamento. No entanto, muito recentemente um protocolo “verde” de formação da ligação amídica foi reportado, independentemente, por Das et al. e Mukhopadhyay et al., o qual se baseia na reação direta de ácidos carboxílicos e aminas catalisada por nanopartículas de γ -Al₂O₃.^{1,2} Contudo, o mecanismo molecular associado à interveniência da γ -Al₂O₃ permanece ainda desconhecido. Neste estudo, cálculos de estrutura eletrônica e teoria do estado de transição foram empregados para a investigação do mecanismo molecular de formação da ligação amídica pela reação direta entre aminas e ácidos carboxílicos catalisada por γ -Al₂O₃.

MÉTODOS

Os cálculos foram feitos em nível DFT/B3LYP/6-31G(d,p). Neste estudo, foram empregados dois modelos de descrição para a superfície do óxido, a saber, modelo de aglomerados (cluster) e modelo híbrido ONIOM com o método semiempírico AM1 para a descrição do sistema real, (Al₂O₃)₃₄. Os cálculos foram feitos com o programa Gaussian09. Utilizou-se como modelo para o ácido fórmico a molécula de ácido fórmico, enquanto a amina foi representada pela metilamina.

RESULTADOS E DISCUSSÃO

Com o modelo mais sofisticado de representação do óxido (ONIOM B3LYP/6-31G(d,p):AM1) caracterizou-se o seguinte mecanismo de formação da ligação amídica: na primeira etapa, os reagentes se adsorvem na superfície (100) do óxido de alumínio. Observa-se que a superfície exerce um papel bastante relevante na orientação das moléculas interagentes. Na segunda etapa, o nitrogênio da amina ataca o carbono da carboxila do ácido fórmico com a simultânea transferência do hidrogênio ligado ao nitrogênio ao oxigênio da carbonila, via TS1, formando o intermediário dihidroxilado metilamino-metanodiol. A energia de ativação do processo é de 44 kcal/mol. A energia do intermediário adsorvido é 25 Kcal/mol maior que a energia dos reagentes adsorvidos. O intermediário, então, sofre um processo (etapa 3) de condensação das hidroxilas levando à sua desidratação, via TS2, resultando na formação dos produtos, adsorvidos (amida e água). A correspondente energia de ativação é 33 kcal/mol maior que a energia dos reagentes adsorvidos na superfície do óxido. A adsorção da água provoca o deslocamento do equilíbrio no sentido dos produtos.

CONCLUSÃO

As energias de ativação para os dois TS associados à formação da ligação amídica pela reação direta do ácido fórmico com a metilamina catalisada pela γ -Al₂O são 44 kcal/mol e 33 kcal/mol, respectivamente.

¹ S. Ghosh, A. Bhaumik, Mondal, J., A. Mallik, S. Sengupta, and C. Mukhopadhyay, Green Chem. 14, 3220, (2012).

² V.K. Das, R.R. Devi, P.K. Raul and A. J. Thakur, Green Chem. 14, 847, (2012).

A Density Functional Theory Study of NO Adsorption on Pd₄ and Pd₄/γ-Al₂O₃ Clusters

Leticia Maia Prates (PG), Maurício Tavares de Macedo Cruz (PQ)

Departamento de Química Geral e Inorgânica, Instituto de Química, Universidade do Estado do Rio de Janeiro, Rio de Janeiro, Brazil
 leticiamaiapr@gmail.com

Keywords: γ-Al₂O₃, palladium cluster, nitric oxide, heterogeneous catalysis, DFT

INTRODUCTION

For the removal of nitric oxide, specifically, the heterogeneous catalysis using Pd particles supported on γ-Al₂O₃ has shown good results. Some studies show that the support plays an important role in the reactivity of supported metals^{1,2}. Therefore, it is important to evaluate how the structure of γ-Al₂O₃ contributes to the process of interaction with the NO molecule. In this work, DFT calculations were performed to obtain geometric, electronic and energetic parameters involved in the adsorption of NO on palladium clusters isolated and supported in alumina.

METHODS

As a first step, a molecule of NO has been optimized in several modes of adsorption on palladium clusters with both planar and tetrahedral arrangements with Pd—Pd distance fixed in 2.751 Å (bulk of palladium). To simulate the interaction between NO and palladium cluster supported, a planar Pd₄ with initial distance of palladium bulk (2.751) was optimized on an Al₁₈O₂₇ cluster. Following, the NO molecule was optimized on different sites containing palladium atoms. All calculations were carried out with the Gaussian 03 program and performed with B3LYP method employing LANL2DZ and 6-311+G(d) basis sets to describe Pd₄ and Pd₄/Al₁₈O₂₇ clusters and NO molecule, respectively. The adsorption energy was calculated with equation 1 and its value was corrected using BSSE correction techniques.

$$E_{NO_{ads}} = E_{(NO/Pd_4/Al_{18}O_{27})} - [E_{(NO)} + E_{(Pd_4/Al_{18}O_{27})}] \quad (1)$$

RESULTS AND DISCUSSION

The NO molecule adsorbs on Pd₄ agglomerates with bridge mode on planar, and with atop mode on tetrahedral, with adsorption energies of -42.2 kcal.mol⁻¹ and -30.6 kcal.mol⁻¹, respectively. When Pd₄ is supported (Al₁₈O₂₇), the NO

molecule adsorbs preferentially in atop mode, with adsorption energy of -25.8 kcal.mol⁻¹, when the first layer of the Al₁₈O₂₇ cluster is relaxed. This result is in good agreement with experimental results (-27.2 kcal.mol⁻¹)³.

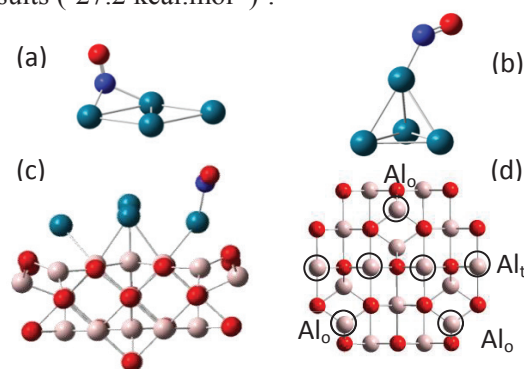


Figure 1. Preferential adsorption mode to NO molecule on (a) Pd₄ planar; (b) Pd₄ tetrahedral and (c) Pd₄/Al₁₈O₂₇ cluster. Al₁₈O₂₇ cluster (d).

For the NO adsorption on Pd₄ clusters isolated, NBO results show that the backdonation is very smaller than donation. However, the presence of alumina significantly increases the backdonation, especially when the molecule of NO adsorbed on Al hexacoordinated with higher coordination number.

CONCLUSIONS

The presence of alumina agglomerate increases palladium ability to transfer electrons to the molecule of NO, but this capability is greater in palladium bond to Al₀ than palladium bound to Al_t.

ACKNOWLEDGMENTS

The authors are grateful for the support given from the CAPES, CNPQ and FAPERJ.

¹ J. W. M. Carneiro and M. T. M. Cruz, *J. Phys. Chem. A*, 112, 8929, (2008).

² K. A. Kacprzak, I. Czekaj, J. Mantzaras, *Phys. Chem. Chem. Phys.*, 14, 10243, (2012).

³ C. -B. Wang, T. -F. Yeh, H. -K. Lin, *J. Hazard. Mater.*, 92, 241, (2002).

Equilibrium and non-equilibrium effects on the local order of water at metallic electrode surfaces

Luana S. Pedroza^a (PQ)

^a CCNH, Universidade Federal do ABC, Santo André, SP, Brasil

Keywords: Ab Initio Molecular Dynamic, solid-liquid interface, DFT, NEGF

INTRODUCTION

The study of liquid/solid interfaces is fundamental in the understanding of electrocatalysis, photocatalysis among other processes associated to new sources of energy. Understanding liquid ordering at the interface involves a detailed study of the nature of the interactions between water-water and water-substrate. A first principles description of all components of the system is the most appropriate methodology in order to advance the understanding of electrochemical processes. In this work we analyze in detail the structural, dynamic and energetic properties of liquid-water interacting with (111) Au and Pd surfaces, with and without the presence of an external potential.

METHODS

We have performed DFT-based ab initio molecular dynamics (AIMD) using the SIESTA code. The simulations were done at ambient temperature, with and without van der Waals interactions. We also present a methodology to study an electrochemical cell in the presence of an external voltage applied to the electrodes. We combine density functional theory (DFT) and non-equilibrium Green's functions methods (NEGF) to provide a more quantitative connection between the macroscopic voltage and the microscopic interfacial charge distribution.

RESULTS AND DISCUSSION

Our results show that the order of water at the interface strongly depends on the metal under consideration. And charge transfer at the interface can affect the local order of the water¹.

We also investigate the adsorption of the water molecule at different orientations on top of Au(111) surface as a function of the applied bias. We find that the position of the most stable configuration changes depending on the absolute value as well as the sign of the applied voltage, as shown in Fig. 1.

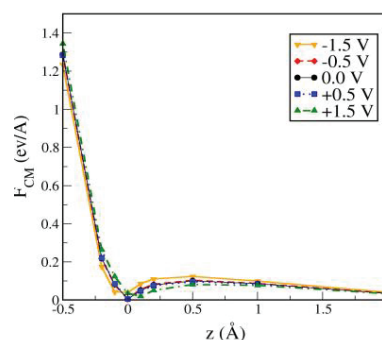


Figure 1. (Au-H₂O) Force at the center of mass as a function of the vertical displacement, for different bias at the electrodes.

CONCLUSIONS

Our results show that the inclusion of the electronic degrees of freedom (in this case, via DFT) is essential to properly describe the interaction of water and metal surfaces in general. We also show that the external potential plays an important role on the structural properties of the water-solid interface and thus in the simulation of electrochemical processes.

ACKNOWLEDGMENTS

This work was done in collaboration with Pedro Brandimarte (IFUSP), Marivi Fernández-Serra (Stony Brook University), Alexandre R. Rocha (IFT-UNESP). The author is grateful for the support given from FAPESP, DOE (USA).

¹ L. S. Pedroza, A. Poissier, M.V. Fernández-Serra, *J. Chem. Phys.*, **142**, 034706, (2015).

Probing the nature of Halogen-Aromatic Interactions by empirical potential

Lucas de Azevedo Santos (PG), Daniela Rodrigues Silva (PG), Teodorico C. Ramalho (PQ)

Federal University of Lavras – Department of Chemistry, 37200-000, Lavras/MG, Brazil

Keywords: Empirical Potentials, DFT-D, Force Field, Halogen Bond, NBO.

INTRODUCTION

Non-covalent weak interactions such as Halogen Bonds have shown to be a very powerful tool in drug design. Actually, they can be the leading figure in several protein-ligand systems¹. However, their nature is not simple to be described by Molecular Mechanics. In this line, there are a few empirical potentials being developed to improve the force fields accuracy. Nevertheless, these potentials do not consider the cases when the electrostatic factor is not favored². In this work, the interaction of benzene and s-triazine is a model to understand the nature of halogen-aromatic interactions as well as to reveal how the empirical potentials can be developed to attend these systems.

METHODS

The parallel between quantum and molecular mechanics was carried out by PES calculations with DFT-D3 and UFF methods. The s-triazazine is reported in Fig 1. The NBO analysis was used to evaluate the electronic and steric contributions for the interaction.

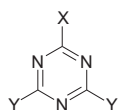


Figure 1. s-Triazine structure (X=Br, Y=H,NO₂).

RESULTS AND DISCUSSION

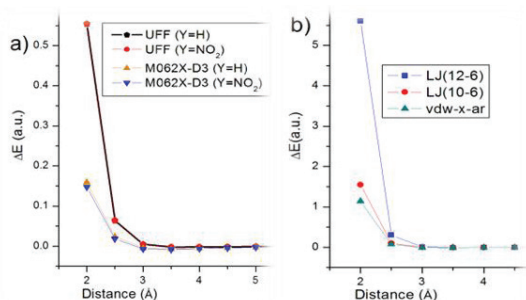


Figure 2. s-Triazine-Benzene interaction results: a) Uff versus m062x-d3/6-31+ and b) The new

potential (vdw-x-ar) plotted in comparison with Lennard-Jones potentials when Y=H.

Fig 2a shows the dissemblance between m062x-d3 and Uff PES. The crucial points lie at low range interactions. At 2.0Å, $\Delta E_{M062x} = -100.03$ kcal.mol⁻¹ and $\Delta E_{UFF} = -347.8$ kcal.mol⁻¹. When Y=NO₂, the positive charges on σ -hole are intensified, increasing the electrostatic repulsion with the centroid of benzene ring. However, when ΔE_{UFF} remains almost the same ($\Delta E_{UFF} = -347.64$ kcal.mol⁻¹), the DFT method detects a significant energy stabilization ($\Delta E_{M062x} = -92.6$ kcal.mol⁻¹). This feature can happen due to the orbital contribution to these interactions through $\pi_{C-C} \rightarrow \sigma^*_{C-Br}$ transitions, which can be noticed, for instance, at 3.0Å and 2.0Å with energies equal to 0.63 and 15.72kcal.mol⁻¹ respectively, when Y=H.

$$E_{vdw-x-ar}(r) = \gamma \left\{ \frac{r_e - (\delta/6 \cos \theta)}{r} - 2 \frac{r_e}{r + ((1+\delta)2^{1+\delta}/25r) \cos \theta} \right\} \quad (1)$$

Results from the new developed potential (1) are shown in Fig 2b. Besides the low range energy minimization, the new equation can predict the variation of σ -hole charge (δ) and its position regarding the interaction axis.

CONCLUSIONS

Directly, this work shows that in some cases, the Halogen Bonds do not depend only on attractive electrostatic interactions due to the σ -hole. Although, the σ -hole charge can be directly related to the σ^*_{C-Br} energy level, that can also be affected by electron withdrawing groups. The orbital contribution must be taken in account and applied to empirical potentials.

ACKNOWLEDGMENTS

Special thanks to CAPES, FAPEMIG and CNPQ.

¹ R. Wilcken et al., J. Med. Chem., 56, 1363-1388, (2013).

² L. A. Santos et al., J. Phys. Chem. A, 118, 5808-5817, (2014).

³ L. Du et al., J. Comp. Chem., 34, 2032-2040, (2013).

Multiple Pathways in the Hydrolysis of Phosphate Esters Catalysed by a Synthetic Model of Catechol Oxidase - Catalytic Promiscuity in Biomimetic Systems.

Lucas F. Esteves (PG), Hélio F. dos Santos (PQ), Luiz A. S. Costa (PQ)

Núcleo de Estudos em Química Computacional (NEQC), Dep. de Química, ICE, Universidade Federal de Juiz de Fora, Juiz de Fora, MG, CEP 36036-900
lu_fa_es@hotmail.com

Keywords: Metalloenzymes, Biomimetic Models, DFT, Catalytic Promiscuity

INTRODUCTION

Metalloenzymes are a broad class of enzymes which contains essential metal ions. Mimetic models for the active site of metalloenzymes have been designed in the last years to mimic the structure of the active site, using ligands similar to those in the real systems.

Two examples related to the present work are: the synthesis of di-copper complexes which mimic the catalytic activity of type-3 copper enzymes (catechol oxidase)¹ and several model complexes to mimic the catalytic activity of purple acid phosphatase².

In this work a study of the hydrolytic cleavage of a model substrate for biological phosphate esters, *bis*-(2,4-dinitrophenyl)phosphate (BDNPP), by a mimetic model of catechol oxidase (catalytic promiscuity) was conducted comparing the possible paths for this cleavage. The chemical process which is under investigation is presented on Figure 1.

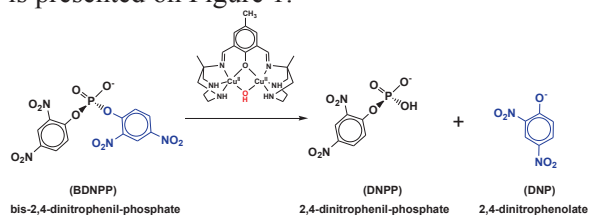


Figure 1. Cleavage of BDNPP by a mimetic model of catechol oxidase.

METHODS

All the transition states were optimized in gas phase at the B3LYP/6-31G(d)/LANL2DZ level and characterized as a saddle point in the PES by having a single imaginary frequency. Reaction intermediates were obtained through IRC calculations at the same level and the solvent effect were evaluated within the PCM model using water as a solvent.

RESULTS AND DISCUSSION

The mechanism by which phosphate esters are hydrolytically cleaved is still an open question in chemistry, due to large number of possibilities for this cleavage. This work presents three transition

states for the first step of the reaction, which are showed on Figure 2 together with some important bond lengths and the values for the single imaginary frequency.

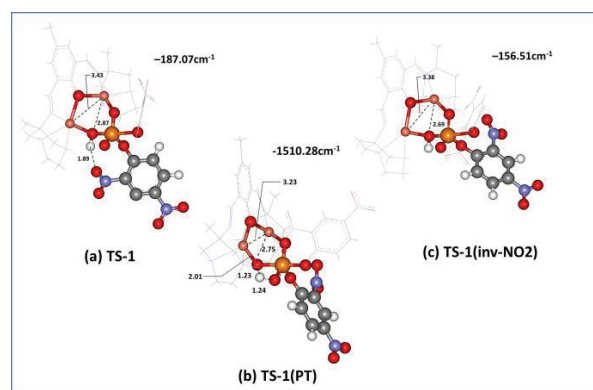


Figure 2. Optimized structures for TS-1.

The stabilities for the obtained structures related to the reaction intermediate obtained from the IRC calculation are very different for each structure, being the TS-1 (Fig. 2a) the most stable. In the TS-1(PT) (Fig. 2b), the phosphate ester cleavage occurs by a different mechanism, involving a proton transfer reaction during the nucleophilic attack. The TS-1(inv-NO₂) (Fig. 2c) differs from TS-1 in the position of the DNP group.

CONCLUSIONS

This work describes different mechanisms in the cleavage of phosphate ester reaction catalyzed by mimetic models. It is the first attempt to describe, theoretically, the catalytic promiscuity in biomimetic systems.

ACKNOWLEDGMENTS

FAPEMIG, CAPES, CNPQ, RQ-MG and UFJF.

¹ Selmezi, K. *et al.* Coordination Chemistry Reviews, 2003, 245, 191-201.

² Desbouis, D. *et al.* Coordination Chemistry Reviews, 2012, 256, 897-937.

³ REY, N. A. *et al.* International Journal of Quantum Chemistry, 2010, 10, 1432-1442.

Effect of Intramolecular Hydrogen Bond OH \cdots O in 1,3-butanediol and 3-methoxybutanol

Lucas José Karas¹ (PG), Patrick Rodrigues Batista¹ (PG), Renan Vidal Viesser² (PG),
 Luciano Nassif Vidal¹ (PQ), Paulo Roberto de Oliveira¹ (PQ)

¹Federal University of Technology – Paraná, Curitiba-PR

²Chemistry Institute, University of Campinas, Campinas-SP
 lucaskaras@gmail.com

Keywords: Intramolecular Hydrogen Bond, Conformational Analysis, Theoretical Calculation

INTRODUCTION

Intramolecular hydrogen bonds (IAHB) are responsible for stabilizing interactions of important structures to life, as carbohydrates and DNA. Good prototypes for systems containing strong IAHB are compounds that have two hydroxyl groups.^{1, 2}

Oliveira and Rittner³ showed that the increase in the volume group OR [R = CH₃, CH₂CH₂CH₃ and CH(CH₃)₂] increases the strength of IAHB for *cis*-3-alkoxycyclohexanols. Therefore the aim of this study was to analyze the influence of IAHB in conformational stability of 1,3-butanediol and 3-methoxybutanol through theoretical calculations and IR.

METHODS

1,3-butanediol (1,3-BDIOL) and 3-methoxybutanol (3-MBOH) compounds were studied. The optimization and frequency calculations for possible conformers were made with Gaussian09 software using the M06/DEF-2QZP. For the most stable structures were performed NBO study and topological analysis with AIMALL software. IR analyses were made in 0.01; 0.03 and 0.1 mol L⁻¹ using CCl₄ as solvent.

RESULTS AND DISCUSSION

Theoretical calculations shown an energy difference of 0.61 kcal.mol⁻¹ between the most stable conformer containing IAHB (g'gg't) and the most stable without IAHB (tgg'g) for the 1,3-BDIOL. For the 3-MBOH the difference between the more stable conformer with IAHB (g'gg't) and more stable without IAHB (tg'g't) was 0.28 kcal.mol⁻¹.

NBO, QTAIM and frequency calculations shown that there is an increase in the strength of IAHB of 1,3-BDIOL for 3-MBOH. There is an

increase in the transfer of electron (LP_O→σ*_{O-H}) of 4.58 kcal mol⁻¹ for 1,3-BDIOL and of 4.76 kcal for 3-MBOH. The topological analysis with QTAIM showed that there is an increased of E_{IAHB} of 1,3-BDIOL (0.0114 a.u.) for 3-MBOH (0.0115 a.u.). Frequency calculations showed a large increase in Δν (O-H_{free} to O-H_{bonded}) of 75 to 113 cm⁻¹, respectively.

The IR experimental results (Figure 1) agree with the theoretical results showing an increase of 82 cm⁻¹ for 1,3-BDIOL to 103 cm⁻¹ to 3-MBOH. The IR analysis also showed the influence of concentration. OH stretching of IAHB decrease in larger concentrations and the OH stretching of intermolecular hydrogen bond increase.

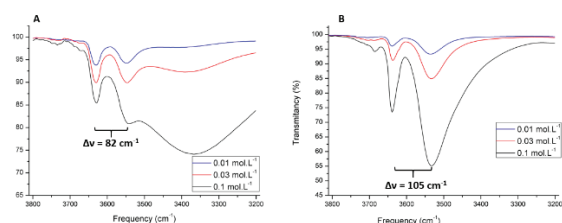


Figure 1. IR spectra of 1,3-BDIOL (A) and 3-MBOH (B) in 0.01; 0.03 and 0.1 mol.L⁻¹.

CONCLUSIONS

The study showed that the structure containing IAHB are more stable for 1,3-BDIOL and 3-MBOH. Furthermore, the increase in the substituent group increases the strength of the IAHB OH \cdots O.

ACKNOWLEDGMENTS

The authors are grateful for the support given from CAPES, LQT-UTFPR and POCL-UNICAMP.

¹ Kozuch, Sebastian; Bachrach, Steven M.; Martin, Jan M. L. J. Phys. Chem. A, 118, 293, (2014)

² Das, Prasanta; Das, Puspendu K.; Arunan, E. J.

Charge Transfer and Excitation Energy of TICT Molecules upon Solvation

Lucas Modesto-Costa^a (PD), Itamar Borges Jr.^a (PQ)

^aDepartamento de Química, Instituto Militar de Engenharia, Praça General Tibúrcio, 80, 22290-270
Rio de Janeiro, Brazil

Keywords: Charge Transfer, ab initio ADC(2) wave function, COSMO solvation model, Torsion potential

INTRODUCTION

Twisted Intramolecular Charge Transfer (TICT) effects are commonplace in molecules bearing an electron donor and acceptor pair connected by a single bond.¹ Their fluorescence spectra have two bands: a localized excited state and intermolecular charge transfer (CT). Upon torsion these bands may shift in energy. Moreover, absorption/emission spectra of TICT molecules depend on solvent polarity and relaxation. TICT molecules have been used as benchmark for several quantum chemistry methods and solvent descriptions.² The most studied TICT molecule, the 4-N,N-dimethylaminobenzonitrile (DMABN), was studied in this work. A DMABN derivative with an increased donor chain that shows a large dependence of solvent polarity,³ *trans*-ethyl *p*-(dimethylamino) cinnamate (EDAC), was also investigated. Absorption spectrum of both molecules were investigated using a continuum model. Excitation energies, dipole moments and charge transfer values as function of the dihedral angle were computed.

METHODS

The ground state geometry was optimized using MP2. For the excited states the ab initio wave function algebraic diagrammatic construction method to second order, ADC(2), was used in combination with the SV(P) Gaussian basis set. Solvent effects were included using the conductor-like screening continuum solvation model COSMO in two versions: in the excited states are optimized. The first three excited states were investigated. ADC(2) method known to describe accurately CT effects and does not have the inherent problems that DFT in describing such effects. Three different solvents with distinct polarities were considered, namely, benzene, DMSO and water.

RESULTS AND DISCUSSION

For planar DMABN, the computed S_1 and S_2 gas phase transition energies are respectively 4.51 eV and 4.77 eV in good agreement with

experiment (4.25 eV and 4.65 eV¹). After vertical excitation, the molecule twists. In gas phase and upon solvation in benzene, the S_1 and S_2 excited states intersect at an angle of about 30°. For the polar solvents water and DMSO, this intersection disappears. This effect is reversed in EDAC molecule. The use of COSMO model that optimizes the excited state mainly affects the twisted structures.

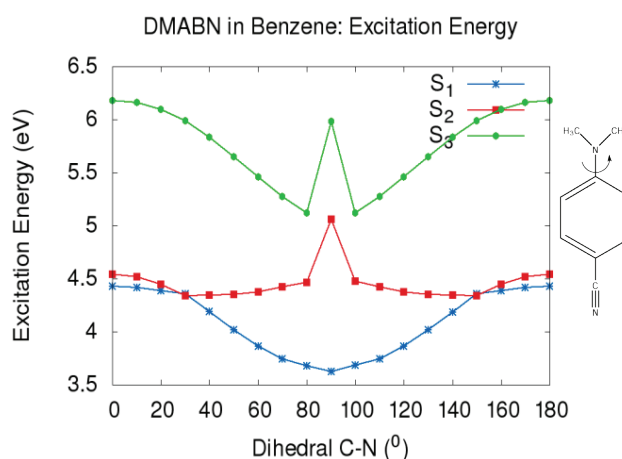


Figure 1. Torsion potential curves of DMABN first three excited states solvated in benzene.

CONCLUSIONS

Gas-phase vertical transitions are well described by the ab initio ADC(2) method. The change of intersection position depends on the solvent polarity as expected. Emission calculations of both molecules are underway and will be presented at SBQT.

ACKNOWLEDGMENTS

The authors are grateful for the support given from the CAPES and CNPQ.

¹ Z.R. Grabowski, K. Rotkiewicz, W. Rettig Chem. Rev. **103**, 3899 (2003).

² A. B. J. Parusela, Phys. Chem. Chem. Phys., **2**, 5545 (2000)

³ T.S. Singh, S. Mitra, J. Colloid Interface Sci. **311**, 128 (2007).

All-electron segmented contraction basis sets of triple zeta valence quality for the fifth-row elements

L.S.C. Martins (PG), F.E. Jorge (PQ) and S.F. Machado (PQ)

Universidade Federal do Espírito Santo
 lucas.qcgroup@gmail.com

Keywords: TZP and TZP–DKH basis sets; fifth-row elements; B3LYP-DKH2 calculations; atomic and molecular properties

INTRODUCTION

Segmented all-electron contracted triple zeta valence plus polarization function (TZP) basis sets for the elements Cs, Ba, La, and from Hf to Rn are constructed¹ for using in conjunction with the non-relativistic and Douglas-Kroll-Hess (DKH) Hamiltonians. Using the B3LYP hybrid functional, the performance of the TZP-DKH basis set is assessed for predicting atomic ionization energy as well as spectroscopy constants of fifteen compounds. Here, we will discuss only one of them.

METHODS

The Hartree-Fock (HF) and restricted open-shell Møller-Plesset perturbation theory (ROMP2) methods were used to construct the non-relativistic TZP basis set, namely: [9s5p4d1f] for Cs and Ba; [9s5p5d2f1g] for La; [9s6p5d3f1g] for Hf, Ta, Os, Au, and Hg; [9s5p5d3f1g] for W, Re, Ir, and Pt; and [9s8p5d3f1g] for Tl to Rn. The relativistic set was obtained from the TZP set by re-optimizing the values of the contraction coefficients using the second-order DKH Hamiltonian.

RESULTS AND DISCUSSION

Spectroscopic constant results obtained at the DKH2-B3LYP level of theory are listed in Table 1. For comparison, experimental² and other theoretical results are also included.

For TiCl, our results are very similar to the previously published theoretical data by other authors. For example, Metz *et al.*³, using the 21-valence-electron relativistic pseudo potential (RPP)-CCSD(T)/[6s6p4d3f2g] procedure, found excellent agreement with us. Their SO effect estimates on r_e , ω_e , and D_e were -0.011 Å, 1 cm⁻¹, and -0.684 eV. One can verify that the DKH2-B3LYP/TZPDKH + SO results (2.462 Å, 286.5

cm⁻¹, and 3.917 eV) give excellent accordance with the experiment².

Table 1. Theoretical and experimental bond length (r_e in Å), harmonic vibrational frequency (ω_e in cm⁻¹), and bond energy (D_e in eV) for the ground state.

		TZP-DKH ^a	Previous theoretical results ³	Expt. ²
TiCl (¹ Σ ⁺)	r_e	2.473	2.497	2.48483
	ω_e	285.5	282	283.75
	D_e	4.601	4.448	3.835

^a DKH2-B3LYP calculation. Basis set generated in [4] and in this work (fifth-row elements).

CONCLUSIONS

In general, the DKH2-B3LYP/TZP-DKH spectroscopic constants compare well with those obtained from higher level of theory.

For compounds containing main group elements, the addition of the SO corrections to the DKH2-B3LYP/TZP-DKH results always improve the agreement with experiment.

With few exceptions, the accordance between the theory and the experiment is good.

ACKNOWLEDGMENTS

We thanks to CNPQ, CAPES, and FAPES.

¹ L.S.C. Martins, F.E. Jorge, and S.F. Machado, *Mol. Phys.* (2015) DOI:10.1080/00268976.2015.1040095.

² D.R. Lide, editor, *CRC Handbook of Chemistry and Physics*, 75th ed. (CRC, London, 1994).

³ B. Metz, M. Schweizer, H. Stoll, M. Dolg, and W. Liu, *Theor. Chem. Acc.* 104, 22 (2000).

⁴ F.E. Jorge, A. Canal Neto, G.G. Camiletti and S.F. Machado, *J. Chem. Phys.* 130, 064108 (2009).

Chemoselectivity of the molybdenum oxodiperoxo complexes in oxidation reactions

Lucelma Pereira de Carvalho^a (IC), Marcus Vinicius Pereira dos Santos^a (PQ), Juliana Angeiras Batista da Silva^a (PQ), Ricardo Luiz Longo^b (PQ)

^aCentro Acadêmico do Agreste, Universidade Federal de Pernambuco

^bdQF - Centro de Ciências Exatas e da Natureza, Universidade Federal de Pernambuco

Keywords: Oxo-diperoxo Complexes, DFT, Oxidation Reactions, Activation Energy

INTRODUCTION

In recent years, many procedures were proposed for oxidations from sulfides to sulfoxides. Although, few of them are highly chemoselective to produce sulfoxide without to obtain the next level oxidation product, i. e., sulfone. Experimentally, it has been shown that the molybdenum oxodiperoxo complexes, $[Mo(O_2)_2L_1L_2]$, M = Mo and W, L_1 = pyrazole or N-oxo of pyridine, L_2 = H₂O or silica, adsorbed onto silica gel are highly selective yielding only sulfoxide product.¹ However, the mechanistic reasons for this selectivity still remain unknown.

Quantum chemical (QC) methods can be useful to understand the behavior of oxygen transfer reactions, and proposing mechanisms to explain the observed chemoselectivity in sulfide oxidation reactions.² Thus, in this work, we investigated the chemoselectivity of these reactions by determining its activation energies (E_a) in different substrates (alkenes, sulfur, and selenium, very susceptible to the oxidation process). The following substrates were chose: $R_1-S-(CH_2)_nCH=CH-R_2$, $R_1-Se-(CH_2)_nCH=CH-R_2$, ($n = 0$ ou 1), where the groups R_1 e R_2 can be electron donor and/or withdrawing can modify and control the chemoselectivity of the reaction.

METHODS

Our group has performed earlier studies in order to obtain all molecular structures of the reagents and products considered in this work. Critical points in the PES have been characterized by Hessian matrix and the transition state by Intrinsic Reaction Coordinate (IRC) analysis. We have used B3LYP/6-311+G(2df,2p) method for all atoms, except for Mo, which were employed the following recipes: B3LYP/X, with X, basis set (BS) and effective core potential (ECP) = LanL2DZ, Def2-SVP, Def2-TZVP, Def2-QZVP, cc-pVDZ-PP and cc-pVTZ-PP. All calculations were performed with Gaussian 09 program (Rev. D.01).

RESULTS AND DISCUSSION

In order to find out the appropriate QC method for these systems, we have obtained the free energy activation profile for the following reaction through two reactions pathways (oxidation of sulfur and oxidation of double bond): $[Mo(O_2)_2OPH_3] + CH_3-S-CH_2CH=CH_2$. These results were compared to Sensato *et al.* results (2005), and all scheme B3LYP/X produce values with great agreement to the literature results,² except for X = LanL2DZ option. Since Def2-SVP is the lower demand BS, this one was chose to proceed with studies. The free energy activation profiles for substrates showed that the transition state for the oxidation of the heteroatom (S and Se) has lower barrier height than the oxidation of alkene. The difference between these barriers is not affected when we increased the side chain of the substrates. Such results are in agreement with experimental results of oxidation reactions involving sulfides.

CONCLUSIONS

Our results show that the chemoselectivity of the molybdenum oxodiperoxo complexes towards oxidation reactions of sulfides is less affected changing the functional groups R_1 and R_2 , in agreement with the experiments. However, for substrates with selenium, the oxidation of the selenium atom is still preferred than the alkenes functionality.

ACKNOWLEDGMENTS

The authors would like to thank the FACEPE, CAPES and CNPq for the grant and scholarships.

¹F. Batigalha, M. Z. Hernades, A. G. Ferreira, I. Malvestiti and Q. B. Cass, *Tetrahedron*, 57, 9669, (2001).

²F. R. Sensato, R. Custódio, E. Longo, V. S. Safont and J. Andrés, *Eur. J. Org. Chem.*, 2406, (2005).

On the Interaction Energy among Propellant Components: A Carbon Black Model

Luiz F.A. Ferrão^{a*} (PQ), José A.F.F. Rocco^a (PQ), Francisco B.C. Machado^a (PQ)

^aDepartamento de Química, Instituto Tecnológico de Aeronáutica. (*ferrao_lfa@yahoo.com.br)

Keywords: DFT, M06-2X, PM6, ONIOM, Carbon spheres, Hybrid rocket, Paraffin

INTRODUCTION

The development of chemical propulsion, mainly by the increase of its efficiency has a central role in the progress of the aerospace propulsion in 21st century. Nowadays this development is possible, since the control of materials increased up to nanometric scale, allowing the synthesis of new propellants with superior performance and low environmental impact. From the quantum chemical point of view, there are three main characteristics to take in account in the development of propellants and its components: (1) Their energy content; (2) The chemical interaction among the components and; (3) The energy release in combustion and decomposition. In this work we are concerned about the chemical interaction between the fuel (paraffin) and the additive (carbon black) used in hybrid rocket propellants. Specifically, we constructed a model to describe the surface of carbon black and its interaction with weak adsorption systems (CH_4), in order to evaluate the capabilities of such model to describe interaction energies involved among propellant components.

METHODS

The Carbon black macromolecule is an agglomerated collection of carbon spheres, in which each sphere is made of graphitic carbon flakes that typically form broken concentric layers emanating from the core of the sphere¹. We constructed a minimal model for the carbon black surface, consisting of two layers of a graphene fragment in a graphitic stacking geometry. Each layer has a mean diameter of 2 nm, representing the typical size of a carbon flake.

The three layers ONIOM methodology was employed to describe the model: The high and medium level layers consisted in DFT within M06-2X approximation with triple and double zeta basis sets, respectively, while in the low level layer a semi-empirical method was used. The high-level contained the 4 central rings and the

considered molecule for adsorption (CH_4), while the mid-level contains all adjacent rings of the high layer, comprising 14 rings of the graphene outer layer. All other atoms and the entire inner layer are described with the low-level semi-empirical method.

RESULTS AND DISCUSSION

From the low-level semi-empirical methods considered (MNDO, PM3 and PM6), only PM6 presented an attractive stacking energy between the graphene layers, although with only 10% of the experimental value. Since the stacking energy does not vary significantly during the considered processes, this does not represent an issue for the model. The low-level should only represent a geometrical constraint, while the mid and high levels recover the largest part of the interaction energy. Figure 1 shows the calculated and experimental values of the distance and adsorption energy of methane over the flake surface.

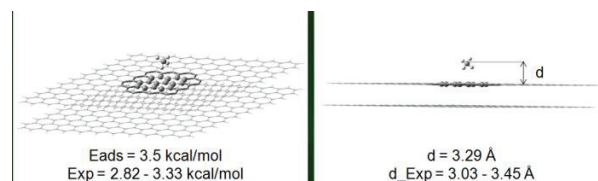


Figure 1. CH_4 adsorption on the CB flake model, obtained with DFT/Semi-empirical ONIOM methodology. Experimental values are given in reference².

CONCLUSIONS

The simulations performed in this work reveal the capability of the methodology to describe physical adsorptions, in agreement with the experiments,

ACKNOWLEDGMENTS

Supporters: CAPES, FAPESP and CNPQ.

¹Deshmukh, A. A., Mhlanga, S. D. and Coville, N. J. Mater. Sci. Eng. R Reports 70, 1–28 (2010).

²Vidali, G., Ihm, G., Kim, H.-Y. and Cole, M. W. Surf. Sci. Reports 12, 135–181 (1991).

Secondary Structure Stabilization of three different peptides by glycerol/water mixtures using molecular dynamics.

Weverson R. Gomes,^a(PG), Luiz C.G. Freitas^a(PQ)

gomeswr@gmail.com

^a *Departamento de Química, Centro de Ciências Exatas e Tecnologia, Universidade Federal de São Carlos, Rodovia Washington Luiz, km 235, C. P. 676, São Carlos, SP, CEP 13565-905, Brazil*

Keywords: Molecular dynamics, peptides, secondary structure, glycerol.

INTRODUCTION

Several experimental evidences have been collected regarding the effects of solutes that may act either as a stabilizing agent or as a denaturing agent. For instance, trifluoroethanol¹, some salts², sugars and polyols³ are known to stabilize proteins in aqueous solutions, whereas guanidine hydrochloride⁴ and urea⁵ act as denaturing agents. Polyhydric alcohols and sugars are among the best stabilizing agents for proteins in aqueous solution.

Molecular dynamics have been performed to investigate the secondary structure stabilization of three different peptides sequence, having 16 glycines, serines and alanines in zwitterionic α -helix conformation at glycerol/water binary mixtures (0:100, 50:50 and 80:20 v/v composition).

METHODS

All simulations were conducted in the NpT (constant number of particles, pressure and temperature) ensemble with Berendsen and V-rescale couple to pressure and temperature bath, respectively. Standard periodic boundary conditions were considered, a 1.2 nm cut-off for the non-bonded interactions and long-range correction was used. The motion equations were integrated using the leap-frog algorithm with a time step of 0.8 fs. The potential energy surface was described using the OPLS-AA force field for the peptide and glycerol, and the TIP4P model for water. The box was built with packmol filling it in a triclinic box. The initial structures of the peptide solutions were optimized by energy minimization runs using steepest descent and then conjugate gradient algorithm to obtain an energy gradient below 100 kJ.mol⁻¹.nm⁻¹. Thenceforth 2 ns NpT calculation was performed with peptide been fixed with a force constant of 1000.0 kJ.mol⁻¹.nm⁻² over all atoms. Finally, a 15 ns trajectory was obtained

and in the analyses was performed excluding the first 10 ns. All calculations were performed using Gromacs 4.5.5.

RESULTS AND DISCUSSION

The peptides are more stabilized by glycerol relative to water due to the hydrogen bonding interaction of glycerol three hydroxyl group with amine and carbonyl groups from backbone peptide and hydroxyl groups from side-chain (for serine). This stabilization mechanism can be associated to the simultaneous hydrogen bonding of a glycerol molecule with different amino acids of a given peptide.

It is observed that the peptide secondary structure is more stabilized with the increase of glycerol molecules in the mixture. Therefore, an augment in the glycerol concentration increase the probability of hydrogen bonding between peptides and glycerol molecules leading to stabilization of the α -helix structure.

CONCLUSIONS

Compared to pure water, the increase of glycerol molar fraction in mixture raises the stabilization of the three peptides studied here. The stabilization process is related to the higher number of hydrogen bonding between glycerol molecule and different aminoacids of the same peptide, therefore preserving the α -helix structure.

ACKNOWLEDGMENTS

The authors are grateful for the support given from the CAPES and CNPq.

¹ F.D. Soennichse, J.E. Van Eyk, R.S. Hodges, B.D. Sykes, *Biochemistry* 31 (1992) 8790.

² T. Arakawa, S.N. Timasheff, *Biochemistry* 21 (1982) 6545.

³ J.F. Back, D. Oakenfull, M.B. Smith, *Biochemistry* 18 (1979) 5191.

⁴ J. Fitter, S. Haber-Pohlmeier, *Biochemistry* 43 (2004) 9589.

⁵ K.A. Dill, D. dShortle, *Annu. Rev. Biochem.* 60 (1991) 795.

Cyclization of lapachol in acidic aqueous media: regioselectivity and interconversion mechanism study

Maicon Delarmelina¹ (PG), Gláucio B. Ferreira¹ (PQ), Vitor F. Ferreira² (PQ), José Walkimar de M. Carneiro¹ (PQ)

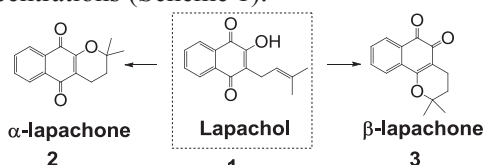
¹Departamento de química inorgânica, IQ, UFF, Outeiro de São João Batista s/n, Niterói, RJ

²Departamento de química orgânica, IQ, UFF, Outeiro de São João Batista s/n, Niterói, RJ
mdelarmelina@hotmail.com

Keywords: lapachol, 1,4-naphthoquinone, DFT, cyclization mechanism, regioselectivity

INTRODUCTION

Intramolecular cyclization reactions of lapachol can produce α - and β -lapachone which have value as potentially cytotoxic quinone compounds. The lapachones are selectively obtained by use of either diluted or concentrated acidic media, and the interconversion equilibrium between these isomers can also be controlled using different acid concentrations (Scheme 1).



Entry	Solvent	α : β	Yield
1	HCl	1 : 0	70% ¹
2	H ₂ SO ₄	0 : 1	80% ¹

Scheme 1. Experimental conditions for preparation of α - and β lapachones.

DFT calculations were employed to compute the pathway connecting lapachol to the lapachones considering the effect of the acid strength in aqueous solution.

METHODS

Geometry optimizations and vibrational frequency calculations were carried out with Gaussian 09 using B3LYP/6-31++g(d,p) and the continuum solvent model (PCM) with water as solvent together with explicit solvation. Basicity ($-\Delta G$) and protonic affinity ($-\Delta H$) of lapachol were calculated to evaluate the preferential protonation sites in acidic media. Energy parameters for cyclization reaction were also calculated.

RESULTS AND DISCUSSION

Di-protonated and tri-protonated lapachol may be formed in HCl and H₂SO₄ depending on the different acid concentration. Di-protonated lapachol affords mainly α -lapachone by kinetic control (**Figure 1 – A**). Tri-protonated lapachol affords exclusively β -lapachone derivative by thermodynamic control (**Figure 1 – B**), once the reverse process is feasible.

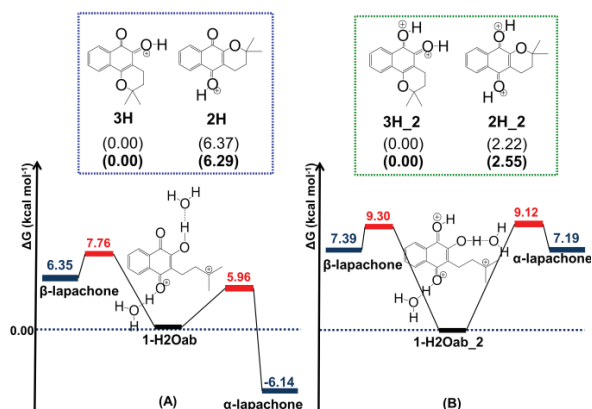


Figure 1. Variation of Gibbs free energy for di- (A) and tri-protonated (B) lapachol cyclization. All values are in kcal mol⁻¹.

CONCLUSIONS

Activation barriers for cyclization are all below 10 kcal mol⁻¹. Regioselective formation of α - and β -lapachone derivatives is dominated by kinetic and thermodynamic control via cyclization of the di- and tri-protonated forms of lapachol, respectively.

ACKNOWLEDGMENTS

The authors are grateful for the support given from FAPERJ, CAPES and CNPQ

¹C. Salas, *et al*, Bioorg. Med. Chem. 16, 668, (2008).

A Software for Designing SCC-DFTB Repulsion Parameters Automatically: The Framework for Automatization of SLAKO Parameterization (FASP)

Maicon P. Lourenço^{a*} (PQ), Maurício C. Silva^b (PQ), Matheus Quintão^a (IC), Hélio A. Duarte^a (PQ)

^a GPQIT - Department of Chemistry – ICEX - Universidade Federal de Minas Gerais - 31.270-901 Belo Horizonte, MG, Brazil.

^b Centre for Molecular Simulation – University of Calgary – Calgary, Alberta, Canada.

Keywords: parameterization, framework, automatization, SCC-DFTB, SLAKO, DFT.

*maiconpl01@gmail.com

INTRODUCTION

FASP program was developed with the aim of making the complex process of parameterizing the SCC-DFTB repulsion energy (E_{rep}) (essential for geometry and reaction energies) that involves a huge number of files, data and variables in a straightforward manner. The parameterization is fully automatic and the users only have to provide adequate references. The FASP also provides the reusability of the electronic part of the SLAKOs^{1,2} available in the literature while reparameterizing the original E_{rep} for describing other systems. The results of the E_{rep} parameterization for C, H, O, N are presented. FASP will be the first tool freely available for the community that deals with the parameterization automatically.

METHODS

The SCC-DFTB energy is $E = E_{bnd} + E_{SCC} + E_{rep}$. E_{bnd} is the sum over all occupied orbital energies², E_{SCC} is the Self-Consistent-Charge (SCC) energy and $E_{rep}(R_{AB})$ is the repulsion energy: $E_{rep}(R_{AB}) = E_{DFT}(R_{AB}) - (E_{bnd}(R_{AB}) + E_{SCC}(R_{AB}))$ (Fig. 1)².

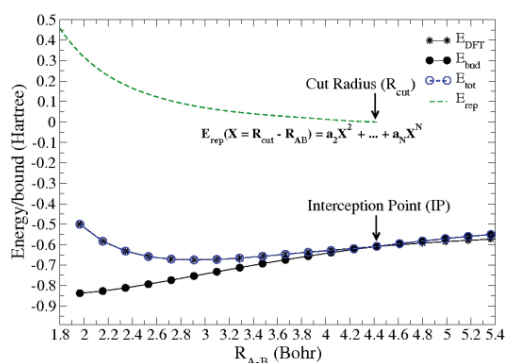


Figure 1. DFT (E_{DFT}) and SCC-DFTB ($E_{bnd} + E_{SCC}$) potentials and the polynomial which describes the E_{rep} all as a function of the interatomic distances (R_{AB}).

RESULTS AND DISCUSSION

Table 1 shows a comparison of the geometrical parameters for typical organic molecules and figure 1 shows a comparison of the mean error bars for 24 organic reactions with parameters obtained using different electronic part of SLAKOs.

Table 1. Bond length obtained with DFT (PBE/TZP) and SCC-DFTB (FASP, mio, matsci) approximation, all values are expressed in Å.

Property	PBE/TZP	current ^a	mio	matsci
Propyne				
C—C	1.456	1.480	1.462	1.453
C≡C	1.215	1.211	1.209	1.206
Acetic Acid				
C—C	1.506	1.533	1.499	1.511
C—O	1.373	1.398	1.385	1.447
C=O	1.217	1.227	1.213	1.216
Pyridine				
C—C	1.398	1.423	1.400	1.395
C=N	1.344	1.359	1.339	1.330
Nitric Acid				
N—O	1.449	1.449	1.419	1.332
N=O	1.222	1.234	1.208	1.235
O—H	0.984	0.978	0.998	0.974

^a Obtained by FASP using the SLAKOs developed by Wahiduzzaman et al.¹

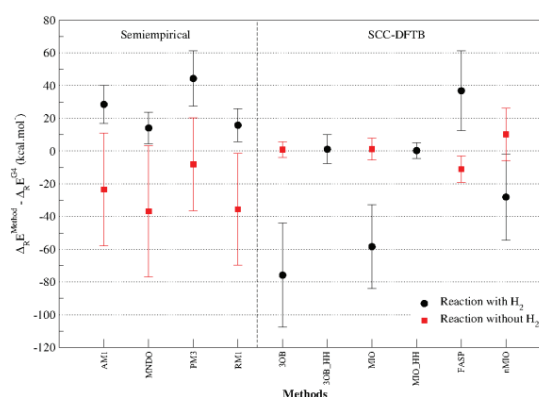


Figure 2. Description of 24 organic reactions computed by semiempirical methods and several SCC-DFTB parameters set compared to G4 method.

CONCLUSIONS

The FASP has proved to be an efficient software for developing E_{rep} parameters by taking into account both geometries and reaction energies during the automatic procedure.

ACKNOWLEDGMENTS

We are grateful for the support given from FAPEMIG, CAPES, CNPQ and INCT ACQUA.

¹Wahiduzzaman et al., J. Chem. Theor. Comp., 9, 4006, (2013);

²Oliveira et al., J. Braz. Chem. Soc., 20, 1193, (2009);

³www.dftb.org.

Estudo por Dinâmica Molecular de PVA em água com variação de parâmetros ambientais

Maíra Theisen (PG), Hubert K. Stassen (PQ), Rosane M. D. Soares (PQ)

Instituto de Química – Grupo de Química Teórica - UFRGS
 e-mail: theisen.maira@gmail.com

Palavras-chave: Dinâmica Molecular, PVA, Temperatura.

INTRODUÇÃO

O poli(vinil álcool) (PVA) é um polímero que tem sido bastante estudado para a síntese de hidrogéis. Hidrogéis são redes tridimensionais formadas por cadeias poliméricas hidrofílicas que possuem boa capacidade de reter água.¹ Existe uma classe de hidrogéis que respondem a estímulos do ambiente, são os chamados hidrogéis responsivos. Estes materiais tem sido bastante estudados para aplicações médicas e farmacêuticas.²

PROCEDIMENTO EXPERIMENTAL

Inicialmente foram obtidas as cargas atômicas através de cálculos quânticos utilizando a metodologia Merz-Kollman (MK). Estas cargas foram ajustadas com RESP e então utilizadas no campo de força AMBER aplicado nas simulações de Dinâmica Molecular (DM). Foram realizadas mudanças na temperatura do sistema a fim de se estudar o comportamento responsivo do polímero. As análises realizadas foram de Função de Distribuição Radial (RDF), Desvio Quadrático Médio (RMSD) e Raio de Giro (Rg).

RESULTADOS E DISCUSSÃO

O sistema analisado continha o polímero PVA com 42 unidades monoméricas. Primeiramente o sistema foi simulado na temperatura de 298K. Foram feitas simulações a 280K e 310K, partindo-se da configuração já equilibrada do primeiro sistema. A estrutura do polímero foi construída de forma linear, no entanto, ao longo da simulação foi observado que a estrutura se dobra e permanece desta forma até o final da simulação (figura 1).

As ligações de hidrogênio formadas entre os grupos hidroxila do polímero e a água foram fiscalizadas através das análises de RDF

(figura 2). Foram encontradas as distâncias de 0,184 nm para a ligação H(polímero)-O(água) e 0,191 nm para O(polímero)-H(água).

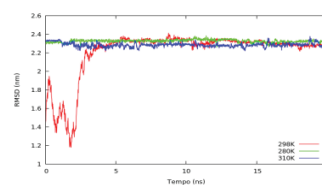


Figura 1. RMSD para o PVA em água a diferentes temperaturas.

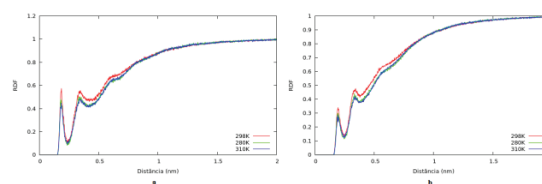


Figura 2. RDF para as três temperaturas: a) H(polímero)-O(água), b) O(polímero)-H(água).

CONCLUSÕES

Conseguiu-se atingir um estado equilibrado para o sistema inicial em poucos ns, e o comportamento foi mantido com a mudança da temperatura. As ligações de hidrogênio não apresentaram mudança significativa com a mudança da temperatura. Os próximos passos seriam o estudo do PVA utilizando o pH como variável e a elaboração do hidrogel de PVA.

AGRADECIMENTOS

Os autores agradecem o apoio dado pelo Conselho Nacional de Desenvolvimento Científico e Tecnológico (CNPq).

¹ Jonker, A. M.; Löwik, D. W. P. M.; van Hest, C. M. Chem. Mater., 24, 5, 759-773, 2012.

² T. J. Deming, Prog. Polym. Sci., 32, 858, (2007).

Metaloenzimas Envolvidas na Hidrólise de Compostos Organofosforados: Uma abordagem teórica via modelos de sítios ativos para Zn(II)-Zn(II), Cd(II)-Cd(II) e Zn(II)-Cd(II) de *Pseudomonas diminuta* (pdPTE)

M. A. Chagas^a (PG), W. R. Rocha^b (PQ)

^{a,b} Universidade Federal de Minas Gerais (UFMG), Av. Presidente Antônio Quadros, 31.270-901, Belo Horizonte, Minas Gerais, Brasil

Palavras chave: Modelos de sítios ativos de proteínas, Hidrólise de triésteres de fosfato, DFT, Dinâmica Molecular Clássica

INTRODUÇÃO

Fosfotriesterases (PTEs) e fosfatase ácida púrpura (PAP), de forma geral, são enzimas que apresentam nos sítios ativos centros metálicos dinucleares M-M contendo íons de metais de transição como Zn²⁺, Co²⁺, Cd²⁺ e Mn²⁺, para as PTEs, e Fe(III)-M(II), sendo M=Fe, Zn ou Mn, para PAP, respectivamente. Estas enzimas hidrolisam ésteres de organofosforados, como inseticidas e agentes de guerra química. Neste estudo modelos de sítios ativos destas enzimas serão investigados visando uma nova abordagem e proposta mecanística para a hidrólise triésteres de fosfato.

METODOLOGIA

Utilizando a teoria do funcional de densidade (DFT) empregou-se os funcionais B3LYP, X3LYP, TPSSH e M06. A estrutura cristalina 1HZY foi utilizada sendo a estrutura do sítio ativo I (Figura 1) constituída de dois íons zinco (Zn²⁺-Zn²⁺) e seus ligantes da primeira esfera de coordenação, incluindo o íon hidróxido em ponte, as quatro histidinas (His55, His57, His201 e His230), Lys169 e Asp301. O conjunto de funções de base 6-31G(d,p) para os átomos de C, H, O, N e P (substrato) e a base LANL2DZ para os elétrons de valência do Zn e pseudo potencial LANL2DZ para os elétrons de caroço foi utilizado. O efeito do meio solvente foi avaliado usando o método IEFPCM (SCRF=SMD) utilizando constantes dielétricas $\epsilon = 80$ e $\epsilon = 4$ (valor padrão utilizado para o entorno de cavidades de sítios ativos em proteínas). IOP (3/124=3) para incorporar efeitos de dispersão de longa distância. Usou-se o programa Gaussian09.

RESULTADOS E DISCUSSÃO

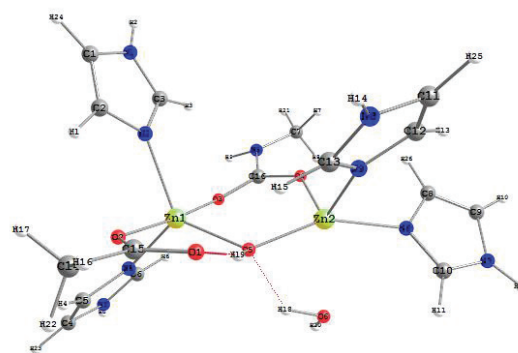


Figura 1: Sítio ativo I otimizado via DFT/B3LYP para o sistema PTE/Zn(II)-Zn(II) .

Os resultados estruturais fornecidos pelas otimizações estão em bom acordo com os dados de raio-x.¹ No entanto, cálculos serão realizados mantendo-se algumas coordenadas congeladas durante novas otimizações, para simular restrições conformacionais do ambiente protéico. A natureza da interação entre o sítio ativo mais exposto ao solvente (Zn2) e moléculas de água será investigada.

CONCLUSÃO

Durante o simpósio os sistemas Zn-Zn, Cd-Cd e Zn-Cd serão discutidos. Serão realizadas dinâmicas moleculares clássicas destes sistemas utilizando o modelo de íon não ligado empregando o programa AMBER14.

AGRADECIMENTOS

CNPq, FAPEMIG, INCT Catálise, RQ-MG

¹ Benning, M. M, Shim, H, Raushel, F. M, Holden, H. M, Biochemistry, 40, 2712, (2001).

A MRCI comparative study of the electronic states of AsX^+ ($\text{X}=\text{F}, \text{Cl}, \text{Br}$ and I)

Marcelo A. P. Pontes^a (PG), Marcos H. de Oliveira^{a,b} (PG), Luiz F. A. Ferrão^a (PQ), Joaquim D. Da Motta Neto^c (PQ), Orlando Roberto-Neto^d (PQ) e Francisco B. C. Machado^a (PQ)

^a Instituto Tecnológico de Aeronáutica, São José dos Campos, SP, Brazil

^b Instituto Federal do Paraná, Curitiba, PR, Brazil

^c Universidade Federal do Paraná, Curitiba, PR, Brazil

^d Instituto de Estudos Avançados, São José dos Campos, SP, Brazil

e-mail: marcelop@ita.br

Keywords: AsX^+ radicals, electronic states, MRCI calculations, molecular constants.

INTRODUCTION

AsX ($\text{F}, \text{Cl}, \text{Br}$ and I) molecules belong to the halimino radical series, and their cations are isovalent with the NF^+ , NCl^+ , PF^+ and PCI^+ molecules.¹⁻³ The AsCl^+ ion has been obtained in the eighties when Coxon *et al.*^{4,5} observed the visible $\text{A}^2\Pi_{1/2} \rightarrow \text{X}^2\Pi_{1/2}$ band. Later, Kim and Hirst⁶ calculated spectroscopic constants for all states of the lowest dissociation asymptote at the CASSCF and MRCI levels. Recently, we have characterized the AsCl radical.⁷

METHODS

We used CASSCF and MRCI to characterize the low-lying electronic states of the AsX^+ radicals. The CASSCF (7,8) has 7 electrons in 8 active orbitals, consisting of the np electrons and orbitals plus one extra b_1 and b_2 virtual orbitals, within C_{2v} symmetry. The ns valence electrons and orbitals were kept doubly occupied for all atoms. The aug-cc-pV5Z basis set was used for all atoms, for As, Br and I the ECP was used. The CASSCF/MRCI calculations were carried out using the MOLPRO program and the molecular constants have been calculated by solving the radial equation using the INTENSITY code. The dissociation energies were calculated within the supermolecule approach with the asymptotic limit energies calculated at $30.0 a_0$.

RESULTS AND DISCUSSION

Table 1 shows the energy order of the excited electronic states of AsX^+ radicals.

Table 1. Energy order of the excited electronic states of AsX^+ radicals.

Halogen	electronic state (increase order)
F	$\text{X}^2\Pi, (1)^2\Sigma^+, (1)^4\Pi, (1)^2\Pi, (1)^4\Sigma^-$
Cl, Br, I	$\text{X}^2\Pi, (1)^4\Pi, (1)^2\Pi, (1)^4\Sigma^-, (1)^2\Sigma^+$

The first excited state $(1)^2\Sigma^+$ of AsF^+ is the fourth excited state for the other molecules.

Table 2 shows the molecular constants of the $\text{X}^2\Pi$ states of ionic molecules. Equilibrium distances are increasing, while vibrational frequencies and dissociation energies are decreasing monotonically in the order $\text{F} \rightarrow \text{I}$. For AsCl^+ , the experimental and theoretical equilibrium distance 2.031⁵ and 2.055⁶ Å, and the vibrational frequency 527.7⁵ and 519.4⁶ cm^{-1} are in very good agreement with our results (in bold).

Table 2. $\text{X}^2\Pi$ molecular constants of AsX^+ .

Halogen	F	Cl	Br	I
r_e (Å)	1.669	2.044	2.192	2.397
D_e (eV)	4.70	4.03	3.75	3.63
ω_e (cm^{-1})	839.8	520.3	376.2	304.9
$\omega_e x_e$ (cm^{-1})	3.65	1.47	0.93	0.73

CONCLUSIONS

We characterized the low lying states of AsX^+ ($\text{F}, \text{Cl}, \text{Br}, \text{I}$) using CASSCF/MRCI method providing a set of molecular constants. For AsCl^+ , the calculated molecular constants for the ground state are in good agreement with previous available experimental^{4,5} and theoretical⁶ results.

ACKNOWLEDGMENTS

The authors would like to thank CNPq and FAPESP for partial research support.

¹ G.S. Kim, D.M. Hirst, Mol. Phys. 85(3), 463, 1995.

² G.S. Kim, D.M. Hirst, Mol. Phys. 86(5), 1183, 1995.

³ Z. Zhu, W. Yu, J. Sun, D. Shi, Mol. Phys. 112(21), 2827, 2014.

⁴ J.A. Coxon, S. Naxakis, A.B. Yamashita, Spectrochim. Acta. 41A(12), 1409, 1985.

⁵ J.A. Coxon, P.G. Hajigeorgiou, P.I. Presunka, Spectrochim. Acta. 45A(2), 281, 1989.

⁶ G.S. Kim and D.M. Hirst, Chem. Phys. Lett. 264, 134 (1997).

⁷ M.A.P. Pontes, M.H. de Oliveira, L.F.A. Ferrão, J.D. Da Motta Neto, O. Roberto-Neto, F.B.C. Machado, Chem. Phys. Lett. 634, 66, 2015.

Effect of 1,10-Phenanthroline Aromaticity in Carboxylic Acids: GIAO Calculations and ^1H NMR Spectroscopy

Márcia K. D. L. Belarmino (PG), Camila M. B. Machado (PG), Nathália B. D. Lima (PG) and Gustavo L. C. Moura (PQ)

Departamento de Química Fundamental, Universidade Federal de Pernambuco, Recife - PE.

Keywords: GIAO, ^1H NMR, Hydrogen Bonds, DFT, 1,10-phenanthroline, carboxylic acids.

INTRODUCTION

Hydrogen bonding influences the functionalities of molecular species, as well as the understanding of several physical properties, such as energetic stabilities, structural properties and the vibrational properties¹⁻². In this work, we examine the pronounced effects associated with the process of formation of the hydrogen bonds as they appear in the chemical shifts of the acidic hydrogens in the complexes between 1,10-phenanthroline and benzoic acid in stoichiometric ratios 1:1 and 1:2, PHEN:ACID. Subsequently, we studied the NBO charges transferred due to hydrogen bonds in these complexes.

METHODS

We performed B3LYP/6-31++G(d,p) calculations to optimize the geometry of the hydrogen bonded complexes, followed by the GIAO method to predict the acidic hydrogen chemical shift. As reference, TMS was also calculated with the same methodology. We also prepared solutions of the 1,10-phenanthroline, the carboxylic acids, and their 1:1 and 1:2, PHEN:ACID, mixtures, all dissolved in CDCl_3 . Further, the experimental ^1H NMR chemical shift values were obtained using a Unity Plus 400 MHz Varian equipment.

RESULTS AND DISCUSSION

Figure 1 shows the calculated, δ^{GIAO} , and experimental, δ^{NMR} , chemical shifts for the acidic hydrogen of the 1:1 and 1:2 complexes. We also show the shielding effect in the acidic hydrogen due hydrogen bonds in the complexes by the difference between the values of the chemical shifts obtained for the acidic hydrogen, both in the complex as well as in the acid dimer ($\Delta\delta = \delta^{\text{in complex}} - \delta^{\text{in acid dimer}}$). The pronounced effect in the 1:1 complex, $\Delta\delta^{\text{GIAO}}$ and $\Delta\delta^{\text{NMR}}$ can be explained by the transferred NBO charge, ΔQ^{NBO} .

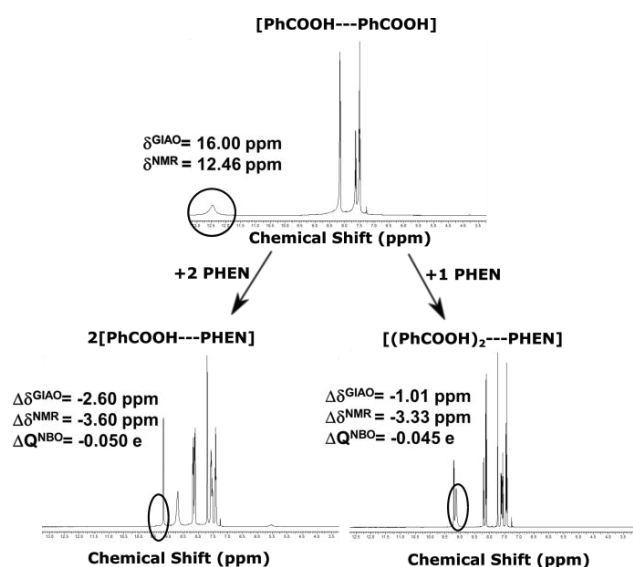


Figure 1. Calculated and experimental chemical shifts of acidic hydrogen nucleus of the benzoic acid (δ^{GIAO} and δ^{NMR}), the shielding effect due hydrogen bonds in complexes 1:1 and 1:2, PHEN:ACID, ($\Delta\delta^{\text{GIAO}}$ and $\Delta\delta^{\text{NMR}}$) and the NBO charges transferred, ΔQ^{NBO} , due hydrogen bonds.

CONCLUSIONS

The GIAO calculations agree with the ^1H NMR experiments in predicting a shielding of the acidic hydrogen of the hydrogen bonded complexes between 1,10-phenanthroline and benzoic acid in ratios 1:1 and 1:2, PHEN:ACID, being the 1:1 complex the most affected.

ACKNOWLEDGMENTS

The authors are grateful for the support given from the CNPQ and FACEPE/PRONEX.

¹ Belarmino, M. K. D. L., Santos, V. F. D. C., Lima, N. B. D., J. Mol. Mod., 20, 2477, (2014).

² Belarmino, M. K. D. L., Lima, N. B. D., J. Theo. and Comp. Chem., 12, 1350044, (2013).

Effects of the complexation energy on the thermochemistry and kinetics of oxidation reactions with oxidiperoxo complexes

Marcio Marcos da Silva^a (IC), Marcus Vinicius Pereira dos Santos^a (PQ), Juliana Angeiras Batista da Silva^a (PQ), Ricardo Luiz Longo^b (PQ)

^a*Centro Acadêmico do Agreste, Universidade Federal de Pernambuco*

^b*Departamento de Química Fundamental, Universidade Federal de Pernambuco*

Keywords: Oxo-diperoxo complexes, DFT, ECPs, basis sets, activation energy.

INTRODUCTION

Oxo-peroxo metal complexes, $[MO(O_2)_2L_1L_2]$, M = Mo and W, L_1 = pyrazol or N-oxo of pyridine, L_2 = H₂O or silica, oxidize unsaturated sulfides to the corresponding sulfoxides and these to sulfones, chemoselectively.¹ Despite their importance and studied, some aspects of the mechanistic reasons for this selectivity remain unknown. Electronic structure methods can be useful to understand this behavior and provide mechanistic information. Intrinsic Reaction coordinate (IRC) analyses are essential to assure that the transition state (TS) connects the proper reactants and products. In addition, the effects of complexation between the oxidant and the substrate should be taken into account in estimating the free energies profiles properly. However, these complexation effects are usually not considered and, in this work, we are investigating the complexation effects on these reactions.

METHODS

The TS structures were characterized by their Hessian matrices for seven processes¹. The IRC analysis from the TS structure provided the reaction path from the reactant to the product. We employed the B3LYP functional and the 6-311+G(2df,2p) basis sets for all atoms, except for Mo that the following basis sets were used LanL2DZ, Def2-SVP and dhf-SVP. All calculations were performed with Gaussian 09 program (Rev. D.01).

RESULTS AND DISCUSSION

To illustrate, in Table 1, we present the values of activation ($\Delta^\ddagger G$) and reaction ($\Delta_r G$) free energies of processes I and II. Pathways I and II are the double bond and sulfur atom oxidations: $[Mo(O_2)_2OPH_3] + CH_3-S-CH_2CH=CH_2$.

Table 1. Free energies (kcal mol⁻¹) of activation ($\Delta^\ddagger G$) and reaction ($\Delta_r G$). The complexation effects results are labeled with (*).

Mo basis set	Process	$\Delta^\ddagger G$	$\Delta_r G$
dhf-SVP	I	27.3	-33.2
	II	19.3	-31.5
	I*	20.1	-38.4
	II*	11.8	-41.5
Sensato et al. ¹	I	26.4	-34.4
	II	19.0	-33.5

Process II has lower $\Delta^\ddagger G$ than process I, thus the oxidation of the sulfur atom is kinetically favored compared to the oxidation of the double bond. Whereas, process II is more spontaneous than process I, namely, $\Delta_r G(I) < \Delta_r G(II) < 0$. However, when the complexation step is taken into consideration process II becomes kinetics and thermodynamically favored. This same trend is observed for LanL2DZ and Def2-SVP basis sets. Noteworthy the excellent results provided by the dhf-SVP compared to the more complete designed basis set for Mo by Sensato et al.¹

CONCLUSIONS

Complexation effects decrease the activation energies and they make reactions more spontaneous. Additional calculations are in progress for other systems to corroborate this trend.

ACKNOWLEDGMENTS

The authors would like to thank the FACEPE, CAPES and CNPq for the grant and scholarships.

¹ F. R. Sensato, R. Custódio, E. Longo, V. S. Safont, J. Andrés, *Eur. J. Org. Chem.*, 2406, (2005).

Beryllone: a Novel Divalent Beryllium Lewis Base

Felipe Fantuzzi^a (PG), Marco A. C. Nascimento^a (PQ)

^a *Dpto. Físico-Química, Instituto de Química, Universidade Federal do Rio de Janeiro*

Keywords: Beryllium, Chemical Bond Theory, Generalized Valence Bond, Density Functional Calculations, Main-Group Elements

INTRODUCTION

The chemistry of divalent carbon(0) species, or carbenes, has recently gained intense theoretical and experimental developments. A highlight of this improvement was the theoretical prediction by Frenking¹ – and further synthesis by Bertrand² – of carbodicarbenes, $C(NHC)_2$, as a new type of CL_2 compound. The dative bonds between the ligands and the central carbon atom makes the compound act as a double Lewis base, since the four valence electrons of the central carbon are retained as lone pairs.

In this work, quantum chemical methods have been applied to propose a new class of divalent beryllium(0) species, analogous to carbenes, in which the central beryllium atom has one lone pair. The calculations were performed in order to highlight the nature of the Be-L chemical bond, and to obtain thermochemical properties of this novel type of Lewis base.

METHODS

Generalized Valence Bond (GVB) calculations at the perfect-pairing (PP) approach were used to study the nature of the chemical bond in $Be(N_2)_2$, a prototype for the beryllone species. All valence electrons were treated at the GVB-PP level, while the core was described by a Restricted Hartree-Fock wave function. Density functional calculations with dispersion correction were applied to the BeL_2 systems, in order to characterize their structures and stabilities, and to obtain the proton affinities and complexation to BH_3 . The classes of ligands comprise different types of N-heterocyclic carbenes and phosphines, as well as CO and N_2 . The programs VB2000 and Jaguar were used in this work.

RESULTS AND DISCUSSION

Figure 1 shows some selected GVB-PP orbitals of $Be(N_2)_2$. One could see that the bonding between Be and N is of a dative type, in which the

electron pair is oriented from the N to the Be. Figure 1 also shows the beryllium lone pair, evidencing the Lewis base nature of the compound.

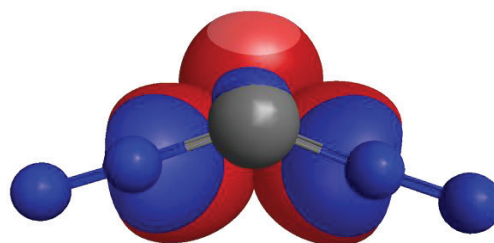


Figure 1. Six valence GVB orbitals of the $Be(N_2)_2$ system, highlighting the dative bonds between Be and N, and the Be lone pair.

For the beryllone compound in which the ligand is an imidazole-2-ylidene, the proton affinity and the ΔG for BH_3 complexation at B3LYP/6-31G** are 319.4 and -32.9 kcal mol⁻¹. In comparison, the respective values for the analogous carbene at MP2/TZVPP//BP86/SVP are 254.2³ and -26.1⁴ kcal mol⁻¹.

CONCLUSIONS

The calculations reveal the nature of the Be-L bonding in beryllone species, and show that it acts as a Lewis base.

ACKNOWLEDGMENTS

The authors are grateful for the support given from CAPES, FAPERJ, and CNPq.

¹ R. Tonner, G. Frenking, *Angew. Chem. Int. Ed.*, 46, 8695, (2007).

² C. A. Dyker, V. Lavallo, B. Donnadieu, G. Bertrand, *Angew. Chem. Int. Ed.*, 47, 3206, (2008).

³ R. Tonner, G. Heydenrych, G. Frenking, *ChemPhysChem*, 9, 1474, (2008).

⁴ S. Klein, R. Tonner, G. Frenking, *Chem. Eur. J.*, 16, 10160, (2010).

Second hyperpolarizability of the lithium salt electride $\text{Li-H}_3\text{C}_4\text{N}_2\text{...Na}_2$

Marcos A. Castro (PQ), Orlando Silveira (PG), Salviano A. Leão (PQ),
 Tertius L. Fonseca (PQ)

Instituto de Física, Universidade Federal de Goiás, CP 131, Goiânia, Goiás 74001-970, Brazil

Keywords: Electrides, Hyperpolarizabilities, Vibrational corrections

INTRODUCTION

Molecular systems with excess electrons have attracted great interest because of their intriguing properties. Electrides are compounds that have been extensively investigated since they have electrons with very diffuse character, which usually leads to large values of the polarizability and hyperpolarizabilities. Recently Ma et al.¹ proposed a new molecule with extraordinary first hyperpolarizability, the lithium salt electride. Calculations performed at the MP2 level showed that replacing a hydrogen atom of the pyridazine for a lithium increases the first hyperpolarizability from 5 to 859 au. This property is further increased to the extraordinary value of 1.4×10^6 au when this molecule is doped with two sodium atoms, yielding the lithium salt electride $\text{Li-H}_3\text{C}_4\text{N}_2\text{...Na}_2$. In this work we complement the work of Ma et al.¹ providing information on the second hyperpolarizability of this system.

METHODS

We have calculated the electronic and vibrational contributions for the second hyperpolarizability of the lithium salt electride. The electronic part was computed through coupled cluster cubic response theory² implemented in the DALTON program at the HF, CCS and CCSD levels. The vibrational corrections were obtained at the MP2 level through two methods: the perturbation theoretical method of Bishop and Kirtman (BKPT)³ and variational methodology (VAR) developed in a previous work⁴ to treat anharmonic systems.

RESULTS AND DISCUSSION

With objective of evaluate the role played by the electronic correlation effects we computed the dynamic second hyperpolarizability related to the

dc-Kerr effect at the HF, CCS and CCSD levels. The static value computed at the CCSD level was 1.1×10^9 au. Dynamic results obtained showed that there is a strong dependence of the computed values in relation to the correlation treatment, indicating that accurate results only could be obtained in a more sophisticated level than CCSD. Results for others nonlinear optical processes were obtained and will also be presented.

The computed values for the vibrational corrections show that the term $[\alpha^2]$ corresponds to little more than 10% of the electronic contribution while the term $[\mu\beta]$ is practically zero. Comparisons between the results obtained by perturbative and variational procedures showed large discrepancies.

CONCLUSIONS

The extremely large value of the second hyperpolarizability of the lithium salt electride, even compared to similar systems, reinforces the statement of Ma et al.¹ that the lithium salt electride has potential for application in nonlinear optics.

ACKNOWLEDGMENTS

The authors are grateful for the support given from the FAPEG, CAPES and CNPQ.

¹ F. Ma, Z.-R. Li, H.-L. Xu, Z.-J. Li, Z.-S. Li, Y. Aoki, F. L. Gu, *J. Phys. Chem. A* 112, 11462 (2008).

² C. Hättig, O. Christiansen, P. Jørgensen, *Chem. Phys. Lett.* 282, 139 (1998).

³ D. M. Bishop, J. M. Luis, B. Kirtman, *J. Chem. Phys.* 108, 10013 (1998).

⁴ O. Silveira, M. A. Castro, T. L. Fonseca, *J. Chem. Phys.* 138, 074312 (2013).

A DFT-D2 study of BTEX adsorption on rutile TiO₂ (110) surface

Marcos dos Reis Vargas^{a,b} (PG), Elton Anderson Santos de Castro^c (PQ), José Roberto dos Santos Politi^a (PQ), João B. L. Martins^a (PQ)

^a Universidade de Brasília, Instituto de Química, Laboratório de Química Computacional, CP 4478, Brasília-DF 70904-970, Brazil.

^b Instituto Federal de Educação, Ciência e Tecnologia de Goiás, Coordenação de Química Tecnológica, Campus Goiânia, 74055-110, Goiânia-GO, Brazil.

^c Universidade Estadual de Goiás (UEG), Química, Formosa-GO, 73807-250, Brazil.

Keywords: BTEX, DFT-D2, Adsorption, TiO₂ rutile

INTRODUCTION

Air pollution is a critical environmental problem in the world, affecting directly the health quality. A typical cause of indoor air pollution is the known volatile organic compounds (VOCs). The major VOCs are the monoaromatic hydrocarbons, such as benzene, toluene, ethylbenzene and xylenes (o-xylene, m-xylene and p-xylene)¹. Altogether, these compounds are known under the acronym BTEX. Rutile TiO₂ is the most abundant polymorphic form, among the natural low index faces the (110) is the most stable. TiO₂ applied to VOCs degradation is a promising technology for the control of these compounds, largely for the BTEX degradation. In this work, we have performed theoretical studies of BTEX adsorption over TiO₂ (110) of rutile.

METHODS

All calculations were performed using DFT with plane wave as basis sets in VASP. Generalized Gradient Approximation (GGA) was used with the exchange and correlation functional Perdew-Burke-Ernzerhof (PBE) with and without the semi-empirical correction proposed by Grimme (PBE-D2). Adsorption of BTEX molecules were studied using supercells of (3x2) of rutile TiO₂ with four layers. Atomic positions for BTEX molecules were fully optimized, while for the TiO₂ surface only the atomic positions of half of the layers were relaxed. For the optimization the Quasi-Newton algorithm was used. The energy cutoff was 400 eV, using a monkhorst pack k-point grid in the first Brillouin zone of 3×3×1. We have performed the study of energy convergence as the criteria for the k point grid. The precision for electronic minimization was set to 10⁻⁵. A vacuum of 20 Å along the z axis was also used.

RESULTS AND DISCUSSION

The most stable configurations found were the BTEX molecules parallel and

perpendicular to the surface with the ring center in a bridge conformation, between bicoordinated oxygen atoms (O_{2C}) and pentacoordinated titanium atoms (Ti_{5C}). This is the BTEX|TiO₂-rutile and BTEX⊥TiO₂-rutile conformation for the (110) do TiO₂ surface. Fig. 1 shows the optimized system for the benzenel|TiO₂-rutile and benzene⊥TiO₂-rutile using PBE functional.

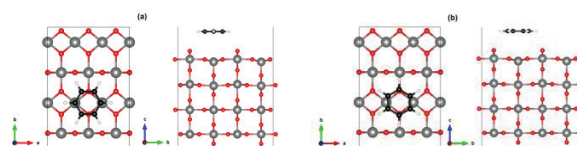


Figure 1. Optimized (a) benzenel|TiO₂-rutile and (b) benzene⊥TiO₂-rutile.

The adsorption energy of BTEX molecules in the rutile TiO₂ surfaces are shown in Table 1.

Table 1. Adsorption energy of BTEX on TiO₂.

E _{adsorption} (kJ/mol)	BTEX TiO ₂ -rutile		BTEX⊥TiO ₂ -rutile	
	PBE	PBE-D2	PBE	PBE-D2
Benzene	25.00	60.04	25.58	60.18
Ethylbenzene	23.83	72.38	21.86	67.28
Toluene	23.59	65.21	22.65	67.45
o-Xylene	18.72	75.19	16.52	67.99
m-Xylene	19.00	77.98	20.68	71.03
p-Xylene	17.19	93.49	17.58	72.62

CONCLUSIONS

The interaction energies using functional with dispersion correction (PBE-D2) show that the calculations using the PBE functional failure in the description of this interaction, underestimating the adsorption energies.

ACKNOWLEDGMENTS

The authors are grateful for the support given from the FAPEG, CAPES, CNPq, PIQS/IFG, CENAPAD-SP and FAPDF.

¹ C. A. Korologos, M. D. Nikolaki, C. N. Zerva, C. J. Philippopoulos, S. G. Pouloupoulos., *Journal of Photochemistry and Photobiology a-Chemistry*, 244, 24 (2012).

The Spin-Orbit effects on the CB, SiB and GeB molecules

Marcos H. de Oliveira^{1,2} (PG), Marcelo A. P. Pontes¹ (PG), Luiz F. A. Ferrão¹ (PQ) Joaquim D. Da Motta Neto³ (PQ), Orlando Roberto Neto⁴ (PQ), Francisco B. C. Machado¹ (PQ)

¹ Instituto Tecnológico de Aeronáutica – ITA, São José dos Campos, SP, Brazil

² Instituto Federal do Paraná – IFPR, Curitiba, PR, Brazil

³ Universidade Federal do Paraná – UFPR, Curitiba, PR, Brazil

⁴ Instituto de Estudos Avançados – IEAv, São José dos Campos, SP, Brazil

Email:marcos.oliveira@ifpr.edu.br

Keywords: Ab Initio, MRCI calculations, diatomic species, spectroscopic constants

INTRODUCTION

Boron is used as *p*-type dopant in carbon, silicon and/or germanium semiconductor devices. The description of CB, SiB and GeB diatomic molecules has previously been performed.¹⁻⁴ However, in this work, we present a systematic comparison of the lowest quartet electronic states of these borides using state-of-art CASSCF/MRCI methodology with extensive basis sets, and including spin-orbit effects

METHODS

In the present work, we have performed CASSCF/MRCI calculations for the low-lying quartet states of CB, SiB and GeB. The spin-orbit states (Ω) step were carried out within Breit-Pauli approximation using the aug-cc-pV5Z-DK basis set, relativistic effects were included. All the steps were carried out as implemented in MOLPRO code, while the molecular constants were evaluated using the INTENSITY software.

RESULTS AND DISCUSSION

In order to complement the electronic description of these species, this work presents the spin-orbit

states for the first time. As far as we know, there is no data to the CB and SiB¹⁻³ at this level of theory. Our main results for to the $(X)^4\Sigma^-$, $(1)^4\Pi$ and Ω states are collected in Table 1. The ground spin-orbit state splitting, in cm^{-1} , is 0.004 and 0.009, 0.022 and 0.154, 0.658 and 6.145 for CB, SiB and GeB, respectively. The avoided crossing gives rise to disturbances in the curvature of the spin-orbit states, it is detected by the minimum shift of the equilibrium distances, vibrational frequencies and dissociation energy.

CONCLUSIONS

Here we report, a complete description of some low-lying electronic quartet states related to the first dissociation channel of CB, SiB and GeB molecules. We also provided the molecular constants for these electronic and spin-orbit states. The main behavior shows the increasing of atomic number decrease the dissociation energy for ground state, while the excitation energy for the first excited quartet increases.

ACKNOWLEDGMENTS

The authors are grateful to CAPES, CNPq and FAPESP for the research support.

Table 1. Molecular constants of the BC, SiB and GeB electronic and Ω states. R_e in Å, T_e and ω_e in cm^{-1} and D_e in eV.

State	Re	Te	ω_e	De	Re	Te	ω_e	De	Re	Te	ω_e	De
	CB				SiB				GeB			
$(X_1)^4\Sigma^-_{1/2}$	1.498	0	1173	4.40	1.920	0	745	3.27	1.999	0	632	2.87
$(X_2)^4\Sigma^-_{3/2}$	1.498	0.004	1173	4.40	1.918	0.022	745	3.27	1.999	0.658	632	2.87
$(X)^4\Sigma^-$	1.498	0.009	1164	4.41	1.918	0.154	746	3.28	1.999	6.145	632	2.97
$(1)^4\Pi$	1.366	9050	1557	3.28	1.809	18672	860	0.97	1.900	20495	390	0.43
$(1)^4\Pi_{-1/2}$	1.366	9065	1549	3.28	1.809	18552	867	0.97	1.892	20342	438	0.40
$(1)^4\Pi_{1/2}$	1.366	9072	1495	3.28	1.809	18574	865	0.97	1.905	20447	402	0.39
$(1)^4\Pi_{3/2}$	1.367	9081	1506	3.28	1.809	18595	865	0.97	1.902	20527	361	0.38
$(1)^4\Pi_{5/2}$	1.367	9089	1506	3.27	1.810	18616	875	0.96	1.918	20619	385	0.37

¹ D. Tzeli, A. Mavridis, J. Phys. Chem. A, 105 (2001).

² A.I. Boldyrev, J. Simons, J. Phys. Chem., 97 (1993).

³ F.R. Ornellas, S. Iwata, J. Chem. Phys., 107 (1997).

⁴ M.H. Oliveira, M.A.P. Pontes, J. D. Da Motta Neto, L.F.A. Ferrão, O Roberto-Neto, F.B.C. Machado. Chem. Phys. Letters, 601 (2014).

Computational study of the interaction between the $[\text{Pb}(\text{H}_2\text{O})_3]^{2+}$ cation with ligands containing oxygen, nitrogen and sulfur donors atoms

Marcos Vinícius M. Meuser^a(IC), Daniel G. S. Quattrociocchi^a(PG), Glaucio B. Ferreira^a(PQ), Leonardo M. da Costa^b(PQ) and José W. de M. Carneiro^a (PQ)

^aUniversidade Federal Fluminense, Outeiro de São João Batista, s/n, 24020-141 Niterói - RJ, Brazil,

^bCentro Universitário Estadual da Zona Oeste -UEZO, Campo Grande, Rio de Janeiro - RJ, Brasil.

Keywords: :Pb(II) aquacation, O, N, S donor ligands, interaction affinity, DFT

INTRODUCTION

The Pb(II) cation is a bioaccumulative heavy metal, that forms harmful adducts in the human body. Its accumulation may result in growth cessation, neurodegenerative diseases, increase of vascular pressure and cancer.¹As the human body does not have efficient mechanisms to eliminate this toxic cation, some chelate medicines are used to detoxification. They interact with the Pb(II)cation occupying all interaction sites and avoiding its binding to biomolecules. After complexation, the metal cation clearance is favored due to the higher hidrosolubility of the adduct, which is more easily eliminated.¹

METHODS

B3LYP/6-311+G(d,p) calculations were performed to study the affinity of 14 monodentated neutral ligands to the Pb(II) cation. Compounds containing O (phosphoryl, ester, carboxylic acid, ketone, aldehyde, amide, ether, alcohol), N (imina, amine and ammonia) and S (tioketone, tioether and thioalcohol) donor atoms were selected as ligands. A hemidirected complex, with coordination number of 4, was simulated with water molecules surrounding the cation ($[\text{Pb}(\text{H}_2\text{O})_4]^{2+}$). In this complex one water molecule was exchanged by a ligand to evaluate the efficiency of the interaction between the ligand and the Pb(II) cation, as showed in Figure 1.

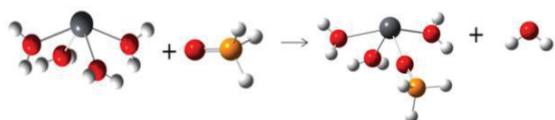


Figure 1. Substitution of one water molecule by the phosphoryl ligand.

RESULTS AND DISCUSSION

Table 1 shows the enthalpy and the free energy for the substitution, the values are negatives, showing a spontaneous and exothermic process. The phosphoryl group has the strongest interaction with the metal cation, followed by ligands with a double bonded interacting atom followed by ligands with a single bonded interacting atom. In the phosphoryl group the phosphorous atom with a large atomic

radius, highly polarizes the electronegative oxygen atom, which increases its charge and strengths the interaction. Following the phosphoryl ligand are the compounds that have a double bond interacting atom, is adjacent to a mesomeric electron donor group, such as amino, metoxyl and hydroxyl. After that, there are the compounds where the interacting atom is adjacent to a methyl group that donates electron by inductive effect. The compounds with the weakest interaction are the one with a single bonded interacting atoms.

Ligands	ΔH	ΔG^{298}	Q_L	HOMO
Phosphoryl	-30.22	-31.17	0.346	-0.297
Ester	-27.20	-26.36	0.335	-0.286
Imine	-25.82	-24.59	0.396	-0.265
Ketone	-17.99	-17.89	0.292	-0.259
Ether	-9.91	-8.92	0.293	-0.265
Thioether	-9.09	-8.27	0.394	-0.224
Alcohol	-7.08	-6.62	0.181	-0.284
Thioalcohol	-2.82	-2.37	0.332	-0.243

Table 1. Energetic and electronic parameters for some ligands.

CONCLUSIONS

Ligands containing oxygen atom have the strongest interaction with the metal center, followed by ligands with nitrogen and sulfur atoms, respectively. The interaction energy has strong correlation with the metal-ligand distance. Energy decomposition analysis shows that both the covalent and the electrostatic components of the interaction are important to determine the strength of the complex. The polarization term was found as the most relevant to determine the affinity of each ligand for the metal center.

ACKNOWLEDGMENTS

The authors are grateful for the support given from the FAPERJ, CAPES and CNPQ.

¹A.A. El-Kahatib, A.K. Hegazy, A.M. Abo-El-Kassem, , Int. J. Phytoremediation. 16, 29, (2014).

PICVib: An Accurate, Fast and Simple Procedure to Investigate Selected Vibrational Modes at High Theoretical Levels

Marcus Vinicius Pereira dos Santos^a (PQ), Yaicel G. Proenza^b (PG), Eduardo C. Aguiar^b (PQ), João Bosco P. da Silva^b (PQ), Ricardo Luiz Longo^b (PQ)

^aCentro Acadêmico do Agreste, Universidade Federal de Pernambuco

^bDepartamento de Química Fundamental, Universidade Federal de Pernambuco

Keywords: energy only, normal modes, frequencies, high level *ab initio*, large molecules, DFT, MP2, CCSD(T), vibration.

INTRODUCTION

Vibrational spectroscopy is a well-known technique for structural characterization and quantitative analysis. From the theoretical point of view, the development of analytical gradients and Hessians for electronic structure methods has enable the application of these methods to a wide range of molecular systems. However, the computational demand (RAM memory, hard disks access and CPU time) for calculating the Hessian matrix is very high compared to the geometry optimization and has become the source of frustration for studying systems at higher levels or studying large systems.

Hence, we have devised an alternative procedure denoted PICVib¹ (Procedure for Investigating Categories of Vibrations) that computes the vibrational normal modes at higher theoretical levels using energy only (single-point) calculations.

METHODS

This procedure were applied to a wide class of molecular systems and vibrational modes using computational methods ranging from semiempiricals to high level *ab initio* such as CCSD(T). All calculations were performed with ACESIII, CFOUR and Gaussian 09 programs.

RESULTS AND DISCUSSION

To illustrate the PICVib results, we predicted the radial breathing mode (RBM, Figure 1) vibrational frequencies of three (8,0) single wall carbon nanotubes (SWCNTs): pristine, C₂H₂@NT and HCN@NT. RBM frequencies are useful for (*n,m*) assignments¹. In Table 1, we present the vibrational frequency and the percentage difference in relation to the analytical calculation in parenthesis. It can be seen good agreement between the analytical and PICVib calculated

Table 1. Vibrational frequencies (cm⁻¹) of the RBM for pristine SWCNTs, with C₂H₂ (C₂H₂@NT) and HCN (HCN@NT) molecules inside its cavity at B3LYP/6-31G(d):AM1 level.

Pristine	C ₂ H ₂ @NT	HCN@NT
370 (+0.5)	371 (-0.5)	373 (0.0)

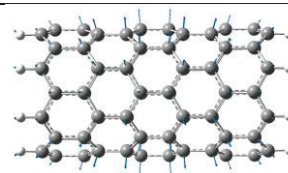


Figure 1. RBM Mode of pristine (8,0) SWCNTs.

Noteworthy that using PICVib, only one normal mode (RBM) was calculated, instead of 330 modes (in pristine case) in traditional calculation.

CONCLUSIONS

The PICVib has an excellent performance (errors smaller than ca. 0.5%), at only a small fraction of the computational demand required for a complete analytical calculation of the vibrational frequencies. The approach is quite general because it can use practically any quantum chemical program and electronic structure method. In addition, it has been generalized for infrared intensities.²

ACKNOWLEDGMENTS

The authors would like to thank the SINAPAD, FACEPE, CAPES and CNPq for the grant and scholarships.

¹ M. V. P. D. Santos et al., J. Comput. Chem., 34, 611–621, 2013.

² M. V. P. D. Santos et al., Phys. Chem. Chem. Phys., 16, 17670-17680 (2014).

Estudo *ab initio* da interação de compostos análogos do alcaloide marinho teoneladina C com o grupo heme [Fe(III)PPIX]:

Marília L.A e Costa^a (IC), Clebio S.Nascimento Jr^a (PQ), Gustavo H.R. Viana (PQ)^b, Luciana Guimarães^a (PQ)

^a Laboratório de Química Teórica e Computacional, Universidade Federal de São João del Rei, São João del Rei, MG

^b Laboratório de Síntese Orgânica, Universidade Federal de São João del Rei, Divinópolis, MG
e-mail: lucianaguimaraes@ufsj.edu.br

Palavras-chave: Malaria, alcaloides 3-alkilpiridínicos, DFT, Fe(III)PPIX.

INTRODUÇÃO

A malária é uma doença provocada pelo protozoário do gênero *Plasmodium*, típica das regiões tropicais e subtropicais. A maior parte dos *Plasmodium* é resistente a um ou mais fármacos empregados atualmente. Uma classe de substâncias marinhas que vem chamando a atenção devido às suas potencialidades como antimaláricos são os alcaloides 3-alkilpiridínicos. Nos últimos anos, o grupo de síntese orgânica da UFSJ vem obtendo bons resultados para a síntese e atividade antimalárica de análogos desses alcaloides (figura 1a). Os análogos tem se mostrado ativos nos ensaios *in vitro* realizados contra cepas do *Plasmodium* resistentes à cloroquina. No entanto, alguns compostos mostraram-se muito mais ativos que outros, e não há até então uma explicação racional para tal fato. Neste contexto, o objetivo deste trabalho é realizar uma análise estrutural e energética do processo de interação entre o grupo heme ferriprotoporfirina [Fe(III)PPIX] (figura 1b) e análogos da teoneladina C previamente sintetizados. Desta forma, busca-se auxiliar na compreensão de como a estrutura do ligante afeta a sua atividade antimalárica.

MÉTODOS

Todas as geometrias foram otimizadas no nível DFT/B3LYP utilizando o Gaussian 09. Diferentes multiplicidades de spin foram avaliadas. As Funções de base 6-31G(d,p) foram usadas para os átomos de Fe, N, O e S envolvidos nas ligações fármaco-receptor. Funções de base mínima STO-3G para os grupos CH_n. Cálculos de frequências vibracionais harmônicas asseguram que todas as estruturas encontram-se no mínimo de energia. As propriedades termodinâmicas energia livre de

RESULTADOS E DISCUSSÃO

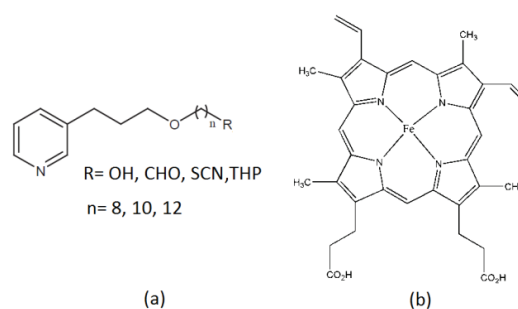


Figura 1. Estrutura geral dos análogos da teoneladina C, com seus respectivos substituintes (b) Estrutura do grupo heme [Fe(III)PPIX]

As estruturas mais estáveis são dupletos. A estequiometria da reação foi contemplada de duas formas: (i) Complexos do tipo 1:1 – 1 grupo [Fe(III)PPIX] e 1 análogo; (ii) Complexos do tipo 2:1 – 2 grupos [Fe(III)PPIX] e 1 análogo. Nos complexos 1:1 foram avaliados a interação do ligante via anel piridínico e via substituinte R. Com os valores de ΔG obtidos, pode-se perceber que os resultados envolvendo o processo de complexação 1:1 não são conclusivos, quando comparados aos valores de IC₅₀. No entanto, os primeiros cálculos para complexos (2:1) indicam uma maior variação do ΔG em função da mudança de substituinte e do tamanho da cadeia carbônica.

CONCLUSÕES

A partir de cálculos B3LYP/GEN observou-se que a interação dos análogos estudados com o grupo heme na estequiometria 1:1 não são conclusivos e devem ocorrer na estequiometria 2:1.

AGRADECIMENTOS

FAPEMIG, CNPq, PIBIC/UFSJ e RQ-MG

Hydrazine decomposition reactions on the small platinum cluster Pt₄

Pelegriani M^{a*} (PQ), Parreira RT^b (PQ), Ferrão LFA^c (PQ), Caramori GF^d (PQ), Machado FBC^c (PQ), Roberto-Neto O^e(PQ)

^a Divisão de Ensino, Academia da Força Aérea, Pirassununga-SP, Brazil

^b Núcleo de Pesquisa em Ciências Exatas e Tecnológicas, Universidade de Franca, Franca-SP, Brazil

^c Departamento de Química, Instituto Tecnológico de Aeronáutica, São José dos Campos-SP, Brazil

^d Departamento de Química, Universidade Federal de Santa Catarina, Florianópolis-SC, Brazil

^e Instituto de Estudos Avançados, Departamento de Ciência e Tecnologia Aeroespacial, São José dos Campos-SP, Brazil

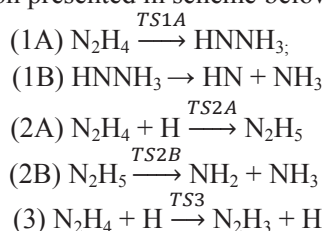
* marinapelegriani101@gmail.com

Keywords: DFT, M06, N₂H₅ species, catalyst, IRC

INTRODUCTION

Hydrazine (N₂H₄) and its derivatives constitute an important group of energetic molecules widely utilized in aerospace applications. Another capability of hydrazine is its use in fuel cells due to its high-density storage of hydrogen. Fuel cells based on hydrazine catalyzed by platinum were tested experimentally with success.¹ An experimental study of the decomposition of hydrazine on Pt(111)² shows that the decomposition of N₂H₄ occurs through the successive breaking of N-H bonds in hydrazine leading to the formation of N₂, and it also detects the desorption of H₂ and NH₃, however it was not evident how the NH₃ molecule is formed. The hydrogenation of N₂H₄ is one of pathways suggested to the NH₃ formation and it can be formed through the N₂H₅ reaction intermediate.

In this work we studied reaction paths for N₂H₄ decomposition presented in scheme below.



For each reaction, energies and barrier heights were studied in both the absence and the presence of the tetrahedral Pt₄ cluster.

METHODS

All geometry optimizations were carried out by using the DFT method, M06. The effective core potential LANL2DZ basis set was employed for the Pt atom and the 6-311++G(d,p) basis set was used for the N and H atoms. Geometry optimizations were carried out with partial constraints, the Pt-Pt distances were kept constant and equal to the experimental bulk distance, 2.775 Å. The IRC procedure identified the connectivity of the

stationary points. The calculations were carried out using the Gaussian 09 code.

RESULTS AND DISCUSSION

The Fig.1 summarizes the results showing the energetic profile for reactions of the scheme in the presence of the Pt₄ cluster.

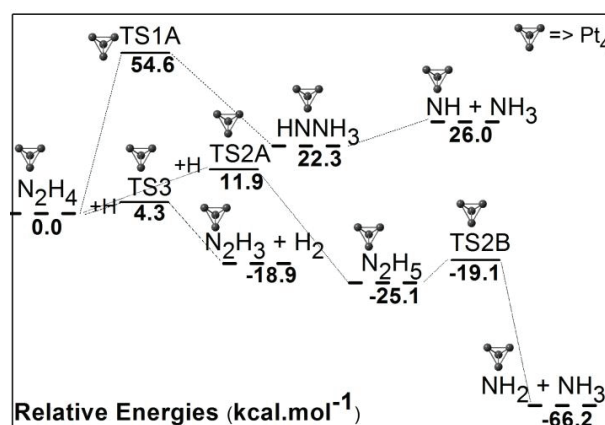


Fig.1 Reaction profile for adsorbed molecules. Relative energies are given in kcal.mol⁻¹.

CONCLUSIONS

The Pt₄ cluster assistance does not affect the energetic parameters in a systematic way. This is the first time that the N₂H₅ species has been characterized in the literature, and the reaction energies suggest the N₂H₅ as a reaction intermediate in pathway to produce ammonia, especially in the Pt₄ presence.

ACKNOWLEDGMENTS

The authors are grateful for the support given from the FAPESP (12/50666-2), CAPES and CNPQ.

¹Yamada, K.; Asazawa, K.; Yasuda, K.; Ioroi, T.; Tanaka, H.; Miyazaki, Y.; Kobayashi, T. J. Power Sources 115, 236, (2003).

²Alberas, D. J.; Kiss, J.; Liu, Z-M.; White, J. M. Surf. Sci. Lett. 278, A71,(1992).

ESTUDO COMPARATIVO DA ATIVIDADE ANTIMALÁRICA DE TRITERPENOS PENTACÍCLICOS

***Marlon Marques V. de Melo Filho^{1a}(IC), Kelson Mota T. Oliveira^{1a}(PQ), Jefferson R. A. Silva^{1b}(PQ), Noam S. Gadelha^{1a}(PG), Aristeu S. da Fonseca^{1a}(PG)**

^{1a}Grupo de Química Teórica e Computacional (GQTC); ^{1b}Grupo de Química de Produtos Naturais e Desenvolvimento de Métodos Analíticos (QPNMA). ¹DQ/ICE – UFAM. Bloco 10, Setor Norte. Av. Rodrigo O.J. Ramos, 6200, Japiim, 69077-000, Manaus – Amazonas.

*e-mail: marlonvieirademelo@gmail.com

Palavras-chave: ácido botulínico, ácido melaleuco, Autodock, DFT

INTRODUÇÃO

A redução da sensibilidade do *Plasmodium sp* a medicamentos antipalúdicos recomendados anteriormente coloca um aumento da carga sobre os programas de controle da malária, bem como sobre os sistemas nacionais de saúde nos países endêmicos. Estudos com Ácido Botulínico contra parasitas *Plasmodium falciparum* in vitro, mostraram resultados expressivos.¹ Quatro moléculas isoladas da *A. amazonicus* no QPNMA, com esqueleto triterpênico pentacíclico, têm mostrado graus diferentes de atividade contra o *P. falciparum*. Três destes compostos são apresentados na literatura como ótimos candidatos para o desenvolvimento de um tratamento mais eficiente contra a malária e outras doenças parasitárias. Os quatro compostos, depois de isolados, foram identificados por meio de análise espectroscópica (ver fig. 1). Suas estruturas foram estudadas por meio de abordagem teórica visando determinar que fatores estruturais e eletrônicos que poderiam ser determinantes no grau de atividade.

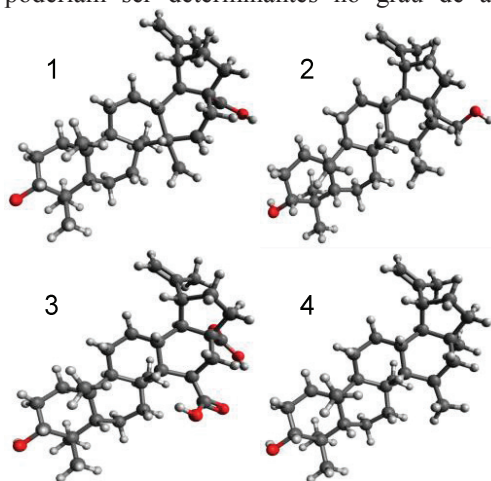


Figura 1. Configuração dos triterpenos em 3D 1-Ácido Betulínico, 2 – Betulina, 3- Ácido Melaleucico e 4- Lupeol

PROCEDIMENTO EXPERIMENTAL

Os cálculos foram realizados utilizando PC INTEL Core™ i5 (4 GB RAM), em plataforma Debian LINUX (Versão 14.0) para calcular as propriedades estruturais e eletrônicas das quatro moléculas. Na otimização geométrica de rotina foi empregado a teoria do funcional de densidade (DFT),

com e a base com bases 6-31G e funcional B3LYP, por meio do Programa Gaussian03. O AutoDock foi utilizado para analisar as possíveis interações existentes dos triterpenos candidatos a fármacos com uma enzima alvo.

RESULTADOS E DISCUSSÃO

A literatura aponta a carboxila como forte candidato responsável pela atividade do ácido betulínico, e a hidroxila nos demais compostos. Estruturalmente os compostos apresentaram grande similaridade em distâncias e ângulos no esqueleto lupânico. Da mesma forma, os resultados demonstraram diferenças mínimas nos mapas de potencial, ou de densidade eletrônica, devido a presença do grupo COOH. O que se faz mais evidente na Betulina que possui uma hidroxila em seu lugar, e ainda assim apresenta boa atividade. Por outro lado, o ácido melaleucico, tendo dois grupos COOH não apresentou experimentalmente nenhuma atividade. Considerando que tanto OH como COOH são responsáveis pela atividade, a explicação para a inatividade do melaleucico deve ser procurada em outros aspectos além do estrutural e eletrônico. Estudando a interação com enzimas digestivas do *P. Falciparum*, foi possível observar que a interação do ácido melaleucico com a enzima alvo não apresentou ligações de hidrogênio, enquanto o lupeol, betulina e ácido botulínico apresentam ligações de hidrogênio, mostrando assim interação com a enzima alvo.²

CONCLUSÃO

É possível compreender que a inatividade do ácido melaleucico ocorre devido a falta de interação com a enzima alvo, mostrando que essa atividade é determinada também pela seletividade enzimática.

AGRADECIMENTOS

FAPEAM, CNPq

1.M. S. de Sá : J. F. O. Costa : R. Ribeiro dos Santos: M. B. P. Soares : Antimalarial activity of betulinic acid and derivatives in vitro against *Plasmodium falciparum*, 2008.
2.World Health Organization, Drugs against parasitic diseases: R&D methodologies and issues. 2003.

Computational Studies on Dodecylsulfate-Quaternary Ammonium Herbicides Ion-Associate Formation in Water: A DFT Study

Kassem Kalife Nege^a (IC), Mateus Ribeiro Lage^a (PG), Jonas Oliveira Vinhal^b (PQ), Ricardo Jorgensen Cassella^a (PQ), José Walkimar de M. Carneiro^a (PQ)

^aIQ, UFF, Campus do Valonguinho, 24020-141, Niterói-RJ, Brasil

^bDQ, UFU - Campus Patos de Minas, 38700-128, Patos de Minas-MG, Brasil
mrlage@id.uff.br

Keywords: DFT, Diquat, Diphenzoquat, Ion-associate, Solvation, Agrochemicals, Herbicides

INTRODUCTION

Agrochemicals have been becoming important to increase the modern agricultural productivity. However, the use of such compounds is the cause of contamination of aquatic systems, considered as one of the main problems in modern society.¹ Chemicals like paraquat, diquat (DQ) and difenzoquat (DF) are largely employed as herbicides in various types of cultures, but this class of compounds has been proved to be toxic.^{1,2,3} In this way, recent works focused in the development of efficient methodologies for the extraction of agrochemicals from water.³ In the present work we report the study of the ion-associate formation from the interaction of dodecylsulfate (DS) ion with diquat and difenzoquat. Understanding the interaction mechanism between such compounds is important for the development of new extraction methodologies.

METHODS

The association of the well-known DFT functional B3LYP with the 6-31G(d) basis set was employed. CPCM solvation model was employed to simulate the effect of the solvent water. The geometry of each isolated ion and of each ion-associate was obtained in the gas phase and in water. Each successful geometry optimization was followed by calculation of the second order Hessian matrix. The results were analyzed in terms of the computed thermodynamic properties.

RESULTS AND DISCUSSION

The final geometries indicate that the ion associate is mainly stabilized by electrostatic interactions, what was confirmed by analysis of atomic partial charges (Figure 1). The interaction energy (IE) was computed according to the equation: $IE = E_{\text{ION-ASSOCIATE}} - (E_{\text{CATION}} + NE_{\text{ANION}})$ and are given in kcal/mol in Table 1.

Table 1. IE per number of DS added (N).

N	DQ (g)	DF (g)	DQ (s)	DF (s)
1	-163.63	-87.73	-6.26	-4.72
2	-256.30	-114.85	-8.10	-6.02
3	-288.93	-91.54	-14.71	-5.21
4	-285.58	-56.76	-14.64	-1.11
5	-243.01	-	-11.90	-

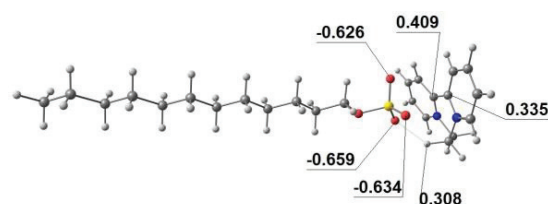


Figure 1. Geometry of DS-DQT ion-associate.

CONCLUSIONS

The results in Table 1 indicate that, for the system containing DQ, increasing the number of DS unities there is an increase in the interaction energy, which is attain the maximum value for 3 or 4 DS unities. For DF the interaction is much weaker and attain the most negative value for two DS unities. This show that for the doubly charged DQ it is needed a higher number of DS unities than for the interaction with DF which has only one positive charge.

ACKNOWLEDGMENTS

The authors are grateful for the support of FAPERJ, CAPES and CNPQ.

¹ O. Núñez, J.-B. Kim, E. Moyano, M. T. Galceran, S. Terabe, J. Chromatogr. A, 961, 65, (2002).

² F. N. Feiteira, L. G. T. dos Reis, W. F. Pacheco, R. J. Cassella, Microchem. J., 119, 44, (2015).

³ J. O. Vinhal, M. R. Lage, J. W. M. Carneiro, C. F. Lima, R. J. Cassella. J. Environ. Mange., 17, 11095, (2015).

Free Solvation Energy of aqueous Aluminium (III) species

Matheus C. Quintão¹ (IC), Guilherme F. de Lima² (PQ) and Hélio A. Duarte¹ (PQ)

1) Grupo de Pesquisa em Química Inorgânica Teórica – GPQIT; Departamento de Química - ICEx, Universidade Federal de Minas Gerais (UFMG), 31.270-901 Belo Horizonte – MG.

2) Instituto de Física e Química; Universidade Federal de Itajubá (UNIFEI), Av. BPS, 1303, Bairro Pinheirinho, Itajubá - MG

Email: mcquintao.qui@gmail.com.

Keywords: Chemical Speciation, DFTB Dynamics, DFT, PCM

INTRODUCTION

Thermodynamics studies in condensed phase are important to comprehension of many chemical processes. For example, the *pKa* of species in solution can be estimated from thermodynamics cycles¹; however, in this methodology, the calculation of $\Delta_{\text{solv}}G$ is a challenge. The shell solvation theory developed by Pliego² considers explicit solvent molecules, placed via molecular dynamics, and continuum method, to evaluate long range effects. In this work we have studied the $\Delta_{\text{solv}}G$ of $[\text{Al}(\text{H}_2\text{O})_6]^{3+}$, $[\text{Al}(\text{OH})(\text{H}_2\text{O})_5]^{2+}$, $[\text{Al}(\text{OH})_2(\text{H}_2\text{O})_4]^+$ and $\text{Al}(\text{OH})_3$ speciation in aqueous medium.

METHODS

The $\Delta_{\text{solv}}G$ was estimated using eq. (1)

$$\Delta\Delta_{\text{solv}}G = \frac{1}{2}\langle U \rangle + \langle \Delta_{\text{solv}}G^{A^+(\text{H}_2\text{O})_n} - \Delta_{\text{solv}}G^{(\text{H}_2\text{O})_n} \rangle \quad (1)$$

on the right hand side, the first term accounts the specific interactions between solute and solvent, while the second term and third terms add the long range contribution. Molecular dynamics (MD) were carried out in deMonNano package from which 4000 structures of a water box were obtained, whereas each structure contains about 54 explicit water molecules. The solvation free energy were estimated using different number of explicit water molecules. The first term of eq. (1) was averaged from 500 equally spaced structures selected from MD. DFT calculation were carried out at PBE/6-31++G** level to evaluate the interaction between the solute and the explicit solvent molecules. The second and third terms were averaged from 50 equally spaced structures using the PCM/HF/6-31++G** method. All calculations were carried out in the software GAUSSIAN09.

RESULTS AND DISCUSSION

By Eq. 1, was calculated the free solvation energy of all species. In a previous analysis, was determined that the value of $\Delta_{\text{solv}}G$ converge between 2 Kcal mol⁻¹ for 30 explicit solvent molecules, as shown in Figure 1. Thus, was obtained a $\Delta_{\text{solv}}G$ around -420.4, -216.7, -90.0 and -73.4 Kcal mol⁻¹ for the species $[\text{Al}(\text{H}_2\text{O})_6]^{3+}$, $[\text{Al}(\text{OH})(\text{H}_2\text{O})_5]^{2+}$, $[\text{Al}(\text{OH})_2(\text{H}_2\text{O})_4]^+$, and $\text{Al}(\text{OH})_3$ respectively.

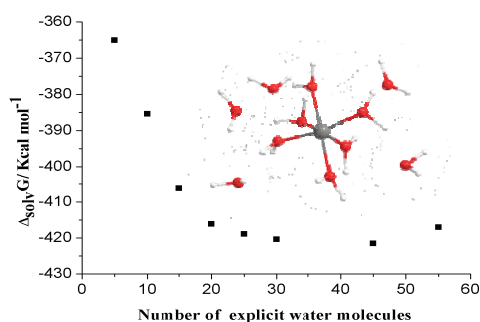


Figure 1. Convergence of $\Delta_{\text{solv}}G$, for $[\text{Al}(\text{H}_2\text{O})_6]^{3+}$.

CONCLUSIONS

The results indicate that the shell solvation energy method in combination with the SCC-DFTB method is adequate for estimating the free solvation energy of aqueous metal species.

ACKNOWLEDGMENTS

The authors are grateful for the support given from the FAPEMIG, CAPES, CNPQ, FINATEC and INCT-ACQUA.

¹ C. P. Kelly, C. J. Cramer, D. G. Truhlar. *J. Phys. Chem. B*, 110, 16066, (2006).

² G. F. Lima, J. R. Pliego Jr, H. A. Duarte. *Chem. Phys. Letters*, 518, 61, (2011).

DFT Approach of CO and NO Adsorption on LaFeO₃ Perovskite Doped with Pd and CoMaurício Tavares de Macedo Cruz (PQ), Leticia Maia Prates (PG)*Departamento de Química Geral e Inorgânica, Instituto de Química, Universidade do Estado do Rio de Janeiro, Rio de Janeiro, Brazil.
cruzmtm@uerj.br*

Keywords: perovskite, intelligent catalysis, self-regeneration, CO and NO adsorption, DFT.

INTRODUCTION

The sintering of metal particles in conventional automotive catalysts is an inherent process which affects its efficiency and increases the demand for precious metals. Studies have proposed that the intelligent catalyst suppresses this problem through a self-regeneration mechanism as response to redox fluctuations in the atmosphere of automobile engine exhaust gases, during fuel combustion. Experimental studies¹ show that LaFeO₃ perovskite doped with Pd, when exposed to reductive atmospheres, Pd particles segregate out of the perovskite structure. As the oxidative atmosphere become, the palladium atoms return to the perovskite structure as cations.² The objective of this study is to evaluate the relationship between composition and catalytic activity of the perovskite LaFeO₃ through DFT calculations for the adsorption of CO and NO on a LaFeO₃ cluster doped with a Pd atom, and, adding a Co atom in different positions.

METHODS

A cubic perovskite an arrangement (LaFe_{0.94}Pd_{0.06}O₃) was simulated by a set of four unit cells containing one atom of Pd doped in the center of the surface (Figure 1a). Then, using the same structure, a Fe atom has been replaced by an atom of Co. As a first step, the two complexes were fully optimized. Next, a CO molecule and a NO molecule were optimized over the Pd atom on the surface of the perovskite clusters, individually. All calculations were described with the PBEV5LYP/LANL2DZ/6-311+G(d) method, where 6-311+G(d) basis sets was used to describe the electrons of NO and CO molecules. During optimization of the complexes, NO and CO were optimized keeping the atoms of perovskite frozen, except the palladium atom.

RESULTS AND DISCUSSION

It was obtained opposite behaviors, comparing the results obtained to adsorption of CO and NO

molecules. The CO adsorption is favored with the presence of cobalt whereas the NO adsorbs strongly when the structure is doped only with palladium. Analyzing the bonding energy for the Pd atom, the Co acts maintaining the Pd atom more fixed in the agglomerate.

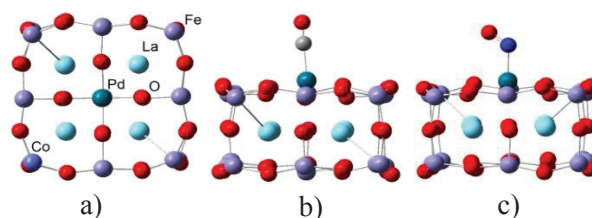


Figure 1. LaFeO₃ perovskite structure optimized doped with Pd and Co: a) pure, b) with CO adsorption, c) with NO adsorption.

Table 1. CO and NO adsorption energy (E_{ad} , kcal.mol⁻¹) and bonding energy for the Pd (E_b , kcal.mol⁻¹) with and without Co.

Perovskite		E_{ad}	Perovskite		E_b
NO	Pd	-41.80	Pd	Pd/Co	-140.02
	Pd/Co	-19.60			
CO	Pd	-16.40	Pd/Co	Pd/Co	-168.33
	Pd/Co	-28.60			

CONCLUSIONS

The perovskites doped with Pd and Pd/Co present opposite behaviors, comparing the results obtained to adsorption of molecules of CO and NO molecules. The presence of Co increases the bonding energy of the palladium atom.

ACKNOWLEDGMENTS

The authors are grateful for the support given from the CAPES, CNPQ and FAPERJ.

¹ M. Uenishi, M. Taniguchi, H. Tanaka, Appl. Catal., B., 57, 267, (2005).

² I. Hamada, A.Uozumi, Y.Morikawa, J. Am. Chem. Soc., 133, 18506, (2011).

All-electron double zeta basis sets for the most fifth-row atoms: Application in DFT spectroscopic

Mauro Lúcio Franco¹ (PQ), Antônio Canal Neto²(PQ), Francisco Elias Jorge²(PQ)

¹Universidade Federal dos Vales do Jequitinhonha e Mucuri, Departamento de Ciências Exatas, 39800-371 Teófilo Otoni, MG - Brasil; e-mail: ml.franco@ufvjm.edu.br

²Universidade Federal do Espírito Santo, Departamento de Física, 29060-900 - Vitória, ES-Brasil; e-mail: canalneto@gmail.com; email:jorge@cce.ufes.br

Keywords: Ab Initio, Spectroscopy, DFT

INTRODUCTION

In recent years, it has become commonplace to supplement experimental studies by quantum chemical calculations. The emphasis of most calculations, commonly performed at some level of density functional theory (DFT). A potential problem in calculations on fifth-row elements is the relatively high computational effort required to treat all the inner shell electrons (1s-4f).

METHODS

Segmented all-electron contracted double zeta valence plus polarization function (DZP) basis sets for the elements Cs, Ba, La, from Hf to Ir, and from Au to Rn are constructed for using in conjunction with the non-relativistic and Douglas-Kroll-Hess (DKH) Hamiltonians, using the B3LYP hybrid functional.

RESULTS AND DISCUSSION

In Table 1, compares theoretical and experimental harmonic vibrational frequencies for some diatomics. Four theoretical models are investigated. For the gold halides, unlike the bond length, the theoretical harmonic vibrational frequencies decrease going from AuF to AuI. This finding is in agreement with the experiment and with the chemical

Table1: Bond lengths (r_e in Å), harmonic vibrational frequencies (ω_e in cm^{-1}).

		DKH2-B3LYP				Expt. ^e
		DZP-DKH ^a	DZP+1d-DKH ^b	ANO-RCC-DZP ^c	UGBS1V ^d	
AuF(¹ Σ^+)	r_e	1.883	1.924	1.964	1.947	1.918
	ω_e	616.9	558.3	518.0	530.5	564
	D_e	3.666	2.800	2.790	2.963	3.01
AuCl(¹ Σ^+)	r_e	2.186	2.224	2.258	2.243	2.199
	ω_e	412.7	374.0	351.3	353.6	384
	D_e	3.520	2.706	2.674	2.779	3.13

^{a,b,d}Present investigation, DKH basis set generated in Refs^{2,3}

CONCLUSIONS

In summary, we have shown that it is possible to construct all-electron basis sets that spend small computational time to carry out atomic and molecular calculations of systems containing many electrons. The basis sets used in this work are available through the internet at <http://www.cce.ufes.br/qcgv/pub/>

ACKNOWLEDGMENTS

FAPEMIG, CNPq, CAPES, UFVJM and FAPES (Brazilian Agencies).

[1]P. Pyykkö, Chem. Rev. 88 (1988) 563.

[2]C.L. Barros, P.J.P. de Oliveira, F.E. Jorge, A. Canal Neto, M. Campos, Mol. Phys. 108 (2010) 1965.

[3]F.E. Jorge, A. Canal Neto, G.G. Camiletti, S.F. Machado, J. Chem. Phys. 130 (2009) 064108.

New Double Zeta Bases Sets for Boron and Carbon Obtained by HF^{Gauss} – GSA

M. D. de Andrade (PQ), A. M. de C. Sobrinho (PQ), L. A. C. Malbouisson (PQ)

Instituto de Física da UFBA – Depto. de Física do Estado Sólido, Salvador – Ba, Brasil
 e-mail: micael@ufba.br

Keywords: Atomic bases optimization, Hartree-Fock Gauss Generalized Simulated Annealing method, stochastic methods.

ABSTRACT

In previous work [1] were constructed new atomic 3G and 6G minimal bases for the first row atoms of the Periodic Table applying a stochastic method, the Generalized Simulated Annealing. Using this approach new Double Zeta (DZ) atomic bases for the Lithium and Beryllium atoms [2], were obtained recently. These new bases were used to calculate Hartree-Fock (HF) and full CI energies, and to calculate the permanent electric dipole [2, 3] and quadrupole [4] moments using the Multi-Reference Hartree-Fock Configuration Interaction (MRHF CI) method. These results were obtained for some molecules formed with first row atoms of the periodic table.

The procedure, designated HF^{Gauss}-GSA method, consists in the direct optimization of the HF functional of the atom, taking simultaneously as variational parameters the coefficients of the atomic orbital expansions in the basis functions and the coefficients and the exponents of the Gaussian functions which define the basis functions set.

By other side the HF equation is not linear and has, in principle, several solutions [5]. So, for each system, can be determined several HF solutions with the adequate point and spin symmetry. With each of the HF extreme we can construct a base of the full CI space in adequate symmetry class. In the MRHF CI method are employed several HF extremes as references to expand the state function.

In this work we are using the HF^{Gauss}-GSA method to obtain new DZ bases for the Boron and Carbon atoms. Were implemented modifications in the HF^{Gauss}-GSA FORTRAN code and in the present stage we are adjusting the best GSA parameters (q_A , q_V and q_T) for the procedure. The new bases obtained with this approach will be

used in MRHF CI calculations for systems involving Boron and Carbon atoms.

¹ M. D. de Andrade, M. A. C. Nascimento, K. C. Mundim, A. M. de C. Sobrinho and L. A. C. Malbouisson. *Int. Journal of Quantum Chemistry*, 108, 2486 (2008).

² A. M. de C. Sobrinho, M. D. de Andrade, M. A. C. Nascimento and L. A. C. Malbouisson. *J. Mol. Model.*, 20, 2382 (2014).

³ (a) L. A. C. Malbouisson, M. G. R. Martins and N. Makiuchi, *Int. J. Quantum Chem.*, 106, 2772 (2006); (b) A. M. C. Sobrinho, M. A. C. Nascimento, M. D. de Andrade and L. A. C. Malbouisson. *Int. J. of Quantum Chem.*, 108, 2595 (2008); (c) L. A. C. Malbouisson, M. D. de Andrade and A. M. de C. Sobrinho. *Int. J. of Quantum Chem.*, 112, 3409 (2012);

⁴ L. A. C. Malbouisson, M. D. de Andrade and A. M. de C. Sobrinho. *Int. J. of Quantum Chem.*, 112, 3409 (2012).

⁵ (a) W. H. Adams. *Phys. Rev.*, 127, 1650 (1962); (b) R. E. Stanton. *J. Chem. Phys.*, 48, 258 (1968); (c) L. A. C. Malbouisson, J. D. M. Vianna. *J. Chim. Phys.*, 87, 2017 (1990); (d) R. M. Teixeira Filho, L. A. C. Malbouisson and J. D. M. Vianna. *J. Chim. Phys.*, 90, 1999 (1993).

Theoretical Investigation of the Formaldehyde Gas-Phase Reaction with Chlorine Atoms

Michel Braga Garcia (PG), Glauco F. Bauerfeldt (PQ)

Departamento de Química, Instituto de Ciências Exatas, UFRuralRJ

Keywords: H₂CO + Cl Reaction, Prebarrier Complex, Variational Transition State Theory

INTRODUCTION

In recent years, an increasing interest in chlorine atom reactions with volatile compounds at atmospheric conditions is observed. Formaldehyde is an important atmospheric compound, for which only few works were dedicated to the determination of rate coefficients and the comprehension of the Cl reaction mechanism.^{1,2} Despite the effort in explaining the reaction energetics and activation parameters for the H₂CO + Cl reaction, the role played by pre-barrier intermediates and satisfactory rate coefficients prediction remain unclear.

In this work, several theoretical methods are employed for studying the H₂CO + Cl reaction path and rate coefficients are predicted from a chemical model explicitly taking into account the participation of a pre-barrier complex. Our main goals are the comprehension of the reaction energetics and the discussion about the reaction mechanism.

METHODS

H₂CO + Cl reaction was studied at *ab initio* (MP2, CCSD and QCISD) and DFT (B2PLYP, BHandHLYP) levels, adopting the aug-cc-pVDZ (ACCD) and aug-cc-pVTZ (ACCT) basis sets. Single point calculations at CCSD(T) and QCISD(T) levels were also performed. Canonical variational rate coefficients were finally calculated in the range from 200 – 500 K.

RESULTS AND DISCUSSION

Molecular properties were predicted for reactants and products of the H₂CO + Cl reaction in reasonable agreement with the literature data, as evidenced by rms deviations lower than 0.05 Å, 5° and 300 cm⁻¹.

Stabilization energies regarding the pre-barrier intermediates have been found in the range from 4.8 to 1.8 kcal mol⁻¹ (the highest value has been

obtained at B2PLYP level and the lowest value, at the MP2 level).

Previous MRD-CI calculations suggested the saddle point relative energy as 0.17 kcal mol⁻¹.⁴ Our results were found in the range from -0.42 to 1.5 kcal mol⁻¹. Inclusion of zero point energy corrections cause these values to decrease, and our resulting B2PLYP value (-0.47 kcal mol⁻¹), agrees with the MRD-CI prediction (-0.5 kcal mol⁻¹).

Canonical variational rate coefficients were predicted at 200 – 500 K. Rate coefficients were predicted (in 10⁻¹¹ cm³ molecule⁻¹ s⁻¹ units, at 298 K) in the range from 0.56 – 54, in agreement with the experimental value (7.8), the best values being: $k_{B2PLYP} = 5.3$, $k_{CCSD} = 2.0$, $k_{QCISD} = 4.7$ and $k_{CCSD(T)/B2PLYP} = 10$. Activation energies are found in the range 0.07 – 0.26 kcal mol⁻¹, whereas our best values vary from 0.02 to 0.23 kcal mol⁻¹.

CONCLUSIONS

In this work, the proposal of a reaction mechanism with explicitly participation of the pre-barrier complex is made and variational rate coefficients were predicted, in good agreement with experimental data. Our results suggest that the reaction dynamics can be satisfactorily described from the mechanism in which the pre-barrier intermediate plays a key role.

ACKNOWLEDGMENTS

The authors thank the support given from CAPES.

¹ J. Liu, Z. Li, C. Sun, J. Phys. Chem. A, 105, 7707 (2001).

² M. Nakamura, K. C. Lin, T. Kasai, Phys. Chem. Chem. Phys., 12, 2532 (2010).

³ M. Gruber-Stadler, J.C. Sellevag, S.R. Mühlhäuser, M. Nielsen, Phys. Chem., 9, 112 (2008).

⁴ R. Atkinson, D. L. Baulch, R. A. Cox, R. F. Hampson, JR., J. A. Kerr, M. J. Rossi, and J. Troe, J. Phys. Chem., 26, 521 (1997).

DFT studies on degradation mechanisms of chlorhexidine

Michele A. Salvador^a (PQ), Camila Pinheiro Souza^b (PQ), Pedro de Lima-Neto^b (PQ), Adriana N. Correia^b (PQ), Paula Homem-de-Mello^a (PQ)

^a Universidade Federal do ABC – Santo André - SP, Brazil

^b Universidade Federal do Ceará – Fortaleza – CE, Brazil

Keywords: Density Functional Theory, Chlorhexidine, Degradation.

INTRODUCTION

Chlorhexidine (CHD) is a cationic drug with germicidal activity against bacteria, yeasts, and molds¹. Its degradation process has been studied to involve formation of toxic products. In acidic conditions, it has been suggested to exist two degradation routes, involving a different number of intermediates, both leading to formation of PCA (p-chloroaniline) as one of the final products. Figure 1 presents the structural form of CHD.

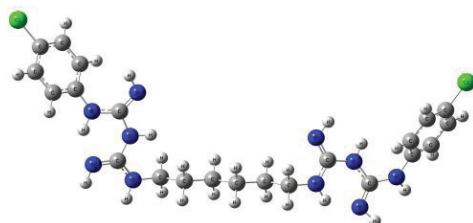


Figure 1. CHD's structure representation.

Literature indicates that such processes start with molecules' initial protonation in different sites, followed by bond breaking, after the incorporation of water molecules. In this work DFT methods were used to evaluate the different routes proposed and also to propose a mechanism for the electrooxidation process.

METHODS

We have made a systematic study of intermediates and products of degradation process using B3LYP hybrid functional and 6-311+G(d) basis set as implemented in Gaussian09 package. We have also employed TD-DFT calculations to evaluate molecular orbitals of CHD.

RESULTS AND DISCUSSION

First of all we have estimated the initial protonation states of CHD. The four nitrogen atoms are not equivalent, and depending on the pH, we have 2 or 4 protonation sites. The symmetry of the highest occupied molecular orbitals is also dependent of this protonation, being HOMO and HOMO-1 degenerated for some cases. In acidic conditions, our calculations demonstrate that the reaction proceeds for several steps until the formation of PCA.

Electrooxidation experiments were conducted in pH = 4, for which we have the fourfold protonated state of CHD. The interaction with magnetite nanoparticles and with nanoparticles recovered with chitosan changes the geometry of the molecule, leading to conformations with more oxidation sites.

CONCLUSIONS

Degradation processes of chlorhexidine have been systematically studied by DFT. Both degradation pathways in acidic medium considered lead to PCA formation, but with different number of intermediates. The electrooxidation mechanism seems to have smaller number of steps, and the interaction between CHD and chitosan helps to create oxidation sites.

ACKNOWLEDGEMENTS

The authors are grateful for the support given from the CNPq, FAPESP and UFABC.

1 Z. Zong, L.E. Kirch, Journal of Pharmaceutical Sciences, 101, 2012.

2 L-H Wang, S.-J. Tsai, Analytica Chimica Acta 441, 2001.

Theoretical Insights of Metallic Ag Growth on α -Ag₂WO₄ upon Electron Irradiation

Miguel A. San-Miguel^a, Juan Andrés^b, Elson Longo^c, Edison Z. da Silva^d

^a Instituto de Química, Unicamp, Campinas 13083-970, Brazil – smiguel@iqm.unicamp.br

^b Departamento de Química Física i Analítica, UJI–Universitat Jaume I, Castelló de la Plana 12071, Spain - andres@qfa.uji.es

^c Instituto de Química, UNESP, Araraquara 14800-900, Brazil - elson.liec@gmail.com

^d Instituto de Física, Unicamp, Campinas 13083-970, Brazil - zacarias@ifi.unicamp.br

Keywords: DFT calculations; Ag Nanoparticles; Transmission Electron Microscopy

INTRODUCTION

The formation and growth of metallic Ag on α -Ag₂WO₄ upon electron beam irradiation is a novel process that has been investigated extensively by different experimental techniques including transmission electron microscopy (TEM), field emission scanning electron microscopy (FE-SEM), energy dispersive spectroscopy (EDS) characterization, among others¹⁻³. This is a widely employed route to produce efficient photocatalysts, ozone sensors and bactericides.

METHODS

Quantum calculations based on the Density Functional Theory (DFT) using the VASP code were carried out on periodic supercells to represent the (100) and (001) surfaces of α -Ag₂WO₄. The geometries were optimized using the conjugate gradient (CG) method and selected structures were also studied using *ab initio* molecular dynamics simulations in the canonical ensemble at 300 K. The Nudged Elastic Band (NEB) method was used to characterize the minimum energy pathways for the diffusion process of Ag atoms.

RESULTS AND DISCUSSION

The nucleation and formation of metallic Ag on α -Ag₂WO₄ is initiated when Ag atoms diffuse from the interior material to the surface. In this work, we have made use of DFT calculations and *ab initio* molecular dynamics simulations to investigate the geometrical and electronic structure of the most favorable surfaces: (100) and (001). This semiconductor exhibits a complex structure, which can be understood as an arrangement of AgO_x (x = 2, 4, 6, and 7) clusters used as constituent building blocks. Thus, the

relaxation process upon cleaving the surfaces from the bulk can induce significant rearrangements. We also show that there are specific Ag atoms in the sub-surface positions that are prone to undergo the diffusion process with very low energy barrier (< 0.1 eV). Furthermore, our results point out that the injection of electrons decreases the activation barrier for this diffusion step [4].

CONCLUSIONS

Our calculations supply an atomistic approach to the local geometry and the electronic structure of the surfaces exposed to the electron beam irradiation and gain insight into the initial stages of the metallic Ag growth on the Ag₂WO₄ surfaces.

ACKNOWLEDGMENTS

The authors are grateful for the support given from the FAPESP.

REFERENCES

- ¹ E. Longo, L. S. Cavalcante, D. P. Volanti, A. F. Gouveia, V. M. Longo, J. A. Varela, M. O. Orlandi and J. Andres, *Sci. Rep.*, 3, 1676 (2013).
- ² J. Andrés, L. Gracia, P. Gonzalez-Navarrete, V. M. Longo, W. Avansi Jr., D. P. Volanti, M.M. Ferrer, P. S. Lemos, F. A. L. Porta, A. C. Hernandez and E. Longo, *Sci. Rep.* 5, 5391 (2014).
- ³ E. Longo, D. P. Volanti, V. M. Longo, L. Gracia, I. C. Nogueira, M. A. P. Almeida, A. N. Pinheiro, M. M. Ferrer, L. S. Cavalcante and J. Andrés, *J. Phys. Chem. C*, 118, 1229 (2014).
- ⁴ W. da Silva Pereira, J. Andrés, L. Gracia, M. A. San-Miguel, E. Z. da Silva, E. Longo and V. M. Longo, *Phys. Chem. Chem. Phys.* 17, 5352 (2015).

Elastic scattering of low-energy electrons by CH₃CN and CN₃NC Isomers

Milton Massumi Fujimoto^a (PQ), Erik V. R. de Lima^a (IC) and Jonathan Tennyson^b (PQ)

^a *Departamento de Física, Universidade Federal do Paraná, 81531-990 Curitiba, PR, Brazil*

^b *Department of Physics and Astronomy, University College London, Gower St., London WC1E 6BT*

Keywords: R-matrix method, CH₃CN and CH₃NC, resonance, cross sections

INTRODUCTION

Molecules containing cyanide and isocyanide groups have many different applications in chemical industries. The CH₃CN (acetonitrile) molecule was detected in the interstellar clouds and can be considered an building block for amino acids. The isomers CH₃CN and CH₃NC (isoacetonitrile) have large permanent dipole moments (> 3 Debye), can form "dipole-bound" molecular anions. Theoretical and experimental studies have shown the existence of "dipole-bonded" anion for CH₃CN. There are also studies of dissociative electron attachment (DEA) for both CH₃CN and CH₃NC in the gas phase. The resonance features are important to understand the DEA mechanism of explain, such as, appearance energies of ions and even fragmentation patterns leading different anions. In this work we report elastic integral cross sections for low-energy (below 10 eV) electron collisions with CH₃CN and CH₃NC.

METHODS

The R-matrix theory¹ is used to describe electron scattering by molecules and the UK polyatomic Rmatrix (UKRMol) codes were employed to calculated the cross sections and quantities of interest in the nuclei-fixed frame. In this method the space is split into an inner and an outer region. The inner region is defined as the space inside of a sphere of radius $r=a$ in which the center-of-mass of the molecule defines the origin of the coordinates. The radius a is chosen in order to have all electronic density of the target molecule inside the sphere. In the inner region, the interactions between the scattering electron and all electrons of the molecule is strong is the inner region, it is important to consider exchange, polarization and correlation effects. The cross sections were calculated in static-exchange (SE) and static-exchange-polarization (SEP) level. Due to the large permanent dipole moment for both isomers, and in order to take into account the

long-range interaction, a Born closure procedure² was employed.

RESULTS AND DISCUSSION

First, we performed a systematic study of the convergence of eigenphase sums and in SE level, we observed sharp resonance feature near 5.0 eV and 5.5 eV for CH₃CN and CH₃NC, then in SEP level the resonance moves to 2.4 and 2.8 eV respectively. Both molecules present another broad resonance at higher energy near 6 eV.

The differential cross sections (DCS) for both molecules are very similar between them. As there is no experimental data available in the literature, we have compared our results with available results for HCN. The magnitude order of DCS are in good agreement.

The integral cross section (ICS)-SEP results have shown that the resonance converges to 2.4 and 2.8 eV and the long-range interactions are dominant effects comparing with polarization. The ICS experimental results for HCN are around 4 times smaller comparing with both isomers, and it could be partially explained by experimental extrapolation method.

CONCLUSIONS

This study presents the first study of elastic cross sections for CH₃CN and CH₃NC. The lower energy resonance (2.4 and 2.8eV) are in reasonably agreement with experimental results. The long-range interactions are dominant comparing with polarization effects.

ACKNOWLEDGMENTS

The authors are grateful for the support given from the UFPR-TN, Fund. Araucária and CNPq.

¹ J. Tennyson, Phys. Rep. 491, 29 (2010).

² I. Rabadan, B.K. Sarpal and J. Tennyson, J. Phys. B: At. Mol. Opt. Phys., 31, 2077 (1998).

Study of Isomer and Conformer effects in electron scattering using R-Matrix

Method

Milton Massumi Fujimoto^a (PQ), Erik V. R. de Lima^a (IC) and Jonathan Tennyson^b (PQ)

^a *Departamento de Física, Universidade Federal do Paraná, 81531-990 Curitiba, PR, Brazil*

^b *Department of Physics and Astronomy, University College London, Gower St., London WC1E 6BT*

Keywords: R-matrix method, CH₃CN and CH₃NC, Alanine conformers, resonance, cross sections

INTRODUCTION

After the discovery of degradation of DNA molecules by low energy electrons, less than 20 eV, many experimental and theoretical studies involving DNA building blocks have been made in gas phase to understand in details the DEA (Dissociative Electron Attachment) mechanism of DNA. In this work we present a study of electron scattering by isomers CH₃CN, CH₃NC and some conformers of amino acid Alanine. The CH₃CN (acetonitrile) molecule was detected in the interstellar clouds and can be considered an building block for amino acids. The isomers CH₃CN and CH₃NC (isoacetonitrile) have large permanent dipole moments (> 3 Debye), can form "dipole-bound" molecular anions. The resonance features are important to comprehend the DEA mechanism and explain, appearance energies of ions and even fragmentation patterns leading different anions. In this work we report a comparison of elastic integral cross sections for low-energy (below 10 eV) electron collisions with CH₃CN, CH₃NC and Alanine conformers. We will discuss some features which are important to take into account to that cross sections.

METHODS

The R-matrix theory¹ is used to describe electron scattering by molecules and the UK polyatomic Rmatrix (UKRMol) codes were employed to calculate the cross sections and quantities of interest in the nuclei-fixed frame. In this method the space is split into an inner and an outer region. The inner region is defined as the space inside of a sphere of radius $r=a$ in which the center-of-mass of the molecule defines the origin of the coordinates. The radius a is chosen in order to have all electronic density of the target molecule inside the sphere. In the inner region, the interactions between the scattering electron and all electrons of the molecule is strong is the inner region, it is important to consider exchange,

polarization and correlation effects. The cross sections were calculated in static-exchange (SE) and static-exchange-polarization (SEP) level. Due to the large permanent dipole moment for both isomers, and in order to take into account the long-range interaction, a Born closure procedure² was employed.

RESULTS AND DISCUSSION

First, we performed a systematic study of the convergence of eigenphase sums and in SE level, we observed sharp resonance feature, then the calculation in SEP level moves the resonance to lower energies.

The differential cross sections (DCS) for these molecules are very similar between them but some cases can be very different. As there are no experimental data available in the literature, we have compared our results with available results of similar molecules. The magnitude order of DCS are in reasonable agreement.

For CH₃CN and CH₃NC the integral cross section (ICS)-SEP results have shown the resonance features and the long-range interactions are dominant effects comparing with polarization. For Alanine molecules the ICS results can be very different depending on the geometry of conformer.

CONCLUSIONS

In this work we have shown the importance of atoms position in isomers and of geometry of conformers in the cross sections. The discussions will be present at the meeting.

ACKNOWLEDGMENTS

The authors are grateful for the support given from the UFPR-TN, Fund. Araucária and CNPq.

¹ J. Tennyson, Phys. Rep. 491, 29 (2010).

Identificando os sítios preferenciais de solvatação da xilose

Miqueias M. Peixoto^a (IC), Clarissa O. da Silva^b (PQ)

^a*miqueiaspeixoto@ufrj.br*

^b*clarissa-dq@ufrj.br*

Palavras chave: Xilose, Sítios de Solvatação, Monossacarídeo, Descrição Teórica, Rotação Ótica.

INTRODUÇÃO

Neste trabalho pretende-se realizar a identificação dos sítios preferenciais de solvatação dos confôrmeros mais estáveis da molécula de xilose em solução aquosa^{1,2}, com a consideração de até duas moléculas de água explícitas. Então, pretende-se avaliar o quanto a consideração destas moléculas explícitas do solvente interfere no equilíbrio anomérico (valores de população dos anômeros em solução), bem como no valor de rotação específica, quando comparados aos valores correspondentes obtidos somente na presença de um método contínuo para a descrição dos efeitos do solvente. Devido à versatilidade que os carboidratos possuem a nível conformacional, a rotação específica ($[\alpha]_D$) será a propriedade intensiva escolhida para a análise destes confôrmeros.

METODOLOGIA

Todos os cálculos de otimização realizados, iniciaram-se a partir das conformações mais abundantes em solução, encontradas em trabalho anterior². A partir destas, explorou-se os efeitos das mudanças conformacionais na distribuição populacional do sistema, quando explicitada uma molécula de água, utilizando o funcional de densidade B3LYP com conjunto de funções de base 6-31+G(d,p). A identificação dos sítios de micro-solvatação obedeceu a um procedimento anteriormente utilizado com sucesso³, e baseia-se na identificação da região molecular onde se encontram os módulos dos maiores valores de carga depositados sobre a superfície da cavidade, que no modelo de contínuo polarizável utilizado, mimetiza a presença do solvente polarizado pela presença do soluto. Este procedimento foi proposto em virtude da interação estabelecida entre soluto e solvente ser de natureza predominantemente eletrostática.

RESULTADOS E DISCUSSÃO

A partir das informações conformacionais adquiridas neste estudo, prosseguiu-se aos cálculos de frequência para a determinação da distribuição populacional do sistema, fazendo uso das geometrias escolhidas nos cálculos de micro solvatação. Com as frequências determinadas e assumindo uma distribuição populacional de Boltzmann, verificou-se uma proporção anomérica ($\alpha:\beta$) de aproximadamente (27:73), conforme segue no gráfico:

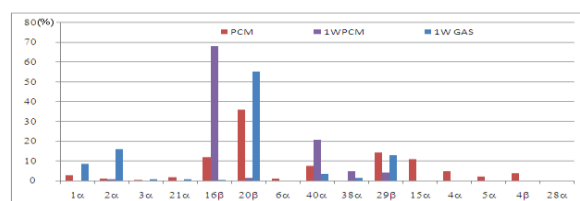


Figura 1. Gráfico de distribuição populacional do sistema em estudo (1WPCM), do trabalho anterior² (PCM) e de nossa análise preliminar (1WGAS).

CONCLUSÕES

Observa-se que há uma mudança na abundância dos confôrmeros entre as descrições apresentadas, porém este fato não interfere de modo definitivo no equilíbrio anomérico $\alpha:\beta$ (Exp.: 37:63; PCM: 34:66; 1WPCM: 27:73). Os cálculos de rotação específica utilizados para validar este estudo, indicam uma inversão de valores com a mudança de descrição ($[\alpha]_D$): PCM = 19,61; 1WPCM = -4,83, onde ($[\alpha]_D$) é dado em $(\% / (\text{dm}(\text{g}/\text{cm}^3)))$. Este fato se deve, não a grandes mudanças nos valores individuais de rotação específica de cada confôrmero analisado, mas devido à alteração na distribuição populacional do sistema micro solvatado.

REFERENCIAS

- ANDRADE, R. R.; Silva, C. O. Mini-Review in Organic Chemistry (MROC) 8, 239 (2011)
- ANDRADE, R. R.; Silva, C. O. Carbohydr. Res. 350, 62 (2012)
- ORLOVA, A. V.; Andrade, R. R.; da Silva, C. O.; Zinin, A. I.; Kononov, L. O. ChemPhysChem. 15, 195 (2014)

Electronic and structural properties of B phase of Nb₂O₅ bulk – A DFT study

Mirele Bastos Pinto (PG), Hélio A. Duarte (PQ) and Heitor A. De Abreu (PQ).

Universidade Federal de Minas Gerais, Departamento de Química – GPQIT, Belo Horizonte
Brazil. e-mail: mirele.quimica@gmail.com

Keywords: Niobium pentoxide, DFT, Plane Waves, QTAIM.

INTRODUCTION

The niobium chemistry is still not well understood, nevertheless niobium compounds have attracted interest in many areas due to its strong surface acidity and stability in aqueous medium for various acid-catalyzed reactions. There are several crystallographic phase of Nb₂O₅ that depends on the temperature and pressure to which the materials are submitted. It has been shown that the B phase (B-Nb₂O₅) can be stabilized at room temperature and pressure^[1]. This phase is monoclinic and has 28 atom/cell^[2]. The understanding of the electronic and structural properties of the bulk and surfaces of Nb₂O₅ is the first step for understanding the catalytic properties of these material at a molecular level. Therefore, the aim of this work is the elucidation of the nature of the chemical bonding and the structural and electronic properties of the B-Nb₂O₅ bulk.

METHODS

All the calculations have been performed through Density Functional Theory (DFT)/plane waves methodology with periodic boundary conditions as implemented in the *Quantum-ESPRESSO package—PWscf*. PBE exchange–correlation (xc) functional with core electrons described by ultrasoft pseudo-potentials were used. A cutoff energy of 60 Ry and charge density cutoff of 400 Ry were used. The k-points density 4x4x4 integrals by Monkhorst and Pack was applied.

RESULTS AND DISCUSSION

The band structure was calculated indicating indirect band gap of 2.6 eV. The experimental gap of this phase is not reported in the literature. For crystalline H-Nb₂O₅ and T- Nb₂O₅ the measured gap was 3.4 eV^[3]. Figure 1 shows the total and site-projected DOS calculated for B-Nb₂O₅. The oxygen atom is the one that most contributes to the states around the Fermi level in the valence band. On the other hand, niobium (*d* orbitals) are the largest contributor to the conduction band. This agrees to the Quantum Theory of Atoms in Molecules (QTAIM) atomic charge analysis which are shown in Table 1. The estimated

positive atomic charge for Nb is reasonable since oxygen atom is more electronegative (χ). The QTAIM topological analysis and ELF indicate ionic character for Nb–O bond.

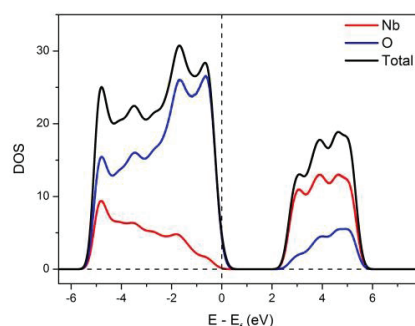


Figure 1. Total and projected DOS over the atoms of Nb₂O₅.

Table 1. Atomic charges in QTAIM analysis. Volume (Borh³) is the volume of the basins occupied by the atoms.

Atoms	Charge	Volume (Borh ³)	χ
O1	-1.07	98.63	3.44
O2	-1.01	92.83	
O3	-1.16	81.51	
Nb	2.72	67.10	1.60
Total		2358.02	

CONCLUSIONS

Structural and electronic calculated properties for the crystalline B phase of Nb₂O₅ bulk are in good agreement with the experimental data. Preliminary results point out the niobium sites as the most acidic, which will be important for the chemical reactivity of the surfaces.

ACKNOWLEDGMENTS

INCT-acqua, FAPEMIG, CAPES and CNPq.

[1] I. Nowak and M. Ziolk, *Chemical Reviews* **99**, 3603-3624, 1999.

[2] T. Ercit, *Miner. Petrol.* **43**, **3**, 217-223, 1991.

[3] S. Pérez-Walton, *et al*, *Phys. Status Solidi B* **250**, **8**, 1644-1650, 2013.

Molecular Dynamics Simulation to design an Enzyme-based Nanobiosensor using Atomic Force Microscopy to detect Glyphosate herbicide

Moacir F. Ferreira Jr.^{1*}, Eduardo F. Franca¹, Fábio L. Leite²

¹ Instituto de Química - Universidade Federal de Uberlândia, Uberlândia – MG, Brasil.

² Universidade Federal de São Carlos, Sorocaba – SP, Brasil.

*jrmoca@gmail.com

Keywords: Potential of mean force, nanobiosensor, glyphosate, molecular dynamics.

INTRODUCTION

The functionalization of atomic force microscopy (AFM) tips with biomolecule is capable of measuring the force of interaction between this biomolecule with the analyte on a substrate, acting thus as a nanobiosensor¹. The potential of mean force (PMF) method is a practical method that can be used to analyze the intermolecular interactions in protein-ligand systems. In this study PMF calculations were performed for determination of the absolute binding free energies for (EPSPs, Shikimate-3-phosphate)-Glyphosate system (figure 1) in order to mimic the interaction between the AFM tip functionalized with the EPSP enzyme and glyphosate.

METHODS

Calculations were performed with the software program GROMACS 4.6² using the NPT ensemble (1 bar and 298K) for 4ns in vacuum. The PMF calculations were carried out using Sterred Molecular Dynamics (SMD) applying to the distance constraints between the GPJ and active site of EPSPs(S3P) a force constant of 367 kJ.mol⁻¹.nm⁻¹, with a constant velocity of 0.001 nm.ps⁻¹.

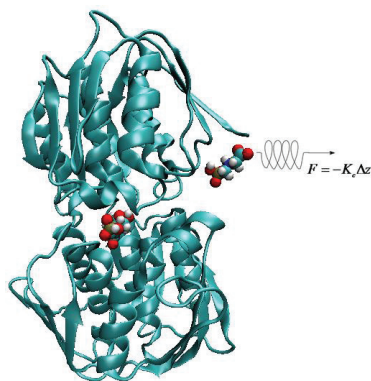


Figure 1: Possible unbinding pathway of glyphosate from the EPSPs active site.

RESULTS AND DISCUSSION

The figure 2 shows the force-extension profiles of the interaction between GPJ and active site EPSPs with the presence of S3P substrate. It is observed that the maximum of force necessary required to remove the herbicide from active site occurs around 2500 KJ.mol⁻¹.nm⁻¹ around 500 ps, from the start of the simulation, which can be attributed to the moment of rupture of the main interactions between residues of enzyme and S3P with the GPJ.

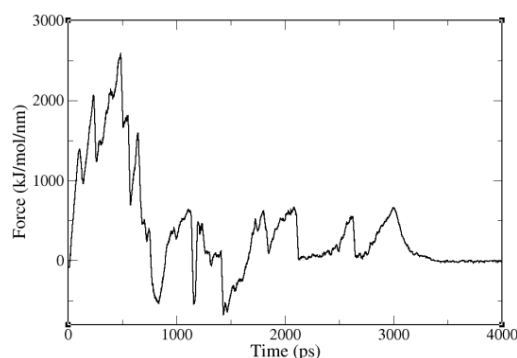


Figure 2: SMD force-extension profiles between GPJ and active site EPSPs-(S3P).

CONCLUSIONS

Obtaining the force of interaction between the GPJ herbicide and the active site of EPSPs-S3P will provide comparative information of the sensitivity of this new biosensor.

ACKNOWLEDGMENTS

The authors are grateful for the support given from the FAPEMIG and Rede Mineira de Química.

¹ E. F. Franca, F. L. Leite, O. N. Oliveira, L. C. G. Freitas, *Phys.Chem.Chem.Phys.* 13, 8894 (2011).

² B. Hess, C. Kutzen, D. van der Spoel, E. Lindahl. *J. Chem. Theory Comput.* 4, 435-447, (2008).

Hybrid QC/MM potential simulations of iron-containing proteins

Murilo H. Teixeira (PG) and Guilherme M. Arantes (PQ)

Depto. Bioquímica - Instituto de Química – Universidade de São Paulo
email: murilo.teixeira@usp.br ; garantes@iq.usp.br

Keywords: Metalloprotein, Heme, Iron-Sulfur clusters, QM/MM

INTRODUCTION

Theoretical studies of proteins containing transition metals require a proper description of the metal unpaired electrons. The reactivity of these metalloproteins is usually correlated with the metal open shell electronic configurations. In this work we simulated two classes of metalloproteins: Myeloperoxidase (MPO) catalysis of chloride to hypochlorite oxidation reaction; and the redox reaction of various iron-sulfur proteins (ISP).

METHODS

Initial configurations for MPO and the ISP proteins rubredoxin, ferredoxin^[1,2] were obtained from crystallographic structures. All protein models were built in a salt neutralized water box. Energies were calculated with either a pure MM force-field or a quantum chemical/molecular mechanical (QC/MM) hybrid potential with several different density functional theory (DFT) functionals. In the QC/MM calculations for MPO, the active site equipped with a heme center and the groups covalently linked to heme were included in the QC region. For the ISPs, the iron-sulfur clusters and its coordinated residues were described in the QC region (Figure 1).

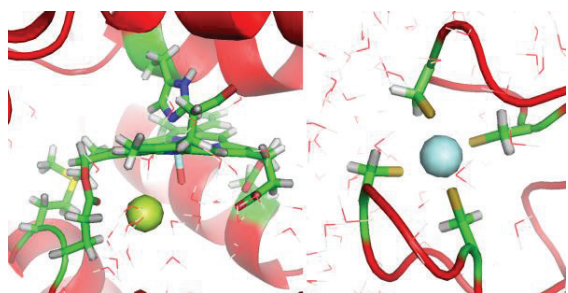


Figure 1. MPO catalytic site (left) and Rubredoxin iron-sulphur center (right). QC and MM regions indicated with ball-stick (green) and cartoon (red) representations, respectively.

Molecular dynamics (MD) simulations were run with a pure MM CHARMM36 force-field. Geometry optimizations and single-point energy calculations were performed along selected structures obtained from these MD trajectories with the hybrid QC/MM potential. Redox free-energies were calculated using the linear

response^[3] approximation. MD simulations were performed with GROMACS version 4.6.7. Hybrid potential calculations were done with the pDynamo library version 1.8 interfaced with ORCA version 3.0.1 for QC calculations.

RESULTS AND DISCUSSION

For MPO, the QC/MM calculations indicate an associative (An+Dn) mechanism with a stable intermediate by 8kcal/mol, in relation to the chloride oxidation reactant. Water molecules with high residence times (2–3ns) were found in MD simulations near the heme group. This is in line with a possible hydration reaction of the heme group proposed in the literature^[2].

For the ISPs, redox potential differences measured experimentally in comparison to the WT protein are 50mV for the L41A mutant and 100mV for the V44A mutant. Using a pure MM force-field, calculated differences are negligible for both mutants, in disagreement with experiment. On the other hand, QC/MM calculations can reproduce the experimental redox potential differences within +/- 10 mV.

The convergence of the redox potential calculations with various DFT functionals, basis sets, and simulation details of the hybrid potential are analyzed.

CONCLUSIONS

Modeling iron proteins is challenging. Hybrid potentials are useful in describing key elements of the electronic structure of active metal centers and may be used for the calculation of experimental observables and reaction mechanisms.

ACKNOWLEDGMENTS

Support from CNPq and FAPESP are acknowledged.

¹ Arantes, G. M. et al. Nat. Commun. 6, 7569 (2015).

² Beinert, H. et al. Science. 277, 653 (1997).

³ King, G. et al. J. Chem. Phys. 89, 859 (1988).

Structure and thermochemical properties of C₆ volatile unsaturated alcohols

Natália Aparecida Rocha Pinto (GR), Stella Maris Resende (PQ)

Laboratório de Química Atmosférica Teórica (LAQAT), Departamento de Ciências Naturais, Universidade Federal de São João del-Rei (UFSJ), São João del-Rei, Minas Gerais, Brasil.

Keywords: ab initio, CCSD(T), thermochemistry, atmospheric chemistry, VOC

INTRODUCTION

A significant class of compounds emitted to the atmosphere is the volatile organic compounds (VOC). The atmospheric oxidation of these compounds leads to the formation of organic aerosols. The presence of these particles in the atmosphere has important environmental consequences, because they are involved in the climate regulation of the planet. Among the oxygenated VOC, the most relevant are the unsaturated alcohols C₄, C₅, C₆ e C₈. Concerning the C₆ alcohols, there are some experimental studies on its atmospheric decomposition.¹ However, structural and thermochemical properties are not known with accuracy. In this work, our aim is to investigate the structural properties of the VOC (Z)-hex-3-en-1-ol (leaf alcohol), (E)-hex-3-en-1-ol, (Z)-hex-4-en-1-ol and (E)-hex-4-en-1-ol and to determine its thermochemical properties.

METHODS

Initially, it was conducted a conformational analysis in order to determine the most stable structure for the species in study. The energy optimization calculations and determination of harmonic frequencies were done at the MP2/cc-pVTZ level. Single point calculations were performed at the MP2/cc-pVDZ, MP2/cc-pVQZ and CCSD(T)/cc-pVTZ levels in order to achieve the limit for an infinite basis set function and a better accuracy to the electron correlation. For the study of the thermochemical properties, isodesmic reactions were used to provide errors minimization. Using values obtained from the literature for the standard enthalpy and Gibbs energies of formation of other species involved in the reactions studied, and the values of standard enthalpy and Gibbs energies of reaction obtained at the CCSD(T)/CBS level of theory, the standard enthalpy and Gibbs energies of formation of alcohols of interest were determined theoretically.

RESULTS AND DISCUSSION

The values calculated for the species of interest are presented in Table 1. Because this is the first determination of these thermochemical properties, there is no data in the literature for comparison. Nevertheless, we can see that the values are intermediate between those already established for hexene and hexanol, which is expected. Furthermore, our results show that (E) isomers are more stable than the (Z) ones, which is also observed for similar compounds.

Table 1. Standard Enthalpy and Gibbs free energies of formation in kJ/mol (298.15 K, 1 atm).

Species	ΔH_f	ΔG_f
(Z)-hex-4-en-1-ol	-117.7	38.7
(E)-hex-4-en-1-ol	-136.3	22.3
(Z)-hex-3-en-1-ol	-132.4	25.5
(E)-hex-3-en-1-ol	-136.4	20.6

CONCLUSIONS

The most stable conformation of the volatile organic compounds (Z)-hex-3-en-1-ol, (E)-hex-3-en-1-ol, (Z)-hex-4-en-1-ol and (E)-hex-4-en-1-ol were determined theoretically, and the standard enthalpy and Gibbs energies of formation for these species were calculated. According to our knowledge, there are no values in the literature for comparison, but the high level of calculation used enables us to say that our results are reliable. This is the first structural and thermochemical characterization of these compounds and these values are will be useful in a future study of the atmospheric decomposition of these compounds.

ACKNOWLEDGMENTS

The authors are grateful for the support given from FAPEMIG and CNPq.

¹ M. E. Davis, J. B. Burkholder, *Atmos. Chem. Phys.*, 11, 3347 (2011).

Europium Luminescence: Electronic Densities and Superdelocalizabilities for a Unique Adjustment of Theoretical Intensity Parameters

Nathalia B. D. Lima^a (PG), José D. L. Dutra^b (PG), Ricardo O. Freire^b (PQ) and Alfredo M. Simas^a (PQ)

^a Departamento de Química Fundamental, CCEN, UFPE, 50590-470 - Recife, PE, Brazil.

^b Departamento de Química, CCET, UFS, 49100-000 - Aracaju, SE, Brazil.

Keywords: Europium luminescence, intensity parameters, LUMPAC, Sparkle Model

INTRODUCTION

We advance the concept that the charges, g_i , and polarizabilities, α_i , for europium complexes, within SOM and Judd-Ofelt theory, can be effectively and uniquely modeled by energy variations resulting from perturbations on the semiempirical electronic wave function of the complex. In our conceptualization, the charges will be determined from first order perturbation theory, and the polarizabilities from second order perturbation theory.

METHODS

All Sparkle calculations were carried out using MOPAC2012, and all RM1 orbital model for europium calculations were carried out by a version of the same software we modified. Subsequently, routines within LUMPAC were then coded to implement the new methodology being advanced here, and will be made available from <http://www.lumpac.pro.br>.

RESULTS AND DISCUSSION

With only three adjustable constants, we introduce expressions that relate the charge factors g_i to electronic densities q_i ,

$$g_i = Q \cdot q_i$$

$$q_\mu = 2 \sum_{i'}^{occ} \sum_p^{N_\mu} |c_{pi'}^\mu|^2$$

and the polarizabilities α_i to superdelocalizabilities SE_σ that we derived specifically for this purpose

$$\alpha_i = SE_i \cdot D + C$$

$$SE_\sigma = 2 \sum_{i'}^{occ} \sum_p \sum_q \frac{c_{pi'}^\sigma c_{qi'}^\sigma}{\epsilon_{i'}}$$

where i' runs over all occupied molecular orbitals of the complex, p and q run over all atomic orbitals of atom μ , and $c_{pi'}^\sigma$ and $c_{qi'}^\sigma$ are the corresponding linear coefficients.

The three constants Q , D , and C , are then adjusted iteratively until the calculated intensity parameters, corresponding to the ${}^5D_0 \rightarrow {}^7F_2$ and ${}^5D_0 \rightarrow {}^7F_4$ transitions, converge to the experimentally determined ones.

From the converged values of the constants, we then define a binary outcome acceptance attribute for the adjustment, and show that when the adjustment is acceptable, the predicted geometry is, in average, closer to the experimental one. This methodology advanced was tested on all thirteen europium complexes whose crystallographic structures could be obtained from the Cambridge Crystallographic Database, and whose values of Ω_2^{exp} and Ω_4^{exp} have been published.

CONCLUSIONS

The procedure advanced in this work, is seemingly a robust one, and leads to a unique set of g and α necessary for the prediction of the intensity parameters. An important consequence is that the terms related to dynamic coupling and electric dipole mechanisms will be unique. Hence, the important energy transfer rates will also be unique, leading to a single predicted intensity parameter for the ${}^5D_0 \rightarrow {}^7F_6$ transition.

ACKNOWLEDGMENTS

The authors acknowledge support from CNPq, FACEPE/PRONEX, FAPITEC/SE and INCT-INAMI.

Design de um catalisador baseado em éter-coroa e ligações de hidrogênio seletivas para promover reações de fluoração nucleofílica

Nathália F. Carvalho* (PG), Josefredo R. Pliego Jr. (PQ)

Departamento de Ciências Naturais, Universidade Federal de São João del-Rei, Campus Dom Bosco, CEP 36300-160, São João del Rei, MG, Brasil

*nathaliaufsj@yahoo.com.br

Palavras-chave: catálise, fluoração, éter-coroa, DFT, solvatação

INTRODUÇÃO

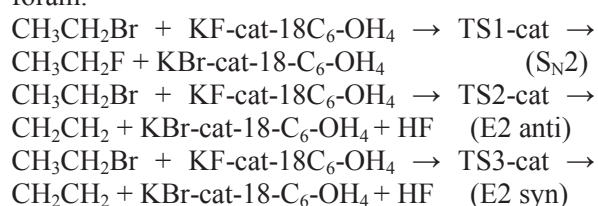
A química orgânica do flúor tem ganhado notoriedade nos últimos anos devido às muitas propriedades que este elemento acrescenta a compostos orgânicos bioativos. A dificuldade em se obter compostos organofluorados se deve em parte à competição com o caminho de eliminação. Uma alternativa viável para a fluoração de haletos de alquila com KF é usar catalisadores de transferência de fase (como um éter-coroa) para promover esta reação em solventes apolares. Neste trabalho, objetiva-se projetar um novo catalisador para este fim.

MÉTODOS

- Otimização e frequência: X3LYP/6-31+G(d)
- Cálculos no ponto: B3PW91/TZVPP (com correção para a dispersão de Grimme¹), MP2/TZVPP e ONIOM (MP4/TZVPP: MP2/TZVPP)
- Efeito do solvente: SMD/6-31+G(d)

RESULTADOS E DISCUSSÃO

Na Figura 1 tem-se a estrutura geral do catalisador proposto. Na Tabela 1 tem-se os dados de ativação e as barreiras de reação para as reações estudadas neste trabalho. Os valores de energia livre incluem o efeito do solvente pelo modelo SMD. Observa-se um pronunciado efeito catalítico que favorece a reação S_N2 sobre os caminhos de eliminação. O estado padrão adotado foi de 1 mol/L para as fases gasosa e líquida, indicado pelo símbolo *. As reações estudadas foram:



Os resultados apontam um favorecimento do caminho S_N2 em relação aos demais. A barreira obtida, entretanto, ainda é alta.

Tabela 1. Barreiras de ativação das reações estudadas em kcal/mol.

Canal	X3LYP/ 6-31+G (d)	B3PW91/ TZVPP	MP4 ^a	ΔG*
S _N 2 sem cat	11,75	11,27	14,24	25,53
E2 anti sem cat	27,82	19,42	23,30	28,56
E2 syn sem cat	4,47	3,04	9,28	19,94
S _N 2 cat	4,30	6,57	6,34	21,71
E2 anti cat	14,16	12,46	14,02	23,85
E2 syn cat	10,75	13,61	16,09	26,85

^a valor obtido pelo método ONIOM (MP4/TZVPP:MP2/TZVPP)

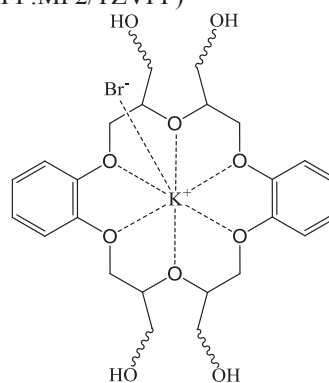


Figura 1. Estrutura geral do catalisador proposto.

CONCLUSÃO

O catalisador proposto é seletivo para reações S_N2, o que é uma importante contribuição na área de fluoração. A análise da cinética global ainda requer um cálculo da energia livre de reação de troca de KBr por KF.

AGRADECIMENTOS

À CAPES, FAPEMIG, CNPQ, UFSJ, e ao LQTC.

¹ S. Grimme, J. Antony, S. Ehrlich and H. Krieg, J.Chem.Phys. 132, 154104/1-19(2010)

Charge, Charge Flux and Dipole Flux Contributions for Infrared Intensities of the Stretching Modes during Protonation

Natieli A. da Silva^a (PG), Roberto L. A. Haiduke^a (PQ)

^a Departamento de Química e Física Molecular, Instituto de Química de São Carlos, USP, São Carlos, SP.
natieli.iqsc@usp.br

Keywords: Lewis bases, infrared intensity, CCFDF model

INTRODUCTION

The chemistry of the interstellar medium is permeated by ion-molecule reactions because, as H₂ is one of dominants species in this environment, the primary ions H₂⁺ and H⁺ are formed initially. The ion-molecule reactions are generally involved in the formation of the most abundant species in that medium. Thus, since simple protonated species are often found in astrophysical environments, the purpose of this study is to apply the Charge - Charge Flux - Dipole Flux (CCFDF) partition model in terms of multipoles from the Quantum Theory of Atoms in molecules (QTAIM)¹ to interpret the infrared intensities of the new B-H stretching modes during protonation of Lewis bases (B).

METHODS

All calculations were carried out with the GAUSSIAN 03 package.² Geometry optimization of molecules such as CO, SO, HNC, FNC, CINC, HCN, FCN, CICN, BrCN, HOCN, HCNO and HONC along with their protonated species were done at the coupled cluster (CCSD) level of theory by applying the cc-pVQZ basis sets. Thus, the vibrational frequencies and infrared fundamental intensities were also calculated from these ground state equilibrium geometries.

The QTAIM charge and atomic dipole were calculated in equilibrium structures of species and also in geometries with atoms shifted by 0.01 Å along the three Cartesian axes. From these atomic charges and dipoles, obtained with the AIMAll program,³ it was possible to calculate the molecular dipole moment derivatives in Cartesian coordinates and charge, charge flux and dipole flux contributions. Finally, the molecular dipole-moment derivatives for each normal vibration mode were used to estimate the infrared intensities by the CCFDF/QTAIM model.

RESULTS AND DISCUSSION

The infrared intensities calculated by CCFDF/QTAIM model show good agreement with those obtained directly at the CCSD/cc-

pVQZ level of theory. The analysis of CCFDF contributions indicates that the charge contribution is predominant when the proton is bound to more an electronegative and less polarizable atoms. However, the charge flux becomes more significant when the proton is bond to the isonitrile carbon.

Furthermore, the square root of infrared intensities for B-H stretchings shows a linear correlation with the atomic charge of the proton obtained by different formalisms (QTAIM, GAPT and Mulliken). The best linear fit between these properties is obtained with the GAPT charges (Figure 1).

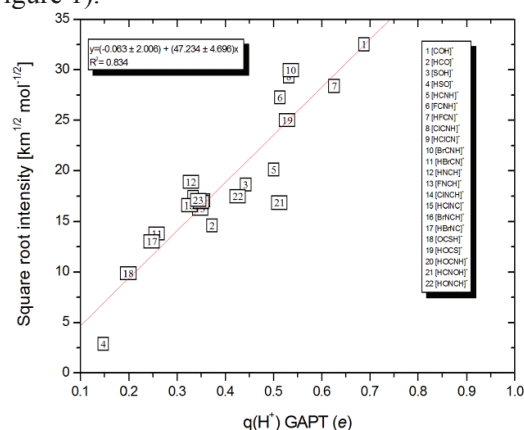


Figure 1 – Graph of the square root of infrared intensities for B-H stretching modes versus GAPT charges for the proton added.

CONCLUSIONS

The infrared intensity for B-H stretching modes can be explained by predominance, in most cases, of the charge contribution.

ACKNOWLEDGMENTS

CAPES and FAPESP (2010/18743-1 and 2014/23714-1).

¹ Haiduke, R. L. A.; Bruns, R. E. *J. Phys. Chem. A*, 2005,109, 2680-2688.

² Frisch, M. J. *et al. Gaussian 03*, Revision D02, Gaussian Inc. Wallingford CT, 2004.

³ Keith T. A., AIMAll (*Version 12.11.09*), TK Gristmill Software, Overland Park KS, USA, 2013, aim.tkgristmill.com.

Simulation of Reactive channels for Inorganic Cycle SNP2 Formation: A Study via *ab Initio* Molecular DynamicsCOUTINHO, N.D.C.^{1,*}(PG), OLIVEIRA, H.C.B.¹(PQ), CARVALHO, V.H.²(PQ)¹ Instituto de Química, Universidade de Brasília, 70904-970, Brasília, Brasil.² Grupo de Química Teórica e Estrutural de Anápolis, Campus de Ciências Exatas e Tecnológicas, Universidade Estadual de Goiás, 75001-970, Anápolis, Brasil)

*nayaradcoutinho@gmail.com

Keywords: Inorganic heterocyclic, BOMD, DFT

INTRODUCTION

Inorganic heterocyclics have aroused great interest in synthetic and computational chemistry in recent years.^{1,2} Recently, Zeng and coauthors synthesized a new aromatic ring compound (cycle SNPNP) through the pyrolysis of SP(N₃)₃.³ In order to understand the formation of this compound, the authors conducted electronic structure calculations indicating the formation of the cycle by dimerization of the SNP and subsequent elimination of a sulfur atom from a six-membered ring (SNPSNP).

In order to get a full description of the mechanism of formation of the cycle-SNPNP, this work proposes to perform a Born-Oppenheimer molecular dynamics, aiming to check the mechanism already proposed and propose other possibilities for cycle formation.

METHODS

The Born-Oppenheimer molecular dynamics simulations were performed using the Gaussian 09 program. First, we used the semiempirical PM6 method. Subsequently, in order to obtain a better description of the energy and make it possible to compare the results obtained by Zeng and coauthors³, we employed the B3LYP/6-311+G(3df) level of calculation. All simulations were developed at 1000 °C, which is the experimental temperature used in the synthesis.

RESULTS AND DISCUSSION

The Born-Oppenheimer molecular dynamics simulations were able to confirm the mechanism proposed by Zeng and coworkers. At 0.50 ps, it was possible to verify the formation of the six-membered cycle. For about 0.50 ps, this compound undergoes several structural conformations, and close to 1.052 ps the release of a sulfur atom and subsequent formation of the

five-membered aromatic ring was observed, as can be seen in Figure 1a.

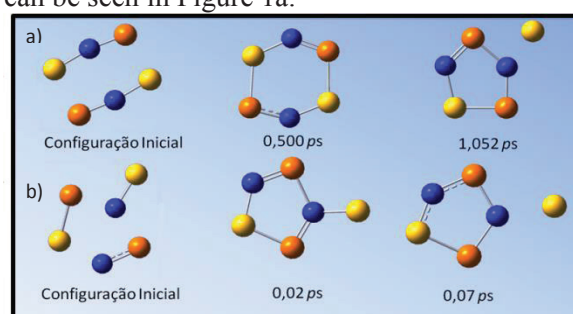


Figure 1. Simulation cycle-SNPNP formation (a) from the dimerization of the SNP and (b) from the reaction between the molecules NP, NS, PS using Born-Oppenheimer molecular dynamics with the semiempirical PM6 method.

Furthermore, calculations were performed to elucidate other possible mechanisms of cycle-SNPNP formation from the other products formed in the pyrolysis of SP(N₃)₃, such as: NP, NS, HN3 and PS. These simulations show that the cycle-SNPNP can also be formed from the reaction between NP, NS and PS, as shown in Figure 1b. The calculations using the B3LYP/6-311+G(3df) level are nearing completion.

CONCLUSION

The Born-Oppenheimer molecular dynamics simulations showed two possible mechanisms for cycle-SNPNP formation from the products of pyrolysis SP(N₃)₃: the first one is formed from SNP dimerization and subsequent elimination of the sulfur atom; the second one is formed by linking NP, NS and PS.

ACKNOWLEDGMENTS

The authors are grateful for the support given from FAPEG, CAPES, CNPQ and FAPDF.

1. He, G.; Shynkaruk, O.; Lui, M. W.; Rivard, E.; *Chem. Rev.* **2014**.
2. Mück, L. a.; Lattanzi, V.; Thorwirth, S.; McCarthy, M. C.; Gauss, J.; *Angew. Chem. Int. Ed.* **2012**, *51*, 3695.
3. Zeng, X.; Li, H.; Sun, H.; Beckers, H.; Willner, H.; Schaefer, H. F.; *Angew. Chemie Int. Ed.* **2015**, *54*, 1327.

Electronic structure studies of Fe₂O₄

Nelson Henrique Morgon^a (PQ)

^a *Instituto de Química, Universidade Estadual de Campinas (UNICAMP) –
morgon@iqm.unicamp.br*

Keywords: Fe₂O₄, Electronic Structure, DFT, CASSCF

INTRODUCTION

In the present work, we carry out a density functional theory (DFT) and complete active space SCF method (CASSCF) study on the electronic structure and chemical bonding in a series of molecular geometries and electronic states of Fe₂O₄. These calculations were performed to elucidate the geometric and electronic structures and the chemical bonding of this molecular system.

METHODS

Theoretical calculations were performed at the DFT level using the B3LYP, PW91, and M06-L exchange-correlation functionals, and at the CASSCF(8,8) level of theory. A number of structural candidates including different spin states and initial geometries were evaluated (C₁, C₂, C_{2v}, D_{2d}, and D_{2h} point groups and singlet and triplet electronic states). The search for the global minima (and fundamental electronic state) was carried out using the basis set adapted to the corresponding Stuttgart effective core potential for Fe atoms and the aug-cc-pVTZ basis set for oxygen atoms. The relativistic effects (mass velocity and Darwin effects), were taken into account via the quasi-relativistic pseudopotentials. The MP2 single point energies were employed to comparison among different methods. All calculations were performed using GAMESS program[1].

RESULTS AND DISCUSSION

The results of the MP2 calculations for the all systems are reported in Table 1.

Table 1. Energies (a. u.) of the electronic states of the Fe₂O₄ system at the DFT and CASSCF levels of theory^(a).

Electronic State	Method	Electronic Energy
D _{2h} (¹ A _g)	M06-L	-547.5748
C _{2v} (¹ A ₁)	PW91	-547.5359
C _{2v} (³ A ₁)	B3LYP	-547.3621
D _{2d} (³ A ₁)	M06-L	-547.3589
C ₂ (³ A)	B3LYP	-547.3573
C ₁ (³ A)	M06-L	-547.3299
C ₁ (³ A)	PW91	-547.3071
C ₂ (³ A)	B3LYP	-547.1948
C _{2v} (¹ A ₁)	B3LYP	-547.1676
D _{2h} (³ A _g)	CASSCF	-547.0114

^(a)The results of the structures having the 10 lowest energies are shown in the table.

COMPARATIVE THEORETICAL STUDIES OF ENERGETIC AND STRUCTURAL PROPERTIES OF BETULINIC AND MELALEUCIC ACIDS AND THE STABILITY OF CLUSTERS OF THESE SPECIAL METABOLITES

Noam Gadelha da Silva^a (PG), Kelson Mota Teixeira de Oliveira^a (PQ), Jefferson Rocha Andrade Silva^a (PQ)

^aDQ/ICE, UFAM, Block 10, North Sector, Avenue Rodrigo O. J. Ramos, 6200, Japiim, 69077-000, Manaus, Amazonas.

Keywords: Computational Chemistry, Structure-Activity Relationship, Clusters.

INTRODUCTION

Drugs such as Betulinic acid gain attention because of their biological activity against several diseases such as various types of cancer, AIDS, and Malaria¹. Many studies indicate the manner in which the drug acts on the disease, but is not detailed about which molecular characteristics have influence in these processes¹. Combined theoretical and experimental studies can lead to answers about the real reason for activity of these biomolecules as inhibitors of diseases, and we can understand more about the structure-activity relationship and other influences on biochemical reactions^{2,3}. In this work, theoretical calculations with the Gaussian 03 program package seek to explain the inactivity of Melaleucic acid, a very similar analogue of Betulinic acid, with just one difference regarding Betulinic acid, which is a carboxylic acid group at C-27 (**Figure 1**).

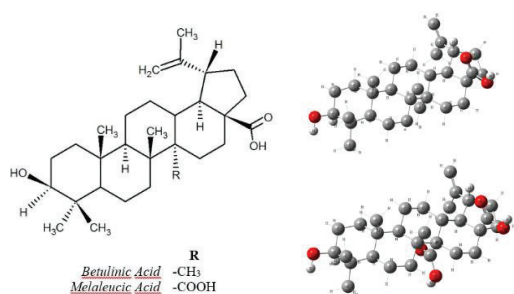


Figure 1. Structure of the substances and optimized geometry given by AM1 calculations.

RESULTS AND DISCUSSION

The methodologies used was semi-empirical AM1 (geometry optimization) and Ab Initio DFT/B3LYP 3-21G and 6-311+G(2d,p) (Single-Point energy and others). To AM1, the stabilizations by intermolecular interactions in systems with two (2MC2) and three (3MC7) molecules of both substances are close (see **Table 1**). In DFT level of theory, 2MC2 systems was not stabilized by these interactions, but the 3MC7

systems was. Structure and charges data indicate that coupling with an enzyme should be similar. A possible explanation to the relative inactivity of Melaleucic acid is the formation of clusters with a large number of hydrogen bonds stabilizing these macrostructures. Melaleucic acid may be forming more stable clusters, and, because of that, the substance tends to interact less with an enzyme active site. A theoretical molecular docking study showed similar affinity of the both substances with a specific enzyme active site (similar work can be seen in reference 2).

Table 1. Principal energetic results given by AM1 and DFT/B3LYP calculations.

Substance	E _T (kcal/mol)	Stab. 2MC2 (kcal/mol)	Stab. 3MC7 (kcal/mol)
Betulinic acid (AM1)	-190.64288	-7.22716	-22.75594
Betulinic acid B3LYP 6-311+G(2d,p)	-877151.98241	4.07525	-16.38562
Melaleucic acid (AM1)	-276.18145	-6.77567	-22.66992
Melaleucic acid B3LYP 6-311+G(2d,p)	-970820.01935	2.25227	-14.27433

CONCLUSIONS

This results indicates very similarity of these substances, and the reason for the difference in the bioactivity could be the possibility of more stable clusters in the Melaleucic acid. Experimental studies can confirm the presence of clusters or the incompatibility of the Melaleucic acid in the enzyme active site.

ACKNOWLEDGMENTS

For the support of FAPEAM and CNPq.

¹M. G. Moghaddam, F. B. H. Ahmad and A. Samzadeh-Kermani. *Pharmacology & Pharmacy* 3 (2012) 119-123.

²P. Bernard, M. Pintore, J. Berthon, J. R. Chrétien. *European Journal of Medicinal Chemistry* 58 (2001) 1-19.

Theoretical Study of Geometric and Electronic Properties of Theophylline Using Car-Parrinello Molecular Dynamics

Núbia Maria Nunes Rodrigues^a (PG), Lauriane Gomes Santin^b (PG), Ademir João Camargo^a (PQ) e Solemar Silva Oliveira^a (PQ)

^a *Campus de Ciências Exatas e Tecnológicas (CCET) – Universidade Estadual de Goiás (UEG)*

^b *Instituto de Física – Universidade de Brasília (UnB)*

keywords: Molecular Dynamics, Car-Parrinello, theophylline.

INTRODUCTION

Theophylline (1,3-dimethyl-7H-purine-2,6-dione) is a dimethylxanthine with similar molecular structure to other methylxanthines such as caffeine and theobromine. Theophylline is an alkaloid and can be found in existing plants in various regions of the world. Theophylline has several pharmacological actions of therapeutic applications. Relaxes smooth muscle, bronchial muscle, stimulate the central nervous system stimulates the heart muscle and kidney acts producing diuresis. Theophylline is one of spasmogens release inhibitors more effective among xanthine. It is found as the main component of prescription medications for the treatment of chronic obstructive pulmonary disease (COPD) and asthma treatment.^{1,2}

METHODS

The structural data of the molecule were conducted at Quantum ESPRESSO program package, which carried out the simulation of the molecular dynamics of Car-Parrinello.³ Calculations were made to a value of 400.000 steps. To maintain adiabaticity system a μ fictitious mass of 400 u.a which proved effective during the whole simulation of dynamic vacuum was used. To reduce the calculation for the electronic subsystem, the pseudopotential ultrasoft Vanderbilt, together with plane waves. The temperature of the ionic subsystem was kept constant using the Nosé-Hoover thermostats to 300 K. The temperature used was the statistical ensemble NVT.

RESULTS AND DISCUSSION

The Map of molecular electrostatic potential and the structural data were also calculated using Density Functional Theory using the theory level B3LYP/6-311++G(2d,p). The interatomic bond

distances with greater variations were: H15-C12, C7-N3, C9=O2, C7-O1 e C13-H17 with relative error, in relation the results with DFT of 1,849 %, 1,598%, 1,480%, 1,482% e 1,809% respectively. The interatomic angles with greater variations were: H14-C12-H16, C12-N3-C9 e H17-C13-N4 with relative error 1,320%, 1,259% and 1,435% respectively. The largest variations of these bond lengths and angles are due possibly to the fact that atoms are more electronegative regions and then it can be assumed that such interaction is outside the full domain of the functional.

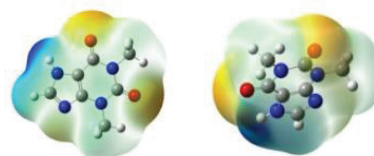


Figure 1. Map electrostatic potential molecular

CONCLUSIONS

The results of the molecular dynamics simulation of Car-Parrinello in theophylline led to obtaining the geometrical values for the distance and angles entre atoms of the molecule. It is observed good agreement between the theoretical results values obtained by DFT. These results allow an interesting study about possible interactions of theophylline in a solvent such as water.

ACKNOWLEDGMENTS

The authors are grateful for the support given from the CAPES.

¹ BARNES, P. J. Theophylline. American Journal of Respiratory and Critical Care Medicine, London, 3 may. p. 901-906, (2013).

² HADZOVIC, E. Roller Compact. of theophylline Doctoral thesis. Faculty of Science of the University of Basel. Bosnia and Herzegovina.

³ CAR, R., PARRINELLO, M. Phys. Rev. Lett. v. 55, n. 22, p. 2471-2474, (1985).

Chemical kinetics of the $\text{CH}_3\text{CH}_2\text{SH} + \text{H}$ abstraction and bond breaking reactions: influence of the methodology on the tunneling effects

Leonardo A. Cunha¹ (IC), Daniely V. V. Cardoso¹ (PG), Luiz F. A. Ferrão¹ (PQ), Rene F. K. Spada¹ (PD), Orlando Roberto-Neto² (PQ)*, Francisco B. C. Machado² (PQ)

¹Instituto Tecnológico de Aeronáutica (ITA), São José dos Campos-SP

²Instituto de Estudos Avançados (IEAv), São José dos Campos-SP

*orlando@ieav.cta.br

Keywords: ethanethiol, rate constant, DFT, MP2.

INTRODUCTION

An unquestionable fact is that organic sulfur compounds play an important role on human daily life.^{1,2} We studied elementary reactions involving the $\text{CH}_3\text{CH}_2\text{SH}$ molecule and the hydrogen atom (R1-A and R1-B: $\text{CH}_2\text{CH}_2\text{SH} + \text{H}_2$; R2: $\text{CH}_3\text{CHSH} + \text{H}_2$; R3: $\text{CH}_3\text{CH}_2\text{S} + \text{H}_2$ and R4: $\text{CH}_3\text{CH}_2 + \text{H}_2\text{S}$). Two different electronic structure methods are employed and the results are compared.

METHODS

The geometries of the stationary points of the minimum energy paths (MEP) for each reaction path were optimized using the BB1K/maug-cc-pV(D+d)Z and MP2/6-311+G(2d,p) methods. The thermochemical properties were refined using the single-point coupled-cluster (CCSD(T)) calculations, followed by the extrapolation to the complete basis set (CBS), which usually gives reliable results when compared with experimental data.²⁻⁴ The thermal rate constants were calculated using the canonical variational transition state (CVT) method including the zero-curvature tunneling (ZCT) and small-curvature tunneling (SCT) corrections. GAUSSIAN G09 and POLYRATE codes were used to carry out electronic structure and rate constants calculations, respectively.

RESULTS AND DISCUSSION

The lowest adiabatic barriers are $1.51 \text{ kcal}\cdot\text{mol}^{-1}$ and $2.34 \text{ kcal}\cdot\text{mol}^{-1}$, respectively, computed with CCSD(T)/CBS//MP2 and CCSD(T)/CBS//BB1K methods (Table 1) for the hydrogen abstraction involving the -SH group (R3). The imaginary frequencies of the transition states of R3 are $822i$ and $1688i$, respectively, calculated with the BB1K and MP2 methods. Calculated thermal rate constants are given in Figure 1. At 298 K, the CVT/SCT rate constants obtained with MP2 method agree well with experimental data^{3,4} and with previous theoretical results.⁵

Table 1. Energetics (kcal/mol) calculated with CCSD(T)/CBS//BB1K and CCSD(T)/CBS//MP2 (in parentheses) methods.

	$\Delta V_a^{G,\#}$	$\Delta H_0^\#$		$\Delta V_a^{G,\#}$	$\Delta H_0^\#$
R1-A	10.63	-3.28	R3	2.34	-17.98
	(10.63)	(-3.15)		(1.51)	(-18.01)
R1-B	11.05	-3.28	R4	3.76	-17.82
	(11.17)	(-3.15)		(3.41)	(-17.41)
R2	6.87	-10.39			
	(6.78)	-(10.06)			

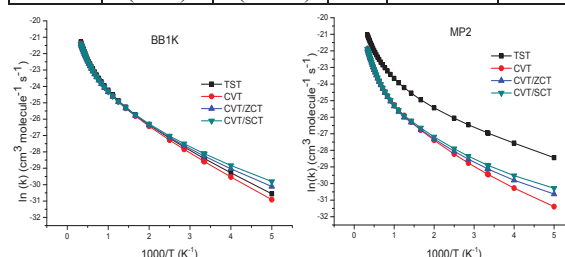


Figure 1. BB1K and MP2 rate constants.

CONCLUSIONS

The MP2 method overestimates the values of the imaginary normal mode frequencies resulting in a sharp potential energy surface and higher values of tunneling coefficients. Despite of the small difference between the adiabatic barriers calculated with the MP2 and BB1K methods, variational effects and SCT corrections play an important role, especially for the rate constants calculated with the MP2 method.

ACKNOWLEDGMENTS

Support: FAPESP, CNPq and CAPES.

¹T.E. Graedel, Chemical Compounds in the Atmosphere, Academic, New York (1978).

²D.V.V. Cardoso et al., J. Mol. Mod., 20, 2449 (2014).

³D. Martin et al., Int. J. Chem. Kinet., 20, 897 (1988).

⁴W.W. Lam et al., J. Photochem. Photobiol.A, 47, 47 (1989).

⁵Q. Zhang et al., Chem. Phys., 324, 298 (2006).

Polysulfides species: formation mechanism in acid and basic environment.

Pâmella V. B. de Pinho^a (G), Maurício C. Silva^b (PQ), Guilherme S. Rodrigues^a (PG),
Guilherme F. de Lima^c (PQ), Hélio A. Duarte^a (PQ)

^a Grupo de Pesquisa em Química Inorgânica Teórica – GPQIT, Departamento de Química – ICEx,
UFMG. 31.270-901 – Belo Horizonte-MG.

^b Centre for Molecular Simulation – University of Calgary - Calgary, AB, Canada.

^c Instituto de Física e Química, Unifei, Av. Bps 1303, Pinheirinho, Itajubá, MG.

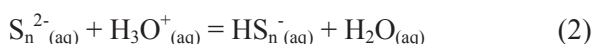
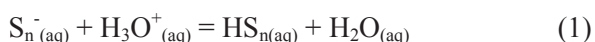
Keywords: polysulfides, stability, formation mechanism, DFT

INTRODUCTION

It is well known that polysulfides are formed during copper extraction based on the chalcopyrite (CuFeS₂) leaching slowing down the rate of dissolution.¹ During the dissolution process, the chalcopyrite is a source of sulfur in the form of disulfide² and sulfur is reduced and polymerized, producing species such as S_n²⁻, S_n⁻, S_n and their protonated forms (HS_n, HS_n⁻ and H₂S_n). These species have never been isolated in aqueous solutions, but their existence is proved based on spectroscopic data analysis in solutions under many conditions.³ The present work has investigated the formation mechanism of different species in different pH of the medium.

METHODS

The S_n (n = 2, 4, 6, 8), S_n⁻ (n = 3, 5, 7, 9, 11), S_n²⁻ (n = 1, 2, ..., 8, 10, 12, 14, 16) and their protonated forms (HS_n, HS_n⁻ and H₂S_n) were completely optimized and the thermodynamic properties were estimated based on the harmonic approximation. The PBE exchange/correlation functional with aug-cc-pVTZ basis sets were used as implemented in GAUSSIAN09. The solvent effects were taken into account based on the SMD model. The thermodynamic stability of the polysulfides ions was quantified by the variation of reaction Gibbs free energy (Δ_rG) of the reactions represented in Equations 1-3.



RESULTS AND DISCUSSION

The protonation reactions were very favorable for the smaller structures (n < 6), as shown in Figure 1. The non-protonated species can only exist in basic environment. Otherwise, non-

protonated long chain polysulfides (n > 6) can exist in basic or neutral environmental.

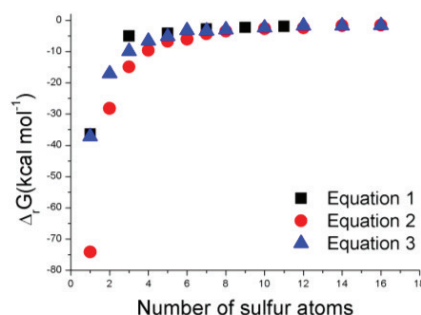


Figure 1. Variation of reaction Gibbs free energy for the chemical reactions in Equations 1-3.

Considering that in basic environment the species S_n²⁻, S_n⁻ and S_n were prevalent and that in acid environment the protonated or double protonated species were prevalent, three mechanisms were proposed. In basic environment, the reactions indicated the formation of large chains. However, in acid environment the reactions indicated the formation of elemental sulfur.

CONCLUSIONS

The proposed mechanism is coherent with the reality of the system. The elemental sulfur is frequently found during the acid dissolution process of chalcopyrite. The structures of the polysulfides, the thermodynamic data and the formation mechanism will be presented in detail.

ACKNOWLEDGMENTS

The authors are grateful for the support given from the INCT-ACQUA, CAPES, CNPQ and FAPEMIG.

¹ C. Klauber, Int. J. Miner., 86, 1, (2008).

² De Lima, G. F. et al, J. Phys. Chem. C., 115, 10709-10717, (2011).

³ D. Rickard, G. W. Luther, Chem. Rev., 107, 514-562, (2007).

Theoretical Studies of $\text{HS}+\text{HX}=\text{H}_2\text{S}+\text{X}$, with $\text{X} = \text{H}, \text{F}, \text{Cl}$ and Br

P R P Barreto (PQ), H O Euclides (IC), A C P S Cruz (PG)

Instituto Nacional de Pesquisas Espaciais (INPE)/MCT, Laboratório Associado de Plasma (LAP), São José dos Campos, SP, CEP 12247-970, CP515, Brazil.

patricia@plasma.inpe.br

Keywords: Reaction Rate, HS, H₂S, Transition State Theory

INTRODUCTION

Chemical models are an important tool in helping us understand various physical and chemical processes in space, the full understanding of the physics and chemistry in molecular sources requires a detailed understanding of chemical kinetics and, in particular, reaction rate coefficients over a wide range of temperatures involving the chemical species in space. In the following year of the discovery of interstellar CH, others additional neutral diatomic hydrides have been discovered in the interstellar gas, such as: OH, H₂, HCl, NH, HF, and SiH, in addition to these neutral molecules, hydride molecular ions have, also, been discovered: CH⁺, OH⁺, SH⁺, and HCl⁺. These diatomic hydrides represent the simplest of interstellar molecules, and may provide key information about the interstellar environment.

METHODS

In this work, we will discuss the theoretical studies of $\text{HS}+\text{HX}=\text{H}_2\text{X}+\text{X}$ and $\text{HS}^++\text{HS}=\text{H}_2\text{S}+\text{X}^+$, with $\text{X} = \text{H}, \text{F}, \text{Cl}$ and Br reaction. The theoretical reaction rate will be compared with the experimental data, for the neutral cases and also the difference among the neutral with the charged cases

The geometries are optimized at MP2/aug-cc-pVTZ using the GAUSSIAN09 program and the energies are obtained at CCSD(T)/aug-cc-pVQZ.

RESULTS AND DISCUSSION

Table 1 present the optimized geometries of the transition state of HSHX systems, with $\text{X}=\text{H}, \text{F}, \text{Cl}, \text{Br}$, neutral or charged ones. It is possible to observe the increase of the HS distance in all cases and the decreases of the HX distances when compared the neutral and charged cases. For the HSH, SHX and

dihedral angle there is not a patterned when compared the neutral and charged cases. Figure 1 compares the reaction rate of the neutral cases and presents the conventional and with tunneling correction the reaction rate.

Table1: Geometry structure of transition state of HS+HX

Neutral	H	F	Cl	Br
r _{HS}	1.3355	1.3346	1.3359	1.3370
r _{HS}	1.4492	1.3903	1.4415	1.5627
r _{HX}	1.0564	1.4494	1.6456	1.6241
a _{HSH}	90.245	93.152	91.437	91.0821
a _{SHX}	174.884	91.519	135.187	145.399
D	0.000	80.824	78.992	76.096
Charged	H	F	Cl	Br
r _{HS}	1.3643	1.3497	1.3457	1.3449
r _{HS}	1.4636	1.5485	1.6680	1.7877
r _{HX}	0.9481	1.1929	1.4364	1.5335
a _{HSH}	99.460	94.932	93.673	93.210
a _{SHX}	74.192	81.473	87.983	87.778
D	0.000	87.846	91.086	91.193

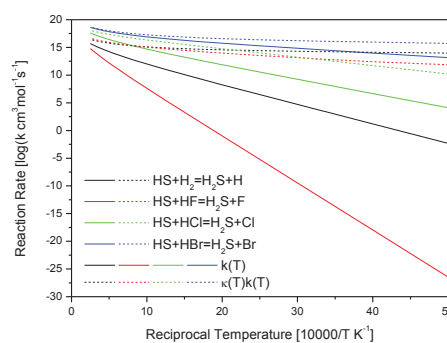


Figure 1. Reaction rate of $\text{HS}+\text{HX}=\text{H}_2\text{S}+\text{X}$, with $\text{X}=\text{H}, \text{F}, \text{Cl}$ and Br .

ACKNOWLEDGMENTS

The authors are grateful for the support given from the FAPESP, CAPES and CNPQ.

Conformational Analysis of 3-amino-1-propanol and 3-N,N-dimethylamino-1-propanol using QTAIM and NBO

Patrick Rodrigues Batista¹ (PG), Lucas José Karas¹ (PG), Renan Vidal Viesser² (PG), Luciano Nassif Vidal¹ (PQ), Paulo Roberto de Oliveira¹ (PQ)

¹Federal University of Technology – Paraná, Curitiba-PR
²Chemistry Institute, University of Campinas, Campinas-SP
patrickrbatista@gmail.com

Keywords: Intramolecular Hydrogen Bond, Conformational Analysis, Theoretical Calculation

INTRODUCTION

The intramolecular hydrogen bonding (IAHB) is a type of interaction that has great influence on conformational preference in molecular systems, sometimes more than steric effects. Oliveira and Rittner^{1,2} showed that the increase in the volume group NRR' [RR = H, RR = CH₃ and R = H, R' = CH₃] increases the strength of the intramolecular hydrogen bond (IAHB) on *cis*-3-aminocyclohexanols. The objective of this study was to analyze the influence of substituent bulk on the strength of IAHB OH \cdots N by theoretical calculations.

METHODS

The conformational analysis of the compounds 3-amino-1-propanol (APOL) and 3-N,N-dimethylamino-1-propanol (DMAPOL) was performed by theoretical calculations. The initial structures were obtained using a conformational search with Tinker program. Optimization and frequency calculations were performed using the theoretical level M062X/aug-cc-pVDZ with Gaussian09 program. Then a statistical thermodynamic analysis was performed to obtain more stable populations and their thermal structures. These structures were subjected to topological analysis QTAIM and NBO.

RESULTS AND DISCUSSION

The results showed that the two compounds showed the IAHB. More stable conformers for APOL and MAPOL showed thermal population of 85.5 and 90.0%, respectively. Gibbs energy (ΔG) of conformers with and without IAHB was of 2.18 and 2.13 kcal.mol⁻¹ for APOL and DMAPOL. The QTAIM identified an IAHB OH \cdots N for the two conformers more stables (Figure 1) with the presence of Bond Path (BP), Bond Critical Point (BCP) and Ring Critical Point (RCP). The results

of dissociation energy of IAHB OH \cdots N showed that the APOL (0.00934 a.u.) makes an IAHB stronger than the DMAPOL (0.00897 a.u.).³ Total electronics Energy Density on BCP of IAHB was of 0.000453 and 0.000834 u.a. for APOL and DMAPOL. These results showed that IAHB for APOL has more covalent character. Hyperconjugative interaction (LP(N) $\rightarrow\sigma^*$ O-H) also showed that the IAHB OH \cdots N for APOL (9.85 kcal.mol⁻¹) is stronger than DMAPOL (8.01 kcal mol⁻¹).

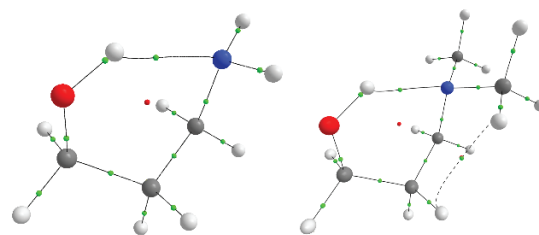


Figure 1. Molecular graphics for APOL and DMAPOL obtained by QTAIM.

CONCLUSIONS

The calculations showed that the 1,3-amipropanols have conformers with a higher thermal population stabilized by IAHB. The higher alkyls substituent favors the increase of 1,3- diaxial steric effect reducing the strength of the IHAB.

ACKNOWLEDGMENTS

The authors are grateful for the support given from CAPES, LQT/UTFPR and LFQO/UNICAMP.

¹ P.R. Oliveira, R. Rittner, J. Phys. Org. Chem., 18, 513 (2005).

² P.R. Oliveira, R. Rittner, Spec. Chem. Acta A, 78, 1599 (2011).

³ E. Espinosa, I. Alkorta, I. Rozas, J. Elguero, Molins, Physical Letters, 336, 457, (2001).

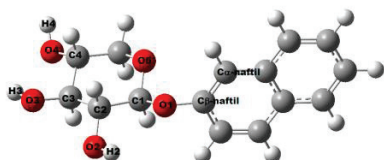
Investigação das conformações mais estáveis da molécula de β -naftilxilosePaula do Nascimento Goulart^a (PG), Clarissa Oliveira da Silva^b (PQ)^{a,b} Dep. De Química – ICE Universidade Federal Rural do Rio de Janeiro Rodovia BR 465Keywords: β -naftil-xilose, *conformers*, DFT, cálculos de estrutura eletrônica, microsolvatação.

INTRODUÇÃO

Xiloses simples substituídas com agliconas hidrofóbicas podem funcionar como iniciadores para a síntese de compostos que recobrem externamente as células tumorais (GAGs).¹ A porção hidrofóbica interfere seletivamente na via biossintética dos GAGs.

METODOLOGIA

Foi realizado um estudo conformacional da β -naftilxilose (figura 1) utilizando a Teoria do Funcional Densidade (B3LYP) com conjuntos de funções de base 6-31G+(d,p)² e 6-311++G(2d,2p)². Para os cálculos em solução metanólica, utilizamos também o modelo PCM(modelo do contínuo polarizável). Investigou-se conformações provenientes da rotação de cada ligação C-O, variando-se o ângulo diedro que define a posição de cada grupo hidroxila, e também variando-se o diedro que define a posição do anel naftil. Sobre o diedro C1-O1-C β -C α (diedro ϕ_{naftil}) foi realizada uma varredura para construção da superfície de energia potencial.

Figura 1- Molécula de β -naftilxilose.

RESULTADOS E DISCUSSÃO

Após a otimização geométrica de todas as 81 possibilidades conformacionais para esta molécula em fase gasosa, foram obtidas 20 conformações. As 12 conformações mais estáveis foram utilizadas na investigação das 6 posições relativas encontradas para o grupo naftil, a partir do estudo realizado (figura 2a). Combinando essas informações, 72 estruturas tiveram a geometria otimizada (figura 2b) e aquelas mais estáveis foram solvatadas.

Após o cálculo de frequência e de rotação específica, os resultados obtidos para os 19 conformers mais estáveis fornecem um valor da rotação específica para a β -naftilxilose de $-70,12^\circ/\text{dm}(\text{g}/\text{cm}^3)$.

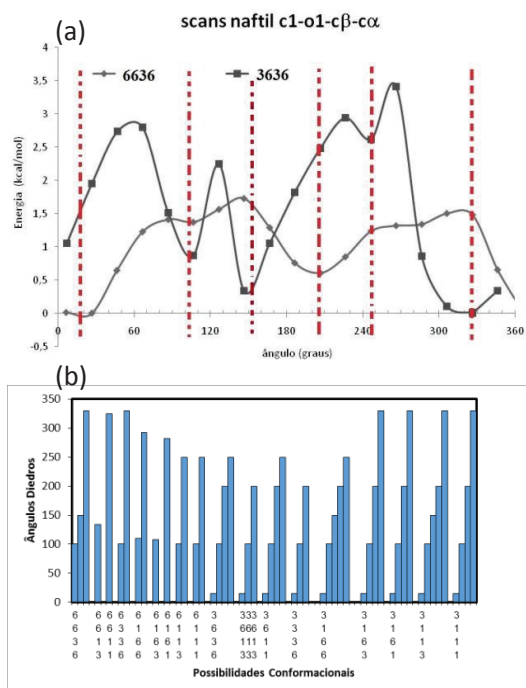


Figura 2-varreduras nos conformers 3636 e 6636(a). E “mapa” com os conformers estáveis encontrados(b).

CONCLUSÕES

O valor da rotação específica obtido nesse estudo para a molécula de β -naftilxilose ($-70,12^\circ/\text{dm}(\text{g}/\text{cm}^3)$) não apresentou boa correspondência com o valor da propriedade obtido experimentalmente ($-32^\circ/\text{dm}(\text{g}/\text{cm}^3)$).³ São introduzidas moléculas de solvente (MeOH) explícitas, para investigar se a consideração de interações específicas soluto-solvente influenciam significativamente no valor da propriedade considerada.

¹ ANNA SIEGBAHN, ULRICA Aili, AGATA OCHOCINSKA, MARTIN, JERK RÖNNOLS, KATRIN MANI, GÖRAN WIDMALM, ULF ELLERVIK. *Bioorganic & Medicinal Chemistry* 19 (2011) 4114–4126.

² CSONKA, G.I. Proper basis set for quantum mechanical studies of potential energy surfaces of carbohydrates. *J. Mol. Struct. (THEOCHEM)*, 2002, 584,1-4; CSONKA, G.I., FRENCH, A.D., JOHNSON, G. P., STORTZ, C. A. *J. Chem. Theory Comp.*, 2009, 5, 679-692

³ Comunicação pessoal com Göran Widmalm.

SAR analysis of phthalocyanines, porphyrins and chlorins using properties obtained with density functional calculations

Fernanda Bettanin^{a,c} (PQ), Káthia M. Honório^b (PQ), Paula Homem-de-Mello^a (PQ)

^a ABCSim, Centro de Ciências Naturais e Humanas, Universidade Federal do ABC, Brazil

^b Escola de Artes, Ciências e Humanidades, Universidade de São Paulo, Brazil

^c Instituto Tecnológico de Aeronáutica – ITA, Brazil

Keywords: PDT, porphyrins, phthalocyanines, chlorins, SAR, DFT, PCM

INTRODUCTION

We have carried out computational studies for some phthalocyanines (Ph), porphyrins (Pc) and chlorins (Ch), Fig. 1. These dyes have a conjugated π -electron system that gives them catalytic, spectrophotometric, magnetic and electrochemical applications. They are vastly used in photodynamic therapy (PDT), a therapy for several types of cancer. [1] The dyes studied here have different substituents (including amine, alcohol, piridine, methyls, ethers, esters, ketones and carboxylic acids), are free or complexed with Al^{+3} , Zn^{+2} and Si^{+4} . We have included in this study three dyes approved for PDT: Foscan[®], used to treat head and neck cancers; Levulan[®], employed in dermatological treatments and urinary bladder cancers; and Visudyne[®], used against ocular vascular disorders.

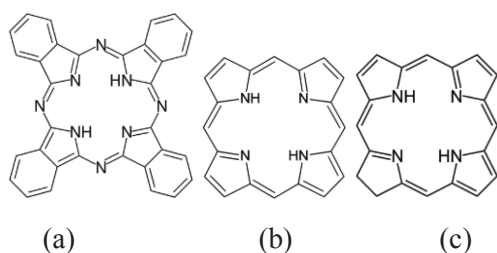


Figure 1. Structures of free (a) phthalocyanine, (b) porphyrin and (c) chlorin.

METHODS

We have studied 37 molecules derived from phthalocyanines, porphyrins and chlorins, including 3 approved drugs: Levulan[®], Foscan[®] and Visudyne[®]. Structures were optimized at B3LYP/LanL2DZ level and electronic properties were obtained with TD-DFT/OLYP/6-31g(d). The solvent effects were added by IEFPCM solvation model. Aiming to better correlate all properties with the differences in those molecules, hierarchical cluster analysis (HCA) and principal components analysis (PCA) were performed.

RESULTS AND DISCUSSION

PDT occurs by the administration of a dye followed by light irradiation. The dye transfers the absorbed energy to molecular oxygen (or other reactive species of oxygen) that may cause irreversible damage to the cell. So, we have studied properties that can influence the interaction with the environment and with the molecular oxygen, such as the absorption wavelength in water (λ) of the Q band, oscillator strength, energies of HOMO and LUMO (Δ_{H-L}), solvation free energy (ΔG_{solv}) in different solvents (to simulate the interaction with lipid bilayer), molecular area and volume, dipole moment.

Using HCA and PCA analyses, we considered the division of the studied molecules into two groups, each of them containing at least one approved drug: (i) the group of Visudyne[®] is composed by free Ph, charged Ph (with pyridine and amine), Ph substituted with ether, carboxylic acid and methyl; and (ii) the group of Levulan[®] and Foscan[®], containing the complexed and substituted phenyl Ph, free Pc and free Ch. The main variables that characterize the Visudyne[®] group were oscillator force, molecular volume and dipole moment. For the other group, ΔG_{solv} and LUMO energy play an important role.

CONCLUSIONS

Electronic and structural properties were used to evaluate different dyes to PDT. PCA and HCA analyses allowed grouping structurally different molecules with approved drugs, indicating that the molecules can be used for the same applications.

ACKNOWLEDGMENTS: FAPESP, CNPq, CAPES, CENAPAD and UFABC.

¹ A. B. Ormond and H. S. Freeman, *Materials*, 6, 817, (2013).

² J. H. Jensen *et al.* *J. Phys. Chem. A*, 109, 6634, (2005).

Adaptive Resolution Simulation of Oligonucleotides

Paulo Augusto Netz^a (PQ), Raffaello Potestio^b (PQ), Kurt Kremer^b (PQ)

^aUniversidade Federal do Rio Grande do Sul, Porto Alegre, Brazil netz@iq.ufrgs.br

^bMax Planck Institute for Polymer Research, Mainz, Germany

Keywords: Nucleic acids, Molecular Dynamics, Multiscale Methods, Coarse Graining

INTRODUCTION

Because of the structural peculiarities, the computational study of DNA demands the use of multiscale simulation methods, in order to describe sequence or conformation-dependent interactions while keeping the global constraints of the whole molecule. The Adaptive Resolution Simulation Scheme (AdResS) [1] is one of the most promising multiscale methods. AdResS couples two systems with different resolution: an atomistic system and a coarse-grained one, using a hybrid region in between. In this work we describe the implementation of AdResS to the simulation of oligonucleotides,

METHODS

The oligonucleotide $d(\text{CGCGAATTCGCG})_2$ [2] was built with X3DNA [3] and simulated using parameters of the AMBER force field [4]. This oligonucleotide and also TIP3P water molecules and ions (Na^+ and Cl^-) are simulated explicitly and surrounded by coarse-grained water and ions [5] in an elongated box setup (X-split AdResS, Figure 1). The interaction potentials were derived by the iterative Boltzmann inversion (IBI) method [6] using VOTCA [7]. The simulations were run using GROMACS [8]. In order to achieve a flat density profile for water and ions through the simulation box, thermodynamic force corrections for all species were applied [9]. The results, regarding density profiles and DNA structural parameters were compared with reference atomistic simulations.

RESULTS AND DISCUSSION

The interaction potentials and thermodynamic force corrections were optimized using simulations of aqueous salt solutions. With the derived parameters, in the simulations of the full system the DNA was kept in the center of the atomistic region and interacts only with the explicit molecules Water and ions, however, can migrate freely in the system and interact with the species in the hybrid and coarse grained regions. The root mean square deviation of the

macromolecule's structure, the density profiles for the species and the geometrical parameters for the DNA are essentially the same as in the atomistic reference simulations. The AdResS simulations performed faster than the reference atomistic simulations, especially if the atomistic region is chosen to be sufficiently small.

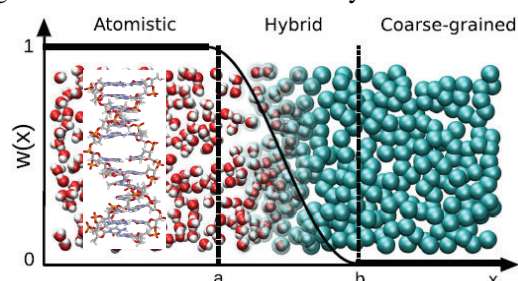


Figure 1. Geometrical setup of X-split AdResS (adapted from [10]).

CONCLUSIONS

The multiscale method AdResS was successfully applied to a complex system, composed by a oligonucleotide (dodecamer) in a salt solution. Despite of some simplifications the use of AdResS resulted in a improvement on the performance of the simulations, without affecting the structural stability of the nucleic acid.

ACKNOWLEDGMENTS

The authors are grateful for the support given from the CNPq, FAPERGS, CAPES and MPG.

- ¹ M. Praprotnik et al. J. Chem. Phys. 123, 224106 (2005).
- ² R. Wing et al. Nature 287, 755 (1980);
- ³ X. J. Lu, W. K. Olson, Nucleic Acids Research 31, 5108 (2003)
- ⁴ Y. Duan et al. J. Comp. Chem. 24, 1999 (2003).
- ⁵ S. Bevc et al. New J. Phys. 15, 105007 (2013)
- ⁶ D. Reith et al. J.Comp. Chem.24, 1624 (2003) .
- ⁷ V. Rühle et al. J. Chem. Th. Mod. 5, 3211 (2009).
- ⁸ S. Pronk et al. Bioinformatics 29, 845 (2013).
- ⁹ S. Poblete et al. J. Chem. Phys. 132, 114101 (2010) .
- ¹⁰ S. Fritsch et. al. Phys. Rev. Lett 108, 170602 (2012)

Pyrite oxidation mechanism in the presence of oxygen and water

Egon C. Santos (PG), Paulo R. G. Gonçalves Júnior (PG), and Hélio A. Duarte (PQ).

Grupo de Pesquisa em Química Inorgânica Teórica – GPQIT; Departamento de Química – ICEx,
Universidade Federal de Minas Gerais (UFMG), 31.270-901 Belo Horizonte-MG.
Email: pgarcs@gmail.com

Keywords: Mineral Sulfides, Pyrite, Acid Mining Drainage, DFT, NEB

INTRODUCTION

Pyrite (FeS_2) is the most abundant and widespread sulfide mineral at the Earth's surface. When it is exposed to the atmosphere and humidity, it is oxidized forming acid and sulfates.¹ This phenomenon is called Acid Rock Drainage (ARD) and, consequently, contributes to the acidification of aquifers. Many works¹⁻³ identified the formation of ARD products on the pyrite, but a molecular view of the mechanism remains to be established. Therefore, the aim of this work is to identify the oxidation mechanism of pyrite.

METHODS

The electronic structure of the systems were calculated by GGA/PBE exchange/correlation approximation of the Density Functional method (DFT) as implemented in Quantum-ESPRESSO package. Following the Monkhost-Pack scheme $1 \times 1 \times 1$ special k-points meshes were carry out for all slabs. The Kohn-Sham (KS) electronic orbitals were expanded in a plane-wave basis set up to a kinetic cutoff of 680 eV (50 Ry). This theoretical approach assures an energy accuracy in less than $0.5 \text{ kcal.mol}^{-1}$ for reactions calculations. Transition states were calculated by CI-NEB (Climbing Image - Nudge Elastic Band) method, and ten images converged to the minimum energy pathway using a convergence criteria of 0.025 eV.Å^{-1} .

RESULTS AND DISCUSSION

Initially the adsorption of water and oxygen molecules were investigated. Water adsorbs molecularly on the pyrite surface, and no dissociative adsorption is favored. The adsorption energy for water was estimated by our theoretical level in $-14.5 \text{ kcal.mol}^{-1}$, in a good agreement with Thermal Programed Desorption analysis,³ which estimates the adsorption energy in about $-10 \text{ kcal.mol}^{-1}$. We check different adsorptions for the oxygen molecule, and the most stable adsorption occurs with the oxygen adsorbed on two iron pyrite surface sites, see Figure 1.

The initial steps of pyrite oxidation is shown in Figure 1. Oxygen molecule adsorbs and oxidizes two Fe(II) pyrite sites to Fe(III). Hydrogen transference occurs from two water molecules adsorbed near oxygen molecule, and four Fe(III)-OH groups forms on the surface. This reaction is energetically favorable ($-42.0 \text{ kcal.mol}^{-1}$) and the activation energy estimated in our calculations is about $2.0 \text{ kcal.mol}^{-1}$. The determinant ARD oxidation step is the formation of the first S-O bond on the surface. Water adsorbs by hydrogen bonding around two OH species and hydrogen transference occurs to formation of two water molecules on the surface. The reaction energy is $-23.3 \text{ kcal.mol}^{-1}$ and activation energy is $11.6 \text{ kcal.mol}^{-1}$ for the last reaction.

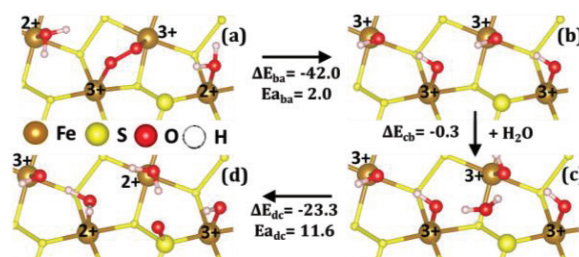


Figure 1. Fragment of the pyrite surface showing the initial oxidation mechanism steps.

CONCLUSIONS

The present study suggests a Fe(II)/Fe(III) redox cycle on the pyrite surface, in accordance with an extensive literature,^{1,2} which predicted that several electron transfer between iron sites would be involved in the oxidation of pyrite. All intermediates proposed in the mechanism were observed by photoelectronic spectroscopies.²

ACKNOWLEDGMENTS

The authors are grateful for the support given from the FAPEMIG, CAPES, CNPq, IFMA and INCT-Acqua.

¹ R. Murphy, E. D. Strongin, *Surf. Sci. Rep.* 64, 1, (2009).

² A. P. Chandra, A. R. Gerson, *Surf. Sci. Rep.*, 65, 9, (2010).

³ J. M. Guevremont, M. A. A. Schoonen, *Environ. Sci. Technol.* 32, 3743, (1998).

Theoretical Study on the Substitution of Tungsten by Vanadium on Keggin Structures $[XW_{12-n}V_nO_{40}]^{-(q+n)}$ X=Si, P; $0 < n < 4$.

Pedro. S. Pinheiro (PG), Alexandre. B. Rocha (PQ), Jean. G. Eon (PQ).

Instituto de Química, Universidade Federal do Rio de Janeiro UFRJ.
pedro.sc.pin@gmail.com

Key words: Keggin structures, Heteropolyanions, DFT.

INTRODUCTION

Heteropolyanions (HPAs) are molecular structures resembling oxide fragments with well defined shape and size¹. Among HPAs, Keggin structures, with $[XM_{12}O_{40}]^{q-}$ general formula, figure as the most relevant specie, counting for 2/3 of the published material about this compounds family, in which about 80% are on catalysis purpose². Substitution of the heteroatom or of the metal (X, or M, respectively) give rise to different relations of acidity, reducing character and stability, tuning its conversion and selectivity on its catalytic activity. The preset work aim to analyze and compare a series of theoretical and experimental data to collaborate to the comprehension of the isomer formation mechanisms on the series $[XW_{12-n}V_nO_{40}]^{-(q+n)}$, with X=Si, P and $0 \leq n \leq 4$, as well as to better interpretation of the vibrational spectra of infrared (IR) and Raman.

METHODS

The geometry optimization and vibrational frequency calculations were performed on DFT/B3LYP and M062X levels. The 6-31G* base set was used on phosphorus and silicon, while 6-31+G* was used on oxygen, and the LanL2DZ effective core potential with relativistic effects implicitly included base set was used on vanadium and tungsten. The polarizable continuum model (PCM) with the integral equation formalism variant (Integral Formalism Polarizable Continuum Model – IEFPCM) was used on the calculations to count for charge stabilization effects due to the aqueous solvent on the studied anions.

RESULTS AND DISCUSSION

There are 47 different possible structures with 0 to 4 M substituents⁴. A good agreement between

calculated geometry and experimental data was reached on the cases where the comparison is valid⁵. Gibbs free energy analyses shows small energy variation among species with same number of substituents, suggesting a thermodynamic factor leading to a observable amounts of different isomers among a given sample. Optimal relative ratio of isomers was shown to be sensitive on the heteroatom choice. Samples with different isomer distribution are expected to generate different IR spectra patterns. The coexistence of species with different number of substituents was shown to be thermodynamically unfavorable on the performed calculations; experimental observation of this coexistence most lie on kinetics factors. Experimental Raman spectrum didn't show characteristic V-O_d bands present on the calculations and need to be further investigated.

CONCLUSIONS

It is thermodynamically expected to observe a isomer distribution on a given sample. Homogeneous distribution of the substituents is energetically favorable. IR bands can be used to differ between different isomer distributions and to identify substitution rate. Predicted characteristics Raman bands are not experimentally observed and need further investigations.

ACKNOWLEDGEMENTS

To my advisors, Alexandre Braga da Rocha and Jean Guillaume Eon. To PGQU/UFRJ, CAPES, CNPq e FAPERJ for the financial suport.

¹ S. W.Benson and O. Dobis, J. Phys. Chem. A, 102, 5175, (1998).

² J. Liu, Z.Li, C.Sun, J. Phys. Chem. A, 105, 7707, (2001). Tsai, P.-Y.; Che, D.-C.;

³ M. Nakamura, K. C. Lin, T. Kasai, Phys. Chem. Chem. Phys., 12, 2532, (2010).

Photo-thermal activation study of ruthenium Keppler-type complexes with focus on the release of the nitrosyl ligand using TD-DFT and AIM theories

Priscila C. Rocha^a (IC), James A. Platts^b (PQ), Luiz Antônio S. Costa^a (PQ)

^aNúcleo de Estudos em Química Computacional (NEQC), Dep. de Química, ICE, Universidade Federal de Juiz de Fora, Juiz de Fora, MG, CEP 36036-900.

^bSchool of Chemistry, Cardiff University, Park Place, Cardiff CF10 3AT, United Kingdom
 priscila_sjn@hotmail.com

Keywords: Ruthenium complexes, nitrosyl, cancer, AIM, DFT

INTRODUCTION

New cancer cases arises every day with frightening statistics and one of the greatest challenges in the treatment in recent years, which is the low selectivity of medicines, inefficiency on the metastatic cells, resistance and toxicity thereof. In this context, ruthenium complexes containing nitrosyl group (NO) has gained ground since the release of nitrosyl inside mitochondria can change the functions of the cell and cause its death.¹ Thus, based on the mechanism (Figure 1), the aim of this study is to use the density functional theory (DFT) to evaluate the reduction and release of the nitrosyl group within the cell, and also apply the theory of atoms in molecules (AIM) to gain details of Ru-nitrosyl interaction.

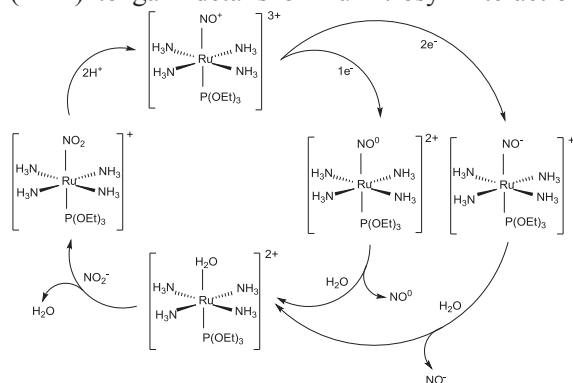


Figure 1: Thermal activation steps of NO in the Ru^{III} complexes, *trans*-[Ru(NO₂)(NH₃)₄P(OEt)₃]²⁺ (Adapted from Tfouni 2012).²

METHODS

All structures were optimized using the B3LYP functional with 6-31G(d) basis set for non-metals and LANL2DZ for the Ru atom. All calculations were carried out in gas and aqueous phase (CPCM). Later, the optimized species were studied using TD-DFT and AIM Bader's theory.

RESULTS AND DISCUSSION

In the reduction step, the loss of an electron ($E^\circ=5.44\text{V}$) is more favorable for its reduction

potential to be greater than the loss of two electrons ($E^\circ=4.56\text{V}$) and the release of the binder NO⁰ energy is lower, compared to NO⁻ release ($\delta\Delta_rG = 85.14 \text{ kcal mol}^{-1}$). From distances of Ru-N bond obtained in DFT, it is observed that the complex [Ru-NO⁰]²⁺ (1.98 Å) the distance is slightly higher compared to [Ru-NO⁻]⁺ (1.95 Å). These data agree with the AIM theory, so that the Laplacian ($\nabla^2\rho$) (Table 1) in the Ru-N bond for complex [Ru-NO⁰]²⁺ is higher than in [Ru-NO⁻]⁺.

Bond	Ru-N	
	$\nabla^2\rho$	DI
[Ru-NO ⁻] ³⁺	1.094	1.422
[Ru-NO ⁰] ²⁺	0.704	1.032
[Ru-NO ⁻] ⁺	0.523	1.123

Table 1: Laplacian and Delocalization Index for Ru-N bonds in selected complexes.

Coordination to Ru alters properties of N markedly, but affects O rather less. N in NO⁺ bound to Ru contains almost a whole electron more than in the free ligand, despite having an almost identical volume, evidence of substantial donation from metal d-orbitals into the empty, low-lying π^* orbitals on N.

CONCLUSIONS

Through the AIM a good approximation was obtained for Lewis structures. All properties are in good correlation with data obtained from TD-DFT. Also, the thermodynamic study allowed energy assessment involving the metal reduction steps and release of NO group. Transitions states are now being studied.

ACKNOWLEDGMENTS

FAPEMIG, RQ-MG, BIC-UFJF.

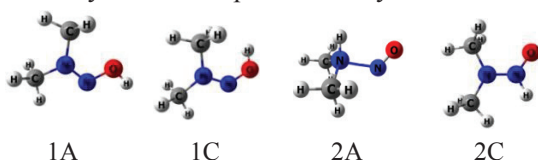
- Adeniyi, A. A.; Ajibade, P. A. *J. Molecular Graphics and Modelling*, 38, 60-69, (2012).
- Tfouni, E.; *et al. Nitric Oxide*, 26, 38-53. (2012).

Protonated N-Nitrosodimethylamine: a comparative MR-CISD and NEVPT2 studyR. B. de Andrade^a(PG), E. Ventura^a(PQ), S. A. do Monte^a(PQ), M. A. F. de Sousa^b(PQ)^aDepartamento de Química, Universidade Federal da Paraíba, João Pessoa, PB 58059-900, Brazil.^bInstituto de Química, Universidade Federal do Rio Grande do Norte, Natal, RN 59072-970, Brazil.railtoncg@gmail.com

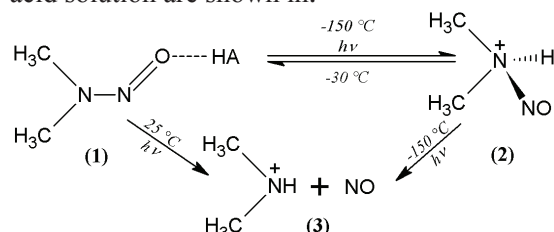
Keywords: Nitrosamine, CASSCF, MR-CISD, NEVPT2.

INTRODUCTION

Nitrosamines are considered carcinogenic and have been detected even in drinking water^[1]. The photolysis is a technique that can be used to treat or even remove these substances^[2]. In high acid concentration N-nitrosodimethylamine (NDMA) become protonated (Figure 1: Ground state conformations of protonated NDMA.) and will not undergo photolysis. Thus, the protonated nitrosamine is a key species in the study of NDMA photostability.

**Figure 1:** Ground state conformations of protonated NDMA.

The main photochemical reactions of NDMA in acid solution are shown in:

**Figure 2:** Main photochemical reactions of NDMA in acid solution (adapted from^[3]).**METHODS**

The CASSCF, MR-CISD and NEVPT2^[4] methods with the aug-cc-pVDZ basis set have been used in the calculations. COLUMBUS^[5] and ORCA^[6] softwares have been used for the first two and for the last method, respectively. The active space consists of the following set of orbitals: $2s_O$, $2s_N$, σ_{XH} , σ_{NN} , π_{NO} , σ_{NO} , n_X , π^*_{NO} , σ^*_{NN} , σ^*_{NO} , σ_{XH}^* , where X = N or O.

RESULTS AND DISCUSSION

Tabela 1 shows the relative energies of the four tautomers of NDMA. The energies shown have been obtained at the CASSCF, MR-CISD and NEVPT2 levels based on CASSCF (14,11) geometries optimized with the aug-cc-pVDZ basis set.

Tabela 1: CASSCF, MR-CISD and NEVPT2 energies (in kcal/mol) of the four tautomers of protonated NDMA.

Structures	CASSCF ^[7]	MR-CISD ^[7]	NEVPT2
1A	0,00	0,00	0,00
1C	11,10	11,34	12,15
2A	-15,41	2,54	1,35
2C	10,92	14,47	15,72

As can be seen from this Table there is good agreement between MR-CISD and NEVPT2 results.

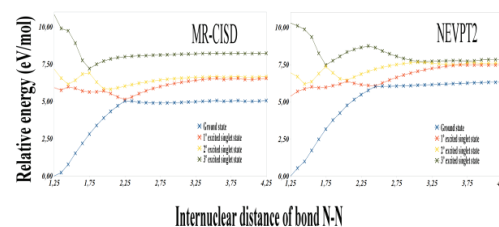
**Figure 3:** Potential energies curves for the first five singlet electronic states of protonated NDMA obtained at the NEVPT2 and MR-CISD levels along the N-N bond distance of structure 1A. The energies shown have been obtained from a relaxed scan.

Figure 3 shows the energies of the first five singlet electronic states of protonated NDMA obtained from a relaxed scan along the N-N distance. As can be seen from this plot there is very good agreement between the results obtained at the MR-CISD and NEVPT2 levels.

CONCLUSIONS

The very good agreement between the MR-CISD and NEVPT2 results suggests the use of the latter method (which has a much lower computational cost) for larger nitrosamines of varied photostability^[8]. Besides, solvent effects (with continuum solvent models) can also be included at the latter level.

ACKNOWLEDGMENTS

The authors are grateful for financial support given from FINEP, CAPES and CNPq.

¹ Lee, C. *et al.*, *Environ. Sci. Technol.* 39, (2005).² Hellebust, S. *et al.*, *J. Phys. Chem. A*, 114, (2010).³ Chow, Y. L. *et al.*, *J. Am. Chem. Soc.* 107, (1985).⁴ Lischka, H. *et al.*, COLUMBUS, an ab initio electronic structure program, release 7.0 (2012).⁵ Angeli, C. *et al.*, *J. Chem. Phys.* 114, 10252(2001).⁶ Neese, F. *et al.*, ORCA-an ab initio, DFT, and Semiempirical Electronic Structure Package. Germany (2015).⁷ Andrade, R. B. *et al.*, *J. Comput. Chem.* DOI: 10.1002/jcc.24007, (2015).⁸ Ohwada, T. *et al.*, *J. Am. Chem. Soc.* 123, 10164-10172, (2001).

Theoretical study of the $H_2 + PtO^+$ reaction by relativistic methods

Régis T. Santiago^a (PG), Roberto L.A. Haiduke^a (PQ)

^a Instituto de Química de São Carlos, Universidade de São Paulo, São Carlos, SP
registantiago@iqsc.usp.br

Keywords: relativistic calculations, transition state, chemical kinetics

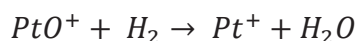
INTRODUCTION

Quantum chemistry has been widely used in kinetics studies of chemical. However, the investigation of the variations caused by relativistic effects over these quantities is still at an early stage.¹

Recently, Tong and co-workers have made a theoretical study about the activation of H_2 by PtO_2^+ and PtO^+ using the Relativistic Effective Core Potential (RECP) method.² Thus, our goal was to analyze the reaction of H_2 with PtO^+ by other relativistic methods: Second-Order Douglas-Kroll-Hess (DKH2) and Zeroth Order Regular Approximation (ZORA).

METHODS

We studied the following reaction:²



All calculations (geometry optimization, vibrational frequency and Intrinsic Reaction Coordinate-IRC) were performed with the ORCA package³ by means of the relativistic approximations DKH2 and ZORA, using Density Functional Theory (DFT) with the B3LYP functional and def-SVP basis sets.

RESULTS AND DISCUSSION

First, through optimization and frequency calculations, it was possible to determine the transition states (TSs) and molecular intermediates (MIs) of the studied reaction. In order to characterize these transition states (Figure 1) we performed IRC calculations.

As one can see, both the relativistic methods chosen here have demonstrated similar reaction coordinate profiles (Figure 2). The activation enthalpy (ΔH_a) associated with the first transition state (TS1) is $16.4 \text{ kcal mol}^{-1}$ according with ZORA and DKH2 approaches. Moreover, the

ΔH_a values obtained from TS2 are around 25 kcal mol^{-1} .

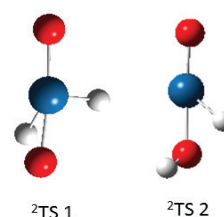


Figure 1: Transition state structures optimized by DKH2 – B3LYP/def-SVP calculations

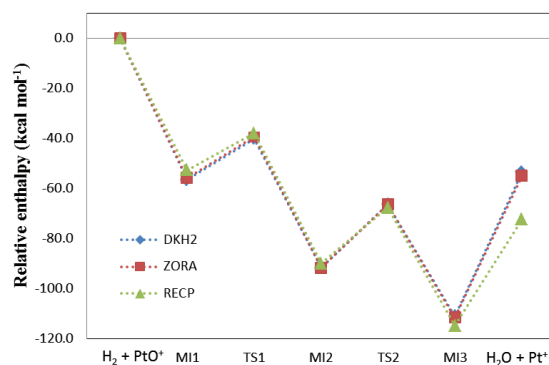


Figure 2: Energetic profile for the reaction $H_2 + PtO^+ \rightarrow Pt^+ + H_2O$

CONCLUSION

The methods used here were able to describe adequately the studied reaction. The activation barriers of the rate determining step obtained by both alternative treatments were very similar.

ACKNOWLEDGMENTS

FAPESP (2010/18743-1 and 2014/23714-1), CNPq and CAPES.

¹ PYYKKO, P. Annu Rev Phys Chem, v. 63, p. 45-64, 2012.

² TONG, Y.; WANG, Q.; WU, D.; WANG, Y. J Theor Comput Chem, v. 9, n. 6, p. 963-974, 2010.

³ NEESE F. The ORCA program system. WIREs Comput Mol Sci 2: p. 73-78. 2012.

Electronic and structural properties of engineering CdSe@TiO₂ nanotubes arrays

R. G. Freitas^a (PQ), R. A. Mendes^a (PG), F. W. S. Lucas^b (PG), M. A. Santanna^b (PG), G. L. C. Souza^a (PQ), L. H. Mascaro^b (PQ), E. C. Pereira^b (PQ)

^aDepartment of Chemistry, Federal University of Mato Grosso, 78060-900, Cuiabá-MT, Brazil

^bDepartment of Chemistry, Federal University of São Carlos, 13560-970, São Carlos-SP, Brazil

Keywords: TiO₂ nanotubes, Rietveld refinement, band structure, density of states

INTRODUCTION

TiO₂ nanotubes emerge as a promising class of semiconductors^[1], especially when tuned with CdSe quantum dots^[1]. TiO₂-anatase crystalline structure can be obtained at 450°C. Therefore, this work describe the structural and electronic parameter for CdSe deposited inside TiO₂NT previously (TiO₂NT-PTT) and later thermally treated (TiO₂NT-LTT).

METHODS

Rietveld refinement^[2] was performed using the General Structure Analysis System program^[3] suite. Based on the results of Rietveld refinement, TiO₂-anatase CIF inputs for the band structure and density of states (DOS) were obtained. DFT calculation for electronic structures of TiO₂ unit cell were carried out within the generalized gradient approximation (GGA) using the PWscf code included in the Quantum-Espresso package^[4]. For this surface, a 4x4x4 Monkhorst-Pack and 49 *k*-points mesh was utilized for energy and electronic calculations.

RESULTS AND DISCUSSION

Rietveld refinement for TiO₂NT-PTT and TiO₂NT-LTT can be observed in Figure 1 with good statistical agreement.

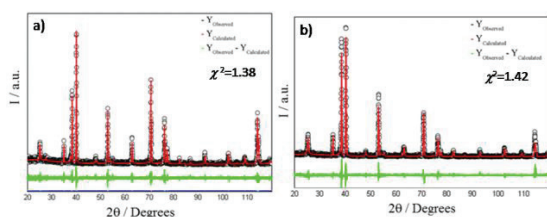


Figure 1. Rietveld refinement for a) TiO₂NT-PTT and b) TiO₂NT-LTT nanostructured materials.

Structural parameter obtained were $a=b=3.756(4)\text{Å}$, $c=9.441(7)\text{Å}$ and $a=b=3.796(2)\text{Å}$, $c=9.502(6)\text{Å}$ for TiO₂NT-PTT and TiO₂NT-LTT respectively.

The band structure and DOS for the TiO₂NT-PTT and TiO₂NT-LTT can be observed in Figure 2. It is possible to notice that the top of valence band is located at point Z for both crystalline structure.

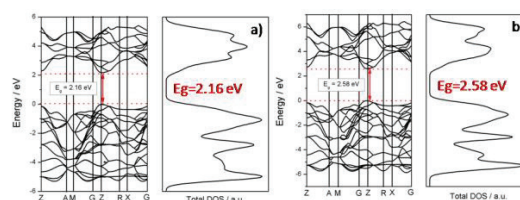


Figure 2. Band structure and DOS obtained for a) TiO₂NT-PTT and b) TiO₂NT-LTT nanostructured materials.

Moreover, direct band gaps can be observed. Experimental band gap values were 2.20eV and 2.65eV for TiO₂NT-PTT and TiO₂NT-LTT respectively. These data are in agreement with theoretical one.

CONCLUSIONS

Electronic structures derived from the models obtained using Rietveld refinement allows calculated electronic energy band gap, as well as energy band structure that were consistent with experimentally determined optical band gap.

ACKNOWLEDGMENTS

The authors are grateful for the support given from the FAPESP, CAPES and CNPQ.

¹ G. A. Grimes, G. K. Mor, TiO₂ nanotubes: synthesis, properties and applications. Springer (2009)

² H. M. Rietveld, Journal Applied Crystallography 2 (1969) 65 ³ A. C. Larson, R. B. von Dreele, Lab. Rep. LAUR 86 (2004) 1

⁴ S. Baroni, S. de Gironcoli, A. dal Corso, P. Giannozzi, Quantum Espresso, <www.quantum-espresso.org>

Aromaticity in Complex Consisting of Thiocarbons ($C_nS_n^{2-}$; $n = 3 \text{ e } 4$)

Eder H. da Silva¹ (PG), Giovanni F. Caramori² (PQ), Renato L. T. Parreira¹ (PQ)

¹ Núcleo de Pesquisa em Ciências Exatas e Tecnológicas, UNIFRAN - Franca - 14404-600, SP, Brazil

² Depto. de Química, UFSC, Campus Universitário Trindade, Florianópolis - 88040-900, SC, Brazil
 renato.parreira@unifran.edu.br / edersilva3@yahoo.com

Keywords: Aromaticity, Thiocarbons, Electronic effects, NICS.

INTRODUCTION

The thiocarbons ($C_nS_n^{2-}$), similarly to the oxocarbons ($C_nO_n^{2-}$), present important optical and photophysical properties.^{1a} The continued interest in the family of thiocarbons is due, in part, to the aromaticity of this class of compounds, which exhibits electron delocalization stabilized by resonance.^{1b} This work presents the study of the species $C_3S_3^{2-}$ (1) and $C_4S_4^{2-}$ (2), isolated and complexed with lithium (Li^+) and calcium (Ca^{2+}) ions, as models for the investigation of the structural and electronic characteristics of this class of compounds.

METHODS

Geometries were optimized at the B3LYP/6-311++G(3df,3pd) level of theory by using the Gaussian09 software. Methods based on magnetic (NICS) and structural (HOMA) parameters were used for the study of aromaticity.² The topological analysis of the electron density was performed with the use of the QTAIM theory.^{4,5}

RESULTS AND DISCUSSION

The studied compounds are shown in Figure 1.

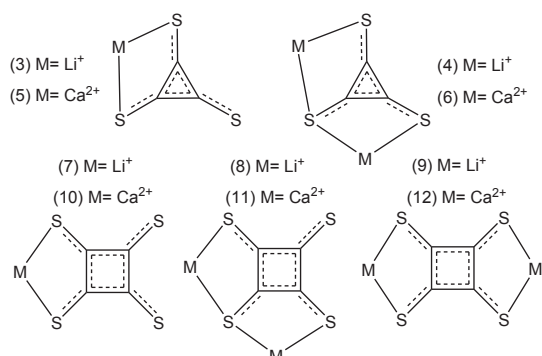


Figure 1. $C_3S_3^{2-}$ and $C_4S_4^{2-}$ complexes.

The NICS values (Table 1) indicate strong aromatic character to the complexes constituted by the $C_3S_3^{2-}$ ion. The increase in the ring size led to a reduction of aromaticity in complexes formed by $C_4S_4^{2-}$ ion. It is observed that the symmetrical coordination with metal ions cause an increase in the aromaticity.

Table 1. NICS and HOMA values.

	NICS(1)	NICS(1) _{zz}	HOMA	EN	GEO
C_6H_6	-10,04	-29,84	0,998	0,002	0,000
1	-9,94	-13,96	0,974	0,026	0,000
3	-9,71	-13,96	0,952	0,037	0,010
4	-9,89	-14,82	0,963	0,028	0,010
5	-7,52 ⁽ⁱⁿ⁾ -9,12 ^(out)	-10,51 ⁽ⁱⁿ⁾ -14,65 ^(out)	0,871	0,107	0,023
6	-8,36	-12,98	0,956	0,044	0,001
2	-2,50	1,26	-0,568	1,568	0,000
7	-2,43	1,23	-0,568	1,440	0,128
8	-2,37	1,55	-0,590	1,317	0,272
9	-3,68	-0,44	-0,194	0,192	0,002
10	-0,97 ⁽ⁱⁿ⁾ 0,53 ^(out)	2,79 ⁽ⁱⁿ⁾ 3,73 ^(out)	-1,052	1,818	0,234
11	-1,37	2,35	-0,991	1,440	0,551
12	-3,09	1,37	-0,123	1,123	0,000

According to the HOMA index (Table 1), only the complexes formed by the $C_3S_3^{2-}$ ion present aromatic character. The anti-aromatic character for $C_4S_4^{2-}$ compounds is related to the long lengths of the C-C bonds (EN term). The Laplacian of the electron density ($\nabla^2\rho_b$) indicates that metal-ligand bonds are classified as type "closed-shell".

CONCLUSIONS

The NICS index showed that the complexes formed by $C_3S_3^{2-}$ ion are aromatic. The complexation with symmetrical pattern promotes slight increase in the aromatic character to the complex formed by $C_4S_4^{2-}$ ions. The metal-ligand bonds were classified as "closed-shell".

ACKNOWLEDGMENTS

FAPESP (2011/07623-8 and 2012/22440-0) and CNPq (grant 470985/2011-9).

¹ (a) A. J. Fatiadi, J. Am. Chem. Soc. 100, 2586 (1978). (b) D. Quiñonero, C. Garau, A. Frontera, P. Ballester, A. Costa, PM Deya, Chem. Eur. J., 8, 433 (2012).

² D. Geuenich, K Hess, F. Köhler, R. Herges, Chem. Rev. 105, 3758 (2005).

³ (a) R. F. W Bader, Atoms in Molecules. A Quantum Theory. Oxford University Press. Oxford, U. K., 1990. (b) R. F. W. Bader, Phys. Chem. A, 102, 7314 (1998).

Influência da Presença de Moléculas do Solvente Explícitas no Estudo Conformacional de Monossacarídeos

Renato Andrade^a (PG), Clarissa Silva^a (PQ).

^a Dep. De Química-ICE, Universidade Federal Rural do Rio de Janeiro, Seropédica, Rio de Janeiro

Palavras-chave: D-lixose, microsolvatação, razão anomérica, amostragem conformacional.

INTRODUÇÃO

A obtenção das conformações absolutas para os carboidratos não é uma tarefa simples. Este fato se deve à liberdade conformacional presente em suas estruturas. Por exemplo, a pentose D-lixose possui razão anomérica ($\alpha:\beta$), em porcentagem, de 72:28. Dentre os 72% de α , 33% estão na forma cadeira 4C_1 e 39% na forma cadeira 1C_4 . Para o anômero β , 22% estão na forma cadeira 4C_1 e 6% na forma cadeira 1C_4 .¹ Mas experimentalmente não se tem acesso às orientações relativas dos grupos hidroxila destas moléculas. Somente estudos teóricos podem chegar a essas orientações relativas para os monossacarídeos.^{2,3} O objetivo deste trabalho é obter teoricamente as conformações absolutas para a molécula de D-lixose em solução aquosa.

METODOLOGIA

Partiu-se de três estruturas otimizadas. Duas para o anômero α (cadeira 4C_1 e 1C_4) e uma para o anômero β (cadeira 4C_1), que correspondem a uma ocorrência de 94% do total. Utilizou-se o programa CONFPO⁴ para gerar todas as 243 possibilidades conformacionais. Cálculos de otimização de geometria e frequência vibracional foram realizados para o sistema com e sem uma molécula de água explícita (1w). Todos os cálculos foram realizados utilizando Teoria do Funcional de Densidade, com o funcional B3LYP e conjunto de funções de base do tipo 6-31+G(d,p). Os cálculos em solução foram feitos utilizando o Modelo de Contínuo Polarizável (PCM).

RESULTADOS E DISCUSSÃO

Partindo de 243 possibilidades conformacionais, chegou-se a 55 conformações. Os resultados de razão anomérica ($\alpha:\beta$) para o sistema em fase gasosa (FG), solução aquosa (PCM), Fase gasosa com uma molécula de água explícita (FG+1w) se encontram na Figura 1.

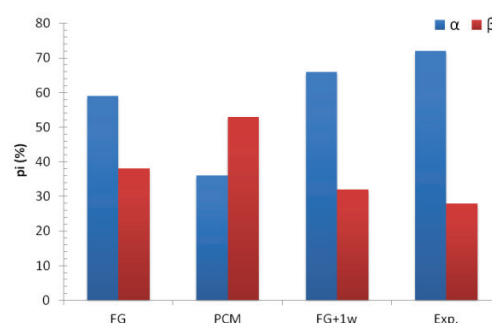


Figura 1: Valores de razão anomérica ($\alpha:\beta$), em porcentagem, para a molécula da D-lixose em fase gasosa (FG), solução aquosa (PCM) e fase gasosa com uma molécula de água explícita (FG+1w).

Na Figura 1, percebe-se a solvatação (PCM) agindo de forma a inverter o sentido preferencial de abundância relativa, colocando o anômero β como aquele mais estável, e se distanciando do resultado experimental. Em FG+1w, há uma melhora no valor de $\alpha:\beta$, aproximando-se este resultado daquele experimental.

CONCLUSÃO

A introdução de uma molécula de água explícita pode ser determinante para a obtenção das conformações mais abundantes envolvidas no equilíbrio anomérico de pentoses em solução aquosa. A próxima etapa do trabalho será a realização dos cálculos em PCM com uma molécula de água explícita (PCM+1w).

Agradecimento

Os autores agradecem ao CNPQ.

¹ K. S. Vijayalakshmi and V. S. R. Rao. *Carbohydr. Res.*, 22, 413-424 (1972).

² Andrade, R. R.; Silva, C. O. *Mini-Rev. Org. Chem.*, 8, 239-248 (2011);

³ Renato R. Andrade, Clarissa O. da Silva, *Carbohydr. Res.*, 350, 62-67 (2012).

⁴ Leandro G. Alves. Renato R. Andrade e Clarissa O. da Silva. (Submetido).

Hydrogen Abstraction from the Hydrazine Dimer by an Oxygen Atom

Rene F. K. Spada^{1*} (PQ), Luiz F. A. Ferrão¹ (PQ), Orlando Roberto-Neto² (PQ),
Hans Lischka^{3,4} (PQ), Francisco B. C. Machado¹ (PQ)

¹*Departamento de Química, Instituto Tecnológico de Aeronáutica, São José dos Campos, São Paulo, Brazil.*

²*Divisão de Aerodinâmica e Hipersônica, Instituto de Estudos Avançados, São José dos Campos, São Paulo, Brazil.*

³*Department of Chemistry and Biochemistry, Texas Tech University, Lubbock, Texas, United States.*

⁴*Institute for Theoretical Chemistry, University of Vienna, Vienna, Austria.*

*rfkspada@gmail.com

Keywords: Hydrazine, Electronic Structure, Chemical Kinetics, Ab Initio, DFT, VTST

INTRODUCTION

The hydrazine molecule (N_2H_4) is used as propellant for the attitude-control jets in spacecraft vehicles, as well as satellites. Some of these spacecrafts are in a low earth orbit, above 180 km with a temperature around 880 K, in an ambient atmosphere where ground-state oxygen is abundant. Although the majority of the propellant is consumed in the chamber, some is ejected unburned into the atmosphere, especially during the engine shutdown.

In an earlier work¹ we investigated the dehydrogenation of the hydrazine monomer. In this work, we considered the hydrazine dimer dehydrogenation through four reaction paths, all of them leading to different isomers of $N_2H_4 \cdot N_2H_3 + OH$.

METHODOLOGY

The thermochemical properties were acquired using the CCSD(T) methodology and the M06-2X DFT functional with the aug-cc-pVXZ (X = T,Q) and the maug-cc-pVTZ basis sets, respectively. The chemical kinetic properties were calculated with the ICVT approach using the dual-level methodology to build the reaction path. The non-classical effects were considered by means of the SCT approximation. Wells in both sides of the reaction (reactants and products) were found and considered in the chemical kinetics calculations.

RESULTS AND DISCUSSION

Considering the energy of the reaction, the M06-2X functional predicts values between -17.8 and -20.0 kcal/mol and the CCSD(T) ones are in the interval from -16.2 to -17.8 kcal/mol. For the reactant well and product well, the M06-2X method predicts higher stabilization energies than the CCSD(T), with the larger difference being

4.2 kcal/mol. As these reaction paths present low barriers, using a high correlated methodology is extremely important. We observed that the DFT functional predicts adiabatic barriers below zero, while the CCSD(T) method returns a negative value only for one reaction path (-0.8 kcal/mol). For the other reaction paths, the adiabatic barriers are equal to 2.2, 3.3 and 1.5 kcal/mol.

The calculated rate constants are in good agreement with the literature.² The measured value is equal to $6.2 \times 10^{-12} \text{ cm}^3 \text{ molec}^{-1} \text{ sec}^{-1}$ and the calculated result for the most important reaction path is $4.0 \times 10^{-12} \text{ cm}^3 \text{ molec}^{-1} \text{ sec}^{-1}$. This reaction path presents a negative temperature dependence in the range of 250 – 400 K. This behavior is also observed experimentally.²

CONCLUSIONS

A reaction path with a negative adiabatic barrier was found and the rate constant exhibits a negative dependence with the temperature below 400 K, agreeing with the experimental measurements.² The rate constant results considering the hydrazine dimer are in better concordance with the experimental results by Vaghjiani² than our results in a previous work¹ considering the hydrazine monomer. Since Vaghjiani measured the oxygen depletion in a hydrazine atmosphere, it suggests that the hydrazine dimer can play an important role in the mechanism of the global $N_2H_4 + O$ global reaction.

ACKNOWLEDGMENTS

The authors acknowledge the research and fellowship support of FAPESP, CNPq and CAPES.

¹ Spada, R. F. K., *et al.*, J. Phys. Chem. A, 119 (9), 1628, (2015).

² Vaghjiani, G. L., J. Chem. Phys., 104, 5479, (1996).

Spectroscopic Study of the Ng-CCl₄, O₂-CCl₄, D₂O-CCl₄ and ND₃-CCl₄ Systems.

Rhuiago Mendes de Oliveira^a (PG), Gabriel Fávero^a (PG), Luiz F. Roncaratti^a (PQ), Geraldo Magela e Silva^a (PQ) and Ricardo Gargano^a (PQ).

^aInstituto de Física, Universidade de Brasília, 70919-970, Brasília, Brazil.

Keywords: CCl₄ molecule, DVR, Dunham's Method, rovibrational energies, spectroscopic constants.

INTRODUCTION

The investigation of dispersion events between carbon tetrachloride molecules (CCl₄) and other atomic and molecular species have been motivated for several reasons¹. In a short way, it is observed that the interaction between CCl₄ and another atom/molecule is characterized by a van der Waals component, since that the polarizability value of CCl₄ ($\alpha = 10, 5 \text{ \AA}^3$) is expected to be much more elevated than a one of a heavy atom, for example ($\alpha = 4,04 \text{ \AA}^3$ for xenon). The CCl₄ molecule shows a high symmetry structure without permanent dipole momentum. In this work we calculated the rovibrational energies and spectroscopic constants of the carbon tetrachloride with a few atoms and molecules systems, such as He-CCl₄, Ne-CCl₄, Ar-CCl₄, O₂-CCl₄, D₂O-CCl₄ and ND₂-CCl₄.

POTENTIAL ENERGY CURVES

The Improved Lennard-Jones model (ILJ)¹, found to be suitable to formulate V(R) for several systems of different nature and at increasing complexity, stands out as an interesting model that eliminates most of the original LJ model inadequacies, particularly those from short and long range. This is accomplished in an elegant fashion through the consideration of a single extra parameter. The ILJ potential functions is given by

$$V(r) = \varepsilon \left[\frac{6}{n(r) - 6} \left(\frac{r_m}{r} \right)^{n(r)} - \frac{n(r)}{n(r) - 6} \left(\frac{r_m}{r} \right)^6 \right]$$

$$n(r) = \beta + 4 \left(\frac{r}{r_m} \right)^2$$

where, ε is the depth of the potential well, r_m the equilibrium distance and $\beta=9$ is a experimental parameter.

RESULTS AND DISCUSSION

Using the ILJ, we obtain the potential energy curves (PEC) for each considered complexes. The spectroscopic constant calculations were

determined by using two different approaches: Discrete Variable Method (DVR) and Dunham's method.

System	Method	ω_e	$\omega_e x_e$	$\omega_e y_e$	α_e	γ_e
He-CCl ₄	DVR	-	-	-	-	-
	Dunham	30.96	9.16	0.24	0.04	0.0002
Ne-CCl ₄	DVR	21.41	2.10	0.03	5.56E-07	-1.86E-08
	Dunham	21.35	2.04	0.01	0.003	6.59E-06
Ar-CCl ₄	DVR	25.58	1.10	0.005	-1.87E-07	-2.88E-08
	Dunham	25.57	1.10	0.004	0.0008	7.26E-07
O ₂ -CCl ₄	DVR	28.06	1.32	0.007	-1.12E-07	-1.00E-08
	Dunham	28.05	1.32	0.005	0.001	1.03E-06
D ₂ O-CCl ₄	DVR	39.72	2.17	0.01	-7.65E-07	-2.70E-09
	Dunham	39.70	2.15	0.01	0.002	2.25E-06
ND ₂ -CCl ₄	DVR	38.34	1.98	0.01	-1.25E-07	-1.75E-08
	Dunham	38.33	1.97	0.009	0.001	1.84E-08

From Table above, one can see an excellent agreement between the Dunham and DVR methods. One another fact that deserves special attention is that the greater contribution of harmonic part (ω_e) happens for the D₂O-CCl₄ massive system.

CONCLUSIONS

In this work, we presented the rovibrational energies and the spectroscopic constants for the systems formed between carbon tetrachloride and others atoms and molecules. Our calculations were based on potential energy curves obtained through molecular beam scattering experiments. The vibrational energy level distribution followed the pattern qualitatively expected from the nature of each system. Furthermore, it was observed that the H₂O₂-He system can remain bonded (only one vibrational state) even with a small depth of the potential well.

ACKNOWLEDGMENTS

The authors are grateful for the support given from the CAPES, CNPq and FINATEC.

¹ L.F. Roncaratti, Quantum effects in molecular scattering experiments: Characterization of the

The influence of the first series of transition elements in the electronic properties of Pd clusters: a study based on Density Functional Theory

Ricardo de Almeida* (PG), Maurício Tavares de Macedo Cruz (PQ)

Departamento de Química Geral e Inorgânica, Instituto de Química, Universidade do Estado do Rio de Janeiro, Rio de Janeiro, Brazil.

*rialmeida@hotmail.com

Keywords: perovskite, intelligent catalysis, self-regeneration, CO and NO adsorption, DFT.

INTRODUCTION

Palladium, in particular is a promising material as catalyst in various applications. Small clusters of Pd are used in automotive exhaust systems to reduce toxic pollutants such as CO, NO and hydrocarbons¹. In this present work was carried out a series of calculations based on Density Functional Theory (DFT) to study the adsorption of NO molecule was used as prototype to interact on the molecular clusters and pure palladium doped with transition metals of the first transition series (Pd₃M and Pd₉M). In this context, the scope of this study was obtained information about possible changes in structural, electronic and energetic parameters of palladium clusters when doped with the first series of transition metals (TM).

METHODS

As a first step, was obtained the preferential spin state for clusters containing four atoms of Pd₄ and Pd₃M (M = Sc, Ti, V, Cr, Mn, Fe, Co, Ni, Cu) with a tetrahedral arrangement with Pd—Pd and Pd—M distances of palladium bulk (2.751 Å). After, these clusters were optimized in the multiplicity of lowest energy. On Pd₄ and Pd₃M clusters a molecule of NO was optimized on two kind of tetrahedral agglomerates: with Pd—Pd (or M) of 2.751 Å and with Pd—Pd(or M) optimized. Following, the palladium cluster was increased to ten atoms, Pd₉M (figure 1b). In all calculations, the transition metal M doesn't interact directly with the molecule of NO. All calculations were performed using the Gaussian 03W program employing BP86/LANL2DZ method for metal clusters and BP86/LANL2DZ/6-311+ G(d) method for complexes with NO molecule.

RESULTS AND DISCUSSION

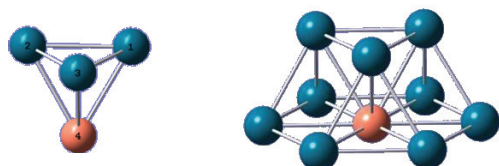


Figure 1. Clusters of Pd₃M and Pd₉M.

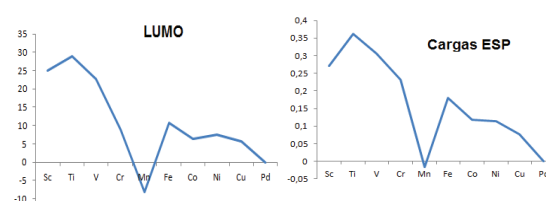


Figure 1. Comparison of trends in atomic charges on the first series atoms and the stabilization energies of the frontier orbitals, for Pd₃M clusters. a) ESP charge, b) LUMO

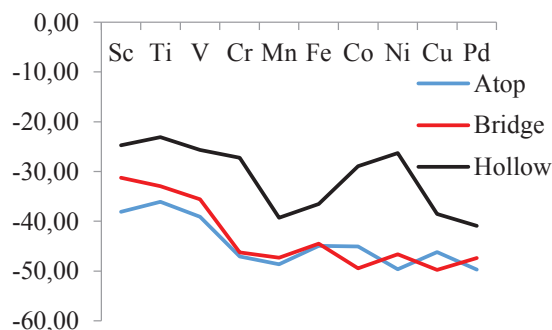


Figure 2: Adsorption energy (kcal.mol⁻¹) for the adsorption modes of NO molecule on Pd₃M.

CONCLUSIONS

The LUMO of the Pd₃M presents the same behavior of the charge ESP on metal dopant M. The NO molecule adsorbs more favorably in Atop mode, regardless of which metal is doping the Pd₃M cluster.

ACKNOWLEDGMENTS

The authors are grateful for the support given from the FAPERJ, CAPES and CNPQ.

¹ B. Kalita and R.C. Deka, Phys. J. D, 53, 51 (2009).

² J. A. Alonso, Science, 100, 637, (2000).

Catalytic hydrogenation of acrylic acid by molybdenum carbide

Ricardo R. Oliveira^a(PG), Victor Teixeira da Silva^b, Leandro Sousa^b, Alexandre B. Rocha^a(PQ)

^aChemistry Institute, UFRJ, Rio de Janeiro, Brazil

^bNUCAT, COPPE, UFRJ, Rio de Janeiro, Brazil

Keywords: **acrylic acid, molybdenum carbide, hydrogenation, DFT**

INTRODUCTION

Hydrogenation of fatty acid is an important step of a larger catalytic fuel production process. These reactions can be catalyzed by molybdenum carbide (Mo₂C), an efficient catalyst cheaper than that based on transition metals. The overall triglyceride transformation proceeds into two steps¹:

- (i) thermal cracking of the triglyceride forming free fatty acids and
- (ii) hydrogenation of the double bonds and of the carboxylic group of the free fatty acid forming n-alkanes.

There are two possibilities in the hydrogenation step, the reaction pathway by double bond addition or by carboxylic group addition. Moreover, the complete mechanism is unknown.

The aim of this work is obtain the reaction path for the hydrogenation step at Density Functional Theory (DFT) level on explicit carbide surface. For this study, acrylic acid was used as fat acid model.

METHODS

All calculation were made at DFT level with Generalized Gradient Approximation (GGA) functional PBE with periodic boundary condition (PBC). The energy cutoff for plane wave basis set was 410 eV.

For geometry optimization the projector augmented wave approximation was used and for the search for minimum energy path with nudged elastic band method (NEB) ultra-soft pseudo-potential approximation was used.

All geometry optimization, self-consistent field (SCF), density of states (DOS) and band energy calculation was done in Vienna Ab initio Simulation Package (VASP) and all NEB calculation were done in Quantum ESPRESSO suite of programs.

RESULTS AND DISCUSSION

Preliminary results show that the hydrogenation by oxygen atom in the carboxyl group is the most

probable pathway, followed by dehydration. The activation energy is about 40 kcal/mol.

The pathway by addition to carbon 2 (see figure 1) is more likely than the pathway by carbon 3.

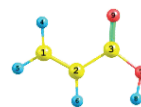


Figure 1. Acrylic acid structure and numeration.

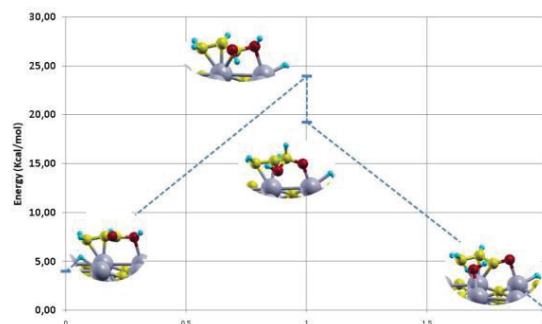


Figure 2. Hydrogenation by oxygen atom in the carboxyl group pathway.

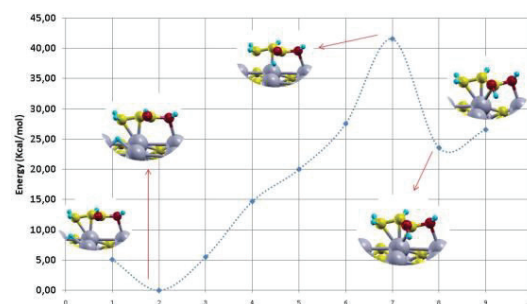


Figure 3. Minimum energy path for hydrogenation by oxygen atom in the carboxyl group obtained with NEB method.

CONCLUSIONS

The previous results show that the hydrogenation by carboxyl group is the most probable pathway for this step.

ACKNOWLEDGMENTS

Authors acknowledge FAPERJ, CAPES, and CNPQ for financial support.

¹ L. A. Souza, J. L. Zotin and V. Teixeira da Silva, Appl. Catal. A, v. 449, p. 105-111, 2012.

Structural Characterization and Theoretical Study of Asymmetric Azines $C_{17}H_{17}N_3O_2$ and $C_{16}H_{16}N_4O_2$.

Ricardo Rodrigues Ternavisk^b (PG), Hamilton Barbosa Napolitano^b (PQ), Ademir João Camargo (PQ), Jhonata de Jesus Silva^a (PG), Francisco Bolivar Correto Machado^b (PQ).

^a *Unidade de Ciências Exatas Tecnológicas, Universidade Estadual de Goiás, Anápolis-GO*

^b *Departamento de Química, Instituto Tecnológico da Aeronáutica, São José dos Campos-SP*
^b*ricardoternavisk@hotmail.com*

Keywords: Azines, crystallography and DFT.

INTRODUCTION

The drug recognition by the bioreceptor of the biomacromolecule is dependent on the drug structure including the spatial arrangement of their functional groups. So, the molecular and supramolecular chemistry analyses helped understanding the effects of molecular structure modifications that increase the drug effectiveness and planning new compounds with desired physical and chemical characteristics¹.

This work aims to discussed the effect of substituent's in the crystalline arrangement of the compounds (1) {(7E, 8E) -2- (4-isopropyl - benzylidene) – 1- (4- nitrobenzylidene) hydrazine} and (2) {(7E, 8E) -1 - (4-nitrobenzylidene) -2 - (4-dimethylamino benzylidene)-hydrazine}.

METHODS

The crystals (1) and (2) were obtained from the initial formation of the hydrazone (E)-1-(4-nitrobenzylidene) hydrazine. In the crystallization step was used the method of slow evaporation of solvent. The structures of the compounds were elucidated by X-ray diffraction experiment on a diffractometer Enraf-Nonius Kappa CCD using Mo $K\alpha$ radiation. The structures was solved, refined and analyzed with OLEX2².

Theoretical calculations can support the understanding of mechanisms that govern the molecular packing due to different substituents at position R1. The level of theory employed was the DFT M06-2X/6-311+G (d,p) as implemented in Gaussian 09 software.

RESULTS AND DISCUSSION

The two structures crystallized in triclinic crystal system and centrossymmetric space group $P\bar{1}$. The molecular geometric parameters of each

compound were provided by the refined structure and compared to optimized ones. The supramolecular arrangement is kept by hydrogen bonds, π - π interactions between the aromatic rings and non classical hydrogen bonds C-H...O. The mapping of the two dimensional projection of Hirshfeld surface (fingerprint) showed the contribution of each type of contacts which occur in the structures. It shows that compound have a network of non classical hydrogen bonds and π - π interactions which stabilizes the crystallographic packing.

CONCLUSIONS

Theoretical calculations on progress will improve the understanding of different substituent effects in R1, providing parameters to study the electrostatic molecular behavior and their effects in packing mechanisms. Also, it can give evidence of interaction mechanisms with active biological sites, assisting the rational design of new substances with biological activity or solid state characteristics that are of interest.

ACKNOWLEDGMENTS

The authors are grateful for the support given from the CAPES.

¹ Barreiro, E. J.; Fraga, C. A. M.; Química Medicinal, As Bases Moleculares da Ação dos Fármacos, 2^a ed; Artmed: São Paulo, Brasil, 2008.

² Dolomanov, O.V.; Bourhis, L.J.; Gideia, R.J.; Howard, J.A.K.; Puschmann, H., OLEX2: A complete structure solution, refinement and analysis program (2009). J.Appl. Cryst., 42, 339-341.

Estimativa teórica da constante de velocidade da reação $\text{CH} + \text{CO} \rightarrow \text{HCO} + \text{C}$ em função da temperatura

Roberto L. A. Haiduke (PQ), Rafael M. Vichiatti (PG), Albérico B. F. da Silva (PQ)

Departamento de Química e Física Molecular, Instituto de Química de São Carlos, Universidade de São Paulo, CP 780, CEP 13560-970, São Carlos, SP, Brasil.
 haiduke@iqsc.usp.br

Palavras chave: estado de transição, cinética, constante de velocidade, correção de Wigner

INTRODUÇÃO

A reação do radical CH com uma vasta gama de moléculas tem sido amplamente estudada experimentalmente ao longo de décadas. Neste sentido, este trabalho apresenta um estudo teórico da cinética do CH com CO, formando os produtos C e HCO em diferentes temperaturas.

METODOLOGIA

As geometrias e correções térmicas dos reagentes, produtos e estado de transição foram calculadas em nível CCSD/cc-pVTZ por meio do pacote Gaussian 09.¹ As energias eletrônicas foram estimadas mediante uma extrapolação de base completa,² segundo resultados em níveis CCSD(T)/cc-pVnZ ($n = \text{Q e 5}$). A pressão de 1 atm foi selecionada e o fator de escala de 0,941³ foi utilizado para correção das frequências vibracionais. Por fim, as constantes de velocidade foram aferidas pela Teoria do Estado de Transição com correção de Wigner para o tunelamento, conforme a expressão

$$k(T) = \frac{k_B T}{h} e^{\frac{-\Delta G_{act}(T)}{RT}} \left[1 + \frac{1}{24} \left(\frac{hc|\omega_i|}{k_B T} \right)^2 \right],$$

onde k_B , h e R são as constantes de Boltzmann, de Planck e dos gases ideais, respectivamente. Além disso, ΔG_{act} é a energia de Gibbs de ativação, T representa a temperatura, c denota a velocidade da luz e ω_i corresponde à frequência imaginária do estado de transição.

RESULTADOS E DISCUSSÃO

A reação $\text{CH} + \text{CO} \rightarrow \text{HCO} + \text{C}$ é endotérmica no sentido direto e a entalpia de ativação necessária para os reagentes se transformarem em produtos varia muito pouco (entre 59,9 e 60,5 kcal mol⁻¹) quando a temperatura aumenta de 300 para 4000K (veja a Tabela 1). Além disso, nesta mesma tabela, a constante de velocidade de tal

reação aumenta consideravelmente de 10⁻⁵⁸ para 10⁻¹⁶ cm³ s⁻¹ no mesmo intervalo de temperatura, indicando claramente que esta reação é processada mais facilmente em altas temperaturas. Infelizmente, ainda não há dados experimentais disponíveis na literatura para serem comparados aos resultados teóricos obtidos neste trabalho.

Tabela 1. Entalpia de ativação, ΔH_a , e constante de velocidade no sentido direto, k_d , da reação $\text{CH} + \text{CO} \rightarrow \text{HCO} + \text{C}$ em função da temperatura.

Temperatura (K)	ΔH_a (kcal mol ⁻¹)	k_d (cm ³ s ⁻¹)
300	60,5	$2,17 \times 10^{-58}$
500	60,2	$1,42 \times 10^{-40}$
700	60,1	$6,44 \times 10^{-33}$
1000	60,0	$3,84 \times 10^{-27}$
1500	59,9	$1,34 \times 10^{-22}$
2000	59,9	$2,73 \times 10^{-20}$
2500	60,0	$6,97 \times 10^{-19}$
3000	60,0	$6,25 \times 10^{-18}$
3500	60,0	$3,07 \times 10^{-17}$
4000	60,0	$1,03 \times 10^{-16}$

CONCLUSÕES

Um estudo teórico-cinético foi realizado para a reação $\text{CH} + \text{CO} \rightarrow \text{HCO} + \text{C}$ e conclui-se que ela é endotérmica no sentido direto e se processa mais rapidamente em altas temperaturas.

AGRADECIMENTOS

Agradecemos ao CNPq pela bolsa concedida e à FAPESP pelo suporte financeiro (2010/18743-1 e 2014/23714-1).

¹ M. J. Frisch et al. Gaussian 09. Gaussian Inc. Wallingford CT, (2009).

² R. F. K. Spada et al., Chem. Phys. Lett., 557, 37, (2013).

³ R. D. Johnson III, NIST Computational Chemistry Comparison and Benchmark Database, (2013).

Rovibrational Energies and Spectroscopic Constants for Buckyball Dimer

Rodrigo Aparecido Lemos Silva^a (PG), Luciano Ribeiro^a (PQ), Valter Henrique Carvalho Silva^a (PQ), Daniel Francisco Scalabrini Machado^b (PG), Heibbe C. B. de Oliveira^b (PQ)

^a QTEA, Universidade Estadual de Goiás, CP 459, Anápolis, GO, Brasil

^b Instituto de Química, Universidade de Brasília, CP 4478, 70919-970, Brasília, DF, Brasil

Keywords: Fullerene Dimers, Diatomic Systems and Spectroscopic Constants

INTRODUCTION

After being discovered by Kroto and co-authors¹ in 1985, the C₆₀ molecule (buckyballs) and other stable fullerenes have opened a completely new field of material research. The dimerization of C₆₀ and other forms² has attracted considerable interest from both experimental and theoretical scientists. Apart from (C₆₀)₂ and (C₇₀)₂ fullerene dimers, many other stable larger ones (C₇₆, C₇₈, C₈₃, etc.) exist.³ In this work, we have built Binding Energies Curves (BECs) from interactions between C₆₀, C₇₀ and C₈₄ fullerenes. In this way, different dimers were studied, such as (C₆₀)₂, (C₇₀)₂ and (C₈₄)₂. Cross-dimers, such as C₆₀C₇₀, C₇₀C₈₄, etc., were studied as well. We have also calculated the rovibrational energies and spectroscopic constants from the BEC by solving the Nuclear Schrödinger Equation and Dunham method as well.

METHODS

Firstly, all BECs (rigid scan) were obtained at the ω B97XD/6-31G(d) level of calculation as implemented in the G09 suite of programs and calculated as following:

$$E_b = E_{Dimer} - (E_{monomer,1} + E_{monomer,2}),$$

where, E_{Dimer} , and $E_{monomer,i}$ are the total energies of dimers and monomer i , respectively. We have evaluated the effect of inclusion of BSSE correction.

The rovibrational energies $E_{v,J}$ were obtained by solving the Nuclear Schrodinger Equation using the Discrete Variable Representation (DVR) method. We have employed the generalized Rydberg of sixth degree (Ryd 6) to represent the effective potential for the nuclei in motion. To ensure the consistency of this approach, the spectroscopic constants care also determined by the Dunham method.

RESULTS AND DISCUSSION

The calculated BEC for the (C₆₀)₂ is depicted in the Figure 1. From this Figure, it is possible to

extract the dissociation energy and the center to center (C₆₀)₂ dimer distance, which is $De_{(C60)2} = 6.54$ kcal/mol and $R_e = 10.06$ Å, respectively. There is a close agreement between our results for the center-to-center (C₆₀)₂ distance and the experimental one ($R_e = 9.91$ Å).⁴

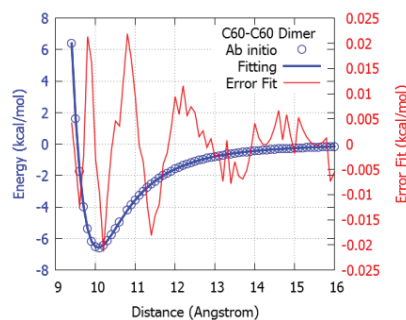


Figure 1. BEC (blue line) of the C60C60 dimer and its error fits (red line).

The spectroscopic constants obtained using the Dunham method for the (C₆₀)₂ dimer are: $\omega_e = 27.32$ cm⁻¹, $\omega_e x_e = 9.24 \times 10^{-2}$ cm⁻¹, and $B_e = 4.61 \times 10^{-4}$ cm⁻¹. The results obtained using DVR and Dunham are in excellent agreement, thus indicating the good quality of our results and the suitability of both approaches to treat these systems.

CONCLUSIONS

In this work we have calculated the rovibrational and spectroscopic constants for dimers and cross-dimers formed by C₆₀, C₇₀ and C₈₄. The current theoretical predictions are expected to be useful in the future experimental investigations.

ACKNOWLEDGMENTS

The authors are grateful for the support given from UEG, UnB, CAPES, CNPQ and FAPEG.

¹ H.W. Kroto, J.R. Heath, S.C. O'Brien, R.F. Curl, and R.E. Smalley, *Nature* **318**, 162 (1985).² H.W. Kroto, *Nature* **329**, 529 (1987).³ H.W. Kroto and D.R.M. Walton, *Chem. Phys. Lett.* **214**, 353 (1993).⁴ M.R. Peterson and A.A. Quong, *Phys. Rev. Lett.* **74**, 2319 (1995).

On the fluxional behavior of [CpMn(CO)₂(σ-alkane)] complexes

Rodrigo Silva Bitzer (PQ), Marco Antonio Chaer Nascimento (PQ)

*Laboratório de Química Teórica e Modelagem Molecular, Instituto de Química,
Universidade Federal do Rio de Janeiro, Brazil
e-mail: rodrigoitzer@gmail.com*

Keywords: manganese, sigma complex, fluxionality, DFT.

INTRODUCTION

The coordination chemistry of alkanes has been widely discussed since the 1970s.¹ Though counterintuitive, alkane complexes have been proposed as unstable intermediates in a number of organometallic transformations.¹ Spectroscopic evidence and crystallographic data have shown that alkane complexes exhibit C-H σ bonds coordinated to metal centers.^{1,2} In effect, fundamental questions concerning the structures and properties of σ-alkane complexes, including their fluxional behavior toward rapid exchange of geminal or vicinal protons, are still challenging.^{2,3} In this work, we have performed a DFT study of the fluxional behavior of [CpMn(CO)₂(σ-CH₄)] (**1**) and [CpMn(CO)₂(σ-C₂H₆)] (**2**).

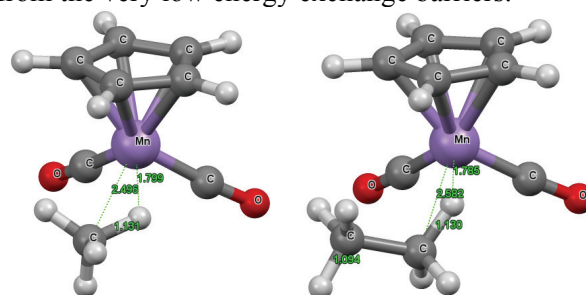
COMPUTATIONAL DETAILS

All calculations have been carried out in the gas phase at the DFT B3PW91-D3/LACV3P**++ level using Jaguar 7.9.⁴ This functional has been chosen because it provides reliable geometries and binding energies for σ-alkane complexes.⁵

RESULTS AND DISCUSSION

IR and NMR spectroscopic pieces of evidence support the formation of σ-alkane complexes from UV photolysis of [CpMn(CO)₃] in liquid alkane.^{2,3} However, a detailed investigation of the structures of [CpMn(CO)₂(σ-alkane)] complexes is lacking.⁶ Methane coordinates to Mn according to the η²-C,H mode (**Figure 1a**). Ethane exhibits two modes upon coordination to Mn, namely η²-C,H and η¹-H (**Figure 1b**). η¹-H-2 is 0.9 kcal/mol less stable than η²-C,H-2. Coordinated C-H bonds are ca. 0.04 Å longer than the uncoordinated ones. According to **Table 1**, all structures exhibit close values for the ν(CH) and ν(CO) vibration modes. η²-C,H-1 and η²-C,H-2 have similar calculated alkane binding enthalpies (ΔH_{bind}): 10.5 and 12.6 kcal/mol, respectively. Calculated ΔH[‡] values for

the exchange of geminal protons are 0.57 (η²-C,H-1) and 0.95 (η²-C,H-2) kcal/mol. They show that the fluxional behavior of both **1** and **2** results from the very low energy exchange barriers.

**Figure 1.** Structures obtained for η²-C,H-1 and η¹-H-2.**Table 1.** Vibrational frequencies (cm⁻¹) calculated for [CpMn(CO)_n] (n = 2 or 3), **1** and **2**.^a

Complexes	ν(CH) _{coordinated}	ν(CO)
[CpMn(CO) ₂]	-	2075, 2017 (1961, 1893)
[CpMn(CO) ₃]	-	2117, 2050 (2035, 1955)
η ² -C,H-1	2644	2066, 2012 (1972, 1908)
η ² -C,H-2	2599	2064, 2010 (1968, 1901)
η ¹ -H-2	2686	2064, 2011

^a Experimental frequencies at 298 K are given in brackets.³**CONCLUSIONS**

This work contributes to the current knowledge of the structure and thermodynamics of [CpMn(CO)₂(σ-alkane)] complexes.

ACKNOWLEDGMENTS

CAPES, CNPq, and FAPERJ.

¹ C. Hall, R. N. Perutz, Chem. Rev., 96, 3125, (1996).² R. D. Young, Chem. Eur. J., 20, 12704, (2014).³ O. Torres et al., Chem. Sci., 6, 418, (2015).⁴ Jaguar, version 7.9, Schrodinger, LLC, New York, NY, 2011.⁵ B. Chan, G. E. Ball, J. Chem. Theory Comput., 9, 2199, (2013).⁶ E. A. Cobar et al., Proc. Natl. Acad. Sci. U.S.A., 104, 6963, (2007).

Theoretical studies of adsorption on the surface of zeolite ZSM-5

Costa, R. J.¹ (PG), Martins, J. B. L.¹ (PQ), Politi, J. R. S.¹ (PQ), Castro, E. A. S (PQ)².

¹ UNB – Universidade de Brasília. (LQC) Laboratório de Química Computacional. (IQ) Instituto de Química. CP 4478. CEP 70904-970. Brasília-DF, Brazil.

² UEG – Universidade Estadual de Goiás, Câmpus Formosa. Rua Nagib Simão S/N. Setor Nordeste 3807250. Formosa-GO, Brazil
e-mail: rogerquim@gmail.com

Keywords: Ab initio calculation, zeolite ZSM-5, Interaction on surface

INTRODUCTION

Chemical reactions involving solid-gas interfaces or solid-liquid are important for varied purposes such as the production of non-renewable resources, materials processing, enhancement of modern technologies, energy production, environmental maintenance and natural resources¹. The potential of these materials is governed by the electronic and structural characteristics of bulk and their surfaces and the interaction with these molecules adsorbed on them. Understanding the process, describe the reaction mechanisms occurring on their surfaces and get control of products can provide important insights for understanding and development of new devices². In the early 1970s, researchers at Mobil synthesized zeolite ZSM-5 (Zeolite Socony Mobil) and found their catalytic properties in hydrocarbon synthesis³. Electronic and structural properties of solids, as the interaction of their surfaces with adsorbent molecules studied can be by electronic structure calculations.

METHODS

Theoretical calculations and relaxation geometries with DFT (Density Functional Theory) method with B3LYP (Becke, three-parameter, Lee-Yang-Parr) 6-31G* based function, PM6 (Parametric Method 6) and MM (Molecular Mechanics) using ONIOM (Our own N-layered Integrated Molecular Orbital and Molecular Mechanics) combining PM6/DFT, PM6/MM, MM/DFT on ZSM-5 zeolite models with 288 atoms (Figure 1-a). A specific pore diameter (Figure 1-b) was chose to be the interactions of molecules of ethanol and calculating the interaction energy in the adsorption process.

RESULTS AND DISCUSSION

The geometry models of ZSM-5 can modify distance values and bond angles between atoms at

the end of the convergence calculations. The relaxation of the whole molecule ZSM-5 is not feasible due to the large number of atoms, thereby starting the method using ONIOM treatment of the system with semi-empirical method or molecular mechanics and the other with DFT can be good results. The interaction of ethanol molecules in optimized designs then provide the information on the catalytic reactivity of aluminosilicate as adsorption energies, bond distances among others.

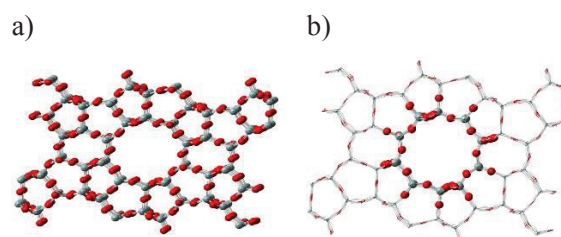


Figure 1. Zeolite ZSM-5 model (a) and specific Pore of adsorption (b).

CONCLUSIONS

Theoretical calculation ab initio of optimization using ONIOM facilitate convergence due to partial treatment of the system. The ethanol interactions in a specific pore of the ZSM-5 model can used to identify and represent the active site of the molecule via data such as bond distances and energies.

ACKNOWLEDGMENTS

The authors are grateful for the support given from the FAPDF, CAPES, CNPQ.

¹ M. Bjørgen; S. Svelle. *J. of Catalysis*, 249, 195–207, (2007).

² J. B. L. Martins, *et al.* *J. of Quantum Chem.*, 112, 3223-3227, (2012).

³ A. M. Christiansen and G. Mpourmpakis. *ACS Catalysis*, 3, 1965–1975, (2013).

Insight into the Spontaneity of Hydrogen Bond Formation between Formic Acid and Phthalimide Derivatives

Rogério V. A. Júnior (IC), Nathália B. D. Lima (PG), and Alfredo M. Simas (PQ)

Departamento de Química Fundamental, CCEN, UFPE, 50590-470 - Recife, PE, Brazil.

Keywords: hydrogen bond, QSPR, phthalimide derivatives

INTRODUCTION

Phthalimide derivatives have been demonstrated to reduce serum cholesterol and serum triglycerides¹ and, as a result, had several of their possible derivatives synthesized with their hypolipidemic activities determined. This set of derivatives also comprise a convenient test set for the study of the multiple factors involved in the energetics of hydrogen bond formation.

Accordingly, we carried out quantum chemical calculations on the hydrogen-bonded complexes formed between a sample of phthalimide derivatives with formic acid (Fig. 1) with the intent of identifying the most important electronic and structural factors related to how their strength and spontaneity vary across the series.

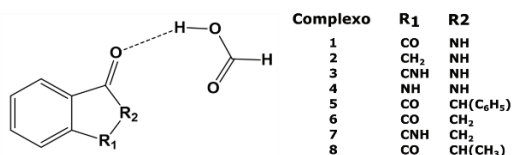


Figure 1. Hydrogen bonded complexes.

METHODS

All eight complexes considered are indicated in Fig. 1. All isolated molecules and possible interaction arrangements have been considered and had their geometries fully optimized at the DFT B3LYP/6-31++G(d,p) level, followed by frequency calculations to determine their Gibbs free energies of hydrogen bond formation using Gaussian 2009. Atomic ZDO charges of both neutral and positively charged isolated phthalimide derivatives to be used in the quantitative structure property relationship part of this work have been computed using RM1.

RESULTS AND DISCUSSION

Our intent with this study was to identify which electronic and structural factors could be playing a role in the differentiation between the hydrogen bond formation Gibbs free energy across the phthalimide derivative series considered.

The most important property explaining the different Gibbs free energy of formation across the series was found to be an electronic property: the difference in the charge at the carbonyl oxygen between the neutral and cationic forms of the phthalimide derivatives, computed by RM1. This is related to the easiness of electron donation by the hydrogen bond acceptor.

The next relevant property was the number of hydrogen atoms that can function as hydrogen bond donors. Finally, the last explaining property was the number of oxygen atoms that can function as hydrogen bond acceptors.

A kernel partial least squares regression, KPLS, of these three variables on the Gibbs free energy of hydrogen bond formation is shown in Fig. 2.

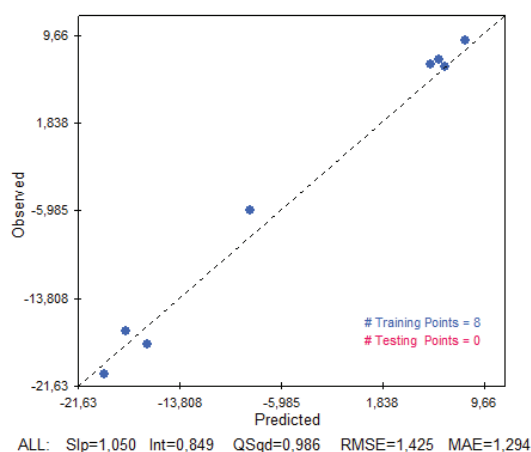


Figure 2. KPLS predicted and theoretical (Obs.) Gibbs free energies of hydrogen bond formation.

CONCLUSIONS

The easiness of electron donation by the hydrogen bond acceptor emerged as the most important property differentiating the spontaneity of hydrogen bond formation in these complexes.

ACKNOWLEDGMENTS

The authors acknowledge support from CNPq, PET-Química UFPE and FACEPE/PRONEX.

Characteristic behavior of carbonyl stretching IR absorption intensities

Wagner Eduardo Richter (PG), Arnaldo Fernandes da Silva (PQ), Roy Edward Bruns (PQ)

Institute of Chemistry, State University of Campinas, Campinas-SP, Brazil.

wagner.richter@iqm.unicamp.br

Keywords: IR intensities, characteristic group, QTAIM, CCFDF, CCTCP.

INTRODUCTION

Vibrational frequencies are readily related to chemical groups and therefore called spectroscopic fingerprints. Infrared intensities, on the other hand, do not show such a characteristic pattern for their numerical values. In this work, the IR intensities of the carbonyl stretches in mono and dicarbonyl molecules are studied using the QTAIM/CCFDF and QTAIM/CCTCP models. Our efforts were directed to understand why this fingerprint feature does not hold for the absorption intensities as for the frequencies.

METHODOLOGY

The theoretical methodology is described in more detail in recent reports by our group^{1,2}. Shortly, one can split the infrared intensity of any vibrational mode in terms of CCFDF contributions as presented in Eq. (1):

$$A_j = A_j^{(C^2)} + A_j^{(CF^2)} + A_j^{(DF^2)} + A_j^{(C \times CF)} + A_j^{(C \times DF)} + A_j^{(CF \times DF)} \quad (1)$$

Due to their high correlation, one can sum the CF^2 , DF^2 and $CF \times DF$ terms in a unique portion called *Charge Transfer-Counterpolarization*, and the $C \times CF$ and $C \times DF$ terms can be summed to form an interaction term:

$$A_j = A_j^{(C)} + A_j^{(CTCP)} + A_j^{(C \times CTCP)} \quad (2)$$

The results show how these two models can reproduce the infrared intensities of several carbonyl stretches with the advantage of a reliable physical interpretation for them.

RESULTS

Figure 1 and 2 summarizes the results obtained in this work for the CCFDF and CCTCP models.

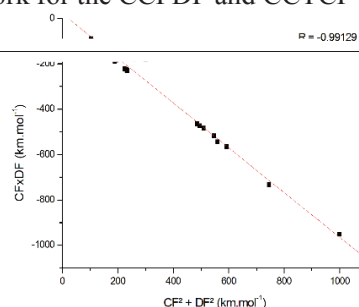


Figure 1. Correlation between the $CF^2 + DF^2$ and $CF \times DF$ yielding an almost perfect cancellation. The term CTCP (of the CCTCP model) is therefore almost null.

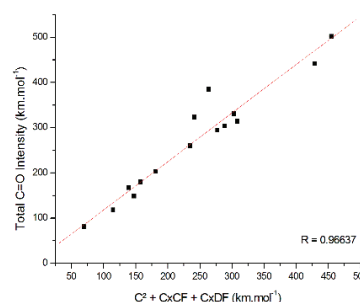


Figure 2. Correlation between the $C + C \times CF + C \times DF$ (on the CCTCP model: $C + C \times CTCP$) and the total intensity of the vibrational modes. The overall agreement is very good.

CONCLUSIONS

The results show that the intensity is widely dominated by the charge term, followed by the $C \times CP$ interaction, while the polarization itself is negligible in almost all cases. Even though the values of the intensities are not characteristic, their contributions behave in a characteristic way among the different molecules. Therefore, the contribution patterns can be visualized as characteristic for this kind of stretch, an unpublished result in the IR research field.

ACKNOWLEDGEMENTS

¹ AF Silva, WE Richter, RE Bruns. *PCCP*, 16, 23224, 2014.

² AF Silva, WE Richter, RE Bruns. *PCCP*, submitted.

Spectroscopic Constants and Rovibrational Energies of the Helium-Antihydrogen System: A Study by Discrete Variable Representation Method

Sandro F. Brito^a (PG), Daniel F. S. Machado^a (PG), Valter H. Carvalho^b (PG), Heibbe C. B. de Oliveira^a (PQ)

^a LMSC, Instituto de Química, Universidade de Brasília, 70919-970, Brasília, DF, Brazil.

^b QTEA, Universidade Estadual de Goiás, 75001-970, Anápolis, Brasil

Keywords: Helium-Antihydrogen, DVR, Rovibrational energies, Spectroscopic Constants

INTRODUCTION

Investigations in the spectroscopy field are intensively made to check CPT symmetry breakdown. This clearly shows the importance of theoretical spectroscopic predictions about the interaction of normal matter and antimatter. In an earlier work, Strasburger *et al*¹ determined the potential energy curve for the $\text{He}\bar{\text{H}}$ interaction in the ground state within the Born-Oppenheimer approximation. In this work we have calculated the rovibrational properties from the Strasburger and Chojnacki PEC (SC PEC) by solving the Nuclear Schrödinger Equation using Discrete Variable Representation Method. The current theoretical predictions are expected to be useful in the future experimental investigations.

METHODS

The rovibrational energies $E_{\nu,J}$ were obtained by solving the Nuclear Schrödinger Equation using the Discrete Variable Representation (DVR) method. Namely, we have evaluated ω_e , $\omega_e x_e$, $\omega_e y_e$, α_e and γ_e spectroscopic constants.

In this work, we have used four different analytical forms to represent the effective potential for the nuclei in motion: generalized Rydberg of sixth degree (Ryd6), Bond-Order of six degree (BO6) and the deformed versions of these potentials by imposing the d -Exponential function ($d\text{Ryd}6$ and $d\text{BO}6$) as well.

RESULTS AND DISCUSSION

Figure 1a shows both the $\text{He}\bar{\text{H}}$ Strasburger and Chojnacki (SC PEC) PEC and fitted PEC with $d\text{BO}6$ analytical function. Figure 1b presents the Rovibrational levels for the $\text{He}\bar{\text{H}}$ interaction obtained using $d\text{Ryd}6$ PEC to represent the effective potential.

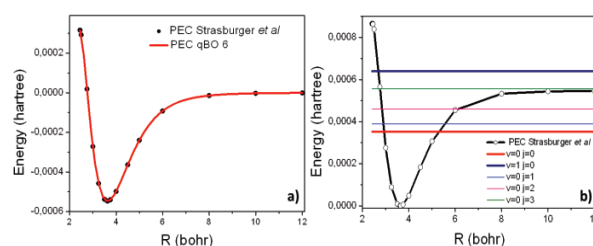


Figure 1. a) Fitted PEC using d-Bond Order as analytical form and b) Rovibrational levels obtained through the PEC described in a).

From this theoretical results, we found bounded states for $\nu = 0$ and $J = 0, 1$ and 2 in agreement with Ref. 2 where for rotational quantum numbers $J \leq 3$ bound states are feasible. The spectroscopic constants shows a fairly agreement independently of the analytical form employed: $\omega_e = 93 \text{ cm}^{-1}$, $\omega_e x_e = 23 \text{ cm}^{-1}$, $\omega_e y_e = 5 \text{ cm}^{-1}$ and $B_e = 5.7 \text{ cm}^{-1}$.

CONCLUSIONS

We found bounded states for $\nu = 0$ and $J = 0, 1$ and 2 in agreement with Ref. 2 where for rotational quantum numbers $J \leq 3$ bound states are feasible. The spectroscopic constants shows a fairly agreement independently of the analytical form employed. For the first time the spectroscopic constants for ordinary matter and antimatter interaction have been calculated and the results will provide a comparison source to further theoretical and experimental works.

ACKNOWLEDGMENTS

The authors are grateful for the support given from the CAPES and CNPQ.

¹ Strasburger, K. and H. Chojnacki. Phys. Rev. Lett., 2002, 88(16): p. 163201.

² Jonsell, S., et al. Phys. Rev. A, 2004, 70(6): p. 062708.

Efeitos Cooperativos Como Abordagem Alternativa ao Tunelamento Quântico no Entendimento do Rearranjo de Hidroximetileno a Temperaturas Ultrabaixas

Sara F. de A. Morais^{a*} (PG), Kleber C. Mundim^a (PQ), Davi A. C. Ferreira^a (PQ)

^a Instituto de Química, Universidade de Brasília, Campus Darcy Ribeiro, Brasília, DF.

*sfam777@gmail.com

Keywords: Efeitos Cooperativos, Rearranjo em Temperaturas Ultrabaixas, CBS-4M, NBO, QTAIM.

INTRODUÇÃO

Carbenos clássicos como o hidroximetileno (HM) apresentam alta reatividade e curtíssimo tempo de meia vida; por isso são espécies difíceis de se isolar. Schreiner e colaboradores¹ conseguiram isolar o hidroximetileno em matrizes de argônio a 11K. Eles observaram que, após a geração do HM, havia a formação de formaldeído e traços de CO e H₂ através de um rearranjo unimolecular de alta energia de ativação (E_a) atribuindo à este o fenômeno de tunelamento quântico. Neste trabalho aplicaremos o mesmo modelo de mecanismo alternativo para o rearranjo do HM, através de efeitos cooperativos e mudanças de molecularidade, que proporcionam uma drástica redução da E_a descrita por Ferreira e colaboradores².

MÉTODOS

Todos os cálculos foram realizados com o método CBS-4M no pacote Gaussian09 considerando o HM como simpleto e neutro. E para tratamentos dos dados de QTAIM foi utilizado o programa AIMAll.

RESULTADOS E DISCUSSÕES

Analisando a coordenada de reação do rearranjo unimolecular (Figura 1) observamos que a formação de formaldeído é cineticamente favorecida em relação a CO + H₂, com uma E_a de +29.06 kcal.mol⁻¹, energia indisponível a 11K. Aplicando o mecanismo bimolecular proposto por Ferreira e colaboradores² verificamos que o rearranjo acontece com uma E_a de -8.06 kcal.mol⁻¹ (Figura 2), essa E_a negativa indica que o processo é extremamente favorável e deve apresentar um complexo de van der Waals, que o antecede, com mais baixa energia, levando a uma E_a positiva menor que 1.0 kcal.mol⁻¹, inferior que a E_a de tunelamento que é 2.91 kcal.mol⁻¹. A análise NBO mostrou uma energia de deslocalização $n_C \rightarrow \sigma^*_{O-H}$ de 47.80 kcal.mol⁻¹ para o rearranjo bimolecular.

de ligação de hidrogênio que proporcionam a evolução por dupla e concertada transferência protônica. Ao contrário, nenhum caminho de ligação foi verificado na evolução unimolecular.

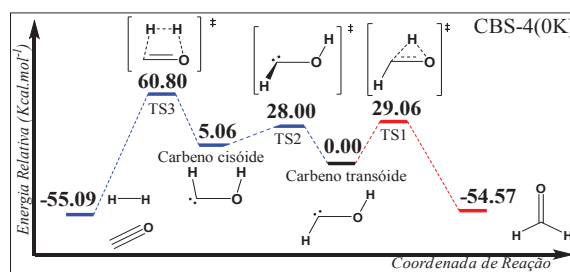


Figura 1. Coordenada de Reação Clássica

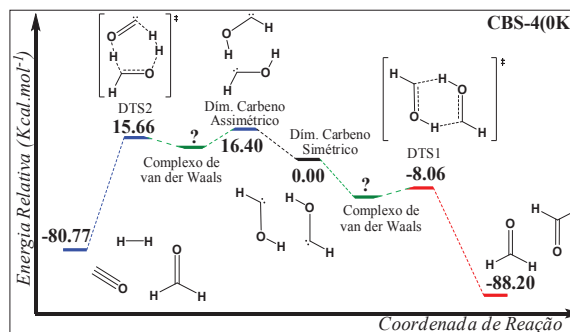


Figura 2. Coordenada de Reação do Modelo Proposto

CONCLUSÕES

Nosso estudo apontou que a formação de dímeros diminui drasticamente a E_a do processo, de modo que, em baixas temperaturas, o rearranjo é conduzido e favorecido pela entropia vibracional do sistema. Assim, a abordagem por efeitos cooperativos se mostrou mais pertinente para esse tipo de fenômeno que o tunelamento quântico.

AGRADECIMENTOS

CAPES, CNPq e IQ/UnB.

¹ P. R. Schreiner et. al., Nature Letters, 453, 906-909, (2008).

² S. F. de A. Morais, K. C. Mundim, D. A. C. Ferreira, Phys. Chem. Chem. Phys., 17, 7443-7448, (2015).

Investigação Teórica do Processo de Inclusão Envolvendo a Prilocaina e o Ácido *p*-Sulfônico Calix[6]areno

Sara Maria Ribeiro de Sousa (PG), Clebio Soares Nascimento Jr. (PQ)

LQTC: Laboratório de Química Teórica e Computacional, Departamento de Ciências Naturais,
 Universidade Federal de São João del-Rei, São João del-Rei, MG.

Email: sarasousa13@yahoo.com.br

Palavras chave: calix[*n*]arenos, complexos de inclusão, prilocaina.

INTRODUÇÃO

Calixarenos¹ podem atuar no encapsulamento de moléculas bioativas, tais como de anestésicos locais (AL) como a prilocaina² (PLC), gerando sistemas supramoleculares de liberação controlada. A PLC possui inúmeras vantagens farmacológicas, porém existe um produto de sua degradação que, quando em altas doses, pode induzir a metemoglobinemia. Além disso, a PLC apresenta baixa solubilidade em diversos solventes. Uma alternativa diante deste problema, que tem sido relatado na literatura, é a utilização de complexos de inclusão, os quais podem minimizar tais efeitos, possibilitando o desenvolvimento de novas formulações, porém com o mesmo princípio ativo³. Neste contexto, no presente trabalho realizou-se um estudo teórico do processo de inclusão molecular da PLC no ácido *p*-sulfônico calix[6]areno (aps-calix6). O objetivo que norteou este trabalho foi o de compreender, no nível molecular, o mecanismo e fatores que influenciam a formação de tais complexos, bem como suas propriedades físico-químicas.

METODOLOGIA

Os cálculos de otimização de geometria e de frequências harmônicas foram realizados em nível semi-empírico PM3. Foram realizados cálculos de energia no ponto utilizando Teoria Funcional da Densidade – BLYP/6-31G(d,p). Para a avaliação do efeito do solvente utilizou-se o método implícito PCM. Foram propostos dois modos de inclusão: Modo A: inserção da parte aromática da PLC na coroa superior do aps-calix6 e o Modo B: inserção pela parte alifática da PLC. Os complexos de inclusão foram estudados considerando a razão molar 1:1.

RESULTADOS E DISCUSSÕES

Os principais resultados deste trabalho encontram-se sumarizados na Figura 1 e Tabela 1.

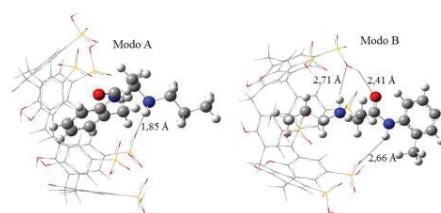


Figura 1. Estruturas otimizadas dos complexos de inclusão aps-calix6...PLC: Modo A e Modo B.

Tabela 1. Propriedades energéticas calculadas para os processos de formação dos complexos aps-calix6... PLC em dois modos de inclusão distintos.

	Gasoso		Aquoso	
	$\Delta E_{(elet-nuc)}$	ΔG	$\Delta E_{(elet-nuc)}$	ΔG
aps-calix6...PLC - Modo A	-11,03	3,26	-6,95	7,35
aps-calix6...PLC - Modo B	-12,02	1,65	-8,78	4,90

Os valores estão em kcal.mol⁻¹ e foram calculados a 298,15K e 1atm.

De acordo com os dados termodinâmicos ilustrados na Tabela 1, percebe-se que os valores de energia de interação (ΔE), nas fases gasosa e aquosa, são ligeiramente menores para o Modo B, fato esse que pode ser explicado pelo número de ligações de hidrogênio formadas. Porém, analisando-se os valores das energias livre de Gibbs (ΔG) em fase gasosa e aquosa, pode-se confirmar que o complexo mais estável, de fato, é o aps-calix6...PLC Modo B.

CONCLUSÕES

Verificou-se no presente trabalho, por meio da metodologia sequencial BLYP/PM3, que o complexo aps-calix6...PLC - Modo B foi o mais estável devido fundamentalmente ao maior número de ligações de hidrogênio estabelecidas para esse sistema.

AGRADECIMENTOS

FAPEMIG, CAPES, CNPq, RQ-MG

¹CRAGG, P.J. *Supramolecular Chemistry*. 2010.

²ARANTES, L. M. *et al.*, *Mag. Reson. Chem.*, 2009, 47, p.757-763.

³CABEÇA, L. F. *et al.*, *Mag. Reson. Chem.*, 2011, 49, p. 295–300.

Investigation of Chemical Bonds of the Interactions Cation- π in Ruthenophanes

Sergio Emanuel Galembeck (PQ) and Renato Pereira Orenha (PG)

Departamento de Química, FFCLRP, Universidade de São Paulo, 14040-901, Ribeirão Preto - SP

Keywords: Cation- π Interaction, IQA, ELF, NBO

INTRODUCTION

The interaction between the cyclophanes and the metal cations is extremely relevant due, for example, be related the biomimetic catalysis, selectivity and transportation of ions, and molecular recognition.¹

METHODS

From of optimized geometry of $[\text{Ru}(\eta^6\text{-C}_{16}\text{H}_{16})(\text{NH}_3)_3]^{2+}$ with the BP86/def2-TZVP computational model containing ECP-28 for the Ru atom, the NBO, QTAIM, IQA and ELF methods were used to the analysis of electron density.

RESULTS AND DISCUSSION

In the first place, the geometry parameters of compound studied (Fig. 1) shows that the most nearly carbon atoms of Ru are C(10) and C(14), followed by C(11) and C(13) (Fig. 1). Already, C(9) and C(12) has the longest r(Ru-C) bond lengths.

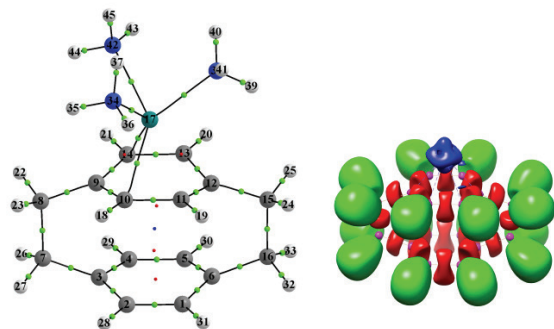


Figure 1. QTAIM topological map and 3D basins representation (ELF=0.721).

Furthermore, at the ELF method the delocalization index between the V(Ru) basins and V(C,C) disynaptic basins occurs involving, mainly, the C(10) and C(14) atoms (Fig. 1). However, the electron delocalization is more deep between the V[Ru,C(11)] and V[Ru,C(13)], monosynaptic basins localized nearly to C(11) and C(13), to V(Ru).

Besides, from of NBO method, the highest order second energy stabilization of structures arises of donation $\pi \text{ C-C} \rightarrow d_{\pi}$ or $d_z^2 \text{ Ru}$ (Fig 2.). Since it is important highlight that the main involved are C(10) and C(14), due the highest overlap between the natural bond orbitals.

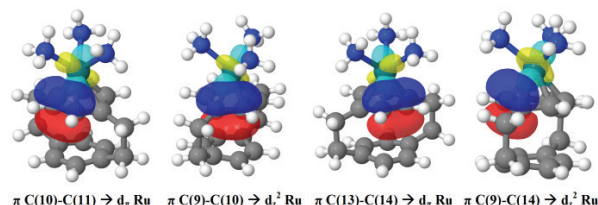


Figure 2. Main NBOs interactions (Isovalue=0.04).

Another point, the QTAIM method shows BCPs only between Ru and C(10) or C(14) (Fig. 1). Where, the negative and nearly to zero H(r) factor indicates that there is low covalent character for these chemical bonds.

Finally, the IQA method highlighted the interactions between Ru with C(11) and C(13) as the most stabilizers due mainly the lower values of inter-electronic and inter-nuclear repulsion than the showed by Ru with C(10) and C(14), despite of higher electrons-nuclei energies.

CONCLUSIONS

Therefore, the interactions between Ru with C-C occurs main from C(10) and C(14), but, the metal establishes more stable interactions with the electron density localized in C(11) and C(13).

ACKNOWLEDGMENTS

The authors thank CAPES/PROAP, CNPq (grants 481560/2010-6 and 304447/2010-2), and FAPESP (grants 2008/02677-0 and 2011/20351-7) by financial support, besides Ms. Ali Faez Taha by technical assistance.

¹ G. F. Caramori, L. C. Garcia, D. M. Andrada and G. Frenking, ORGANOMETALLICS, 33, 2301, (2014).

Solvent Effect on the Structure and Electronic Transition Energy of Enrofloxacin

Queiroz, Nayhara B. D. F. ^{a*} (IC), Alcantara, Isabella C. (IC)^b Garcia, M. V. R. (PG)^a, Preza, Sergio L. E. (PQ)^a, Amaral, Marcos S. (PQ)^a

^a *Laboratório de Modelagem Molecular, INFI, UFMS, Campo Grande, MS - *e-mail: nayharaqueiroz@gmail.com*

^b *Laboratório de Tecnologias Farmaceuticas, CCBS/Fármacia, UFMS, Campo Grande, MS*

Keywords: enrofloxacin, molecular dynamics, solvation

INTRODUCTION

Antibiotics are natural or synthetic compounds able to inhibit growth or cause death of fungi or bacteria¹. The enrofloxacin (ENR), a fluoroquilona broad spectrum derived from nalidixic acid, is used in the treatment of various infectious diseases but especially in the treatment of urinary tract, respiratory system and skin diseases, and is intended for dogs, cats and poultry. We studied the ENR isolated in water in order to assess structural changes and interactions with the environment that affect its energy transition.

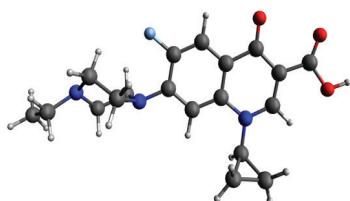


Figure 1 – Neutral 3D Enrofloxacin structure.

METHODS

The 3D structure of the neutral drug was optimized by Hartree-Fock method with basis 6-31G. The Molecular Dynamics (MD) was performed using the NAMD² software for 10ns with 1fs step, the temperature was 310K with NpT ensemble. Structural analyzes were made through the RMSD, RMSF and formation of hydrogen bonds. Finally the electronic transition energies were obtained using the computational package ORCA using ZINDO method. The experiments were made on Evolution 60-Thermo Scientific spectrophotometer at room temperature.

RESULTS AND DISCUSSION

In Figure 2, the RMSD graph (a) shows that the system has already been in equilibrium at the beginning of MD. By RMSF (b), we can observe the great mobility of atoms they do hydrogen bonds (HB), except O and N attached to aromatic ring, which have higher rigidity. This is important for

evaluation of the interaction with the solvent, monitored by HB graph between water and drug, where we observe the presence of at least 1 HB during MD and may be made up to 7 connections, but with low probability. The graph (d) show the curves of optical absorption of the drug at acidic pH (3.4) where the molecule is in its neutral state and also the transition energy graph for all frames MD. We can see that the maximum absorbance are not next between the experimental and calculated, possibly because it does not take into account the participation of water in obtaining energy electronic transition.

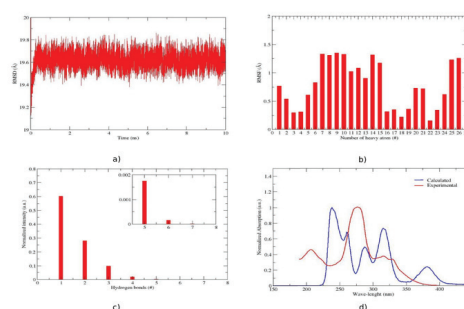


Figure 2 – RMSD(a), RMSF(b), HB(c) and Electronic Absorbance(d) graphs.

CONCLUSIONS

The molecule has in its neutral form, a low interaction with water, however, we believe that the micro-solvation of important regions of the structure can be critical for the electronic transition energies of the molecule. The next step is to do the same type of study to the charged form of the drug, which is found at physiological pH.

ACKNOWLEDGMENTS

The authors are grateful for the support given from the CNPq and FUNDECT.

¹ GUIMARÃES, Denise O., et al. *Quimica Nova*, v.33, n.3, p.667-679, 2010

² NAMD. <http://www.ks.uiuc.edu/Research/namd/>. [S.l.]: Technical report, 2015.

Computational Simulation of C60 Embedded in Amino Acid Ionic Liquids

Sidney R. Santana (PQ), Jefferson L. Medeiros (IC),
Dayse N. Moreira(PQ)

*Departamento de Ciências Fundamentais e Sociais, Centro de Ciências Agrárias,
Universidade Federal da Paraíba, Campus II, 58397-000, Areia, PB, Brasil.
email: santanasidney@cca.ufpb.br*

Keywords: Semiempirical Methods, Molecular Dynamics, Intermolecular Interactions.

INTRODUCTION

Nowadays, ionic liquids have been employed in the most wide applications in technological fields such as chemical industry, electrochemistry, optics, environmental chemistry, medicine and nanotechnology¹. These systems have been comprised by complexes ions maintained in an equilibrium between the electrostatic and sterical forces. Focusing a biotechnological development, amino acids have been used into such ionic liquids templates. So, amino acid ionic liquids (AAIL) have been attained a special attention in the scientific community by its possibility to be added to that landscape such as one more challenge in the developments in biosensors and biomaterials². In the other corner of this challenge, light fullerenes have been appointed such as a probably alternative to the development into biomedical fields, in particular, C60. But, its hydrophobicity is one of the great problems that have to be overcoming³. In this sense, this work explores a variety of computational methods to evaluate what is the most important chemical interactions between these two systems pledging to describe the limits of that forces.

METHODS

Molecular dynamics simulations using semiempirical methods have been employing in ten AAIL that has been chosen to make interactions with the same number of HSO₄⁻ anions with and without C60 using CP2K program⁴. The NVT ensemble was chosen to produce 10ps molecular dynamics with a timestep of 1 fs in the room temperature. The geometries has been optimized by each 10 fs.

RESULTS AND DISCUSSION

We found until 15 kcal/mol of difference in the energies formation of the pairs [AAIL+][HSO₄⁻], but until 75 kcal/mol in the conformational analysis energies variations, when we compare some conformers. During the molecular dynamics the snapshots have been showing the migration of groups to the C60 surface suggesting some chemical reactivity due a polarization of this kind of fullerene in the ionic liquids. During the simulation a huge H-bond network has been formed.

CONCLUSIONS

A complex H-bond network seem to be one the main factor of the structural stability. These structure is affected by the volume and number of these pairs the presence of C60. The C60 presented some polarization in the AAIL chemical environment turning it into a reactive specie in this medium following the trends pointed in the classical molecular dynamics of similar systems.³

ACKNOWLEDGMENTS

The authors are grateful for the support given from the UFPB, CAPES and CNPQ.

¹ R. Caminiti, L. Gontrani (Eds), *The Structure of Ionic Liquids*, Springer, New York, 2014;

² P. D. de Maria, *Ionic Liquids In Biotransformations And Organocatalysis*, John Wiley & Sons, New York, 2012;

³ E. E. Fileti, V. V. Chaban, *J. Phys. Chem. Lett.* 5, 1795, (2014).

⁴ J. Hutter, M. Iannuzzi, F. Schiffmann and J. VandeVondele, *WIREs Comput Mol Sci* 2014, 4, 15 (2014)., <http://www.cp2k.org>

OH radical initiated oxidation of the volatile organic compound 3-methyl-3-buten-1-ol under atmospheric conditions

Stella Maris Resende (PQ), Sara M. Ribeiro de Sousa (PG)

Laboratório de Química Atmosférica Teórica (LAQAT), Departamento de Ciências Naturais, Universidade Federal de São João del-Rei (UFSJ), São João del-Rei, Minas Gerais, Brasil.

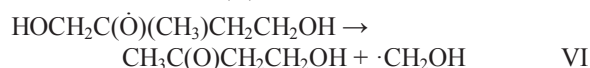
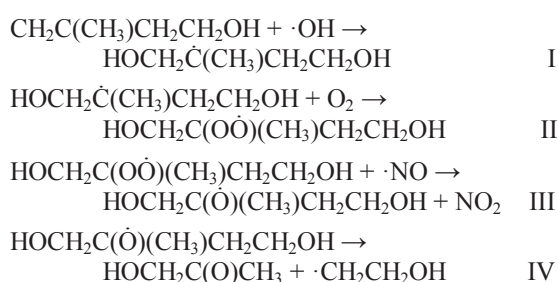
Keywords: ab initio, thermochemistry, atmospheric chemistry, VOC

INTRODUCTION

Unsaturated alcohols are important constituents of the volatile organic compounds (VOC) emissions. Products of its atmospheric decomposition can lead to the formation of secondary organic aerosols, which are involved in the climate regulation of the planet. The reactions of a lot of unsaturated alcohols with the atmospheric oxidants OH, NO₃ and Cl have been studied, but investigations about mechanism or product determination are scarce, because these reactions generate several intermediate radical whose decomposition can occur in several steps. In this way, performing a thermochemical study may be useful to determine the viability of possible steps before a kinetic investigation. In this work, we have investigated the thermochemistry of the atmospheric decomposition of the 3-methyl-3-buten-1-ol by ·OH radical, considering several steps of reaction.

METHODS

All species were optimized and frequencies calculations were done at the MP2/cc-pVTZ level of theory. Single point calculations were done at the MP2/cc-pVDZ, MP2/cc-pVQZ and CCSD/cc-pVTZ levels in order to achieve the limit for an infinite basis set function and a better accuracy to the electron correlation. In this way, our best level of calculation is CCSD/CBS. Based on mechanisms proposed to similar reactions, the following reaction steps were considered:



RESULTS AND DISCUSSION

The enthalpies and Gibbs free energies of reaction for the six steps investigated are presented in Table 1. Steps I to III are exothermic and spontaneous. Considering that they are consecutive, we can say that this sequence of steps will be exothermic and spontaneous too. Steps IV to VI represent different possibilities of decomposing the radical HOCH₂C(·O)(CH₃)CH₂CH₂OH and they are competitive. Although the three steps being spontaneous, only the Step IV is exothermic, indicating that it may be preferential.

Table 1. Reaction enthalpies and Gibbs free energies for the reaction steps investigated.

Step	ΔH _r / kJ mol ⁻¹	ΔG _r / kJ mol ⁻¹
I	-116.4	-75.2
II	-127.5	-74.5
III	-17.1	-20.7
IV	-2.8	-60.8
V	16.5	-37.8
VI	30.7	-33.7

CONCLUSIONS

The thermochemistry of the first steps of the reaction of atmospheric decomposition of the 3-methyl-3-buten-1-ol with ·OH radical was investigated theoretically. Our results show that steps I to III can be occur consecutively. Concerning considering the competitive steps (IV to VI), only step IV is thermodynamically feasible. Kinetic studies are in progress.

ACKNOWLEDGMENTS

The authors are grateful to FAPEMIG and CNPq.

Kinetic Analysis of the 2,5-Dimethylfuran Combustion Chemistry

Suelen S. da S. F. Pessanha (IC), Alessandra Rohr Fernandes de Amorim (IC), Gladson de Souza Machado (PG), Glauco F. Bauerfeldt (PQ)

Departamento de Química, Instituto de Ciências Exatas, UFRuralRJ

Keywords: 2,5-Dimethylfuran, Combustion Chemistry, Rate Analysis, Sensitivity Analysis, Kinetic Simulation

INTRODUCTION

Biofuels, which can be obtained from renewable and abundant resources, have received much attention. Several molecules can be produced from biomass, however furan derivatives have received special attention.¹⁻³ Among these, 2,5-dimethylfuran (DMF) is a promising substitute for gasoline in a future scenario. A systematic study assessing the combustion profile of DMF and comparison with other typical fuels is, therefore, necessary.

In this work, a combustion model for DMF is evaluated, through numeric simulations.

METHODS

The combustion model is based on an available mechanism,⁴ which consists of 1456 reactions (in a total of 2820 steps, considering the reversible reactions) and 274 species. The corresponding differential equations were numerically solved using the DVODE method available in the Kintecus ® software.⁵ Rate Analysis (RA) has been performed in order to identify the most important reactions to the initiation of the mechanism and to the ignition. Simulations have been performed varying the equivalence ratio ($\phi = 0.5$, $\phi = 1.0$ and $\phi = 1.5$), initial temperature (1300 – 1800 K) and total pressure (1 – 4 bar).

RESULTS AND DISCUSSION

An important parameter for the evaluation of a combustion profile is the ignition delay time. In this work, this parameter has been calculated as the maximum point in the curve representing the first derivative of the system temperature in relation to the time. Ignition times were found in the range from 70 – 1700 μ s, increasing as the temperature decreases, in an Arrhenius-like trend. Our results were also found in good agreement with experimental data.

It can also be noted that the ignition time decreases as the DMF concentration increases. Moreover, ignition time is also shown to decrease as the total pressure increases and as the equivalence ratio decreases.

From the rate analysis, the combustion is initiated, at 1×10^{-8} s, from unimolecular dissociation reactions leading to ring opening and H atoms formation. Hydrogen atoms further reacts with DMF via H-abstraction channels. The importance of these reactions increase with time and H-abstraction reactions are shown to be the dominant channels at around 5×10^{-6} s. Moreover, H-abstraction channels initiated by OH reactions with DMF are also found among the most important steps at instants close to the ignition time (5.6×10^{-4} s).

CONCLUSIONS

The good agreement of our simulated combustion profile and the experimental results support the adoption of this chemical model for further studies aiming the evaluation of DMF as a biofuel in specific engine conditions.

ACKNOWLEDGMENTS

The authors thank the support given from CAPES.

¹ B. Sirjean, R. Fournet, Phys. Chem. Chem. Phys. 15, 596–611 (2013).

² J. M. Simmie, W. K. Metcalfe, J. Phys. Chem. A. 115, 8877–8888 (2011).

³ K.P. Somers *et al.*, Combustion and Flame 160, 2291-2318 (2013).

⁴ B. Sirjean, R. Fournet, P-A. Glaude, F. Battin-Leclerc, W. Wang, M.A. Oehlschlaeger, J. Phys. Chem. A. 117, 1371–1392 (2013).

⁵ Ianni, James C., Kintecus, Windows Version 5.00, 2014, www.kintecus.com.

Second hyperpolarizability of the lithium salt of pyridazine calcium doped

Li–H₃C₄N₂...Ca

Suélcio Marques (PG), Marcos A. Castro (PQ), Salviano A. Leão (PQ),
 Tertius L. Fonseca (PQ)

Instituto de Física, Universidade Federal de Goiás, CP 131, Goiânia, Goiás 74001-970, Brazil

Keywords: Alkalide, Electride, Hyperpolarizabilities

INTRODUCTION

During the past twenty years a great deal of work has been carried out to study the nonlinear optical properties of many different types of materials. At molecular level, hyperpolarizabilities are the properties that govern nonlinear optical processes and, as such, much attention has been given to their evaluation.

A new class of compounds with excess electrons, called alkalides, have been synthesized experimentally. These compounds have attracted great attention due to their broad potential application in materials with nonlinear optical responses. It has been shown that the weakly bound excess electrons play a crucial role in the large values of the hyperpolarizabilities.

The main objective of this study is to provide information of the second hyperpolarizability lithium salt of pyridazine calcium doped Li–H₃C₄N₂...Ca, an alkalide molecule proposed by Wang et al.¹ with extraordinary value of the first hyperpolarizability.

METHODS

We have calculated the static and dynamic hyperpolarizabilities of the lithium salt electride calcium doped employing the coupled cluster quadratic and cubic response theories² implemented in the DALTON program at the SCF, CCS and CCSD levels. We did a study to get the most suitable basis set of functions to calculate the optical properties. The optimized basis set consists of the cc-pVTZ basis set augmented with some diffuse and polarization functions. Test calculations showed that f-type functions present in the original basis set are unnecessary, so they were removed in the final basis set.

RESULTS AND DISCUSSION

The static values computed at the CCSD level for the first and second hyperpolarizabilities were 1.52×10^4 au and 4.34×10^6 au, respectively. We calculate the second hyperpolarizability related to the dc-K effect at the SCF, CCS and CCSD levels and the results showed that there is a strong dependence of the computed values in relation to the correlation treatment. The computational cost to calculate the second hyperpolarizabilities related to the dc-SHG and THG nonlinear optical processes using the basis set optimized proved to be very large. To workaround this problem, we chose to use the expansion obtained by Bishop and De Kee³ in combination with the less expensive results obtained for the dc-Kerr and IDRI processes.

CONCLUSIONS

We realize that this molecule has a large value of second hyperpolarizability. A strong indication that this molecule can be used in nonlinear optical materials.

ACKNOWLEDGMENTS

The authors are grateful for the support given from the FAPEG, CAPES and CNPQ.

¹ Y.-F. Wang, J. Huang, L. Jia, and G. Zhou, *Journal of Molecular Graphics and Modelling* 47, 77–82 (2014).

² C. Hättig, O. Christiansen, P. Jørgensen, *Chem. Phys. Lett.* 282, 139 (1998).

³ D. M. Bishop and D. W. D. Kee, *Journal of Chemical Physics* 104, 9876–9887 (1996).

Molecular properties and spectroscopy along the phase diagram

Marcelo H. Cardenuto^a, Kaline Coutinho^a, Benedito J. C. Cabral^b, Sylvio Canuto^a (PQ)

^aInstituto de Física, Universidade de São Paulo, São Paulo/SP, Brazil

^bDepartamento de Química e Bioquímica, Fac. de Ciências, Universidade de Lisboa, Lisboa, Portugal

Keywords: Dielectric constant, Hybrid QM/MM method, normal and supercritical conditions, critical point

INTRODUCTION

The combination of quantum mechanics with molecular modeling is a powerful tool for studies of simple and complex liquids. In addition, it may also be used to study the spectroscopic and reactivity of molecules in solution, a situation that is germane in chemical laboratories. The understanding of the solvent effects is thus a major concern in the rationalization of experimental results.

METHODS

In the last two decades theoretical treatments have been developed to incorporate solvent effects. An important direction of research uses some sort of computer simulation to perform hybrid calculations. This is generally called QM/MM method, because both classical and quantum methodologies are employed. Conventional QM/MM methodology can be so costly that normally only a small fraction of the system is indeed treated by quantum mechanics. A systematic procedure based on a sequential Monte Carlo (or Molecular Dynamics) quantum mechanics (S-QM/MM) methodology has been developed in our group [1] that treats the solvent as an explicit liquid system. Different applications [2] have been made including absorption and emission spectra, NMR parameters, vibrational circular dichroism, chemical reactivity, etc. As long as the thermodynamic condition can be imposed this opens a large avenue for applications in other parts of the phase diagram. Hence, we have also addressed the technologically and environmental friendly condition of supercritical fluids.

RESULTS AND DISCUSSION

Several applications will be shown indicating the accuracy of the calculated results. In particular we discuss the structural aspects of supercritical CO₂ and its role on the

spectrum of para-nitroaniline as obtained from Born-Oppenheimer Molecular Dynamics[3].

More recently we have pointed our focus to the vicinities of the critical point. Theoretical studies of the critical behavior of fluids have been conducted mostly by universal scaling functions and renormalization theories. We have given the first explicitly calculated values of the dielectric constant in the close vicinity of the critical point ($T > T_c$). Thus, the behavior of the dielectric constant, only slightly above the critical point, is determined using first-principle quantum mechanical calculations for the first time. Our multiscale results[4] obtained by combining statistical mechanics and first-principle quantum mechanics indicate that the dielectric constant of Ar only 2K above T_c and around the critical isochoric (0.531 g/cm³) becomes density-independent (Fig. 1).

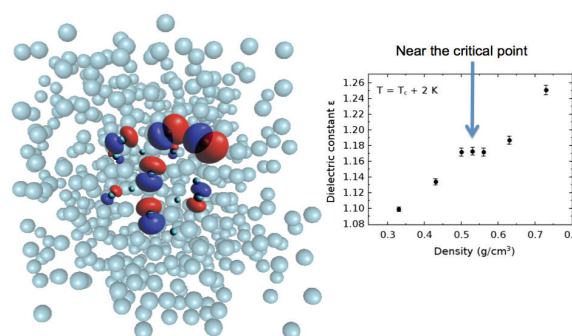


Figure 1. Change of the dielectric constant of Ar.

ACKNOWLEDGMENTS

The authors are grateful for the support given from the FCT in Portugal, BioMol/CAPES, CNPq and FAPESP in Brazil.

¹ S. Canuto, Ed., Solvation Effects on Molecules and Biomolecules. Computational Methods and Applications. Springer (2008).

² See S. Canuto home page: <http://gfmf.if.usp.br/>

³ B. Cabral *et al* 2015 *J. Chem. Phys.* 142, 024504.

⁴ M. Hidalgo *et al* 2015 *Phys. Rev. E.* 91, 032115.

Study of the Impact of the Central Atom on the Geometrical Parameters of Phthalocyanines

Tamires Lima Pereira^a (PG), Antonio Marcos Silva Santos^a (PG), Demétrio Antonio da Silva Filho^a (PQ)

^aInstitute of Physics, University of Brasilia, 70.917-970, Brasília, Brazil.

Keywords: Phthalocyanine, Structural-Properties relationships.

INTRODUCTION

In recent years, studies of phthalocyanines (Pcs) and its derivatives have attracted great interest because of their unique properties of this class of molecules. By varying the central atom (usually a metal), a variety of molecules have been designed for different applications in organic electronics. For example, Pc and its derivatives have been used in electrochromic display devices, organic light emitting diodes (OLEDs), organic photovoltaics (OPVs) and organic field effect transistors (OFETs). In this study, we analyzed the impact of the central atom on the geometrical properties of phthalocyanines. This study should shed light into the suitability of specific derivatives for a given technological application.

METHODS

We start by extracting the X-Ray geometries metallophthalocyanine (MePcs) molecules from Cambridge Structural Database (CSD). In order to speed up the theoretical calculations, we removed long alkyl chains by $-CH_3$ groups. We then use the Gaussian 09 program suite with the B3LYP/6-31G** method to compute the energy and optimize the geometry of such molecules.

RESULTS AND DISCUSSION

We show that the distance between the center metal atom of the molecule (Figure 1), taking the average between the inner four nitrogen atoms indicated that there was little or no change of this distance by optimization. This distance has been analyzed for a set of molecules before and after optimization. A careful analysis has also been performed to understand the impact of each atom on the structure of the Pc cage.

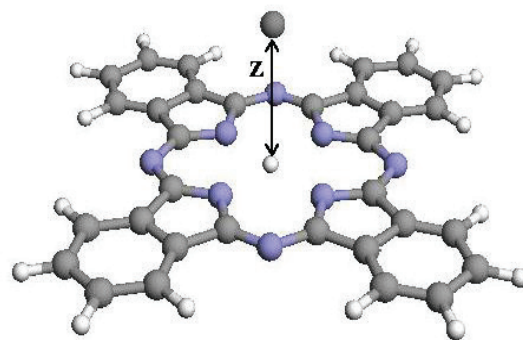


Figure 1. Distance central metal atom at the center of the phthalocyanine molecule.

CONCLUSIONS

In this work, we analyze the impact of the central atom of the geometry on the structural properties of phthalocyanines and its derivatives. Our preliminary results indicated that some central atoms deform quite drastically the geometry of the Pc molecule whereas others only mildly change its properties.

ACKNOWLEDGMENTS

The authors are grateful for the support given from the University of Brasília and from the Brazilian Research Councils CNPq and CAPES.

¹ Ruan, C., Mastryukov, V., Fink, M., Journal of Chemical Physics, 111, 3035-3041 (1999).

OH Addition Reactions to 1-pentene and 1-hexene: A Multi-Path Variational Transition State Study.

Tatiane Nicola Tejero (IC), Luís Gustavo de Moraes (IC), Glauco F. Bauerfeldt (PQ)

Departamento de Química, Instituto de Ciências Exatas, UFRuralRJ

Keywords: 1-pentene + OH Reaction, 1-hexene + OH Reaction, Variational Transition State Theory

INTRODUCTION

Hydroxyl radical addition reactions to alkenes is described by a mechanism taking into account the reversible formation of a π -type prebarrier complex (π -PC), followed by the addition steps, which can lead to different products, considering the addition of the OH radical to each carbon atom at the double bond. Moreover, the π -prebarrier complex may also show distinguishable conformations, which refer to the upward or downward OH attack to the double bond.¹ The reactant itself may also show several conformers and the single mechanism described above may be attributed to each single conformer. The collection of the distinct mechanisms composes the so-called multi-path case.²

The central question is how important are the distinct mechanisms for the less abundant conformers to the description of the global kinetics? In this work, this question is first explored by examining two cases, the 1-pentene + OH and 1-hexene + OH reactions, aiming the prediction of accurate rate coefficients.

METHODS

The chemical reactions were studied at the DFT level, adopting the BHandHLYP functional and the aug-cc-pVDZ (ACCD) basis set. Theoretical calculations include geometry optimizations and vibrational frequencies and reaction paths calculations. Canonical variational rate coefficients were calculated in the range from 200 – 500 K.

RESULTS AND DISCUSSION

Molecular properties were predicted for each conformer of 1-pentene and 1-hexene and relative abundances, at 298 K, were calculated on the basis of the Boltzmann distribution.

For the most stable conformers, π -PC and saddle points (SP) were located at the

BHandHLYP/ACCD level. For instance, along the 1-hexene + OH reaction path, the prebarrier complexes lie 3.25 and 1.95 kcal mol⁻¹, below isolated reactant, for the upward and downward OH additions, respectively. Saddle points for OH addition to the central and terminal carbon atoms show relative energies 0.18 and 0.38 kcal mol⁻¹, respectively (upward OH addition) and 0.05 and 0.76 kcal mol⁻¹, respectively (downward OH addition). Similar values were obtained for 1-pentene + OH energy profile.

BHandHLYP/ACCD rate coefficients for both reactions have been calculated at 200 – 500 K, neglecting the contribution of the less stable conformers of the alkenes. Room temperature rate coefficients for 1-pentene + OH and 1-hexene + OH reactions are predicted as 1.25×10^{-12} and 9.04×10^{-13} cm³ molecule⁻¹ s⁻¹, respectively. These values are underestimated by 20 and 40 times, comparing to the experimental values.^{3,4}

CONCLUSIONS

The results obtained so far indicate that the BHandHLYP/ACCD level reasonably predicts the room temperature rate coefficients and a satisfactory picture of the reaction mechanism and energy profile has been achieved at this level of theory. Nevertheless, the contribution of other conformers may be important in order to achieve a better agreement with the experimental value, and such evaluation represents a work in progress.

ACKNOWLEDGMENTS

The authors thank CNPq.

¹ T. S. Barbosa *et al.* PCCP 17, 8714-8722 (2015).

² T. Yu, J. Zheng, D. G. Truhlar. J. Phys. Chem. A, 116, 297-308 (2012); J. Zheng, D. G. Truhlar, Faraday Discuss. 157, 59-88 (2012).

³ R. Atkinson, S. M. Aschmann, Int. J. Chem. Kin., 16, 1175-1186 (1984).

⁴ M. R. McGillen *et al.* PCCP, 9, 4349-4356 (2007).

Maghemita dopada com cobre (Cu- γ -Fe₂O₃) para aplicação em reações Fenton heterogêneo: estudo experimental e teórico

Teodorico Castro Ramalho* (PQ), Maíra dos Santos Pires (PG), Livia Clara Tavares Lacerda (PG), Telles Cardoso Silva (PG), Silviana Corrêa (PG), Francisco Guilherme Esteves Nogueira (PG), Eduardo Pereira da Rocha (PG), Mateus Aquino Gonçalves (PG).

Laboratório de Modelagem Molecular. Departamento de Química. Universidade Federal de Lavras, Campus Universitário. CEP 37200-000, Lavras-MG, Brasil

*teo@dqi.ufla.br

Palavras-chave: Maghemita, catálise, DFT

INTRODUÇÃO

Maghemita (γ -Fe₂O₃) é um mineral de forte caráter magnético, que apresenta uma estrutura espinélio inverso. Este material é utilizado em várias áreas, incluindo a catálise.¹ Suas propriedades físicas e químicas podem ser ajustadas mediante alteração dos íons metálicos inseridos na rede cristalina. Neste sentido, a dopagem com cobre (Cu) se mostrou promissora para catalisadores em reações de degradação de compostos orgânicos em reações Fenton Heterogêneo.² Tendo em vista a importância desse mineral para catálise, o objetivo deste trabalho é o estudo das propriedades estruturais e eletrônicas da maghemita dopada com Cu (Cu- γ -Fe₂O₃), além de propor seu mecanismo para degradação de H₂O₂ e geração dos radicais hidroxilas, espécies reativas em reações Fenton. Para isso, foram aplicadas técnicas experimentais, além de cálculos computacionais em condições periódicas utilizando o método DFT.

MÉTODOS

O material FeCu300 foi preparado pelo método dos precursores poliméricos a 300 °C.³ Os cálculos teóricos foram realizados em condições periódicas com o método DFT utilizando o funcional OPBE e função de base TZP no programa BAND. As superfícies da maghemita pura e dopada foram otimizadas no intuito de analisar a influência da substituição isomórfica do Cu na barreira de ativação.

RESULTADOS E DISCUSSÃO

Por DRX, a predominância da fase (Cu- γ -Fe₂O₃) foi observada por meio da caracterização pelo plano de índice (311). O parâmetro de rede $a = 8.33$ também confirma a presença da fase maghemita. Na Figura 1 está apresentado o mecanismo de degradação do H₂O₂ para os dois catalisadores (maghemita pura e dopada).

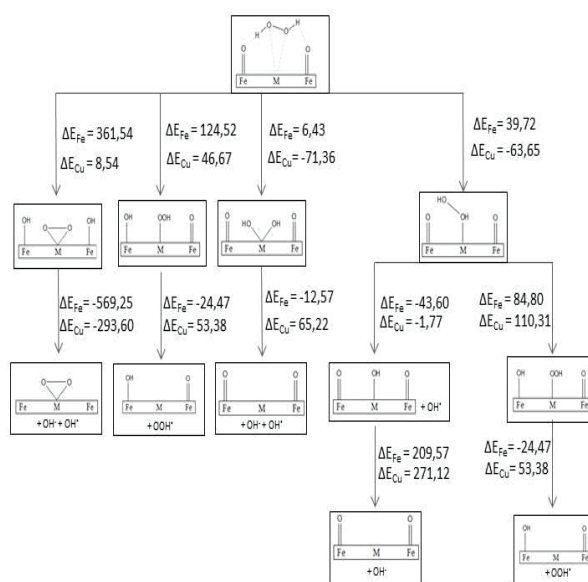


Figura 1. Mecanismo de degradação de H₂O₂ pelas superfícies, com valores de energia (Kcal/mol) para as respectivas etapas de formação dos intermediários. Sendo, M=Cu para catalisador dopado e M=Fe para catalisador puro.

CONCLUSÃO

A Cu- γ -Fe₂O₃ foi sintetizada com sucesso, permitindo análise satisfatória de DRX. Os valores de energia obtidos pelo mecanismo teórico apontaram que, a superfície modificada é mais promissora para aplicação em reações Fenton Heterogêneo se comparada à superfície pura.

AGRADECIMENTOS

CNPQ e CAPES.

¹Goulart, A.T.; et al. Phys. Chem. Miner. 1996, 25, 63.

²Romero, E.; Soto, R.; Durán, P.; Herguido, J.; Penã, J.A. Int. J. Hydrogen Energy. 2012, 37, 6978.

³Tu, H.; et al. J. Power Sources. 2011. 196, 3109.

Theoretical Study of the Mechanism of Co-Mutagenicity of AminoPhenylNorharman

Thayná Borges da Silva (IC), Alberto dos Santos Marques (PQ)

Universidade Federal do Amazonas, Laboratório de Tecnologia com Moléculas Bioativas, LTMB, Departamento de Química, Av. General Rodrigo Otavio, 6200, Coroado I, CEP: 69077-000, Manaus, AM, E-mail: marquesalbertods@gmail.com.

Keywords: Aminofenilnorharman, Co-mutagenicity, Norharmane, Aniline

INTRODUCTION

The aminofenilnorharman [9-(4'-amino-phenyl)-9H-pyrido[3,4-b]indol], APNH, is a new mutagenic, endogenous and probably carcinogenic *in vivo*, produced by the reaction of co-mutagenic norharman (9H-pyrido [3,4-b]indole), NH, with the aniline in *S. typhimutium* TA98 of S9-mix. The mechanisms of appearance of the mutagenicity of APNH¹ were analyzed using abinitio calculations of total energy, HOMO/LUMO energies, bond orders, and atomic charges. The calculations were made for the isolated molecule, and without taking into consideration the complex factors involved in biological activity, or the effect of the solvent. The analyzed molecules were: aniline and NH, and their derivatives produced by enzymatic reactions; APNH; and metabolites N-OH-APNH and NO-PNH.

METHODS

The SPARTAN10 program was used and for all calculations the crystallographic structures of molecules were used as input, and when necessary, the geometries of the molecules were optimized using Hartree-Fock method and 6-31G* basis function. The excitation energies were calculated using the Time-Dependent Density Functional Theory (TD-DFT), using B3LYP functional and 6-31G* basis function.

RESULTS AND DISCUSSION

The optimization of the geometry of APNH showed that the molecule is non-planar; NH was approximately perpendicular to the plane of the aniline. The higher order of aniline binding is (0.931), which corresponds to the C(4)-H(1) bond and that of NH is (0.842), which corresponds to the C(9)-H, bond and these are the atoms that are involved in the formation of APNH. The carcinogenic chemical agents are electrophilic species, their LUMO orbital must have a relatively low energy. Calculations of LUMO energies showed that the NH, APNH, and

metabolites are electrophilic species, but that aniline is not. For example, aniline is 0.25 eV; APNH, -0.89 eV; N-OH-APNH, -0.98; and NO-PNH, -2.85 eV; the latter two species are the most electrophilic. The atomic charges of APNH showed that the charge of N(3), which belonged to aniline, ranges from -0.791 to -0.432 in N-OH-APNH formation, and to -0,060 in NO-HNP formation. So it can be considered that there is formation of free radicals through the removal of the H atom from NH₂, from APNH, and from N-OH-APNH. The total energy of the molecules decreases in the following order: aniline>NH>APNH>N-OH-APNH>NO-NHP indicating that APNH has lower energy than its formers and that the metabolites may be intermediate species of the metabolism of APNH, because they are more stable than APNH.

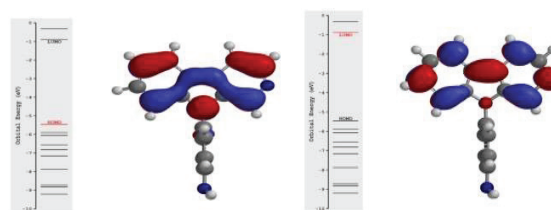


Figure 1. Optimized molecular structure of APNH: Left, HOMO; and Right, LUMO.

CONCLUSIONS

The results showed APNH does not have a planar structure; the electronic transitions are more localized in NH. The formation of the metabolites of APNH occurs in the N of aniline by the removal of H; which was justified by the analysis of the atomic charges, and of the bond orders, which have shown to be more electrophilic than APNH. The mechanism of co-mutagenicity of APNH is related to the enzymatic reaction of its formation and its metabolites.

ACKNOWLEDGMENTS

The authors thank the support given by FAPEAM and CNPQ.

¹ R. Nishigaki, et al., *Mutat. Res.* 562, 19, (2004).

Quantum Reactive Scattering Study of the $\text{Mu} + \text{Li}_2$, $\text{D} + \text{Li}_2$, and $\text{T} + \text{Li}_2$ Isotopic Reactions

Thiago F. da Cunha(PG), Henrique V. R. Vila(PG), Rhuigo Mendes de Oliveira(PG),
Geraldo M. e Silva(PQ), Ricardo Gargano(PG)

*Instituto de Física, Universidade de Brasília.
CP04455, Brasília, DF, CEP 70919-970, Brazil
gargano@unb.br*

Keywords: Isotopic reactions, potential energy surface, quantum reactive scattering, reactivity probabilities

INTRODUCTION

This work presents an exact quantum investigation of the reactive scattering process $\text{X} + \text{Li}_2 \rightarrow \text{LiX} + \text{Li}$, with $\text{X} = \text{D}$, T , and Mu in the ground state with total angular momentum equal zero. This study has been carried out with a developed potential energy surface (PES)[1], which has been fitted from the *ab initio* energies determined with a full CI calculation for the 6-311G(2df,2pd) basis set and also through a pseudo potential representing the Li atom.

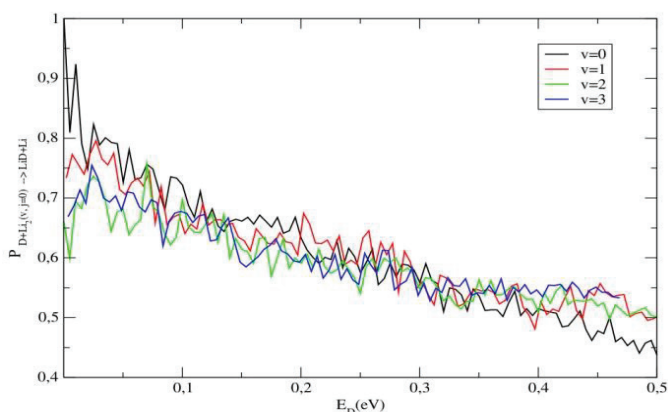
METHODS

Analytical representations of the $\text{X} + \text{Li}_2$ PES, with $\text{X} = \text{D}$, T and Mu , were obtained using a Bond Order (BO) polynomial expansion for both two and three-body terms, in agreement with the standard many-body method. Due to the fact that the considered reaction is highly exothermic (about 33.66 kcal/mol), a great number of rovibrational states and quadratures has been taken into account (even for low energies) in order to accurately describe its dynamical properties. The time-independent nuclear Schrödinger equation has been solved by means of the ABC program[2]. This code is ideally suited to calculating detailed state-to-state quantities - such as the state-resolved differential cross-sections - in which the quantum states of the reactants, as well as those of the products, are specified at the same time. ABC simultaneously expands the wave functions of all three possible chemical arrangements in the Delves hyper-spherical coordinate system.

RESULTS AND DISCUSSION

Reaction probabilities (RP) as a function of the translational energy of reactant (Deuterium) for

the purely rotational excitation of the molecule Li_2 (considered in the vibrational states $v=0, 1, 2$, and 3) are shown in the figure below. From this figure



one can note that the system's reactivity is higher when the Deuterium translational energy is low. The same trend was observed for the RP for the purely vibrational excitation of the molecule Li_2 . Furthermore, we observed that greater the reduced mass of the diatomic product, the greater the reactivity of the system. This result is consistent with the fact that the greater the mass of the diatomic product, the greater the ro-vibrational coupling states between reactant and product.

ACKNOWLEDGMENTS

The authors are grateful for the support given from the CAPES, CNPq and FINATEC.

¹ Maniero A. M., Acioli P. H., e Silva G. M., Gargano R. *Chemical Physics Letters*, v.490, p.123-126, (2010).
² Skouteris D., Castillo J. F., Manolopoulos D. E. *Computer Physics Communications*, v.133, p.128, (2000).

Challenges for the *ab initio* simulation of the spectra of large molecules: Absorption and fluorescence spectra of poly(p-phenylenevinylene) oligomers

Thiago Messias Cardozo^a (PQ), Adélia A.J. Aquino(PQ)^b, Mario Barbatti(PQ)^c, Itamar Borges Jr.(PQ)^d, Hans Lischka(PQ)^b

^a Instituto de Química, Universidade Federal do Rio de Janeiro, Avenida Athos da Silveira Ramos, 149, 21941-909 - Cidade Universitária - Rio de Janeiro, RJ, Brazil.

^b Dep. of Chemistry and Biochemistry, Texas Tech University, Lubbock, Texas 79409-1061, USA.

^c Max-Planck-Institut für Kohlenforschung, Kaiser-Wilhelm-Platz 1, D-45470 Mülheim an der Ruhr, Germany

^d Departamento de Química, Instituto Militar de Engenharia, Praça General Tibúrcio, 80, 22290-270 Rio de Janeiro, Brazil.

Keywords: PPV, photovoltaics, spectra simulation, ADC(2)

INTRODUCTION

Poly(p-phenylenevinylene) (PPV) oligomers (Figure 1) are widely studied as model systems for electroluminescent and photovoltaic material design. Most *ab initio* studies have focused on the smaller PPV oligomers, due to the rapidly increasing computational cost along the oligomer series.

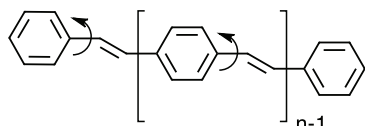


Figure 1. Structure of (PV)_nP oligomers

In this work, we tackle the problem of simulating spectra for these large molecules with *ab initio* methods. We show that obtaining a qualitatively correct description of the spectra of these species becomes feasible with a judicious selection of model, basis set and approximations.

METHODS

Ground state calculations were done at the RI-MP2 level, and excited state calculations with the RI-ADC(2) level, with both SV and SV(P) basis set. The spectra were simulated with the nuclear ensemble method. Electronic structure calculations were done with the TURBOMOLE 6.5 program and the spectra simulations were carried out with the NEWTON-X program.

RESULTS AND DISCUSSION

The simulated spectra show a trend of decreasing photon energy along the series. The

shapes of the spectra are quite close to available experimental data¹, but the predicted photon energies are considerably higher. This difference can be attributed to a number of effects which can be independently estimated.

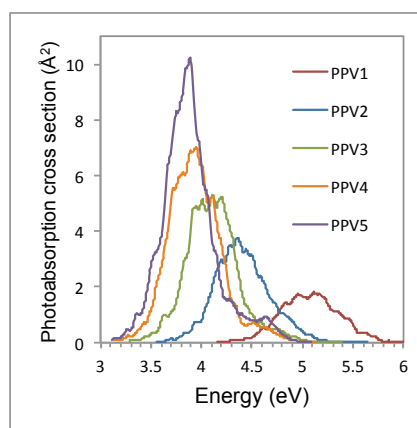


Figure 2. Absorption of (PV)_nP oligomers

CONCLUSIONS

The simulated spectra are shown to reproduce some important features and trends of the experimental spectra. The differences in the photon energy can be independently estimated.

ACKNOWLEDGMENTS

The authors are grateful for the support given from CAPES.

¹ Rauscher, U.; Bassler, H.; Bradley, D. D. C.; Hennecke, M. Phys Rev B, 42, 9830, (1990)

Substituent Effect in the Mesoionic Ring on Optical and Electric Properties of Mesoionics Compounds

Thiago O. Lopes^a (PG), Grazielle S. Pereira^a (PG), Guilherme R. de Oliveira^b (PQ), Heibbe C. B. de Oliveira^a (PQ)

^a LMSC, Instituto de Química, Universidade de Brasília, 70919-970, Brasília, DF, Brazil.

^b LQSA, Instituto de Química, Universidade Federal de Goiás, 74001-970, Goiânia, Brasil.

Keywords: Mesoionic rings; MP2 Calculation; TD-DFT.

INTRODUCTION

Material science has given great attention to a new type of organic material class called mesoionic compounds. The interest in this type of materials is due to their photoluminescence, conductivity, low cost, faster optical response, greater versatility, ability to adjust their structure according to their nonlinear optical property and optical nonlinear susceptibility comparable to other conventional materials. In a previous paper, Simas *et al.*¹ reported a semi-empirical investigation for a series of mesoionic compounds varying the atoms in the mesoionic ring. Emphasis was dedicated to analyzing the second hyperpolarizability results. The main goal of this work is to study the effect of substituents on the electric and optical properties of these molecular systems. To achieve this goal, we have used highly accurate *ab initio* and DFT methods.

METHODS

The mesoionics rings studied in this work were generated from the variation of atoms O or S in positions R₁, R₂ and R₃ of Figure 1. We have followed the same nomenclature adopted by Simas *et al.*¹

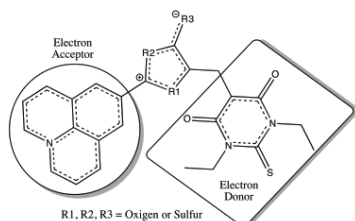


Figure 1. Structures of push-pull compounds with (a) mesoionic ring bridges generated from varying O and S atoms in R₁, R₂ and R₃ positions.

For all compounds, the geometries were fully optimized at the MP2/6-31G(d) level of theory. Dipole moments, linear polarizabilities and first hyperpolarizabilities were calculated numerically using the Field Finite (FF) method at the MP2/6-31+G(d) level. Simulated absorption spectra were obtained at the TD-PBE1PBE/6-311+G(2d,p) level. All calculations were performed in gas phase and DMSO as solvent (implicit treatment).

All calculations were performed using the G09 suite of programs.

RESULTS AND DISCUSSION

Figures 1-3 show results for Band Gap, dipole moment and wavelength of maximum absorption for all mesoionic compounds calculated in gas phase and in solvent as a medium.

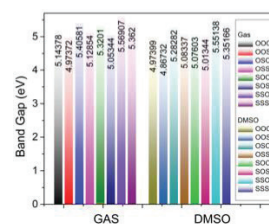


Figure 2. Band gaps values for all mesoionic compounds studied in this work.

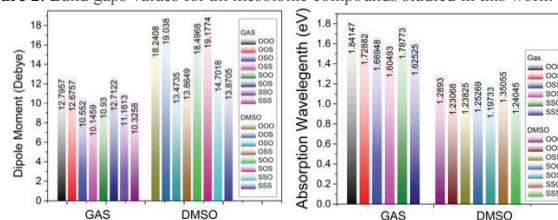


Figure 3. Dipole moments (left) and wavelength of maximum absorption (right) of mesoionics Rings.

From these Figures, we can note a huge dependency of molecular properties as a function of the effect of the substituents in the mesoionic ring.

CONCLUSIONS

In summary, a series of mesoionic compounds had their electronic properties calculated. MP2 and TD-DFT calculations revealed very interesting features of the new structures, allowing a rational design of a candidate to be applied in nonlinear optics technologies.

ACKNOWLEDGMENTS

The authors are grateful for the support given from UFG, UnB, CAPES, CNPQ, FAPDF and FAPEG.

¹ SILVA, Andréa M. S. et al.; **J. Braz. Chem. Soc.**, São Paulo, v. 16, n. 3b, p. 583-588, June 2005.

Relaxation of Optically Excited States of p-Nitroaniline

Valdemir Ludwig (PQ) and Zélia M. da Costa Ludwig (PQ)

Universidade Federal de Juiz de Fora (UFJF), ICE, Dep. de Física; Brasil.

Keywords: Intersystem crossing, Para-nitroaniline,

INTRODUCTION

The photophysics of para-nitroaniline (PNA) has been extensively studied by experimental techniques¹. The most intense absorption band of PNA was composed by a HOMO-LUMO charge transfer transition. Two strong bands were observed in gas-phase, the first 4.24 eV and the second absorption band at 5.66 eV². The intramolecular charge transfer makes this transition very susceptible to the solvent polarity. In water, the maximum was located at 3.25 eV, a shift of about 1.0 eV. Another characteristic feature is the absence of fluorescence; instead, a very fast nonradiative process is proposed, on which the lowest-lying triplet state is populated, via an intersystem crossing, and phosphorescence emission³ is observed. In this work, we examine the photoinduced processes of PNA in the gas phase and in water by theoretical calculations.

METHODS

Ground and excited states (singlets and triplets) potential energy surfaces were computed as function of the $-\text{NO}_2$ torsional coordinate. The DFT method, with the B3LYP functional, and 6-31G(d,p) basis sets were employed to calculate the ground state geometries. The non-equilibrium vertical excitation energies in gas phase and water were computed at the TD-B3LYP/NE-IRFPCM/6-31++G(d,p) level of theory.

RESULTS AND DISCUSSION

Figure 1 displays the potential energy surfaces computed as function of the torsional angle in water solvent. It suggests that the vertical excitation leads to the first excited state H-L (S1), which evolves barrierless to an ISC with the T2 state, in a region characterized by a nuclear configuration with the $-\text{NO}_2$ at 90°. From that, the T1 state is populated via a crossing between the T2 and T1 state, giving rise to the observed phosphorescence.

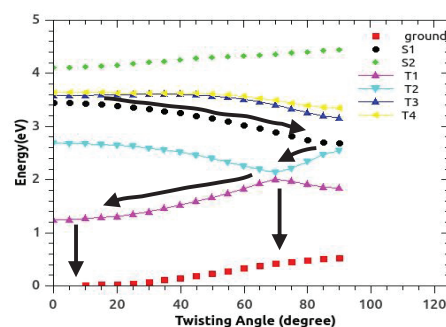


Figure 1. Potential energy surfaces for the ground and excited states: singlets (S1, S2) and triplets (T1, T2, T3 and T4) in water.

CONCLUSIONS

The photophysical events of PNA in water have been investigated by using the DFT/PCM method. The contributions of the hydrogen bonding on the electronic structures of PNA have also been studied. The solvation stabilizes the charge-transfer excited state, which becomes the S1 state. With these results, we propose a photophysical mechanism to explain the phosphorescence observed experimentally.

ACKNOWLEDGMENTS

The authors are grateful for the support given from the FAPEMIG and CNPQ.

¹ A. M. Moran and A. M. Kelley, *Journal Chemical Physics*, 115, (2001), 912-924.

² S. Millefiori, G. Favini, A. Millefiori, and D. Grasso, *Spectrochim. Acta Part A*, 33 A, (1977), 21 – 27.

³ W. Schuddeboom, J. M. Warman, H. A. M. Biemans and E. W. Meijer, *J. Phys. Chem.* 100, (1996), 12369-12373.

Estudo Teórico das bases catalíticas β -isocupreidina e Quinidina na Reação Assimétrica Morita-Baylis-Hillman

Verônica M. Nascimento¹(PG), Renan S. Galaverna²(PG), Gabriel Heerdt²(PG), Marcos N. Eberlin²(PQ), Fernando Coelho²(PQ), Ataulpa A. C. Braga¹(PQ)

¹Instituto de Química – USP. Av. Prof. Lineu Prestes, 748 - Butantã - São Paulo - SP

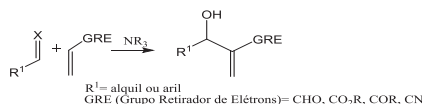
²Instituto de Química – UNICAMP. Caixa Postal 6154 – Campinas, SP-CEP:13083-970

*veronica@iq.usp.br

Keywords: Morita-Baylis-Hillman, DFT, regioseletividade.

INTRODUÇÃO

A reação Morita-Baylis-Hillman (MBH), ilustrada no Esquema 1, apresenta muitas vantagens como método sintético, dentre elas as mais relevantes são sua natureza organocatalítica¹. É uma reação de condensação entre carbonos eletrofílicos sp^2 , geralmente um aldeído, e a posição α de uma olefina contendo grupos retiradores de elétrons (GRE), catalisada por uma amina terciária ou fosfina, levando à formação de uma nova ligação σ C-C, juntamente com um novo centro estereogênico.



Esquema 1: Escopo geral da reação MBH.

O objetivo deste trabalho é investigar os diferentes rendimentos enantioméricos entre os catalisadores β -isocupreidina (β -ICD) e quinidina na reação MBH, observadas experimentalmente.

MÉTODOS

Todas as otimizações estão sendo realizadas com aplicação do GAUSSIAN 09. Os cálculos sob nível M06-2X/6-31+G(d,p)², incluindo na otimização o efeito do solvente através do método de solvente contínuo SMD.

RESULTADOS E DISCUSSÕES

Os estudos se basearam em uma busca conformacional, em dimetilformamida, dos reagentes acrilato de 1,1,1,3,3,3-hexafluoroisopropila (HFIPA), *p*-nitrobenzaldeído, β -ICD, quinidina e dos conformeros da reação. Na Figura 1 estão apresentadas as geometrias dos estados de transição (ET) dos mesmos estereoisômeros com β -ICD e quinidina na etapa de adição aldólica.

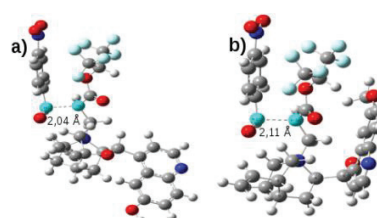


Figura 1: Geometria dos ETs dos enolatos Z com centros enantioméricos S (carbono do enolato) e R (C do aldeído). a) β -ICD, e b) Quinidina.

Observa-se nas geometrias dos ETs uma grande diferença na disposição dos anéis aromáticos das bases catalisadoras, o que pode ser entendida pela menor liberdade de rotação da β -ICD com relação à quinidina. O estudo desse mecanismo de reação ajuda a entendermos melhor os dados experimentais, onde foi obtido cerca de 91% de rendimento enantiomérico na presença da base β -ICD, enquanto que, ao se usar quinidina, obteve-se uma mistura racêmica.

CONCLUSÃO

A rigidez dos anéis aromáticos do catalisador β -ICD pode ser um dos fatores que influencia na alta enantiosseletividade observada experimentalmente. As ferramentas da química computacional podem levar à avanços na compreensão do mecanismo de reações assimétricas MBH.

AGRADECIMENTOS

CNPQ, LCCA/CENAPAD e ao processo 2015/01491-3 (FAPESP)

1. P. Verma; R.B. Sunoj; *Org. Biomol. Chem.* **2014**,12, 2176-2179.
2. Y. Zhao, D. G. Truhlar, *Theor. Chem. Acc.* **2008**.120, 215-241.

Theoretical Study on Electron Collisions with Dimethyl Disulfide

Victor A. S. da Mata^a (PG) and Gabriel L. C. de Souza^a (PQ)

^aFederal University of Mato Grosso, Department of Chemistry, 78060-900 Cuiabá-MT, Brazil
E-mail: victorssantana.93@hotmail.com

Keywords: Electron Scattering, dimethyl disulfide, Cross Sections

INTRODUCTION

Disulfide bridges (*RS-SR*) can be formed in some metabolic processes. It is known that the cleavage of a given bond can be induced by electron interaction via different mechanisms.¹ In order to understand the physical phenomena that occurs in electron-biomolecules interactions, one needs to know the quantities associated to the cleavage process initiated by the electrons interacting with building blocks, e.g., the electron-molecule (*e⁻-molecule*) cross sections for a wide energy range.

In this work, we computed several *e⁻-molecule* cross sections, in the 1-300 eV energy range, for a molecule that can be a good prototype for studying large biochemistry systems: the dimethyl disulfide (DMDS). More specifically, Differential and Integral cross sections (DCS and ICS, respectively) for elastic scattering, as well as Momentum Transfer and Total Absorption cross sections (MTCS and TACS, respectively) were probed.

METHODS

The present study made use of a complex optical potential given by:

$$U_{\text{int}} = U_{\text{st}} + U_{\text{ex}} + U_{\text{cp}} + iU_{\text{ab}}$$

In our calculation, static (U_{st}) and exchange (U_{ex}) potentials are derived directly from a Hartree-Fock SCF target wavefunction. The parameter-free model potential introduced by Padial and Norcross² is used to account for correlation-polarization (U_{cp}) contributions while the model potential developed by Lee *et al.*³ is used for describing the absorption effects (U_{ab}). With the referred interaction potential, the scattering equations are solved iteratively using the Padé's approximant method, as in the manner described by Lucchese *et al.*⁴

RESULTS AND DISCUSSION

In Fig. 1 we show our calculated Differential Cross Sections (DCS) for elastic *e⁻-DMDS* scattering at 100 eV along with experimental data taken from Sugohara *et al.*⁵ Unfortunately, there is no experimental data available in the literature for the molecule of interest. Thus, experimental results for the isoelectronic molecule, tetramethylsilane (TMS), are presented for comparison purposes.

Computed results of *e⁻-DMDS* DCS present similar trend to what is observed in the case of the measured *e⁻-TMS* DCS. In addition, the DCS magnitudes are practically the same for all the angular region covered by the measurements.

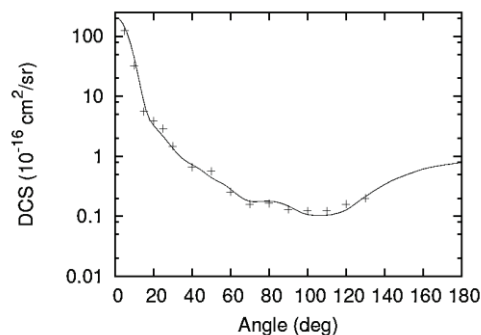


Figure 1. DCS for elastic scattering at 100 eV. Solid line: Present results for *e⁻-DMDS*; Crosses: Experimental data from Sugohara *et al.*⁵ for *e⁻-TMS*.

CONCLUSIONS

This work can aid to fulfil the existent lacuna on *e⁻-DMDS* collisions. Up to our knowledge, there are no experimental or theoretical study on *e⁻-DMDS* scattering in a wide energy range available in the literature. Provided results can be useful for basic and/or applied issues in the future. Additional results will be presented at the Conference.

ACKNOWLEDGMENTS

The authors thank CAPES and CNPq.

¹ L. Sanche *et al.* Science, 287, 1658 (2000).

² N. T. Padial and D. W. Norcross. Phys. Rev. A, 29, 1742 (1984).

DMBE potential energy surface for the $1^2A'$ excited state of the ClO_2 system

Vinícius C. Mota^a (PQ), Osvaldo B. M. Teixeira^b (PQ), José Manoel Garcia de la Vega^b (PQ)
and António Joaquim de Campos Varandas^c (PQ)

^a Departamento de Física, Universidade Federal do Espírito Santo

^b Departamento de Química Física Aplicada, Universidad Autónoma de Madrid

^c Departamento de Química, Universidade de Coimbra

Keywords: global potential energy surfaces, multiconfigurational calculations, basis set extrapolation

INTRODUCTION

Since Cl_xO_y molecules have been suggested to play an important role in the ozone depletion, a significant amount of experimental data have been gathered, followed by several theoretical studies, mostly focusing on investigating the kinetics of the $\text{Cl}+\text{O}_2$ and $\text{O}+\text{ClO}$ reactions as well as of the ClOO and OCIO fragmentation mechanism¹⁻⁵. Given the atmospheric relevance of ClO_2 and lack of similar work, we have recently published⁴ a global Double Many-Body Expansion⁶ (DMBE) potential energy surface (PES) for its ground state based on multireference *ab initio* data jointly with Complete Basis Set (CBS) extrapolation⁷. In the sequence the DMBE PES has been employed for studying the $\text{O}+\text{ClO}$ reaction mechanism⁵, with the results showing significant discrepancy with the available experimental data. It has been suggested⁵ that the reaction dynamics calculations would be missing the $\text{ClO}_2(1^2A')$ contribution, which may be as important as the ground state for the theoretical rate of reaction. However, a global PES for the $\text{ClO}_2(1^2A')$ system is not available. In this presentation we report the steps towards the construction of a global DMBE⁶ PES for the $\text{ClO}_2(1^2A')$ system based on multireference *ab initio* data jointly with CBS extrapolation⁷.

METHODS

Global PESs are of central importance to an accurate description of chemical reactions within the Born-Oppenheimer formalism⁶. To obtain them we start by mapping the relevant part of the configuration space via high level multiconfigurational *ab initio* methods⁸ employing correlated consistent basis sets⁹ jointly with accurate CBS extrapolation schemes⁷. The data is thenceforth modeled using the well known DMBE theory⁶, which allows for the proper treatment not only of the interaction region of the configuration space but also of all the long range properties relevant for the title system. As usual in

DMBE theory, accurate Potential Energy Curves (PECs) are obtained first and used to provide the triatomic energy points, which are fitted in order to ensure also a perfect merging of the PES with the PECs at the asymptotic limits. The final DMBE PES therefore provides not only an accurate description of any relevant stationary states but also of all long range forces involved, making them specially suitable for reaction dynamics and spectroscopic calculations.

RESULTS AND DISCUSSION

Ab initio calculations have been performed at the multi-reference configuration interaction (MRCI)⁸ level of theory, using the full valence complete active space self-consistent method (CASSCF) and cc-pVXZ (X=T,Q) basis sets⁹ to model the PES for the $1^2A'$ state of the ClO_2 system. The computed *ab initio* energies for the diatomics ClO and O_2 were extrapolated to the CBS limit using an appropriated correlation scaling formalism⁷. Then, the corresponding PECs were calibrated within the DMBE formalism¹. For the triatomic grid data we also start by extrapolating the obtained energy points to the CBS⁷, resulting in approximately 2000 geometry points covering all the chemically relevant regions of the PES including the atom-diatom limits. In order to take into account the correct long-range behavior of the $\text{ClO}_2(1^2A')$ PES, the main electrostatic contributions involving dipole and quadrupole interactions have been included for both $\text{Cl}-\text{O}_2$ and $\text{O}-\text{ClO}$ channels. To properly model the data for the title system we follow the DMBE theory and treat the 3-atom term separately, ensuring both an accurate fit and the proper merging of the PES with the PECs at the asymptotes, as required for any accurate reaction dynamics calculations to be performed using the PES.

CONCLUSIONS

The global form is still on its preliminary shape, and we hope to report soon the most

Absorption Spectra Shift of Tetrasubstituted Phthalocyanine due to Dimerization: evaluation of the environment

Vinicius Fernandes (IC), Maurício D. Coutinho Neto (PQ), Paula Homem-de-Mello (PQ)

ABCSim – Centro de Ciências Naturais e Humanas, UFABC – Santo André – SP – Brazil
fernandes.vinicius@aluno.ufabc.edu.br, mauricio.neto@ufabc.edu.br, paula.mello@ufabc.edu.br

Keywords: Phthalocyanine, Dimerization, Photodynamic Therapy, DFT, COSMO.

INTRODUCTION

Researches in PDT (photodynamic therapy) are very broad, and covers theoretical and experimental approaches, with emphasis on the physical and chemical investigation of new compounds. Within the variety of chemical families, some phthalocyanines are already approved to use, as the drug Photosens® employed for the treatment of skin and endobronchial lesions^{1,2}. In this work, we simulated a phthalocyanine tetrasubstituted and also complexed with Zn⁺² using (TD)DFT to investigate the changes at aggregation energy by sliding, stacking, and rotation of monomers to form dimers, and the respective influence in the light absorption behavior.

METHODS

The first step was to optimize the geometry of ZnPcOH (Fig. 1) molecule in gas-phase with BLYP/def2SVP methodology.

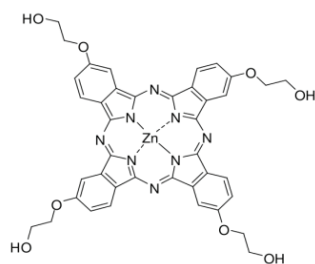


Figure 1. Phthalocyanine structure of ZnPcOH.

To build the potential-energy curves for the interaction between monomers we performed unrelaxed scans of sliding, rotation, and stacking in gas-phase. The aggregation energy (ΔG_{Agg}) was calculated using the thermodynamical cycle of monomer (M) desolvation, dimer (D) formation, and dimer solvation in DMSO using implicit method COSMO.

$$\Delta G_{\text{Agg}} = 2\Delta H_{\text{gf}} + \Delta G_{\text{DMSO}}(\text{D}) - 2\Delta G_{\text{DMSO}}(\text{M})$$

The absorption spectra were obtained by means of TD-DFT at the most favorable geometries of dimers.

RESULTS AND DISCUSSION

Geometry optimization of monomers lead to planar structures. Table 1 displays the aggregation energy (ΔG_{Agg}) for the first proposed dimer.

$2\Delta H_{\text{gf}}$	$\Delta G_{\text{DMSO}}(\text{D})$	$2\Delta G_{\text{DMSO}}(\text{M})$	ΔG_{Agg}
-0,14766553	-0,05773955	-0,08171583	-0,04197342

Table 1. Thermodynamical cycle for ZnPcOH optimized dimer (Δ in a.u.).

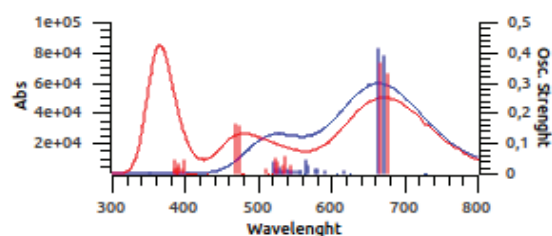


Figure 2. Shift in ZnPcOH absorption spectra due to the dimerization. Red line is monomer absorption and blue is dimer absorption.

CONCLUSIONS

The results confirm the experimental evidence of dimerization due to the coupling of the inner phthalocyanine rings, and the expected disadvantage of dimerization caused by DMSO interactions. These values are welcomed for comparison between the thermodynamic states. Aggregation has a negative effect on B band, making it non-absorptive, and intensifies the Q band absorption.

ACKNOWLEDGMENTS: FAPESP, CNPq and CAPES.

¹ ALLISON, R. R. et al. *Photodiagnosis and photodynamic therapy*. 1, 27-42. 2004;

² OLIVEIRA, T.K. et al. *J. Org. Chem.* 74, 7962-5. 2005.

A Theoretical Model for Chiral-Induced Spin Selectivity

Vladimiro Mujica

Department of Chemistry and Biochemistry, Arizona State University

The striking experimental observation that organic chiral molecules can act as electron spin polarizers, despite the fact that this type of behavior is usually associated with atoms with large atomic number, has received considerable attention. The experimental observation has been made in a variety of electron energy regimes, namely in photoemission and STM, and it is very robust, indicating a fundamental process that is intimately related to the combined effect of molecular chirality and an enhancement of spin-orbit interaction.

In this contribution I will discuss the current status of the theory, particularly the explicit connection between spin polarization and electron transmission^{1,2,3,4,5}, which is crucial to explain the experimental observations that the longitudinal polarization depends on the number of turns of helical molecules and the existence of spin selection.

References

- (1) Sina Yeganeh, Mark A. Ratner, Ernesto Medina and Vladimiro Mujica
 “Chiral Electron Transport: Scattering Through Helical Potentials”
 J. Chem. Phys. 131 (2009) 014707.
- (2) Ernesto Medina, Floralba López, Mark A. Ratner and Vladimiro Mujica
 “Chiral Molecular Films as Electron Polarizers and Polarization Modulators”
 EPL, 99 (2012) 17006
- (3) Rosenberg, Richard; Symonds, Joshua; Kalyanaraman, Vijayalakshmi; Markus, Tal; Orlando, Thomas; Naaman, Ron; Medina, Ernesto; López, Floralba; Mujica, Vladimiro
 "Kinetic Energy Dependence of Spin Filtering of Electrons Transmitted Through Organized Layers of DNA"
 J. Phys. Chem. C 117 (2013), 22307-22313
- (4) S. Varela, E. Medina, F. López and V. Mujica
 “Inelastic Electron Scattering From a Helicoidal Potential: Transverse Polarization and the Structure Factor in the Single Scattering Approximation”
 J. Phys: Cond. Matte. 26 (2014) 015008
- (5) Ernesto Medina, Luis A González-Arraga, Daniel Finkelstein-Shapiro, Bertrand Berche, Vladimiro Mujica, “A Continuum model for chiral induced spin selectivity in helical molecules”, arXiv preprint arXiv:1501.06201. To appear in Journal of Chemical Physics.

Atomic decomposition of carbonyl stretching IR absorption intensities

Wagner Eduardo Richter (PG), Arnaldo Fernandes da Silva (PQ), Roy Edward Bruns (PQ)

Institute of Chemistry, State University of Campinas, Campinas–SP, Brazil.
wagner.richter@iqm.unicamp.br

Keywords: IR intensities, atomic contributions, QTAIM, CCFDF, CCTCP.

INTRODUCTION

The description of a molecular property in terms of its constituent parts, the atoms, is the ultimate desire of almost all chemists. In this work, we report an atomic decomposition of infrared intensities for the carbonyl stretch in a set of several mono and dicarbonyl compounds, looking for trends in their contributions and novel interpretations of the vibrational phenomena.

METHODOLOGY

The general methodology is described in recent reports¹ and is essentially a matrix transformation from the APT's Cartesian space to the normal coordinate space, for each atom in the molecule individually. This transformations yields N (the number of atoms) terms which can be related with effective charges. Those terms can be evaluated for each vibrational mode as well for the sum of all modes, being in this case closely related with the Crawford's G Sum Rule².

RESULTS

Table 1. Atomic contributions to the intensities plus their percentages of the total intensity.

Molecule	km.mol ⁻¹		%	
	C	O	C	O
F ₂ CO	337.0	89.6	76.2	20.3
Cl ₂ CO	208.6	104.8	66.4	33.4
Br ₂ CO	192.3	111.5	63.3	36.7
HF ₂ CO	184.3	74.8	70.9	28.8
HCICO	209.4	109.2	64.8	33.8
HBrCO	242.2	133.8	62.9	34.8
HCOOH	211.9	91.7	64.1	27.7
H ₂ CO ₃	323.7	110.6	64.5	22.0
CH ₃ COOH	186.4	84.3	63.4	28.7
Acetone	94.6	54.7	63.6	36.8
Acetaldehyde	97.6	54.7	65.3	36.6
Formaldehyde	56.7	34.4	69.9	42.3
Glycoaldehyde	77.2	46.7	65.2	39.5
Glyoxal	99.6	71.8	59.4	42.8
Methylglyoxal	108.6	74.9	60.3	41.6
Diacetyl	123.7	80.4	60.7	39.5

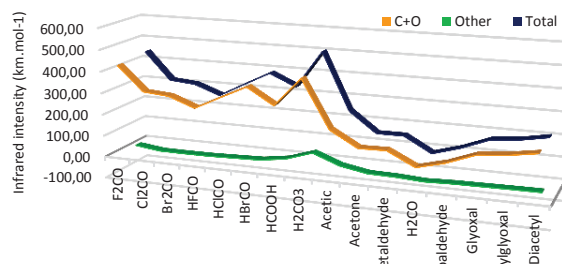


Figure 1. Carbon and oxygen intensities versus the total intensities of the mode (blue).

It is easily seen that almost all the infrared intensity of the carbonyl stretch is concentrated on the carbon and oxygen atoms. Figure 1 makes it very clear since the yellow line, representing the sum of the carbon and oxygen intensities closely follows the blue line (the total intensity). The green line, representing all the intensity allocated on the “other” atoms (all the atoms but C or O) is near zero in all cases except for the acids, where there is a reasonable concentration of intensities on the acidic hydrogens.

CONCLUSIONS

One can conclude that the atomic contributions to infrared intensities provide a very useful tool for interpreting vibrational phenomena. Even though the values of the contributions vary in a wide range for both carbon and oxygen atoms among the molecules, their proportions to the total intensity are remarkably constant; moreover, almost all the intensity is concentrated on these two atoms. These observations are general and the values of the proportions are just slightly affected by the chemical groups attached to the carbonyl in a way somewhat related to the electronegativity of those groups.

ACKNOWLEDGEMENTS

The authors thank FAPESP and CNPq for financial support, scholarships and a fellowship.

¹ AF Silva, WE Richter, RE Bruns, *PCCP*, submitted.

² WT King, GB Mast, PP Blanchette. *JCP* 56, 4440 (1972).

Estudo teórico da adsorção de gases leves nas MOFs SIFSIX-2-Cu e SIFSIX-2-Cu-i

Walber Gonçalves Guimarães Junior^a (PG), Guilherme Ferreira de Lima^a (PQ).

^aLaboratório de Química Computacional (LaQC) - Instituto de Física e Química, Universidade Federal de Itajubá, Av. BPS, 1303, Pinheirinho, Itajubá – MG CEP: 37500-903
juniorcavs@hotmail.com

Palavras-Chaves: Redes Metalorgânicas, Adsorção de gases leves, Ondas planas.

INTRODUÇÃO

Com a ação antropogênica, a concentração de gases estufa, na atmosfera, atingiu níveis jamais observados na história do planeta. Entre as medidas adotadas para a diminuição das concentrações estão as técnicas de captura e sequestro de gases. Materiais porosos com adsorção seletiva são de interesse para aplicações nessa técnica. Entre os materiais estudados, as estruturas metalorgânicas são bastante interessantes por terem grande área superficial, cerca de $3140 \text{ m}^2 \text{ g}^{-1}$. Dentro dessas, a família de materiais SIFSIX-2-Cu, a estrutura SIFSIX-2-Cu-i é a atual recordista na capacidade de adsorção de CO_2 .^[1] Esse trabalho tem como objetivo investigar a adsorção seletiva de CO_2 nesses materiais através de cálculos DFT com condições de contorno periódicas.

METODOLOGIA

A otimização estrutural de ambas as redes metalorgânicas foram executadas no programa PWscf usando o funcional PBE e ondas planas. A energia de corte das ondas planas e a malha de pontos k utilizadas foram determinadas através da avaliação da convergência de valores de energia de interação de alguns gases e de propriedades estruturais. Utilizou-se uma energia de corte de 50 Ry nas ondas planas e uma malha de $2 \times 2 \times 2$ pontos k na primeira zona de Brillouin.

RESULTADOS E DISCUSSÃO

A Figura 1 mostra a cela unitária da MOF SIFSIX-2-Cu. Os parâmetros de rede foram avaliados e mostraram bom acordo com os dados experimentais, com erros em torno de $0,2 \text{ \AA}$ (Tabela 1). Funções termodinâmicas relativas ao processo de adsorção são calculadas para avaliar os melhores sítios de adsorção do CO_2 e outros gases leves e serão apresentados.

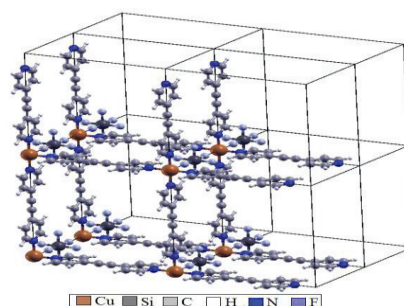


Figura 1. Estrutura otimizada da MOF SIFSIX-2-Cu.

Tabela 1. Comparação dos parâmetros de rede Experimental e Calculada em Angstroms (Å).

Parâmetros de rede	Experimental ^[2]	Calculada
<i>a</i>	13,633	13,748
<i>b</i>	13,633	13,748
<i>c</i>	7,970	8,305

Dados relativos à estrutura da MOF SIFSIX-2-Cu-i, bem como dados relativos à adsorção de gases em seu poro serão apresentados.

PERSPECTIVAS

Cálculos DFT com condições periódicas, são capazes de fazer uma boa descrição geométrica da MOF SIFSIX-2-Cu. Cálculos da energia de adsorção dos diferentes sítios permitirão compreender melhor o mecanismo de adsorção de gases leves nesses materiais.

AGRADECIMENTOS

FAPEMIG, CAPES, CNPq, PPGMQ-MG, RQ-MG e INCT-ACQUA.

¹ NUGENT, P. et al. *Nature*, (2013), Vol. 495.

² ZHEQUI, L.I. *Russian Journal of Applied Chemistry* (2014), Vol. 87.

Conformational Analysis of 1,2-Ethandiol through NBO, QTAIM and NCI Methods

Wesley G. D. P. Silva (G), Josué M. Silla (PG), Matheus P. Freitas (PQ)

^a Federal University of Lavras, Department of Chemistry, P.O. Box 3037, 37200-000, Lavras, MG.
wsilva@quimica.ufla.br

Keywords: Conformational analysis, 1,2-Ethandiol, NBO, QTAIM, NCI.

INTRODUCTION

The presence of intramolecular hydrogen bond (IHB) in vicinal diols has been studied by several groups and it is still under discussion.¹ Since 1,2-ethandiol (1,2-ED) is the simplest molecule containing vicinal hydroxyl groups, it can be an useful model for understanding the influence of hydrogen bond in the conformational equilibrium of this sort of molecules (Figure 1). Earlier studies showed that there is a *gauche* preference in 1,2-ED, which was assigned as due to IHB between the two hydroxyl groups, but this is not consensual.^{1,2} Based on the divergences among different investigations, the present work proposes the conformational analysis of 1,2-ED through NBO, QTAIM and NCI methods to investigate the presence of IHB.

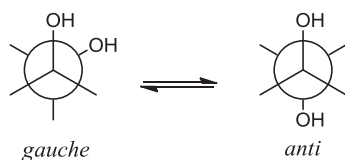


Figure 1. Conformational equilibrium of 1,2-ED.

METHODS

All 27 possible geometries of 1,2-ED were optimized at the B3LYP/6-311G++(d,p) level and frequency calculations were carried out to guarantee that imaginary frequencies were absent. NBO analysis were performed at the same level of theory in the gas phase and implicit DMSO, including deletion of all antibonding and Rydberg-type orbitals using the Gaussian 09 program. QTAIM analysis was carried out to search for possible hydrogen bonds using AIMALL program. Non-covalent interactions (NCI) method was performed using the NCIPLOT program.

RESULTS AND DISCUSSION

The optimization calculations confirmed the *gauche* preference for 1,2-ED both in the gas phase and implicit DMSO. According to NBO calculations, the *gauche* conformation is favored by hyperconjugation relative to the *anti* one by 9.3

(gas) and 14.9 kcal mol⁻¹ (implicit DMSO). However, such a stabilization was not found to be due to the $n_{\text{O}} \rightarrow \sigma_{\text{O-H}}^*$ interaction (IHB), but rather to antiperiplanar interactions usually invoked to explain the *gauche* effect ($\sigma_{\text{C-H}} \rightarrow \sigma_{\text{C-O}}^*$). QTAIM analysis did not show any bond-path between O...H(O), indicating the absence of IHB in 1,2-ED. On the basis of some controversial cases in the literature,² in which a BCP cannot be found in compounds where IHB is expected, the NCI method was applied. Figure 2 shows the NCI isosurface and the respective plot of RDG vs $\text{sign}(\lambda_2)\rho$. The isosurface shows a single circular volume between the two OH moieties due to the collapse of both regions of interaction in the intramolecular bonding and the plot illustrates the presence of two peaks. The peak on the negative sign represents attractive interactions (IHB), while the other belongs to repulsive interactions (ring formation). These interactions are nearly equivalent and, therefore, the overall result of the OH...OH approximation is an interaction neither attractive nor repulsive.

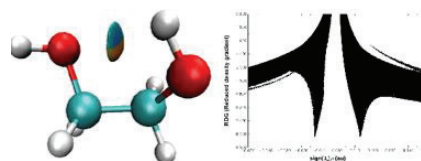


Figure 2: NCI isosurface and plot of RDG vs $\text{sign}(\lambda_2)\rho$ for 1,2-ED.

CONCLUSIONS

All three methods (NBO, QTAIM and NCI) converged to the same result with respect to the role of IHB as stabilizing force of the *gauche* conformation in 1,2-ED: it is absent or, at least, not strong enough to rule the conformational equilibrium of 1,2-ED.

ACKNOWLEDGMENTS

Authors are thankful to CNPq and FAPEMIG.

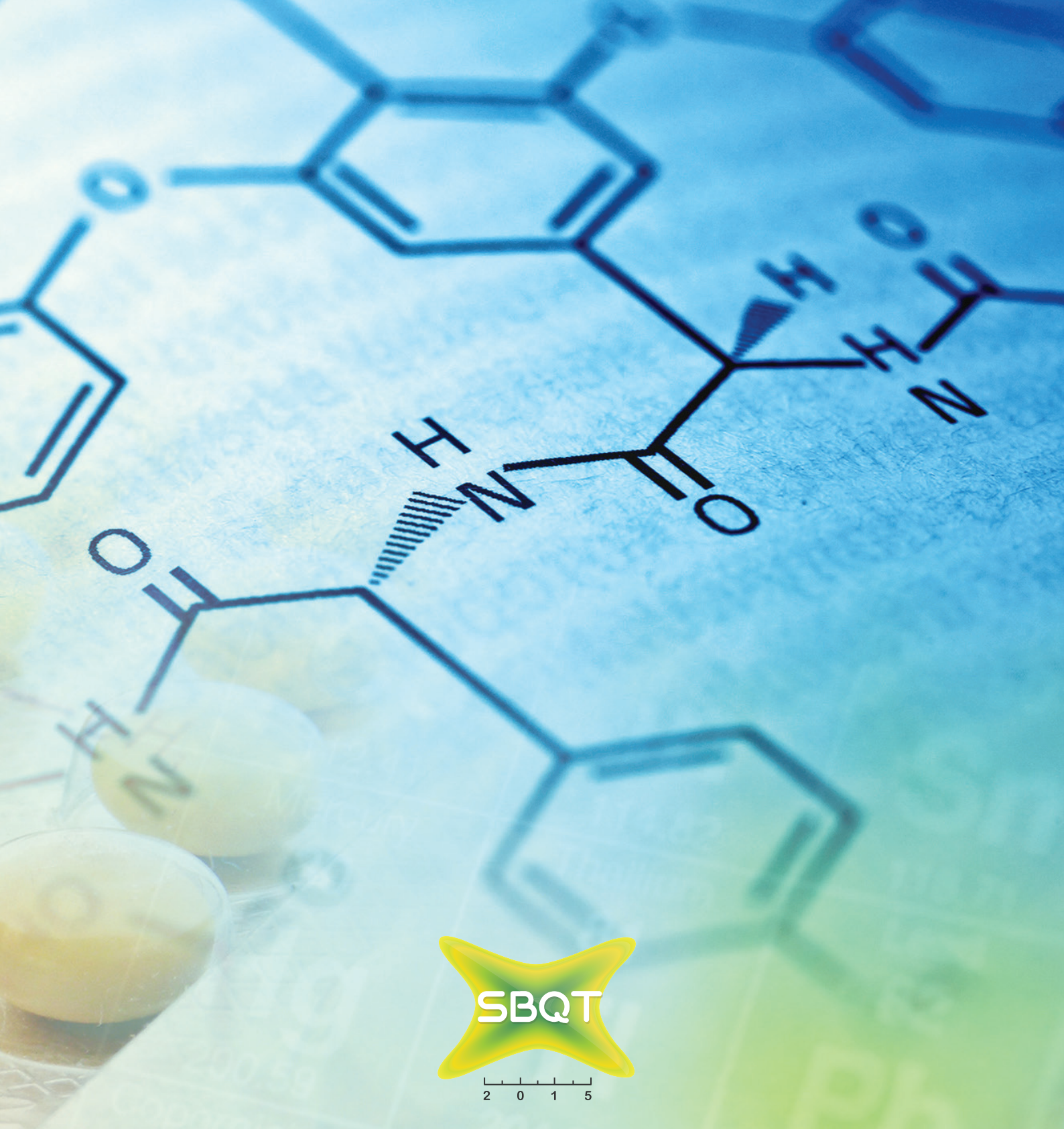
¹Das, P. et al. *J. Phys. Chem. A* **2015**, 119, 3710-3720.

²Lane, J. R. et al. *J. Chem. Theor. Comput.* **2013**, 9, 3263-3266.

LISTA DE PARTICIPANTES

PARTICIPANTE	INSTITUIÇÃO	PARTICIPANTE	INSTITUIÇÃO
Acássio R. Santos	UFRN	Eduardo C. Aguiar	UFRPE
Adalberto V. S. de Araújo	IQUSP	Eduardo F. Franca	UFU
Ademar D.M. Neto	IQ-UnB	Eduardo P. Rocha	UFLA
Ademir João Camargo	UEG	Egon C. Santos	UFMG
Adilson L.P. Silva	UEMA	Elaine H. T. Oliveira	UF
Agenor M. Andrade	UEPG	Eliezer F. Oliveira	UNESP
Alberto S. Marques	UFAM	Elizabeth L. M. Miguel	UFSJ
Alessandra Albernaz	UnB	Elizete V. do Monte	UFPB-(National Committee)
Alessandra S. Kiametis	UnB	Ellen V. D'alessandro	UFSJ
Alex G. Taranto	UFSJ	Emerson Boschetto	UFSCar
Alexandre A. Leitão	UFJF	Emília V. F. Aragão	IQ-UnB
Alexandre M. Carauta	FTESM-RJ	Erica Liandra - Salvador	UFABC
Alfredo M. Simas	UFPe (Scientific Committee)	Erika H. Nozawa	UF
Aline A. Oliveira	USP	Eugenio F. Souza	UFRJ
Aline C. Baruqui	UFRJ	Ezequiel F. V. Leitão	UFPB
Aliny A. Reis	UF	F. M. Bickelhaupt	VU Amsterdam
Aluizio G. Silva	UFPE	Fabio L. P. Costa	UFG
Ana C. F. Albuquerque	UFRJ	Fabiola F. P. Lopes	UF
Ana P. S. Cruz	INPE	Fabricio Carvalho	UFABC
Ana G. C. Oliveira	UnB	Fátima C. A. Correia	UF
Ana Paula Carregal	UFSJ	Fátima M. P. Rezende	UFL
Ana Paula Oliveira	UEG	Felipe C. T. Antônio	UFABC
Ana V. P. Abreu	UnB	Felipe D. S. Vilhena	UFF
Anderson H. Lima	UFPA	Felipe F. Soares	UFRJ
Anderson J. L. Catão	UFSCar	Felipe M. Fernandes	IQ-UFRJ
André F. Moura	UFSCar	Felipe S. Carvalho	UFV
André G. Oliveira	IME	Felipe V. Z. Assad	UNIFESP
André H. Barbosa	UFF-(National Committee)	Felippe M. Colombari	UFSCar
André M. Henriques	UFF	Fernanda Bettanin	UFABC
Andrés Reyes	UNC-Colombia	Fernando R. V. Ferreira	UERJ
Andriele S. Prado	IF-UnB	Fernando Steffler	UFMG
Antenor J. P. Neto	UFABC	Filipe B. Lima	UFRPE
Antonio C. Borin	USP	Flávio Olimpio	UEG
Antonio L. S. Júnior	UFMG	Francisco C. Machado	ITA
Antonio M. S. Santos	UnB	Francisco C. Lavarda	FIS-UNESP
Antonio C. Sobrinho	IF-UFBA	Francisco E. Jorge	UFES
Arno Veldhorst	USP	Frederico B. Sousa	UF
Arsênio P. V. Neto	UnB	Frederico T. Silva	UFPE
Asdrubal L. Blanco	UFSCar	Gabriel S. Fernandes	UNESP
Ataualpa A. C. Braga	USP	Gabriel L. C. Souza	UFMT
Bárbara D. L. Ferreira	UFMG	Gabriel M. Zanotto	UFRGS
Brenda S. Pauletti	UnB	Gabriela D. Silva	UFABC
Breno Galvão	CEFET	Gabriela Zavatti	UF
Breno R. L. Galvão	CEFET	Gabrielle G. Silva	UnB
Bruna L. Silva	UF-Itajubá	Gerd B. Rocha	UFPB
Bruno M. Servilha	USP	Gesiel G. Silva	UnB
Bruno N. C. Tenório	UFRJ	Gessenildo Rodrigues	UFPB
Bruno S. Leite	UFRPE	Gisele F. Castro	UEAM
Camila D. A. B. Silva	UnB	Gladson S. Machado	UFRRJ
Camila M. B. Machado	UFPE	Glauco F. Bauerfeldt	UFRRJ
Camila S. Avelar	UNIFESP	Gleiciane L. M. Pinheiro	UFPA
Carla G. Fonseca	UFJF	Graziele S. Pereira	UnB
Carla V. Soares	UFJF	Guelber C. Gomes	UFPA
Carlos E. Silva	UFG	Guilherme A. Canella	IQ-SCar/USP
Carlos E. Silva	UNICAMP	Guilherme F. de Lima	UNIFEI
Carlos E. T. Magalhães	UFOP	Guilherme K. Gonzatti	UFRGS
Carlos E. V. Moura	UFRJ	Guilherme L. Chinini	Unicamp
Carlos M. Cavalcante	UFRPE	Guilherme M. Arantes	IQ-UnB
Cassiano M. Aono	UFABC	Gustavo H. L. Souza	UFPE
Cayo E. M. Gonçalves	UFMG	Gustavo J. Costa	UTFP
Célia F. Guerra	VU Amsterdam	Gustavo L. C. Moura	UFPE
Charles A. O. Rocha	UnB	Gustavo O. Silva	UEG
Christina T. Borges	UF-Itajubá	Hamilton B. Napolitano	UEG-(Local Committee)
Clarissa O. Silva	UFRRJ	Heibbe C. B. Oliveira	IQ-UnB
Claudia Fileto	UF	Heitor A. Abreu	UFMG-(National Committee)
Clebio S. N. Júnior	UFSJ	Hélcio J. Batista	UFRPE
Cleiton D. Maciel	UFABC	Hélio A. Duarte	UFMG
Cleuton S. Silva	UNICAMP	Henrique A. Rodrigues	UFLA
Corey Alan Petty	ITA	Henrique O. Euclides	INPE
Cristiano E. L. Júnior	UFPE	Hubert Stassen	UFRGS
Cristina A. Barboza	UNICAMP	Hugo G. Machado	UEG
Dana Nachtigallova	IOC- AS CR	Inara de Aguiar	UFMT
Daniel A. B. Oliveira	UFT	Iran da L. Sousa	UNICAMP
Daniel F. S. Machado	UnB	Isabella M. S. Rosado	UF
Daniel S. Quattrocchi	UFF	Isaque G. Medeiros	UFPA
Daniel J. Ribeiro	UFRJ	Ítalo C. Anjos	UFPB
Daniela R. Silva	UFL	Ítalo P. Lima	UnB
Daniely V. V. Cardoso	ITA	Ítamar B. Junior	IME
Danillo P. Valverde	UFG	Ivan E. V. Coelho	UFSJ
Danilo S. Olivier	FFCLRP	Jakler N. Nunes	UFF/IME
Davi A. C. Ferreira	UnB	Jhonata J. Silva	UEG
David Fuks	BGU-Israel	João L. Martins	UnB-(National Committee)
David L. Azevedo	UnB	João S. Monteiro	UFF
David Willian O. Sousa	UFRJ	Joaquim D. M. Neto	UFRP
Deiver A. Teixeira	IFMT	José S. Freitas	UFAL
Demétrio S. Filho	IF-UnB (Local Committee)	José D. L. Dutra	UFPE
Deyse G. Costa	UFV	José S. Politi	UnB
Diego F. S. Paschoal	UFJF	Josefredo R. P. Jr.	UFSJ
Diesley Martins	UFU	Josene Maria Toldo	UFRGS
Edison F. Junior	UFABC	Joyce K. L. Vale	UFPA
Ednilson Orestes	UFF	Júlia F. Haiduke	UF
Eduardo C. Vaz	UEG	Juliana C. M. Silva	UFMG
Eduardo da Conceicao	UFRJ	Juliana de O. Mendes	UFRJ

PARTICIPANTE	INSTITUIÇÃO	PARTICIPANTE	INSTITUIÇÃO
Juliana F. Lopes	UNIFEI	Pamella V. B. Pinho	UFMG
Julio G. Correia	CETEM/ MCTI	Patricia B. Gusmão	IQ - UERJ
Julio S. Silva	UFPE	Patricia R. P. Barreto	INPE
Júlio C. Maia	UFPB	Patrick R. Batista	UTFPR
Kalil Bernardino	UFSCar	Paula N. Goulart	UFRRJ
Kaline Coutinho	IF- USP (Co-Chair)	Paula H. Mello	UFABC-(National Committee)
Kayo F. Silva	UFPE	Paulo A. Netz	UFRGS
Kelson M. T. Oliveira	UFAM	Paulo Mc. C. Oliveira	UFPE
Kleber C. Mundim	IQ-UnB (Chair)	Paulo R. Oliveira	UTFPR
Lais S. Barbosa	IQ-UnB	Paulo R. G. Júnior	UFMG
Lais P. Machado	UFRRJ	Pedro S. Pinheiro	IQ - UFRJ
Larissa T. Jesus	UFS	Pooria Farahani	IQ-USP
Lars G. M. Pettersson	LNCC	Priscila C. Rocha	UFJF
Laurent E. Dardenne	LNCC	Railton B. Andrade	UFPB
Lauriane G. Santin	UnB	Regis C. Leal	UNICAMP
Leandro O. Duarte	UFG - ICET	Regis T. Santiago	USP
Leandro R. Franco	UFG	Renan A. P. Ribeiro	UEPG
Lenin J. D. Soto	PUC	Renan F. Guerra	UFU
Leonardo Baptista	UERJ	Renata R. Nunes	UFSJ
Leonardo F. de Oliveira	UFMT	Renato B. Pontes	IF-UFG
Lethícia R. Santos	UNIFESP	Renato G. F. Sobrinho	UFMT
Letícia M. Prates	UFRRJ	Renato L. T. Parreira	UNIFRAN
Luana S. Pedroza	UFABC	Renato R. Andrade	UFRRJ
Lucas C. Santana	UF-Itajubá	Rene F. K. Spada	ITA
Lucas de A. Santos	UFL	Rhuiago M. Oliveira	UnB
Lucas F. Esteves	UFJF	Ricardo Almeida	UERJ
Lucas José Karas	UTFPR	Ricardo L. Longo	DQ-UFPE
Lucas M. Costa	IME	Ricardo O. Freire	UFS
Lucas C. Martins	UFES	Ricardo R. O. Junior	UFRJ
Lucelma P. Carvalho	UFPE (UFPE)	Ricardo R. Ternavisk	ITA
Luciano A. Leal	IF - UnB	Roberto L. A. Haiduke	IQ-UFSC
Luciano N. Vidal	UTFPR	Rodrigo A. L. Silva	UEG
Luciano Ribeiro	UEG	Rodrigo S. Bitzer	IQ/UFRJ
Luciene B. Silva	UFSCar	Rodrigo M. D. Ledo	UnB
Luiz Henrique Lacerda	UEPG	Rodrigo S. Bitzer	UFRJ
Luiz A. R. Júnior	UnB	Rogério J. Costa	UnB
Luiz A. S. Costa	UFJF	Rogério S. K. Asano	UF
Luiz C. Malbouisson	IF-UFBa	Rogério V. A. Júnior	UFPE
Luiz C. Zonetti	UNESP	Rosemberg F. N. Rodrigues	UEG
Luiz F. A. Ferrão	ITA	Roy E. Bruns	UNICAMP
Magaly M. Brandão	UF	Sandro F. Brito	IQ-UnB
Maicon Delarmelina	OSJB	Sara F. A. Morais	UnB
Maicon P. Lourenço	UFMG	Sara M. R. Sousa	UFSJ
Maira Theisen	UFRGS	Sara S. Brito	UnB
Marcelo A. Chagas	UFMG	Selma F. Bazan	UNIFEI
Marcelo A. O. Pontes	ITA	Sergio E. Galembeck	USP
Márcia L. Belarmino	UFPE	Sergio E. Preza	UFMS
Marcilio N. Guimarães	UFBA	Shella Cristina S. Costa	UFMS
Marcio M. Silva	UFPE	Sidney R. Santana	UFPP
Marco A. C. Nascimento	IQ-UFRJ (Scientific Committee)	Solemar S. Oliveira	UEG-(Local Committee)
Marcos M. Castro	UFG	Stella M. Resende	UFSJ
Marcos R. Vargas	IQ - UnB	Suelen S. F. Pessanha	UFRuralRJ
Marcos H. Oliveira	IFPR	Suélmo M. S. Filho	IFG
Marcos V. M. Meuser	UFF	Sylvio Canuto	IF-USP (Scientific Committee)
Marcus V. P. Santos	UFPE	Taina G. Barros	UFPA
M. Suely P. Mundim	IF-UnB (Local Committee)	Tamires L. Pereira	UnB
Marília L. A. Costa	UFSJ	Tatiane N. Tejero	UFRuralRJ
Marina Pelegrini	AFA	Teodorico C. Ramalho	UFLA
Marlon V. M. Filho	GQTC - UFAM	Terttu I. Hukka	TUT-Finland
Masaki Nozawa	UF	Thayná B. Silva	UFAN
Mateus A. M. Paiva	CEFET-MG	Thiago F. Cunha	UnB
Mateus R. Lage	UFF	Thiago M. Cardozo	IQ - UFRJ
Matheus C. Quintão	UFMG	Thiago O. Lopes	IQ - UnB
Mauricio D. Coutinho	UFABC	Valdemir Ludwig	UFJF
Mauricio G. Rodrigues	UNICAMP	Valter H. Carvalho	UEG
Mauricio T. M. Cruz	UERJ	Vanildo M. L. Braga	UFSJ
Maurício V. Teijido	Fac.Química/Udelar	Verônica M. Nascimento	IQ-USP
Mauro B. Amorim	UFRJ	Victor A. S. Mata	UFMT
Mauro L. Franco	UFVJM	Victor V. Ferreira	UFRJ
Micael D. Andrade	IFUFBa	Vincenzo Aquilanti	UNIPG-Italy
Michel B. Garcia	UFRuralRJ	Vinicius C. Mota	UFES
Michele A. Salvador	UFABC	Vinicius Fernandes	UFABC
Michell O. Almeida	UFABC	Vitor H. M. Silva	IQ-USP
Miguel A. San-Miguel	IQ - Unicamp	Vladimiro M. Hernandez	Arizona University, USA
Milene A. R. Oliveira	UFSCar	Wagner B. de Almeida	UFF (Scientific Committee)
Milton M. Fujimoto	UFPR	Wagner E. Richter	UNICAMP
Miqueias M. Peixoto	UFRRJ	Walber G. G. Júnior	UF-Itajubá
Mirele B. Pinto	UFMG	Washington B. Silva	UnB
Mitca H. T. Oliveira	UF	Wesley G. D. P. Silva	UFLA
Moacir F. F. Júnior	UFU	Weverson R. Gomes	UFSCar
Murilo H. Teixeira	IQ-USP	William K. Nitschke	UFRGS
Naomi H. T. Oliveira	UF	Yago S. Sousa	UEG
Natália A. R. Pinto	UFSJ	Yoelvis Orozco-Gonzalez	BGSU-USA
Natália M. Silva	IQ-UFSJ	Yuri A. Aoto	ITC-Universität Stuttgart
Nathália B. Lima	UFPE		
Nathalia F. Carvalho	UFSJ		
Natieli A. Silva	USP		
Nayara D. C. Carvalho	IQ - UnB		
Nelson A. N. Alencar	UFPA		
Nelson H. Morgon	UNICAMP		
Noam G. Silva	UFAM		
Núbia M. N. Rodrigues	UEG		
Orlando R. Neto	IEA/DCTA		



AGRADECIMENTOS

